

TECHNOLOGY UTILIZATION

(NASA-SP-5113) NONDESTRUCTIVE TESTING:
A SURVEY (Southwest Research Inst.)
283 p MF \$0.95; SOD HC \$3.25 Domestic
Postpaid CSCI 14D

N73-28517
THRU
N73-28528
Unclas
G1/15 69889

NONDESTRUCTIVE TESTING

A SURVEY



1

NONDESTRUCTIVE TESTING

A SURVEY

Prepared under contract for NASA
by Southwest Research Institute



Technology Utilization Office 1973
NATIONAL AERONAUTICS AND SPACE ADMINISTRATION
Washington, D.C.

NOTICE • This document is disseminated under the sponsorship of the National Aeronautics and Space Administration in the interest of information exchange. The United States Government assumes no liability for its contents or use thereof.

For sale by the Superintendent of Documents,
U.S. Government Printing Office, Washington, D.C. 20402
Price \$3.35 domestic postpaid or \$3.00 GPO Bookstore
Stock Number 3300-00471
Library of Congress Catalog Card Number 72-600247

Foreword

Both standard and developmental methods for nondestructive evaluation (NDE) are reviewed in this survey. The high reliability required for aerospace components has been one factor in the increasing development of more effective methods, but many other sectors of industry are making use of these improvements. Major fields of NDE (the use of liquid penetrants, magnetic particles, X-ray radiography, ultrasonic vibrations, and eddy currents) have reached a high state of development. Less widely used techniques in industry include strain sensing, neutron radiography leak detection, heat (thermal or infra-red methods), and the use of microwaves, acoustic emission and holography.

The principles involved are discussed and typical applications are given. Advantages and disadvantages are listed, NASA contributions are summarized, and an attempt is made to present practical considerations.

The National Aeronautics and Space Administration established its Technology Utilization Program to disseminate knowledge derived from aerospace research so that the private sector and various public agencies could benefit. Information is collected and evaluated in terms of its potential utility. This survey is one of a series of documents designed to aid in the dissemination and use of such developments.

The information in this survey is based on an examination of pertinent literature from NASA and its contractors, and discussions with scientists in the field. A comprehensive reference and bibliography will aid the reader who seeks further details.

Director
Technology Utilization Office

1

Contents

	Page	
Chapter 1. INTRODUCTION.....	1	✓
C. Gerald Gardner		
Chapter 2. LIQUID PENETRANTS.....	7	✓
Richard L. Pasley		
Physical Principles.....	10	
Penetrant Systems.....	13	
Inspection Procedures.....	14	
Specifications and Standards.....	19	
Description of Commercially Available Equipment.....	20	
Selecting a Penetrant System.....	22	
NASA's Utilization Contributions.....	22	
Chapter 3. ULTRASONICS.....	27	✓
Byron E. Leonard and C. Gerald Gardner		
Elementary Principles.....	28	
Ultrasonic Testing.....	34	
NASA Contributions.....	39	
Chapter 4. RADIOGRAPHY.....	63	✓
C. Gerald Gardner		
Basic Principles.....	65	
Safety.....	70	
X-Ray Equipment.....	71	
Gamma-Ray Equipment.....	73	
Selection of Radiographic Equipment.....	75	
Radiographic Film.....	77	
Interpretation of Radiographs.....	83	
Special Radiography.....	85	
Neutron Radiography.....	89	
NASA Contributions.....	90	
Chapter 5. EDDY-CURRENT TESTING.....	101	✓
Richard L. Pasley and James A. Birdwell		
Physical Principles.....	102	
Electrical Circuitry.....	106	
Eddy-Current Test Equipment.....	108	
Selecting an Eddy-Current Inspection Method.....	113	
Advantages and Limitations.....	116	
Chapter 6. THERMAL AND INFRARED TESTING.....	119	✓
Robert E. Engelhardt and William A. Hewgley		
Physical Principles.....	119	
Thermal Detectors and Methods.....	122	
Contact Thermographic Methods.....	124	
Noncontact Thermographic Detectors and Methods.....	131	
Contact Thermometric Methods and Materials.....	136	
Noncontact Thermometric Instruments.....	137	

	Page
Chapter 7. MICROWAVE TECHNIQUES.....	141 ✓
William L. Rollwitz	
Physical Principles.....	142
Applications of Microwave Techniques.....	150
Chapter 8. MAGNETIC TESTING.....	165 ✓
Richard L. Pasley and John R. Barton	
Physical Principles.....	167
The Magnetic-Particle Method.....	181
Magnetic-Hysteresis Measurements.....	187
Magnetic Field Perturbation.....	190
Electric Current Perturbation.....	191
Limitations and Advantages.....	192
Chapter 9. LEAK TESTING.....	195 ✓
Robert E. Engelhardt	
Physical Principles.....	196
Relationships of Leak-Testing Methods and Instrumentation.....	200
Details of Leak-Testing Methods and Instrumentation.....	204
Strategy of Leak Testing.....	216
NASA Contributions.....	220
Chapter 10. STRAIN SENSING.....	225 ✓
Robert R. King and Felix N. Kusenberger	
Physical Principles.....	228
Brittle Coatings.....	229
Photoelastic Coatings.....	239
Resistance Strain Gages.....	248
Chapter 11. DEVELOPMENT METHODS.....	263 ✓
C. Gerald Gardner	
Acoustic Emission.....	263
Coherent Light Methods.....	265
Ultrasonic Holography.....	268
BIBLIOGRAPHY.....	269

CHAPTER 1

Introduction**C. Gerald Gardner**

Man has always been concerned with the quality and reliability of the things he fashions for himself, the products of his technology. Moreover, he has continually sought to improve upon his immediate senses as instruments by which to test these products. Archimedes' jubilant "eureka" was evoked not primarily because he had discovered the principle of flotation, but rather because that discovery afforded him a means of determining whether his king's newly made gold crown had been unduly alloyed with silver. In this respect, the most gifted technologist of antiquity was concerned with what today is called nondestructive evaluation (NDE).

While man's concern with nondestructive evaluation has always been manifest, his skills and implements for this task have generally lagged behind his technology. Indeed, most of the NDE methods presently used were developed within the past half century; some are less than a decade old. Moreover, until quite recently, NDE was commonly regarded as a production shop activity, a mixture of craft and lore, the province of the skilled tradesman; rarely (as in the case of Archimedes) was it an area of concern for the engineer or scientist. As long as serviceability and safety could be secured by an engineering approach based on overdesign with large safety factors, such an

unsophisticated approach to NDE was acceptable. But, with the advent of the modern technological era, the need has arisen for components and structures of unprecedented efficiency, the design of which requires that the constituent materials are exploited close to their ultimate capability. Such a design approach requires both a greatly improved understanding and exploitation of the engineering properties of classical materials, and the development and use of new materials including nonmetallics and composites. With these developments has come the need for commensurate improvements in the technology of nondestructive evaluation.

By the close of World War II, the "big five" NDE methods (liquid penetrant testing, magnetic particle testing, X-ray radiography, ultrasonic testing, and eddy-current testing) had reached a high, though not definitive, state of development. The post-war years brought the introduction of nuclear power plants, jet-powered aircraft, rocket-powered ballistic missiles, unmanned spacecraft, and finally manned spacecraft. These developments required further refinement of the big five NDE methods, as well as of strain sensing and leak detection. The development of entirely new methods, including thermal and infrared testing, microwave testing, acoustic emission testing, and holographic testing, was also stimulated. Most

of these refinements and new developments are based on advanced physics and electronics; their development was brought about by the efforts of highly trained scientists and engineers as well as skilled technicians.

The contemporary period in NDE development is characterized not only by the introduction of novel, sophisticated technical approaches, but also by a trend away from hand operations and toward substantially automated inspection systems. By greatly reducing the time required for inspection and by eliminating the uncertainties typically associated with "operator dependence" of hand operations, such automated systems are, in many cases, proving to be cost-effective despite their greater initial cost. Thus progress in systems engineering, electromechanical design, signal processing, information theory, computer technology, and cybernetics are increasingly prominent aspects of NDE development.

The aerospace industries and government agencies concerned with aerospace development are making significant contributions to the development and growth of NDE. Among these the National Aeronautics and Space Administration (NASA), through its several Centers and many of its contractors, is a significant contributor. NASA's contributions to NDE are, of course, by-products of its primary mission, the development of advanced aerospace vehicles and the exploration of space. The extraordinary efficiency and reliability of modern aerospace structures has been achieved in no small measure because of the systematic, painstaking programs of reliability and quality assurance (R&QA) that have accompanied their development and production. In these R&QA programs, nondestructive evaluation is a significant factor, though certainly not the only one. NASA's influence on NDE technology is both indirect and direct—indirect in the sense that its needs have stimulated developments by suppliers, and direct in the sense of explicit research and development efforts by both NASA Centers and NASA contractors. Many NASA-sponsored advances in NDE technology have potential applications outside the aerospace field, and this

survey is intended to serve primarily as a medium for the dissemination of these developments and for their transfer to nonaerospace applications.

Throughout industry, popular demand for a greater degree of quality, reliability, and safety in all products is currently focusing attention on NDE. The automotive and trucking industry, the railroad and high-speed ground transportation industry, the pipeline industry, and the shipbuilding industry all stand to profit from advances in NDE technology. The electric utility industry, the construction industry, the home appliance industry, and the food industry likewise are recognizing that NDE, properly implemented, can more than pay for itself through improvements in product uniformity, fewer rejections, and reduced incidence of in-service failure.

Typically, the responsibility for recognizing the need for, and assessing the potential cost-benefit impact of, a new or revised NDE program in industry rests primarily at the level of middle management. For members of middle management with such responsibility, a general working knowledge of the available NDE methods and their capabilities and limitations has become a virtual necessity. It is to this audience that this Technology Utilization Survey is principally addressed. While it is in no sense intended to be a textbook or treatise, it is hoped that it will serve the need of middle management for an overview of the field of NDE. Although a general technical faculty on the part of the reader has been supposed, no expertise in nondestructive evaluation has been assumed.

In addition to this introduction, the survey contains nine chapters each of which deals with a major NDE method, with a concluding chapter on several methods still being developed. Each of the nine major chapters contains a brief synopsis of the fundamental principles and practical procedures in standard use; the contributions made by NASA Centers and contractors are then presented against this background. These synopses are restricted in scope to the essentials required for a general understanding of the significance of the NASA con-

tributions subsequently presented. In presenting these contributions, emphasis has been placed on basic principles and practical applications rather than on details of implementation.

The primary documentation on which this survey is based consists of pertinent NASA technical notes, technical memoranda, and contractor reports. The survey is not intended as a substitute for these referenced documents, but as a summary and guide. Readers who find a contribution of potential use to them should refer to the referenced document(s) for further, more detailed information.

Of the numerous NASA contributions described herein, one in particular should be noted. Recognizing that a successful NDE program depends crucially on the knowledge and skill of practicing technicians, NASA has, through a contractor, prepared a series of instructional materials in each of the most widely used NDE methods (refs. 1 to 18). A training handbook is provided for each method, which can be used as a classroom text, together with one or more manuals of the so-called programmed type. These manuals are suitable for self-study, and are designed to lead the student step-by-step to an understanding of the principles, apparatus, and procedures of an NDE method. When used as part of a systematic training program conducted by competent instructors, and including a period of supervised apprenticeship, these materials provide the

student with the knowledge and experience necessary for expert application of the method at the technician level. These books (available from the American Society for Nondestructive Testing) may prove to be NASA's most significant contribution to the practice of NDE.

Table 1-1 presents in brief outline a comparison of selected NDE methods. It contains for each method the basic property sensed or measured, some typical applications, and the most notable advantages and limitations of the method. This table (of which many similar versions are in circulation) is necessarily incomplete, and is intended to serve only the purpose of orientation. It should not be relied on for making critical assessments of the potential application of a method to a specific NDE task.

Historically, the term "nondestructive testing" has been widely used. Some have preferred the term "nondestructive inspection." The *Ad Hoc* Committee on Nondestructive Evaluation of the National Materials Advisory Board (ref. 19) has stated that "the term nondestructive evaluation (NDE) is considered more appropriate . . . since: (1) this discipline also requires the evaluation of test results and inspection; (2) the words 'testing and inspection' do not properly imply the theoretical aspects of this field; and (3) the name (nondestructive evaluation) is more succinct and descriptive." The recommendation of the NMAB *Ad Hoc* Committee has been adopted for this survey.

TABLE I-1.—Comparison of Selected NDE Methods

Method	Chapter	Properties sensed or measured	Typical flaws detected	Representative application	Advantages	Limitations
X-ray radiography...	4	Inhomogeneities in thickness, density, or composition.	Voids, porosity, inclusions, and cracks.	Castings, forgings, weldments, and assemblies.	Detects internal flaws; useful on a wide variety of materials; portable; permanent record.	Cost; relative insensitivity to thin laminar flaws such as fatigue cracks and delaminations; health hazard.
Neutron radiog: raphy.	4	Compositional inhomogeneities; selectively sensitive to particular atomic nuclei.	Presence, absence, or mislocation of internal components of suitable composition.	Inspection of propellant or explosive charge inside closed ammunition or pyrotechnic devices.	Good penetration of most structural metals; high sensitivity to favorable materials; permanent record.	Cost; relatively unportable; poor definition; health hazard.
Liquid penetrants...	2	Material separations open to a surface.	Cracks, gouges, porosity, laps, and seams.	Castings, forgings, weldments, and components subject to fatigue or stress-corrosion cracking.	Inexpensive; easy to apply; portable.	Flaw must be open to an accessible surface; messy; irrelevant indications often occur; operator dependent.
Eddy-current testing.	5	Anomalies in electric conductivity and, in cases, magnetic permeability.	Cracks, seams, and variations in alloy composition of heat treatment.	Wire, tubing, local regions of sheet metal, alloy sorting, and thickness gaging.	Moderate cost; readily automated; portable; permanent record if needed.	Conductive materials only; shallow penetration; geometry sensitive; reference standards often necessary.
Microwave testing...	7	Anomalies in complex dielectric coefficient; surface anomalies in conductive materials.	In dielectrics: dishonds voids, and large cracks; in metal surfaces: surface cracks.	Glass-fiber-resin structures; plastics; ceramics; moisture content; thickness measurement.	Noncontacting; readily automated; rapid inspection.	No penetration of metals; comparatively poor definition of flaws.
Magnetic particles...	8	Anomalies in magnetic field flux at surface of part.	Cracks, seams, laps, voids, porosity, and inclusions.	Castings, forgings, and extrusions.	Simple; inexpensive; senses shallow subsurface flaws as well as surface flaws.	Ferromagnetic materials only; messy; careful surface preparation required; irrelevant indications often occur; operator dependent.

Magnetic field testing.....	8	Anomalies in magnetic field flux at surface of part.	Cracks, seams, laps, voids, porosity, and inclusions.	Castings, forgings, and extrusions.	Good sensitivity to and discrimination of fatigue cracks; readily automated; moderate depth penetration; permanent record if needed.	Ferromagnetic materials only; proper magnetization of part sometimes difficult.
Ultrasonic testing.....	3	Anomalies in acoustic impedance.	Cracks, voids, porosity, and delaminations.	Castings, forgings, extrusions; thickness gaging.	Excellent penetration; readily automated; good sensitivity and resolution requires access to only one side; permanent record if needed.	Requires mechanical coupling to surface; manual inspection is slow; reference standards usually required; operator dependent.
Sonic testing.....	3	Anomalies in low-frequency acoustic impedance or natural modes of vibration.	Disbonds, delaminations, larger cracks or voids in simple parts.	Laminated structures; honeycomb; small parts with characteristic "ring".	Comparatively simple to implement; readily automated; portable.	Geometry sensitive; poor definition.
Ultrasonic holography.	3	Same as ultrasonic testing.....	Same as ultrasonic testing.....	Inspection of small, geometrically regular parts.	Produces a viewable image of flaws.	Cost; limited to small parts; poor definition compared to radiography.
Infrared testing.....	6	Surface temperature; anomalies in thermal conductivity and/or surface emissivity.	Voids or disbonds in non-metals; location of hot or cold spots in thermally active assemblies.	Laminated structures; honeycomb; electric and electronic circuits.	Produces a viewable thermal map.	Cost; difficult to control surface emissivity; poor definition.
Strain gages.....	10	Mechanical strains.....	Not used for flaw detection.....	Stress-strain analysis of most materials.	Low cost; reliable.....	Insensitive to preexisting strains; small area coverage; requires bonding to surface.
Brittle coatings.....	10	Mechanical strains.....	Not commonly used for flaw detection.	Stress-strain analysis of most materials.	Low cost; produces large area map of strain field.	Insensitive to preexisting strains; messy-limited accuracy.
Optical holography..	11	Mechanical strains.....	Disbonds; delaminations; plastic deformation.	Honeycomb; composite structures; tires; precision parts such as bearing elements.	Extremely sensitive; produces map of strain field; permanent record if needed.	Cost; complexity; requires considerable skill.
Leak detection.....	9	Flow of a fluid.....	Leaks in closed systems.....	Vacuum systems; gas and liquid storage vessels; pipage.	Good sensitivity; wide range of instrumentation available.	Requires internal and external access to system; contaminants may interfere; can be costly.

REFERENCES

1. ANON.: Introduction to Nondestructive Testing. NASA CR-61204, 1968. (N68-28776)
2. ANON.: Liquid Penetrant Testing. NASA CR-61205, 1968. (N68-28777)
3. ANON.: Magnetic Particle Testing. NASA CR-61206, 1967. (N68-28778)
4. ANON.: Ultrasonics: Vol. I—Basic Principles. NASA CR-61209, 1967. (N68-28781)
5. ANON.: Ultrasonics: Vol. II—Equipment. NASA CR-61210, 1967. (N68-28782)
6. ANON.: Ultrasonics: Vol. III—Applications. NASA CR-61211, 1967. (N68-28783)
7. ANON.: Eddy Current: Vol. I—Basic Principles. NASA CR-61207, 1967.
8. ANON.: Eddy Current: Vol. II—Equipment, Methods, and Applications. NASA CR-61208, 1967.
9. ANON.: Radiography: Vol. I—Origin and Nature of Radiation. NASA CR-61212, 1967. (N68-28784)
10. ANON.: Radiography: Vol. II—Radiation Safety. NASA CR-61213, 1967. (N68-28785)
11. ANON.: Radiography: Vol. III—Radiographic Equipment. NASA CR-61214, 1967. (N68-28786)
12. ANON.: Radiography: Vol. IV—Making a Radiograph. NASA CR-61215, 1967. (N68-28787)
13. ANON.: Radiography: Vol. V—Film Handling and Processing. NASA CR-61216, 1967. (N68-28788)
14. ANON.: Liquid Penetrant Testing: Classroom Training Handbook. NASA CR-61229, 1967. (N68-28791)
15. ANON.: Magnetic Particle Testing: Classroom Training Handbook. NASA CR-61227, 1967. (N68-28789)
16. ANON.: Ultrasonic Testing: Classroom Training Handbook. NASA CR-61228, 1967.
17. ANON.: Eddy Current Testing: Classroom Training Handbook. NASA CR-61230, 1967. (N68-28792)
18. ANON.: Radiographic Testing: Classroom Training Handbook. NASA CR-61231, 1967. (N68-28793)
19. ANON.: Nondestructive Evaluation—A Report of the National Materials Advisory Board. Publication NMAB-252, National Academy of Sciences—National Academy of Engineering (Washington, D.C.), June 1969. (Available from the National Technical Information Service, Springfield, Va.)

CHAPTER 2

Liquid Penetrants

Richard L. Pasley

Liquid-penetrant inspection is a process for locating defects that are open to the surface in solid, essentially nonporous materials by observing the presence of entrapped highly visible liquids. These liquids penetrate surface openings, remain there during a rinsing operation, and then emerge to the surface after a thin coating of absorbent material, which acts as a developer applied to the article under test. The visibility of the trace amount of liquid withdrawn from a defect into the coating is greatly enhanced by a special additive in the penetrant. The additive may be either a very bright dye, the color of which contrasts with that of the absorbent coating, or a compound that strongly radiates visible light under invisible ultraviolet illumination.

In practice, the liquid-penetrant-inspection procedure usually comprises six basic steps:

- (1) Cleaning of the article to be inspected
- (2) Application of the penetrant to the article
- (3) Removal of excess penetrant
- (4) Application of an absorbent coating (developer) to the surface of the article
- (5) Visual inspection of the article, and interpretation of flaw indications
- (6) Post-inspection cleaning

These steps are further discussed in ensuing sections; certain special penetrant systems combine or even omit some of these basic steps.

Liquid-penetrant inspection has become popular throughout industry, and today is probably the single most widely employed nondestructive testing method. It is popular because it has a wide range of applications, is comparatively easy to employ, and requires only a modicum of special training or technical ability for its routine use. Within its normal application, penetrant inspection has proved to be both sensitive and reliable in the hands of properly trained and experienced technicians. Its fundamental limitation is, of course, that it is useless for detecting flaws that are present within the body of an article, but not open to its surface.

Perhaps the earliest application of liquid-penetrant inspection was by blacksmiths who, in the fabrication of ironwares, noticed stains caused by quenching liquids seeping out of quench cracks. Liquid-penetrant inspection, as it is practiced today, however, had its beginning with the development of the "oil and whiting" process in the railroad industry. In this process, such railroad hardware as locomotive parts, rail car axles, wheels, and couplers were first coated with a thin liquid consisting of a mixture of kerosene and heavy, dark lubricating oil. The excess liquid was then removed from the surface of the part, leaving the oil mixture entrapped in cracks and similar surface flaws. A coating of a white chalk and alcohol mixture was then applied to the surface of the part.

When the alcohol evaporated, the part was left with a thin, uniform film of dry, white powder coating its surface. The part was then struck with a hammer or similar tool to force or jar the entrapped oil from the defects, thus staining the white coating (ref. 1).

Although, in principle, the oil and whiting process would work on both ferrous and non-ferrous metal parts, the method was apparently used only on steel parts. When the magnetic-particle method for inspecting ferromagnetic materials was introduced, the oil and whiting method began to decline in popularity, and, by 1940, had been largely displaced by the magnetic-particle method (ref. 2).

The next significant advancement in penetrant inspection was the addition of black-light inspection to the process. After a penetrating oil was allowed to seep into surface discontinuities, the surface of the article under inspection was cleaned quickly with a solvent, then viewed under ultraviolet light. Oil fluoresces, or glows, emitting a pale blue light when illuminated by ultraviolet (so-called "black") light; hence, the visibility of the traces of oil migrating out of very small surface defects was substantially enhanced. Usually both the oil and the article being inspected were heated to increase penetrating effectiveness, thus giving rise to the name "hot-oil method." Although this development marked an improvement in liquid-penetrant processes, it was, by modern standards, low in sensitivity because of the faintness of the oil's fluorescence; consequently, it had only limited use (ref. 2).

With the onset of World War II, an urgent need, especially in the aircraft industry, was generated for improved nondestructive test methods, which accelerated the development of liquid penetrants. In 1941, Robert C. Switzer and Joseph L. Switzer developed an improved penetrant test by introducing a highly fluorescent additive into a specially compounded penetrant liquid. Under black light, the resultant material emitted a brilliant yellow-green fluorescence, which exhibited high contrast when viewed in a darkened room. The yellow-green hue was close to the color range to which the normal eye is most sensitive, and thus proved

to be ideally suited for the visual detection of small defects. Commercial fluorescent penetrant systems were quickly introduced and immediately accepted by industry (ref. 3).

About the same time that fluorescent penetrants were being developed, the Switzers also thought of using brilliant colored dyes which would be visible under ordinary white light. Contributions in this direction were also made by Tabor de Forest (ref. 4). Because of the difficulty in providing black-light inspection for large welded structures, the welding industry offered a good market for penetrants with visible dyes. This and similar industrial requirements prompted the commercial development and widespread use of colored (usually red) dye penetrants.

Although attempts were made to formulate penetrants with water as the liquid vehicle, such formulations originally were found to be much inferior to penetrants with an oil base. The convenience of using oil-base penetrants was greatly increased with the development of formulations containing an emulsifying agent in the penetrant material itself. This made the penetrant material washable by ordinary tap water. Such self-emulsifiable penetrant systems of the fluorescent type were the first to have wide commercial success.

During the early 1950's, the so-called post-emulsifiable penetrant systems were developed, in which the former practice of adding an emulsifying agent to the penetrant liquid itself was abandoned. Instead, a separate step was introduced in which an emulsifying agent was added after the liquid penetrant had been applied. This post-emulsifying technique proved markedly superior to the use of self-emulsifiable penetrants in detecting comparatively wide and shallow defects such as scratches or gouges. It also competed favorably with the self-emulsifiable penetrants in revealing small defects such as cracks (ref. 2).

The current demand for aerospace hardware of near 100-percent reliability, as well as the large-scale use of new engineering materials, has continued to stimulate the development of liquid-penetrant materials and methods. Materials that are safe for use on surfaces in contact

with liquid oxygen have been developed. Others have been formulated that are compatible with titanium, nickel, and other alloys. Methods of permanently recording penetrant-inspection indications and penetrant materials with controlled ranges of sensitivity have been introduced. Promising alternatives to the standard post-emulsification system are available; some of which are treated in this chapter. There is every indication that new advances will occur as the manufacturers of penetrant materials respond to the challenges of advancing technology. The same is true of penetrant inspections.

The most important advantage of the penetrant method is its relative simplicity and economy. With very little investment in equipment, supplies, and operator training, an excellent liquid-penetrant inspection capability can be established. Other advantages are listed below.

(1) The method will accommodate articles of many sizes and shapes.

(2) Automation can be used to provide rapid, uniform inspection of large quantities of similar objects.

(3) Many penetrant materials are available to suit a wide range of special purposes.

(4) The penetrant method is comparatively easily and quickly learned.

(5) In the hands of trained and experienced technicians, the method has less tendency to give false indications than many competing techniques.

The principal limitation of nondestructive testing by liquid penetrants, as noted earlier, is that it can detect only those discontinuities having an opening to the surface. Thus, the penetrant method is suited for detecting surface cracks, seams, tears, pits, laps, and porosity. (Another type of defect for which penetrants are sometimes used is leaks in piping and containers. Leak testing with liquid penetrants is discussed in another chapter.) Some of the principal disadvantages of liquid-penetrant inspection are listed below.

(1) The effectiveness of the method depends on the skill and vigilance of the inspector; it is operator dependent.

(2) Porous surfaces tend to absorb pene-

trants, thus producing an undesirable background which will mask defect indications.

(3) In general, penetrants are not useable at very hot or very cold temperatures; i.e., below about 40° or above 120° F.

(4) The liquid materials may be contaminated by water, dirt, and other foreign substances, rendering the method ineffective.

(5) If penetrant or developer material affects subsequent processes, such as painting or etching, special post-inspection cleaning may be required.

Other standard nondestructive test methods that can detect surface flaws include magnetic-particle, eddy-current and ultrasonic testing, and radiography. Less frequently used than these standard methods, magnetic-field perturbation and electric-current injection also compete with liquid-penetrant testing as methods of detecting surface flaws. In general, radiography is far less sensitive than liquid penetrants in detecting fine surface flaws, and, generally, is more costly. For the inspection of ferromagnetic articles, magnetic-particle testing is comparable in sensitivity to that by liquid penetrants, and, when dry magnetic powder is used, has the advantage of being faster and less messy. The magnetic particle method, however, is inapplicable to nonferromagnetic articles; in this respect, the liquid-penetrant method complements the magnetic-particle method. In the hands of a skilled technician, ultrasonics approaches liquid penetrants in its ability to detect surface flaws. Compared with liquid-penetrant inspection, however, the use of ultrasonics for scanning any appreciably large area is usually prohibitively time-consuming and costly. Eddy-current inspection for surface cracks has about the same deficiency in rate of inspection as ultrasonics, and, with a few exceptions, is less sensitive than liquid-penetrant inspection. Both the magnetic-field-perturbation method (for ferromagnetic articles) and the electric-current-injection method have been shown to be generally more sensitive than the liquid-penetrant method. Their use, however, is generally restricted to the inspection of a large number of articles of similar size and shape,

thus justifying a semiautomatic and comparatively expensive inspection machine.

PHYSICAL PRINCIPLES

The penetrant inspection method depends on a liquid that can effectively wet the surface of a solid article, flow over that surface to form a continuous and reasonably uniform coating, and migrate into cavities that are open to the surface. The cavities of interest are, of course, usually exceedingly small, and the surface opening may be quite invisible to the unaided eye. The ability of a given liquid to flow over a given surface and enter surface cavities depends principally on the following factors:

- (1) The cleanliness of the surface
- (2) The geometry of the cavity
- (3) The size of the cavity
- (4) The surface tension of the liquid
- (5) The ability of the liquid to wet the surface.

The cohesive forces between the molecules of a liquid cause a surface tension. An example of the influence of surface tension is the tendency of free liquid, such as water droplets, to contract into a sphere. In such a droplet, the surface tension is, of course, counterbalanced by the internal hydrostatic pressure of the liquid. When the liquid comes into contact with a solid surface, the cohesive force responsible for surface tension competes with the adhesive force between the molecules of the liquid and the solid surface. These forces jointly determine the contact angle θ , which the liquid makes with the surface (fig. 2-1). If it is less than 90° , the liquid is said to wet the surface, or to have good wetting ability.

Closely connected with wetting ability is the familiar phenomenon of capillary rise or depression (fig. 2-2). If the contact angle, which the liquid makes with the wall of the capillary tube, is less than 90° (i.e., if the liquid wets the tube wall), the liquid meniscus in such a tube is concave, and the liquid rises in the tube. If, on the other hand, the liquid does not wet the tube wall, the meniscus is convex, and the liquid is depressed in the tube. In the case of capillary rise illustrated here, the meniscus does not pull

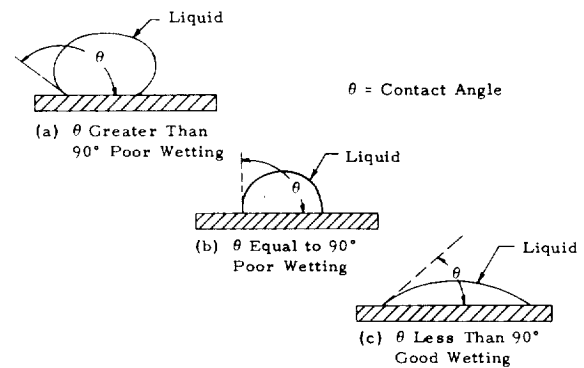


FIGURE 2-1.—The contact angle, θ , is the angle between the liquid and solid surfaces.

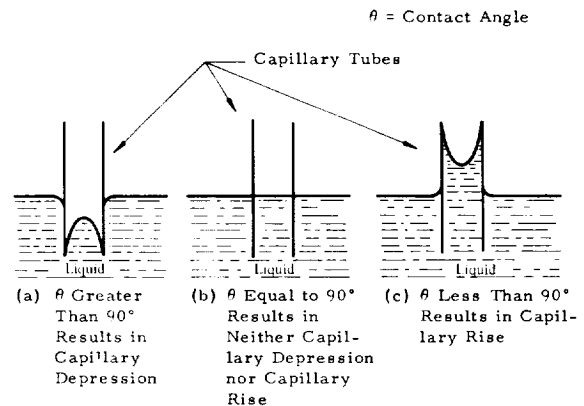


FIGURE 2-2.—The rise or depression of liquids in small vertical capillary tubes is determined by the contact angle, θ .

the liquid up the tube; rather, the hydrostatic pressure immediately under the meniscus is reduced by the distribution of surface tension in the concave surface, and the liquid is pushed up the capillary by the hydraulically transmitted pressure of the atmosphere at the free surface of the liquid outside the capillary. In fact, figure 2-3 clearly shows that if T is the surface tension (i.e., the force per unit length of surface edge), and r is the capillary radius, then the net force on the liquid column, due to surface tension, is $2\pi rT \cos \theta$; this must equal the weight of the vertical liquid column, which is $\pi r^2 \rho g h$, where ρ is the mass density of the liquid, h is the height of the liquid column, and g is the acceleration due to gravity. This leads to the equation:

$$2\pi rT \cos \theta = \pi r^2 \rho g h$$

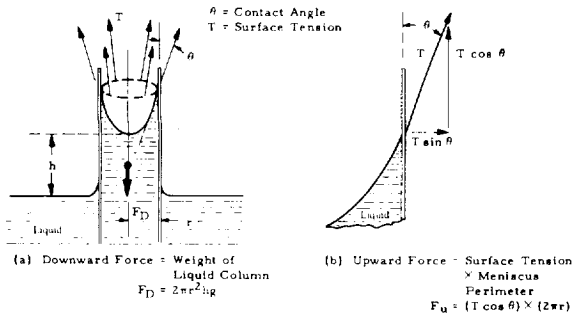


FIGURE 2-3.—The forces involved in capillary rise are the downward force from the weight of the liquid column and the upward force from surface tension along the meniscus perimeter.

This simplifies to the basic equation of capillary rise:

$$h = \frac{2T \cos \theta}{r \rho g}$$

Thus the height to which the liquid rises is directly proportional to the surface tension of the liquid and to the cosine of the angle of contact; it is inversely proportional to the density of the liquid and to the radius of the capillary. If, as in figure 2-4, the capillary tube is closed rather than open, a wetting liquid will still rise in the tube; but now there exists an extra pressure due to the air and vapor compressed in the

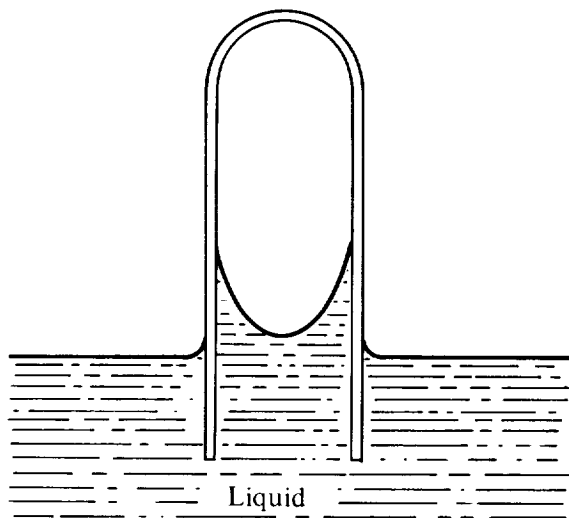


FIGURE 2-4.—The rise and depression of liquids in closed capillary tubes are affected by the compressed air entrapped in the closed end.

closed end of the tube, and the capillary rise is not as great.

These examples of liquid-surface wetting and capillary rise illustrate the basic physical principles by which a penetrant may enter fine surface discontinuities. It must be recognized, however, that the practical circumstances encountered in the use of liquid penetrants are somewhat more complex than these examples may suggest. Cracks, for example, are not capillary tubes; but the basic interaction between a liquid and a solid surface, which is responsible for capillary rise, is also responsible for the migration of penetrants into fine surface openings. Thus, a high-surface tension in a penetrant, combined with a small angle of contact and low density, is generally desirable.

It is noteworthy that the viscosity of the liquid is not a factor in the basic equation of capillary rise. Viscosity is related to the rate at which a liquid will flow under some applied unbalanced stress; in itself, it has a negligible effect on penetrating ability. In general, however, very viscous liquids are unsuitable as penetrants because they do not flow rapidly enough over the surface of an article; consequently, they require excessively long periods of time to migrate into fine flaws.

Another desirable property of a liquid penetrant is its ability to dissolve an adequate amount of a suitable dye or fluorescent compound. Finally, the liquid must be compatible with a suitable solvent or emulsifier (if it is to be water-washable).

The foregoing discussion should make it clear that the development of practical penetrant materials has entailed solving a wide range of technical problems. The successful development of a modern oil-base, self-emulsifiable, fluorescent penetrant of high sensitivity and low volatility, and which is chemically stable over a practical temperature range, tolerant of minor contamination, and safe both for the user and the material on which it is used (at a reasonable price), is indeed a noteworthy achievement.

Just as it is important that a penetrant enter surface flaws, it is also important that the penetrant emerge from the flaw after the superficial coating is removed from the penetrant. It is a

seeming paradox that the same interaction between a liquid and a surface that causes the liquid to enter a fine opening is also responsible for its emergence therefrom. The resolution of the paradox is simple: once the surface has been forcibly freed of the excess penetrant by the washing operation and is again clean, it becomes accessible to the entrapped liquid, which, under the effect of the adhesive forces between liquid and solid, spreads over the newly cleaned surface until an equilibrium distribution is attained, as illustrated in figure 2-5.

Although in some cases the amount of penetrant in the surface bead at equilibrium is sufficient to be detected visually, sensitivity is vastly increased by the use of a so-called developer. The common developer is an extremely fine, fluffy powder. When applied as a thin coat to a surface immediately following the removal of excess superficial penetrant, it forms a sponge-like system of very fine, random capillary paths. If the penetrant contacts the powder, the powder then competes with the freshly cleaned surface of the inspected item for the penetrant liquid as it flows out of the flaw. If the developer is properly designed, it readily absorbs the liquid, and, under favorable condi-

tions, can literally clean the flaw and the surrounding surface of the penetrant liquid. The liquid continues to migrate by capillary action, spreading through the developer until either an equilibrium is reached or the liquid evaporates, leaving behind a residue of visible dye or fluorescent material. This migrating action is shown schematically in figure 2-6. The visibility of the dye is greatly increased by the spreading or enlargement of the indication, and also by the contrast between the color of the dye (usually red) against the color of the developer (usually a flat white). In the case of fluorescent penetrants, the enlargement of indication is effective in increasing sensitivity, but, of course, the color of the developer no longer plays so important a role.

It should be noted that the developer is a mixed blessing. The enlargement of indication, due to spreading in the developer, inevitably causes a reduction in resolution, which makes it difficult to discriminate between two separate flaws that are close together. Also, the migration of the penetrant in the developer dilutes the visible dye or fluorescent additive; and, if the thickness of the developer coating exceeds a certain optimum value, the detectability of a flaw will, in general, be reduced.

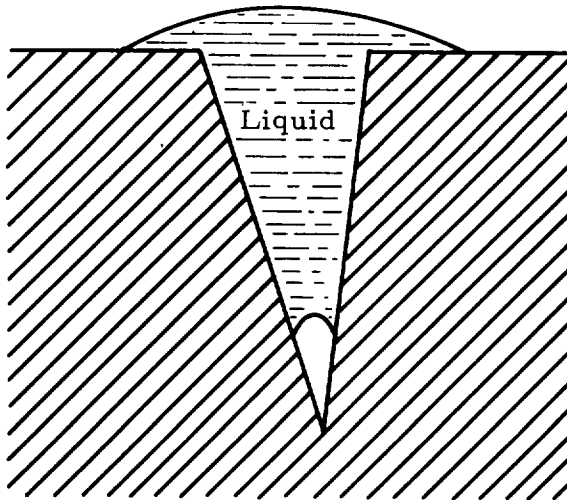


FIGURE 2-5.—After the excess penetrant has been removed from the surface, the penetrant liquid remaining in a crack will emerge and form a bead on the surface.

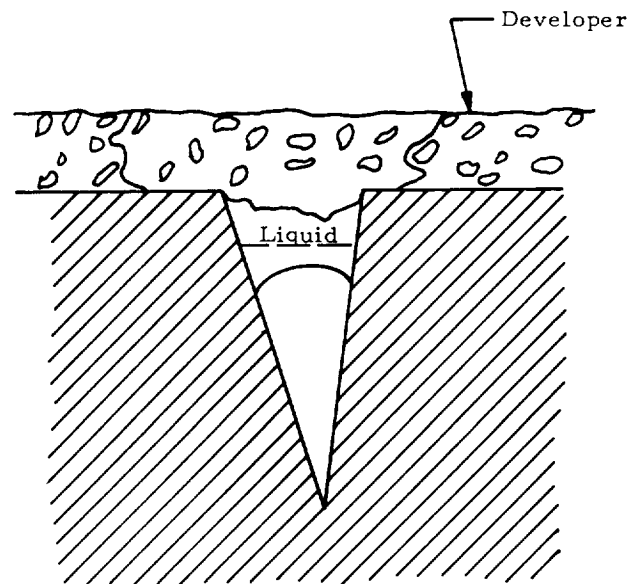


FIGURE 2-6.—Schematic of powder developer action.

PENETRANT SYSTEMS

Classification of Penetrant Systems

The expression "penetrant system" is used here to denote a particular set of materials that have been specifically formulated in combination to perform a penetrant inspection; it does not refer to a set of mechanical devices or other apparatus which may be necessary in the process. The most commonly used liquid-penetrant systems are customarily categorized according to the criteria below.

(1) The type of additive used to make the penetrant visible; thus colored-dye penetrants are distinguished from fluorescent penetrants.

(2) The rinse medium used to remove the superficial coat of wet penetrant from an article; thus water-washable penetrants are distinguished from the solvent-removable penetrants.

(3) The need for a separate emulsifier; thus *self-emulsifiable* penetrants are distinguished from *post-emulsifiable* penetrants. The self-emulsifiable penetrants have an added constituent, an emulsifying agent, which makes them miscible with ordinary water without further treatment. The post-emulsifiable penetrants require, as a separate step in the inspection procedure, the addition of an emulsifying agent directly to the penetrant on the surface of an article under inspection.

Other characteristics which differentiate penetrant systems are listed below.

(1) *Nature of the liquid base of the penetrant.* The most common penetrants are formulated with oil bases. However, there are also now available water-base penetrants; water-soluble-base penetrants (which do not require an emulsifier), such as glycol-base penetrants; and penetrants whose bases form gels when water is added in certain proportions.

(2) *Type of developer required in the penetrant system.* Some systems have wet developers, others, dry developers, and some have no developers at all. In cases of large surface openings, penetrant material will emerge to the surface in sufficient amounts to be easily detected without the use of a developer. Also, highly sensitive penetrant systems have been introduced that are specifically intended to be used without devel-

opers. Developers are discussed in some detail later in this chapter.

(3) *Specific type of inspection for which the penetrant system is formulated.* Thus, there are special penetrant systems for leak detection, for inspection of electronic circuits, etc.

(4) *Sensitivity of the penetrant system.* In some cases, it is useful to be able to select a penetrant that is comparatively insensitive to flaws smaller than a certain size. Several manufacturers now offer penetrants in a graded range of sensitivities.

Developers

A properly designed developer causes penetrant material to emerge from small surface openings and spread through the developer material. This spreading action enlarges the area covered by penetrant material, thereby enhancing the visibility of the penetrant indication. There are two principal classes of developers—powder-particle developers and dilution-expansion developers. The powder-particle developers further comprise three types: (1) the dry developers, (2) the aqueous wet developers, and (3) the nonaqueous wet developers. The dry developers are special light fluffy powders that will cling to dry metallic surfaces. Figure 2-7 illustrates the application of powder developers. Aqueous wet developers are suspensions of powder in water to which wetting agents have been added. The nonaqueous wet developers are powders suspended in a volatile organic liquid. Developer powders must, of course, be insoluble in the penetrant.

With fluorescent penetrants, the aqueous wet developers and the dry developers are generally preferred, whereas nonaqueous wet developers are usually used with visible dye penetrants. Wet developers are best suited for use on very smooth surfaces to which dry developers adhere poorly; when a large number of small articles are to be inspected; or when wide, shallow discontinuities are sought. Dry developers are generally preferred for inspecting rough surfaces; sharp fillets, holes and threaded articles; and very large articles.

The so-called dilution-expansion developers



FIGURE 2-7.—Small parts in a wire basket are dipped into a dry fluffy developer (ref. 2). (Courtesy of Magnaflux Corp.)

are liquid or plastic film materials that do not contain particulates. After the developer is applied, the penetrant diffuses into the liquid developer so that it is simultaneously diluted and expanded in the film, thus becoming more visible to the test operator. If the plastic form is used, the developer will set and freeze the penetrant in a film which may be stripped from the part surface and used as a recording of the penetrant indication. Strippable developers are further discussed in an ensuing section of this chapter.

INSPECTION PROCEDURES

Basic Steps

Except in certain penetrant systems that require no developer, the penetrant-inspection process involves six basic steps:

- (1) Cleaning of the article to be inspected
- (2) Application of the penetrant
- (3) Removal of excess penetrant
- (4) Application of developer to the surface of the article (not required for some recently introduced systems)

(5) Visual inspection of the article and interpretation of indications

(6) Post-inspection removal of residue materials.

The details of each step depend on the particular penetrant system being used. For instance, the post-emulsifiable-penetrant method requires the addition of an emulsifying agent as part of the wash operation for removal of excess penetrant. Flow charts illustrating the sequence of steps for the most commonly used penetrant systems are shown in figures 2-8, 2-9, and 2-10. Each of the basic steps is discussed more fully in the remainder of this section.

Cleaning Methods

For effective penetrant inspection, the surface of an article must be free of rust, scale, welding flux, grease, paint, oily films, and dirt. The complete removal of such contaminants is quite important because if anything is left on the surface which will prevent the penetrant liquid from entering a defect, the inspection will be ineffective. Some of the common cleaning

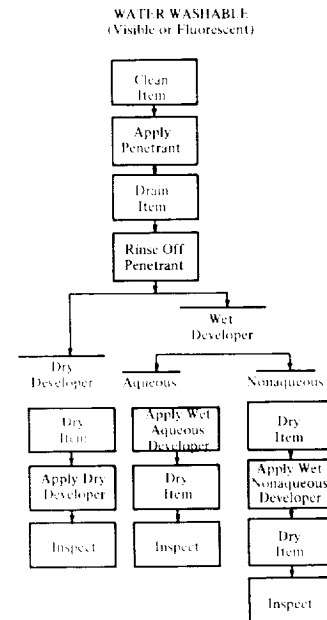


FIGURE 2-8.—Procedures for water-washable liquid-penetrant systems.

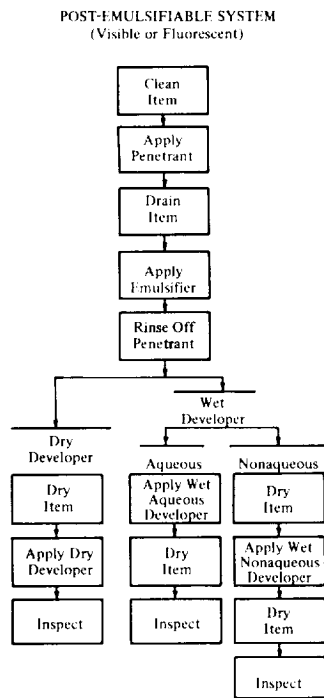


FIGURE 2-9.—Procedures for post-emulsifiable liquid-penetrant systems.

SOLVENT-REMOVABLE SYSTEM
(Visible or Fluorescent)

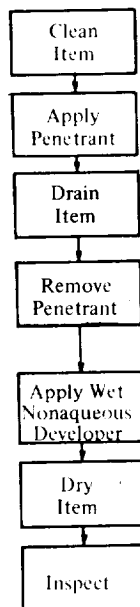


FIGURE 2-10.—Procedure for solvent-removable liquid-penetrant systems.

methods and their recommended applications are as follows (ref. 5) :

(1) *Detergent cleaning* (or washing with soap and water) is generally recommended for removing superficial materials and contaminants from surface and void areas. Rags and brushes are commonly used with a detergent cleaner to wash or scrub a surface. Brushes with wire bristles should generally not be used, as the bristles may actually close the surface openings of some small defects.

(2) *Cleaning with organic solvents*, such as naphtha or alcohol, is recommended for removing grease and oils. This method is generally inadequate for solid soils embedded in void areas.

(3) *Vapor degreasing* is recommended for removing heavy oils, grease, and organic soils. The article is suspended in a container at the bottom of which a quantity of chlorinated solvent is being heated and vaporized. Hot vapors condense on the article and dissolve the contamination. For inorganic soils, detergent cleaning is generally superior to this method.

(4) *Descaling solutions*, such as hydrochloric acid, nitric acid, or hydrofluoric acid (depending on the base metal), are recommended for removing oxide films and oxide scales. The descaling solution chosen must be used with care to prevent degradation of the article being cleaned. The articles should be thoroughly rinsed and dried after descaling.

(5) *Paint remover* is recommended for stripping away paint from the article's surface. Either solvent paint removers or hot-tank alkaline strippers may be used, as appropriate. The articles should be thoroughly rinsed and dried after paint removal.

(6) *Ultrasonic cleaning* is recommended for use in conjunction with any of the above cleaning materials. The ultrasonic agitation improves cleaning efficiency and decreases cleaning time.

(7) *Abrasive blasting* is sometimes used to remove resistant incrustations of carbon, rust, and scale. This type of cleaning, however, can result in filling surface discontinuities with abrasive or the crust material, or in peening the surface of the base material, thus possibly

closing some discontinuities. Hence, this method should be used only with due caution, if at all.

(8) *Air firing* (i.e., heating in a clean, oxidizing atmosphere) is sometimes useful for removing moisture or light organic soil from ceramic articles.

Penetrant Application

Proper application of the penetrant to an article includes thoroughly and uniformly wetting with the penetrant the region of the surface to be inspected, and maintaining the coating wet for a prescribed minimum time (so-called dwell time), during which the material migrates into the surface flaws. Dwell times generally recommended for many different combinations of materials, surface flaws, and penetrants may be found in references 2 and 3. Temperature affects penetrating action; however, for most materials the manufacturer's recommended dwell times are valid for the range of 60° to 90° F. For temperatures between 30° and 60° F, the dwell time should generally be lengthened to at least twice those recommended. Application of liquid penetrants at temperatures below 30° F is not recommended, because some of the liquids associated with the system could solidify. For temperatures in the range of 90° to 120° F, the nominal dwell times may be shortened to periods determined experimentally with a representative specimen. During the dwell time, the article need not be continually sprayed or brushed with penetrant, nor must it remain submerged in the penetrant solution. If the penetrant begins to dry, however, it will lose its penetrating ability; hence, the operator should periodically test for dryness during the dwell time, and, if necessary, prevent drying by re-spraying, rebrushing, or redipping.

Excess Penetrant Removal

Proper removal of excess penetrant is an important step. Failure to remove all excess penetrant will leave a confusing background, which will interfere with accurate defect indications. Moreover, overwashing (i.e., removing penetrants from defects) during the rinse operation

will exclude any chance of obtaining a defect indication. Hence, the method of penetrant removal must be chosen to suit the article being inspected, the penetrant material used, and the type of defect sought.

Excess penetrants are removed by using either water or a solvent. Oil-base water-washable penetrants and post-emulsifiable penetrants are both readily removed by a properly used water rinse. Water is an excellent washing medium for these materials because it will not dissolve the unemulsified penetrant, and does not tend to penetrate into small defects and rinse out the entrapped penetrant.

Spraying and wiping are the usual methods of removing excess penetrant and water. Of these two methods, spraying is usually preferable. Special nozzles for this purpose have been designed, which generate a stream of coarse droplets. Usually, the best washing action is achieved by directing the spray stream at an angle of approximately 45° with the article's surface. Such a spray has the effect of cutting through the penetrant film by impact, getting under it, and then rolling it off the surface (ref. 2).

An interesting variation on the standard water wash is the use of a so-called inhibited wash mixture in which the wash water is combined with a chemical compound that modifies the washing properties of standard water-washable penetrants by inhibiting the emulsification process in a controlled manner. Such wash mixtures are less prone to remove penetrant from surface cracks than water alone (ref. 6).

Penetrants are sometimes removed simply by wiping with a dry, absorbent cloth or paper towel. This method is comparatively slow and messy, and requires an abundance of rags or towels. Moreover, if water buckets are used, the wash water must be continually kept clean; otherwise penetrant liquid will contaminate the wash water and ruin its effectiveness as a rinse. The advantage of this method, however, is that, when done with reasonable skill, penetrant will not be removed from any defects unless the defects are extremely large and shallow.

Since solvent-removable penetrants are designed to be used with specific solvents, they

should be removed only with the material recommended by the manufacturer, and only by wiping. The solvent liquid, if used as a bath or spray, tends to dilute or wash out the penetrant entrapped in defects. Prior to applying the solvent, excess penetrant should be wiped from the article's surface with absorbent towels. After this, the article's surface should be wiped with clean towels dampened with the recommended solvent (ref. 7).

Emulsifying agents are used to facilitate the removal of penetrant materials with some wash medium, usually water. The emulsifying agent used with post-emulsifiable penetrants should blend with the penetrant material on contact. It must also spread through the penetrant sufficiently slowly to permit time-of-contact control by the test operator, but not so slowly as to delay inspection.

Emulsifiers are usually supplied in two viscosity ranges. The lower-viscosity emulsifiers are preferred for articles of irregular shape or with rough surfaces, because they readily flow over surface irregularities, threads, fillets, and the like. The higher-viscosity emulsifiers, on the other hand, tend to act more slowly, enabling the user to control with some precision the depth of emulsification before rinsing. Hence over-emulsification resulting in the unwanted removal of penetrant from shallow relatively open flaws can more readily be prevented. Special emulsifiers, whose chemical composition is compatible with their use on specific reactive alloys, are also available.

After the penetrant's dwell time has elapsed, the emulsifying agent is applied either by dipping the article into an emulsifier bath, by pouring the emulsifier over the article, or by spraying. Emulsifiers should not be applied with a brush, since the stroking action of the bristles may remove penetrant from shallow or scratch-like defects. After the emulsifier has been applied, the article should be left untouched while the emulsifying agent spreads through the penetrant liquid. The period of time allowed for this spreading action (called emulsifying time) is the most critical step in the post-emulsifiable penetrant process. If the penetrant-emulsifier solution is rinsed too soon and the emulsifier

hasn't had time to spread over the article's surface, the excess penetrant cannot be properly removed. On the other hand, if the emulsifier is left on the article too long, it will spread into surface defects causing all the penetrant, including that in defects, to wash away during the excess-penetrant-removal step. Emulsifying time should be specified by the penetrant manufacturer. Recommended emulsification dwell times usually range from a few seconds to a maximum of 5 min for fluorescent penetrants; in the case of visible dye penetrants, dwell times are usually only a few seconds. Generally, because so many factors are involved, emulsifying times are best determined beforehand, by experiment, for the article (and defects) under investigation (ref. 8).

After the penetrant-removal process, the test operator should determine if he has achieved thorough penetrant removal. If fluorescent penetrants are used, the operator should examine the article under black light. If visible penetrants are used, the test operator should wipe the article surface with a dry cloth and examine the cloth for traces of penetrant. If the surface is not completely free of excess penetrant, the article should be completely reprocessed, beginning with the initial cleaning operation.

Developer Application and Drying

Dry developers are usually applied by dipping the article into a bin of loose fluffy powder, as previously illustrated in figure 2-7, or by gently blowing the powder onto the article with soft hand-squeezed rubber "puff bottles." The dry developers should be applied lightly and evenly over the entire surface, and, because they are in powder form, their application is usually best done in a booth equipped with an air circulation and filtration system. The powder will not appear to adhere to the article, but a sufficient amount will remain and act to bring out indications. Excess powder should be removed by lightly shaking, tapping, or blowing the article. The test operator must be careful, however, not to remove too much powder as this may ruin the effectiveness of inspection (ref. 2).

The wet aqueous developers are applied by dipping the article into a vat of the liquid mix-

ture, or by spraying the developer onto the article with commercial compressed-air or airless-spray systems. This developer should be applied so as to achieve a smooth, uniformly thin coating of powder when the developer liquid has evaporated. Care must be taken to avoid concentration of developer in hollow open areas of the article. After the wet aqueous developer has been applied, the article is dried.

Wet nonaqueous developers are applied by the same methods of dipping or spraying used for the wet aqueous developers. Nonaqueous developers are used primarily with visible penetrants where a flat-white background is essential. The article is first dried and then a fairly heavy coat of developer is applied; the coat should be heavy enough to provide a satisfactory background for visible indications (ref. 2).

For drying the article, practically any method is acceptable, provided the part is not overheated or contaminated with foreign materials during the process. Circulating hot-air driers are generally preferred because the drying process is hastened, the temperature can be controlled, and the developer dries in an even coat. The drying temperatures are usually set at 200° to 225° F for maximum drying efficiency. The articles should remain in the drier only long enough to dry water off the surface. The danger of leaving the article in the drier too long is that the penetrant itself may evaporate, thereby ruining the sensitivity of the inspection. For the same reason, the drying-oven temperature should generally not be allowed to exceed 250° F (ref. 7).

The length of time the developer is allowed to remain on the article surface before inspection begins is called the development time. Since entrapped penetrant is being pulled out of the defects by capillary action in the developer, the development time should be sufficiently long to allow the dye indication to appear. This may range from a few minutes for large flaws to an hour or longer for very small flaws.

Visual Examination and Interpretation of Indications

The phase of penetrant inspection requiring the greatest skill and experience is the actual

visual examination and interpretation of developed indications. The inspector must be fully aware of the capabilities and limitations of the penetrant system that is being used, and he must have thorough and competent knowledge of the article being inspected. In particular, he must know the kinds of flaws to expect, their likely locations, and the likelihood that an unusual flaw may occur. Moreover, he must be able to discriminate between a genuine flaw indication and any spurious, or false, indication that may occur because of either improper handling of the various steps in the penetrant procedure, or a peculiarity in either geometry or surface properties of the article under inspection. Such skill comes only with a thorough understanding of the penetrant process and adequate experience in its use. Both formal instruction and an adequate on-the-job apprenticeship are necessary to ensure optimum reliability.

Adequate and proper lighting and an appropriate, well-designed, and comfortable facility for visual examination are important. Moreover, the work schedule of the inspector should be devised to reduce eye fatigue and loss of alertness. At the visual inspection stage, haste may cause not only waste (in the form of unnecessarily rejected articles), but possibly disaster by passing an article unfit for its intended service.

Restoration of Inspected Articles for Storage or Service

After an article has been examined and passed by an inspector, it is usually necessary to remove all residual inspection materials and, in some cases, to protect the surface by applying either light oil, packing grease, or other coating. Painting or plating may be called for in certain cases.

Rejected articles should be either discarded or subjected to proper rework. Rejected articles should be clearly and appropriately tagged or otherwise marked to prevent their accidental reentry into service. If a rejected article is considered expendable waste, it should be destroyed. Salvageable articles should be properly reworked, and again inspected to insure the effectiveness of the rework.

SPECIFICATIONS AND STANDARDS

In the present context, the term *specification* refers to a written statement expressing in detail one or more of the following: (1) a specific requirement for liquid penetrant inspection; (2) the penetrant system or systems that must be used in an inspection; (3) special procedural regulations; (4) appropriate acceptance-rejection criteria; and (5) a list of qualifications required of inspection personnel. The term *standard* is sometimes used in referring to an item in the above list of types of specifications that may be referred to collectively as specifications and standards. However, the term *standard* is also used in another distinctive sense, namely, a material, test object, or test arrangement that has been agreed on as a basis of comparison for some penetrant parameter. It is in the latter sense that the term *standard* is used in this discussion.

A number of U.S. Government agencies have issued specifications referring to some aspect of penetrant inspection. In addition, several professional societies concerned with engineering practice and quality assurance have also issued penetrant-inspection specifications. Table 2-1 lists a representative selection of current specifications; a more complete list may be found in reference 9.

To date, there are no widely accepted standard penetrant indications for comparison purposes, although progress in this direction is being made. The principal obstacles are: (1) variations due to differences of technique of penetrant use; (2) variations in visual acuity and discrimination among inspectors; and (3) the difficulty of accurately and reproducibly simulating a useful range of types and sizes of flaws. Among the various proposed approaches to flaw simulation, the only one that has so far achieved any significant degree of acceptance is the so-called cracked-aluminum-block penetrant comparator. In this approach, a small standardized aluminum-alloy bar is heated in a gas flame so as to produce a symmetric thermal gradient from the center to the edges of the bar; at a specified temperature of the center, the bar is quenched in cold water, producing a more or less symmetric distribution of cracks, the dimensions of which are large near the bar's center and become progressively smaller near the edges. A shallow slot is sawed in the cracked face of the bar, dividing it into two halves, each having a comparable pattern of cracks and range of crack sizes. The two halves of the block are then inspected according to one of the two penetrant systems that are to be compared. (The two penetrant systems are often of the

TABLE 2-1.—Selected Representative Liquid Penetrant Inspection Specifications

Issuing Agency or Organization	Date	Title
Atomic Energy Commission (AEC)-----	1969	Nondestructive Evaluation, Supplementary Criteria for Use of ASME Sec. III and USASI B31.7. Div., Reactor Dev. and Tech. (ref. 10).
American Society of Mechanical Engineers (ASME).	1968	Sec. IX. Boiler and Pressure Vessel Code (Welding Qualifications) (ref. 11).
American Society for Testing and Materials (ASTM).	1965	E 165-65. Standard Methods for Liquid Penetrant Inspection (ref. 12).
Department of Defense (DOD)-----	1962	MIL-STD-410A. Qualification of Inspection Personnel (ref. 13).
Department of Defense (DOD)-----	1964	MIL-I-25135 and Amendment 3. Penetrant Inspection Materials (ref. 14).
Department of Defense (DOD)-----	1969	MIL-I-6866B and Amendment 2. Penetrant Method of Inspection (ref. 8).
Society of Automotive Engineers (SAE)---	1965	AMS 2645F. Fluorescent Penetrant Inspection (ref. 15).
American Society for Nondestructive Testing (ASNT).	1968	SNT-TC-1A (1968 Edition) Supplement D. Recommended Practice for the Training, Qualification, and Certification of Liquid Penetrant Testing Personnel (ref. 16).

same type, the test being made as a means of maintaining the quality of a penetrant system.) Figure 2-11 shows a typical cracked block with indications. A detailed account of the cracked-block test, as specified by the American Society for Testing and Materials, may be found in reference 8. The cracked-block comparison test has its limitations, the most important being that, in practice, such comparisons have rather poor repeatability.

It has not been possible to develop a widely useful atlas of photographs representative of flaw indications, because, in general, indications do not photograph faithfully (especially fluorescent indications). Types and sizes of flaws vary greatly, and the indications themselves vary due to minor differences of operator technique. In some specialized instances, collections of reference photographs of indications have been used effectively. One such case is discussed later in this chapter. Sketches of typical penetrant indications, such as those in figure 2-12, are not used as standards, but simply as aids to assist students or inexperienced inspectors.

DESCRIPTION OF COMMERCIALY AVAILABLE EQUIPMENT

Commercially available liquid-penetrant-inspection equipment may be classified in three general categories: (1) portable equipment, (2) general-purpose stationary equipment, and (3) special-purpose stationary equipment. The choice among these three is determined by such



FIGURE 2-11.—Typical cracked aluminum block with indications (ref. 3). (Courtesy of Magnaflux Corp.)

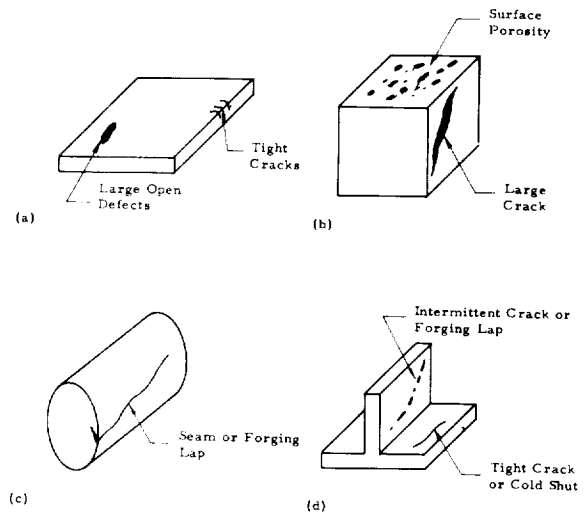


FIGURE 2-12.—Typical liquid-penetrant indications.

factors as the size, configuration, and number of the articles to be tested and their physical location. Lists of commercial penetrant equipment and suppliers may be found in the March 1969 edition of *Materials Evaluation* (ref. 17) and in the *Thomas Register* (ref. 18) under the category "Penetrants."

Portable equipment for penetrant inspection is small, lightweight, and relatively inexpensive; it can be hand carried to almost any inspection location. Portable kits for fluorescent or visible penetrants are available, or they can be assembled by the user. Such kits should contain everything necessary for inspection, and should include, as a minimum, cleaning solvents, penetrant materials, emulsifying agents, developing materials, and a liberal number of rags and brushes. If fluorescent penetrant inspection is required, a portable black light must be included in the kit. Packaging of cleaning solvents, penetrant material, emulsifying agents, and developer materials in aerosol spray applicators has become very popular; such applicators are now used almost exclusively in the portable penetrant-inspection kits. Dry developers are usually packaged in soft pliable rubber or plastic bottles, which can be squeezed briskly to puff the dry developer on the article.

General-purpose stationary equipment provides for all penetrant-inspection functions in a single self-contained unit. The inspection proc-

esses are generally manual except for heavy articles. There is little practical limitation on the type or shape of articles that can be inspected except for maximum size. The general-purpose stationary equipment provides stations for (1) dipping the article into the penetrant; (2) draining the penetrant from the coated article; (3) rinsing off excess penetrant; (4) drying; (5) applying developer; and (6) visual examination. A station for cleaning the article before applying penetrant is usually necessary; it should be located away from the inspection materials to reduce the likelihood of accidental contamination of inspection materials. Small general-purpose units may be capable of processing only a few articles per hour; larger units are capable of processing production quantities of some articles. An illustration of a general-purpose stationary unit is shown in figure 2-13 (ref. 19).

Special-purpose stationary equipment is designed to process articles automatically at production-line speeds with a minimum of manual operations. Such equipment is generally mechanized complete with conveyor systems and special-handling fixtures for the article to be inspected. Properly designed, the special-purpose stationary equipment is the fastest, most economical, and most uniform method of penetrant inspection. It has, however, the disadvantage that it can handle only one or a few similar types of articles. An example of special-purpose stationary equipment is shown in figure 2-14 (ref. 20).

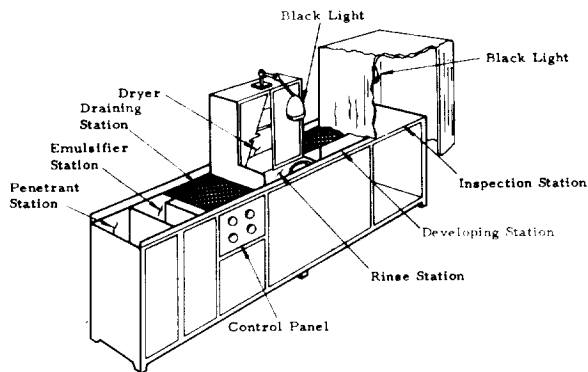
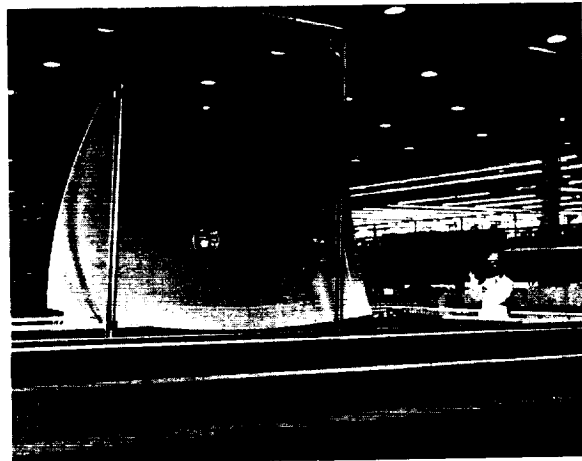
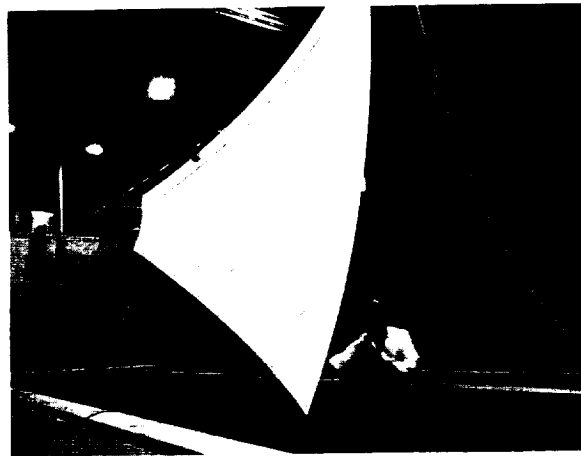


FIGURE 2-13.—View of a general-purpose stationary liquid-penetrant-inspection unit. (Courtesy of General Dynamics.)



(a) Base Segment



(b) Gore Segment

FIGURE 2-14.—Special-purpose stationary liquid-penetrant units for inspecting the Saturn V-S-1C booster. (Courtesy of the Boeing Co.)

Proper lighting is a requirement of all three of the above categories of equipment. White light, or ordinary visible light, may be obtained from any of a number of sources including sunlight, incandescent lamps, and fluorescent lamps. Black light, however, can be economically obtained only from a few sources. The most popular source of black light is the enclosed mercury-vapor arc lamp because of its high radiation output. Following closely in popularity are special ultraviolet-light fluorescent lamps. The ultraviolet illumination obtainable from such lamps is not as high as the output of the mercury-vapor arc lamp; how-

ever, fluorescent lamps can be easily battery-powered, permitting fluorescent penetrant inspection in locations where power-line electricity is not available.

SELECTING A PENETRANT SYSTEM

Selecting a penetrant system for a given inspection requirement is, in most cases, reasonably straightforward; in some instances, however, the choice may be complicated by a number of conflicting considerations. Consider, for example, the task of inspecting for fatigue cracks on the surface of a large pressure vessel permanently located in an open area. The large area to be inspected would, on the basis of economy, suggest a self-emulsifiable water-washable system. Unless it is convenient to carry out the inspection at night, a visible dye penetrant is indicated. On the other hand, the requirement for assurance of vessel integrity may be great enough to rule out as inadequately sensitive the self-emulsifiable system; moreover, the difficulty of supplying wash water, or of satisfactory disposal of run-off may argue against the water-washable system. In this case, a solvent-removable visible-dye system would probably be the best choice. Each new inspection task will usually have some novel aspects which clearly cannot be fully anticipated by the testing specialist. Consequently, no specific formula for selecting a penetrant system will be applicable in all situations. Good practice, however, will require that the following questions be answered.

(1) Is the inspection task suited to penetrants in general?

(2) Does the nature of the material(s) from which the article to be inspected is fabricated place any constraints on the selection of a penetrant system?

(3) Does the end use of the article to be inspected place any constraints on the use or choice of penetrants? (A case in point is the inspection of a surface that is to be wetted by liquid oxygen.)

(4) What sensitivity will be required? (That is, what is the size and configuration of the smallest flaws that must be reliably detected?)

(5) What is the size, geometry, and portability of the article to be inspected?

(6) How many articles of the same type are to be inspected?

(7) If it is not feasible to transport the article(s) to be inspected to an appropriate facility, under what environmental conditions must the inspection be conducted?

(8) To what extent is time a constraint?

(9) To what extent is cost a constraint?

(10) What personnel (in terms of skill) are available to conduct the inspection?

Some important general criteria relevant to the selection of penetrant systems are displayed in table 2-2. While this table reflects sound general practice, it should be used critically. In all cases, the actual selection of a penetrant system for a given inspection task should be made by a properly qualified expert.

NASA'S UTILIZATION AND CONTRIBUTIONS

Liquid Penetrants

Liquid-penetrant inspection has been used extensively by NASA Centers and NASA contractors as a part of the overall quality assurance programs associated with the development of launch vehicles, unmanned scientific satellites and space vehicles, and manned space vehicles. Such inspections have involved essentially the routine application of commercially available materials and equipment, without any special development of either. Figure 2-15 illustrates a typical penetrant inspection.

Two uncommon features of certain applications of penetrants by NASA and its contractors are noteworthy: (1) the frequent requirement for 100-percent inspection, and (2) the large physical size of certain hardware components requiring penetrant inspection. By way of illustration, figure 2-14b shows the penetrant inspection of a gore segment destined for incorporation by welding into the propellant tankage of the first stage of a Saturn V launch vehicle.

LOX Compatible Materials

Early in the space exploration program, it was recognized that certain constituents of commonly used penetrant-inspection materials were

TABLE 2-2.—*Some Criteria for Selecting Penetrant Systems (ref. 8)*

Type	Water washable	Post emulsifiable	Solvent removable
Visible dye penetrants	<ul style="list-style-type: none"> a. Lowest in sensitivity. b. Suited for large surface areas. c. Suited for large quantities of similar objects. 	<ul style="list-style-type: none"> a. Higher sensitivity than water-washables. b. Suited for large surface areas. 	<ul style="list-style-type: none"> a. Where water rinse is not feasible. b. For spot inspections. c. Recommended for small quantities of similar articles.
Fluorescent penetrants	<ul style="list-style-type: none"> a. Lowest in sensitivity of fluorescent penetrants. b. Suited for large surface areas. c. Suited for large quantities of similar objects. d. Suited for deep, narrow discontinuities. e. Recommended for rough surfaces (i.e., sand castings). 	<ul style="list-style-type: none"> a. Higher sensitivity than water-washable fluorescent penetrants. b. Suited for large quantities of similar articles. c. Suited for parts contaminated with acid, chromates, or other chemicals that will harm water-washable penetrants. d. Suited for wide, shallow discontinuities. e. Suited where different levels of sensitivities are required. f. Suited for parts which have defects contaminated with in-service soils. g. Suited for stress, intergranular, or grinding cracks. 	<ul style="list-style-type: none"> a. Higher sensitivity than solvent-removable visible penetrant. b. Where water rinse is not feasible. c. For spot inspections. d. Recommended for small quantities of similar articles.

shock sensitive in the presence of liquid oxygen. Even trace amounts of these materials, left as residues on surfaces and in superficial cracks of surfaces that would be LOX wetted, would have represented an unacceptable hazard. As a consequence, penetrant manufacturers quickly responded by modifying the formulation of penetrant materials to reduce their LOX sensitivity to acceptable levels (ref. 21).

Strippable Developers for Permanent Records

A major advantage of radiography is that it naturally provides an essentially permanent record of an inspection, which can, if the need arises, be reviewed after an inspection has been completed. A radiographic indication of a weldment flaw and a radiograph of the same area after reworking to remove the flaw, for example, together provide a valuable quality assurance record. In certain instances, the value of liquid-penetrant inspection would be greatly enhanced if a permanent record of indications

like that of a radiograph were possible. Free-hand sketches, photographs, and written descriptions of indications serve this purpose rather poorly. The obvious value of a permanent record of liquid-penetrant indications has stimulated considerable effort toward this end. A NASA contractor approached the problem by discarding the conventional powder developer, and substituting a transparent plastic material dissolved in a volatile liquid, which can be sprayed on the surface. This solution wets the surface, adheres to it, and develops penetrant indications by dissolving penetrant trapped in flaws. The penetrant spreads through the thin plastic layer by diffusion rather than by capillary action. The volatile vehicle evaporates at a controlled rate, leaving behind a somewhat tough, flexible, dry film with the indications set in it. This film may be physically strengthened by spraying on additional layers of a transparent flexible plastic such as vinyl. When properly dried, the film may be stripped from the surface, leaving it quite clean; the film itself



FIGURE 2-15.—Penetrant inspection of Apollo command module. (Courtesy of North American Rockwell Corp.)

provides a record of indications. Some users report that these developers (and compatible penetrants) have substantially greater resolution than powder developers, with no appreciable loss in sensitivity. Various versions of this new system are now commercially available (refs. 6 and 21), though they have not yet been widely used. A photograph of a strippable developer is shown in figure 2-16 (ref. 6). Some users report that indications stored in the stripped film continue to diffuse after the stripping, ultimately losing their usefulness. Another recognized limitation of the strippable developers is that their use is restricted to essentially flat surfaces or large, gently curved surfaces; the films do not strip well from small articles of complex shape.

Although photographs of liquid-penetrant indications have a number of deficiencies and are not generally used, one NASA contractor

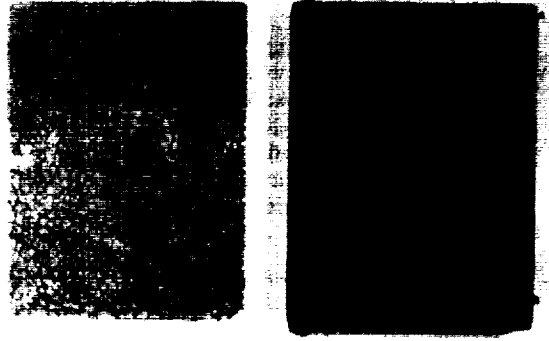
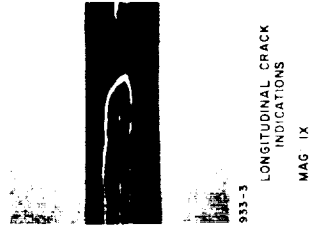
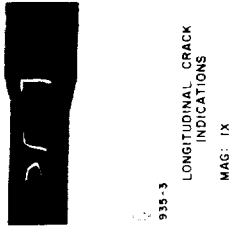
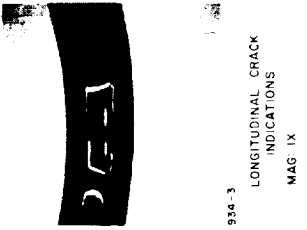
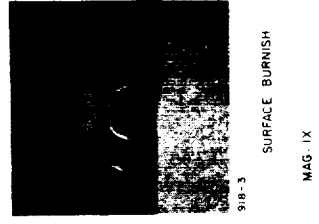
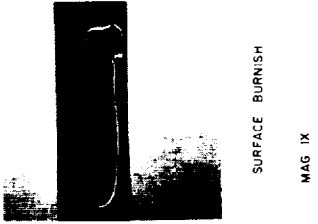
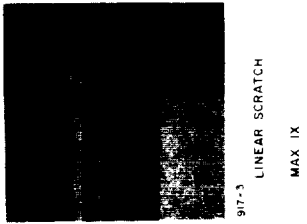
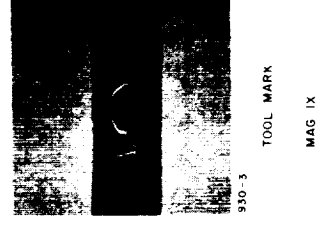
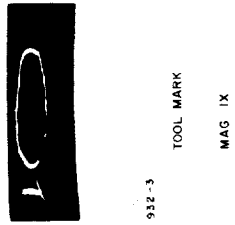
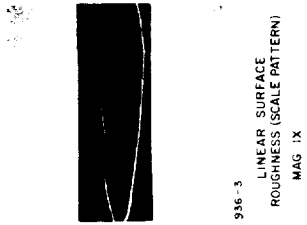
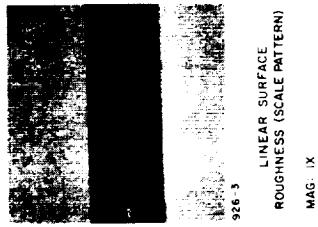
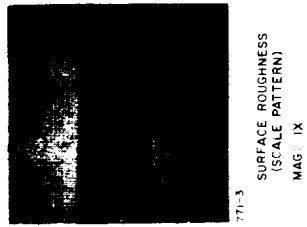


FIGURE 2-16.—A strippable developer is shown alongside the specimen after having been removed. The developer may be stored as a record of the test result. (Courtesy of Shannon Luminous Materials Co.)

has developed a set of reference photographs of penetrant-indicated flaws that occur in Inconel-X tubing used in the manufacture of liquid-fuel rocket engines (ref. 22). Figure 2-17 shows some typical examples taken from this set of reference photographs.

Finally, NASA, through one of its contractors, has furnished the nondestructive-testing community with two substantial aids to personnel training in the use of liquid penetrants. *The Class Room Training Handbook—Liquid Penetrant Inspection* (ref. 7) is a comprehensive text covering the elements of liquid-penetrant testing at a level suitable for technicians. A supplementary programmed handbook for self-study, entitled *Liquid Penetrant Testing* (ref. 19) is also available. These documents, in conjunction with the NASA document, *Introduction to Nondestructive Testing* (ref. 23), provide essentially complete textual material for a thorough course of instruction and study in liquid-penetrant testing. They are, of course, best used under competent supervision by a qualified instructor, and in conjunction with a period of supervised apprenticeship.

ACCEPTABLE INDICATIONS



REJECTABLE INDICATIONS

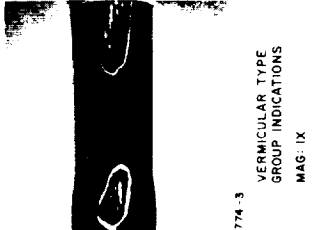
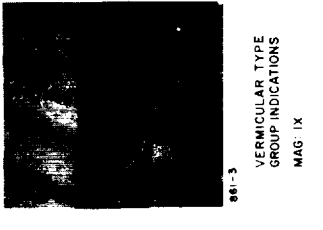
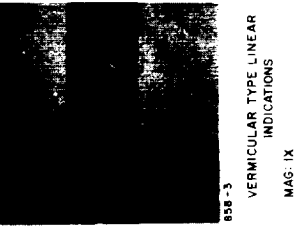
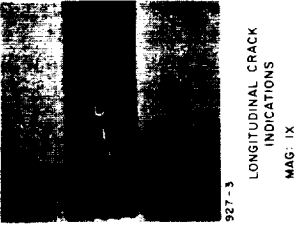


FIGURE 2-17.—Inspection standards for fluorescent penetrant inspection of Inconel-X tubing. (This reproduction has been reduced approximately 2½ times; used by permission of North American Rockwell Corp.)

REFERENCES

1. ANON.: Special Technical Publication No. 223. Record of Symposium on Nondestructive Tests in the Field of Nuclear Energy, American Society for Testing and Materials (Philadelphia, Pa.), Mar. 1958, p. 127.
2. BETZ, CARL E.: Principles of Penetrants. First ed., Magnaflex Corporation, Chicago, Ill., 1963.
3. McMASTER, ROBERT C., Ed.: Nondestructive Testing Handbook, Vol. I, The Ronald Press Co., 1963, pp. 6.1, 6.7 and 6.27.
4. THOMAS, W. E.: An Analytic Approach to Penetrant Performance. Nondestructive Testing, Vol. 21, Nov.-Dec. 1963, p. 355.
5. ANON.: 1969 Book of ASTM Standards, Physical and Mechanical Testing of Metals—Metallography, Nondestructive Testing, Fatigue, Effect of Temperature, Part 31. American Society for Testing and Materials (Philadelphia, Pa.), May 1969, p. 619.
6. ALBURGER, JAMES R.: Penetrants, 1969. Proceedings of the Seventh Symposium on Nondestructive Evaluation of Components and Materials in Aerospace, Weapons Systems and Nuclear Applications, (Sponsored by South Texas Section, American Society for Nondestructive Testing, Inc. and Southwest Research Institute) Apr. 23-25, 1969, p. 52. (Available from Western Periodicals Co., North Hollywood, Calif.)
7. ANON.: Classroom Training Handbook—Liquid Penetrant Testing. NASA CR-61229, 1968, p. 9-4. (N68-28791)
8. ANON.: Inspection, Penetrant Method of, Military Specification. MIL-I-6866B (ASG), Feb. 26, 1964, pp. 3-5.
9. ANON.: Commonly Used Specifications and Standards for Nondestructive Testing. Materials Evaluation, Aug. 1968, pp. 30A-35A.
10. ANON.: Nondestructive Evaluation, Supplementary Criteria for Use of ASME Section III and USASI B31.7. Division Reactor Development and Technology, AEC, 1969.
11. ANON.: Boiler and Pressure Vessel Code (Section IX). ASME, 1968.
12. ANON.: Standard Methods for Liquid Penetrant Inspection. ASTM Designation, E165-65, 1965.
13. ANON.: Qualification of Inspection Personnel (Magnetic Particle and Penetrant). MIL-STD-410A, Aug. 13, 1962.
14. ANON.: Inspection Materials, Penetrant. Military Specification, MIL-I-25135C (ASG), Oct. 21, 1959, and Amendment 3, June 1, 1964.
15. ANON.: Fluorescent Penetrant Inspection. SAE Material Specification AMS 2645F, July 1, 1948; revised Feb. 15, 1965.
16. ANON.: Supplement D, Liquid Penetrant Testing Method. ASNT Recommended Practice, No. SNT-TC-1A, 1968.
17. ANON.: Trade Names of Nondestructive Test Equipment and Materials. Materials Evaluation, Mar. 1969, pp. 33A-38A.
18. ANON.: Thomas Register. Thomas Publishing Company (New York), 1969.
19. ANON.: Liquid Penetrant Testing. NASA CR-61205, 1968, pp. 4-8 through 4-10. (N68-28777)
20. MUSSEY, C. W.: Nondestructive Testing of Saturn V-S-1C Booster Welds. Paper presented by ITT Research Institute at 2nd Symposium on Nondestructive Testing of Welds, Illinois Institute of Technology (Chicago, Ill.), Jan. 30-Feb. 1, 1967, p. 219. (Available in microfiche from AIAA, Number A69-18798.)
21. ANDERSON, R. E.; AND POE, R. F.: Evolution of Penetrants Used on the Apollo and Saturn S-II Programs. American Society for Nondestructive Testing, 28th National Conference (Detroit, Mich.), Oct. 14-17, 1968. (Available in microfiche from AIAA, Number A68-45207.)
22. SANTORO, E. C.; AND JOHNSON, C. M.: A Nondestructive Test to Detect Intergranular Surface Attack on Inconel-X Thrust Chamber Tubing. Materials Evaluation, vol. 24, Jan. 1966, pp. 30-38.
23. ANON.: Introduction to Nondestructive Testing. NASA CR-61204, 1968. (N68-28776)

CHAPTER 3

Ultrasonics

Byron E. Leonard and C. Gerald Gardner

The term *ultrasound* refers to sound waves having a frequency greater than 20 kHz (20 000 cps), roughly the upper limit of sound frequencies to which the human ear responds. *Ultrasonics* refers to the body of scientific knowledge and practical lore associated with the generation, propagation, detection, and use of ultrasound. Although the use of audible sound as a means of testing the quality of manufactured articles is ancient (for example, the testing of swords, bells, glassware, etc., by their ring), the practical use of ultrasound is quite recent, having been developed almost entirely since 1900. During the 1930's, O. Mulhauser, A. Trost, and R. Pohlman of Germany and S. Sokoloff of Russia experimented with various schemes to detect internal flaws in a solid body by the transmission of ultrasound through the body. The first known practical success of ultrasonics was in detecting submarines during World War I. In 1940, F. A. Firestone of the University of Michigan invented the ultrasonic reflectoscope, the forerunner of the modern pulse-echo test system, which operates by generating a succession of ultrasonic pulses, each of short duration, and thence detecting the echoes from subsurface discontinuities in solids. The reflectoscope revolutionized ultrasonic testing by making it possible to test an object from one surface, and to determine (within certain

limits) the size of the flaw and its depth beneath the surface.

Ultrasonic testing is now a primary means of nondestructive evaluation (NDE). Of the big five NDE methods, only ultrasonics and radiography can reveal flaws which are substantially subsurface; the others (penetrant testing, magnetic-particle testing, and eddy-current testing) are restricted to the detection of surface, or slightly subsurface, flaws. Because the propagation of ultrasound is essentially a mechanical phenomenon, it is especially suited to determining characteristics of engineering materials. The major NDE applications of ultrasonics include flaw detection, thickness measurement, and characterization of metallurgical structure. The principal advantages of ultrasonics are

- (1) Its ability to penetrate to substantial depths in many important materials
- (2) Its ability to test from one surface only
- (3) Its sensitivity in the detection of minute flaws
- (4) Its comparative accuracy in determining flaw size and depth
- (5) Its electronic operation which enables rapid and substantially automated inspection.

The chief disadvantages are

- (1) Its manual use requires technicians of considerable native ability, training, experience, and motivation.

(2) It is intrinsically a small-area-coverage method—large area coverage requires complex mechanical scanning or the use of numerous transducers in an array.

(3) Its use, in general, requires a good, essentially direct mechanical coupling to the article to be tested, a requirement which is often difficult to meet in practice.

The discussion of ultrasonic testing in this chapter is necessarily severely restricted in scope. The elementary principles involved in ultrasonics are briefly surveyed; the treatment is not exhaustive or detailed, and is intended only to make the remainder of the chapter intelligible to readers unfamiliar with the subject. The references provide for their detail. The types of instrumentation in general use, their modes of operation, and the conventional techniques of their use in NDE are presented in introductory fashion. Finally, a number of selected contributions to ultrasonic testing made by NASA centers and their contractors are presented with a view to making them of practical help to those outside the aerospace industry.

Also included in this chapter are a few examples of sonic testing, that is, testing in which sound waves of audible frequency are used. While the instrumentation for sonic testing often differs somewhat from the corresponding ultrasonic instrumentation, the underlying principles are similar.

ELEMENTARY PRINCIPLES

Sound waves propagate to some extent in any material that is elastic; that is, if a particle (or small volume element) of the material is displaced from its equilibrium position by any applied stresses, internal forces tend to restore the system to its original equilibrium. A confined fluid (gas or liquid) or a solid has such elastic properties. Because of the mechanical coupling between adjacent regions of the material, a displacement at one point induces displacements at neighboring points, and so on, thus propagating a stress-strain wave. The actual displacement of matter that occurs in ultrasonic waves is, of course, quite small.

Elastic waves are categorized according to

the mode of particle displacement involved. The basic types of waves which propagate in the bulk of a material are longitudinal waves, in which the displaced particles vibrate back and forth along a direction parallel to the direction of wave propagation, and transverse waves, in which the displaced particles vibrate in a direction perpendicular to that of wave propagation. Longitudinal waves are also called compressional waves; transverse waves are sometimes called shear waves. Figures 3-1 and 3-2 illustrate the particle displacements occurring in longitudinal and transverse waves, respectively. Waves involving more complicated modes of particle displacement will be discussed later.

In general, gases and liquids do not strongly support a mechanical shear; hence, while longitudinal (compressional) waves readily propagate through them, transverse (shear) waves do not. Solids, on the other hand, support both longitudinal and transverse waves.

A complete description of a sound wave must specify the displacement of each particle in the medium as a function of time. For longitudinal or transverse waves of sufficiently small amplitude, each particle vibrates in simple harmonic motion, and the displacements vary throughout the medium in a simple, regular manner described by a sinusoidal function of the form

$$d = D \sin \left[2\pi \left(\frac{x}{\lambda} - \frac{t}{T} \right) + \phi \right] \quad (1)$$

where d is the particle displacement, D is the wave amplitude (the maximum value of the displacement), x is the equilibrium position of the particle (measured along a line in the direction of wave propagation), λ is the wavelength,



FIGURE 3-1.—Particle displacement for a longitudinal sound wave.

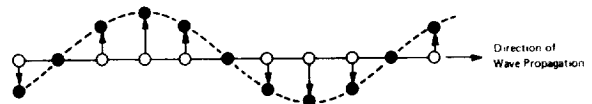


FIGURE 3-2.—Particle displacement for a transverse sound wave.

t is the time at which the displacement is considered, T is the period of particle vibration, and ϕ is an angle (called the initial phase) determined by the initial conditions. Figures 3-3 and 3-4 illustrate the significance of equation (1). Waves described therein are called pure harmonic waves.

During the period T , a particular wave crest will advance a distance λ ; the velocity of propagation, v , is therefore equal to λ/T . The reciprocal of T is called the frequency, f , of the wave. Hence, the important elementary relation is

$$v = f\lambda \tag{2}$$

The quantity $[2\pi (x/\lambda) - (t/T) + \phi]$ is called the phase of the particle motion. An imaginary surface drawn through the medium connecting all particles having the same phase is called a wave front. A sound wave may be thought of as a regular succession of wave fronts, uniformly separated from one another by a distance λ , all propagating with speed v . The shape of a wave front depends on how the sound waves are produced. Spherical wave fronts, for example, might be produced by a sphere whose radius alternately expands and contracts. Wave fronts

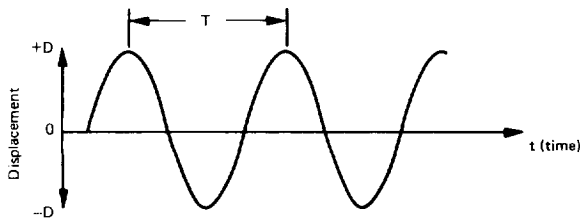


FIGURE 3-3.—Vibratory particle displacement at a fixed point in a material for a harmonic sound wave. (T =period of vibration; D =amplitude of vibration.)

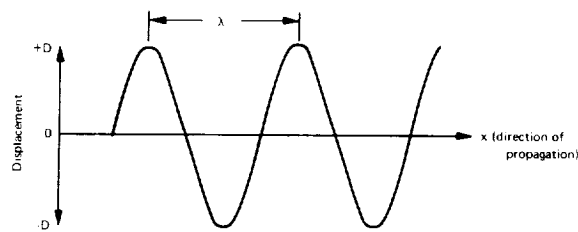


FIGURE 3-4.—The spatial variation of the displacement at a fixed time for a plane harmonic sound wave. (λ =wavelength; D =amplitude of vibration.)

which are flat over most of their surface (plane waves) may be produced by a vibrating flat piston, the diameter of which is large compared to the wavelength λ .

An important property of sound waves of small amplitude is their superposability; the instantaneous displacement of a particle in a region through which two or more sound waves are propagating is determined by simply combining vectorially the displacements corresponding to each of the waves. When two or more waves combine so as to produce displacements in the same sense, they are said to interfere constructively; if their respective displacements are in opposite senses, they interfere destructively.

Because waves of small amplitude satisfy the superposition principle, it is possible to resolve a complex sound wave into a set of simpler waves; harmonic plane waves are especially useful for this. An arbitrary compressional-wave train may be represented by superposing harmonic, plane-compressional waves of appropriate wavelength, amplitude, and phase. Shear waves may also be resolved into harmonic components. Because of the directed character of transverse displacement, however, it is normally necessary to include two separate harmonic plane waves for each wavelength. Their respective directions of transverse displacement are at right angles to one another. Thus shear waves are said to be polarized, the direction of polarization being that of the transverse vibrations.

In NDE (as well as other applications), it is often useful to create short bursts of ultrasound, which propagate through a medium as a wave packet. In the simplest case, such a burst may be regarded as a sinusoidal wave train of finite spatial extent, and having sharp leading and trailing edges (fig. 3-5). Such a wave packet

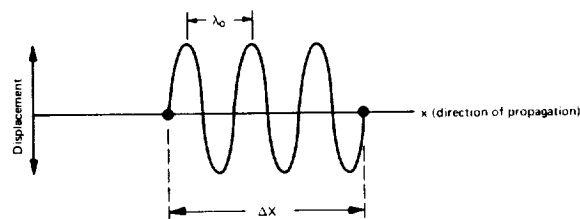


FIGURE 3-5.—An idealized ultrasonic-wave packet.

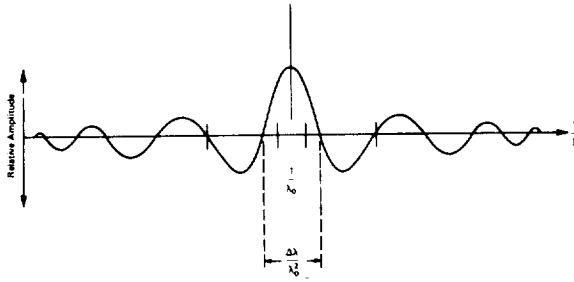


FIGURE 3-6.—The relative amplitudes of harmonic components present in the wave packet represented in figure 3-5. (The amplitude is shown as a function of the reciprocal of wavelength rather than the wavelength directly.)

can be formed only by superposing an infinite number of pure, infinitely extended harmonic components, each with the proper relative phase and amplitude. Figure 3-6 is a graphical representation of the relative amplitudes of the harmonic components required to make up the wave packet illustrated in figure 3-5. The harmonic component of largest amplitude is, of course, of wavelength λ_0 . There is, however, significant amplitude at wavelengths above and below λ_0 . The range of wavelengths, $\Delta\lambda$, over which there is appreciable amplitude may be shown to satisfy the approximate equation:

$$(\Delta x)(\Delta\lambda) \simeq \lambda_0^2 \quad (3)$$

This simple equation is quite important; it is valid for any wave packet whose spatial breadth is Δx , regardless of the packet's detailed shape. The most important implication of equation (3) is that, as the breadth of a wave packet becomes smaller, the range of wavelengths making it up becomes greater; an infinitely short wave packet with equal amplitude contains harmonic components of all wavelengths from zero to infinity. Later it will be shown that this property has important consequences for the resolving power of an ultrasonic test system.

A short ultrasonic wave packet will not, in general, retain its initial shape as it propagates. Harmonic components of different wavelengths travel at different speeds; as the packet propagates, its harmonic components tend to get out of step, destroying the precise phase relationship required to form the packet, and thereby causing it to broaden and to lose its initially

sharp leading and trailing edges. This effect is referred to as dispersion.* It can be shown that a material is dispersive only if it absorbs energy from a wave packet as it propagates. Dispersion is greatest for wavelengths at which attenuation is greatest.

When an ultrasonic wave propagating in a medium encounters an interface with another medium, reflection, refraction, and mode conversion may occur. The simplest case, that of normal incidence, is illustrated in figure 3-7. If the incident wave is of amplitude A_0 , the reflected wave of amplitude A_1 , and the transmitted wave of amplitude A_2 , the following relations hold:

$$\frac{A_1}{A_0} = \frac{\rho_2 v_2 - \rho_1 v_1}{\rho_1 v_1 + \rho_2 v_2} \quad (4)$$

$$\frac{A_2}{A_0} = 1 - \frac{A_1}{A_0} = \frac{2\rho_2 v_2}{\rho_1 v_1 + \rho_2 v_2} \quad (5)$$

Here, ρ_1 and ρ_2 are, respectively, the densities of materials 1 and 2, and v_1 and v_2 are the respective sound velocities. Equations (4) and (5) hold for either longitudinal or compressional waves if the corresponding velocities are used. The quantity (ρv) is an important parameter of a material; it is called the characteristic impedance. The amplitudes of the reflected and transmitted wave are thus determined by the ratio of the characteristic impedances, $r = \rho_2 v_2 / \rho_1 v_1$. When r is unity, no reflection occurs; when it is much greater than unity, reflection is nearly total.

Elastic waves transport energy; for a plane harmonic wave, it may be shown that the intensity (energy/unit time/unit area) of such a wave is given by the relation:

$$I = \frac{1}{2} (\rho v) (2\pi f)^2 A^2 \quad (6)$$

where f is the frequency, A is the amplitude, and (ρv) is the characteristic impedance of the medium. Equations (4), (5), and (6), together with the definition of characteristic impedance

*Some writers on NDE use the term *dispersion* to mean the diffuse scattering of a wave; such usage is, however, not standard.

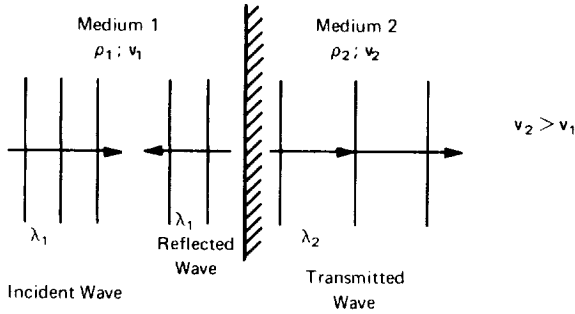


FIGURE 3-7.—A plane harmonic elastic wave normally incident upon a plane interface between two materials of differing acoustic properties.

ratio, r , may be combined to give the intensity reflection coefficient, R , and the intensity transmission coefficient, T :

$$R = \frac{I_1}{I_0} = \left(\frac{r-1}{r+1} \right)^2 \quad (7)$$

$$T = \frac{I_2}{I_0} = \frac{4r}{(r+1)^2} \quad (8)$$

where

I_0 = incident intensity

I_1 = reflected intensity

I_2 = transmitted intensity and,

r = ratio of characteristic impedances.

The sum ($R + T$) is, of course, unity.

When a plane harmonic wave is incident on a plane interface at an angle of incidence other than zero, mode conversion occurs; whether the incident wave be longitudinal or transverse, both longitudinal and transverse waves will be reflected and transmitted. The angles of reflection and refraction satisfy a generalized form of Snell's law:

$$\frac{\sin \theta_i^l}{v_i^l} = \frac{\sin \theta_r^l}{v_r^l} = \frac{\sin \theta_t^l}{v_t^l} = \frac{\sin \phi_i^t}{v_i^t} = \frac{\sin \phi_r^t}{v_r^t} \quad (9)$$

Here the angles are defined according to figure 3-8. The superscripts on the velocities denote the relevant medium; the subscripts distinguish between longitudinal (l) and transverse (t) wave modes. If the incident wave is transverse rather than longitudinal, equation (4) still applies if θ_i^t and v_i^t are substituted for θ_i^l and v_i^l , respectively, in the first term. The general equa-

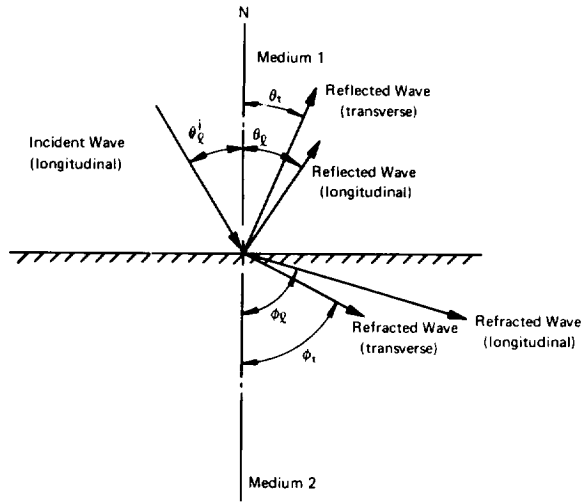


FIGURE 3-8.—A plane harmonic longitudinal wave incident upon an interface at an angle of incidence θ_i^l . (Both longitudinal and transverse waves are reflected and refracted (mode conversion).)

tions relating the amplitudes of the reflected and refracted waves to the amplitude of the incident wave are rather complicated functions of the angle of incidence and the wave velocities, and will not be presented here. Some special cases, however, are of interest.

An important practical application of mode conversion is the conversion of longitudinal waves into transverse waves for ultrasonic-inspection purposes. The refracted longitudinal wave may be effectively eliminated from medium 2 by adjusting θ_i^l so that θ_r^l just exceeds 90° . The value of θ_i^l for which this occurs is called the first critical angle of incidence. From equation (9), one sees that the first critical value of θ_i^l is given by

$$(\theta_i^l) \text{ First critical} = \sin^{-1} \left(\frac{v_i^l}{v_r^t} \right) \quad (10)$$

The first critical angle is illustrated in figure 3-9.

If θ_i^l is increased still further so that the angle of refraction of the transmitted shear wave is equal to 90° , no energy enters the bulk of medium 2. Instead, a complex (partially longitudinal, partially transverse) wave mode propagates along the interface between the two media. If medium 1 is a liquid such as water,

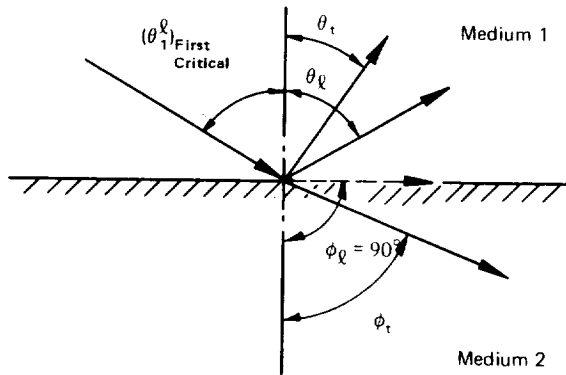


FIGURE 3-9.—First critical angle of incidence of a longitudinal wave. (Only the refracted transverse wave enters the bulk of medium 2.)

and medium 2 is a typical metal, this surface wave is rather rapidly attenuated. If, however, medium 1 is air, the surface wave (called a Rayleigh wave) propagates readily along the surface of a metal, and is very useful for ultrasonic inspection for such surface flaws as cracks. Rayleigh waves tend to follow the curvature of the metal surface without reflection unless the radius of curvature is comparable to or smaller than the wavelength of the Rayleigh wave. Figure 3-10 illustrates a frequently used arrangement for generating Rayleigh waves. Note that, so far as the critical angle is concerned, medium 1 is the plastic wedge, not air.

In general, mode conversion occurs whenever an elastic stress wave encounters a discontinuity in elastic properties. This effect is often an unwanted (if unavoidable) source of energy loss from the mode of interest, as well as being a source of spurious waves in a material being tested. Internal reflection and mode conversion within coupling angle-wedges (fig. 3-10) may

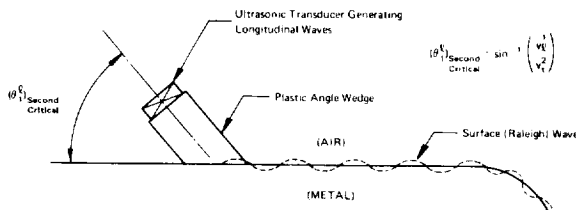


FIGURE 3-10.—Mode-conversion method for generating Rayleigh waves on the surface of a metal component. (The waves tend to follow the surface, even if it is curved. Reflection of the wave occurs at surface discontinuities.)

adversely affect the performance of the attached transducer. On the other hand, as has been shown, mode conversion can, under favorable circumstances, be turned to useful advantage in ultrasonic testing.

In the foregoing discussion, the media bearing the elastic waves were assumed to be infinite in extent and homogeneous except for the change in characteristic impedance across their common plane interface. In finite bodies, of which one or more characteristic dimensions are comparable to the wavelength of an elastic wave propagating in them, complex wave modes may occur. Important among these are Lamb waves that are supported by thin plates (fig 3-11). Characteristic complex waves may also be excited in thin rods. Both plate waves and rod waves are useful in ultrasonic testing.

Like all forms of wave motion, elastic waves are subject to diffraction; that is, when the wave encounters a discontinuity with an edge, it will, in effect, bend around that edge. Figure 3-12 illustrates this effect with a wave passing through a circular aperture in an otherwise non-transmitting barrier. Because of constructive and destructive interference, the amplitude of the waves on the diffraction side of the barrier is not uniform over a wave front. It actually varies greatly, and vanishes at certain characteristic positions. In the case of a pure harmonic incident plane wave, the intensity of the diffracted wave along the axis of the aperture varies according to the graph shown in figure

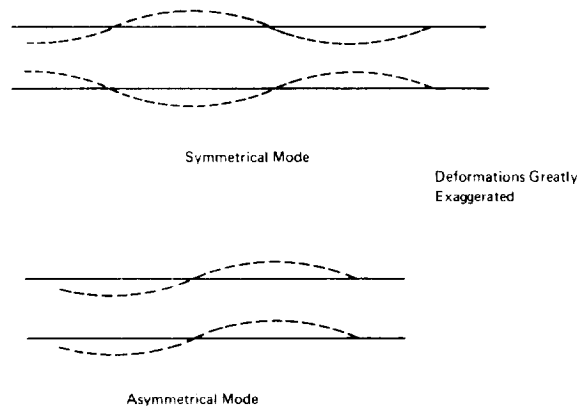


FIGURE 3-11.—Symmetrical and asymmetrical Lamb waves in plates.

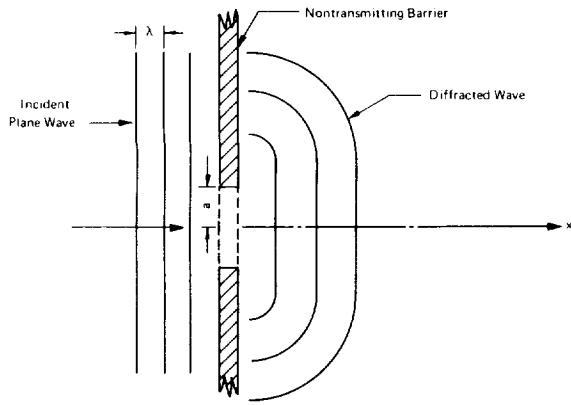


FIGURE 3-12.—Diffraction of a plane wave on passing through a circular aperture.

3-13. The region where $x < a^2/3\lambda$ is usually referred to as the near-field region; the region beyond is called the far-field or Fraunhofer diffraction region.

The distribution of sound intensity off the aperture axis is quite complicated in the near-field region. In the far-field region, however, it is somewhat simpler; figure 3-14 illustrates its general features. The angles at which the first and second intensity nulls occur are given, respectively, by the relations:

$$\psi_1 = \sin^{-1} \left(1.22 \frac{\lambda}{D} \right) \quad (11a)$$

$$\psi_2 = \sin^{-1} \left(2.23 \frac{\lambda}{D} \right) \quad (11b)$$

The half-power angle, i.e., the angle at which the intensity of the main lobe falls to 0.707

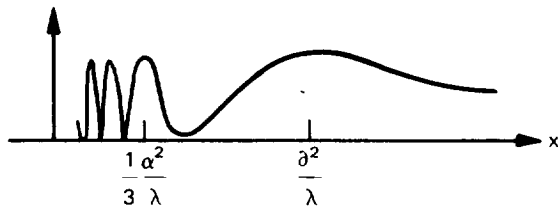


FIGURE 3-13.—Relative intensity, I , as a function of the distance along the axis of the circular aperture shown in Figure 3-12. (Note the intensity nulls caused by destructive interference near the aperture.)

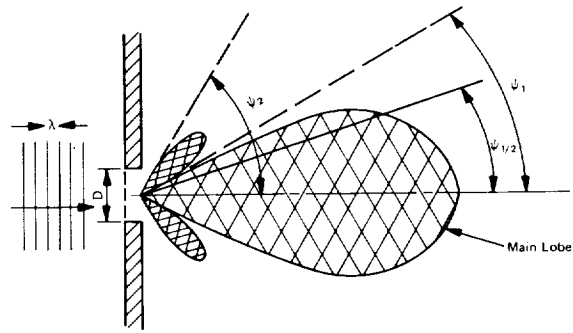


FIGURE 3-14.—Far-field intensity profile of an ultrasonic beam produced by diffraction by a circular aperture. (The pattern shown corresponds to the case in which $\lambda/D = 1/2.44$.)

times its maximum value, is given by the formula:

$$\psi_{1/2} = \sin^{-1} \left(0.72 \frac{\lambda}{D} \right) \quad (12)$$

If λ/D is greater than $1/1.22$, there are no secondary lobes. The smaller the ratio λ/D , the better collimated the diffracted beam is, i.e., the less pronounced are the effects of diffraction. The foregoing discussion of diffraction, in particular that of equations (11) and (12), applies only at distances from the aperture greater than $a^2/3\lambda$. The off-axis, near-field intensity pattern is more complicated.

The diffraction of ultrasound by a circular aperture has another important application in ultrasonics: a circular transducer produces ultrasonic waves, which, for most practical purposes, behave like waves diffracted through a circular aperture. Thus, if a transducer is to produce a well-collimated beam, free of possibly troublesome side lobes, its diameter must be large compared to the wavelength of the ultrasonic wave it produces in the medium to which it is coupled. For simple disc-shaped transducers, the far-field beam diameter cannot be less than the diameter of the transducer itself; hence, narrow beams require both small diameter transducers and very short ultrasonic wavelengths.

Ultrasonic-beam profiles can be altered by the use of acoustic lenses, usually attached directly to the transducer. The operation of acoustic lenses is analogous to that of optical lenses. For

best performance, the lens material must have the same acoustic impedance as that of the transducer and the material to which it is coupled; however, the velocity of sound in the lens must be substantially different from that of the medium. Figure 3-15 illustrates the operation of an acoustic lens. Beyond the focal point of the lens the ultrasonic beam again diverges; thus, focused beams are most sensitive to flaws at the focal point.

The velocity of ultrasound is greater in metals than in water. Hence, a converging beam in water, incident upon a plane metal surface, will be further focused (fig. 3-16).

The above discussion of diffraction effects is based on the assumption that the ultrasound is a continuous pure harmonic wave; i.e., its amplitude is not a function of time. This, of course, excludes the very important case of ultrasonic pulses. A short pulse, it will be recalled, is actually made up of a spectrum of pure harmonic components over a range of wavelengths. Consequently, neither the instantaneous nor time-averaged near-field and far-field intensity

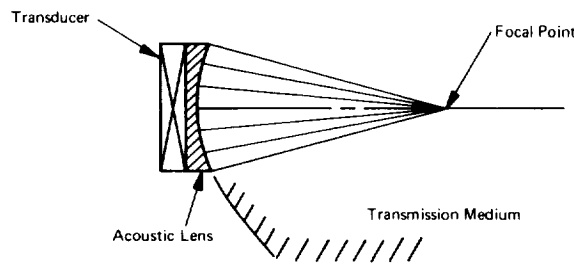


FIGURE 3-15.—Focusing effect of an acoustic lens. (The velocity of ultrasound in the lens is greater than that in the transmission medium.)

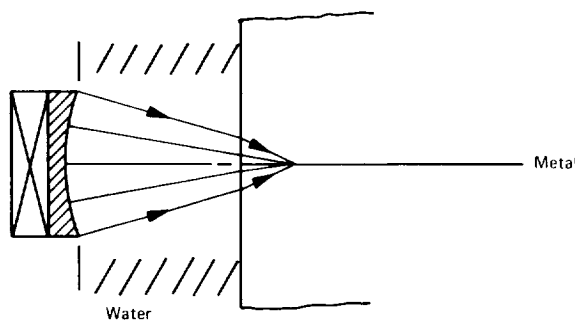


FIGURE 3-16.—Foreshortening of focal distance by a metal.

profile is precisely as illustrated in figures 3-13 through 3-16. When they are required, beam profiles of pulses are usually determined empirically.

ULTRASONIC TESTING

Basic General-Purpose Test Unit

General-purpose ultrasonic test units comprise the essential modules listed below.

(1) *A pulsed oscillator*, which, when electronically triggered, generates a burst of alternating voltage. The principal frequency of the burst, its duration, the profile of the envelope of the burst, and the burst repetition rate may be either fixed or adjustable depending upon the flexibility of the unit.

(2) *A sending transducer* to which the voltage burst is applied, and which mechanically vibrates in more or less faithful compliance with the applied alternating voltage. When appropriately coupled to an elastic medium, the transducer thus serves to launch ultrasonic waves into the medium.

(3) *A receiving transducer*, which serves to convert ultrasonic waves that impinge upon it into a corresponding alternating voltage. In the "pitch-catch" mode, the sending and receiving transducers are separate units; in the "pulse-echo" mode, a single transducer alternately serves both functions.

(4) *A receiver* that amplifies and (if desired) demodulates the received signal.

(5) *A display oscilloscope* with which the user can observe the wave-form of signal voltages at various points in the system.

(6) *An electronic clock* or timer which serves as a source of logic pulses and reference voltage wave forms. The timer governs the internal operation of the system as a whole.

The unit will also include a power supply. Additional features, which are often included in test units, are electronic compensation for loss of signal amplitude caused by attenuation of the ultrasonic pulse in the medium under test; and electronic gates, which monitor the return signal for pulses of a selected amplitude, and which occur within a selected time delay range (corresponding to flaws of a certain size at a pre-

scribed depth range). Other refinements are available, especially in the areas of signal processing and automatic interpretation, and in the interfacing of the unit with mechanical scanning systems.

Scan Modes

The A-scan presentation (fig. 3-17) simply provides for an oscilloscope display of: (1) the envelope of the initial voltage pulse applied to the transmitting transducer (the "main bang"); (2) the envelope of the voltage pulses generated by the receiving transducer as reflections are received, and (3) a timing trace (if available). The ordinate of the oscilloscope trace is proportional to pulse amplitude, and the abscissa is proportional to elapsed time (which may be related to transmission time in the test medium). It is common practice to adjust the display so that the "main bang" is just off the oscilloscope presentation; the pulse from the front surface reflection appears at the start of the oscilloscope trace, and the pulse from the back surface reflection appears at the far right of the oscilloscope trace. Thus, the location of pulses resulting from echoes from a flaw with respect to the two surface echo pulses enables the operator to gauge

the depth of the flaw. The amplitude of a pulse representing an echo from a discontinuity cannot be simply related to the size or severity of the flaw; only when there is sufficient auxiliary evidence as to the general nature of the flaw is this possible.

The B-scan presentation is illustrated in figure 3-18. Here, the internal vertical sweep (y-axis) of the oscilloscope spot is triggered by the timer. The beam is deflected horizontally (x-axis) in synchronism with the usually linear scanning motion of a pulse-echo transducer. The intensity of the oscilloscope spot is modulated in proportion to the amplitude of the received echo signal. If the resulting oscilloscope pattern is to be observed visually, the phosphor of the screen must be of the persistent type, and the scanning of the transducer must be repeated periodically to renew the image. The image itself represents a one-dimensional slice through the specimen, with the profile of discontinuities appearing as corresponding discontinuities in the oscilloscope screen pattern.

In practice, the B-scan system has serious deficiencies. Limits of phosphor persistence times restrict the scan range; the more persistent phosphors tend to produce a smeared image, reducing resolution. Various alternatives to the cathode-ray oscilloscope as a means of displaying B-scan presentations have been tried without notable success. Consequently, the B-scan presentation is seldom used.

The C-scan presentation provides a plane view of a slice of the specimen at a selected depth below the surface. The essentials of the system are

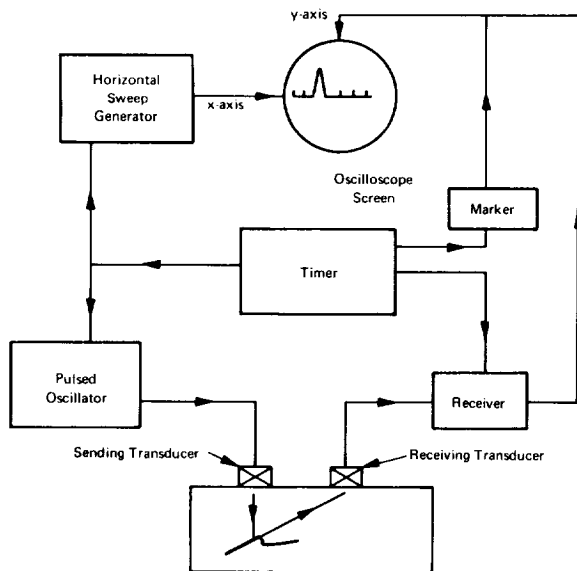


FIGURE 3-17.—Main features of a basic general-purpose ultrasonic test unit in the A-scan mode.

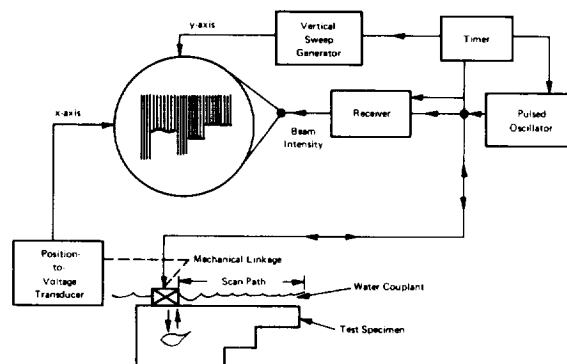


FIGURE 3-18.—Basic features of B-scan system with a persistent-phosphor cathode-ray oscilloscope display.

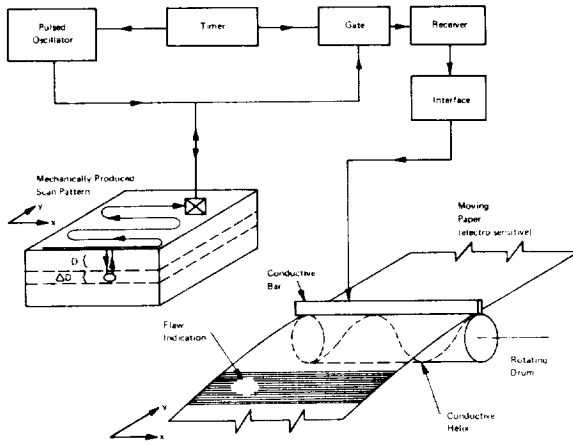


FIGURE 3-19.—A pulse-echo C-scan presentation system. (Here a permanent record is made with a helix-drum recorder. The rotation of the drum is electromechanically coupled with the transducer-scan-pattern mechanism. A flaw within the sensitivity zone ΔD , at depth D , appears as a region of reduced intensity on the electrosensitive paper. Other forms of recorders are also used to produce C-scan records.)

illustrated in figure 3-19. Although a persistent-phosphor oscilloscope could, in principle, be used for the C-scan presentation, in practice, other means of recording the presentation are superior. Usually some form of electromechanical recorder producing a permanent paper record is used.

For C-scan operation, the ultrasonic test unit must be equipped with an electronic gate that samples the received echo for a selected period, starting at a selected elapsed time after the initial transmitted pulse. The elapsed time selected is proportional to the distance from the depth to the top of the inspected slice of the test specimen, and the length of time the gate is open is proportional to the thickness of the inspected slice. When used in conjunction with a large-aperture focused transducer, the C-scan system is capable of generating a detailed record of well-resolved discontinuities. The outstanding disadvantage of the C-scan presentation is that it produces a two-dimensional plane view of discontinuities within a given depth range, but does not provide information from other depths unless the material is scanned repeatedly at successively greater depths.

Ultrasonic Transducers

Virtually all ultrasonic testing is presently done by using ultrasonic transducers of the piezoelectric type. A piezoelectric crystal mechanically deforms when an electric field is applied to it. The mode of deformation depends upon the direction of the applied electric field with respect to the crystalline axes. Conversely, if a piezoelectric material is deformed by the application of external mechanical stresses, it becomes electrically polarized and produces a voltage difference between certain regions of its external surface. Hence, a piezoelectric crystal can be used both as a generator and as a receiver of ultrasonic vibrations.

Piezoelectric materials now in use include quartz, lithium sulfate, and such ceramic materials as lead zirconate titanate and barium titanate. Each of these has peculiar advantages and disadvantages. Quartz, once used almost universally, has outstanding chemical, electrical, thermal, and mechanical stability, but is comparatively inefficient and tends toward internal mode conversion. Lithium sulfate, though quite efficient, especially as a receiver, is very fragile, water soluble, and limited to temperatures below 165° F. Ceramics are the most efficient ultrasound generators, are moisture tolerant, and can be used up to about 300° F. They are, however, mechanically weak, they age with use, and are subject to some internal mode conversion.

The basic active element of a transducer consists of a slab of piezoelectric material sandwiched between thin conductive electrodes, forming a capacitor. This assembly is housed in a protective casing on which electrical connectors are mounted. The unit may also include a backing material that serves to damp the mechanical vibrations of the crystal; in the case of the angle-beam transducer, a plastic wedge may be incorporated in the assembly. For use in water, the entire unit must be hermetically sealed, including the connecting electrical wires or cables. Schematic diagrams of two typical transducer designs appear in figure 3-20. Transducers are available in a wide variety of sizes and functional designs. Focused transducers incorporate an acoustic lens directly in the assem-

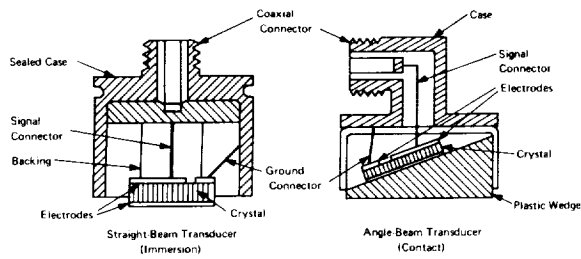


FIGURE 3-20.—Cross-sectional views of a straight-beam transducer and an angle-beam transducer.

bly. In dual-element transducers, two crystals—one for transmitting, the other for receiving—are mounted in the same housing assembly. For certain applications, one face of the piezoelectric crystal may be exposed for direct coupling to a metal surface, the inspected metal itself serving as the ground-potential electrode. The selection of the proper transducer or combination of transducers is extremely important for successful ultrasonic testing, and should be done by a qualified specialist.

Coupling Techniques

In order for ultrasound to be launched into a material, the vibrating element of a transducer must be mechanically coupled to it. In contact testing, a very thin layer of fluid between the active surface of the transducer and the surface of the substrate material usually serves as a coupling medium, or couplant. Mixtures of glycerine, water, and a wetting agent are commonly used on smooth surfaces. Light oils (with a wetting additive), greases, or pastes are used on less smooth surfaces. The messiness and inconvenience of “wet” couplants motivate a continuing search for effective “dry” couplants. Thin layers of certain synthetic elastomeric materials are satisfactory dry couplants for some applications.

A major difficulty with contact testing is the difficulty it poses for continuous scanning of the transducer over the surface of the test specimen. When continuous scanning of appreciable surface area is required, immersion testing is usually done. In this method, the article to be tested is immersed in a tank of water. A submersible transducer is then placed in suitable proximity

to the surface of the test article; the water itself serves as the ultrasonic couplant. Immersion tanks of various sizes, and equipped with electromechanical devices for manipulating the transducer and generating various scan patterns, are commercially available.

Since many articles for which a scanning inspection is desirable cannot conveniently be immersed, there is a great incentive to develop alternate means of coupling for scanning transducers. Two techniques, the bubbler and wheel transducer, are illustrated in figure 3-21. The water-bubbler technique (fig. 3-21(A)) has the disadvantage that the overflow must be disposed of in some manner. The wheel transducer (fig. 3-21(B)), though free of the main shortcoming of the bubbler, is, in most applications, less efficient as a coupler. The transducer inside the wheel can be arranged so that the incident compressional wave is at either normal incidence for generating compression waves, or a critical angle for generating shear waves or surface waves.

Reference Standards

By far the most difficult aspect of ultrasonic testing is the task of interpreting ultrasonic indications of internal discontinuities. To provide some assistance in the interpretation of such indications, reference standards have been developed. Such standards serve two important purposes. They enable the operator to check, adjust, and calibrate his test equipment periodically; and by judicious comparison of the ultrasonic indications of an unknown discontinuity with those produced by selected reference standards, the operator may assess the nature and significance of the discontinuity in question.

The most commonly used reference standards

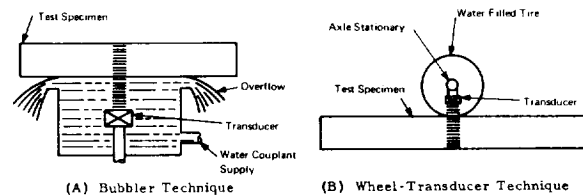


FIGURE 3-21.—Bubbler and wheel-transducer techniques for coupling scanning transducers.

are blocks with flat-bottom holes drilled in them. A set of "area-amplitude" blocks comprises a number of blocks, all of the same dimensions, each with a hole drilled into it of the same depth, but of progressively larger diameters throughout the set. When a transducer is coupled to the surface opposite that into which the hole is drilled, it senses a circular discontinuity, provided the effective diameter of the ultrasonic beam is greater than the maximum diameter of the drilled hole.

A set of "distance-amplitude" blocks comprises cylindrical blocks, all of the same diameter, and ranging in length from about 1 to 6 inches. A flat-bottom axial hole of exactly the same diameter and depth is drilled into each block; thus the depth from the undrilled surface to the discontinuity presented by the bottom of the drilled hole is progressively greater through the set of blocks. Distance-amplitude blocks are used in adjusting the circuit which electronically compensates for signal attenuation due to varying depth (on test units having this feature). For flaw-size evaluation, multiple sets of distance-amplitude blocks are used; each set has the flat-bottom hole of progressively larger diameter. Other reference standards in common use are the American Society for Testing and Materials (ASTM) basic set, which also has flat-bottom-hole drilled blocks, and the International Institute of Welding reference block.

Reference blocks must be used with great caution; only a well-trained, experienced ultrasonic inspector, thoroughly familiar not only with the use of the references themselves, but also with the characteristics of the particular article being inspected (material, type, size, and location of flaws, etc.), should attempt to use them as an aid in interpreting flaw indications.

Resonance Testing

The thickness of plate-like regions of a specimen can often be measured accurately and conveniently by ultrasonic resonance. The principle involved is illustrated in figure 3-22. A generator, variable in frequency over a suitable range, and a means of sensing the power input to the transducer are employed. As the frequency of the oscillator passes through a value

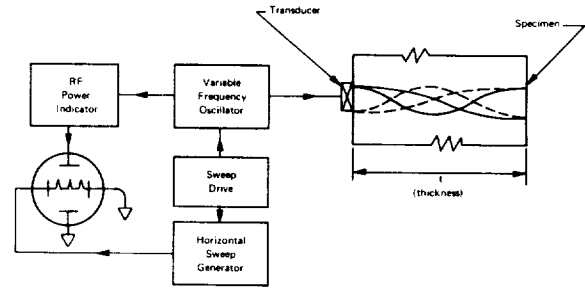


FIGURE 3-22.—An automatic resonance system. (Vertical peaks occur on the oscilloscope trace when the oscillator frequency corresponds to a resonant frequency of the specimen.)

for which the thickness of the material is an integral number of half-wavelengths of the ultrasound in the material, vibrational antinodes occur at the surfaces of the material, and the material vibrates in resonance with the transducer. At this frequency, the power drawn from the radio frequency oscillator increases sharply, so that an appropriate power meter can be used to sense the occurrence of resonance. Thus, for the resonant condition, the following equation holds:

$$n \frac{\lambda}{2} = t \quad (13)$$

where:

t = the specimen thickness

λ = the wavelength of the ultrasound

n = an integer.

Since the wavelength, λ , is not known directly, it may be expressed in terms of the frequency, f , and the velocity, v , (which must be known). Since $\lambda = v/f$, the foregoing equation becomes

$$\frac{nv}{2f} = t \quad (14)$$

If two consecutive resonance frequencies, f_1 and f_2 , are determined, the relations then become

$$\frac{nv}{2f_1} = t \quad (15)$$

$$\frac{(n+1)v}{2f_2} = t \quad (16)$$

Elimination of the integer, n , between these two equations gives the final result:

$$t = \frac{v}{2(f_2 - f_1)} \quad (17)$$

Commercial ultrasonic resonance-thickness gauges usually provide for automatic sweeping of the frequency of the oscillator, and an oscilloscopic or other visual indication to determine the occurrence of resonance.

Resonance testing is sometimes used to detect laminar flaws in plate-like specimens. It is also a convenient and accurate means of measuring the velocity of ultrasound in a specimen whose thickness is known.

Sensitivity and Resolution in Ultrasonic Testing

In ultrasonic testing, the term *sensitivity* refers to the ability of a particular system to produce a clear indication of the presence of a discontinuity. Sensitivity is thus measured in terms of the smallest discontinuity that the system can detect. The term *resolution* refers to the ability of the system to give separate, distinct indications corresponding to spatially separate discontinuities. Both sensitivity and resolution are usually measured by using a series of successively smaller, spatially localized, synthetic flaws.

When a discontinuity is detected by reflection of ultrasound, sensitivity is generally improved by:

- (1) Increasing the intensity of the incident ultrasonic beam
- (2) Increasing the intrinsic sensitivity of the receiver crystal (i.e., using a crystal that generates a higher voltage for a given applied stress)
- (3) Decreasing the mismatch between the acoustic impedance of the receiver crystal and the material under inspection
- (4) Increasing the effective surface area of the receiver
- (5) Increasing the electronic amplification of the output of the receiver crystal
- (6) Decreasing the ratio of the ultrasound wavelength to the effective dimension of the discontinuity.

There are practical limits to which each of these can be carried; for example, decreasing the wavelength of the ultrasound may cause attenu-

ation so great that the effect of increased reflection from the discontinuity is offset, or raising the gain of the receiver amplifier may create greater electronic noise, nullifying the increased sensitivity.

To improve the resolution of a system requires two separate considerations. The first concerns the range or depth of a discontinuity in the test material. If depth is gauged by the length of time required for the round-trip between transducer and discontinuity, then, two discrete flaws will not be detected separately unless one is deeper than the other by an amount approximately equal to the spatial length of the ultrasonic wave packet. This breadth is, in turn, approximately equal to the rf pulse duration times the ultrasound velocity. Therefore, to improve resolution in range (or depth), the rf pulse duration must be shortened. To resolve two adjacent localized discontinuities having the same range requires that either the transmitted beam must be sufficiently narrow to illuminate only one of the discontinuities, or the effective cone of sensitivity of the receiving crystal must be sufficiently narrow to discriminate between the two discontinuities. In both cases, resolution is improved by increasing the ratio λ/D ; here, D is the effective diameter of either crystal and λ is the maximum ultrasound wavelength having significant amplitude in the wave packet. In the usual pulse-echo technique, a single crystal serves as both sender and receiver; therefore, the reception cone is essentially the same as the transmission cone. If the discontinuity is in the near-field zone of either transducer, special consideration is required.

NASA CONTRIBUTIONS

NASA centers and contractors routinely make extensive use of ultrasonic and sonic methods of NDE. The effectiveness of these methods as tools of quality and reliability assurance depends on the knowledge and skill of the technicians employing them. As an aid to the training of such technicians, NASA has prepared a series of manuals that comprehensively cover the state of the art of instrumentation and test procedures (refs. 1 through 4).

This series comprises three volumes of programmed instructional material, and an accompanying textbook. Together, these volumes constitute a thorough course in both principles and practice at the level generally required of inspection personnel.

Many of the reliability and quality assurance problems encountered in the space program have created special requirements for NDE methods and instrumentation. Whenever possible, these requirements have been met by industrial contractors. In other cases, exploratory work has first been conducted at NASA centers, with subsequent developmental work, where warranted, being pursued by a contractor. The results of some of these efforts, selected on the basis of their possible utility outside the aerospace industries, are described in ensuing sections of this chapter.

Water-Column Probe for Mechanized Ultrasonic Scanning

Ultrasonic inspection of weldments in critical structures is sometimes a mandatory supplement to X-radiography. To be maximally effective, such inspection must approach 100-percent coverage; i.e., the entire weldment region must be inspected. In production circumstances involving great lengths of weldment, a mechanized ultrasonic scanning system is a virtual necessity. Such was the case with the Saturn V booster stage S-IC propellant tanks, which involved joining aluminum plates by butt welds. Preliminary feasibility studies established that 2.25-megacycle shear-wave ultrasonic inspection was more effective than radiography in the detection of flaws associated with lack of both penetration and fusion in the weldment. The large size of the items to be inspected precluded the use of an immersion tank for continuous ultrasonic scanning; the bubbler technique was also considered impractical. Faced with this problem, workers at the George C. Marshall Space Flight Center developed a "water-column probe" suitable for continuous scanning.

The basic concept of this probe is illustrated in figure 3-23 (ref. 5). A conventional immersible straight-beam transducer was mounted

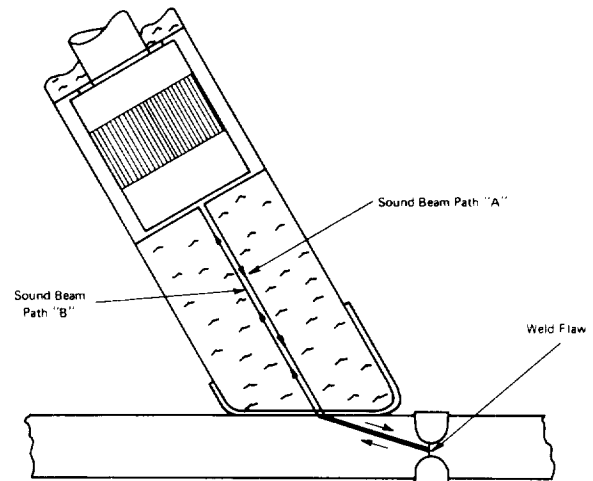


FIGURE 3-23.—NASA water-column probe for mechanized scanning.

in a water-filled cylinder, one end of which was cut at an angle appropriate for launching shear waves, and closed with a stretched urethane rubber diaphragm, or boot. A thin layer of water (supplied by an auxiliary spray) served as a couplant between the rubber boot and the aluminum plate; the water also served as a lubricant enabling the boot to slide over the aluminum surface. Urethane rubber was used for the boot because of its exceptional resistance to abrasion. A cross-sectional view showing the details of the water-column-probe assembly appears in figure 3-24 (ref. 5). To suppress irrelevant indications caused by reflections at the water-column-boot interface, the cylinder was lined with a layer of neoprene rubber, which effectively attenuated these reflected waves.

Figure 3-25 is a schematic diagram showing the essential features of the complete inspection system. A mechanical fixture was devised

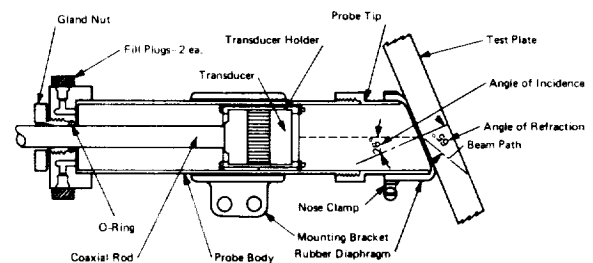


FIGURE 3-24.—Details of the NASA water-column probe.

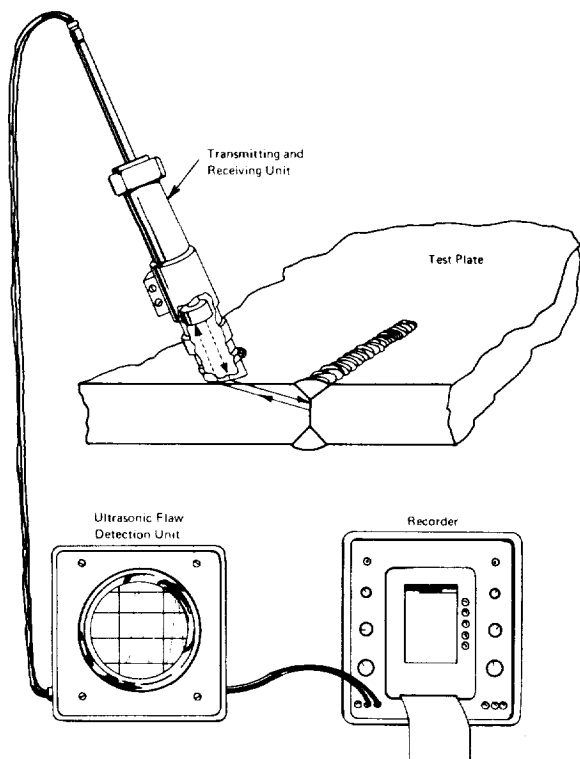


FIGURE 3-25.—Mechanized ultrasonic scanning system.

to hold the probe in contact with the aluminum surface while allowing it to be scanned parallel to a weldment; this fixture also carried the spray that continuously dampened the aluminum surface as the probe moved across it. Further technical details, including the results of a thorough study of the characteristics of the shear-wave beam emitted by the probe may be found in reference 5.

Ultrasonic Detection of Fatigue Cracks

Structural metals develop cracks when they are subjected to cyclic stress; above some rather well-defined peak-stress value characteristic of the specific material, the induced cracks propagate to failure within some statistically determined number of stress cycles. The material is therefore said to fatigue. Studies have shown that a specimen may fail comparatively rapidly once fatigue cracks become detectable by any presently available means; for such materials, most of the "fatigue life" is expended prior to this stage of crack development.

When a component is operated under a cyclic stress regime corresponding to a limited fatigue life, safe operation can be assured only if the component is removed from service as soon as possible after detectable fatigue cracks form. While safety considerations require that a component be removed from service before there is a significant probability of its failing, economic considerations argue for keeping the component in service as long as it is consistent with safety. There is thus a double incentive to develop practical methods of NDE for detecting fatigue cracks at the earliest possible stage of their development. Such methods are also needed in the continuing laboratory investigations of the physical mechanisms involved in fatigue. Ultrasonic techniques have been, and continue to be, intensively investigated for such applications.

At NASA Lewis Research Center, the capabilities of the ultrasonic shear-wave technique for detecting and measuring the length of fatigue cracks in notched-sheet fatigue specimens were investigated (ref. 6). Commercial A-scan instrumentation with time-gating and output-integrating circuitry for strip chart recording was used. Since both sensitivity and resolution are important, the highest practical frequency was called for. It was experimentally determined to be 5 MHz with the available equipment. Both the pulse-echo technique and the through-transmission (pitch-catch) technique were investigated.

A special transducer design was developed for the pulse-echo application. The design is shown schematically in figure 3-26(a). The plastic shear-wave wedge was so designed that the reflected compressional wave internal to the Lucite wedge was transmitted via an extension to a second transducer operating as a receiver only. This feature served two purposes. The internally reflected wave was effectively prevented from interacting with the primary transducer; and by monitoring the internally reflected wave with the secondary receiving transducer, changes in the coupling at the interface between the wedge and the metal specimen could be monitored.

The transducer design employed for through-

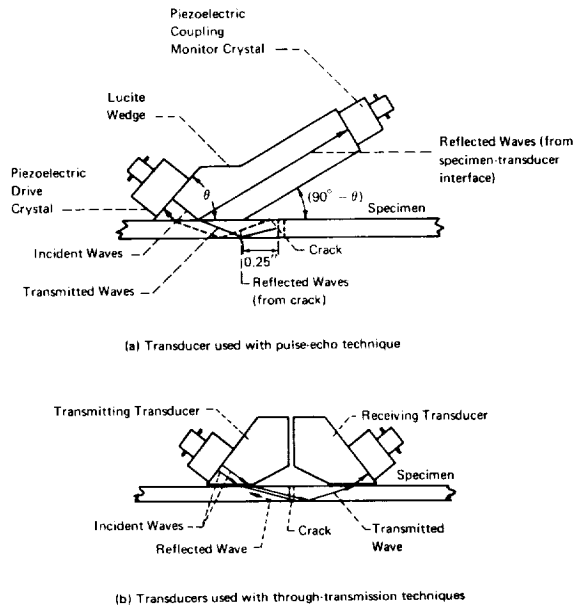


FIGURE 3-26.—Ultrasonic transducers used with crack-detection device.

transmission is illustrated in figure 3-26(b). Space limitations prevented the use of secondary coupling-monitoring crystals. The couplant material used in this investigation was a molybdenum disulfide lubricant normally employed to prevent seizure of mating parts at high temperature. This unconventional couplant material was reported to be quite efficient. The shear-wave beam profile in the specimen was determined by measuring the energy reflected from a 0.050-in. slot in an aluminum plate as the transducer was moved laterally past the slot. After the region of maximum sensitivity of the transducer was determined, the transducer was subsequently mounted on fatigue specimens so as to utilize this region to advantage.

A brief study was made to determine the effect of crack orientation on the amplitude of echo pulses. The results obtained are summarized in table 3-1; they were applied to explain observed differences in ultrasonic reflection from fatigue cracks the surfaces of which lie at different angles with respect to the direction of the incident ultrasonic wave. They illustrate the extreme importance of flaw orientation in ultrasonic testing.

TABLE 3-1.—Output Voltage as Function of Flaw Orientation (ref. 6)

Flaw	Orientation Angle, deg	Normalized Output Voltage
	ψ	
	0	1.00
	10	0.96
	30	0.96
	45	0.74
	ψ	
	0	1.00
	30	0.81
	45	0.75
	α	
	0	1.00
	10	0.92
	30	0.30
	45	0.00

Five materials were employed in the study: unalloyed aluminum; 6061-T6 aluminum alloy; 2014-T6 aluminum alloy; mild steel; and Inconel. The specimens (of conventional design) were subjected to axial tensile fatigue.

The sensitivity of the pulse-echo system to crack size was studied by selective destructive examination of specimens. On the first clear indication of a crack, the selected specimen was removed and sectioned for metallographic microscopic examination. As expected, the ultrasonic system was most sensitive when the specimen was under maximum tensile load, which opened any cracks present.

The investigators summarized their results as given below.

(1) With the reflection technique, fatigue cracks ranging from 0.0005 to 0.005 in. in length were detected during fatigue testing of the more ductile materials (i.e., pure aluminum, mild steel, and Inconel); cracks ranging from 0.0005 to 0.0025 in. in length were detected in the less ductile materials (6061-T6 and 2014-T6 aluminum alloys).

(2) In the sharply notched specimens utilized in this investigation, cracks were detected within approximately 1 to 3 percent of total specimen life for all of the materials considered over the range of stresses considered.

(3) The reflection technique was more sensitive to the detection of minute fatigue cracks than was the through-transmission technique. Thus, it was possible to detect much smaller cracks with the reflection technique.

(4) The through-transmission technique gave consistently reproducible output voltages for cracks on the order of 0.062 to 0.082 in. in 2014-T6 aluminum. This reproducibility was better than that obtained with the reflection technique for similarly long cracks. The through-transmission technique thus appears to be better suited for measuring the length of cracks greater than about 0.010 in.

(5) The effects of crack orientation on output voltage with the reflection technique was studied by means of slots machined into flat plates. Slot surfaces normal to the direction of the ultrasonic waves produced the greatest output voltage. The farther the slot surface deviated from a position normal to the wave-propagation direction, the smaller the output, even though the slot surface area, when projected on a plane normal to the wave, was constant.

An ultrasonic technique has been developed and used to observe the formation and growth of fatigue cracks in notched cylindrical specimens subjected to reversed axial-fatigue loading (ref. 7). The system used was generally similar to that described in the foregoing discussion. However, the transducer employed was a 7 MHz longitudinal-wave transducer. Longitudinal waves were transmitted back and forth along the axial direction of the specimen. Circumferential cracks around a 0.300-in.-diameter notched specimen were induced by cyclic loading. The depth of initially detectable cracks ranged from 0.0005 in. to 0.004 in.

Automatic Monitoring of Fatigue-Crack Growth

An important aspect of fatigue is the rate at which a fatigue crack, once formed, grows. The study of fatigue-crack growth would be greatly facilitated if a convenient means of continu-

ously and automatically monitoring the size of a growing crack in a fatigue specimen could be found. An ultrasonic approach to this problem has been investigated by a NASA contractor (ref. 8). The investigation consisted of continuously monitoring the position of the tip of a lengthening through-crack in a thin-plate fatigue specimen. The basic features of the technical approach used are shown in figure 3-27. The reflector plate shown in the figure was ultrasonically coupled to the specimen by a thin film of vacuum-pump oil. The angle-wedge surface-wave probe was water-coupled to the specimen. One dimensional mechanical scanning of the probe was achieved with a lead screw driven by a servomotor. Each pulse emitted by the probe resulted in two echoes; one from the tip of the crack and another from the reflector plate. By a dual gating and integrating system, the amplitudes of the crack echo and the reflector echo were continuously compared. An error signal derived from this electronic comparison was supplied as feedback to the servomotor control. When the overall system was appropriately tuned and adjusted, the control loop continuously repositioned the probe to maintain its position relative to the tip of the lengthening crack. The system was essentially an exploratory developmental version. The principles involved should lead to a considerable refinement of the monitoring device, including a two-dimensional scan system for fol-

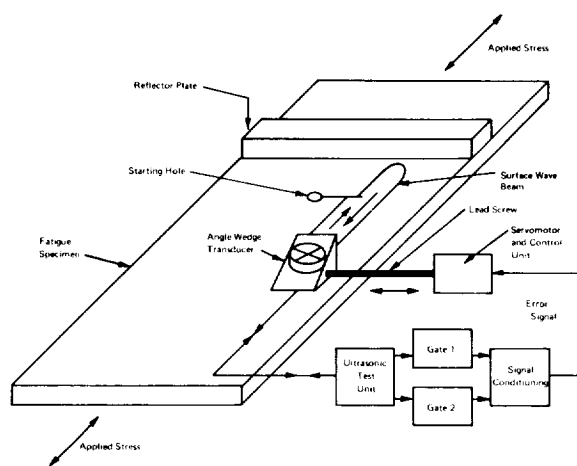


FIGURE 3-27.—Schematic of an automatic system for monitoring fatigue-crack growth.

lowing a crack when its direction changes as it lengthens.

Ultrasonic Detection of Stress-Corrosion Cracking

The development of high-strength aluminum alloys for aerospace applications has resulted in significantly improved strength-to-weight ratios. Many of these alloys, unfortunately, are highly susceptible to stress-corrosion cracking, a process in which the simultaneous and cooperative effects of corrosion and applied or residual mechanical stresses lead to the initiation and growth of cracks. Stress-corrosion cracking may occur at stress levels far below the nominal strength of the material, and may proceed at a rate orders of magnitude greater than the usual rate of corrosion in the absence of mechanical stress. Consequently, there is a strong incentive to develop methods of non-destructively detecting and evaluating stress-corrosion cracking at the earliest possible stage. Since the process begins on the metal surface, it is natural to investigate ultrasonic surface waves (Rayleigh waves) in solving this NDE problem. Such studies have been conducted by NASA, both in-house and through its contractors.

Two general approaches have been explored. The first is to correlate the rate of attenuation of a surface-wave packet as it propagates over a test region; the other is to sense discrete cracks by the pulse-echo method. A limited survey of the attenuation approach as applied to 2219-T31 aluminum (which is quite susceptible to stress-corrosion cracking), and to 2219-T81 aluminum (which is comparatively resistant to stress-corrosion cracking) was conducted at Marshall Space Flight Center by using 5-MHz waves. The results suggested that, while the attenuation was a very sensitive indication of surface condition, it was quite difficult to distinguish the effects of stress-corrosion cracking from those of ordinary corrosion taking place in the absence of stress (ref. 9).

A somewhat more detailed investigation for 7075-T6 aluminum alloy was conducted by a NASA contractor (ref. 10). The alloy that was studied is highly susceptible to stress-corrosion cracking. The specimen geometry and the posi-

tion of the angle-wedge pulse-echo transducer employed is shown in figure 3-28. To induce stress-corrosion, a clamp was applied to the ends of a U-shaped specimen, placing the outer fibers of the bend of the specimen in tensile stress. The U-bend portion of the specimen was then made the anode in an electrolytic cell containing a sodium chloride solution. A constant electric current on the order of 0.5 mA/cm² was passed through the cell for a fixed period of time. As a measure of the exposure to this galvanic corrosion environment, the product of the current density and the elapsed time was used. The specimen was periodically removed from the electrolytic cell, thoroughly cleaned, and tested ultrasonically, both with and without the stress-producing mechanical load applied.

To provide a reproducible reference with respect to which surface-wave attenuation could be measured, two reference grooves were machined in each test specimen as shown in figure 3-28 (ref. 10). The size of reference groove 1 was adjusted to provide a pronounced echo, and to transmit most of the energy of the incident surface wave; reference groove 2 was adjusted to produce a readily detectable reflection. Thus, an ultrasonic-wave packet emitted by the transducer, propagates along the surface, is partially reflected by reference groove 1, and continues to propagate over the test region where it is attenuated. The packet was then partially reflected by reference groove 2, passed through

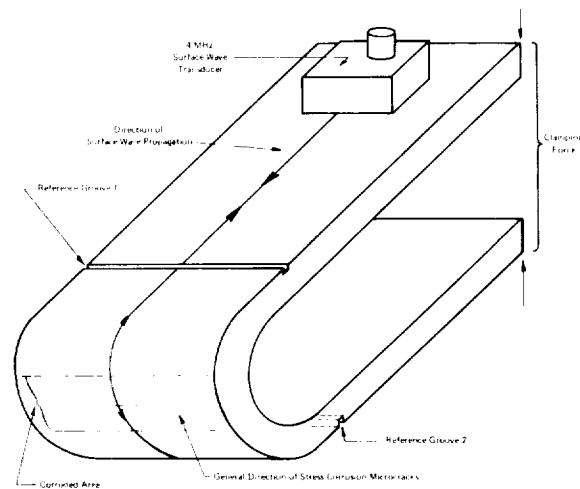


FIGURE 3-28.—U-bend tensile specimen.

the test region where it was further attenuated, thence across reference groove 1, and finally back to the transducer, which now functions as a receiver. For each test, the coupling between the transducer and the specimen and the gain of the receiving amplifier were adjusted to produce the same amplitude for the A-scan echo pulse produced by reference groove 1; the amplitude of the echo pulse produced by reference groove 2 is then a function of the attenuation of the wave packet as it (twice) traverses the test region. As their size increases, stress-corrosion microcracks become sufficiently large to produce individually discernible echoes. It was found that the echoes from such cracks were greatly increased in amplitude when the test was made with the clamping force applied. Photomicrographs verified that the applied tensile stress opened the cracks slightly, greatly increasing the acoustic impedance mismatch.

In figure 3-29, the results of the study are summarized in graphical form. In this case, the attenuation produced by stress-corrosion cracking was appreciably greater than that produced by corrosion alone.

Incidental to the study just described, an interesting and useful result was obtained from reflectivity of artificial defects in the form of transverse grooves produced with a jeweler's saw. For a wavelength, which is long compared

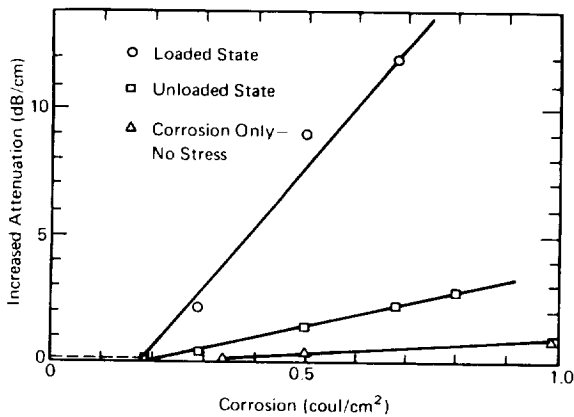


FIGURE 3-29.—The increase in Rayleigh wave attenuation caused by corrosion for three types of stress-corrosion cracking. (Shown are samples still under stress, after release of stress, and corroded with no stress. The samples were corroded when stressed to 90% of their yield strength.)

to the width of the groove, it was found that the relative amplitude of the reflected pulse was proportional to $\exp(-C/D)$, where D is groove depth, and C is a constant that depends on the wavelength of the surface wave. The results for 4 MHz (wavelength equal to 0.028 in.) are shown in figure 3-30.

Ultrasonic Determination of Residual Stress

A number of operations by which structural metal components are formed leave the metal in a state of residual stress. If a rectangular bar is permanently deformed by bending, for example, one surface will be left in a state of tensile stress, and the opposing surface will be left in compression. The residual-stress distribution present in a component depends in a complex way on its thermomechanical history. In some cases, controlled residual stress is beneficial, and may be deliberately induced; for example, shot-peening of a metal surface may be used to induce compressive stress, and thus achieve greater resistance to crack propagation. In other cases, residual stress may be very deleterious, especially with alloys susceptible to stress corrosion. Some nondestructive means of determining the magnitude and direction of residual stress is thus highly desirable. If a material is in a state of residual stress, the atomic-scale crystalline lattice of the metal is strained; that is, it is geometrically distorted with respect to its perfect crystal configuration. For fine-grained polycrystalline metals, the strain is generally homogeneous over the volume of a grain, but usually varies somewhat from grain to grain. The average bulk strain is obtained by averaging the lattice strain over a small region containing many grains. The average bulk

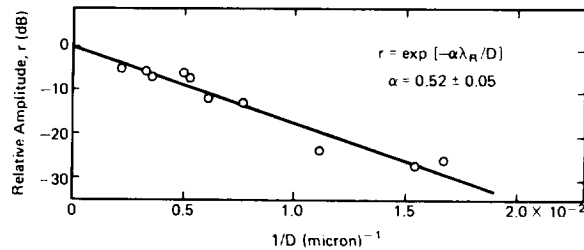


FIGURE 3-30.—Reflection of Rayleigh waves from artificial grooves as a function of depth.

stress is generally presumed to be related to the averaged bulk strain in accordance with a generalized three-dimensional form of Hooke's law.

One approach to the nondestructive determination of residual stresses is the measurement of crystalline-lattice strains by X-ray diffraction. Although usually regarded as the "absolute" method, this approach has several disadvantages. First, it is somewhat complicated requiring precision apparatus operated by highly skilled personnel. Second, the presence of X-rays constitutes a health hazard. Finally, the method is intrinsically limited to sampling a small region of the surface of a specimen. A more practical alternative method is clearly desirable. One possibility is the use of the strain-dependence of the velocity of ultrasonic waves. Through one of its contractors, NASA has explored this possibility (ref. 11).

The velocity with which an ultrasonic wave of prescribed frequency and vibrational mode propagates through a crystalline lattice is determined by the elastic constants and density of the material. For most purposes, only the so-called first-order elastic constants need be considered; in this approximation, however, the ultrasonic-wave velocity is independent of lattice strain. If higher order corrections are made, the wave velocity does depend slightly on the strain. In the case of shear waves, these corrections generally depend on the direction of polarization of the wave; the material is then said to be birefringent with respect to shear waves. There are thus two distinct approaches to lattice-strain (and consequently stress) determination with ultrasonics. On one hand, an attempt can be made to measure the very small stress-induced change in the velocity of some single-wave mode. On the other hand, the difference in velocity of two shear waves of mutually orthogonal polarization possibly can be determined. In either case, grave experimental difficulties can be expected, since the effect is very small. Moreover, objections to the approach can be raised on the ground that, in traversing a finite region, a wave may encounter some zones that are compressively stressed and other zones that are in tension, thereby giving an approxi-

mate null effect. Nevertheless, it has seemed worthwhile to investigate the approach.

Two approaches to stress measurement by the direct measurement of stress-induced changes in the velocity of propagation were investigated by the NASA contractor. These are called the modified time-of-flight system and the frequency-null system.

Modified time-of-flight system.—A simplified block diagram of this system, used to measure stress-induced changes in the velocity of ultrasonic surface waves, is shown in figure 3-31. As illustrated, two pulses are launched simultaneously; one in the test specimen, and one in a similar reference material used as a delay line. When each pulse arrives at its respective receiving transducer, it is amplified and displayed by one trace of a dual-trace oscilloscope. To position the pulses correctly on the face of the oscilloscope, the horizontal trace is triggered immediately before the arrival of the pulses; correct timing of the trigger is obtained with a variable-delay trigger external to the oscilloscope. Triggering of the lower trace may be staggered with respect to that of the upper trace by means of the variable-delay trigger internal to the oscilloscope.

In operating the modified time-of-flight system, the horizontal-sweep rate of the oscilloscope is so set as to display the received pulses with the oscillations of the rf carrier clearly resolved. With a test specimen in the stress-free (mechanically unloaded) condition, the path length of the ultrasonic delay line is mechanically adjusted to bring the upper trace roughly

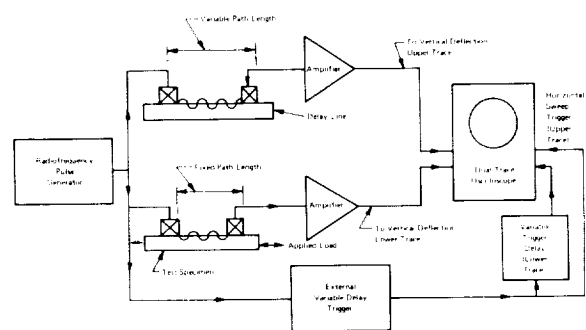


FIGURE 3-31.—The modified time-of-flight system used to measure stress-induced changes in the propagation time of ultrasonic surface-wave packets.

into coincidence with the lower trace. The external variable-delay trigger is then adjusted to delay the trigger pulse by approximately the same value as the ultrasonic propagation time; this has the effect of positioning the pulse traces conveniently on the oscilloscope face. At this point, the horizontal-sweep rate is increased to spread out the two traces, and thus make any phase difference between them visually apparent. The internal trigger delay is then adjusted to bring the traces precisely into phase as judged by visual comparison. The test specimen is then stressed by applying a load. The stress-induced change in the surface-wave velocity causes a change in the propagation time of the pulse; this in turn is evidenced in a change in the phase of the lower-trace oscilloscope display relative to that of the upper trace. The variable-delay trigger internal to the oscilloscope is then adjusted to restore the phase of the lower trace with respect to the upper trace. The internal delay trigger, which is directly calibrated, is capable of resolving 10^{-9} sec. The modified time-of-flight system was normally operated at between 3 and 10 MHz, with a pulse duration in the range of from 1 to 10 μ sec, and a repetition rate of 1 kHz.

For certain applications, the modified time-of-flight system can be operated in a manner somewhat different from that just outlined. It can, for example, be operated without the ultrasonic delay line, provided some alternative reference signal is used. It can also be used with a single transducer operating in the pulse-echo mode, provided an appropriate electronic switch is used to alternate between the send-receive functions.

Frequency-null system.—A simplified block diagram of the frequency-null system is shown in figure 3-32. The master pulse generator generates a train of rectangular pulses with a width that may be varied between 2 and 10 μ sec; the pulse repetition rate may be varied between 3 and 12 kHz. A continuous rf signal is supplied by the oscillator at a frequency which may be varied between 6 and 8 MHz. A precision frequency meter indicates its frequency. The rf signal is fed to each of two linear gates. Pulses from the master pulse generator open Gate 1 for

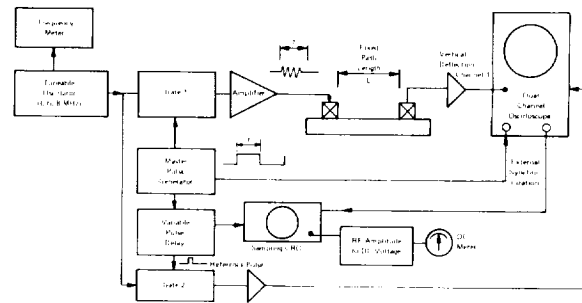


FIGURE 3-32.—The frequency-null system for measuring surface-wave velocity.

the duration of each of the rectangular pulses. The output of Gate 1 is thus a train of rf pulses of the same duration as that of the rectangular control pulse, and with a pulse repetition rate equal to that of the master pulse generator. These rf pulses are then amplified and fed to an ultrasonic transducer coupled to the test specimen. The ultrasonic waves launched in the test specimen are received by a second transducer, from which the output is amplified and fed to the vertical-deflection amplifier of one channel of a dual-channel oscilloscope.

To provide a reference signal, the output of the rf oscillator is fed to a second linear gate, Gate 2. Pulses from the master pulse generator are fed to a variable-delay pulse unit, which generates one pulse of a fixed 1.5- μ sec duration for each pulse emitted by the master pulse generator. The 1.5- μ sec pulse may be delayed from 5 to 30 μ sec with respect to the leading edge of the rectangular pulse which initiated it. The 1.5- μ sec pulse controls Gate 2 from which the output is a train of rf pulses of 1.5- μ sec duration and a repetition rate equal to that of the master pulse generator. These short rf pulses are amplified and fed to the vertical amplifier of channel 2 of the dual-channel oscilloscope. This then displays on a single trace the algebraic sum of the signals present in channels 1 and 2. To insure that the horizontal sweep of the oscilloscope is synchronized with the arriving rf pulses, the leading edge of pulses from the master pulse generator triggers the horizontal sweep.

To operate the null-frequency system, the gains of the vertical amplifiers of channels 1 and 2 are adjusted until their respective signals are of equal amplitude. The variable pulse de-

lay is adjusted until the center of the shorter pulse coincides with the center of the longer pulse. The frequency of the rf oscillator is then adjusted until the signals in channels 1 and 2, respectively, are out of phase by 180° , i.e., until they mutually cancel one another over their region of overlap. Sufficiently precise adjustment of the phase cannot be achieved merely by visual observation of the dual-channel oscilloscope display. In order to achieve adequately sensitive adjustment, the mixed signals of channels 1 and 2 are taken from the external output of the dual-channel oscilloscope and fed to a sampling oscilloscope, which is adjusted to display the mixed signal only over the duration of the reference pulse. The output of the sampling oscilloscope is fed to a circuit that converts the signal amplitude to a proportional dc voltage, which is monitored on a sensitive dc voltmeter. When the frequency of the rf oscillator is correctly adjusted for mutual correlation in channels 1 and 2 of the signals, the dc voltmeter reads zero.

The velocity of an ultrasonic pulse as it travels over a fixed path length of the specimen can now be determined by advancing the frequency of the oscillator until the next higher frequency at which a null on the dc meter occurs. In progressing from one null to another, the number of ultrasonic wavelengths accommodated by the path length, L , must increase by exactly one. Suppose the number of wavelengths originally accommodated in L were N_0 , corresponding to the radiofrequency, f_0 , and ultrasonic wavelength, λ_0 . Thus, the following relation is obtained:

$$N_0\lambda_0 = L = (N_0 + 1)\lambda_0'$$

The wavelength, λ , is equal to the ultrasonic velocity, v_0 , divided by frequency, giving the equation:

$$N_0 \left(\frac{v_0}{f_0} \right) = (N_0 + 1) \left(\frac{v_0}{f_0 + \Delta f} \right)$$

This equation may be manipulated to give the equivalent equation,

$$\Delta f = \frac{f_0}{N_0}$$

from which can be obtained

$$\Delta f = \frac{f_0\lambda_0}{N_0\lambda_0} = \frac{v_0}{L_0}$$

The result is

$$v_0 = (\Delta f)L_0$$

While it is possible to determine Δf with considerable precision, L_0 cannot ordinarily be determined with great accuracy since the area of the ultrasonic transducers in contact with the surface of the specimen is of appreciable size.

The procedure for measuring a stress-induced change in ultrasonic velocity is first to achieve a frequency null for the stress-free situation; second, to apply the stress that will destroy the original frequency null; and, third, to alter the frequency of the oscillator again to achieve a frequency null. In this case, the number of wavelengths contained in the path length L is the same for both null frequencies. Hence, the following relation is established:

$$\frac{f_0}{v_0} = \frac{f_0 + \Delta f}{v_0 + \Delta v}$$

or equivalently,

$$\frac{\Delta f}{f_0} = \frac{\Delta v}{v_0}$$

Thus, the change in null frequency is proportional to the change in ultrasonic velocity.

Measurement of applied uniaxial bulk stress using birefringence of shear waves.—As previously discussed, the velocity of a shear wave in a uniaxially stressed medium depends on the direction of wave polarization with respect to the stress axis. The modified time-of-flight method was used to demonstrate the detectability of this effect. The experimental arrangement in which the pulse-echo technique was employed is illustrated in figure 3-33. The axis of vibration of the crystal surface was determined in a separate experiment. A wax with a low melting point served as couplant.

Specimen materials included the aluminum alloys 2014-T6, 2219-T87, 6061-T651, and 7075-T651. For the latter material, the measured stress-induced time delays for the two shear-wave modes are shown graphically in figure 3-34 (ref. 11).

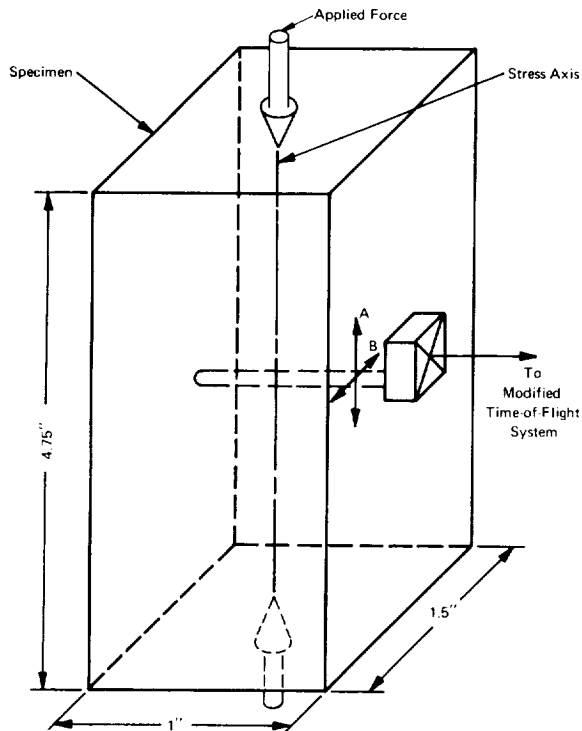


FIGURE 3-33.—Arrangement for measuring shear-wave birefringence induced by uniaxial stress. (The velocity of shear waves, with polarization respectively parallel to A and perpendicular to B, is measured as two functions of applied stress. The ultrasonic frequency used was 7 MHz.)

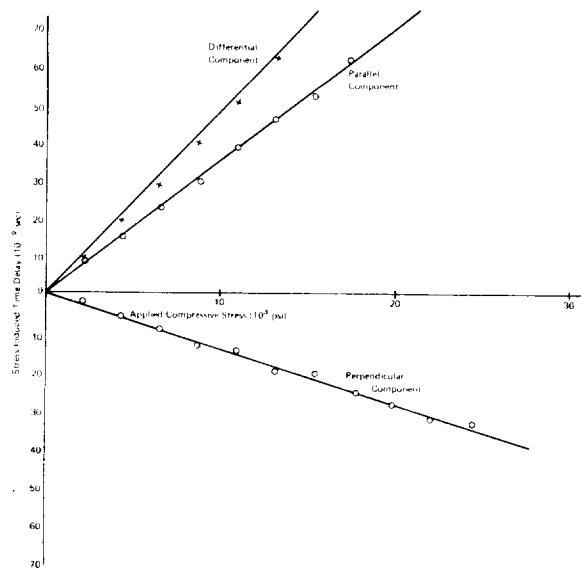


FIGURE 3-34.—Time-of-travel versus applied stress of components of a shear wave in 7075 alloy.

Measurement of stress using surface waves.— Two surface-wave transducers of the pitch-catch type were devised. The first of these is known as the knife-edge transducer (fig. 3-35). Longitudinal waves generated by the sending element are launched toward the knife edge that contacts the surface of the specimen. It was found that the knife edge would generate surface waves, which propagate at right angles to the edge. The receiving element was similar. The knife edges were not sharp, but flattened to a width equal to approximately one-half the wavelength of the surface waves generated in aluminum specimens. The purpose of the knife-

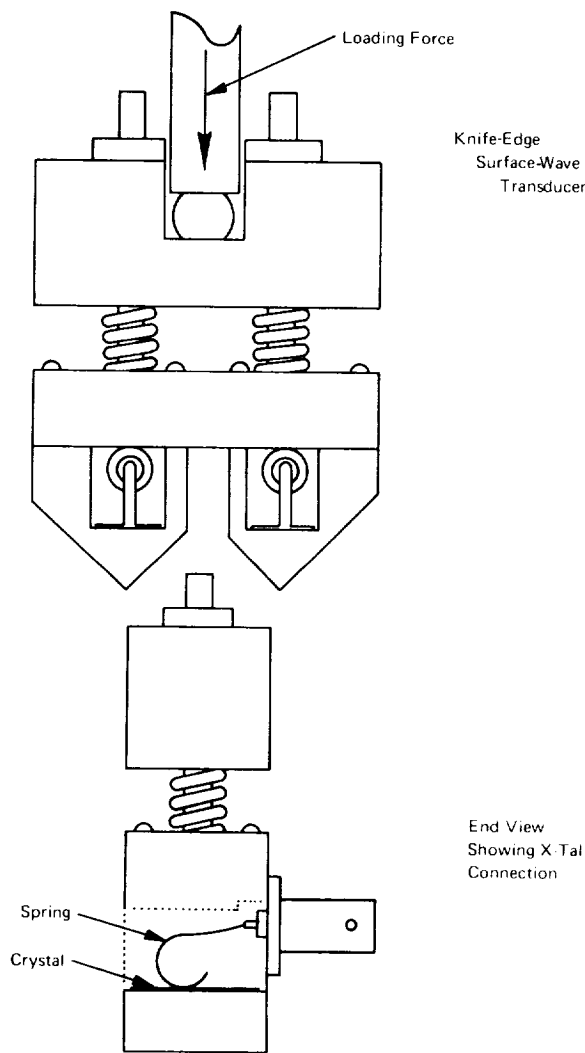


FIGURE 3-35.—Configuration of the knife-edge surface-wave transducer assembly (ref. 11).

edge configuration was to provide a precisely defined separation between the sender and receiver. Satisfactory operation of the knife-edge transducer required that it be firmly pressed against the specimen surface; an external loading fixture was used.

Another type of transducer was called the double-wedge transducer (fig. 3-36). This dual-element surface-wave transducer works on the conventional angle-wedge principle, wherein a longitudinal wave is incident upon the plastic-aluminum interface at the second critical angle. Both the sending and receiving crystals were mounted on opposite ends of a single double-wedge-shaped block of acrylic plastic. To enable it to sustain mechanical loading needed for adequate coupling, the plastic block was reinforced by a closely fitted metal housing.

Both the knife-edge transducer and the double-wedge transducer were used with no

couplant other than the direct mechanical contact effected by pressing the transducer assembly against the surface of the specimen. Both transducers were used exclusively with the frequency-null system. Measurements of stress-induced changes in surface-wave velocity were made by using the compressive loading arrangement previously illustrated in figure 3-33. The surface-wave transducer was placed in the same general position as the shear-wave transducer previously used, and oriented so that the surface waves propagated parallel to the axis of applied stress. The results obtained for 6061-T651 aluminum alloy are shown graphically in figure 3-37; similar results were obtained for the other specimens.

Because surface waves are confined to a surface layer approximately one wavelength in thickness, it is to be expected that the effective stress which affects the surface-wave velocity is the average stress in a one-wavelength thickness of the surface. If a stress gradient exists normal to the surface, the average effective stress will depend on the wavelength of the surface waves used. To test this idea, a rectangular bar specimen was bent in a standard four-point bending arrangement, thereby inducing a uniform tensile stress in the convex surface. The magnitude of the stress decreases with depth, reaching zero at the middle of the beam, and

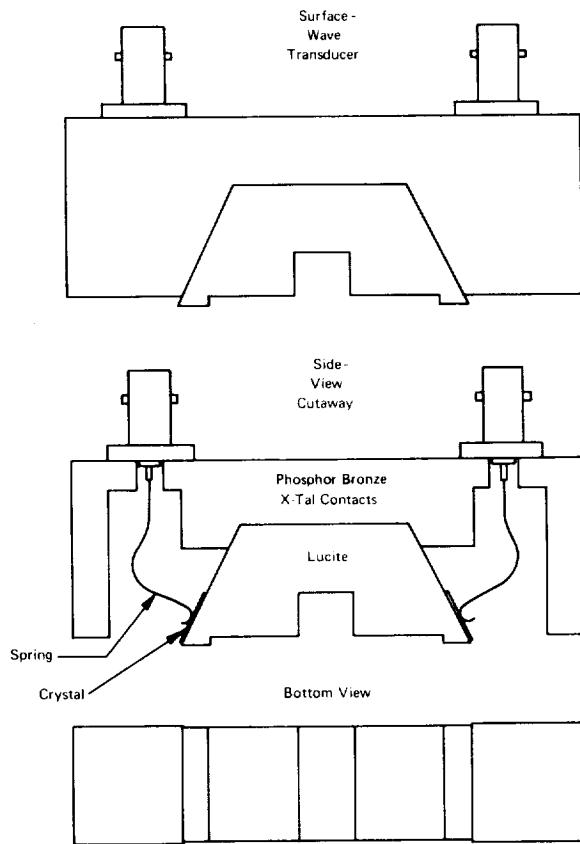


FIGURE 3-36.—Configuration of Lucite surface-wave transducer assembly (ref. 11).

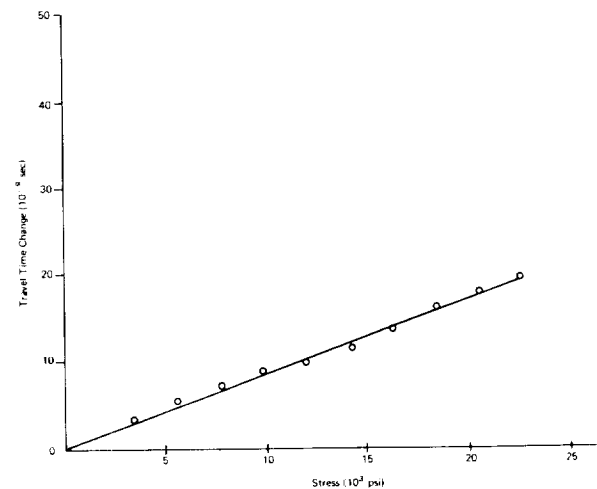


FIGURE 3-37.—Change in time-of-travel (over a 1.5-in. path length) of surface waves vs stress in a uniaxially loaded sample of 6061 alloy (ref. 11).

reverses in sign at greater depths so that the opposite (concave) surface is in compression. The double-wedge surface transducer was mounted on the surface in tensile stress, and the apparent stress measured at frequencies of 1, 3, 5, and 7 MHz. The results showed the apparent stress to be progressively smaller with increasing wavelength (decreasing frequency), and in reasonable quantitative agreement with the hypothesis that the effective stress sensed by a surface wave is the mean stress over a depth of one wavelength.

Effects of preferred grain orientation.—Tests reveal that the ultrasonic properties of a stress-free polycrystalline metal are essentially isotropic, provided that the grains (which are small single crystals) are randomly oriented throughout the volume of the metal. The ultrasonic properties of a single crystal, however, are distinctly anisotropic, especially with shear-wave propagation. For example, in a single crystal of pure aluminum (the symmetry of which is cubic), the velocity of a shear wave propagating in the direction of a cube diagonal is approximately 7.5% greater than the velocity of a shear wave propagating in the direction of a cube edge. Furthermore, a single crystal generally is birefringent with respect to shear waves. In a single crystal of pure aluminum, the velocity of a shear wave propagating in the x-y direction and polarized in the z direction is approximately 10.5% greater than the velocity of a similar wave polarized at right angles to the z direction. In order for a polycrystalline material to be effectively isotropic to ultrasound, three conditions must be met:

(1) The wavelength of the ultrasound must be long compared to the dimensions of the grains.

(2) The grains must be randomly oriented.

(3) There must be no preferred direction created by an applied or residual stress.

The process by which many metal components are manufactured sometimes introduces a preferred grain orientation. This is especially true of rolling operations used in the production of aluminum plate. It can be expected, therefore, that specimens cut from such plates, even when free of applied or residual stress, will

exhibit an apparent stress when tested ultrasonically. Tests conducted by the NASA contractor studying ultrasonic methods of stress measurement confirmed this expectation. This circumstance creates grave difficulties in interpreting the results of ultrasonic stress measurements.

Residual stress studies.—An extensive investigation of specimens of butt-welded aluminum alloy plates was conducted. The general character of the residual stress distribution in such specimens was known from previous studies based on destructive test wherein a specimen is dissected into appropriate pieces and measurements are made of the strain experienced by each piece upon removal from the parent specimen. The detailed results of the NASA contractor's studies are too extensive to summarize here. In general, the ultrasonic measurements were found to be in qualitative agreement with expectations, but many unresolved ambiguities remained at the close of the study. The contractor's report should be consulted for further details (ref. 11).

Delta Technique for Aluminum Welds

The delta technique is a variant of the familiar dual-transducer pitch-catch technique; its name is derived from the fact that the transmitter, flaw, and receiver are conceived to be located respectively at the vertices of a triangle, the shape of which is approximately that of the Greek capital letter delta. The basic arrangement and principle of operation are illustrated in figure 3-38 (ref. 12). The standard immersion water-couplant, mode-conversion technique is used to produce a transmitted shear wave that illuminates the test region of the specimen. The receiver is positioned directly above the test region and is thus sensitive mainly to waves which are longitudinal in the test specimen.

The interaction of the incident shear wave with a real internal flaw is quite complicated. In addition to simple reflection, which is, in general, attended by mode conversion, complex local vibrations of the flaw region are excited. The precise nature of the local vibrations de-

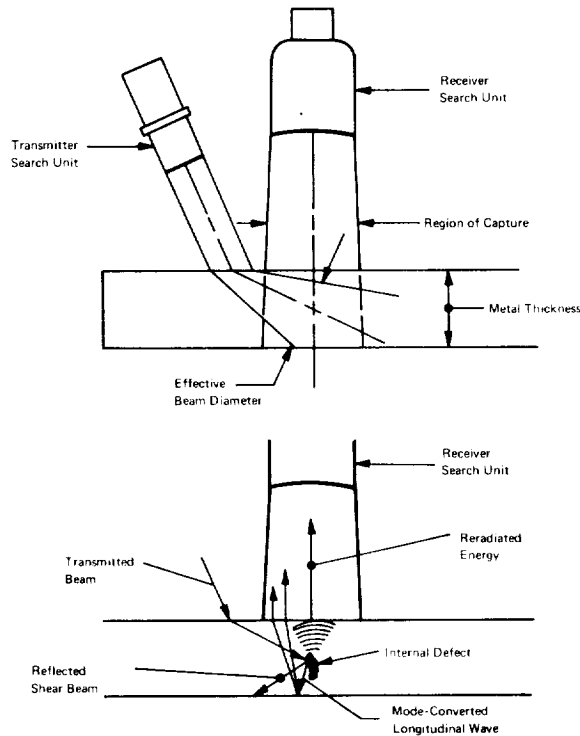


FIGURE 3-38.—Search unit relationship in the basic delta configuration.

depends on the detailed size, shape, and local mechanical properties of the flaw. In simple terms, the flaw may be thought of as a local ultrasound antenna that is excited by the primary incident beam. This complex process, by which the incident beam is scattered, is present in all ultrasonic testing; the various test techniques are distinguished from one another on the basis of just which component (or components) of the scattered ultrasound is utilized by the receiver. The delta technique exploits mainly the longitudinal wave that is reradiated by a flaw.

Because of the potential advantages that the delta technique appeared to hold for flaw detection in aluminum butt weldments, NASA contracted with a commercial firm to evaluate the technique for this application. Three configurations were employed in the study: (1) the basic delta configuration illustrated in figure 3-38; (2) a dual-transmitter arrangement in which two independent transmitters illuminated the flaw region; and (3) a four-transmitter array

configuration. In the multitransmitter configurations, care was taken to match the output of each transducer of the array. Tests were conducted in an immersion water tank; conventional C-scan fixtures and instrumentation were employed. Specimens (which were supplied by NASA) consisted of 6-by-30-in. panels, each with a central butt weld parallel to the long dimensions. Materials used were 2014 and 2219 aluminum alloys, ranging in thickness from 0.15 to 1.0 in. The weldments were deliberately made to contain typical production flaws, including lack of penetration, lack of fusion, gas porosity, foreign matter inclusions, and microfissures. Extensive radiographic inspection and destructive metallographic inspection were conducted to provide a basis for evaluating the delta technique C-scan flaw indications.

The major difficulty encountered in the study was the occurrence of weld-crown noise. Spurious flaw indications were traced to the effects of the irregular as-welded weld crown; scarfing or blending of the crown greatly reduced this effect. The basic single-transmitter delta configuration was found to be considerably less affected by the undressed weld crown, and therefore appeared to be the best choice for weld inspection.

The results of the water-tank test are summarized in table 3-2. Based on these results, the delta-scan technique would appear to be more sensitive than radiography.

For high-speed automatic scanning of production weldments, immersion tank testing is generally impractical. To overcome this difficulty, the contractor demonstrated that the basic delta-scan transducer arrangement could be incorporated in an otherwise conventional commercially available water-filled wheel. For limited local inspection, an encapsulated hand-held probe was devised. For further details, the contractor's report should be consulted (ref. 12).

Acoustic Inspection of Honeycomb Materials

In the design of modern aerospace vehicles, honeycomb-core sandwich-type materials are extensively utilized. Fabrication of these materials involves adhesively bonding thin metal

TABLE 3-2.—Comparison of Delta-Scan Flaw Indications With Results of Radiography and Destructive Inspection (ref. 12)

As-welded sections	Defect occurrence in 341 sections	Number detected by		Percentage detected by		Percentage improvement by Delta
		Delta	X-ray	Delta	X-ray	
Lack of penetration.....	77	54	28	70	36	94
Lack of fusion.....	31	31	27	100	87	15
Porosity >0.010" diam.....	30	27	24	90	80	13
Porosity <0.010" diam.....	88	40	28	45	32	41
Cracks.....	6	5	4	80	66	21
Microfissuring.....	16	16	2	100	13	670

Blended weld sections	Defect occurrence in 53 sections	Number detected by		Percentage detected by		Percentage improvement by Delta
		Delta	X-ray	Delta	X-ray	
Lack of penetration.....	5	4	2	80	40	100
Lack of fusion.....	22	22	18	100	82	22
Porosity >0.010" diam.....	5	5	4	100	80	25
Porosity <0.010" diam.....	19	11	10	58	53	9
Cracks.....	0	-----	-----	-----	-----	-----
Microfissuring.....	2	2	1	100	50	100

face plates to a metal or nonmetallic honeycomb core. Major problems encountered with these materials include the occurrence of regions in which a face plate is disbonded from the core, or regions in which the adhesive fails to develop its minimum acceptable strength. The high reliability required of aerospace vehicles, therefore, calls for NDE techniques capable of finding and characterizing these flaws. An extensive research and development program to meet this need has been conducted by NASA. As part of this effort, an extensive survey was conducted of the pertinent technical literature through mid-1966, and industrial firms and individual authorities were consulted regarding possible technical approaches. The results of this survey, including an annotated bibliography, have appeared as a NASA contractor's report (ref. 13).

Detection of Honeycomb Unbonds by Acoustic Impedance

Technical aspects of the Saturn vehicle necessitated an NDE technique for evaluation of honeycomb disbonds having features that (1) require access to only one side of the honeycomb

panel, and (2) require the mechanical scanning device be portable. Associated electronic instrumentation and C-scan recorders were conceived to be remote. Five candidate approaches were evaluated:

- (1) Ultrasonic pulse-echo
- (2) Sonic and ultrasonic spectral analysis
- (3) Intermodulation between low- and high-frequency vibrational modes of the panel
- (4) Measurement of the natural decay time of vibrational modes
- (5) Measurement of low-frequency mechanical impedance

With the exception of the intermodulation approach, each of these proved to be generally feasible; however, the impedance method appeared to show the greatest promise for meeting all objectives.

Ultrasonic impedance testing depends basically on the electronic sensing of small changes in the ac electrical impedance presented to the signal generator supplying power to the piezoelectric transducer. These changes are, of course, induced by the ultrasonic load placed on the transducer, the load being determined by the

acoustic impedances of the system to which the transducer is coupled. In the study presently under consideration, preliminary feasibility studies were carried out with conventional immersion water coupling with the aim of using a water-filled ultrasonic wheel in the final system. The load on the transducer thus depended on the length of the water path and the orientation of the transducer with respect to the honeycomb panel surface. The nominal beam orientation was 90° (i.e., normal to the surface). The piezoelectric crystal used in the study was selected from several commercially available ceramic materials, mounted in an appropriate submersible housing, and its beam profile determined. Frequencies involved in the study are in the 20- to 35-kHz range.

Four candidate electrical systems for sensing the changes in loading of the transducer were evaluated. These included a constant-current bridge, a constant-voltage bridge, a rectified-crystal detection system, and a piezoelectric-oscillator self-tuned (POST) system. Block diagrams of the four systems are shown in figure 3-39 (ref. 14). The impedance bridge system is a nulling system wherein the crystal is balanced against an adjustable rc circuit. Variable loads

applied to the bridge affect the bridge balance in terms of impedance. The constant-voltage system maintained the crystal voltage at 10 V, and allowed measuring the changes in crystal current with an rf milliammeter. The constant-current bridge utilized a 55-W power amplifier to maintain a reference voltage of 10 V on the crystal.

The rectified-crystal detector system excites the crystal through a series resistance from an oscillator adjusted to the frequency of maximum sensitivity for the crystal. The ac voltage developed across the loaded crystal is rectified, filtered, and adjusted by feedback to variable power supply. The honeycomb disbonds caused an impedance change in the crystal which was measured with a dc voltmeter.

The POST system was designed to self-tune the detection crystal to a natural vibrational frequency of the composite, thereby eliminating the need for frequency scans to determine the optimum sensitivity. This was accomplished by two methods. The first method consisted of isolating a portion of the crystal's electrode surface for feedback; the second employed a separate small crystal mechanically driven by the detection crystal for feedback. Both methods were tested and proved satisfactory. The pickup signal was amplified, phase-adjusted, and fed back for crystal-drive excitation. The POST system oscillated at the frequency where the detection crystal produces the maximum mechanical vibration. The feedback gain and phase circuits were used to trigger levels or stop the crystal oscillation. Of the four systems tested, the POST system was selected as being most promising for further development.

Following an extensive calibration program in which specially prepared honeycomb test panels were used, the optimized breadboard system was applied to automatic scanning of Saturn honeycomb composites by using a prototype water-filled rubber-tire ultrasonic wheel. This system was evaluated through correlation of its results on test panels with the findings of destructive tests. The results of these tests supported a recommendation that a shop-worthy version of the breadboard system be developed.

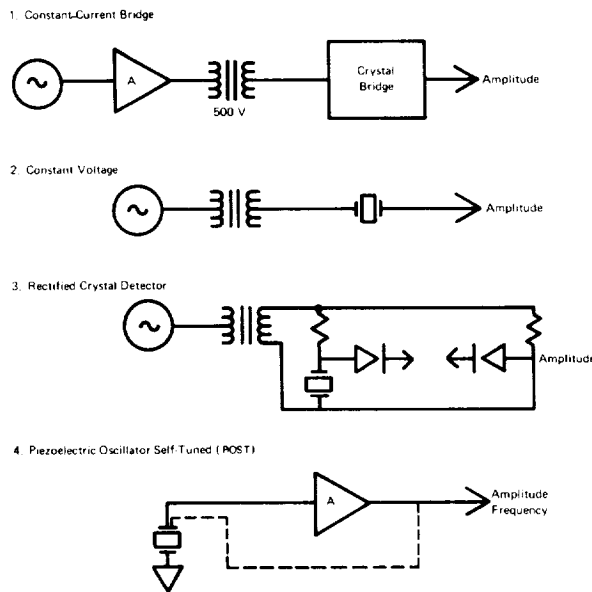


FIGURE 3-39.—Circuits for sensing changes in transducer power levels.

Determination of Honeycomb Adhesive Bond Strength

Apart from regions of total disbond between core and face sheet, regions in which the adhesive fails to develop its nominal strength also compromise the load-bearing capacity of honeycomb plates. Locating such weak regions nondestructively poses a technical problem considerably more formidable than that of locating disbonds. The heart of the problem is that a weak bond region presents no sharp, well-defined discontinuity in any specimen readily susceptible to nondestructive measurement. Even today the problem has not been satisfactorily solved.

One approach to this problem was selected by NASA as potentially applicable to the inspection of large honeycomb propellant tanks used in space vehicles (ref. 14). Following a survey of the literature on adhesively bonded structures, it was concluded that bond weakness occurring in practice was caused by the failure of the adhesive to develop its full cohesive strength rather than its failure to adhere to the joined surfaces. Thus, candidate NDE approaches must be aimed at determining the viscoelastic properties of the thin layer of adhesive itself. The only possible avenue of approach seemed to be through the vibrational properties of the honeycomb sandwich material. A mathematical analysis indicated that a viable NDE method should determine either the amplitude of vibration of a localized vibrational mode which stressed the adhesive, or the excitation bandwidth of a localized vibrational mode as the frequency of a coupled exciter is swept through resonance with the vibrational mode. Characteristic frequencies of localized vibrational modes in representative honeycomb materials were determined by the core cell dimensions and the number of cells affected by the degraded adhesive. Expected upper frequencies were approximately 100 kHz for a $\frac{3}{16}$ -in. cell, and 1 kHz for a $\frac{3}{4}$ -in. cell; the lower frequency expected was of the order of a few Hertz. Two technical problems were paramount: (1) the need to find a satisfactory method of exciting the vibrational modes of the structure without unacceptably loading it (i.e., without direct me-

chanical coupling), if possible; and (2) the requirement for a method of accurately measuring the amplitude of the vibratory excursions of the face sheets.

The approach selected for in-depth evaluation was based on a device called a Displacement Oriented Transducer (DOT). The DOT has two components—an axially symmetric electromagnetic driver and a displacement sensor capable of resolving the small differences in vibrational amplitude associated with regions of weak bonding. The electromagnetic driver is essentially a flat coil of wire that carries an alternating current of variable frequency. The coil couples with a metal substrate through the induction of eddy currents; by Lenz's law, the coil and the substrate will repel one another. Thus, the substrate is given a push twice during each alternating current cycle. (An alternate type of exciter, an interrupted air-stream pulser, proved less successful than the electromagnetic type.)

The DOT system is basically a vibration analysis method using high level, automatically variable frequency excitation forces in a metallic structure and detecting microinch displacements. The simplified block diagram shown in figure 3-40 illustrates its major components and functional operation (ref. 14). The excitation unit comprises an automatic swept-frequency

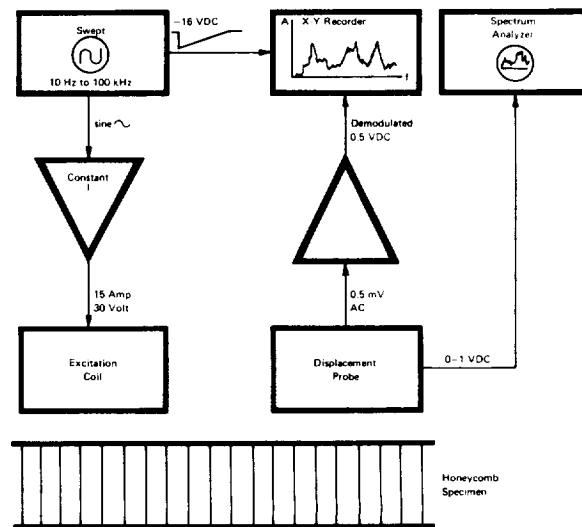


FIGURE 3-40.—The DOT bond-strength system.

source, a power amplifier, and an electromagnetic transducer. Excitation levels are available up to 15 A at 30 V over the 10-Hz to 20-kHz frequency range. An operational amplifier is used to compare the input sine-wave signal with a feedback signal proportional to the transducer current to correct for coil impedance changes and ensure constant-current drive over the operating frequency range. The driver can produce force levels of approximately 8 psi in the aluminum face sheet materials at the high excitation levels. The vibration-response detection system was developed using a commercial fiber-optic displacement instrument with a displacement sensitivity of 5 $\mu\text{in.}/\text{mV}$ over a dc to 40-kHz frequency range. The fiber-optic probe was accurately positioned coaxially in the excitation transducer. The displacement instrument was modified to provide an amplified and demodulated ac output signal proportional to the measured dynamic displacement amplitude; this signal was monitored directly on the oscilloscope display of a spectrum analyzer, and could be plotted with a pen recorder as a function of the excitation frequency. Other system components included an auxiliary heater-controller system, temperature recorders and indicators, and a digital frequency counter.

The DOT system is calibrated by response measurements on composite materials of known strength; either a resonance-response amplitude, frequency, or half-bandwidth parameter was measured. The DOT is either operated noncontact or supported on the composite with rings or three-point contacts. The composite was swept with frequencies of selected excitation levels until a significant response was indicated. Particular frequency resonances related to the geometry effects of the test system were ascertained, and only those resonances associated with the damping of the composite were used for measurements.

To test the basic hypothesis of the method, the DOT system was used to measure the vibrational response to the driver as the frequency of excitation was swept over the range in which resonances were theoretically expected to be. The results for a particular specimen are shown graphically in figure 3-41 (ref. 14). The ex-

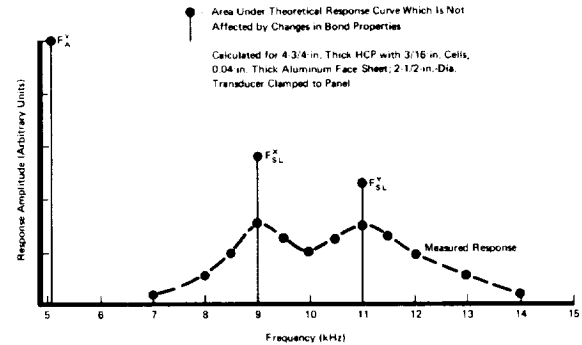


FIGURE 3-41.—Frequency response of adhesive-bonded honeycomb panel from 5 to 15 kHz.

pected resonances are distinctly apparent; however, the breadths of the resonances are orders of magnitude greater than the breadth theoretically expected for the damping action of the adhesive itself; other damping mechanisms evidently predominate. Thus, the attempt to measure bond strength by means of the characteristic energy dissipation of the adhesive was frustrated.

The only apparent alternative was in some way to relate bond strength to the amplitude of resonant vibration under constant excitation conditions. Statistical variation in the response of good bonds was found to be substantial, thus precluding a straightforward approach. However, from an analysis of the kinetics of adhesive curing, it was hypothesized that a weak bond, when heated, should show changes in response because of thermally induced curing. The response of a strong bond, already well cured, should be comparatively less affected by heating. Pursuing this idea, the DOT system was applied to specimens heated in an oven. The procedure was to measure the amplitude of a prominent peak resonance as a function of temperature and of bond strength. The test verified that the amplitude of resonance peaks generally tended to increase as the temperature was raised; however, the increment in resonance amplitude did not appear to depend greatly on bond strength.

In the course of the oven tests, it was observed that the frequency at which a given peak resonance occurred tended to shift with temperature, and that the shift depended upon bond strength. The data were therefore analyzed to determine the change in resonant frequency per

unit rise in temperature as a function of bond strength. Representative results are shown graphically in figure 3-42 (ref. 14). Following these results, which were considered promising, the DOT system was modified to provide an electrical heater, which surrounded the basic probe assembly.

Further evaluation was conducted under laboratory conditions with the DOT driver employed to heat a local area of the composite by eddy-current effect and supplemented by a guard-type resistance heater integrally mounted around the DOT periphery. The heated area was approximately 6 in. in diameter. Tests were conducted at intervals of 10 to 15 min, allowing temperature stabilization. A preliminary evaluation showed that clamping of the specimen was not necessary for damping measurements above 0.8 kHz. Further, the application of heat from only one side of the composite reduced the response peak amplitudes by only 25%, which still permitted a reasonable signal-to-noise level.

The same specimen series tested in the oven was retested by the heater-augmented DOT system. The measurement method included a fre-

quency scan to determine response frequencies related to the composite properties and unaffected by either the specimen geometry or support. Vibration response measurements were made at four or five temperatures after thermal stabilization. The response peak amplitudes were recorded as a function of frequency over a range of the driving coil current of from 5 to 15 A.

The peak response amplitude data at a 15-A drive were plotted as a function of bond strength as shown in figure 3-43 (ref. 14). The amplitude-strength relationship is in accord with the previously obtained oven-test data and shows a proportionately increasing response amplitude with increasing strength. Figure 3-44 shows the dependence of response frequency with strength as predicted and as observed in the oven-test data (ref. 14). It was therefore concluded that the transition from the oven tests to laboratory self-heating conditions was successful.

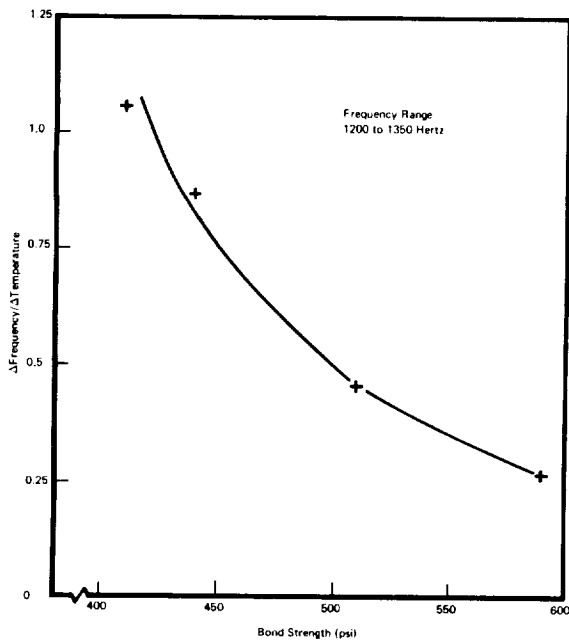


FIGURE 3-42.—Change of high-frequency resonance as a function of test temperature and bond strength (0.02-in. facing sheets).

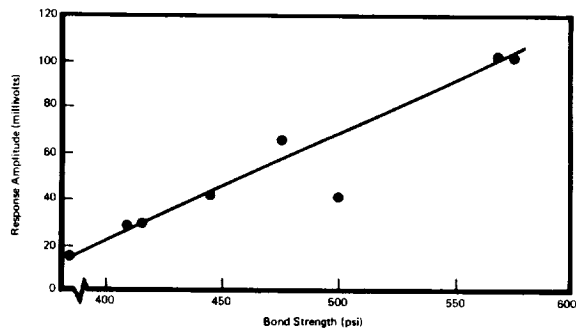


FIGURE 3-43.—DOT vibration response data obtained from self-heated unclamped honeycomb composites (0.063-in. facing sheets).

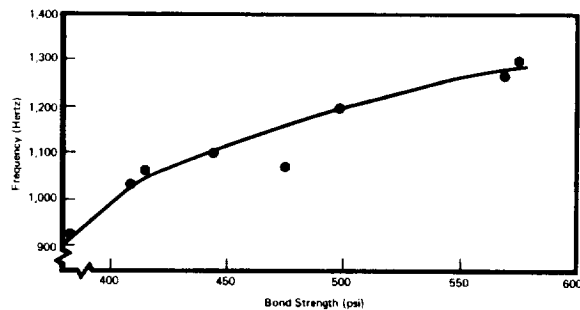


FIGURE 3-44.—DOT vibration response frequency vs bond strength (0.063-in. facing sheets).

The thermally assisted DOT approach to the evaluation of bond strength of honeycomb material has many drawbacks, not the least of which is the time required for thermal stabilization. The inherent complexity of the approach makes it difficult to implement. Moreover, the physical mechanisms by which adhesives cure, gain strength, age, and degrade are still only poorly understood. The problem of NDE bond strength, though broached, remains one of the challenges of the field.

Honeycomb Structure NDE By Through-Transmission of Sound

Another approach that NASA has investigated for testing honeycomb for disbonds is that of straightforward through-transmission of airborne sound (refs. 14, 15, and 16). A block diagram of a system devised for possible application to assembled tanks is shown in figure 3-45 (ref. 14).

Disbond sensitivity tests proved successful on 1- and 1 $\frac{3}{4}$ -in.-thick honeycomb composite specimens. Figure 3-46 shows a typical frequency

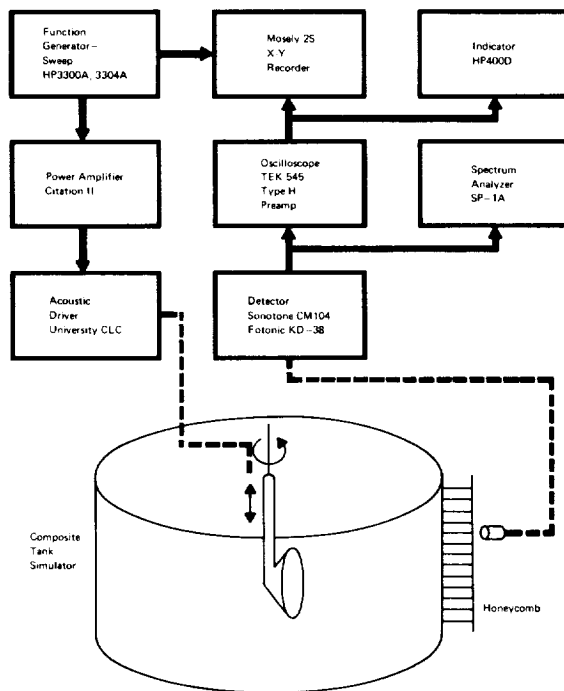


FIGURE 3-45.—Prototype system for inspection of honeycomb by through-transmission of airborne sound.

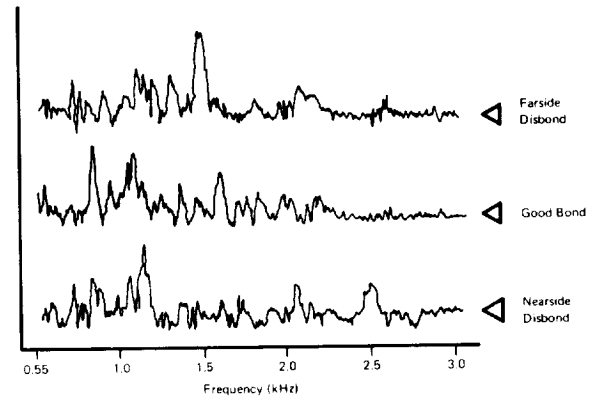


FIGURE 3-46.—Frequency response record from 0.5 to 3.5 kHz for 1 $\frac{3}{4}$ -in. honeycomb composite with square disbonds.

response recording. It is apparent that there are characteristic differences between the spectra of known disbonds and well-bonded areas. In figure 3-46, for example, spectral peaks due to nearside disbonds (on the external adhesive layer of the tank) in the 1 $\frac{3}{4}$ -in. composite are clearly identifiable at 2.05 and 2.37 kHz (ref. 14). The farside disbond (adhesive layer adjacent to the tank wall) is clearly identifiable at 1.295 and 2.05 kHz. The farside disbond response at 2.37 is minimal, thereby suggesting the feasibility of discriminating between disbonds located at either of the two adhesive interfaces.

Based on the frequency response data, selected frequencies were evaluated for disbond detection by using hand scanning techniques. The background noise within the laboratory area, however, was quite high because of leakage and reverberation of the tank simulator. The microphone was installed in a convenient stainless-steel tube approximately 3 in. in diameter by 10 in. in length with glass fiber insulation to reduce side noise pickup. This technique essentially converted the omnidirectional microphone to a single-direction detector with about a 10-deg. reception arc. The same insulation was also applied to the tank simulator in areas not containing composite specimens. Hand scanning for disbond detection was facilitated by spraying either a light Teflon* film or dusting a fine powder on the face sheet.

*Registered trade name of E. I. du Pont de Nemours and Co.

Hand scans were made at test frequencies selected on the basis of the previously obtained frequency response data. In most instances, a significant amplitude response was noted for each type of disbond. In addition, the disbonds were detected by selected frequency bands swept at rates up to 10 kHz. The disbonds were identifiable primarily by amplitude variations of the modulated envelope on the oscilloscope. The detection data also could be correlated by observing phase changes in the display waveform. The hand scanning tests proved the feasibility of air-couple techniques for detecting relatively gross disbonds at both adhesive layers.

Similar tests were conducted by employing the fiber-optic-displacement measuring system used in the DOT system. The measured disbond sensitivity data showed reasonably comparable results. The fiber optic system, however, required resetting at each test location on the composite specimens for reflectivity adjustment, whereas the microphone was readily hand-scanned.

The development of the air-couple technique has made it possible to determine the following performance parameters:

(1) The acoustic source-detector technique was proven suitable for the detection of disbonds at both adhesive interfaces in sizes ranging from 3-in. squares to 1-in. isosceles triangles in Saturn-type composites.

(2) The differing frequency-response characteristics of near and farside disbonds provided the clue to determining the particular adhesive layer containing a disbond.

(3) Acoustic attenuation measurements showed the feasibility of using conventional loud speakers and microphones under the proper conditions to perform disbond detection tests in a tank at distances up to 16.5 ft.

The disbond-detection sensitivity was found to be a function of test frequency. Measurements at the low-frequency ranges were made difficult by major tank wall vibration and a driving of the entire contact-type microphone-housing assembly. The higher-frequency responses, from 1.0 to 2.4 kHz, proved to be most successful. The response peaks for a series of disbonds in a specimen covered rather broad frequency

bands of approximately 50 to 100 Hz. Swept-frequency techniques proved to be effective means of detecting the disbonds.

Ring-Beam-Wheel Surface-Wave Search Unit

Rapid ultrasonic scanning over large surface areas of materials is often desirable. One approach to rapid scanning using ultrasonic surface waves is the so-called ring-beam wheel developed by a commercial firm under a NASA contract (ref. 17). The approach used involves two key developments:

(1) An annular-shaped transducer crystal and ultrasound reflector capable of launching circular surface waves when water-coupled to a metal surface

(2) An approximately spherical water-filled rubber tire, which contacts a metal surface over an essentially circular-shaped area of contact.

From several candidate transducer designs, the one illustrated in figure 3-47 was selected for development. The conical-shaped compressional wave beam produced by the transducer assembly impinges on the water-(tire)-metal interface at the second critical angle, thus, generating surface waves that propagate radially outward from the contact area. The transducer is operated in the conventional pulse-echo mode. An electronic gate operating during the receiving phase is set to receive echoes originating from points within a circular annulus with a minimum radius just greater than the radius of the circular area of contact between the tire and the

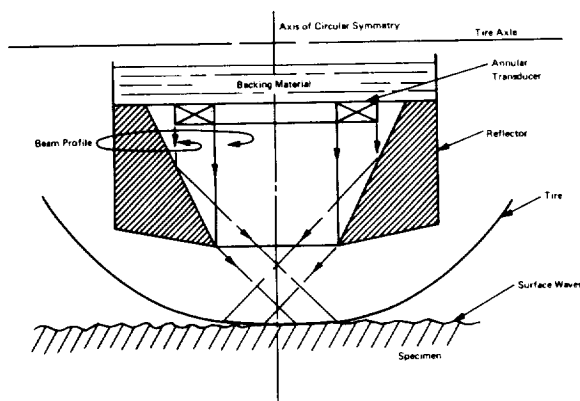


FIGURE 3-47.—Cross-sectional view of a ring-beam-wheel surface-wave search unit.

metal surface; hence, the term *ring beam*. An A-scan presentation reveals the radial distance of a flaw from the center of the ring, but does not indicate its azimuthal position.

A prototype version of the ring-beam-wheel surface-wave search unit was delivered to NASA by the manufacturer. Documentation regarding its evaluation by NASA is unavailable at this writing.

Ultrasonic Testing in the Space Environment

Anticipating the eventual requirement for NDE techniques and instrumentation suitable for application to vehicles and structures in space, NASA has conducted a preliminary study to determine which techniques are the best candidates. Ultrasound was considered a prime candidate. NASA sought to determine the effects of a simulated space environment on basic ultrasonic materials and components (ref. 18, parts I, II, and III; ref. 19).

An evaluation of various types of fluid couplants was conducted to determine which would be most suitable for in-space ultrasonic inspection. The original objective of this area of the program was to select a couplant that would be compatible with the space environment and not leave a greasy film residue after evaporation from the surface of the test object. The basic properties considered for couplants were the stability of the couplant with respect to acoustic energy transmission, the vapor pressure or rate of sublimation loss, and the change in viscosity. The temperature range considered was -100° to $+160^{\circ}$ F and the vacuum level was 10^{-7} torr.

It was found that silicone-base fluids offered the greatest potential for space application. These fluids are chemically inert and compatible with a wide range of materials, both metallics and nonmetallics, and exhibit desirable characteristics when exposed to a high-vacuum or oxygen environment. They also have excellent thermal stability, which enables them to withstand temperatures from -100° to $+450^{\circ}$ F. Because their viscosity is fairly constant, they provide more uniform sound transmission over a wider temperature range than do conventional fluids. They also offer excellent resistance to

oxidation and have a very low surface tension. However, their vaporization rates are in the range of 0.00001 to 0.02 g/hr, which means an oily film would probably remain for a significant length of time following the inspection.

Transducers were then evaluated. The objective of this preliminary testing was to select transducers that would enable inspection of defects of small size, and to define the practical limits of their use in a space environment. The parameters investigated were temperature (room temperature to 140° F), pressure (atmospheric to 10^{-5} torr), and transducer material. Defect resolution and sensitivity were measured with standard equipment and techniques. To obtain the desired test temperature, thermally insulated heater tapes were wrapped around the dead-weight-loaded transducer and test-block interface.

Temperature was recognized as the most critical factor because of three primary problems that arise when exposing piezoelectric materials to elevated temperatures. First, the epoxy cement bonding the crystal to its base begins to soften, leading to broken connections and misalignment. Second, the difference between the thermal coefficients of expansion of the piezoelectric material and the back-up damping material, respectively, is usually quite large; consequently, exposure for any appreciable length of time can cause cracked crystals. Third, the activity of most piezoelectric material decreases with increased temperature, causing reduced output energy and a consequent reduction of echo signal strength.

The three transducer materials evaluated were: lithium sulphate, quartz, and lead zirconate titanate. Lithium sulphate was chosen because it is among the most efficient of all known receivers of ultrasonic energy. The overall voltage performance ratio (i.e., transmitting and receiving) is approximately 28 times greater than that of quartz. The electrical impedance of lithium sulphate is only slightly lower than that of quartz, making it easier to drive with standard ultrasonic instrumentation. Little or no aging has been experienced with lithium sulphate, and it has one of the lowest mode conversions of any of the standard

piezoelectric materials. The disadvantages of its use are that it is highly soluble in water and must be completely protected at all times by some type of plastic or metallic case, and that the crystal's useful upper operating temperature is approximately 167° F.

Quartz transducers were selected for evaluation because quartz can operate at temperatures of approximately 800° F. It also has excellent mechanical and electrical stability and resistance to aging. Quartz is insoluble and has good resistance to abrasion. It is a strong, rugged transducer material. On the other hand, it is susceptible to mode conversion, and it is the least efficient generator of acoustic energy of any of the common piezoelectric materials.

Lead zirconate titanate is classified as a ceramic. It can operate at temperatures up to 580° F. The ultrasonic sensitivity of the material is very high. The piezoelectric constants of the ceramics are usually higher than that of quartz. The low elastic quality of the material is a disadvantage.

The first series of transducer-material tests consisted of establishing a constant test temperature, initiating vacuum pump-down, and recording a standard defect-signal amplitude after reaching equilibrium. A 10-min equilibration was selected, because previous tests had tentatively indicated that this time was necessary for stabilizing pressure (10^{-4} torr). This procedure was followed for each transducer material at each test temperature (85°, 120°, and 140° F.). A constant gain setting was used throughout the tests. Results indicated that lithium sulphate, lead zirconate titanate, and quartz are respectively less sensitive, based on signal amplitude, over the temperature range tested; and as temperature increases for relatively constant vacuum, sensitivity decreases significantly. Lithium sulphate appeared to be the least affected by temperature.

To evaluate further the time-temperature-vacuum effect on the transducer materials, a second series of tests was performed in which the effect on sensitivity of time-in-vacuum at a constant temperature was measured. The tests were similar to the first series with the excep-

tion that the temperature was held constant; measurements of signal amplitude were taken every few minutes for a total time-in-vacuum of 60 min. At atmospheric pressure, the sensitivity decreased significantly with temperature. Temperature and time-in-vacuum also had a significant effect on sensitivity. At 140° F, the stability of the lithium sulphate transducer appeared to break down. However, following the 140° F temperature run, as the temperature was reduced to 120° F, the sensitivity of the material (still under vacuum) gradually returned to and stabilized at the value observed in the originally stabilized 120° F transducer test. On further cooling under vacuum, the sensitivity rose, stabilizing at approximately the original room temperature value. To check the repeatability of this test data, the 120° F test cycle was rerun the following day, and the results agreed well with the original data. The test was then continued for an additional 7 hr at constant vacuum and temperature without any observed change in the sensitivity. At the end of the accumulated 8 hr of test time, further changes in the temperatures were made, and the resulting data agreed with the original data.

A similar series of tests was run using the lead zirconate titanate and quartz transducers. Stability of the lead zirconate titanate was good over the entire temperature range. The expected drop in sensitivity with temperature and time in thermal vacuum did occur. The observed effects, however, were apparently reversible.

In summary, the NASA contractor drew these conclusions.

- (1) As temperature is increased from room temperature to 140° F, ultrasonic sensitivity decreases.

- (2) As the pressure is reduced to the order of 10^{-4} torr, sensitivity decreases, but at room temperature it may regain this initial loss.

- (3) Under thermal-vacuum, as temperature increases, sensitivity decreases; and for a stable material, the sensitivity stabilizes with time.

- (4) For operation in the temperature range anticipated for space applications, the lead zirconate titanate transducer is recommended, based on its better thermal stability.

REFERENCES

1. ANON.: Classroom Training Handbook—Ultrasonic Testing. NASA CR-61228, 1965.
2. ANON.: Ultrasonics. Vol. I—Basic Principles. NASA CR-61209, 1967. (N68-28781)
3. ANON.: Ultrasonics. Vol. II—Equipment. NASA CR-61210, 1967. (N68-28782)
4. ANON.: Ultrasonics. Vol. III—Applications. NASA CR-61211. (N68-28783)
5. EVANS, RAYMOND; AND MACDONALD, J. A.: Development of Mechanized Ultrasonic Scanning System. NASA TM X-53598, 1967.
6. KLIMA, STANLEY J.; LESCO, DANIEL J.; AND FRECHE, JOHN C.: Application of Ultrasonics to Detection of Fatigue Cracks. NASA TM X-52109, 1965. (N66-18328)
7. KLIMA, STANLEY J.; AND FRECHE, JOHN C.: Ultrasonic Detection and Measurement of Fatigue Cracks in Notched Specimens. NASA TN D-4782, 1968.
8. HOPPE, FRANK J.; AND INMAN, NELSON: Development of Nondestructive, Automatic Technique for Monitoring and Recording of Fatigue Crack Growth. NASA CR-66320, 1967.
9. CLOTFELTER, W. N.; BANKSTON, B. F.; AND ZACHARY, E. E.: The Nondestructive Evaluation of Stress-Corrosion Induced Property Changes in Aluminum. NASA TM X-53772, 1968.
10. CORDELLOS, A. D.; BELL, R. O.; AND BRUMMER, S. B.: Use of Rayleigh Waves for the Detection of Stress-Corrosion Cracking (SCC) in Aluminum Alloys, Materials Evaluation, vol. 27, Apr. 1969, pp. 85-90.
11. BENSON, ROBERT W.; CHAPMAN, J. RONAND; HUFFMAN, HAROLD F.; AND PEARSALL, SAMUEL H.: Development of Nondestructive Methods for Determining Residual Stress and Fatigue Damage in Metals. Robert W. Benson and Associates, Inc. (Nashville, Tenn.), Mar. 8, 1969.
12. HANNAH, K. J.; CROSS, B. T.; AND TOOLEY, W. M.: Development of the Ultrasonic Delta Technique for Aluminum Welds and Materials. NASA CR-61952, 1968.
13. MARTIN, G.; MOORE, J. F.; AND ROCKE, J. W.: Development of Nondestructive Testing Techniques for Honeycomb Heat Shields, Vol. I and Vol. II. North American Aviation, Inc. (Los Angeles), Nov. 1966.
14. MARTIN, GEORGE; AND MOORE, J. F.: Design, Development, and Fabrication of Portable Instrumentation for Nondestructive Testing of Composite Honeycomb Materials. North American Rockwell Corp. (Los Angeles), Feb. 3, 1969.
15. CLOTFELTER, W. N.: Acoustic Techniques for the Nondestructive Evaluation of Adhesively Bonded Composite Materials. NASA TM X-53219, 1965.
16. ANON.: Nondestructive Testing: Trends and Techniques. Proceedings of the Second Technology Status and Trends Symposium, NASA SP-5082, 1966.
17. MURDOCH, A. M.: Development of a Ring-Beam Wheel Surface Wave Search Unit. NASA CR-76361, 1966.
18. ZORAN, W. A.: Nondestructive Testing for Space Applications. Final Report, Parts I, II and III, NASA CR-90042, CR-90043, and CR-90044. (N68-10953, N68-10792, and N68-10958)
19. BEAL, JAMES B.: Nondestructive Testing—Applications in the Outer-Space Environment. Materials Evaluation, vol. 26, no. 5, 1968, pp. 69-78.

CHAPTER 4

Radiography

C. Gerald Gardner

A radiograph is basically a two-dimensional picture of the intensity distribution of some form of radiation, projected from a source (ideally, a point source), and which has passed through a material object that partially attenuates the intensity of the radiation. Voids, changes in thickness, or regions of different composition will, under favorable circumstances, attenuate the radiation by different amounts, producing a projected "shadow" of themselves. The basic elements of the radiographic process are shown in figure 4-1 (ref. 1). Three forms of penetrating radiation are presently used in radiography: X-rays, gamma rays, and neutrons. X-rays were the earliest of these to be used.

X-rays were accidentally discovered in 1895 by Wilhelm K. Roentgen, at the University of Wurtzburg, Germany. While studying the phenomena of electric discharges through rarefied gases, he observed a new type of radiation that could penetrate material opaque to light; he called it X-radiation because of its peculiar and unknown nature. When Roentgen announced his discovery, nearly everyone having a high-voltage gaseous discharge tube tried taking X-ray pictures of such things as human limbs and metal objects. These efforts were not very successful, however, since the tubes of that time usually failed when the high voltages necessary

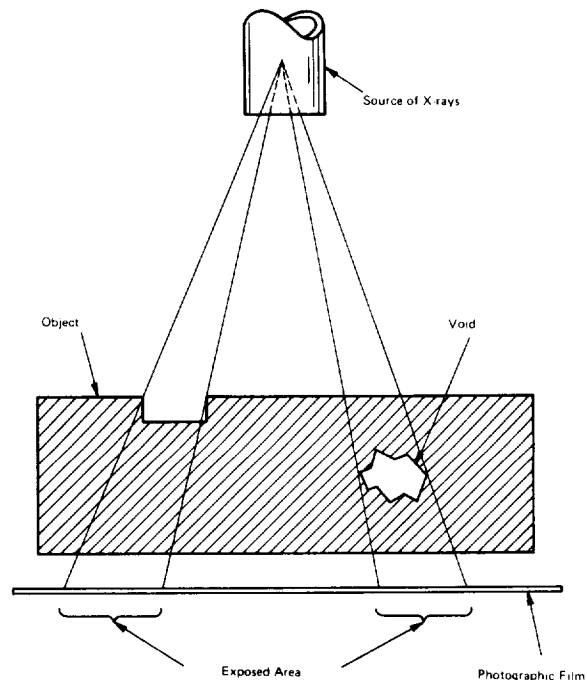


FIGURE 4-1.—Diagram of radiographic process.

to produce X-rays of suitable penetrating power were applied. Moreover, the electric generating devices used then produced very little current. This meant that long exposure times were required. The early radiographer was forced to use ordinary glass photographic plates

that were not favorable to radiography. These and other factors retarded the development of radiography until about 1912.

The development was accelerated when, in 1912, William D. Coolidge perfected a new type of X-ray tube that could operate at higher voltages and carry more current than previous tubes, resulting in X-radiation of greater intensity and penetrating power. Although radiography was used to some extent during World War I for various inspection purposes, it was not until the 1920's that its potential as a practical nondestructive testing method was proven.

In 1922, radiographic equipment with a Coolidge tube that could operate at 200 000 V (200 kV) with a current of 5 mA was installed at the Army Ordnance Arsenal at Watertown, Massachusetts. With the installation of this equipment, pioneer efforts were made which led to the first real accomplishments in industrial radiography. Watertown Arsenal personnel found that up to 3 in. of steel could be radiographed under manufacturing conditions with the new equipment. Today, almost all metal forming and joining operations rely heavily on radiography. Prior to the use of radiography, casting defects, for example, if discovered at all, were not found until the machining phase of manufacturing; this resulted in a loss of time, material, and money. Now, the foundryman and radiographer work hand in hand. When a part is to be cast, a pilot casting procedure is set up, and the part is cast and radiographed. If the radiograph shows the part to be defective, changes are made in the casting technique and the part is recast. This process is repeated until a satisfactory procedure, yielding sound castings, is developed. A continuing quality check is kept by inspecting a number of castings selected at random out of a given lot.

In 1932, a new Coolidge X-ray tube that would perform continuously at 300 kV and 8 mA became available. As technology advanced, X-ray equipment with 1000-kV tube ratings became possible. Then, with the development of the Van de Graaff generator and the betatron, multimillion-volt units were designed. Today, X-ray units, called linear accelerators, have ratings up to 100 million volts.

In recent years, technological advancements in film emulsion and strip film have made possible far greater industrial use of radiography. In addition, both government and industry are emphasizing continued effort toward the improvement of filmless radiographic techniques (e.g., fluoroscopy, xeroradiography, and television).

With the development of practical means of producing artificial radioisotopes after World War II, radiography using radioactive gamma-ray sources has become technically and economically feasible, and now plays a significant role in NDE. More recently, neutron radiography has been introduced, which has unique capabilities for revealing hydrogenous materials surrounded by metals. As practical, portable neutron sources become available, neutron radiography will undoubtedly become more widely used.

Radiographic inspection is superior to other NDE methods in a number of applications. For example, it can provide a permanent visual representation of the interior of the test object. Under favorable conditions, radiographic inspection as a quality control procedure can conserve time and materials as given below.

(1) It reveals, nondestructively, the internal nature of a material, and can be used to separate acceptable items from unacceptable ones after standards for acceptance have been established.

(2) It discloses errors in the manufacturing procedure and process control in sufficient detail to indicate necessary corrective action.

(3) It discloses structural unsoundness, assembly errors, and concealed mechanical malfunctions, thereby reducing the unknown or variable factors in a design during the development phase.

(4) It is also useful in preventative maintenance and failure analysis.

The costs of industrial X-ray films and their handling and processing are relatively high in comparison to other inspection methods. Radiography of material that is small, easily handled, of simple geometry, and which otherwise lends itself to high rates of inspection, can be accomplished economically. Large items, complex geometries, materials which are difficult to

handle, and cases in which the radiographic equipment must be brought to the material are all factors that increase costs of inspections substantially. For example, the cost of radiographic inspection of such small metal components or assemblies as transistors and relays can be held to a low percentage of the value of the materials; on the other hand, the cost of complete inspection of critical metal parts or the preventative maintenance inspection of an assembly can sometimes exceed the cost of the material.

The successful economic use of radiography lies in timely development studies and in-process control followed by the wise use of spot-checking and statistical sampling. Of course, the cost of inspection is insignificant when compared to the cost in lives, money, and time, if failure of a material or component could cause the loss of a major item and result in a catastrophe.

Radiographic inspection has several inherent limitations. Since radiation traveling in straight lines from a source must intercept a film at nearly right angles, the efficient examination of some items of complex geometries is prevented. These conditions can preclude proper orientation of the film, or subject the film to the adverse effects of scattered radiation or image distortion. It is often desirable to determine the condition of a specific area that is surrounded by component materials or items; in these instances, inspection could be impossible because of the confusion created by superimposed images.

The information recorded on a radiograph is obtained because of density differences brought about by differential absorption of the radiation. These density differences, unless gross in nature, must be oriented almost parallel to the direction in which the radiation is traveling. Discontinuities of small volume, such as laminar-type flaws, will often be undetected because they do not present a sufficient density differential to the radiation. Fortunately, this limitation is countered to some extent since the probable orientation of fractures can be approximately predicted and the radiographic setup oriented accordingly. However, the very nature of laminations precludes their ready detection,

and radiographic inspection is seldom used to locate this type of flaw.

Penetrating radiation is attenuated in relation to the thickness of material. As material thickness is increased, the time required to obtain sufficient information on the film also increases. For a given energy (penetrating power) of X-rays or gamma radiation, a maximum thickness exists beyond which the use of radiography is not economically practical. Radiographic equipment of higher maximum energy could be obtained, but costs increase markedly because of the barriers required to protect personnel from the harmful effects of the radiation, as well as the greater cost of larger equipment.

The standards of reliability and quality assurance characteristic of modern aerospace structures make rigorous demands on radiography. Through programs conducted by its Centers and its various contractors, NASA is both a major user of radiographic technology and a significant contributor to its advancement. In this chapter, some of these contributions, selected for their potential usefulness outside the aerospace industry, are reviewed.

BASIC PRINCIPLES

The synopsis of the principles of radiography presented here is brief and as nontechnical as possible. It is intended to serve only as a helpful background for the nonspecialist who wishes to consider the potential usefulness of NASA contributions subsequently presented. The discussion is based primarily on references 1 and 2.

Nature of Radiation

Both X-rays and gamma rays are electromagnetic radiation, differing from each other and from radio-frequency waves and visible light only in their wavelengths. The portions of the electromagnetic spectrum to which these radiations are conventionally assigned are indicated in figure 4-2. X-rays and gamma rays of the same wavelength are physically identical. The name "gamma rays" is generally applied to electromagnetic radiation emitted from radioactive atomic nuclei.

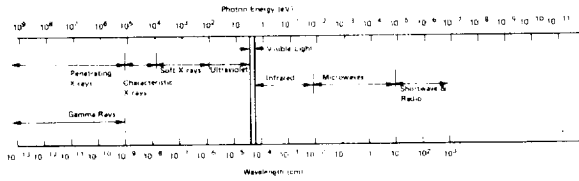


FIGURE 4-2.—The electromagnetic spectrum.

X-rays are produced in two ways. The first way is to rapidly accelerate (or decelerate) an electrically charged particle. Usually an electron is slowly accelerated to a high velocity, and then rapidly decelerated by collision with the atoms in a solid target material. The X-radiation so produced is called *Bremsstrahlung*, a German word meaning “braking radiation.” The other method of producing X-rays is to remove one of the tightly-bound orbital electrons belonging to an atom, thus producing an ion in an excited state. As the orbital electrons of the excited ion rearrange themselves, X-rays are emitted. Such X-rays are found to occur with particular wavelengths that are characteristic of the atomic number of the particular ion emitting them; hence they are called characteristic X-rays.

Like all forms of electromagnetic radiation, X-rays transport energy in packets called *quanta* or *photons*. The energy, E , borne by a single photon is related to its frequency, f , by Planck’s formula, $E = hf$, where h is Planck’s constant.

Electrons used to produce X-rays are usually accelerated by a suitable electric field. The kinetic energy acquired by an electron accelerated between two points with electrical potential difference of 1 volt is called an electron volt (eV). In terms of this unit of energy, the relation between the energy borne by a photon and its wavelength is

$$E(\text{eV}) = \frac{12400}{\lambda} \quad (1)$$

Here, λ is expressed in angstroms, the angstrom being equal to 10^{-8} cm.

When X-rays are produced by collision of high-speed electrons with a target, a continuous spectrum of *Bremsstrahlung* X-rays results, ranging in wavelength from infinitely long (in principle) to a certain minimum wavelength,

λ_{min} , corresponding to a maximum photon energy E_{max} . The maximum photon energy corresponds exactly to the energy of the electrons impinging on the target. If this energy exceeds that of the characteristic X-rays of the target atoms, some of the target atoms are ionized and their characteristic X-rays are emitted. The spectrum of X-rays emitted respectively by tungsten and molybdenum targets when bombarded by 35-keV electrons ($1 \text{ keV} = 10^3 \text{ eV}$) are shown in figure 4-3. This energy is great enough to excite the characteristic radiation of molybdenum, but not that of tungsten which requires about 70 keV.

Gamma rays are derived from certain radioactive isotopes. In contrast to X-rays produced by the bombardment of a target with electrons, isotopic gamma rays corresponding to a particular decay process and all characteristics of the isotope in question have essentially the same energy. Some isotopes emit several gamma rays, each of different, but sharply defined, energy.

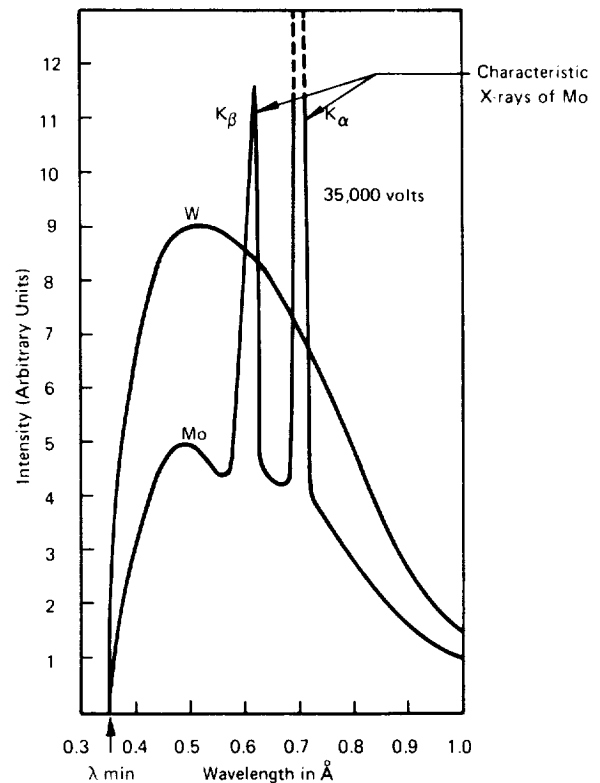


FIGURE 4-3.—X-ray spectra from tungsten and molybdenum targets, respectively, for 35-keV excitation.

The strength of a gamma-ray source is measured in terms of the number of nuclei which decay (emit one or more gamma rays) each second. A 1-curie source undergoes 3.7×10^{10} disintegrations per second. The strength of the source declines exponentially with time; the time required for its strength to drop to one-half its initial value is called its half-life.

Interaction of X-rays and Gamma Rays with Matter

When an X-ray or gamma-ray photon penetrates a substance, one of three primary processes may occur. First, the photon may be absorbed completely by an atom, thereby ejecting an orbital electron, and leaving behind an excited ion. The ejected electron quickly expends its energy by collisions with the electrons of other atoms. The originally excited ion in turn becomes neutralized, emitting its own characteristic radiation. This process is called the photoelectric effect. Second, the incident photon may collide with a peripheral atomic electron, lose part of its energy to the electron (which recoils), and continue to propagate in a new direction with reduced energy. This process is referred to as Compton scattering. Finally, if the incident photon has sufficient energy, a portion of that energy may be converted into the mass of an electron and a positron; the excess energy appears as kinetic energy of the electron-positron pair. The minimum photon energy at which such pair production occurs is just over 1 million electron volts. Depending on the energy of the incident photons, all three of the foregoing processes may contribute to the attenuation of the beam.

If a narrow, well-collimated beam of monoenergetic X-ray or gamma-ray photons is directed against a thin sheet of material, the intensity of the beam (as measured by an appropriate detector that indicates the number of photons per square centimeter per second in the beam) will show an attenuation of the beam intensity. It is found that the attenuation follows the law:

$$I = I_0 e^{-\mu x} \quad (2)$$

where I_0 is the incident intensity, I is the trans-

mitted intensity, x is the thickness of the attenuator, and μ is a factor called the linear attenuation coefficient. The value of μ depends on the energy of the incident photons and the elemental composition of the attenuator.

It is sometimes convenient to divide μ by the density, ρ , of the attenuator. The ratio, μ/ρ , is called the mass attenuation coefficient. The thickness, x , may then be multiplied by ρ to give the number of grams of the attenuator material behind 1 cm² of its surface area. Thus the quantity, ρx , for a flat plate may be determined merely by measuring its area and weighing it, often a more accurate procedure than trying to measure its thickness. A graph of μ/ρ versus photon energy for aluminum is shown in figure 4-4; the general shape is characteristic of intermediate atomic number metals. In general, the higher the energy of the incident photons, the lower the value of the mass attenuation coefficient; i.e., the higher the energy, the greater the penetrating power.

The linear attenuation coefficient measures the probability per unit thickness that a photon in the primary beam will be removed from that

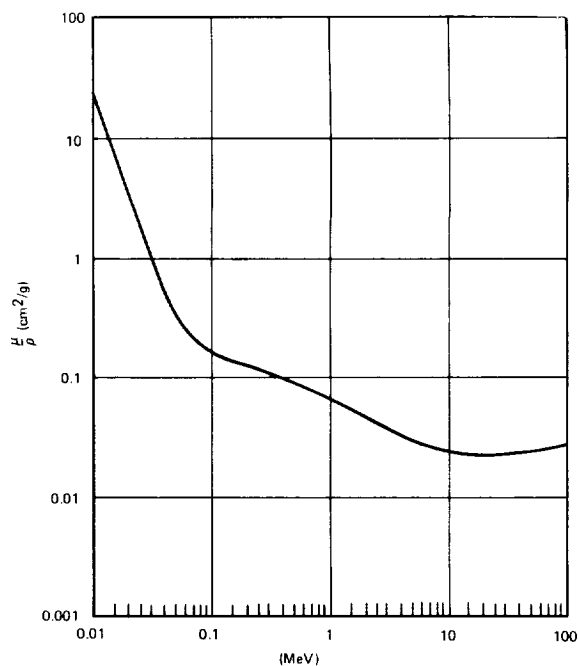


FIGURE 4-4.—Mass attenuation coefficient for photons in aluminum.

beam. It must be understood, however, that not all of the energy removed from the primary beam is deposited in the attenuator. Some of the secondary radiation, especially that resulting from Compton scattering, will escape from the attenuating material. Some of this scattered radiation is directed parallel to the transmitted primary beam, and may affect whatever may be placed behind the attenuator (including a film cassette).

Production of X-rays

X-radiation is produced when some form of matter is struck by a rapidly moving, negatively charged electron. Three basic requirements must be met to produce this condition:

- (1) A source of electrons
- (2) A means of directing and accelerating electrons
- (3) A target for the electrons to bombard

If a suitable material is heated sufficiently, some of the electrons in the material will become so thermally agitated that they will boil off, escape from the material, and surround it in the form of a cloud. This cloud of electrons will hover about or return to the emitting material (cathode) unless some external force pulls it away. The fundamental law of electrostatics states that like charges repel each other and unlike charges attract each other. Thus, a strong unlike or positive charge (on an anode) is used to produce an attracting force to move the electrons from the cathode to the anode, creating a flow of charge, or current, between them. It is important that this movement be conducted in a good vacuum; otherwise, the electrons would collide with gas molecules causing ionization and loss of energy.

To create X-rays, it is necessary that the electrons strike some substance. In the X-ray tube, a solid material is used for the target. The higher the atomic number of the target material, the higher the efficiency of X-ray production. Unfortunately, only a small percentage of the kinetic energy available in the electron beam is converted into X-radiation; the remaining energy is converted into heat that must be dissipated by the target material.

The intensity of X-rays produced in an X-ray tube by the collision of the electrons with the target is directly proportional to the tube current and is, in general, a function of the cathode-to-anode voltage raised to a power greater than 2.5. The efficiency of X-ray production is quite low at low voltages as demonstrated by the following relationship:

$$E \text{ (approx)} = \frac{ZV}{10^7} \quad (3)$$

where

E = efficiency in percent

Z = atomic number of target material

V = tube voltage (volts).

Therefore, the higher the atomic number and the tube voltage, the greater the efficiency of X-ray output. It can be seen from this approximate formula that even at 300 000 V the efficiency of X-ray production is only about 3% for a Z of 100. This means that 97% of the input energy to the tube is dissipated as heat.

Radiation Intensity

The measure of radiation emission from an X-ray tube is stated in roentgens (defined in terms of the response of a standard ionization chamber) at a fixed distance for a stated period of time. For convenience, the current flowing through the tube is taken as a measure of the output of the X-ray machine. Because this current flow is directly proportional to the radiation emission, it can be used as one of the exposure constants for a given machine, and the intensity is often stated in milliamperes or microamperes.

Reference to radiation intensity should describe it at a specified distance from the source. Such reference to distance is essential because the intensity diminishes as the square of the distance from the source. If the distance from a given source is doubled, the quantity of radiation is required to cover four times the original area, and the intensity is therefore reduced to one-fourth the original value, and conversely. Because intensity changes with the square of the distance, the relationship is termed the "inverse-square law," and this law is used extensively in computing industrial radiographic

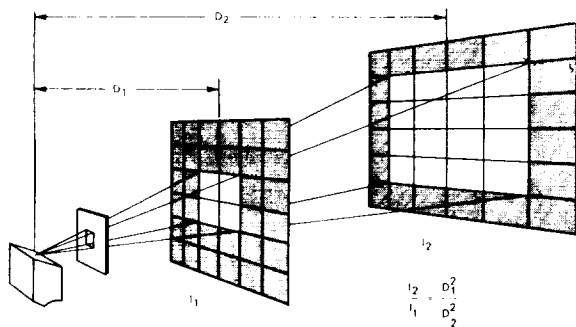


FIGURE 4-5.—Diagram of the inverse-square law.

exposures. Figure 4-5 (ref. 2) is a diagrammatic representation of the inverse-square law, expressed mathematically as

$$\frac{I_2}{I_1} = \frac{D_1^2}{D_2^2} \tag{4}$$

Radiation Quality

The quality of X-rays or gamma rays is often referred to as the effective energy, wavelength, or penetrating power. The radiation from an X-ray tube is a heterogenous spectrum of wavelengths. The minimum wavelength in angstroms ($1 \text{ \AA} = 10^{-8} \text{ cms}$) generated in this spectrum is equal to 12 400 divided by the tube voltage:

$$\lambda_{\text{min.}} = \frac{12\,400}{V} \tag{5}$$

where

λ = wavelength in angstroms
 V = volts.

Changing the X-ray voltage changes the minimum wavelength produced in the spectrum. The wavelengths of maximum intensity are produced at the voltage that is approximately two-thirds of the highest voltage used. The relationship between the voltage applied to an X-ray tube to accelerate the electrons and the penetrating power of the X-rays is shown in figure 4-6 (ref. 1). Figure 4-7 illustrates the distribution of the intensity of X-rays emitted in relation to the applied voltage (ref. 2). Note that increasing the intensity of X-rays at a given maximum applied voltage raises the output curve but does not change its shape (distribution). On the other hand, the effect of in-

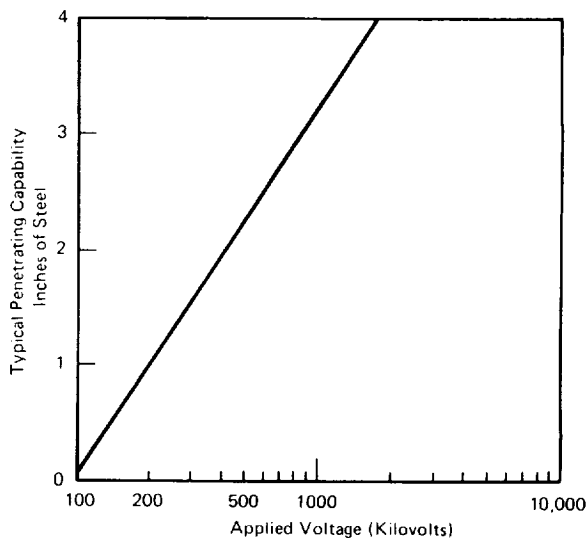


FIGURE 4-6.—Effect of increasing voltage on the penetrating capabilities of an X-ray beam.

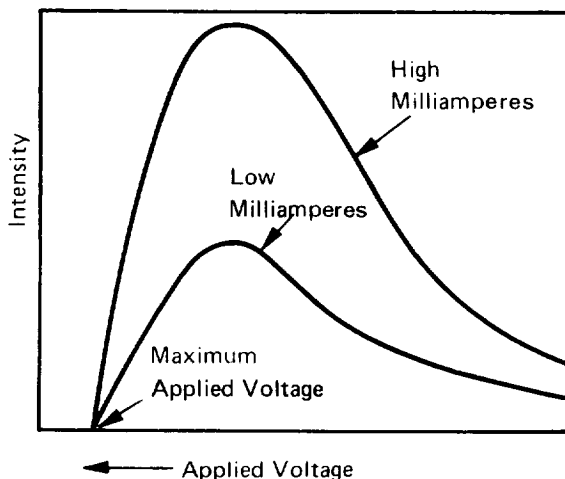


FIGURE 4-7.—Distribution of radiation from an X-ray tube.

creasing the maximum applied voltage is shown in figure 4-8 (ref. 2). Here, the penetrating ability increases (wavelengths become shorter) and the intensity of the radiation increases.

The quality of the radiation obtained from a radioisotope source is a characteristic of the isotope involved and is constant. For example, cobalt 60 emits radiation of only two specific wavelengths that correspond respectively to photon energies 1.17 MeV and 1.33 MeV.

X-ray and gamma-ray beam quality is usually expressed in terms of the thickness of some

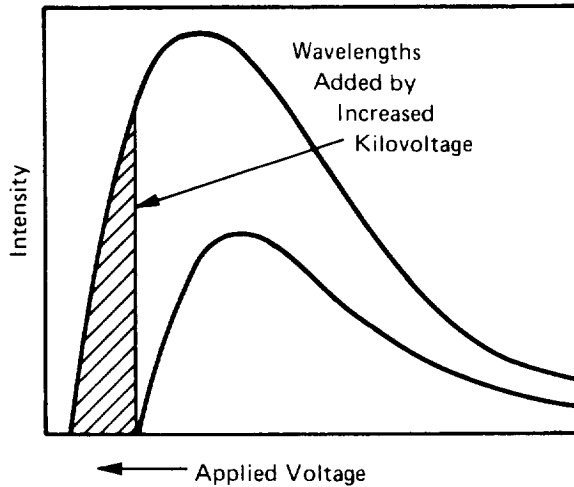


FIGURE 4-8.—Effect of increasing voltage on the quality and intensity of an X-ray beam.

reference attenuator material (e.g., aluminum, copper, and iron) required to reduce the intensity of the beam to one-half its original value. This thickness is referred to as the half-value layer (HVL). Two half-value layers of absorber will reduce the intensity of the beam by a factor of one-fourth only if the radiation is essentially "monochromatic," i.e., if it comprises only a narrow band of wavelengths. This is generally true of gamma-ray sources, but is not true of X-ray sources.

The half-value layer may be expressed in terms of the linear attenuation coefficient, μ , of the reference material by the relation:

$$\text{HVL} = \frac{0.693}{\mu} \quad (6)$$

Scattered Radiation

Figure 4-9 indicates the complexity of the absorption and scattering of X-rays or gamma rays (ref. 1). Because of these characteristics, any material subjected to the radiation field will, in turn, generate more secondary or scattered radiation, some of which will reach the radiographic film. If scatter is sufficiently intense, it results in a foggy appearance in the radiograph, obscuring the desired image. Filters, diaphragms, grids, masks, and other radiation blocking devices are utilized to minimize this undesirable effect. Any material in the

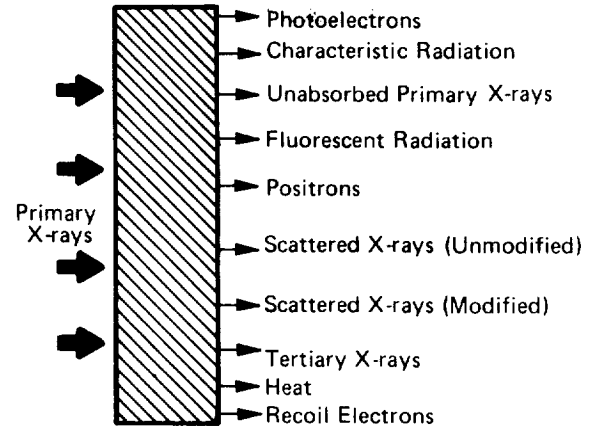


FIGURE 4-9.—Complex effect of primary X-rays.

beam, whether specimen, cassette, table, walls, or floor, receiving direct radiation is a source of scattered radiation.

Alteration of beam quality with filters.—The variation of attenuation coefficients with wavelength provides an easy means of reducing the proportion of soft rays in an X-ray beam. This is accomplished by passing the X-ray beam through a convenient thickness of a filtering material such as aluminum, copper, or lead. The softer components of the beam are almost eliminated, while the hard radiation is reduced by less than about 50%, depending on the thickness of the filter. The soft radiation is generally undesirable because it does not penetrate the specimen to help form the X-ray image, but it is very active in producing a type of scatter undercut. The effect of a filter on the quality of an X-ray beam is shown in figure 4-10 (ref. 1).

SAFETY

All forms of penetrating radiation are potentially hazardous to human health. However, when industrial radiography is conducted under controlled conditions by expert personnel, such personnel can be adequately protected. Radiography should never be undertaken by unqualified personnel or with improper equipment or facilities. All states in the U.S. exercise regulatory power over all forms of industrial radiography, and have established limits of short-term and long-term exposure for personnel, as well as standards for radiographic installations.

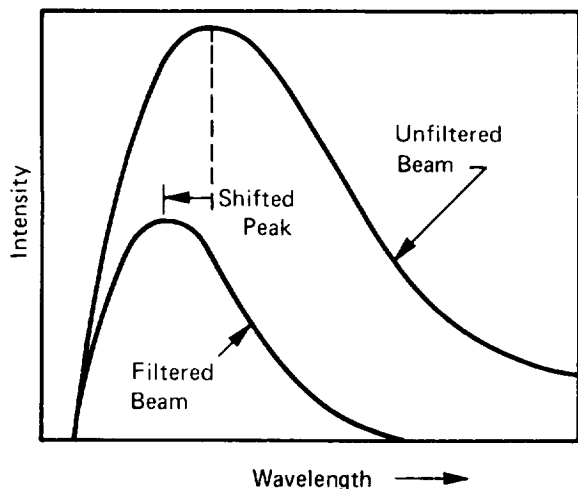


FIGURE 4-10.—Effect of filter on the intensity and quality of an X-ray beam.

X-RAY EQUIPMENT

Prior to 1912, X-rays were produced in gas-filled tubes. The process involved splitting gas molecules into ions and electrons with the application of high voltage. The resulting positive ions were drawn to the negative cathode and the electrons were set free by the ionic bombardment of the cathode. The electrons were then accelerated toward the anode (target), and X-radiation was produced by their absorption at the anode. The cathode usually consisted of an aluminum rod with a cup-shaped end that tended to focus the emitted electrons toward the anode. The electron supply, and thus the X-ray emission, was contingent on the gas content of the tube. Provision was made to inject gas into the tube automatically. However, the intensity of the X-ray emission was highly erratic. Further, the presence of gas in the tube limited the voltages that could be applied because of the tendency of arc-over (breakdown) between cathode and anode. Thus, the wavelength of the X-rays was long and they had little penetrating power. From the standpoint of industrial radiography, the early gas-filled tube was inadequate.

The introduction by Coolidge of the incandescent cathode (heated metallic filament) was a major contribution to the improvement of X-ray equipment, which all is still being used. A schematic of the early type Coolidge tube is

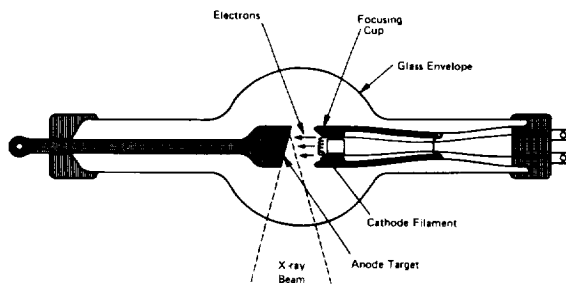


FIGURE 4-11.—Coolidge-type X-ray tube.

shown in figure 4-11 (ref. 1). Most modern tubes are refinements of this early type. Such refinements have been directed toward more consistent emission, longer life, and more efficient shaping and focusing of the electron beam. The incandescent cathode requires an evacuated (vacuum) tube. This prevents oxidation or burning of the heated filament, and allows the application of high accelerating potentials.

Accelerating Potential

Modern X-ray equipment uses a combination of tube rectifier and iron-core transformer to develop accelerating potentials up to about 500 kV (fig. 4-12) (ref. 1). Beyond 500 kV, the size and weight of the iron-core transformer becomes prohibitive. Recognition of this limitation led to the development of the resonant transformer, which does not have an iron core; instead, the core is practically all air. The high-voltage multicoil secondary is designed to resonate at a relatively low frequency, from 180 to 200 Hz, producing an efficient transfer of energy from primary to secondary. This principle of high-voltage generation is used in apparatus of 250 to 4000 kVp (peak kilovoltage) range.

X-ray units which contain resonant-type

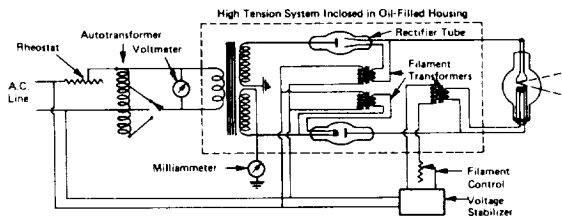


FIGURE 4-12.—Simple rectified circuit for X-ray machine.

transformers are very useful but do have some drawbacks. Although the unit may be rated at 1000 kVp, the actual radiation spectrum is broad and contains a large amount of radiation developed at energies much lower than this peak value. The fluctuation of exciting potential varies the velocity of the accelerated electrons and creates a focusing problem, resulting in a focal spot larger than optimum.

A smaller source size and a more coherent X-ray spectrum was achieved with the development of an effective electrostatic generator (Van de Graaff generator). Such generators are used for voltages from 500 to 6000 kVp.

Electron acceleration by means of applied potential reaches an efficiency peak at about 6 MeV. The development of magnetic induction systems (betatrons), wherein electrons are orbited in a magnetic field, provided a means of extending the electron velocity to progressively higher values with the resultant emission of extremely short wavelength, highly penetrating X-rays. The betatron is a unit which accelerates electrons by magnetic induction. The design of this unit is based on the principle of the transformer wherein a secondary current is induced in one coil by a primary current in another coil. When an alternating current is supplied to the primary coil, a strong variation in the magnetic field is produced in the core of the secondary, which is actually a doughnut-shaped vacuum chamber. Electrons are injected into the chamber as the magnetic field starts to increase, and are accelerated by the voltage induced by the increase in the magnetic field. The electrons travel in a circular path inside the doughnut, increasing their energy on each lap. The electrons circle through the doughnut many thousands of times in one cycle. When the field strength is no longer increasing and is about to decrease, the electrons are ejected by applying a pulse of current in an auxiliary coil to alter the magnetic field. The high-energy electrons are directed to the target and produce X-rays. Betatrons for industrial radiography usually operate in the 20 to 30 MeV range.

A simpler, high-velocity electron accelerator has also been adapted for industrial radiography. This device, the linear accelerator

(LINAC), uses a straight length of waveguide tubing. Radio-frequency energy is coupled with this waveguide to accelerate the electrons that are injected into the system and onto a target. The electron velocity attained in a linear accelerator is a function of the length of the waveguide. The length of waveguide required to attain electron velocities equivalent to values used in industrial radiography is a matter of a few meters. LINACS for industrial radiography usually operate in the 5 to 15 MeV range.

X-ray Source (Target)

The third essential part of an X-ray tube is the target that absorbs the high-velocity electrons and converts their kinetic energy to X-radiation. Three factors are involved in the design of the target: heat dissipation, the shape of the emitted X-ray beam, and the quantity of the X-radiation produced.

Early X-ray tubes used targets of molybdenum or tungsten positioned at a small angle to the cathode to project the X-ray beam as shown in figure 4-13 (ref. 1). To avoid melting the target, it was necessary to disperse the electrons over a wide area of the target, which required large source sizes. Target design has evolved through the development of massive copper heat absorbers and rotating anodes to the present-day system of liquid or gas cooling. Prior to forced-cooling systems, tungsten was the compromise between conversion efficiency (high

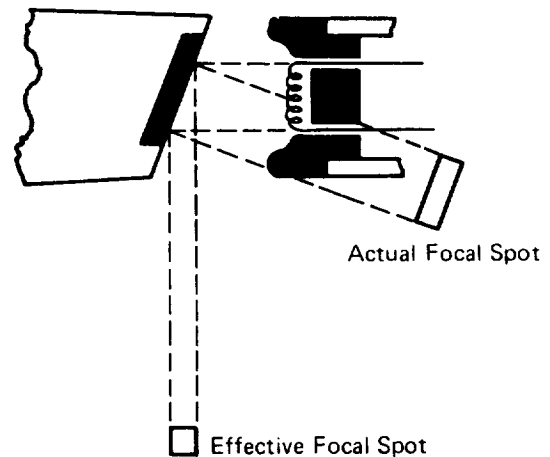


FIGURE 4-13.—Effective vs actual focal spot.

atomic number) and high strength at high temperature. Modern X-ray equipment uses tungsten, gold, and platinum targets.

The shape of the X-ray beam emitted from the target has been the subject of considerable development. As soon as the heat dissipation problem was solved, it was found possible to construct thin targets that would emit X-rays in the forward direction (transmitted beam) as well as to the sides (reflected beam). By selected positioning of the target within the tube structure, almost any beam configuration could be obtained to suit a variety of applications (fig. 4-14) (ref. 2). To restrict the actual radiation developed in the target to its effective beam, it is common design practice to place thick, lead absorbers or diaphragms around the tube.

Image sharpness.—As shown in figure 4-15, the sharpness of the film image is determined by the size of the radiation source and the ratio of the source-to-specimen distance and specimen-to-film distance. Optimum geometrical sharpness of the image is obtained when the radiation source is small, the distance from the source to the specimen is relatively great, and the distance from the specimen to the film is small.

Image distortion.—Two possible causes of film image distortion are shown in figure 4-16 (ref. 2). If the plane of the specimen and the plane of the film are not parallel, image distortion will result, as it will if the radiation beam is not directed perpendicular to the plane of the film. Whenever distortion of the film image is unavoidable, as a result of physical limitations, it must be remembered that all parts of the

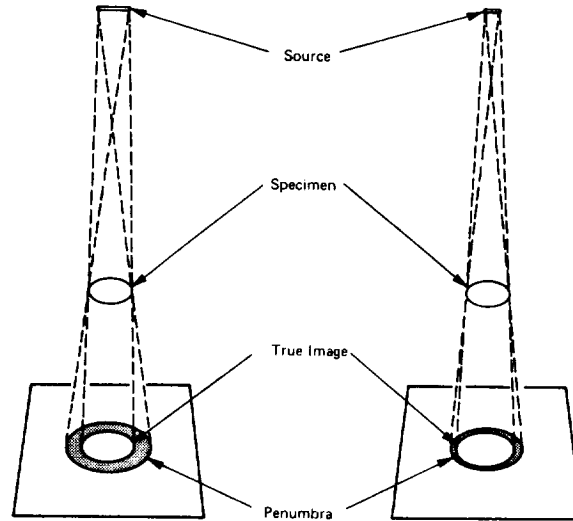


FIGURE 4-15.—Effect of source size on image sharpness.

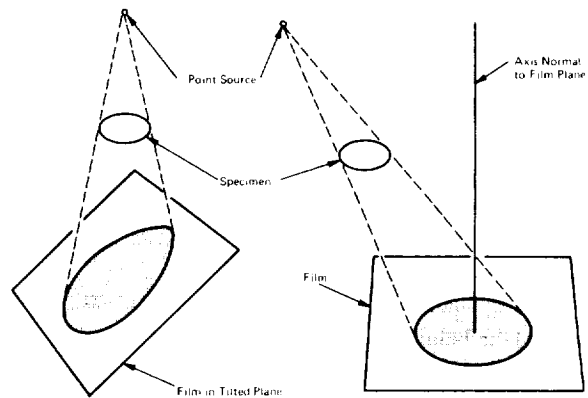


FIGURE 4-16.—Sources of image distortion.

image are distorted; otherwise, an incorrect interpretation of the radiograph may be made.

GAMMA-RAY EQUIPMENT

Storage and Deployment of Source

Gamma-ray equipment is designed to provide (1) a radiation-safe storage container and (2) a system for the remote handling of the radioisotope source.

The sensitivity of gamma radiography depends mainly on the radioisotope being used, and only to a small degree on the design of the storage-handling equipment. Personnel safety and inspection economics, however, require effi-

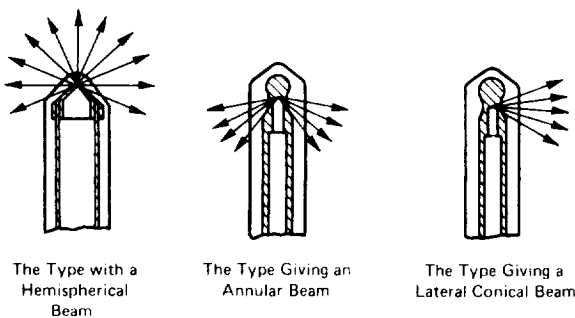


FIGURE 4-14.—Positioning the target within the anode tube to obtain various beam configurations.

cient and safe equipment. Cognizant state and federal agencies require that all equipment used to store and handle those radioisotopes that are under their jurisdiction meet certain standards of safety.

To afford protection from gamma radiation when a radioisotope is not in use, a mass of heavy metal (lead or uranium) is fabricated with a passage leading to its geometric center, where the radioisotope is stored. The amount of metal used is predetermined to reduce the radiation at the surface to a safe level. Containers are designed specifically for the maximum of activity of a given radioisotope or combination of radioisotopes.

All radioisotopes used in industrial radiography are encapsulated within a metallic protective housing. This housing is usually a thin stainless steel sheath and is often protected by an aluminum cover. Encapsulation:

- (1) Prevents abrasion of radioactive metals such as cobalt 60
- (2) Prevents spillage of radioactive salts such as cesium 137
- (3) Prevents leakage of radioactive gas
- (4) Lessens the possibility of loss or accidental mishandling
- (5) Provides a means for attachment of rods and wires used for moving the source.

Removal of the encapsulated source from the storage container may be accomplished by one of three methods according to the design of the system.

Manual pole handling.—The manual pole method is the simplest and least expensive. Its use is limited to low-activity sources where sufficient protection is afforded by distance. The length of the pole must be chosen as a compromise between convenient operation and the safety of distance. Because the source is inserted and withdrawn from the same source opening, the source container consists simply of a hole drilled into the absorbing mass and a plug to seal the hole. The pole can be attached to the source by either a magnet, a screw, or a hook. The manual pole method is to be avoided whenever possible.

Cable-drive handling.—This method is designed with the source capsule securely fixed to

the end of a flexible steel cable (fig. 4-17) (ref. 1). The cable passes over a crank-driven wheel in a remote manual control unit that is used to advance or retract the source from a safe distance. The source and control cable travel within a plastic-covered steel guide tube that both protects the assembly and permits positioning of the source. The container unit has either a V- or S-shaped passage through which the cable drive can push out or pull back the source. The midpoint of either passage is the maximum safe position. Signal lights operated by microswitches may be used to indicate the location of the source capsule. Another means of showing source position is a length index giving the amount of cable that has passed through the control system.

Pneumatic drive handling.—This method affords a third means of transferring the source capsule from container to exposure position. Except for the way the capsule is propelled, the general design is similar to the cable-driven method.

Some gamma-ray equipment does not require the removal of the source from the container. Rather, a cone section of container is designed to swing away, permitting the unobstructed escape of radiation. Actuation of the cone, both opening and closing, is accomplished from a safe position behind the container. Such equipment is referred to (somewhat improperly) as a radioisotope camera.

Gamma-ray Beam Configuration

When a radioisotope source is removed from its container, the beam of radiation is emitted spherically. This is known as panoramic projection and is convenient for making many simultaneous exposures. If the source remains in the container and gamma rays are permitted to escape through an opening, it is known as conical or directional projection. This method is used when it is desired to reduce the radiation hazard, when radiography is performed in confined quarters, and when extremely active sources are employed. The merit of this beam-restriction device stems from the reduction of possible radiation hazard to operating personnel and the

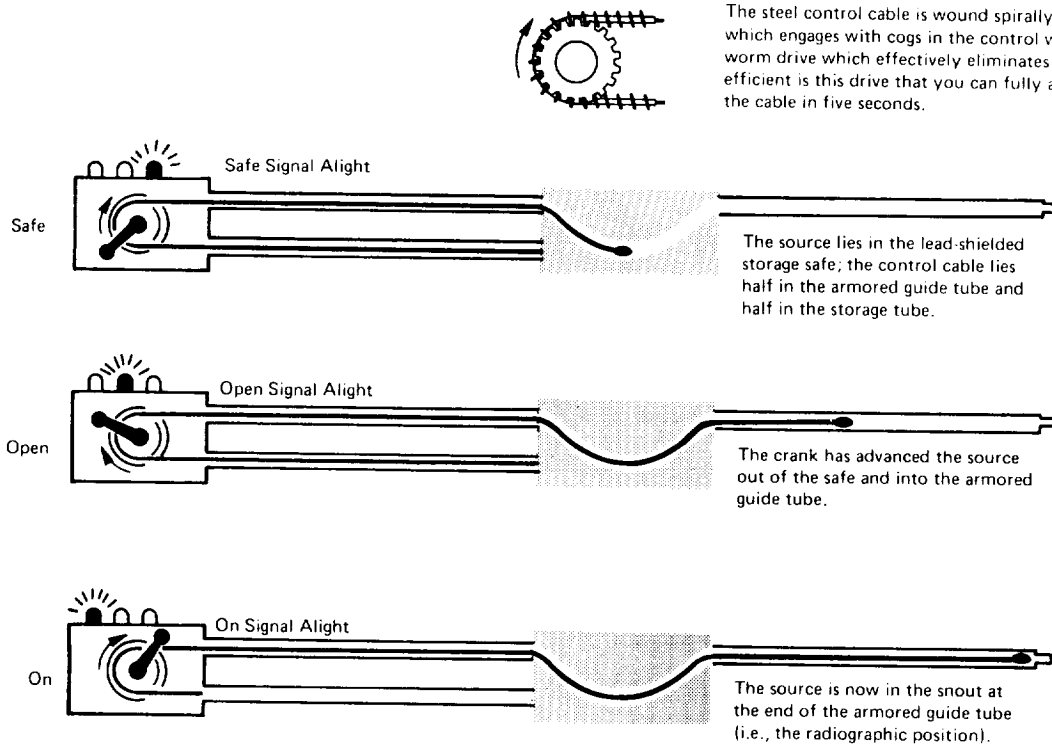


FIGURE 4-17.—Cable-drive source handling method.

improvement of radiographic quality brought about by the reduction of scattered radiation.

SELECTION OF RADIOGRAPHIC EQUIPMENT

Analysis of Inspection Task

Prior to selecting radiographic equipment, the NDE task to be accomplished must be analyzed. The range of tasks to which radiographic equipment might be applied must be determined. Primarily, this range can be usefully expressed in terms of maximum and minimum thicknesses of given materials or components to be inspected. Consideration must also be given to the size and weight of material, the steps in the production process where inspection is best suited, and the quantity of material to be inspected in a given time.

Second, it is necessary to consider the types of irregularities to be encountered. The possibility of effectively and economically locating such flaws by radiography will conclude the analysis. If the analysis affirms that radiography is the

correct inspection method, then effort can be turned to selecting the most suitable equipment.

The thicknesses and types of material to be examined will dictate the X-ray potential or gamma-ray energy necessary to achieve efficient penetration. The type of manufacturing facility and the bulk, weight, and quantity of products to be inspected will establish the equipment requirements. The relationship between radiation energy (expressed in terms of exciting potential) and material thickness are shown in table 4-1 (ref. 1). Table 4-2 gives representative applications for the several categories of equipment according to voltage rating (ref. 1).

Factors in the Selection of X-ray Equipment

Within the requirements established by the analysis of the inspection task the specific machine that will perform most satisfactorily must be selected. Selection will be based on five principal factors: radiation quality, radiation output, source size, range of operation, and re-

TABLE 4-1.—*Relationship Between Voltage and Steel Thickness*

Voltage	Steel thickness (in.)
175 kV	$\frac{1}{8}$ -1
250 kV	$\frac{1}{4}$ -2
1000 kV	$\frac{1}{2}$ -4
2000 kV	$\frac{3}{4}$ -8
15 MeV	$\frac{3}{4}$ -14

TABLE 4-2.—*Relationship Between Voltage and Radiographic Application*

Voltage rating	Typical applications
50 kV -----	Wood, plastics, textiles, leather, and grain. Diffraction and microradiography.
100 kV -----	Light metals and alloys. Fluoroscopy of food stuffs, plastic parts and assemblies, and small light alloy castings.
150 kV -----	Heavy sections of light metals and alloys, and of thin sections of steel or copper alloys. Fluoroscopy of light metals.
250 kV -----	Heavier sections of steel or copper. (Fluoroscopy is not generally used at this voltage.)
1 to 2 MeV ..	Radiography of very heavy ferrous and nonferrous sections.

liability. The last factor, reliability, is beyond the scope of this chapter; the other factors will be discussed briefly.

Radiation quality.—The choice is made to attain the optimum compromise between (1) the ease of penetration at higher energies resulting in shorter exposure times and (2) the greater radiation absorption at lower energies resulting in better contrast and improved radiographic quality. It is usually best to obtain a unit that will emit a spectrum containing a large portion of the short wavelengths corresponding to the peak exciting potential. With such a unit, it is still possible to operate at the lower energies to get the longer wavelength X-rays that improve radiographic contrast.

However, if the unit does not deliver a good quantity of the more penetrating X-rays indicated by the peak potential rating, the only way to reduce the exposure time is to obtain other equipment of higher exciting potential. Thus, when comparing two X-ray machines that are generally equal in design, the machine which produces radiation with the larger half-value thickness in a given material at a given peak voltage is the most efficient.

Radiation output.—When comparing two X-ray machines that are generally equal in design, the machine with the highest output in roentgens is the more suitable. For comparison purposes, all factors concerned with the roentgen measurement must be equivalent. The output is expressed in terms of roentgens per hour at a distance of 1 meter (RHM).

Source size.—For a given quantity of X-rays, the smaller the target area still capable of providing a useful quantity of radiation, the better the sensitivity.

Range of operation.—The ability of an X-ray machine to operate efficiently over a range of exciting potentials is a significant factor. However, the width of the operating range is determined rather sharply by several factors. For example, the inherent absorption in the walls of the X-ray tube and machine housing requires special design to obtain a usable quantity of radiation at low energies. These special features are costly and usually are not required at higher energies. X-ray machines designed to operate at maximum potentials of 150 or 300 kV are generally of limited usefulness below 70 kV.

Selection of Gamma-ray Equipment

For comparable radiation energies, gamma rays may generally be substituted directly for X-rays with satisfactory results. However, the fact remains that the wider spectrum (and therefore lower energy radiation) obtained from X-ray equipment usually gives superior radiographic sensitivity.

From an economic point of view, the initial cost of gamma-ray equipment is generally less, and maintenance is somewhat lower. Maintenance cost is restricted primarily to replacement of the radioisotope source as it weakens

through atomic disintegration. The lower radiation intensity as compared to X-rays and the more simplified method of operation often obviate the need for costly shielded installations, especially in the high-energy field. However, this same factor, lower radiation intensity, works adversely to increase the inspection time. The use of gamma rays approaches its maximum economic efficiency when: (1) the inspection rate is low; (2) the material to be inspected is similar in design and thus advantage can be taken of the radial, annular emission to make numerous simultaneous exposures; and (3) the anticipated duration of the inspection need is short.

Certain specific types of inspection are especially suited to gamma-ray radiography. For example, radiography accomplished in confined areas of enclosed fabrications, such as pipes, tanks, and internal ship structures, is much more suited to the small isotope source in comparison to the more bulky X-ray tube. The absence of power requirements is another factor that makes the use of gamma-ray equipment for field inspection more advantageous than other types.

The selection of a radioisotope for a particular task or area of inspection is based principally upon two characteristics: radiation energy and source size. The selection of radiation energy is accomplished in the same manner and for the same purpose as with X-ray equipment. In comparison to X-ray sources, the monochromatic nature of gamma-ray sources requires a greater compromise between penetration time and radiographic sensitivity.

The size of the source available with radioisotopes is determined by the "specific activity" (i.e., the actual percentage of the element that has been made radioactive) and the quantity of radioisotope involved (i.e., the number of curies). Some representative physical sizes of gamma-ray sources with respect to the elements concerned and quantity of activity are given in figure 4-18 (ref. 2).

Table 4-3 contains important characteristics of some radioisotopes commonly used in sources for gamma-ray radiography (ref. 1).

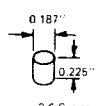
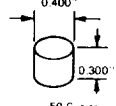
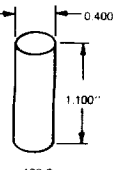
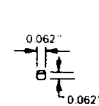
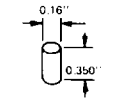
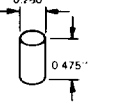
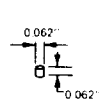
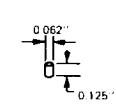
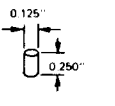
Source	1 RHM	20 RHM	70 RHM
Cesium 137	 2.6 Curies	 50 Curies	 180 Curies
Cobalt 60	 0.75 Curies	 15 Curies	 50 Curies
Iridium 192	 1.8 Curies	 35 Curies	 130 Curies

FIGURE 4-18.—Typical source sizes and RHM outputs.

RADIOGRAPHIC FILM

Effect of Radiation on Film

An X-ray film is basically a sheet of transparent, blue-tinted, cellulose derivative material, coated on either one or both sides with a photosensitive emulsion. The emulsion consists of gelatin in which is dispersed very fine grains of silver halide salts, primarily silver bromide. The emulsion is about 0.001 in. thick on either side of the film. When the silver halide grains are exposed to radiation, they become sensitized. When they are subsequently treated with a chemical solution (developer), a reaction takes place causing the reduction of the silver salts to black, metallic silver. It is this silver, suspended in the gelatin, which constitutes the image. The film is left in a developer solution long enough to allow the sensitized grains to be darkened, that is, reduced to metallic silver. If the film is developed too long, unexposed grains will also be reduced, and the film will be uniformly darkened or fogged. After the film has been developed, it is placed in a weak acid solution to stop the action of the developing solution. The film is then placed in a fixing bath, commonly called "hypo," which dissolves all the undeveloped salts and leaves only the metallic silver or dark grains in the emulsion. The hypo also contains

TABLE 4-3.—*Characteristics of Radioisotopes*

Isotope	Cobalt 60	Iridium 192	Thulium 170	Cesium 137
Half-life	5.3 yr	75 days	130 days	30 yr
Chemical form	Co	Ir	Tm ₂ O ₃	CsCl
Gammas, MeV	1.33, 1.17 14.4	0.31, 0.47, 0.60 5.9	0.084, 0.052 0.032*	0.66 4.2
Practical Sources				
Curies	20	50	50	75
RHM	27	27	0.1	30
Approx diam	3 mm	3 mm	3 mm	10 mm

* Varies widely because of high self-absorption

agents that harden the emulsion to make it more durable. Finally, the film is thoroughly rinsed in running water to remove all traces of the various solutions, and then dried. When the processed film is viewed in front of a strong light, those areas of the film that were not exposed to light or X-rays are relatively transparent, while those areas exposed to X-rays contain metallic silver and are dark or opaque.

Film Types

The wide range of conditions and the variety of materials encountered in industrial radiography have led to the development of several specific types of films. Basically, there are three grades of film for industrial radiography: coarse grain, fine grain, and extra-fine grain. The fine and extra-fine grain film give the highest contrast or quality, but require relatively long exposure times. The coarser grain films do not give quite as good quality as the finer grain films, but they need only relatively short exposure times.

Commercial X-ray film is available in two basic forms: (1) sheet film, of various standard dimensions, which may be coated with the photosensitive emulsion on only one side, but which is normally supplied coated on both sides of the film; and (2) roll film of various widths and practically unlimited length. This second form is especially useful for radiographing circum-

ferential areas. In addition to these two basic forms, custom-tailored shapes are supplied by most manufacturers on request.

Film Density

Film density refers to the quantitative measure of film blackening; for radiographic purposes the term *density* alone is generally used. Density is defined as the common logarithm of the ratio of light intensity incident upon one side of a radiograph to the light intensity transmitted through the radiograph. For example, when the silver deposited in the emulsion allows 1/10 of the incident light to pass through the radiograph, the ratio is 10:1. The logarithm of 10 is 1; thus by definition the density is 1. If only 1/100 of the incident light passed through the radiograph, the ratio is 100:1 for which the logarithm and, therefore the density, is 2. The general formula is

$$\text{Density } (D) = \log_{10} \left[\frac{I_o \text{ (incident light)}}{I_t \text{ (transmitted light)}} \right] \quad (7)$$

Radiographic Exposure

X-ray exposure.—Since X-ray output is directly proportional to both milliamperage and time, it is directly proportional to their product. This product, known as the exposure, is ex-

pressed algebraically as $E = Mt$, where E is the exposure, M is the tube current in milliamperes, and t is the exposure time in minutes or seconds. Hence, the amount of radiation from a given source will remain constant if the exposure remains constant, no matter how the individual factors of tube current and exposure time are varied. This permits specifying X-ray exposure in terms of milliamperere-minutes or milliamperere-seconds, without stating the specific values of tube current or time.

The kilovoltage applied to the X-ray tube affects the quality of the X-ray beam. As the kilovoltage is raised, X-rays of shorter wavelength and hence of more penetrating power are produced. Referring back to figure 4-8, note that in the higher kilovoltage beam there are some shorter wavelengths that are absent from the lower kilovoltage beam. Thus, raising the kilovoltage not only increases the penetration, but also increases the intensity, sometimes to a great extent.

Gamma-ray exposure.—The total amount of radiation emitted from a gamma-ray source during a radiographic exposure depends upon the source strength (usually stated in curies or millicuries) and the time of exposure. For a particular radioactive isotope, the intensity of the radiation is approximately proportional to the strength of the source in curies. Analogous to X-ray exposure, the gamma-ray exposure (E) may be stated $E = Mt$, where M is the source strength in curies or millicuries, and t is the exposure time. Since gamma-ray quality is fixed by the nature of the particular radioactive isotope, there is no variable to correspond to the kilovoltage factor encountered in X-radiography.

Since a gamma-ray source is constantly losing strength, a correction must be made in order that the correct strength (in curies) is used. The frequency of correction depends upon the rate at which strength is lost (half-life). For radiographic isotopes, the original strength and date of conversion are furnished by the supplier. The strength for any subsequent time can be readily calculated, knowing the original strength and half-life of the isotope.

Film Characteristic Curves

The characteristic curve, sometimes referred to as the sensitometric or H and D curve (after Hurter and Driffeld), expresses the relationship between the exposure applied to a photographic film and the resulting photographic density. Such curves are obtained by giving a film a series of known exposures, determining the densities produced by such exposures, and then plotting density against the logarithm of relative exposure. Characteristic curves for several typical films are represented in figure 4-19 (ref. 1).

Relative exposure is used because there are no convenient absolute units suitable to all kilovoltages and scattering conditions with which to express radiographic exposures. Hence, the exposures given a film are expressed in terms of some particular exposure, thus giving a relative scale. The use of the logarithm of the relative exposure, rather than the relative exposure itself, has a number of advantages. It compresses

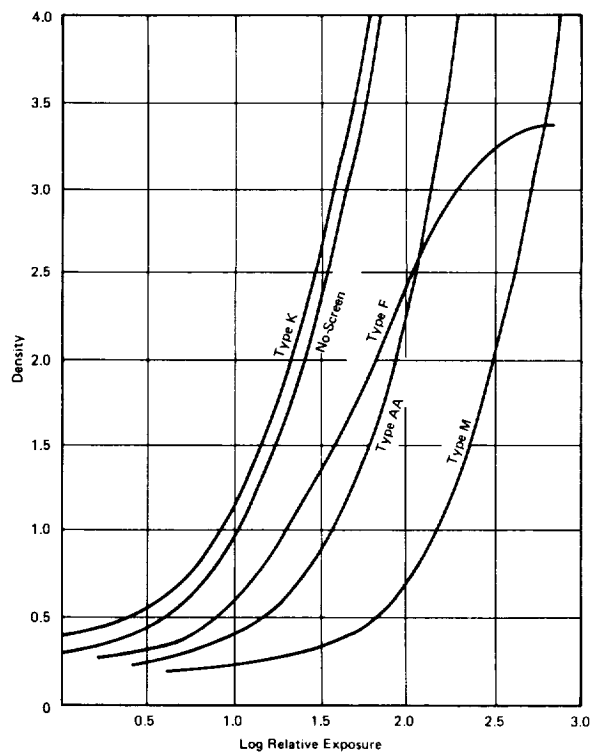


FIGURE 4-19.—Characteristic curves for various radiographic films.

an otherwise long scale. Also, in radiography, ratios of exposures are usually more useful than the exposures themselves. Any two exposures having the same exposure ratio will be separated by the same interval on the log relative exposure scale, no matter what their absolute exposures may be.

The slope, or steepness, of the characteristic curve for X-ray film, changes continuously along its length. The density difference corresponding to a difference in specimen thickness depends on the region of the characteristic curve on which the exposures fall. The steeper the slope of the curve in this region, the greater will be the density difference, and, hence, the greater will be the visibility of detail.

If the gradient of the characteristic curve is greater than 1.0, the intensity ratios, or subject contrasts, of the radiation emerging from the specimen are amplified in the radiographic reproduction; the higher the gradient, the greater is the degree of amplification. Thus, at densities for which the gradient is greater than 1.0, the film acts as a contrast amplifier. Similarly, if the gradient is less than 1.0, subject contrasts are effectively diminished in the radiographic reproduction.

A minimum density is often specified for radiographs, not because of the importance of a particular density, but rather because of the gradient associated with the specified density. The minimum useful density is that at which the minimum useful gradient is obtained. In general, gradients lower than 1.0 should be avoided.

The ability of a film to amplify the subject contrast is of the utmost importance. Otherwise, many small differences in the subject could not be made visible. This gain in contrast is utilized in practically all industrial radiography. It is especially significant in radiography with very penetrating radiations that produce low subject contrast. High radiographic contrast depends greatly on the enhancement of subject contrast by the film.

The shape of the characteristic curve is, for practical purposes, independent of the quality of X-radiation or gamma radiation. Therefore, a characteristic curve made with any radiation

may be applied to exposures made with any other, and the same is true of values of gradient or average gradient derived from the curve. The influence of kilovoltage or gamma-ray quality on contrast in the radiograph is, therefore, due primarily to its effect on the subject contrast, and only very slightly to any change in the contrast characteristics of the film. Radiographic contrast can also be modified by choice of a film of different contrast, or by use of a different density range with the same film. Contrast can also be affected by the degree of development, but, in industrial radiography, films are developed to their maximum, or nearly maximum contrast.

Film Speed

It has been shown that the contrast properties of a film are governed by the shape of the characteristic curve. The other significant value obtained from the characteristic curve is the relative speed, which is governed by the location along the log E axis of the curve in relation to the curves of other films.

Speeds of radiographic films are usually expressed in terms of the reciprocal of the exposure required to achieve a certain density. Additionally, since there are no units of X-ray exposure conveniently applicable to industrial radiography, speeds are expressed in terms of one particular film, whose relative speed is arbitrarily assigned a value of 100.

In figure 4-19, the curves for various films are spaced along the log relative exposure axis. The spacing of the curves arises from the differences in relative speed; the curves for the faster film lying to the left of the chart, those for the slower films lying toward the right. From these curves, relative exposures to produce a fixed density can be determined, and the relative speeds will be inversely proportional to these exposures. For most industrial radiographic purposes, a density of 1.5 is an appropriate level at which to compute relative speeds, although where all work is done at high densities and the radiographs are viewed on high-intensity illuminators, a density of 2.5 is more suitable. Relative speed values, derived from figure 4-19, for the two density levels are given in table 4-4

TABLE 4-4.—*Relative Speeds and Exposure Values Derived From Figure 4-19*

Film	Density = 1.5		Density = 2.5	
	Relative speed	Relative exposure to give $D=1.5$	Relative speed	Relative exposure to give $D=2.5$
Type M.....	40	17	45	14
Type AA.....	170	4	170	4
Type F.....	250	3	170	4
Type K.....	700	1.0	650	1.0
No-screen.....	550	1.3	530	1.2

(ref. 1). As indicated in the table, the relative speeds computed at the two densities are not the same, a result of the differences in curve shape from one film to another.

Although the shape of the characteristic curve of a film is practically independent of changes in radiation quality, the location of the curve along the log relative exposure axis, with respect to the curve of another film, does depend on radiation quality. Thus, if curves of the type shown in figure 4-19 were prepared at a different kilovoltage, the curves would be differently spaced, that is, the film would have different speeds relative to the film that had been chosen as a standard of reference. This difference is attributed primarily to the efficiency of radiation absorption of a film at different photon energies.

The reciprocity law.—It has been assumed in the preceding discussions that an exact compensation for a decrease in exposure time could be made by increasing the intensity of the radiation. A radiographer therefore could reduce exposure time by 20%, if he increased the radiation intensity an equal amount either by shortening the source-to-film distance or by increasing the output of the X-ray source. This direct compensation is termed the reciprocity law and is valid when using direct X-ray or lead-screen exposure techniques. Stated mathematically, for a given exposure (E), the values of intensity (I) and time (t) can be varied at will if their product ($I \times t$) is not changed.

The reciprocity law fails when fluorescent screens (to be discussed below) are used. This failure is due to the radiographic film emulsion that is sensitive not only to the amount but also the brightness of the fluorescent light. The de-

crease in film exposure (density) will be small and cause little difficulty until the X-ray intensity is altered considerably. When the X-ray intensity is altered by a factor of 4 or more, it is usually necessary to change the total exposure inversely by approximately 20% to compensate for this deviation from the reciprocity law.

Technique Charts

Because the wavelength determines the penetrating quality of X-rays, the techniques used with any X-ray machine vary, and require special attention. It is usually necessary to develop data that are pertinent to radiographing various materials and thicknesses of these materials with a particular machine. Such data, when in convenient form, expedite the selection of correct techniques. The general techniques published by X-ray machine vendors are only approximate and seldom satisfactory for direct application.

Industrial radiographic techniques should be based upon the sensitivity required to discern the probable or expected flaws. Technique charts are usually designed as graphs of intensity-time (exposure) vs material thickness at a given radiation energy. A radiographer then selects the lowest energy that will provide an economical exposure for a given thickness. Figure 4-20 (ref. 2) shows a representative technique chart.

The basic information contained in a technique chart may be modified to suit desired changes in technique without redoing all of the exposures required to construct the original chart. Examples of such modifications are given below.

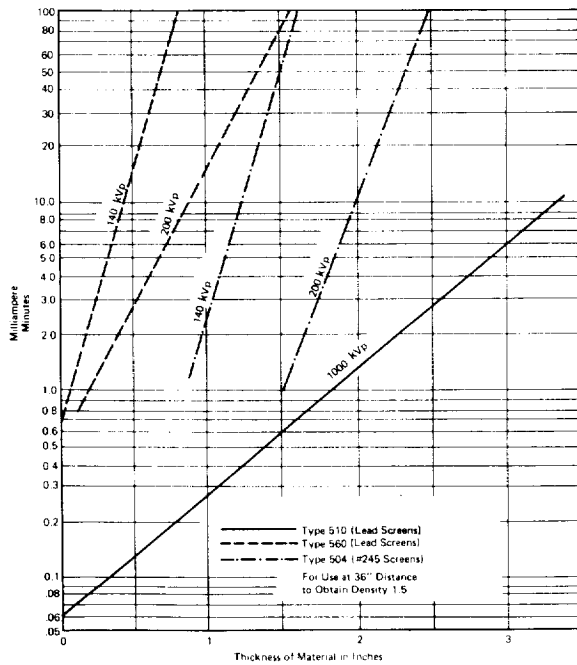


FIGURE 4-20.—Technique chart: time and intensity vs thickness of material (steel) at constant potential.

(1) The change in exposure required by the use of a different film may be calculated and a second set of exposure values developed and applied to the same graph.

(2) The change in exposure required by a change in source-to-specimen distance/specimen thickness (d/t) ratio can be computed through the use of the inverse-square law and a second set of exposure values developed for the same curve.

(3) A technique chart for a new alloy (of the same base material) can be developed by making a single exposure at a given thickness and comparing the density thus obtained with the original alloy. The original curve may then be shifted vertically to indicate the technique for the new alloy.

The radiation energy spectrum is unique for a particular radioisotope. Therefore, only one series of exposures is required to obtain a gamma-ray technique chart for a given material. Except for size and radiation intensity, little difference exists between different sources of the same isotope. It is possible, therefore, to apply the same technique charts to any source of the

isotope. Thus, technique charts published and distributed by isotope vendors can usually be modified to be compatible with the desired application.

Radiographic Screens

When an X-ray or gamma-ray beam strikes a film usually less than 1% of the energy is absorbed. Since the formation of the radiographic image is primarily governed by the absorbed radiation, more than 99% of the available energy in the beam performs no useful photographic work. Obviously, any means of more fully utilizing this wasted energy, without unduly complicating procedure, is highly desirable. Two types of radiographic screens, lead foil and fluorescent, are used to achieve this end.

Lead-foil screens.—Lead foil in direct contact with the film has three principal effects.

(1) It increases the photographic action on the film, largely by reason of the electrons emitted and partly by the secondary radiation generated in the lead.

(2) It absorbs the scattered radiation of longer wavelength more than the primary radiation.

(3) It intensifies the primary radiation more than the scattered radiation.

The quality of the radiation necessary to obtain an appreciable intensification from lead screens depends on the type of film, the kilovoltage, and the thickness of the material through which the rays pass. In the radiography of aluminum, for example, the thickness must be about 6 in. and the voltage as high as 120 kV to secure any advantage in exposure time with lead screens. In the radiography of steel, lead screens begin to give appreciable intensification with steel thicknesses in the neighborhood of $\frac{1}{4}$ in. and at voltages of 130 to 150 kV. In the radiography of $1\frac{1}{4}$ -in. steel at 200 kV, lead screens permit an exposure of about one-third that without screens (i.e., an intensification factor of 3). With gamma rays, the intensification factor of lead screens is about 2. Lead-foil screens, however, do not detrimentally affect the definition or graininess of the radiographic image to any appreciable degree, pro-

viding the lead foil and film are in intimate contact.

Fluorescent screens.—Certain chemicals fluoresce, that is, have the ability to absorb X-rays and gamma rays and emit light. The intensity of the light emitted depends upon the intensity of the incident radiation. The compounds most commonly used for intensifying screens are calcium tungstate and barium lead sulfate. They are finely powdered, mixed with a suitable binder, and coated in a thin, smooth layer on a special cardboard support to form a screen. For the exposure, the film is placed between a pair of these screens. The net photographic effect on the film is the sum of the direct effect of the X-rays and the effect of the light emitted by the screens. In the radiography of 1/2-in. steel at 150 kV, the exposure is about 1/125 as much with screens as without them. In the radiography of 3/4-in. steel at 180 kV, intensification factors of several hundred have been achieved experimentally. At this latter condition, the intensification factor has about reached its maximum and it diminishes both for lower voltage and thinner steel, and for higher voltage and thicker steel. Using radium or cobalt-60 gamma rays for very thick steels, the factor may be 10 or less.

Fluorescent screens give poorer definition in the radiograph, compared to a radiograph made directly or with lead-foil screens. For this reason, they are seldom used except when economy demands the shorter exposure times their use allows. The poorer definition is caused by the spreading of the fluorescence emitted from the screens.

Film Processing

In processing film, the latent image produced by exposure to X-rays, gamma rays, or light, is made visible and permanent. Processing is carried on under subdued light, of a color to which the film is relatively insensitive. The film is first immersed in a developer solution that causes the areas exposed to radiation to become dark, the amount of darkening for a given degree of development depending upon the degree of exposure. After developing, the film is rinsed,

preferably in an acid bath, to stop development. The film is next put into a fixing bath, which dissolves the undarkened portions of the sensitive silver salts, and then is washed to remove the fixing chemicals and dissolved salts. Figure 4-21 illustrates the step-by-step procedure used for the tank processing of X-ray films (ref. 1).

Machine processing.—Where the volume of work is large, automatic processing machines may be used to reduce the darkroom manpower required. Processing machines move films through the various solutions according to a predetermined schedule. Manual work is limited to the routine of loading and unloading the machine.

INTERPRETATION OF RADIOGRAPHS

Sensitivity and Definition

A radiograph is useless unless properly interpreted. Optimum interpretation requires a thorough knowledge of the entire procedure that has produced the radiograph at hand—setup parameters, exposure parameters, film type, intensifying screens used, film development parameters, and the characteristics of the item radiographed. In addition, the interpreter must be thoroughly experienced, and have at his disposal suitable reference radiographs.

The two basic overall parameters that the interpreter must know in regard to a given radiograph are the radiographic sensitivity and the definition which have been achieved. Radiographic sensitivity is measured in terms of the minimum percentage of the thickness of the subject item that corresponds to the least discernible change in photographic density of the final radiograph. Definition refers to the smallest size (in lateral dimension) flaw of given (equivalent) thickness. Both sensitivity and definition are established by the use of penetrameters.

Penetrameters

A penetrometer is a device whose image on a radiograph is used to determine radiographic quality level (sensitivity). It is not intended for use in judging the size or for establishing ac-

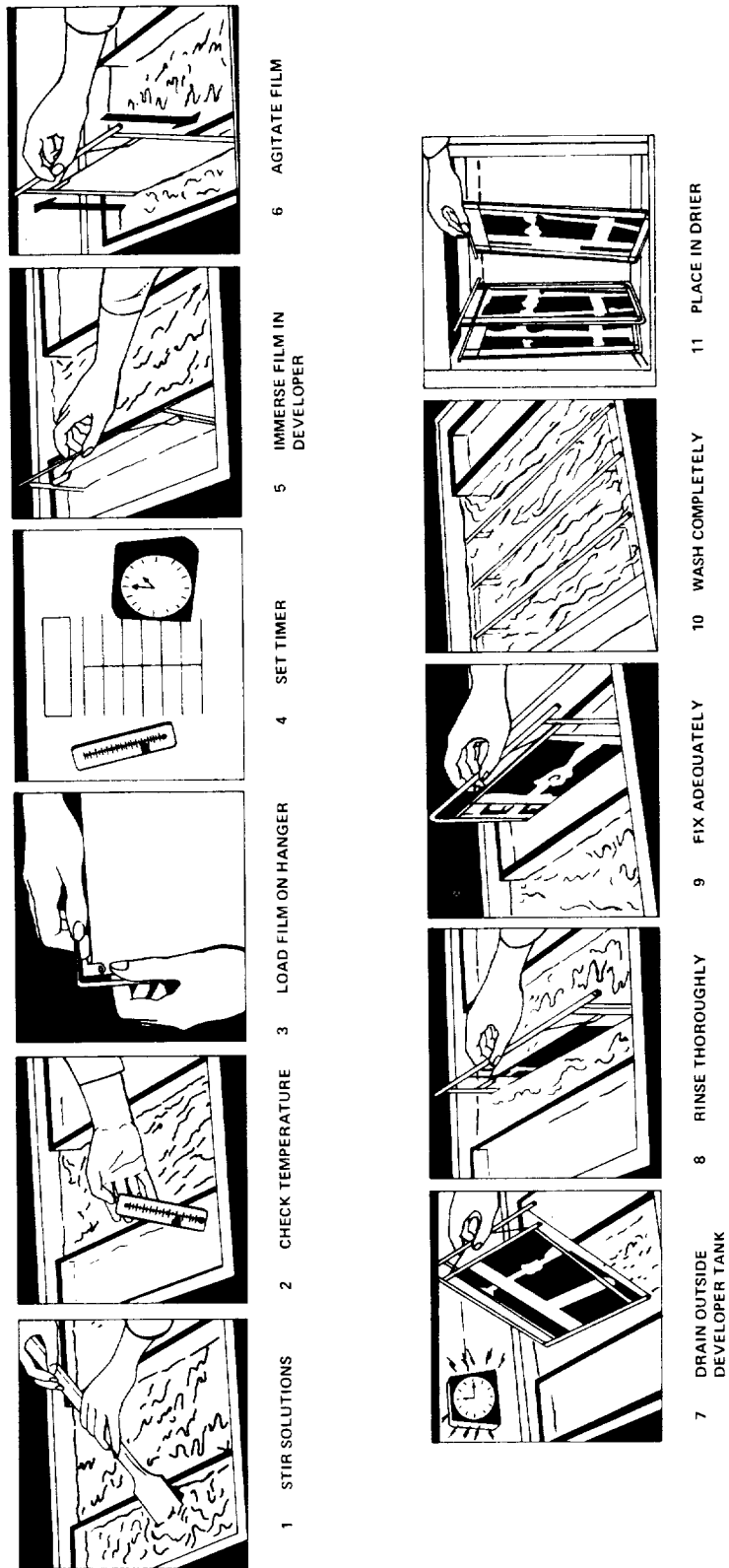


FIGURE 4-21.—Step-by-step processing of film.

ceptance limits of discontinuities. The standard penetrameter is a rectangle of metal with three drilled holes of set diameter, which is composed of material identical, or radiographically similar, to the material being radiographed. Each penetrameter is identified by a lead number (ID no.) that gives the maximum thickness of material for which the penetrameter is normally used (fig. 4-22) (ref. 2). The thickness (T) of the standard penetrameter is 2% of the thickness denoted by the ID no., and the hole diameters are $1 \times T$ (1T), $2 \times T$ (2T), and $4 \times T$ (4T). The standard 1.0-in. penetrameter has a 1.0 ID no. and hole diameters as shown in figure 4-22. A standard 2% sensitivity requires the technique to image the penetrameter whose thickness is 2% of T_m (the maximum thickness of the section to be radiographed), and the 2T hole of the penetrameter (penny). Other sensitivities (quality levels) are shown in table 4-5 (ref. 2). Penetrameters of different types have been devised for special uses, such as the wire penetrameters used in the radiography of small electronic components. In all cases, however, the penny is designed to

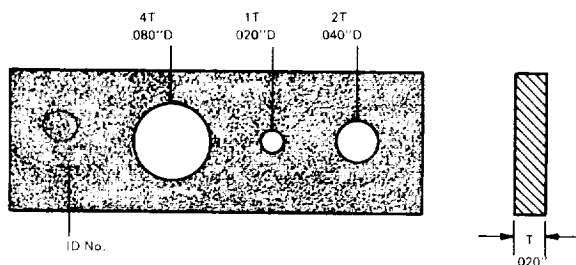


FIGURE 4-22.—Standard penetrameter for 1-in. material.

TABLE 4-5.—Radiographic Quality Levels (Sensitivity)

Sensitivity, %	Quality level	Penny "T" as % of T_m	Perceptible hole diam
0.7	1-1T	1	1T
1.0	1-2T	1	2T
1.4	2-1T	2	1T
2.0	2-2T	2	2T
2.8	2-4T	2	4T
4.0	4-2T	4	2T

determine the radiographic quality level, usually referred to as sensitivity.

SPECIAL RADIOGRAPHY

Fluoroscopy

Fluoroscopy is the direct conversion of X-ray patterns to visible light patterns by means of fluorescent screens. Direct fluoroscopy is relatively fast and inexpensive and is in widespread use despite certain disadvantages. It is generally used to scan a product for gross internal discontinuities or abnormal conditions. The advantages of this inspection system are given below.

- (1) An instantaneous visualization of the X-ray shadowgraph is possible.
- (2) The cost of inspection is materially less than film radiography on a per unit basis.
- (3) The system is fast and can be easily adapted to production lines.
- (4) Operators can be easily trained.

The disadvantages of this inspection system are:

- (1) Relatively poor sensitivity
- (2) Dependence on human vision.

The principal parts of a fluoroscopic unit are (1) an X-ray generator, (2) an X-ray sensitive fluorescent screen, and (3) a protective X-ray barrier.

Image brightness is a direct function of X-ray intensity at a given kilovoltage. This characteristic limits the image contrast of fluoroscopy to somewhat less than that obtained with industrial film, since the film responds to X-rays on a logarithmic scale.

Fluoroscopic sensitivity is a function of X-ray image contrast and the resolving power of the entire system. The resolving power of fluoroscopy is a function of the grain size of the screen and the geometry. A reduction of inherent filtration in the X-ray beam by using a thin beryllium window on the tube improves the contrast and increases the brightness. This effect is most easily seen on light alloy materials with an equivalent thickness less than $\frac{1}{2}$ in. of aluminum. For thicker sections of aluminum, the advantage of the beryllium window is re-

duced because of the absorption of radiation in the object. The response of fluoroscopic screens to various X-ray voltages indicates a peak at approximately 100 kVp.

Fluoroscopic screens are available with a grain size that will allow a presentation of approximately one to two lines per millimeter. This compares with approximately 30 to 40 lines/mm with radiography, using lead screens and a high-speed film. Because of this screen characteristic, the only alternative for improvement of sensitivity is by magnification of the image produced by an X-ray tube with a small focal spot. The low-light output of the fluoroscopic screen and the relatively large grain size continue to be a limitation of industrial fluoroscopy.

The sensitivity of the fluoroscopic inspection has been the limiting factor in its universal application. In general, with standard commercial equipment, a sensitivity of 6% to 8% is obtained. With special screens and tubes having small focal spots of less than 1 mm, sensitivities of 3% have been reported.

The eye is the sole registering medium in fluoroscopy, and as a registering device lacks accuracy. Vision is a variable thing considered from the standpoint of a single individual and is much more of a variable when considered from the standpoint of a number of individuals. The human eye must accommodate itself to the brightness of illumination to see effectively. Fluoroscopy should not be attempted until the operator has spent at least 20 min in total darkness. At ordinary daylight brightness levels, most individuals have no difficulty in distinguishing brightness differences between adjacent areas in which these differences are as small as 2 percent. As the brightness decreases below daylight levels, the minimum perceptible differences become greater and variations between individuals become more pronounced. As the brightness level gets lower and lower, the difference in brightness levels must be greater and greater if the eye is to detect a difference. A contrast of 30% to 100% must be present to be readily visible at brightness levels used in fluoroscopy.

Television Radiography

Closed-circuit television systems that are sensitive to X-rays have been developed. The use of closed-circuit television for X-ray imaging has the advantages of instantaneous image reproduction, and of protection for observing personnel from exposure to ionizing radiations. An instantaneous viewing system of X-ray images permits considerable reduction in production inspection costs. Film radiography, which has been the ultimate method for visualizing an X-ray image, has the advantage of high resolution and contrast sensitivity, but the disadvantage of being time-consuming and expensive. The television X-ray image system provides images equivalent to the best fine-grain radiographic film. This system uses a small-diameter, X-ray sensitive television camera tube to detect X-radiations that penetrate the object under inspection (fig. 4-23) (ref. 1). With a small-diameter camera-tube sensing area and the large-diameter picture-tube screen, the X-ray

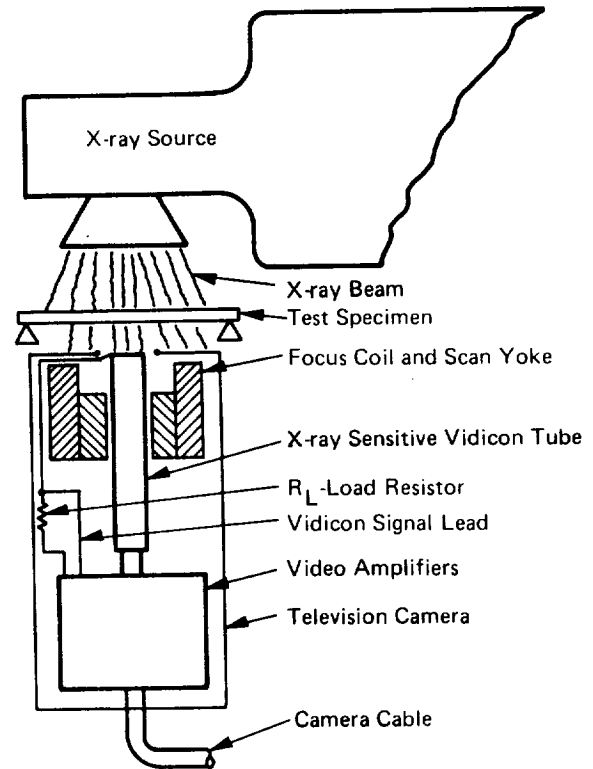


FIGURE 4-23.—Relative positions of X-ray source, test specimen, and television camera.

image is magnified by an amount equal to the ratio of their respective diameters.

The X-ray sensing camera tube is similar in size and appearance to the conventional photoconductive vidicon tube. Special window and target materials have been employed to provide the desired response to the penetrating radiation. Tubes have been built with glass windows of various thicknesses, and with beryllium windows. Beryllium-window tubes have shown much more sensitivity than glass-window tubes because of the inherent transparency of beryllium to X-rays. Glass windows of 0.090- to 0.065-in. thickness have been used. The tube transforms the X-ray image into an electric signal in a manner similar to that by which the light sensitive vidicon tube transforms an optical image into an electric signal.

The system is ideally suited for inspecting electronic-printed board assemblies. Small components magnified 30 times are readily observed on the television screen. Conditions such as solder porosity, lack of solder in terminals, porosity in semiconductors, contamination of diodes, partially broken wires, and breaks in copper conductors on printed-circuit boards are readily observed. Other small enclosed assemblies, such as wristwatches or relays, can be inspected to observe the movement of gears, springs, ratchets, and contacts. Material thicknesses are limited to the equivalent of about $\frac{1}{2}$ in. of steel.

Xeroradiography

Xeroradiography is a combination of X-radiography and electrostatics. The X-ray image is recorded in the form of a distribution of electrostatic charge on a special plate. The recording plate consists of a backing, usually aluminum, which has been given a coating of amorphous selenium. In the dark, this selenium coating will accept and hold an electrostatic charge, but, when exposed to light or radiation, the charge decays. The rate of decay is proportional to the intensity of the radiation to which it is exposed. This sensitivity to radiation produces the X-ray picture on the charged plate. The various steps involved in making a xeroradiograph are shown in figure 4-24 (ref. 1).

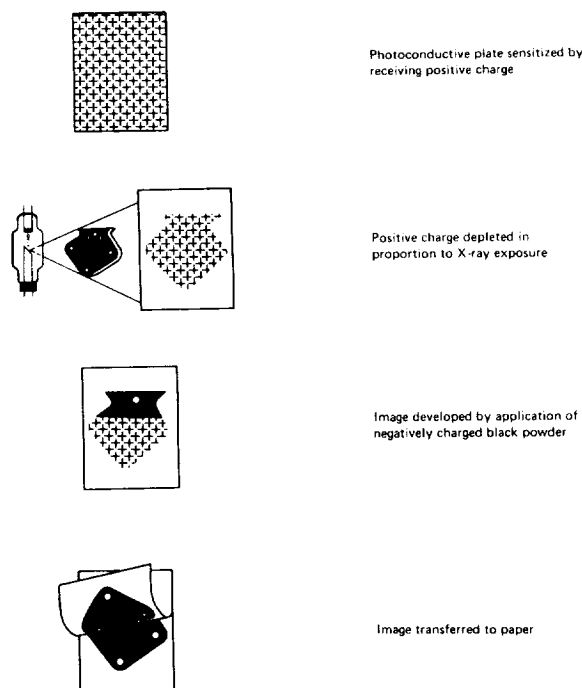


FIGURE 4-24.—Processing of a xeroradiograph.

A potential advantage of xeroradiography is the speed with which a xeroradiograph can be made.

In both sensitivity and definition, xeroradiographs are inferior to corresponding radiographs. This fact, together with the recent introduction of Polaroid* “instant” development films for radiography, has resulted in xeroradiography being little used. However, a principle similar to that of xeroradiography is used in X-ray image storage and intensification panels now being developed by a NASA contractor, which will be discussed in a later section of this chapter.

Stereoradiography

A single radiographic image does not possess perspective. Therefore, it cannot give the impression of depth, or indicate clearly the relative positions of various parts of the object along the direction of vision. The stereoscopic method, designed to overcome this deficiency of a single radiograph, requires two radiographs made

*Registered tradename of the Polaroid Corp.

from two positions of the X-ray tube, separated by the normal distance between human eyes. These radiographs are viewed in a stereoscope, a device which, by an arrangement of prisms or mirrors, permits each eye to see only one of the pair of stereoradiographs. As in ordinary vision, the brain fuses the two images into one in which the various parts stand out in striking relief in their true perspective and in their correct spatial relation. The conditions of viewing the radiographs should be exactly analogous to the conditions under which they were exposed; the two eyes take the place of the two positions of the focal spot of the X-ray tube, and the radiographs, as viewed in the prisms or mirrors, occupy the same position with respect to the eyes as did the films with respect to the tube during the exposure. The eyes see the X-ray representation of the part just as the X-ray tube "saw" the actual part (fig. 4-25) (ref. 2).

The stereoscopic method is not often used in industrial radiography, but occasionally it can be of considerable value in localizing defects, or

in visualizing the spatial arrangements of hidden structures.

Pulsed X-Ray Radiography

The development of pulsed X-ray radiography makes it possible to inspect high-speed events in opaque materials. This type of inspection is used primarily in support of developmental efforts such as gathering information relative to ballistics, explosives, and structural materials.

Equipment is available which is capable of producing 10^7 R/sec (at tube surface) in short bursts on the order of 0.2μ sec and at energies of 300 kV. Similar equipment is designed for operating at energies as high as 600 kV. Electrons are obtained via a cold cathode using the principle of field emission, and the accelerating potential is built up and released in a pulse. Power dissipation reaches several hundred megawatts with a current flow of between 1000 and 2000A. Effective focal-spot sizes are on the order of several millimeters wide and generally have a length several times greater than their width. The X-rays are developed in fractional microsecond bursts and therefore are capable of arresting motions having velocities of many thousand feet per second. The recycling time is normally several minutes, which precludes effective cineradiography using such sources. However, several such X-ray tubes positioned correctly can be pulsed sequentially to obtain progressive information.

Cineradiography

Sequential radiographs made under conditions that permit them to be projected or viewed in a manner analogous to "movies" are called cineradiographs. Problems connected with film shielding (to prevent unwanted exposure), film transport, image size, and source strength have slowed the development of film-type cineradiography. Closed-circuit television viewing of fluoroscope screens is not useful for cineradiography of high-speed phenomena; the response time of the fluoroscope screen is simply too long. However, the introduction of the television image tube that is sensitive to X-rays, together

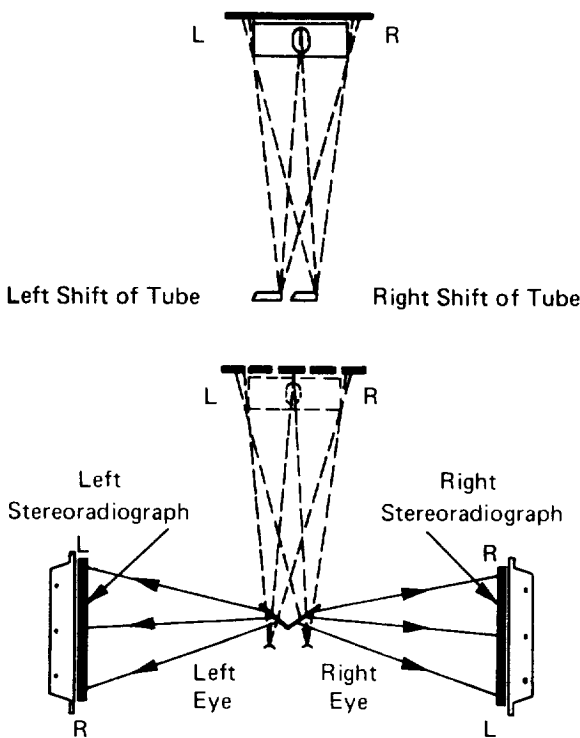


FIGURE 4-25.—Stereoscopic radiography.

with closed-circuit television systems and video tape recorders have made cineradiography practical for some special applications.

NEUTRON RADIOGRAPHY

Neutrons are electrically neutral particles that are constituents of all atomic nuclei except ordinary hydrogen. Neutrons are liberated by various nuclear reactions, including nuclear fission. Unlike X-rays and gamma rays, the neutron does not significantly interact with the electrons in matter. Rather, it interacts directly with the atomic nucleus, either by elastic collision (like billiard balls), or by being absorbed by the nucleus, where it may subsequently induce a nuclear decay process. The linear attenuation coefficient of neutrons (which is related to the probability of nuclear interaction) varies greatly with (1) the particular isotopes (specified by atomic number and atomic mass) making up the absorber and (2) the kinetic energy (or speed) of the incident neutrons. The first of these characteristics is in striking contrast to the corresponding case for X-rays or gamma rays in which the linear attenuation coefficient for photons of a given energy depends solely upon atomic number (i.e., number of orbital electrons), and increases smoothly with increasing atomic number. Figure 4-26 illustrates this by comparing the linear attenuation coefficient, μ , for 130-keV

X-rays with the values of μ for 0.05-eV neutrons, as a function of atomic number. The extraordinarily high neutron attenuation exhibited by hydrogen (H), lithium (Li), boron (B), cadmium (Cd), gadolinium (Gd), samarium (Sm), and europium (Eu), as compared with the attenuation produced by the common metals aluminum (Al), iron (Fe), copper (Cu), and titanium (Ti), and also the heavy elements such as lead (Pb), makes it possible to produce neutron radiographic images of very small amounts of the good neutron attenuators imbedded in thick sections of the poor neutron attenuators.

Ordinary radiographic film is only weakly sensitive to neutrons. Hence, some other material that can interact with neutrons and produce secondary radiation to which film is sensitive must be used. For example, a material such as lithium strongly absorbs "slow" (~ 0.05 eV) neutrons, and immediately disintegrates into an alpha particle (helium nucleus) and a tritium nucleus. The alpha particle is an efficient ionizer, and, when the lithium is in direct contact with a photographic plate, the emitted alpha particle can "expose" the emulsion. Alternatively, the lithium can be mixed with a material such as zinc sulfide which, when affected by the alpha particles from the lithium, "scintillates," that is, emits light, thereby exposing the light-sensitive emulsion.

"Direct" neutron radiography (fig. 4-27a) is accomplished using a prepared cassette in which radiographic film is in contact with neutron-sensitive screens. "Indirect" neutron radiography (fig. 4-27b) involves the use of a neutron-absorbing plate, or screen, which becomes radioactive under the influence of neutrons. The image is stored in the form of a pattern of

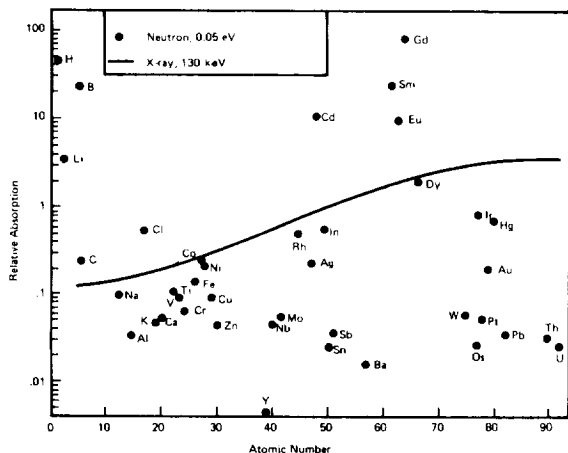


FIGURE 4-26.—Comparison of attenuation of X-rays and neutrons as a function of atomic number.

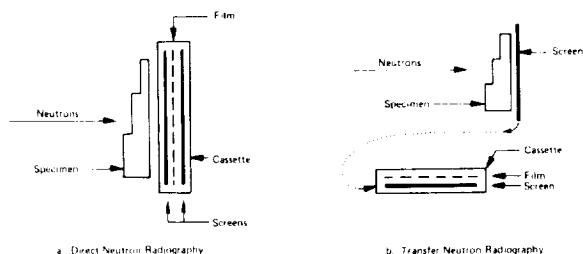


FIGURE 4-27.—Neutron radiography processes.

radioactive nuclei. The screen is then placed in contact with a radiographic film that is exposed by the radiation produced as the radioactive nuclei in the screen decay.

Neutrons for radiographic use are derived from (1) nuclear reactors, (2) nuclear accelerators, and (3) radioactive isotope sources. In reactors, neutrons result from fission of the fuel-element nuclei. Accelerators produce neutrons with accelerated charged particles to induce nuclear reactions in which neutrons are emitted. Isotope sources make use of the gamma radiation produced by certain radioactive nuclei to induce neutron-emitting reactions in a secondary element mixed with the radioactive one (there are no radioactive nuclei which directly emit neutrons in useful quantities).

For most radiographic applications, it is necessary to moderate the neutrons, that is, reduce their average energy to that of a gas at a moderate temperature; an energy of 0.05 eV is representative. In addition, since the "thermalized" neutrons do not radiate from even an approximate point source, it is necessary to collimate the neutrons, using neutron absorbing materials, to give a reasonably unidirectional beam of a diameter at least as great as the diameter of the desired radiograph. This procedure is very wasteful of neutrons, and low beam intensity, particularly for nonreactor sources, is a major shortcoming. Intensive development is being made in this area, however, and portable nonreactor sources of practical intensities may be expected in the near future.

The major practical application of neutron radiography to date is to various ordnance devices where a hydrogenous material (the explosive or propellant) must be examined while inside a closed metal casing. Another promising application is the detection of hydrogen dissolved in metals susceptible to hydrogen embrittlement.

NASA CONTRIBUTIONS

Training Handbook and Instruction Manuals

Satisfactory radiography can be accomplished only by well-trained, thoroughly experienced, conscientious technicians. The stringent

standards of reliability and quality assurance imposed by NASA upon its contractors and its own Centers, and the corresponding shortage of adequately qualified technicians, have resulted in the production of an advanced type of training for such personnel. Under a NASA contract, a complete course in radiography, in the form of "programmed" lessons for the student and an accompanying classroom handbook, has been developed. The programmed manuals make use of a modern self-instruction format comprising text, test questions, and review instructions that provide the student with continuous feedback regarding his progress. The textbooks for this course of instructions comprise the following:

Radiographic Testing: Class Room Training Handbook (ref. 2)

Radiography. Volume I—Origin and Nature of Radiation (ref. 3)

Radiography. Volume II—Radiation Safety (ref. 4)

Radiography. Volume III—Radiographic Equipment (ref. 5)

Radiography. Volume IV—Making a Radiograph (ref. 6)

Radiography. Volume V—Film Handling and Processing (ref. 7).

These documents, when used in conjunction with a program of instruction and laboratory exercises supervised by a qualified instructor and followed by a suitable period of competently supervised apprenticeship, provide a sound training basis for industrial radiographers.

X-ray Laminography

Laminography is a method of radiography that allows one in effect to radiograph a thin interior section of a thick specimen without physically sectioning it. Laminography depends upon smearing the unwanted features of a radiograph while keeping the desired portion of the image in sharp register (refs. 8 and 9). This is achieved by synchronously rotating both the film and the specimen during exposure (fig. 4-28) (refs. 8 and 9). As the specimen is rotated, the film is also rotated so that the pro-

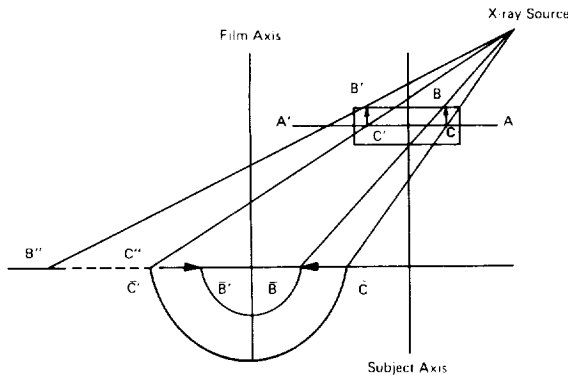


FIGURE 4-28.—Operating principles of the axial transverse laminography.

jection of the tail of the arrow (indicated in the specimen) remains in a fixed position on the film plane. On the other hand, projections of points from other planes of the specimen do not remain in register; hence their image on the film is smeared out. The subject layer, a sharp image of which is to be recorded, will be a plane parallel to the film, and passing through the point of intersection of the axis of rotation of the sample and a line joining the source and the axis of rotation of the film. As suggested by figure 4-28, a shallow angle of incidence of the X-ray beam is desirable to achieve good vertical resolution. Resolution of detail in the imaged plane depends on (1) accuracy of parallelism between the specimen and film planes, (2) deleterious effects of finite source size, and (3) misalignment of the X-ray source with respect to the plane defined by the axes of rotation of the sample and the film. From a mathematical analysis of the effect of these factors, the NASA contractor estimated that for the laminograph which they constructed, image resolution would be limited to 0.0025 inch.

In the laminograph constructed by the NASA contractor, a commercial microfocuss X-ray machine with a focal spot approximately 1.5 mils in diameter was used. The low power of this source necessitated long exposure times. The rotating tables for specimen and film, respectively, were supported at three symmetrically located points on their respective rims by precision bearings in contact with a 45° bevel machined and ground into the rim. The tables

themselves were precision machined and ground from a low-distortion steel. The tables were rotated by a motor-driven rubber rim contacting the rims of the two tables. Changing the compression of the rubber rim produced a small variation in the driving ratio allowing precise synchronism to be achieved. A rotation rate of 0.5 rpm was used. The specimen wheel was recessed to receive the specimen. A simple vacuum hold-down incorporated in the film wheel produced the necessary film flatness. Single emulsion film was used since the slight separation between layers of double emulsion film results in a deterioration of image sharpness. The major difficulty encountered in using this laminograph proved to be the maintenance of precise mechanical alignment.

A continuous scanning laminograph was designed and a prototype version constructed under NASA sponsorship (ref. 10). Basically, the machine required replacing the X-ray film with a fluorescent screen, the introduction of suitable optical elements to derotate the image of the screen, and the use of closed-circuit television for viewing the image. The prototype version of the machine accommodated circuit boards with maximum dimensions of 12×12×0.5 inches. Three overall magnifications were available: 0.2×, 1×, and 4×. At the smallest magnification, a large area (one-fourth of the board) of the printed circuit board can be viewed. The resolution of the system in this mode is severely limited by the television resolution and only gross detail could be observed. In the 1× mode, reasonable detail was available, but only an area 1.24×1.24 in. could be viewed. In the 4× mode, the viewed area was only 0.3×0.3 in., but the resolution was about 0.001 inch. This small viewed area represents the most serious compromise which had to be made in the design and was dictated by the goal of 0.001-in. detail resolution. State-of-the-art image orthicons achieve a resolution of about 250 line-pairs/in., a factor of 4 less than required. If the available resolution had been equivalent to 1000 line-pairs/in., a viewed area of at least 1×1 in. would have been possible, materially reducing the complexity of the instrument, greatly increasing the speed and

ease of inspection, and virtually assuring that a useful instrument could be developed.

Individual layers are selected by moving the X-ray source in a vertical direction. Scanning is achieved by programming the X-ray source and movements of the television camera through a logic control unit. Any selected volume of the sample may be inspected and the scanning will be performed automatically. The display unit is a high-resolution 14-in. monitor. The scan sequence can be manually overridden if a longer view of a given area is required. A completely manual mode is available in which scanning is controlled by the operator. Readouts for each of the position encoders are provided so that return to a previous position is achieved readily. Permanent recording of the inspection is achieved by making use of a Polaroid camera attached to an auxiliary 7-in. monitor that is also used for initial setup and fine focusing. Although the laminograph is very versatile in its operation, it achieves this at the expense of considerable complexity. The control requirements are extensive and operation will require some skill for efficient utilization.

One of the major goals of this design effort was the replacement of some presently used inspection techniques by a much faster 100% inspection tool. This goal was achieved although the solution is not an ideal one. The major limitation is that inspection still involves the human factor, and as yet no completely satisfactory definition of flaws has been formulated. In addition, a restriction is still present because of the limited speed of inspection, which is imposed, in a large degree, not only because of the necessity of visual inspection, but also because of the design itself. This design limitation imposes a time lag of a minimum of 2 sec on the movement of the scan from one position to the adjacent position. For a board of maximum size to be inspected at 4 \times magnification, the time for a complete scan would be several hours. Clearly, an inspection time of several hours is meaningful only if nearly 100% quality assurance can be achieved or if this time is substantially shorter than the time involved in applying conventional methods. In general, the latter is true while the former is not. It is known that

in the inspection of printed-circuit boards all flaws cannot be observed.

The laminograph method could be significantly improved with detailed resolution and a faster inspection time. Both of these improvements could be achieved if an image tube having a resolution of 5000 lines were developed. Much of the present optical system could then be discarded and more area would be displayed on the monitor.

Radiographic Absorptive Additives

A technique that can sometimes be employed to increase the radiographic detectability of discontinuities is the use of auxiliary materials which have comparatively high attenuation for X-rays. The approach is based on medical diagnostic radiography in which fluids containing barium compounds are sometimes introduced into the alimentary canal. Barium has a much higher mass absorption coefficient for low energy X-rays than does tissue. Hence, those portions of the alimentary canal containing the barium-rich fluid are clearly outlined when the abdominal region is radiographed or fluoroscoped.

The possibility of improving radiography for inspection of bonded honeycomb structures by combining a radiographically absorptive additive with the adhesive used in bonding honeycomb panels was investigated by a NASA contractor (ref. 11). To be applicable, the additive had to be: (1) highly absorptive to X-rays, (2) chemically inert, (3) obtainable as a finely divided powder for dispersion in the adhesive resin, and (4) economical. Additives found to meet these requirements were lead oxide (PbO), barium carbonate (BaCO_3), bismuth oxide (Bi_2O_3), and antimony oxide (Sb_2O_3). Lead oxide proved to have an adverse effect on the viscosity of the resin in the hot-melt condition. Barium carbonate was eliminated because of its low tolerance to humidity.

A destructive test program revealed that, in general, the additives did somewhat degrade the strength properties of the bonded honeycomb. It was concluded, however, that the improvement in radiographic detectability of adhesive voids was so great that further effort to find

compatible adhesive-additive combinations would be warranted.

Another potential application of X-ray absorptive additives is in the radiographic inspection of articles made of carbon. Such an application has been studied by a NASA contractor using the Algol II-B rocket motor (ref. 12). This rocket is fabricated with a solid carbon annular insert in the throat of the nozzle, and small cracks and internal flaws in this insert adversely affect the performance of the nozzle. Since the carbon is porous on a microscopic scale, it was hypothesized that an inviscid liquid would impregnate the nozzle and collect in cracks and macropores. The additive chosen was carbon tetrachloride (CCl_4), a promising candidate since chlorine has a much higher mass attenuation coefficient than does carbon, it is a liquid of low viscosity, and it should be chemically inert with carbon. The main disadvantages are its volatility and toxicity, requiring strict safety precautions.

Following an initial X-ray survey, a specimen nozzle insert was weighed (137.9 lb), placed in a 55-gal. drum, covered with carbon tetrachloride, sealed, and allowed to soak for 64 hours. On removal and reweighing, it was found to have absorbed 3.5 lb of the liquid. To prevent excessive evaporation of the liquid from the insert during further radiography, it was sealed in a polyethylene bag.

A second radiographic survey of the impregnated insert was then made. Numerous flaws were detected, and flaw indications were subsequently correlated with findings of a destructive examination of the insert. The contractor concluded that the effectiveness of the additive had been demonstrated, but that further work would be required in order to establish flaw detection thresholds.

On completion of the radiographic inspection, the insert was oven-dried for 8 hr at 200° F. Weighing of the dried insert indicated essentially total removal of the carbon tetrachloride. Mechanical flexure tests of specimens cut from the test insert indicated that the material had suffered no apparent detrimental effects.

An interesting twist on the use of X-ray absorptive additives is the use of "disappearing"

materials. For example, if the abutting surfaces of the edges of aluminum plates being butt-welded are plated with a thin layer of copper, proper welding results in the solution of the copper in the weld metal. If lack of fusion occurs, some of the copper will remain undissolved. Since copper has a higher mass absorption coefficient than does aluminum, the radiographic opacity of the weld flaw is greatly enhanced (ref. 9).

Penetrators for Evaluation of Threshold Detection Level of Crack-Like Flaws in Aluminum Weldments (ref. 13)

Aerospace requirements for high-strength hardware have emphasized the problem of flaw detection in flight vehicle structures. Of particular concern has been the requirement for greater quality and reliability in critical welded components used in cryogenic liquid propellant tankage. The types of flaw that are most likely to exist in a critical weldment prior to service are well known. However, what is generally not known and most difficult to determine has been the size of the flaw, particularly when the flaw has been identified as a weld crack. Detection of cracks, combined with the determination of the crack sizes, would provide quantitative data useful in fracture mechanics estimates of the service life of critical components of structures operating at cryogenic temperatures (e.g., pressure vessels and ducting).

One area that has received much attention is the design of penetrators as semiquantitative indicators of the radiographic sensitivity of any given radiographic technique. However, the major effort along this line has been devoted to radiographic evaluation of materials of thickness greater than $\frac{1}{4}$ in. A NASA contractor evaluated the threshold detection capabilities of a fixed radiographic technique in detecting subsurface crack-like defects in $\frac{1}{4}$ -in. 2014-T651 aluminum weldments.

Several penetrator designs are used throughout the industry as indicators to measure the radiographic quality level or evaluate those parameters influencing radiographic sensitivity. The designs are presently based on the

ability of an experienced film interpreter to resolve radiographic images produced by drilled holes, wires, tapered and parallel slits, and spheres.

Of prime interest in this program was the ability of a given radiographic technique to resolve small weld cracks and to define the detection capabilities in quantitative terms with respect to crack length, width, and depth. The closest approximation to the configuration of a naturally occurring weld crack that has been achieved to date is the taper or parallel slit technique. In this technique, cracks are simulated by placing two identical machined shims next to each other, and, by varying the arrangement and thickness of the shims, various slit dimensions (simulating width and depth of cracks) can be obtained.

To satisfy the requirement of determining the detection capabilities of internal or subsurface weld cracks for a specific radiographic technique, a penetrameter with predetermined crack or slit dimensions (width, depth, and length) can be sandwiched between the welds of two test plates previously machined from the test material being investigated. Finally, by using several of these plaque-type penetrameters (whose crack or slit dimensions are graduated and fixed in terms of width, depth, and length) and sandwiching them between matched sets of welded test plates, the vanishing point of the slit for each penetrameter can be determined by experienced film interpreters. Thus, with a specific set of penetrameters applied to a given material, material thickness, and radiographic technique, slit width and slit depth can be used to establish the minimum slit dimensions that are discernible under a given set of test conditions. The test data then provide a reliable and reproducible reference for either establishing or maintaining a satisfactory radiographic quality level for detecting internal crack-like weld defects. It is important to note that these special penetrameters were not designed either to indicate the type or size of weld cracks or to establish limits of acceptability.

Four weld-test panels possessing a minimum amount of radiographic indications, distortion, and variation in bead width were selected to

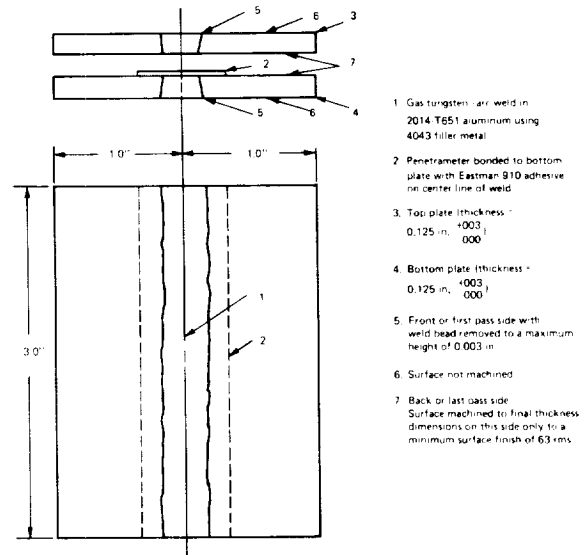
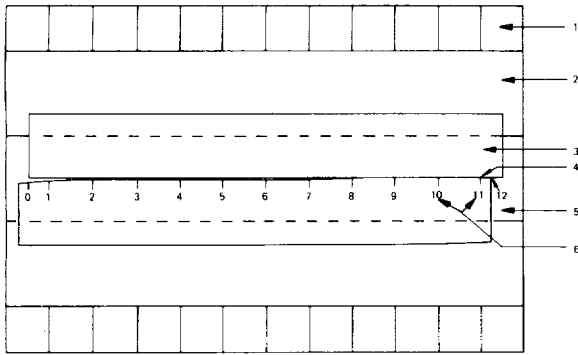


FIGURE 4-29.—Penetrameter test block.

obtain twenty test blocks ($\frac{1}{8} \times 2\frac{1}{2} \times 3\frac{1}{4}$ in.) suitable for the standard penetrameter test. Each plate was then matched and paired with respect to bead width, radiographic quality, and center line of the weld, forming ten matched sets of penetrameter test blocks, which were then finish machined (fig. 4-29). Each test block was measured for thickness across the weld, X-rayed separately, and the best five blocks were selected for the slit-type penetrameters.

Five tapered slit-type penetrameters were prepared from 1100-H18 aluminum foil in thicknesses of 0.001, 0.002, 0.003, 0.004, and 0.005 inch. Foil strips of each thickness and approximately $\frac{1}{2}$ in. wide and 3 in. long were machined with a single-point diamond-capped fly cutter to provide flat, square, parallel edges. The foil strips and the bottom test plate were thoroughly cleaned to remove all loose dirt and grease. The foil strips were then bonded to the bottom plate with Eastman 910 adhesive to form a tapered slit (fig. 4-30). The width of the tapered slits varied between 0.0047 and 0.0067 in. at the open end. Lead marking strips were adhesively bonded to the edges of the bottom test plate, and lines $\frac{1}{4}$ in. apart were scribed into the strip with a height gage to permanently locate the slit width measurements and provide a scale for



1. Lead marker with lines equally spaced 1/4 in. apart
2. Bottom half of penetrameter test block
3. Aluminum foil 0.001 in. thru 0.005 in. thick bonded to block with Eastman 910 adhesive to form slit
4. Slit with edges machined square and flat
5. Weld
6. Numbers indicate the location of slit-width measurements and, with the exception of locations 0 and 12, are aligned with the lead markers

FIGURE 4-30.—Slit-type penetrameter on bottom half of test block.

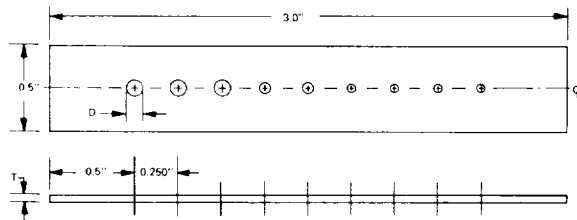
measuring slit lengths on the radiographs. The width of the slits was measured at 100× or 500× by using a metallurgical microscope and a Ramsden filar eyepiece. This equipment provides a means of measuring to the nearest 0.000020 inch. The average of three readings was taken at each of 12 locations for each of the slit-type penetrameters.

Five graduated hole-type penetrameters were also prepared from 1100-H38 aluminum foil in thicknesses of 0.001, 0.002, 0.003, 0.004, and 0.005 in. as shown in figure 4-31. Hole diameters varied between 8 times and 0.2 times the thickness of the penetrameter and were microdrilled to provide cleanly bored holes. Cleaning, bonding, and measuring procedures were identical to those procedures used in the preparation of the slit-type penetrameters.

Based upon the experimental test data obtained during this investigation, the conclusions listed below were drawn.

(1) It was demonstrated that penetrameters designed to simulate crack depths between 0.001 and 0.005 in. can be prepared by using tapered slits and special fabrication techniques, and that equally thin hole-type penetrameters with straight, clean-bored hole diameters equal to T/3 are now within the present state of the art.

(2) Based on the average readings of five analysts, the minimum slit dimensions detectable in the 1/4-in. aluminum welds for the fixed



T, Mils	D in Mils For Hole								
	1	2	3	4	5	6	7	8	9
5	40	20	10	5	4	3	2	1.5	1.0
4	32	16	8	4	3.2	2.4	1.6	1.2	
3	24	12	6	3	2.4	1.8	1.2	0.9	
2	16	8	4	2	1.6	1.2	0.8	0.6	
1	8	4	2	1	0.8	0.6	0.4	0.3	

NOTES

1. Holes shall be equally spaced 0.250 ± 0.010 in. and shall be drilled true and normal to the surface.
2. Holes shall not be recessed or chamfered and shall be clean and free of burrs.
3. Hole diameter tolerances shall be as follows:
 - a. 0.040 in. thru 0.004 in. plus or minus 5%
 - b. 0.003 in. thru 0.001 in. plus or minus 10%
 - c. less than 0.001 in. close as practical.
4. Diameter (D) of holes 1 thru 9 to be equivalent to 8T, 4T, 2T, 1T, 0.8T, 0.6T, 0.4T, 0.3T, and 0.2T, respectively, where T equals penetrameter thickness.
5. Material shall be 1100-H18 aluminum alloy foil.

FIGURE 4-31.—Graduated hole penetrameters.

radiographic technique, and with slits normal to the X-ray beam, were as follows:

- (a) 0.0008 × 0.005 in.
- (b) 0.0012 × 0.004 in.
- (c) 0.0016 × 0.003 in.
- (d) 0.0025 × 0.002 in.

(3) Factors controlling the minimum detectable slit widths were, in order of importance:

- (a) Density variations within the weld area
- (b) Visual acuity of the analysts
- (c) Slit depth
- (d) X-ray beam angle
- (e) Penetrameter location.

(4) Based on the average values determined for resolvable slit dimensions, the following relationships exist.

(a) Minimum detectable slit width increased as the slit depth decreased 0.005 to 0.001 in. and the X-ray beam angle increased from 0° to 20°.

(b) For any given slit depth between 0.002 and 0.005 in., the minimum detectable slit width was not significantly influenced by an X-ray beam angle between 4° and 10°.

(c) With few exceptions, the location of the penetrameter within the test block had little

or no significant effect on the resolution of slit images.

(5) Based on a comparison of the minimum and maximum values obtained for slit lengths, the vanishing point of the tapered slit image varied considerably from analyst to analyst and is believed to be the largest single factor contributing to the scatter in the test data. Slit length measurements were found to vary between $\frac{1}{4}$ and $1\frac{1}{4}$ in. with the largest variation occurring in slit depths 0.003 in. or less and at an X-ray beam angle greater than 15° . The differences in slit-length measurements were more consistent and did not exceed $\frac{1}{2}$ in. for slit depths of 0.005 and 0.004 in. and at X-ray beam angles of 0° , 5° , 10° , and 15° .

(6) When the minimum detectable slit widths were plotted as a function of slit depth, the slope of the straight line drawn through all data points varied between -0.70 and -0.81 indicating that unsharpness was a significant factor in the resolution of the slit image. This was particularly evident for slit depths less than 0.004 and 0.005 in.; at X-ray beam angles of 0° , 5° , and 10° , the slope of the line drawn through these data points approaches the ideal value of -0.50 , where the unsharpness factor is negligible.

(7) The average analyst could resolve at least one or more round hole images in 0.003, 0.004, and 0.005 in. thick graduated hole-type penetrameters located in the weld. The minimum hole diameter perceptible to all analysts was the 27 hole in the 0.004 in. thick penetrometer. It is believed that density variations within the weld area were a major factor in reducing the visibility of the hole image by the average film reader.

(8) The dark linear indications found during the radiographic examination of these simulated production welds were attributed to the diffraction and/or reflection effect resulting from the preferred orientation of large dendritic grains. It is believed that radiographic images of tight cracks or microfissures oriented parallel to the dendritic grains would be completely masked by these indications, particularly if the defect dimension were similar to those investigated in this test program. There-

fore, such cracks would be unresolvable under the most refined technique and by the most experienced film interpreters.

Digital Computer Processing of Radiographs

In order to obtain pictures of the lunar surface and the Martian surface from unmanned space vehicles, the picture is subdivided into many discrete picture elements (pixels). The brightness (or photographic density) of each pixel is then sequentially measured by photometric means, and the reading is converted to a binary number that is then transmitted from the spacecraft to the Earth where it is received and recorded. Since the exact sequence in which the pixels were encoded is known, the recorded information can be reconverted to a picture either by a cathode-ray oscilloscope or by an intensity modulated spot of light scanning a photographic plate.

The great scientific value of such pictures makes it desirable to obtain the maximum possible amount of information from them. To do this, scientists at the Jet Propulsion Laboratory devised a system for processing the received data to achieve improvements in the quality of the reconstructed pictures. The system employs a large-scale digital computer in which the data for each pixel is examined, compared with the data for surrounding pixels, and altered according to certain mathematical rules of digital filtering. In this way, several aspects of the reconstructed picture can be altered, including its overall density, the exaggeration or suppression of density gradients, and the subtraction or addition of a prescribed density pattern. Remarkable improvement in detail definition, density range, and contrast are obtainable. The ultimate resolution is set by the dimensions of each pixel.

The potential of this system for the enhancement of radiographs was recognized virtually from its inception. Within the past several years, its usefulness has been demonstrated both on medical diagnostic radiographs and on industrial NDE radiographs. Commercial firms have now developed similar digital enhancement systems and have also applied them to radiographs.

Radiographic images are converted to a form suitable for computer processing by means of a cathode-ray tube or equivalent scanner. A light beam is passed through the transparency line by line and converted to an electric signal. The amplitude of this electric signal is measured and digitized 500 000 times (optional) for each square inch of transparency. This digitized signal is recorded on magnetic tape and subsequently fed into a computer. After being processed by the computer, the digitized image is converted to an analog voltage that is used to modulate the intensity of an electron or light beam. This beam strikes a phosphor and the resulting emitted light exposes a film in a line by line manner. Thus, the processed or enhanced image is converted back to a transparency.

Two major methods are used to enhance the digitized image. One method is simply to subtract unimportant information from the picture on a point-by-point basis. This is done by using two radiographs taken at different times. Only changes, like the growth of cracks, will show in the resultant "difference" image.

A second image-enhancement method involves the use of two-dimensional spatial filtering concepts, a full discussion of which is beyond the scope of this survey. In brief, this method involves mathematically decomposing an image into superposed periodic density patterns; to enhance certain features of the image, the amplitudes of these periodic density patterns are modified and the modified patterns again superposed to give an enhanced image.

A related method is based on correlation concepts. Here the final density assigned to each pixel by the computer program is based on a probabilistic estimate that the assigned density logically fits in with the total pattern in surrounding pixels.

Figure 4-32 is a digitally enhanced photograph showing the fusion zone of a weldment made with 2014-T6 aluminum alloy and 4043 filter wire. The photograph shows what appears to be a hairline crack or a filamentary oxide inclusion running transverse to the weld; the original radiograph gave no indication of this discontinuity. Sectioning of the specimen and metallographic inspection confirmed the

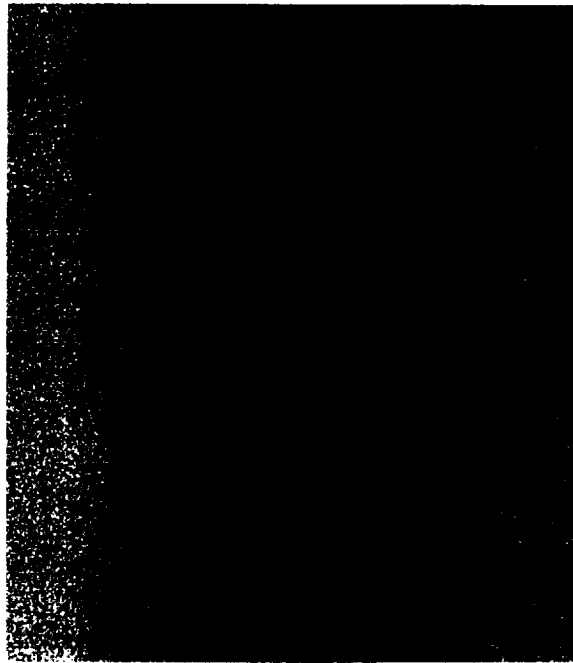


FIGURE 4-32.—Digitally enhanced radiograph. (The oxide line or stringer 0.002 in. in diam was not detected on original radiograph.)

presence of the stringer; figure 4-33 is an enlarged view of a transverse section through the stringer.

The major drawback to the use of digital enhancement of radiographs is the great complexity and cost of the required equipment. With future technical development and the commer-

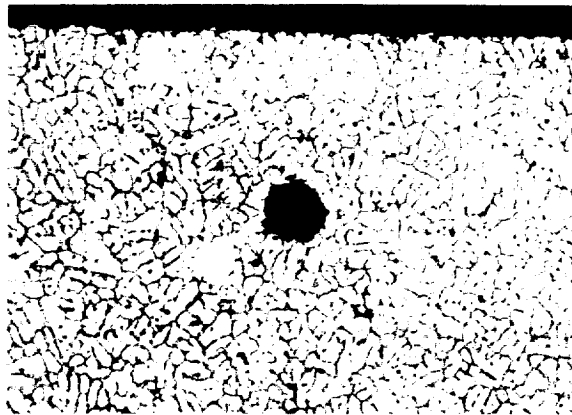


FIGURE 4-33.—Enlarged view of a transverse section through the stringer (200×).

cial demand for such services, the cost should be greatly reduced.

Further information regarding this NASA development may be found in references 14, 15, 16, 17, and 18.

Solid-State Radiographic Image Amplifier and Storage Panel

When a large number of individual radiographs are required for a single inspection, a direct viewing system becomes desirable. A conventional fluoroscope may have inadequate brightness and resolution, while adding an image intensifier may result in a system too cumbersome, intricate, and expensive. Therefore, NASA sponsored the development of a solid-state image amplifier and image-storage system (ref. 19). The system converts input radiation into electric current, amplifies the current which then excites an electroluminescent material to form an output image within a flat, lightweight panel. It also can retain the image for at least 10 minutes.

The system requires no dark adaption by the operator and is quite sensitive. The image quality is reported to be superior to that of a conventional fluoroscope. The system has been successfully tested for X-rays in the 30 keV through 500 keV range.

A panel may be used for an approximate lifetime of 100 hr with an estimated cost of \$1000 for an 8×10 in. plate. At present, no larger plate than 8×10 in. has been produced but no obstacles are presently foreseen in increasing its size. Also, four 8×10 in. plates could be joined by a brace to form a 16×20 in. plate.

One minor disadvantage of the system is that the response time of about a second limits motion studies to slow-moving objects. The advantages, however, are numerous. Less X-ray exposure is necessary and the resolution is better than in most other direct-viewing systems. Also, the cost of each view is substantially less than that of film radiography. Furthermore, the system is simple and lightweight. A complete system, with a radioisotope source, weighs less than 30 lb and can be hand-carried in a small case.

The complete system consists of three major components:

- (1) An image amplifier
- (2) A Thorn image-retaining panel
- (3) A power supply unit.

The Thorn panel is separated from the image amplifier by a microsheet of glass 0.003 in. thick. The X-rays enter through the glass substrate of the image amplifier, and the image is formed in it. The image is simultaneously transferred to the Thorn panel; after a 10 to 20 sec exposure time, the Thorn panel is removed to observe the retained image. The system becomes an instantaneous, direct-viewing device by using just the image amplifier without the Thorn panel.

The image amplifier was developed for NASA based on an approach previously established. The approach used was to sandwich photoconductive (PC) material and electroluminescent (EL) material in alternate layers between two electrodes. CdSe was selected to be the photoconductive material used in conjunction with the contractor's proprietary electroluminescent phosphor. With this type of construction, high-contrast images were obtained. The amplifier requires 120 V rms maximum, 60 to 2000 Hz ac, and 80 mA maximum at 400 Hz, 115 V. The configuration of the image amplifier is shown in figure 4-34. Table 4-6 gives the amplifier's characteristics.

The image storage device was obtained from Thorn Electrical Industries, Ltd., United Kingdom. It is available in varying sizes up to 10×30 in. with larger sizes considered if justified by the application. It consists of a thin metal

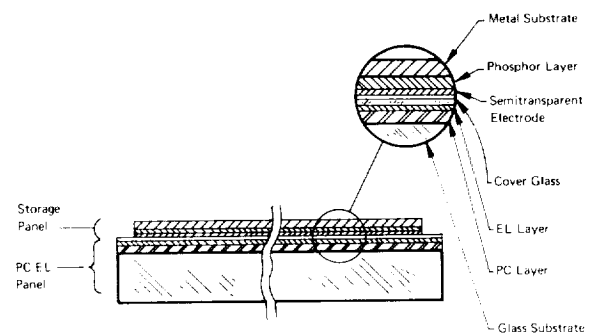


FIGURE 4-34.—Construction of storage radiographic amplifier system.

TABLE 4-6.—*Characteristics of Radiographic Amplifier*

Characteristics	Data
Size of active area.....	7.75×9.75 in.
Size of glass substrate.....	8×10.25 in.
Resolution.....	180 lines/in.
X-ray intensity range.....	0.2 to 20 R/min (60-keV X-ray source).
Max. output brightness.....	7-ft L at 115 V, 400 Hz
Contrast sensitivity.....	3% on .04-in. Al at 50 keV.
Rise-time constant.....	0.5 to 5 sec, depending on X-ray intensity.
Decay-time constant.....	0.1 to 0.5 sec.

plate coated on one side with vitreous enamel layers. If light or X-rays impinge on the coated surface while a potential difference of 60 to 120 Vdc is applied between the front and back electrodes, the plate emits a yellow light where it has been excited. The flowing image may be retained for 10 min or more after the source of excitation has been removed. The image slowly loses resolution, but this loss is not too noticeable for at least five minutes. The image disappears as soon as the potential is removed or polarity is reversed. A few seconds after erasure, the panel can receive another image. This panel increases the system's rise time to 10 to 20 sec and decay time to a maximum of one second.

The power supply consists of two separate, but simple units. The image amplifier requires a power source with a voltage that varies between 0 and 115 V ac and a current of about 200 mA. Optimum contrast sensitivity is easily reached by varying the panel's power-supply voltage. The Thorn panel requires a power source with low power and low dc voltage. The values for the second power supply depend on the size of Thorn panel used.

This system has numerous potential applications. By selecting the right glass substrate, it may be used with visible light, X-rays, ultraviolet light, and near infrared light. As noted, a portable X-ray system may be made by using a radioisotope source. Further development of the system is continuing.

REFERENCES

1. ANON.: *Nondestructive Testing Series—Radiography. Quality and Reliability Assurance Handbook H-55*, U.S. Dept. of Defense, Apr. 1966.
2. ANON.: *Radiographic Testing: Classroom Training Handbook*. NASA CR-61231, 1967. (N68-28793)
3. ANON.: *Radiography: Vol. I—Origin and Nature of Radiation*. NASA CR-61212, 1967. (N68-28784)
4. ANON.: *Radiography: Vol. II—Radiation Safety*. NASA CR-61213, 1967. (N68-28785)
5. ANON.: *Radiography: Vol. III—Radiographic Equipment*. NASA CR-61214, 1967. (N68-28786)
6. ANON.: *Radiography: Vol. IV—Making a Radiograph*. NASA CR-61215, 1967. (N68-28787)
7. ANON.: *Radiography: Vol. V—Film Handling and Processing*. NASA CR-61216, 1967. (N68-28788)
8. HAMRE, HARLAN G. ET AL.: *Nondestructive Testing Techniques for Multilayer Printed Wiring Boards*. NASA CR-67988, 1965. (N66-11764)
9. ANON.: *Nondestructive Testing: Trends and Techniques*. NASA SP-5082, 1967. (N67-23667)
10. MOLEK, R. B.: *Development of a Continuous Scanning Laminograph*. NASA CR-98249, 1968. (N69-16857)
11. PATTON, R. J.: *Incorporation of Additives in Adhesives for Radiographic Inspection of Adhesive Bonded Honeycomb Structures*. NASA CR-60989, 1965.
12. ROBINSON, U. M.: *Investigation of New Radiographic Procedures for NDT of Scout Nozzles*. (NAS1-6935-25) LTV Aerospace Corp., Dallas, Tex., June 30, 1969.
13. TRYON, R. W.: *Evaluation of the Radiographic Threshold Detection Level of Subsurface Crack-Like Defects in Aluminum Welds*. NASA CR-98355, 1968.
14. ANON.: *Digital Computer Processing of X-Ray Photos*. NASA Tech Brief 67-10005, 1967.
15. BILLINGSLEY, FRED C.: *Digital Image Processing Rationale, Supplement D, Progress in Biological Electron Microscope Techniques*. Harper and Row, Publishers, 1969.
16. CAMPBELL, JOHN T.: *JPL Image Processing System Language (the Software System)*. Supplement E. (JPL-951538) IBM/Federal Systems Div.
17. EFRON, EDWARD: *Image Processing by Digital Systems, Supplement F*. Paper presented at Annual Convention of the American Society of Photogrammetry (Washington, D.C.), Mar. 1968.
18. SELZER, ROBERT H.: *Improving Biomedical Image Quality with Computers*. Tech. Rept. no. 32-1336, JPL, Calif. Institute of Technology, Oct. 1, 1968.
19. SZEPESI, ZOLTAN; NOVICE, MICHAEL; AND KEETON, THOMAS: *Solid-State Radiographic Image Amplifiers*. NASA CR-102299, 1968.

|

CHAPTER 5

Eddy-Current Testing

Richard L. Pasley and James A. Birdwell

Eddy-current inspection is a method of locating surface or subsurface flaws in electrically conductive materials, and evaluating such material characteristics as hardness, heat-treat condition, and other metallurgical conditions. The test article is brought into a time-varying electromagnetic field that induces electric current. Typical currents of this sort resemble in form the eddies in flowing streams of turbulent water; hence, they are called eddy currents. The amount of electrical current flowing in these eddies is determined by the electrical conductivity of the test object as well as the frequency and amplitude of the applied electromagnetic field. These eddy currents in turn create their own electromagnetic field, which may be sensed either through its effects upon the primary excitation coil, or by means of an independent sensor. In nonferromagnetic materials, the secondary electromagnetic field depends simply upon the eddy currents; however, with ferromagnetic materials, additional magnetic effects occur that usually are of sufficient magnitude to overshadow the direct eddy-current fields. These magnetic effects result from the magnetic permeability of the test material, and may be virtually eliminated by magnetizing the material to saturation in a static magnetic field. In the case where the permeability effect is not removed, the inspection method is perhaps best categorized as magnetic-field testing. The con-

vention to be followed here is that any form of test making use of predominantly ferromagnetic effects, regardless of whether eddy currents are present, will be regarded as a magnetic-field test method, and will be discussed in the chapter entitled "Magnetic Field Testing."

Eddy currents were discovered some time before anyone thought of using them for nondestructive inspection. Early evidence of eddy currents was presented in 1824 by Gambey, who noted that the oscillations of a suspended bar magnet were rapidly damped whenever a copper plate was held under it. The following year, Arago showed that a magnetic needle suspended above a spinning metal disc was deflected in the direction of rotation. About this same time, Jean B. Foucault, who is generally credited with the discovery of eddy currents, demonstrated that such currents exist in a copper disc moving in a strong spatially nonuniform magnetic field. Thus, eddy currents are sometimes called Foucault currents (ref. 1).

The first mention of an eddy-current-related method of nondestructive testing appears to be that of D. E. Hughes, who in 1879 used the sound of a ticking clock, a microphone, and an induction coil to induce eddy currents in different metals and alloys. The electrical impulses from the microphone caused by the clock ticking were passed through a pair of series-connected coils. Eddy currents were thus induced in

objects placed between these coils. Hughes listened with a telephone receiver and noted what adjustments were necessary to make the sound disappear whenever he made changes in material size, shape, or composition (ref. 2). From 1879 until the late 1920's no significant achievement in eddy-current testing was reported. At this time, under the direction of Cecil Farrow, a steel company began eddy-current testing on a tonnage basis (ref. 3).

In 1948, an institute in Reutlingen, Germany, began pioneer work in developing modern eddy-current instrumentation. Techniques were evolved for separating types of defects based on phase discrimination. In 1949, a completely new use for eddy-current testing was introduced by H. G. Doll. His method, called induction logging, was used for measuring the electrical conductivity of geological strata at various depths in oil-well bore holes (ref. 4).

Today, numerous versions of eddy-current test equipment are commercially available. Much of this equipment is useful only for exploratory tests or for inspecting parts of simple geometry; however, specially designed equipment is used extensively in inspection of production quantities of metal sheet, rod, pipe, and tubing.

As a nondestructive testing tool, eddy-current inspection complements the other standard methods for detection of: (1) surface and subsurface flaws, (2) irregularities in material structure, and (3) variation in chemical composition in metallurgy. Compared with liquid penetrants, eddy-current methods are not as sensitive to small, open flaws; however, they have the advantage over liquid penetrants in that they are faster, they do not require cleanup operations, and, especially, they can respond to subsurface flaws. Compared with the magnetic-particle method, eddy-current methods are not as sensitive to small flaws, but they have the advantage of being effective with both ferromagnetic and nonferromagnetic metals. Ultrasonic methods are superior to eddy-current methods for resolving small flaws and detecting flaws located well below the surface; however, eddy-current methods do not require mechanical coupling to the specimen as does

ultrasonics. Compared with radiographic methods, eddy-current techniques are faster but generally not as sensitive to small, deep subsurface flaws.

Some of the inherent limitations of eddy-current test methods are: (1) depth of inspection below the material surface is limited depending upon the test frequency, (2) eddy currents are influenced by many material variables, which often yield ambiguous test results, and (3) most test instruments must be manned by well trained operators.

PHYSICAL PRINCIPLES

Electric eddy currents have no sources or sinks (in the hydrodynamic sense), but flow in paths which close upon themselves. The generation of eddy currents in two simple cases of practical importance is illustrated in figures 5-1 and 5-2. The main factors in determining the magnitude and direction of eddy currents

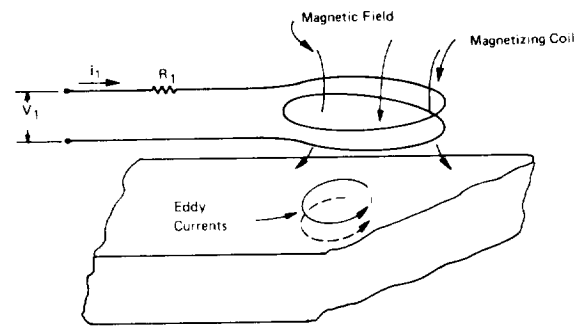


FIGURE 5-1.—Eddy-current flow generated in a flat surface by a time-varying magnetic field.

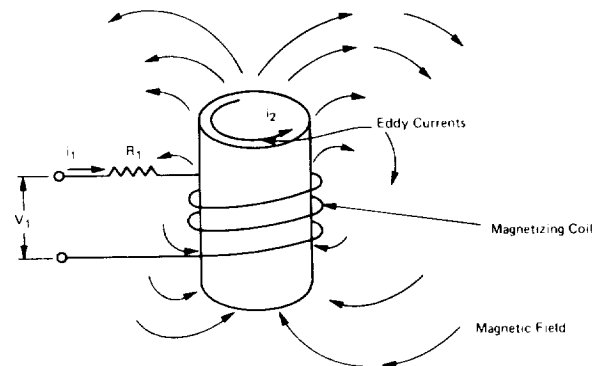


FIGURE 5-2.—Eddy-current flow generated in a cylindrical object by a time-varying magnetic field.

induced by harmonically varying magnetic fields are:

- (1) The geometrical shape of the applied field
- (2) The amplitude of the applied field
- (3) The frequency of the applied field
- (4) The geometry (size and shape) of the article under test
- (5) The location and orientation of the test article with respect to the applied field
- (6) The electrical conductivity of the test article (including inhomogeneities in this property)
- (7) The magnetic permeability of the test article.

Even a very small change in any one of these parameters can have a marked effect on an eddy-current indication. Moreover, for practical testing purposes, it is usually necessary that all save one of these parameters (i.e., the parameter of interest in the test) be either rigorously controlled or accurately established.

From an analytical point of view, it is desirable to predict theoretically the eddy-current-generated field corresponding to a given test arrangement. In principle, Maxwell's equations are an adequate basis for such predictions, but, in practice, only a very few idealized cases can be handled adequately by this approach. Hence, eddy-current design work is largely empirical.

Two distinct approaches to eddy-current testing are in use. The first is called the single-coil approach, in which some property of the test article is inferred by noting the relative amplitudes and phases of the voltage and current flowing in a wire coil (the "probe") carrying some nominal time-varying current. The second approach is to introduce a second sensor (usually an inductive coil or a Hall-effect device) that can sense both the applied field and the secondary field arising from induced eddy currents. In this case, properties of the test article are inferred from the effects of the eddy currents on the secondary sensor. Numerous variations of these two basic schemes have been explored, and many of them have been incorporated in both commercial and custom apparatus.

The Basic Single Coil Systems

The objective in using the single coil system is to measure the change in the apparent ac impedance of the test probe, which is caused by inductively coupling the probe to the test article. The elementary circuit equivalent to a single coil probe (self-capacitance is neglected for simplicity), is shown in figure 5-3. When a steady-state alternating current of the form $I(t) = I_0 \cos \omega t$ is established in the coil, the voltage across its terminals is of the form $V(t) = V_0 \cos(\omega t + \delta_0)$. The voltage amplitude, V_0 , and its phase, δ_0 , relative to the phase of the current, are determined by the ohmic resistance, R_0 , of the coil, its self inductance, L_0 , and the parameters, I_0 and ω . Furthermore, if V_0 and δ_0 can be measured experimentally, the parameters R_0 and L_0 can be computed from the measured values. From elementary circuit theory, the equations connecting V_0 and δ_0 with R_0 and L_0 are found to be

$$R_0 = \frac{V_0}{I_0} \cos \delta_0 \tag{1}$$

and

$$\omega L_0 = \frac{V_0}{I_0} \sin \delta_0 \tag{2}$$

An elementary ac circuit analog representing the probe inductively coupled to a test article is shown in figure 5-4. The test article is simulated by a self-inductance L_1 shorted by a resistance, R_1 . The coupling between the probe and the test article is represented by the mutual inductance, M . For a prescribed probe, the effective value

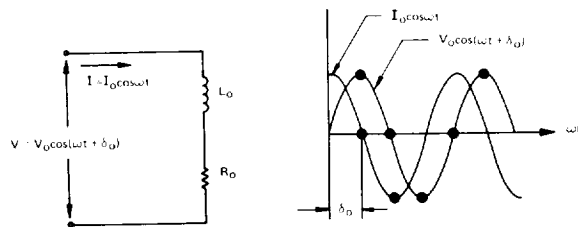


FIGURE 5-3.—The equivalent circuit of a single-coil probe, represented by an inductor, L_0 , which is the self-inductance of the coil, and a resistor, R_0 , which is the dc resistance of the coil wire. (A sinusoidal voltage across the coil will differ in phase from the current flow by the amount, L_0 .)

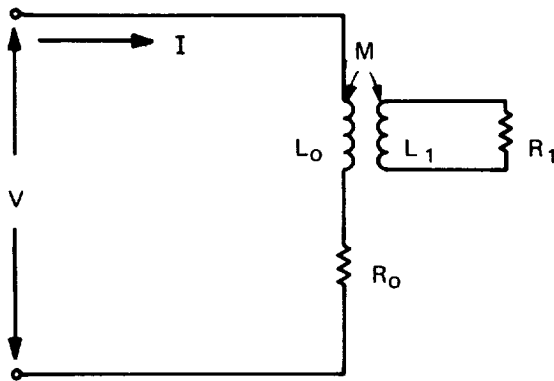


FIGURE 5-4.—The equivalent circuit of a wire coil inductively coupled to a test article. (Represented by an inductor, L_1 , shorted by a resistor, R_1 , coupled to the test coil, L_0 , by the mutual inductance, M .)

of M depends upon the size and shape of the test article and its location and orientation with respect to the probe. It also depends strongly upon the permeability of the test article, but not upon the conductivity of the test article unless the conductivity is inhomogeneous.

Relative to making measurements at the probe terminals, all that can be observed are changes in V_0 and δ_0 (a constant current amplitude, I_0 , and frequency, ω , being assumed). These, in turn, may be related theoretically to shifts in the values of R_0 and ωL_0 . From elementary ac circuit theory, it can be shown that the shift ΔR in the value R_0 , and the shift $\omega\Delta L$ in the value of ωL_0 are given by the equations:

$$\Delta R = \frac{M^2 \omega^2 R_1}{R_1^2 + \omega^2 L_1^2} \quad (3)$$

and

$$\omega\Delta L = \frac{-M^2 \omega^3 L_1}{R_1^2 + \omega^2 L_1^2} \quad (4)$$

The significance of these two equations is made more apparent by connecting them to two equivalent equations. Dividing ΔR by $\omega\Delta L$ gives the equation:

$$\Delta R = -\frac{R_1}{\omega L_1} \omega\Delta L \quad (5)$$

an equation from which the mutual inductance M has been eliminated. On the other hand, if

the variable R_1 is eliminated between equations (3) and (4), the resulting equation is

$$(\Delta R)^2 + \omega\Delta L + \frac{1}{2} \frac{M^2 \omega^2}{L_1} = \frac{1}{4} \frac{M^4 \omega^4}{L_1^2} \quad (6)$$

The physical significance of equations (5) and (6) is clarified by graphically illustrating ΔR as a function of $\omega\Delta L$ for various assumed values of R_1 , L_1 , and M . A family of such graphs is shown in figure 5-5. Equation (5) represents a family of straight lines of negative slope ($-R_1/\omega L_1$); equation (6) represents a family of circles with centers on the negative $\omega\Delta L$ axis, each circle passing through the origin of coordinates tangent to the ΔR axis.

Figure 5-5 shows how it is theoretically possible to distinguish the effects of a variation of conductivity of a test article (other factors being held constant) from effects due to changes in coupling between the probe and the test article (e.g., geometrical changes, unless the magnetic permeability of the test article is variable). Thus, at point P , a change in conductivity alone corresponds to a significant change of ΔR and a comparatively small change in the value of $\omega\Delta L$. On the other hand, a change in coupling

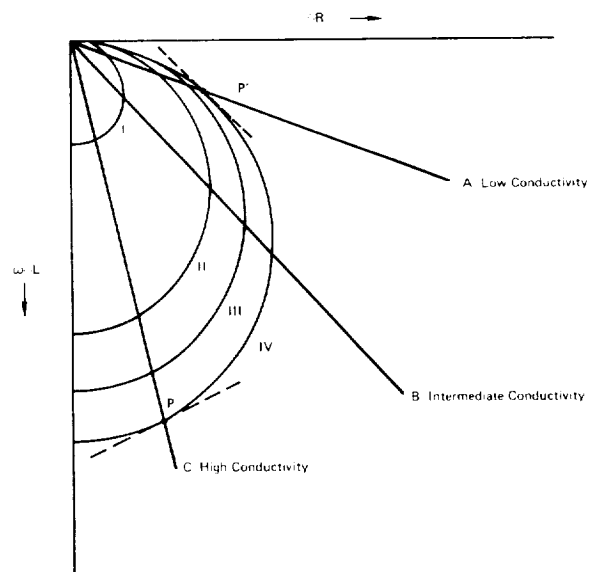


FIGURE 5-5.—The effects of variations of conductivity of a test article and those due to changes in coupling of the probe to the test article. (These effects may be distinguished by measuring ΔR or $\omega\Delta L$.)

(e.g., a change from curve III to curve IV), with no change in conductivity (i.e., along line *C*), has the opposite effect. In contrast, at point *P'*, a change in conductivity or coupling produces similar changes in both ΔR and $\omega\Delta L$, necessitating extremely precise measurements to separate adequately the two effects.

Since the radius of a given circle in figure 5-5 is given by the expression, $M^2\omega^2/2L_1$, it can be concluded that good discrimination between "lift-off" (i.e., geometrical effects) and changes in conductivity of the test article depends upon high conductivity, a high frequency, and close geometrical coupling between probe and test article.

The foregoing discussion in terms of an elementary electric-circuit analog is too simplified for quantitative interpretation of practical eddy-current measurements. An adequate theory, in effect, would have to predict values of *M*, *L*₁, and *R*₁ for a prescribed probe coil and a prescribed test article. This problem has been investigated and results of the study are available for a few simple cases, only one of which will be discussed here—the case of a cylindrical

specimen coaxial with a surrounding closely wound solenoidal test coil; both specimen and coil are assumed to be infinitely long. The results of the calculation (ref. 2) may be presented graphically.

Theory reveals that the coupling parameter (analogous to *M* in the analog circuit) is a factor, $v=a^2/b^2$ (called the "filling factor"), where *a/b* is the ratio of the specimen radius to that of the coil radius. The parameter incorporating the effects of frequency, conductivity, and magnetic permeability is $g=\sqrt{\omega\delta\mu}$, in which *g* is the reciprocal of a length, representing the depth below which eddy currents are less than about one-third surface value (sometimes referred to as the "skin depth"). Some typical skin depths are given in the graph of figure 5-6 (ref. 2). Two families of curves, one corresponding to increments in the parameter, *v*, and the other corresponding to increments in the specimen radius, *a*, for a fixed value of the parameter, *g*, are shown in figure 5-7.

By comparing figure 5-7 with figure 5-5, the similarity is evident. (Note, however, that figure 5-5 shows increments in resistance and

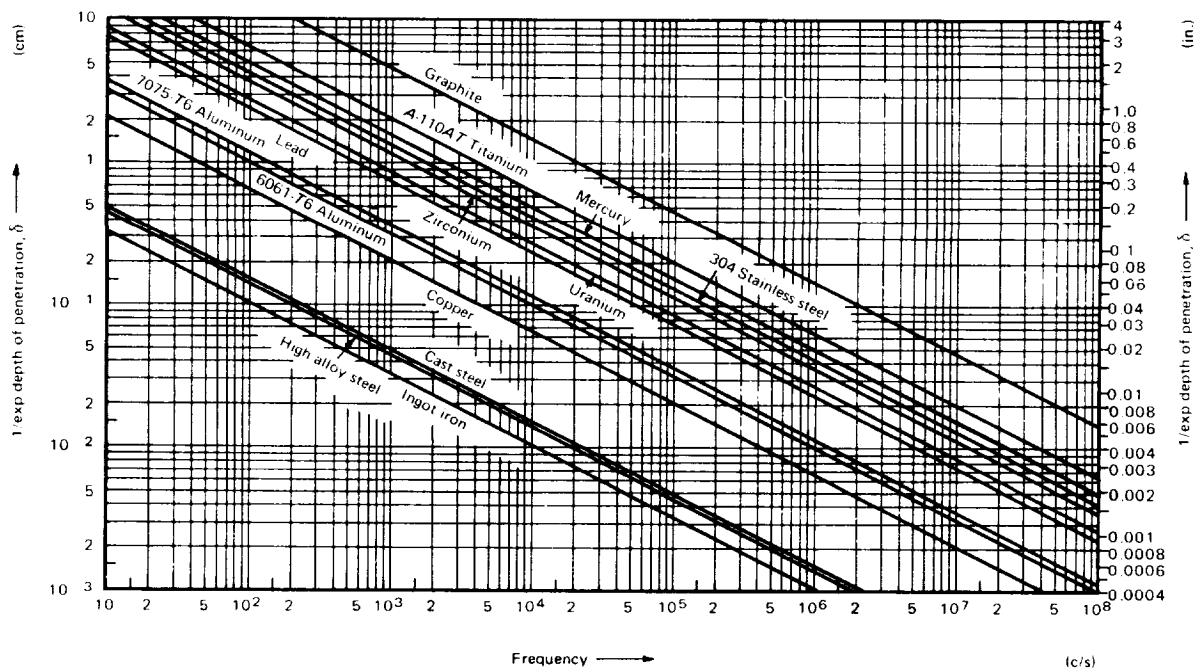


FIGURE 5-6.—Skin depth for frequencies between 10 Hz and 10⁸ Hz in plane conductors of various materials. (Courtesy of The MacMillan Company and Richard Hochschild, Microwave Instruments Co.)

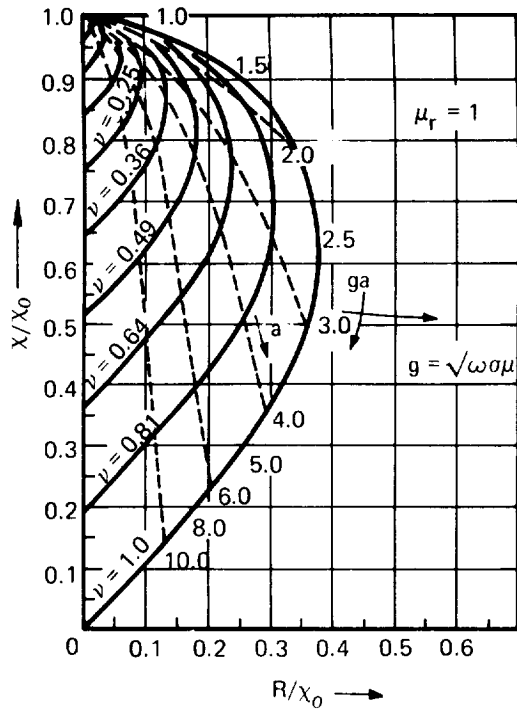


FIGURE 5-7.—Coil impedance for variations in test frequency or conductivity (solid curves) and radius (dashed curves) of nonferromagnetic cylinder surrounded by a long annular test coil. (Courtesy of The MacMillan Company and Richard Hochschild, Microwave Instruments Co.)

reactance components, while figure 5-7 shows the total resistance and reactance components normalized to the reactance, i.e., divided by $X_0 = \omega L_0$, in the absence of a sample.)

The case where the test article is ferromagnetic is represented graphically in figure 5-8. The data are based on the approximations that (1) the permeability is constant (true only for applied fields of very low amplitude), and (2) the filling factor differs negligibly from unity. In figure 5-8, changes in permeability are shown to affect the apparent reactance of the probe coil similar to changes in the radius of the specimen; roughly speaking, lift-off is difficult to discriminate from a permeability decrease. The phase plane effect of discrete flaws, such as cracks, voids, and inclusions, is extremely difficult to estimate theoretically. It is more practical to determine the effects of specific flaws empirically. The operator must be

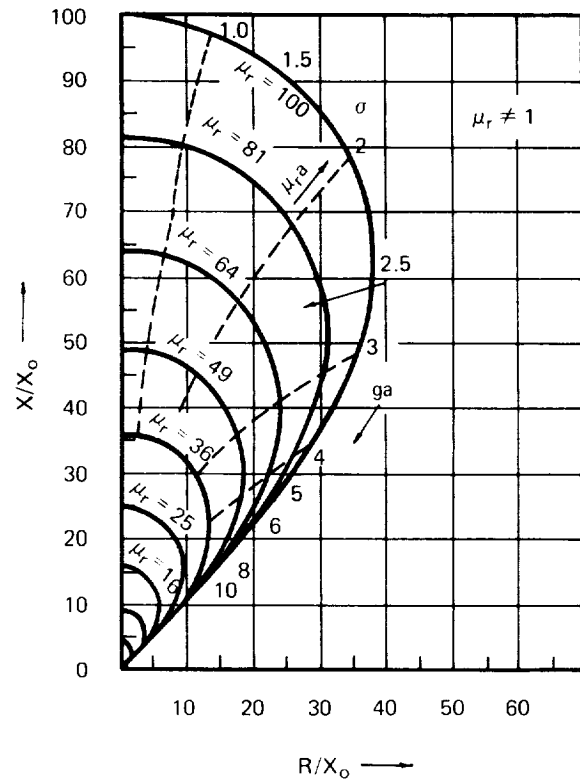


FIGURE 5-8.—Coil impedance for variations in test frequency or conductivity (solid curves) and permeability or radius (dashed curves) of a ferromagnetic cylinder. (Courtesy of The MacMillan Company and Richard Hochschild, Microwave Instruments Co.)

thoroughly familiar with the phase plane "signature" (or whatever corresponding read-out his instrument provides) of various flaws as a probe is passed over them.

The changes in test probe resistance and reactance in terms of flaws or material condition are measured by specially designed electronic instruments. These instruments may be equipped with voltage, current, or phase-measuring circuitry that facilitate measuring probe impedance changes. It is this electrical circuitry that will be discussed in the next section.

ELECTRICAL CIRCUITRY

The impedance changes in a test coil brought about by a crack or inhomogeneity in chemical composition are generally small; for example, on the order of 0.01 percent of the total impedance of the test coil (ref. 5). Measuring this rel-

atively small change with standard absolute impedance-measuring instruments, though possible, is impractical because of the required measuring accuracy. Instead, the test coil is incorporated in some sort of balance network such as an electrical bridge or an electrical filter (fig. 5-9). In a bridge arrangement (fig. 5-9(a)), the test-coil impedance, Z_1 , is compared with the impedance of a standard coil, Z_{STD} . When the bridge is balanced or in its null condition, the potential, V_{ab} , will be zero. For the simple bridge circuit illustrated, the condition of balance may be $R_1/R_2 = Z_1/Z_{STD}$. If the impedance of the test coil is caused to vary slightly, the bridge will be unbalanced, and the voltage, V_{ab} , will increase by an amount depending upon the change of impedance. In the filter arrangement (fig. 5-9(b)), the capacitors, C_1 and C_2 , and the resistor, R_1 , are adjusted in order to tune the circuit for zero (or near zero) output voltage, V_o , for the frequency being used. In the null condition, the circuit acts as a rejection filter for current of the frequency being used. Once having been tuned, any impedance changes in the test coil will detune the

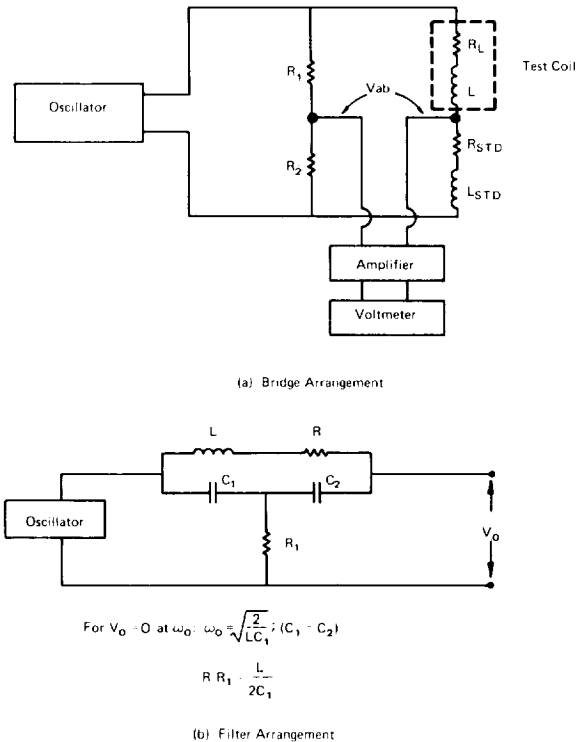


FIGURE 5-9.—Impedance changes of ordinary test coils.

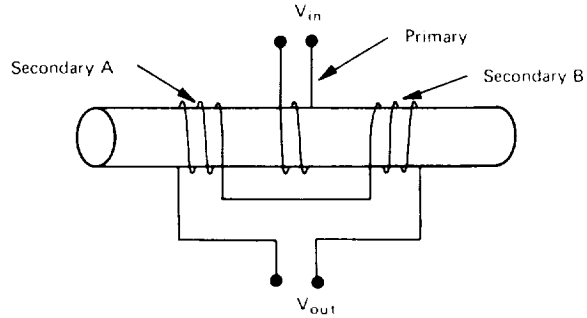


FIGURE 5-10.—The connection of two identical secondary coils in series opposition, causing zero output voltage, V_{out} , whenever identical test material is in both coils.

circuit causing the output voltage, V_o , to increase.

The expected variation in the voltage induced in a secondary coil arrangement of eddy-current testing is extremely small in comparison to the total induced voltage from the magnetizing coil. In the case discussed above, bridge and filter circuits were used, whereas for the case of a primary/secondary test, a differential coil arrangement is used (fig. 5-10). The primary coil establishes the flux in the test item, which generates eddy currents. From the mutual coupling of the primary and the test item, voltages induced in the secondary coils cancel one another and the voltage, V_{out} , tends to be zero (or near zero). Whenever an area containing a discontinuity appears in either of the secondary coils (but not both), the voltage V_{out} will increase.

In some instances, it is desirable to measure the effects of eddy-current flow in a test material by a method that is not dependent upon test coil frequency. Such a measurement using a Hall-effect device is shown in figure 5-11, where

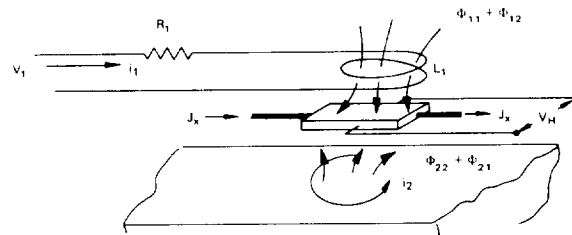


FIGURE 5-11.—A Hall-effect device placed near the generated eddy currents for monitoring changes in the eddy currents caused by discontinuities.

the device has been placed between the magnetizing coil and the test-material surface. The flux just above the surface of the test area of the material is the sum of the flux generated by eddy current, ϕ_{22} , and the flux generated by the primary coil, ϕ_{21} . The voltage, V_H , generated by the Hall-effect device, is found by

$$V_H = R_H \frac{J_x B}{t} \quad (7)$$

where R_H is a characteristic Hall constant of the device material, J_x is the value of a current flowing in the Hall device, t is the thickness of the Hall device, and B is the flux density in the area of measurement. Assuming this device measures over the area A , this equation becomes

$$V_H = \frac{R_H J_x A}{t} (\phi_{22} + \phi_{21}) \quad (8)$$

One successful method of measuring eddy currents with Hall-effect devices is that of so placing the device in the center of the magnetizing coil that its plane is perpendicular to the generating flux. When the magnetizing coil is placed against the test surface, the mutual coupling of the fluxes from the magnetizing coil and the induced eddy currents are both measured. These two interacting fluxes are generally described for this case in terms of the magnetizing field of the coil, which is $H = B/\mu_0$, where μ_0 is the magnetic permeability of air. H_0 is the magnetizing field from the coil. H_r is the magnetic field from the eddy currents, and their vector difference, H_n , is the magnetic field that the Hall-effect device senses. The vector diagram in figure 5-12 illustrates how these fields interact (ref. 6).

Differential arrangements of Hall-effect devices are useful for measuring small changes in eddy currents flowing in the test material. The method for connecting two Hall-effect devices in a differential mode is illustrated in figure 5-13. The amplifiers shown in the figure provide electrical isolation.

EDDY-CURRENT TEST EQUIPMENT

The makeup of eddy-current test equipment ranges from simple portable units to complex automatic or console-type apparatus. Regard-

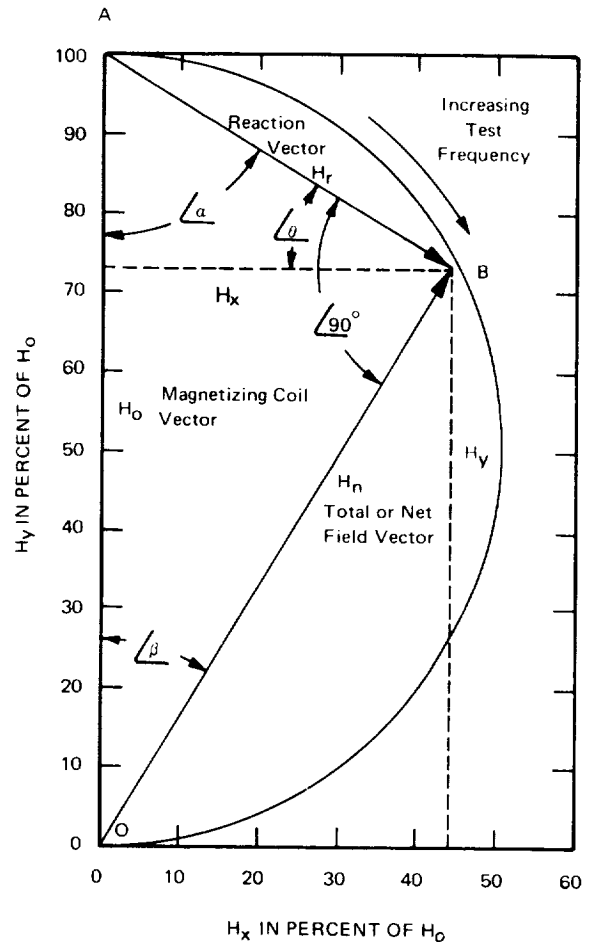


FIGURE 5-12.—The magnetizing field of the coil, H_0 , interacts vectorially with the magnetizing field of the eddy currents, H_r , and results in the net field, H_n . (H_n is measured by the Hall-effect device shown in figure 5-11.)

less of the complexity, however, each system must have at least the following elements:

- (1) A source of magnetic field capable of inducing eddy currents in conductive materials
- (2) A sensor or transducer, sufficiently sensitive to sense minute changes in the magnetic field caused by eddy currents
- (3) A means of interpreting the measured changes in magnetic field, whether it be by monitoring a meter whose reading is proportional to the magnetic field change or an electronic black box that displays readings proportional to phase, magnitude, or modulation of the magnetic field.

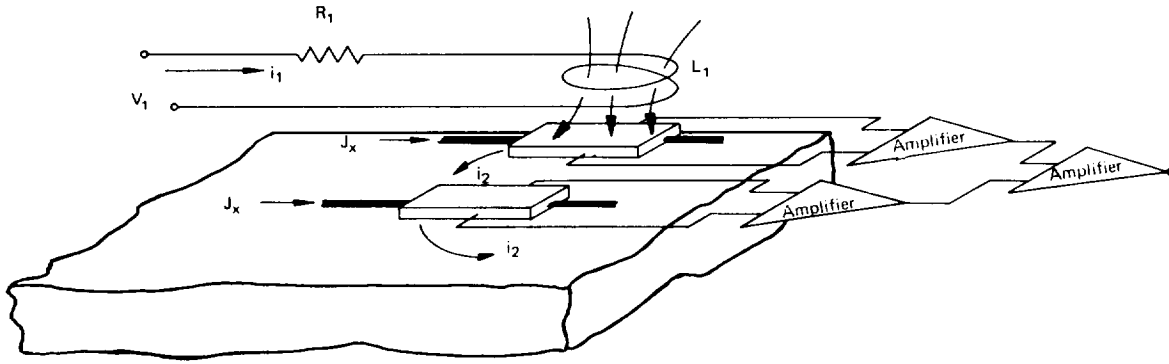


FIGURE 5-13.—Differential connection of Hall-effect devices—a more sensitive means of detecting changes in an eddy-current field than single probes.

Coil Types

In general, all eddy-current units have a coil of wire for generating an alternating magnetic field. These coils may be in the form of long solenoids, short pancake coils, or either ferromagnetic or ferrimagnetic core inductors. In use, they may be placed around, inside, or on the surface of the article being tested. Some typical eddy-current coil configurations are discussed below.

Gap coil.—This type of coil (figs. 5-14 and 5-15) produces a comparatively localized magnetic field. In the coil shown in figure 5-14, shielding is provided by a highly permeable material, usually laminated or made of compressed powder. Another type of gap coil is a wire coil wound on a horseshoe-shaped ferrite or laminated iron yoke so as to shape the magnetic field. The purpose of this coil is to localize the flow of eddy currents in the test object, thereby increasing spatial resolution of flaws. An example of this gap-probe coil is shown in figure 5-15. Here the shape of the probe coil is similar

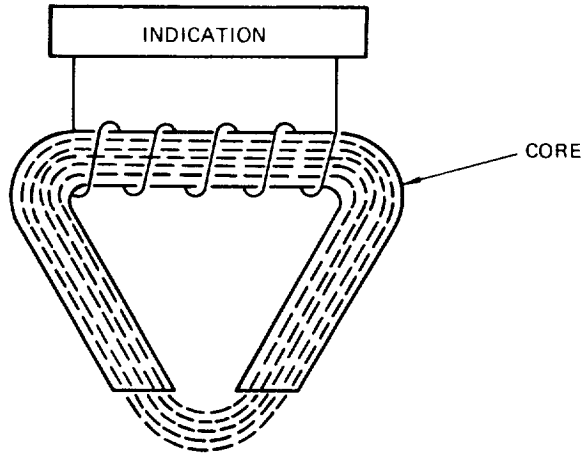
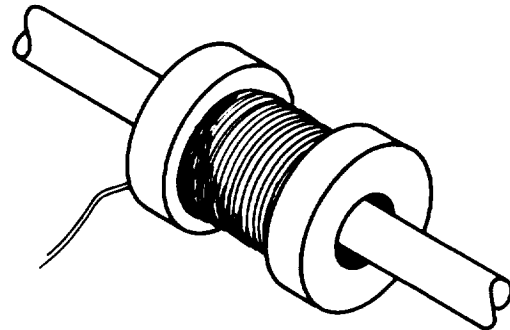
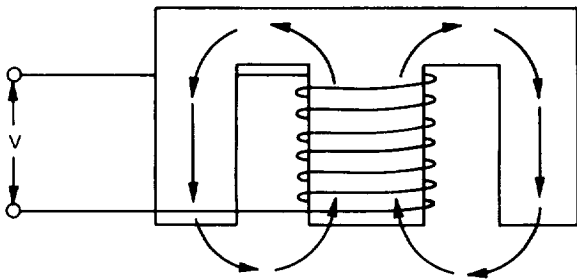


FIGURE 5-15.—Gap probe. (Typical gaps are 0.015 in. wide by 0.125 in. long. They allow very small defects to produce a sizeable indication (ref. 7).)

to that of a magnetic-tape recording head. The shape of the magnetic core, however, can be varied to conform to surface configurations.

Encircling coils.—The encircling coil (fig. 5-16) is so configured as to enclose closely the



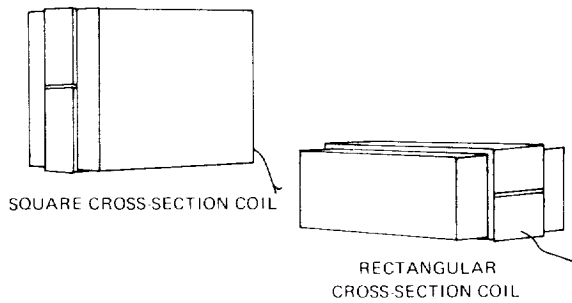


FIGURE 5-17.—Noncircular test coils (ref. 7).

article under test. Such coils should be generally shorter than the test article, for otherwise the test will be undesirably influenced by end effects. The width of the encircling coil, however, will be determined by its intended use. Wide coils covering large areas are used mainly for measuring or monitoring such bulk properties as conductivity, whereas the narrow encircling coils are better suited for locating small discontinuities. Common encircling coils are circular; they may, however, be shaped to fit the test article configuration, as illustrated by the square and rectangular coils shown in figure 5-17.

Probe coils.—The probe coils illustrated in figure 5-18 are intended either for placement directly against the surface of the test article or for insertion inside hollow articles. These coils are wound on nonconductive forms of plastic

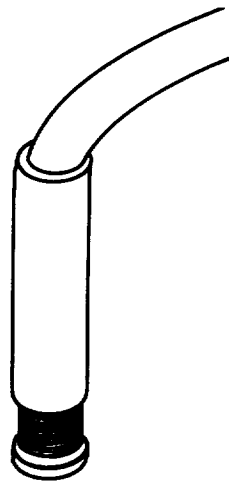


FIGURE 5-18.—Hand-held probe coil.

or phenolic. Some probe coils have cores of ferrite material serving to increase their sensitivity at certain test frequencies.

Direct current saturation coils.—This type of coil (fig. 5-19) is used only for testing ferromagnetic materials. They provide a saturation-level dc magnetic field in the region of an article under test. With dc saturation, the usually undesirable effects of material permeability on the eddy-current test may be substantially removed. Whenever the test material moves through the dc field generated by the saturation coils, eddy currents will be generated. Usually, however, these dc field-induced eddy currents may be disregarded.

The most common method of inducing eddy currents with a coil is to pass an alternating current through the coil so that the resultant magnetic field varies in time. According to the

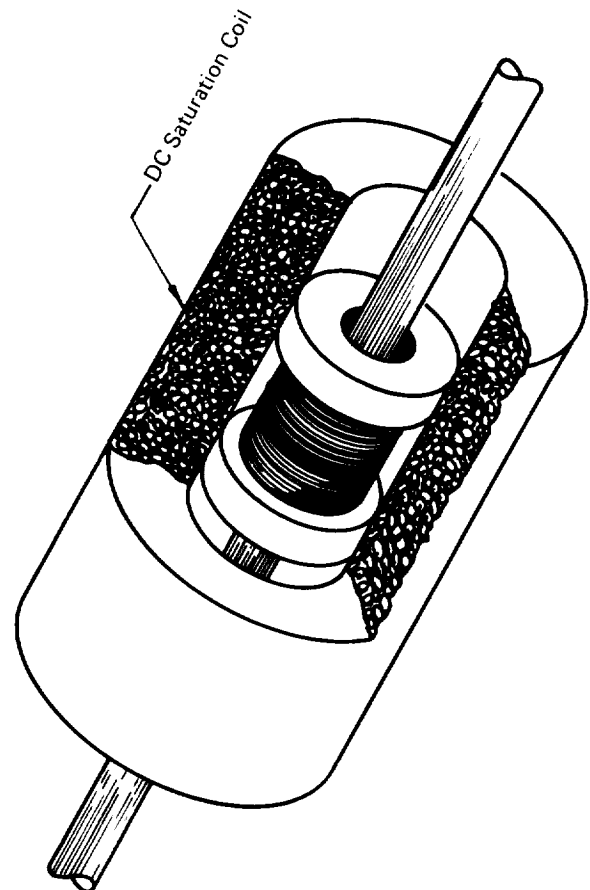


FIGURE 5-19.—Direct-current saturation coil.

intended function and mode of operation, this current may be either sinusoidal or some combination of waveforms. Several different types of current waveforms are shown in figure 5-20. Of these, the single frequency sinusoidal current is most commonly used. Since the magnetizing field varies proportionately to the current, the field also will be sinusoidal. Depending upon the application, frequencies of sinusoidal fields may range from 1 to 2 Hz up to several MHz.

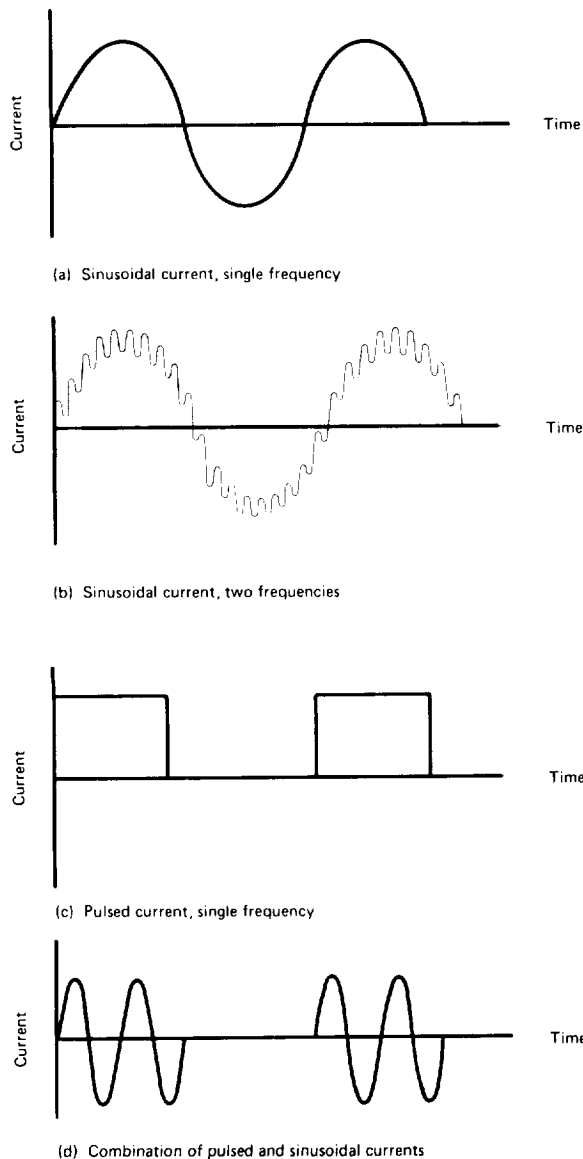


FIGURE 5-20. ---Representative current waveforms used in eddy-current testing.

Some units have two superimposed currents of significantly different frequencies flowing in the same test coil to induce eddy-current flow. For example, one current may vary at the rate of 1 Hz and the other current at 200 Hz. The lower frequency provides conventional eddy-current information, and the higher frequency (being very limited in penetration into the material surface) provides lift-off information, which can be used electronically to compensate for variations in coil-to-specimen spacing.

Pulsed fields have also been used successfully for eddy-current testing. A voltage pulse is impressed on the eddy-current coil, and, after the impressed voltage has subsided, an induced voltage from the decaying eddy currents is monitored. This method takes advantage of the fact that eddy current flow does not start and stop with the pulsed field. Instead, it lags slightly in time after the voltage pulse is gone, and eddy currents will still be flowing for a short time. Further, a pulsed current is made up of a spectrum of frequencies, so that there is a low-frequency component present in the eddy-current information, which is very useful for determining such measurements as the thickness of a plating.

Eddy-Current-Field Measuring Device

At the present time there are three common ways to sense the secondary electromagnetic field produced by eddy currents. These are: (1) measuring the apparent changes in electrical impedance of the coil that generates the primary field; (2) measuring the voltage induced in a separate coil that is sensing the magnetic field through transformer action; and (3) sensing the eddy-current magnetic field directly with a Hall-effect device.

Whenever changes of the eddy-current magnetic field are being monitored by measuring the magnetizing coil impedance, the eddy-current coil may be wound in either an "absolute" or a "differential" form. The distinction between these two forms for the encircling coil, probe coil, and inside coil is illustrated in figure 5-21. In the absolute form, the coil is wound continuously in the same sense and only its im-

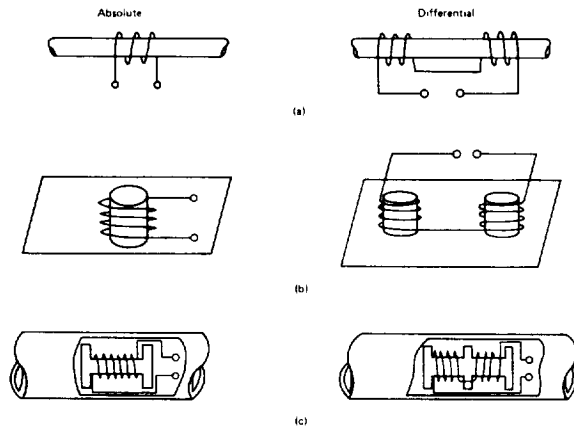


FIGURE 5-21.—Absolute and differential coil-winding arrangements for observing eddy-current effects on test-coil impedance.

pedance is monitored. The differential coil comprises two absolute coils connected in series opposition; because of the canceling effect of this arrangement, impedance changes which are common to both coils are not seen.

Whenever eddy-current changes are being monitored through transformer action with more than one coil, the coils may also be connected in an absolute or differential arrangement as illustrated in figure 5-22. With the absolute arrangement, two coils are wound like

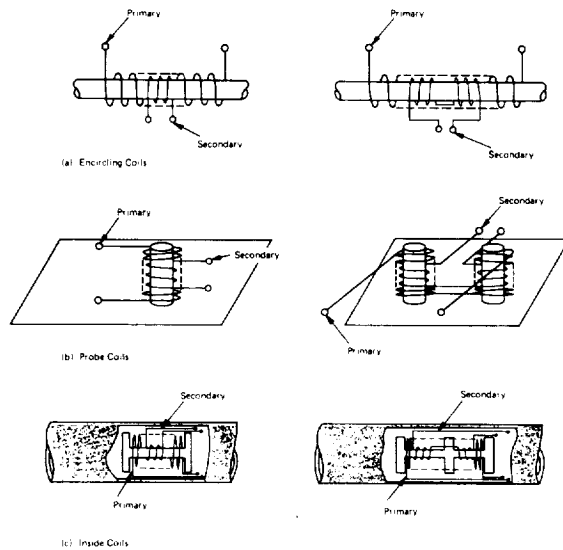


FIGURE 5-22.—Absolute and differential coil-winding arrangements for observing eddy-current effects by measuring voltages induced in secondary coils.

a simple transformer wherein the secondary coil has an induced voltage proportional to the voltage of the primary coil, and eddy-current perturbations in the test specimen cause changes in this secondary-coil voltage. With the differential arrangement, three coils are wound concentrically, one serving as a primary and the other two connected in series opposition serving as a secondary. Whenever there is no defect present with the differential coils, the voltages of the two secondary coils cancel. On the other hand, when the eddy currents in the vicinity of either secondary coil differ from those in the vicinity of the other coil, a voltage difference will be generated at the output terminals.

When Hall-effect devices are used to monitor changes in eddy currents, they also may be employed in either an absolute or differential manner. Since the output voltages of these devices are proportional to the magnetic field being sensed, the changes in eddy current in the absolute arrangement are monitored by noting the fluctuations in the total voltage of the Hall-effect device; whereas, in the differential arrangement, the same magnetic field changes sensed by both elements produce nominally cancelling effects (and a null net-output signal voltage) except when a flaw is sensed. The absolute and differential arrangements for Hall-effect devices were illustrated earlier in figures 5-11 and 5-13.

Interpretation of Eddy-Current Indications

Once eddy currents have been generated and have caused changes in the original magnetizing field which have been detected by one of the methods listed above, the changes may be interpreted by:

(1) *Impedance analysis*.—Measuring net changes in the magnitude of the induced eddy current field.

(2) *Phase analysis*.—Measuring net changes in the time phase of the induced eddy-current field with respect to the test-coil voltage, as well as measuring the magnitude changes.

(3) *Modulation analysis*.—Measuring the rate of change of phase or magnitude of the eddy-current field in instances where the test article is in motion with respect to the test coil.

Measuring only the net changes in magnitude of the induced eddy-current field, whether by observing impedance changes in the test coil or the voltages induced in a secondary coil, is generally referred to as impedance testing. This is the least complicated method of analysis, and could, for instance, use a bridge circuit with the test coil forming one of the bridge legs, and a meter connected to the bridge output terminals.

In the phase-analysis method, electronic circuitry is provided which allows comparison of eddy current field with the voltage applied to the primary test coil. Whenever the test coil is used as one leg of an electrical bridge network, a phase-shifting network and a phase-sensitive voltmeter may be connected to provide phase analysis (fig. 5-23).

Measuring the rate of change of either the phase or magnitude of the eddy-current field is modulation analysis. The chief restriction of this method is that either the test item or the testing coil must be in motion. The method is frequently employed in the inspection of aluminum tubing. Two defective conditions that occur in such tubing are (1) cracks in the base metal, and (2) out-of-tolerance dimensions over a significant length. Referring to figure 5-24(a), it can be assumed that tubing is being inspected by passing it through a pair of encircling coils connected as shown. The recording of the bridge output may appear similar to that shown in figure 5-24(b). By adding electronic filters between the bridge output and the recorder, it is possible to alter the recording so that results from only variables of interest will

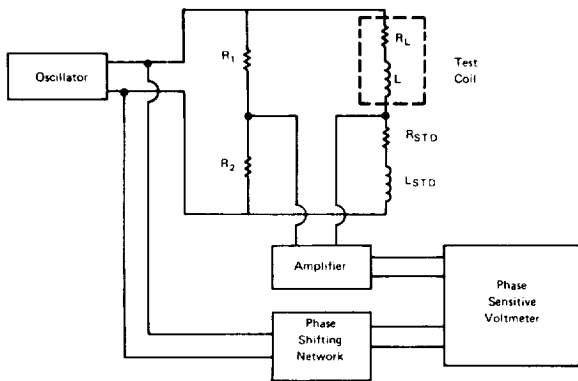


FIGURE 5-23.—Equipment for measuring changes in eddy currents by phase-analysis methods.

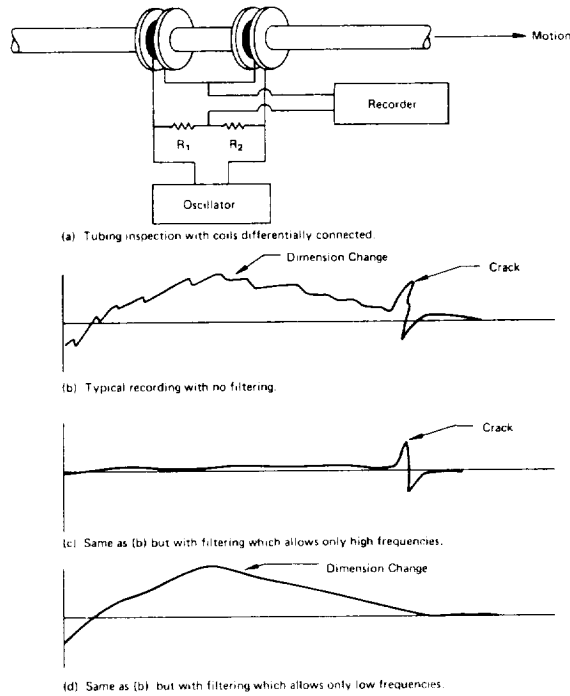


FIGURE 5-24.—The modulation analysis method of eddy-current inspection.

be recorded. For instance, a filter that will pass only high frequencies may be inserted for finding small flaws such as cracks or pits. This type of recording will appear as shown in figure 5-24(c). On the other hand, a filter might be inserted which passes only low frequencies to find gross defects such as dimensional or heat-treat variation. A recording of this might resemble that of figure 5-24(d).

SELECTING AN EDDY-CURRENT INSPECTION METHOD

Choosing the best eddy-current technique and properly applying it requires careful planning. To ensure that the inspection will have the best chance for repeatable success, at least the following steps discussed in the succeeding sections should be performed.

Determining the Optimum Test Frequency

From a knowledge of the test article's material, the expected flaw size, the desired depth of inspection, and the required rate of inspection, it is possible to estimate an optimum eddy-cur-

rent frequency (ref. 8). Charts like those of figure 5-6 should be consulted to determine which frequency will allow inspection at the desired depth. A further consideration in choosing frequency is that if the test article is moving too fast relative to the inspection probe, there may not be sufficient time for a complete cycle of the applied magnetic field. Therefore, there would be inadequate generation of eddy currents while the article is in the test area. From this it is obvious that there is both an upper and lower limit on the test frequency.

When using the eddy-current method to measure surface effects, higher frequencies should be chosen. For example, researchers at NASA's Marshall Space Flight Center successfully related the surface stress corrosion of 7079-T6 and 2219-T31 aluminum to eddy-current measurements. In their experiments, a 6-MHz magnetizing current was used to measure the electrical conductivity of specially prepared samples. Data from their experiments showing electrical conductivity over a 9-day exposure to corrosion are presented in figures 5-25 and 5-26 (ref. 9).

Selection of Instrumentation

Once the test frequency has been established, choice of the instrument will be based on whether or not it can operate at the correct frequency. Some devices operate at one predetermined frequency, whereas others have frequency adjustments. If a single-frequency instrument is to be used, one must be chosen

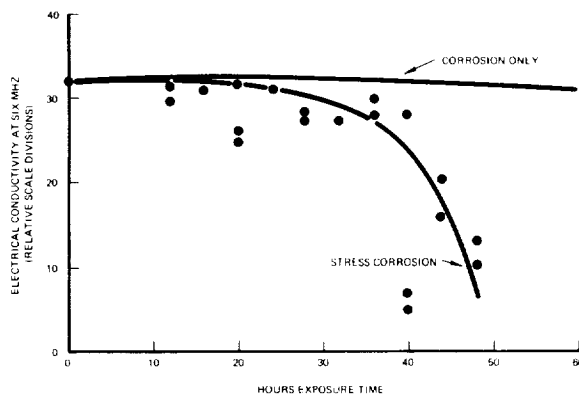


FIGURE 5-25.—Eddy-current conductivity measurements of 7079-T6 aluminum showing degradation by stress corrosion.

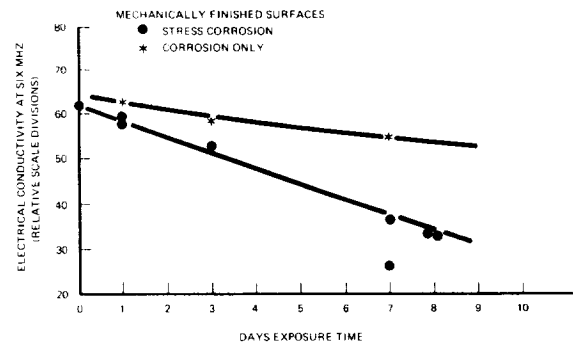


FIGURE 5-26.—Eddy-current conductivity measurements of 2219-T31 aluminum showing degradation by stress corrosion.

having a frequency as close as possible to the optimum frequency for the intended test.

Selection of Test Coil

With most commercial eddy-current equipment, various sizes and shapes of test coils are supplied and are expressly designed for use with that equipment. From these coils, the operator must choose the one which (1) is most closely suited to the geometry of the test article, and (2) is capable of establishing an eddy-current pattern of a size sufficiently small to be consistent with the dimensions of the smallest flaw of interest. Wherever there are no standard coils with the test instrument or the standard transducers are of the wrong geometry for the test article, the user is obliged to design and build a transducer which must (1) be compatible with the instrument, (2) conform closely to the shape of the test article, and (3) be sufficiently sensitive at the required test frequency.

The miniature test coils shown in figure 5-27 are novel examples of coils especially designed for NASA for inspecting plated holes in printed wiring boards (ref. 10).

Automated Scanning

For continuous inspection, if the configuration of the test article permits, the operation may be automated. Ordinarily this will require a mechanism which allows the article to move past the test transducer in a repeatable fashion. Depending upon the sensitivity required, the

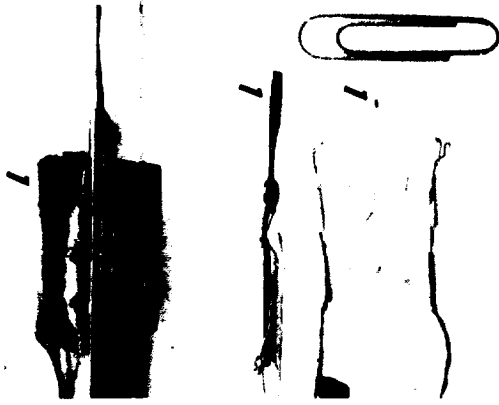


FIGURE 5-27.—Miniature test coils.

mechanism may be either (1) a rudimentary arrangement whereby the test article is simply moved through the magnetic field of the test transducer, or (2) for more stringent requirements, the test article may be precisely positioned and held fixed while an electromechanical

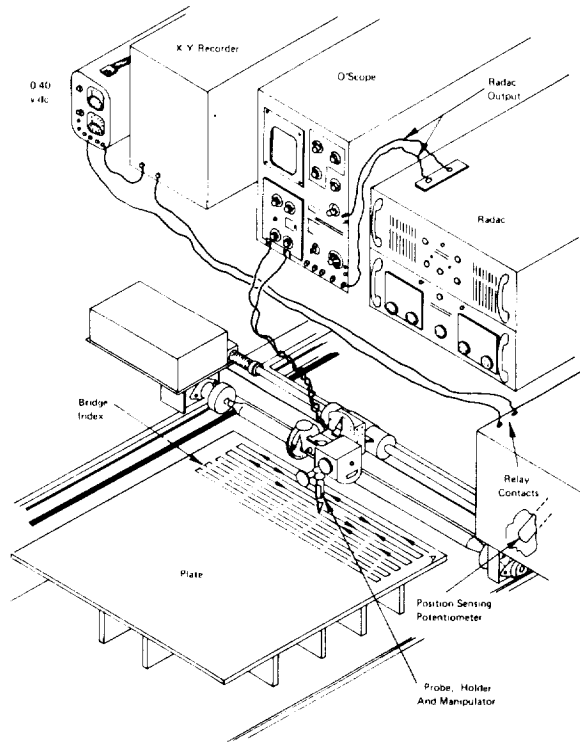


FIGURE 5-28.—Eddy-current fixturing for inspection of cylindrical-tank-wall skin sections of the Saturn V/S-1C first-stage booster. (Courtesy of American Society for Testing and Materials.)

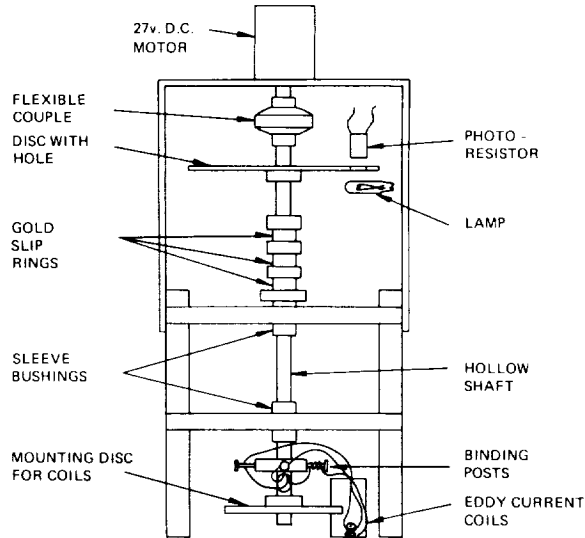


FIGURE 5-29.—A rotating eddy-current probe used to measure the length and depth of discontinuities discovered by the system of figure 5-28. (Courtesy of American Society for Testing and Materials.)

scanning system moves the transducer over it. The latter arrangement reduces the possibility of the transducer detecting movement or misalignment of the specimen rather than flaws.

An example of special fixturing for the inspection of cylindrical-tank-wall skin sections of the first stage booster Saturn V/S-1C is shown in figures 5-28 and 5-29. The contractor, under the direction of Marshall Space Flight Center, assembled this system using off-the-shelf equipment to inspect aluminum skin panels nominally 0.200 in. thick. Inspection is accomplished in two steps. First, surface discontinuities whose depths exceed 5% of the part thickness are located with rapid (120 ft/min) linear scan (fig. 5-28); and second, the length and depth of the discontinuity are measured with a rotating eddy-current probe device shown in figure 5-29 (ref. 11).

Adjustment to a Reference Standard

After the instruments and fixturing have been adjusted and fitted together to form the inspection system, a reference specimen should be passed through the system to verify that the flaw (or variable of interest) may be measured. When inspecting tubing, for example, the mini-

imum defect size should be specified; the reference standard should be a piece of tubing of the same size and material as that being inspected, and should contain defects of the size and type expected to be found in the test specimen. These defects should be at least as small (and some smaller) as the minimum acceptable by the test criteria. Passing the reference standard through the inspection systems will indicate whether the system is capable of locating the required flaws.

Setting the Sensitivity

Upon confirming that the test system can detect the minimum flaw, testing system controls should be so set that test indications of flaws and variations within acceptable limits do not register or actuate any alarm circuits. This operation usually consists of adjusting a threshold level on the instrument panel in such a way that, when the reference standard is placed in the system, flaws below the reject criteria are not detected, whereas flaws of reject size and larger actuate an appropriate alarm or marker. A typical sensitivity control located on an eddy-current instrument panel is shown on the drawing of the MSFC-developed instrument of figure 5-30 (ref. 12). Here the test coil is located inside the instrument housing. The instrument has been used successfully to measure the thickness, up to 14 in., of spray-on foam insulation used on the Saturn V second stage. The foam is backed by the aluminum vehicle skin (ref. 13).

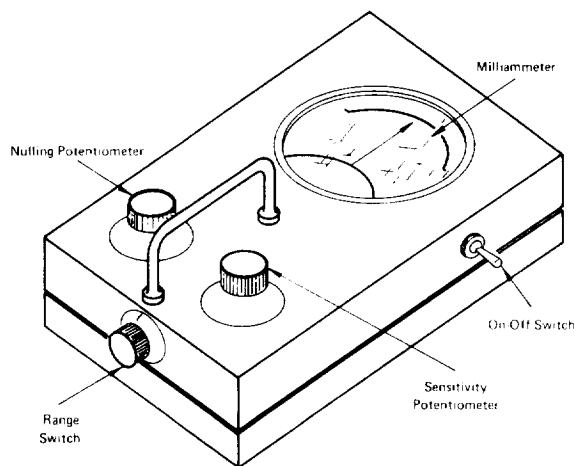


FIGURE 5-30.—MSFC eddy-current instrument.

Testing and Interpretation of Indications

With all the above operations completed, the inspection may begin. Test articles should be introduced into the system in exactly the same manner as that used in establishing the reference standard and setting the sensitivity. Whenever the test instrument indicates that a flaw or some type of undesirable variation is present, an immediate investigation should be made to determine the type of defect and whether or not the part should be rejected. This procedural step is usually needed with eddy-current testing, because there is seldom a simple relationship between output indications and the actual discontinuity within the article. In most cases, it is beneficial to establish a relationship between the eddy-current indication and the magnitude of the variable under investigation. Usually a record of measurements is kept and subsequently plotted as illustrated in figure 5-31, which shows the results of eddy-current measurements of conductivity versus ultimate strength for 2014-T6 aluminum alloy. In this example, data were gathered to provide a quantitative measure of the amount of degradation in the heat-affected zone of dual-thickness weldments used in fabricating the Titan vehicle (ref. 14).

Periodic Verification of Calibration

The test system should be periodically checked to verify the accuracy of the threshold setting on the sensitivity control. This is done by simply passing the reference standard through the system at predetermined time intervals and confirming that the alarms or markers still function as originally adjusted. If the sensitivity has changed, the setting should be corrected, and all material inspected since the last calibration verification should be reinspected.

ADVANTAGES AND LIMITATIONS

The eddy-current method has the advantages listed below.

- (1) Under controlled conditions it provides an accurate measure of conductivity
- (2) The indication of flaws or material condition is immediate

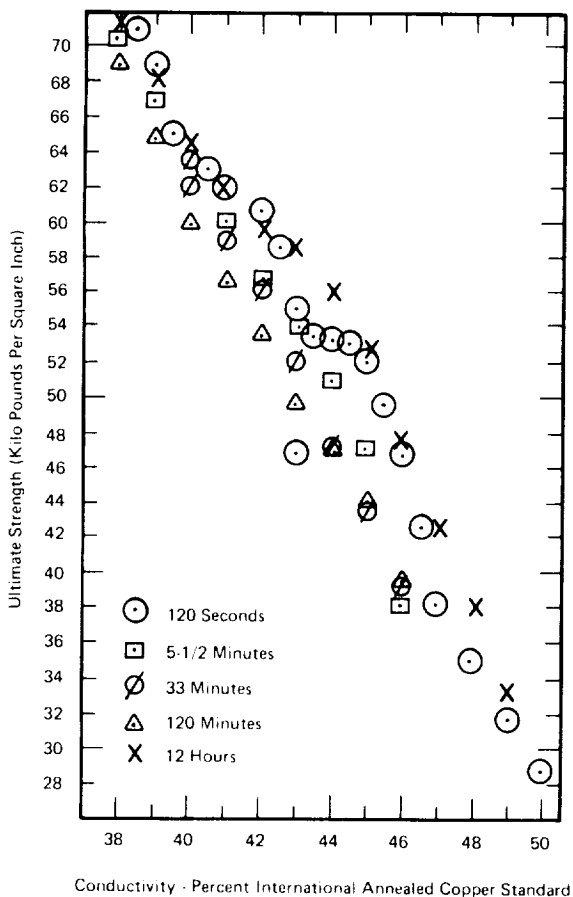


FIGURE 5-31.—Plot of eddy-current measurements of conductivity vs ultimate strength of overheated 2014-T6 aluminum alloy. (Courtesy of Martin Marietta Corp. and the American Society for Quality Control.)

(3) It may be substantially automated
 (4) It is capable of inspecting at high speeds
 (5) With miniature test transducers, the area of inspection can be reduced to detect discontinuities as small as 0.00006 sq in. (ref. 7)

(6) Mechanical contact with the test article is not required, except in special cases.

Limitations of the eddy-current test method include principally the items given below.

(1) Equipment indication is influenced by more than one variable, often making interpretation ambiguous

(2) Because of skin effect, inspection is generally restricted to depths less than about $\frac{1}{4}$ in.

(3) The results of testing ferromagnetic materials may be obscured by changes in the permeability of the test specimen.

REFERENCES

- LIBBY, H. L.: Basic Principles and Techniques of Eddy Current Testing. *Nondestructive Testing*, vol. 14, no. 6, 1956, pp. 12-18 and 27.
- STANFORD, E. G.; AND FEARON, J. H.: *Progress in Nondestructive Testing*. Vol. 1. The Macmillan Company (New York), 1959, pp. 59-109.
- HOLT, R. C.: Eddy Current Testing of Small Diameter Tubing. Knolls Atomic Power Laboratory, General Electric Company, pp. 119-128.
- DOLL, H. G.: Introduction to Induction Logging and Application to Logging of Wells Drilled with Oil Base Mud. *Journal of Petroleum Technology*, vol. 1, no. 6, 1949, pp. 148-162.
- GRANEAU, P.; AND SWANN, S. A.: Electromagnetic Fault Detection on Non-Ferrous Pipes.
- McMASTER, R. C.: A New Eddy Current Nondestructive Test. *Metals Engineering Quarterly*, vol. 6, May 1966, pp. 32-49.
- ANON.: Classroom Training Handbook—Eddy Current Testing. NASA CR-61230, 1967. (N68-28792)
- McMASTER, R. C.: *Nondestructive Testing Handbook*. Vol. I and II. The Ronald Press Company (New York), 1959, p. 36-13.
- CLOTFELTER, W. N.; BANKSTON, B. F.; AND ZACHARY, E. E.: The Nondestructive Evaluation of Stress-Corrosion Induced Property Changes in Aluminum. NASA TM X-53772, Aug. 1968.
- BLANCHE, J. F.: Nondestructive Testing Techniques for Multilayer Printed Wiring Boards. Annual Western Metal and Tool Exposition and Conference, Society for Nondestructive Testing, American Society for Metals, and American Society of Tool and Manufacturing Engineers (Los Angeles), Mar. 1967.
- MUSIL, F. J.: Eddy Current and Ultrasonic Techniques for Inspection of Large Parts. *Journal of Materials*, vol. 2, no. 1, 1967, pp. 65-80.
- ANON.: Detection and Location of Metallic Objects Embedded in Nonmetallic Structures. NASA Tech Brief 68-10183, June 1968.
- BROWN, R. L.: Potential Biomedical Applications of Saturn Nondestructive Test Methods. *J. of the Assoc. for the Advancement of Medical Instrumentation*, vol. 3, no. 5, 1969, pp. 154-161.
- RUMMEL, W. D.: Development and Use On an Eddy Current Conductivity Technique for Monitor of Heat Effects in 2014 Aluminum Alloy Weldments. *Trans. 20th National Conv., American Society for Quality Control*, June 1-3, 1966, pp. 628-639.

|

PRECEDING PAGE BLANK NOT FILMED

CHAPTER 6

Thermal and Infrared Testing

Robert E. Engelhardt and William A. Hewgley

In the comprehensive sense, thermal testing comprises all test methods which depend upon heat sensors. This chapter, however, is restricted to two topics: (1) the detection of defective components or devices which are active heat sources, i.e., they operate at temperatures above ambient, and (2) the detection and characterization of flaws in components or structures that are thermally passive, but which can be nondestructively heated or cooled.

Methodologically, the chapter centers about (1) the measurement of temperature—thermometry and (2) the mapping of isotherms (contours of equal temperature) over a surface—thermography. The techniques fall into two categories: (1) direct contact, in which a thermally sensitive device or material is placed in physical and thermal contact with the article under test, and (2) noncontact techniques that depend upon thermally generated electromagnetic energy radiated from the test article. At moderate temperatures, this is predominantly the infrared. Hence, infrared testing is the most important branch of noncontact thermal testing.

Flaw detection by thermography depends not upon the absolute accuracy of temperature measurement, but rather upon differences in temperature on the surface of the test article. The present workability of thermography for nondestructive evaluation depends on advances in the precision of infrared radiometers, and

improved contact thermographic coatings. Advances in radiometry have been paced principally by the introduction and improvement of solid-state infrared detectors, cryogenically cooled to reduce self-generated noise. Contact thermography has been revitalized by the introduction of low cost liquid crystals and other thermochromic compounds for indicating small thermal gradients in convenient temperature ranges.

As a means of flaw detection, thermography depends upon the occurrence of thermal gradients at the surface of the test article, a flaw being an anomaly in the material's thermal conductivity. For bulk metals, nondestructive test methods using electrical conductivity, magnetic permeability, or ultrasonics are, as a rule, more sensitive than thermography. For certain structures, however, such as bonded honeycomb, or for dielectric materials, thermography is often the method of choice.

PHYSICAL PRINCIPLES

Heat Transfer

Any closed system, with all components in thermal equilibrium, has a single absolute temperature T . Hence, to derive useful information about a component by thermal measurements, a state of thermal nonequilibrium must be pro-

duced in it. Such a state may be invariant with time, or nonstationary (transient or periodic). Thermal testing of thermally passive articles usually involves raising the temperature of a portion of the article above ambient, establishing a steady-state heat flow, and then determining the resulting steady-state temperature distribution. To establish a favorable pattern of heat flow, it is often useful to bring the article into contact with thermal sources, heat sinks, conductors, and insulators. The basic physical laws, applied in designing a thermal test, are those governing the conduction of heat in bulk materials and the transfer of heat from surfaces. While convection may often be of practical importance, it must usually be either suppressed or accounted for arbitrarily.

The basic equation governing the conduction of heat in an isotropic body is

$$\mathbf{I} = -k\nabla T(x, y, z, t) \quad (1)$$

where T is the temperature of the body as a function of time and position within the body, k is the thermal conductivity of the material measured, for example, in

$$\frac{\text{W}}{\sqrt{\text{cm}^2} \cdot \sqrt{^\circ\text{C}/\text{cm}}}$$

\mathbf{I} is the directed heat current (in w/cm^2) and ∇ is the gradient operator. For heat conduction in a single direction along a uniform temperature gradient, equation (1) reduce to the familiar elementary statement:

$$I = k \left(\frac{T_{\text{high}} - T_{\text{low}}}{L} \right) \quad (2)$$

where T_{high} and T_{low} are the temperatures at two points along the direction of heat flow, separated by distance L .

For homogeneous materials, equation (1) is equivalent to the diffusion equation:

$$\rho c \frac{\partial T}{\partial t} = k \nabla^2 T + Q \quad (3)$$

where ρ is the mass density of the material, c is its specific heat, and Q is the amount of heat generated internally in a unit volume of the material.

In most cases an exact solution of equation (3) is practically impossible. The following simplified example in which equation (2) is used serves, however, to illustrate some important points. Consider a thin slab of material, homogeneous except for an isolated defect, as illustrated in figure 6-1. The thermal conductivity of the basic material is represented by k , and that of the imbedded flaw material by k' . For a thermal test, the material is placed in contact with a heat reservoir that maintains the contacting surface at a constant temperature, T_H . The opposite surface is exposed to ambient conditions, which are taken for convenience to be 0°C . Heat is conducted through the specimen, and removed by radiation, conduction, and air convection from the exposed surface. The expected distribution of temperature over the exposed surface is estimated as follows: first, assume that the lateral dimensions of the flaw are large compared to the thickness of the material, thus permitting the lateral heat conduction to be ignored; and second, assume that the temperature of the exposed surface is sufficiently low to allow Newton's law of cooling to be applied. This law is simply a statement that the rate of cooling of a surface is proportional to the difference between its temperature and that of its surroundings, which is found to be true (regardless of the mode(s) of cooling) for small temperature differences. With these approximations the continuity-of-heat-flow equations for the basic material and flaw material become

$$k \left(\frac{T_H - T_i}{l} \right) = hT \quad (4)$$

and

$$k' \left(\frac{T_H - T_i}{l'} \right) = k \left(\frac{T_i - T'}{l} \right) = hT' \quad (5)$$

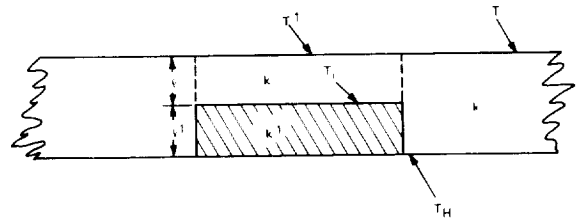


FIGURE 6-1.--Heat-flow parameters in a thin slab containing an isolated defect.

where h is a proportionality constant, the value of which depends upon the details of the cooling mechanism. Equations (4) and (5) lead to the relation:

$$\frac{T' - T}{T} = \frac{\left(\frac{k'}{k} - 1\right)}{\frac{k'}{h\ell'} + \left(1 + \frac{\ell k'}{\ell' k}\right)} \quad (6)$$

As expected, equation (6) indicates that $(T' - T)$ vanishes (i.e., there is no thermal indication of the flaw) if k' equals k or if ℓ' vanishes.

As a concrete example, suppose the flaw is a thin air-filled cavity in a metal, with k' much smaller than k . (The thermal conductivity of air is negligible compared to that of a bulk metal.) For this case, equation (6) reduces to the approximate relation:

$$\frac{T' - T}{T} = \frac{-1}{\frac{k'}{h\ell'} + 1} \quad (7)$$

If the upper surface is cooled entirely by radiant transfer of heat, and if the surface is ideally nonreflective, the cooling parameter, h , has the approximate value 6×10^{-4} W/cm² °C; the thermal conductivity of air is approximately 3×10^{-5} W/cm/cm² °C. Hence, the ratio k'/h , for this example is 5×10^{-2} cm. Equation (7) now reads:

$$\frac{T' - T}{T} = \frac{-1}{\frac{5 \times 10^{-2}}{\ell'} + 1} \quad (8)$$

For $(T' - T)/T$ to have an appreciable value, ℓ' must not be negligible compared to the characteristic length 5×10^{-2} cm. If, for example, ℓ' is equal to this characteristic length, then T' is equal to one-half of T . If ℓ' is one-tenth of this length, T' is 0.91 T . If ℓ' is only 1% of 5×10^{-2} cm, T' differs from T by only 1%.

While the foregoing model is crude, it does emphasize a major technical difficulty encountered in flaw detection by thermal means; what might seem a rather sharp discontinuity may prove to have a weak thermal signature. Equation (7) indicates that for a given value of the ratio k'/ℓ' , the signature is improved by mak-

ing the value of the cooling parameter h as large as possible. The value of h is not appreciably affected by raising the temperature, T_H , of the heated surface of the test article, but is improved by making the surface as nonreflective as possible, and by augmenting radiant cooling by forced circulation of air over the test surface.

Infrared Radiation

Infrared radiation is that portion of the electromagnetic spectrum that ranges from the low end of the visible spectrum to the microwave frequencies. Therefore, the infrared wavelengths range from slightly below 0.7μ (0.6943μ , the wavelength of a ruby laser, is just within the visible range) to around 1000 microns (fig. 6-2).

All bodies at a temperature above absolute zero spontaneously radiate electromagnetic energy. The spectral distribution of the radiation given off is described by Planck's equation:

$$W_\lambda = 2\pi \times 10^{-9} hc^2 / \lambda^5 (e^{hc/\lambda k T} - 1)$$

where

- W_λ = Watt/m²/m μ
- h = Planck's constant = 6.6252×10^{-34} J sec
- c = speed of light = 2.99793×10^8 m/sec
- λ = wavelength, m
- e = natural logarithm base = 2.71828
- k = Boltzman's constant = 1.3804×10^{-23} J/°K
- T = absolute temperature, °K.

This formula evaluates the amount of emitted radiation given off by a body at a given temperature, T , per increment of wavelength, this increment being a millimicron. The graph of the Planck equation for a blackbody at various temperatures is shown in figure 6-3. Figure 6-3 and Planck's equation apply only to blackbodies. A perfect blackbody does not actually exist in nature but is merely a name for a body that absorbs all radiation incident upon it, and con-

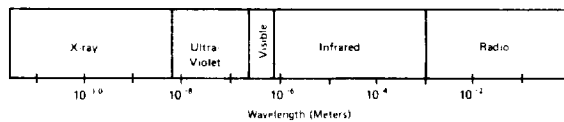


FIGURE 6-2.—The electromagnetic spectrum.

versely emits the maximum possible amount of radiation at any given temperature. By definition, it has an emissivity of unity and is said to be a perfect emitter; all other objects emit at some fraction of a blackbody. Objects made of shiny metal may have an emissivity as low as 0.02, while dull black materials may have an emissivity greater than 0.9.

Referring again to figure 6-3, it is observed that as the temperature rises, the peak radiation shifts toward the shorter wavelengths. This can be determined by observing the color of a body changing from red to yellow to blue as it is heated. This frequency shift is described by Wien's displacement law,

$$\lambda_m = \frac{2897.9\mu}{T}$$

where

λ_m = peak radiation wavelength, μ
 T = absolute temperature, $^{\circ}\text{K}$.

Thus, by the use of the Wien displacement law, wavelength at which the radiation of a body will be at a maximum can be calculated.

The total amount of radiation which a blackbody will emit at a given temperature is the integral of the Planck distribution and is given by the Stefan-Boltzmann equation:

$$W = \sigma T^4$$

where

W = radiated power, W/m^2
 σ = proportionality constant = 5.6699×10^{-8}
 $\text{Wm}^{-2} (\text{K})^4$
 T = temperature, $^{\circ}\text{K}$.

This equation is also used for a very close approximation for bodies that are not black by writing it as

$$W = E\sigma T^4$$

where

E = emissivity.

This equation is not entirely accurate because it implies that the emissivity of a body is independent of its temperature, which is not true. Since emissivity generally changes very little with temperature, however, this equation normally forms the basis for the statement that the

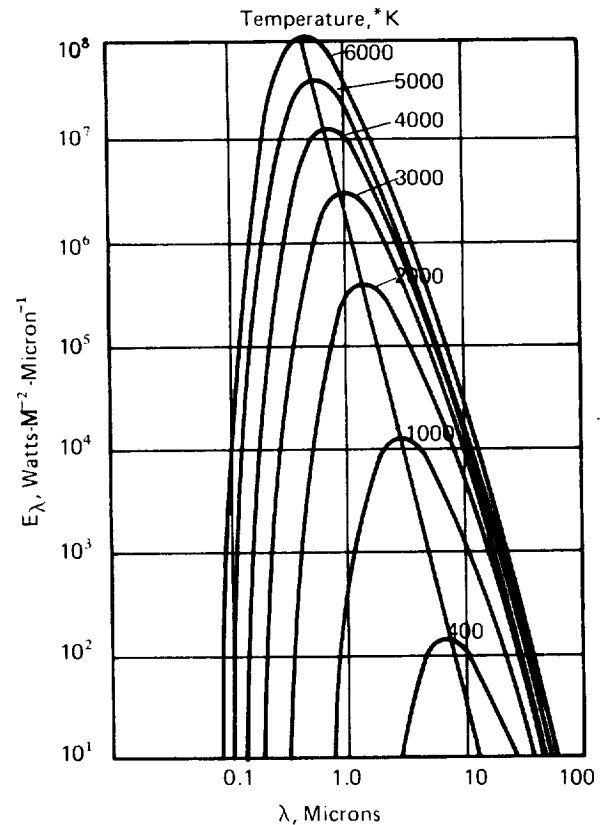


FIGURE 6-3.—Planck blackbody radiation curves.

total radiant energy of a body is directly proportional to the fourth power of its absolute temperature, and is directly proportional to its emissivity.

THERMAL DETECTORS AND METHODS

Finding flaws with thermal nondestructive methods involves detecting an atypical temperature. In some cases it is desirable to measure the absolute temperature; in others only a temperature difference of an area in contrast to the surrounding areas need be detected. In any event, there are many types of temperature-measuring devices and substances that can be used to produce some type of response to the thermal state. Figure 6-4 contains some of the basic methods used to obtain thermographic and thermometric information. This figure is not to be construed as showing all types of temperature-measuring methods, but only those commonly used.

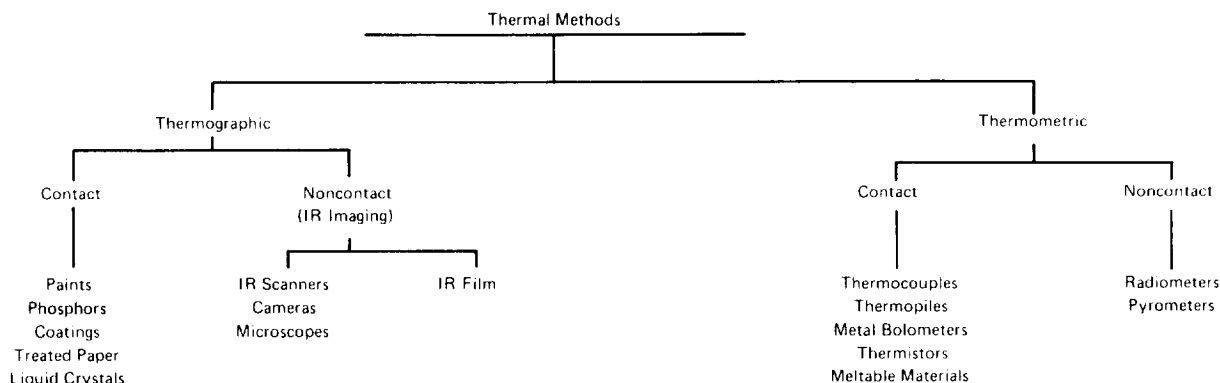


FIGURE 6-4.—Methods used in thermal nondestructive testing.

Testing of Passive Devices

Passive devices must be heated or cooled to obtain thermal intelligence. The presence of a flaw or defect is indicated by a difference in temperature in the vicinity of the flaw. As was shown in the previous section, it is generally true that the greater the impedance to heat flow for the material, the easier will be the detection of a flaw. This is because materials having high heat-flow resistance change temperature more slowly with a fixed thermal input, and therefore equilibrate more slowly. Due to this property, the temperature gradient around the flaw will be greater and longer lived. It also follows that the larger the flaw and the closer it is to the surface, the larger the surface temperature perturbation will be.

Testing of Active Devices

Active devices are self-heating and therefore the emphasis is not directed so much to detecting a temperature difference between one spot and another as it is on measuring the absolute temperature of a spot and comparing it with a predetermined standard or normal temperature. For example, measuring the temperature of a conductor in a microcircuit means very little unless a test has been conducted to establish what the normal operating temperature of that particular conductor should be. That is, the detection of hot spots is unimportant unless the temperature is obviously exceeding the operating limits of the test item.

Contact Methods

The multitudinous contact methods include many types of chemical reactions as well as electrothermal reactions of transducers. For speed and economy, contact coating materials are sometimes used in plastic sandwiches, tapes, and strippable coatings so that they may be easily removed and/or recovered.

In general, coatings produce only qualitative indications of the temperature although some coatings, such as liquid crystals, may be calibrated. Probably the major deficiency of contact materials is that they may, in themselves, alter the heat flow of the surface to be tested. Another disadvantage is that their use is not readily automated (although there is no particular technical difficulty in developing a system that will scan a thermograph and indicate the flaw location). The primary advantage of using contact materials is the low initial investment, particularly if only small areas are to be examined. This cost advantage disappears as the area or number of pieces examined increases. The operator skills required and the effectiveness of contact and noncontact methods in detecting flaws are about equivalent.

Noncontact Methods

Noncontact thermal nondestructive test methods depend on detecting the infrared (IR) radiation emanating from the test object. Although IR detectors have been in existence since IR radiation was first discovered by Herschel in

1800, it was not until after World War II that they were widely used in nondestructive testing. Prior to the middle 1960's, IR was largely restricted to checking active devices with IR transducers and IR film cameras. In the late 1960's, high-speed IR scanning cameras and microscopes became available, making much of the prior equipment and many former techniques obsolete. Rapidly changing temperature transients were readily observed with this new equipment, making it quite useful for viewing passive as well as active devices.

The advantages of IR detectors are that (1) they are noncontacting; (2) the temperature measurement may be made some distance away from test object; and (3) the temperature measurement may be made rapidly. The output of an IR detector (as opposed to contact coatings) is an electrical signal which greatly simplifies automation, recording, and analysis. Variable surface emissivity does cause difficulties since the amount of energy radiated is a direct function of the emissivity, i.e., a surface having an emissivity of 0.5 will radiate one-half the energy of a blackbody at the same temperature.

Detector Sensitivity

Temperature detectors have been developed that will respond to temperature changes on the order of 0.2° C. Because it is difficult to observe a 0.2° C temperature change, the detector must necessarily have a very narrow temperature range. This means that the heat source and the ambient temperature must be well controlled. Another difficulty is the speed of the temperature change. The temperature may change 0.2° C in less than a second or so, making observation and/or detection of the flaw quite difficult. Thus, while the use of highly sensitive detectors may be necessary to reveal the smaller flaws, it may also result in missing some flaws that a less sensitive detector with greater dynamic range would indicate.

Thermal Testing Precautions

There are several precautions that should be taken during thermal testing which are sometimes overlooked. First, the surface should be

uniformly clean. Oily surfaces may reduce or prevent the adherence of contact materials. Some contact materials, such as liquid crystals, are very sensitive to contamination that will either reduce the overall response or cause a shift in color. Contamination will also change the surface emissivity and result in spurious infrared responses.

All contact materials and infrared detectors should be periodically calibrated or checked for sensitivity. While most contact materials have a rather long shelf life, contamination, exposure to strong light, or high humidity, for example, can sharply reduce shelf life. Infrared instruments are subject to drift over time, and they should be calibrated against known temperature standards.

When testing passive devices, heating and/or cooling should be as uniform as possible, and identical on each piece. Reversible coatings (those which may be cycled back and forth through their response temperature) should neither be held for extended periods above their response temperature nor severely overheated; loss in sensitivity will result.

The radiation from a device usually represents only a fraction of the total heat dissipated. Convection and conduction may be responsible for much larger heat losses than radiation; hence they should be held constant during the test. Active devices should be allowed to warm up and stabilize prior to making temperature measurements (ref. 1).

CONTACT THERMOGRAPHIC METHODS

Contact thermographic methods entail coating the surface of the article being tested. The coating will react to a thermal change by changing color or appearance. The reaction may be reversible or permanent. Many reversible coatings are recovered for reuse while nonreversible coatings such as meltable substances are not recoverable. The choice of coating material is governed by the characteristics of both the material and the test article. The following paragraphs provide a summary of coating material characteristics that may aid the reader in making the proper selections.

Paints

Temperature sensitive pigments in the form of paints that will cover a temperature range of 40° to 1600° C have been made. Some of these paints undergo several color transitions as their temperature is raised, and under favorable conditions, an accuracy of $\pm 5^\circ$ C is attainable. These paints have been used effectively to observe the isotherms in the vicinity of a welding operation, for preheating prior to a welding operation, and for the inspection of castings for porosity (ref. 2).

Another type of paint has been developed by Wright-Patterson Air Force Base Materials Laboratory. This compound is composed of a dye formed from the reaction of 5-nitrosalicylaldehyde with 1,3,3-trimethyl-2-methyleneindoline and dispersed in a polyvinyl butyral resin with a titanium dioxide pigment added. It is not necessary to add the pigment if the surface to be inspected is white or light colored. This material may be applied by painting, spraying, or dipping; the surface may be inspected after a drying for one to two hours. A coating thickness of 0.01 to 0.003 in. is required. After drying, the coating is activated with ultraviolet light, which turns the coating a deep purple. Upon heating with hot air the coating rapidly bleaches to white at about 52° C. As the test surface approaches this temperature, a purple and white pattern is produced. The pattern remains stable for several hours if not exposed to heat or excessively bright light. The reaction is reversible and the paint may be reactivated several times without appreciable loss of sensitivity. Using this paint, unbonds as small as $\frac{1}{4}$ in. in diam. have been found in 0.030 in. thick elastomeric materials backed with a water heat sink.

Thermal Phosphors

Thermal phosphors are organic compounds which emit visible light when excited by ultraviolet radiation. The amount of visible light emitted is an inverse function of the temperature of the phosphor. The reason for the decrease in visible-light emission with increased temperatures is not completely understood, but

can be partially explained by solid-state theory. When luminescent molecules are excited with ultraviolet radiation, some of the electrons will be moved to a higher energy level. When the electron returns to the unexcited state, it must lose energy and emits a photon in the process. Because of non-radiative transitions, the emissions, in many cases, are at a lower frequency than the exciting radiation. When the atom or molecule emits or reradiates in the visible range, it either phosphoresces or fluoresces (ref. 3). When a thermal phosphor is heated, the normal return radiation is decreased. This may possibly occur by one or both of the following phenomena. Many electrons may be excited by the thermal input to a high level, thus making this level unavailable to the ultraviolet excited electrons. Or, the thermally induced vibration may induce a nonradiative return from the high-energy level. This nonradiative return is postulated as being a series of small trapping steps between the high-energy level and the ground state (ref. 4).

Figure 6-5 indicates the relative brightness of four thermal phosphors vs temperature (ref. 6).

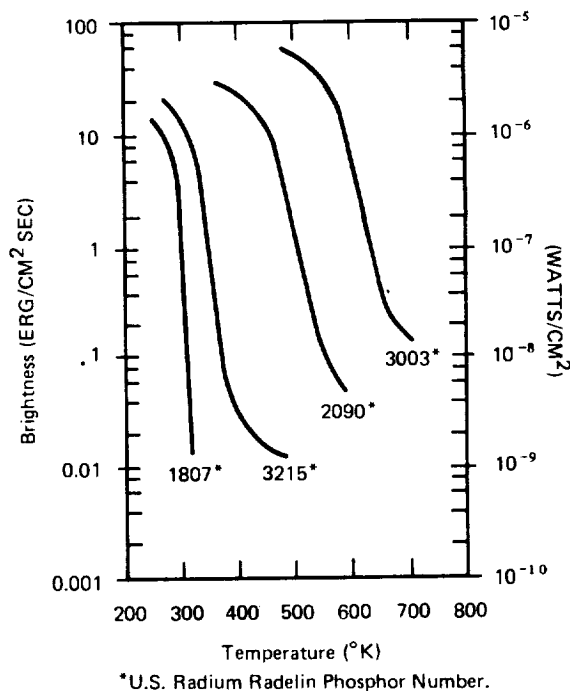


FIGURE 6-5.—Relative brightness of four phosphors vs temperature.

As may be seen, phosphors are available which are useful from room temperature up to 400° C, and some of them have a brightness change of 25%/°C within very limited temperature ranges.

The phosphors may be applied as a paint (refs. 5 and 6), in a tape (ref. 4), a strippable coating (refs. 5 and 6), or the phosphor powder can be directly applied (ref. 7).

The sensitivity of the phosphors will, of course, vary with the intensity of the illumination; however, in one test, a 25 μ thick coating resolved temperature differences of 0.2° C (ref. 6). As with all thermal methods, flaw size, location, and test material characteristics greatly affect sensitivity. One investigator found that the tentative limit for this method was an unbond of 1/2 in. \times 1/2 in. under a 0.032-in. aluminum skin (ref. 5). This finding was based on an inspection of a 4-in. width test item using a hand-held heat gun in a darkened room illuminated by an ultraviolet lamp. This particular inspection used a strippable film that was marked with a felt pen and later peeled from the test item and kept as a permanent record.

An illustrative instance of the use of decomposable or thermally quenched phosphors is in the inspection of soft solder connections. A thermally quenched phosphor is placed in the solder flux. The phosphor selected must have a quench point slightly above the solder melting point. By examining the completed solder joint under ultraviolet light, the presence of fluorescent material would indicate that the phosphor had not been completely thermally decomposed, and, consequently, that the solder joint was a "cold" joint (ref. 3).

Other Temperature-Sensitive Coatings

There are a number of additional temperature-sensitive compounds. Several of which have been employed for nondestructive evaluation are discussed in the following paragraphs.

Thermochromic order-disorder compounds.—Thermochromic order-disorder compounds change color with temperature without breaking chemical bonds (decomposing), as do some organic thermochromic compounds. Two

of the more common compounds exhibiting this effect are Ag₂HgI₄ and Cu₂HgI₄. The color change in the Ag₂HgI₄ compound is caused by the change of an ordered array of the silver and mercury ions in the iodine lattice at low temperatures to a disordered array at high temperatures (ref. 6). The silver-mercury-iodine compound changes color at 50.5° C; the copper-mercury-iodine compound, at 69° C. These compounds change color in a few milliseconds and are very stable so long as they are not held above their transition point for an extended time. Temperature cycling appears to have little effect on their color indications; a sample of Ag₂HgI₄ was cycled 400 000 times without appreciable loss of original indications (ref. 6). These materials are quite expensive; although they may be applied directly to a surface, application by thin plastic sandwiches or tapes greatly reduces the cost per inspection.

Variable surface-tension compounds.—A recent development in thermographic inspection is a material known as Bondcheck. This is a colored fluid which is sprayed on the test item and allowed to dry. Upon heating, it changes viscosity and surface tension. If the surface has warm spots, it is repelled from these warm spots and coalesces in the cool areas. As such, it is not particularly sensitive to the absolute temperature but more to temperature differences on the surfaces. One corporation has indicated that it can be used to detect unbonds in metallic honeycomb material.*

Frost tests.—Frost testing has rather limited application in nondestructive testing, but it can be used as a quick method for determining the presence of gross flaws. In this method the surface of the test object is chilled below the freezing point of water so that a frosted surface is obtained. Visual observation of the frost pattern as it melts will indicate the relatively high- and low-heat conductivity areas and thus determine the flaw locations. The chilling can be accomplished by spraying the surface with a refrigerant gas, such as Freon** or CO₂, or by cold-soaking the test item in a low-temperature

*Magnaflux Corp.

**Registered trade name of E. I. duPont de Nemours and Co.

chamber and then exposing it at room temperature. Frost testing has been used in the testing of nuclear reactor fuel elements consisting of a uranium core bonded to a protective cladding (refs. 2 and 8). Attempts were made to detect unbonds by chilling the elements with CO₂ and then exposing to moist air but the indications were short lived (ref. 8). Diphenyl or acenaphthene, which have a melting point of 93° C, were found to produce a more suitable frost. The fuel elements were sprayed with either of these compounds, giving them a frosty appearance. The elements were then heated by passing them through an induction heating coil. Unbonds were thus indicated by melting of the frost in those areas where the heat conducted to the uranium core was abnormally low. It was found that this test could determine defects of approximately 0.1 sq. in., with a minimum width or length of 0.2 in. However, some rather large defects were not detected by this method.

Treated Papers

A number of thermally sensitive papers can be used in nondestructive testing either by bonding them to the test surface with adhesive or with a vacuum hold-down arrangement. Three of these papers have been evaluated for detecting flaws in a honeycomb sandwich with a glass fiber core and a titanium skin (ref. 6).

Organic coating.—This paper is coated with a meltable organic substance. The paper is black and the coating is white. When the melting temperature is reached, the coating is absorbed in the paper turning it from white to black.

Plastic coating.—A plastic film containing a large number of air bubbles is coated on a paper. The underlying paper is black and the large number of air bubbles in the plastic diffuse the light and give it an appearance of white. Upon heating, the plastic softens and reveals the black paper beneath it. (Such paper is often used in data recorders which have a heated stylus.)

IR copy papers.—These papers contain dye precursors which, when melted, react to produce a colored product. Some general impressions of the performance of these papers can be obtained from table 6-1. It was found that such papers responded most uniformly to radiant

heating, and progressively darkened over a range of temperatures rather than at a single temperature. Tests showed that they could easily detect 1/4-in. square voids beneath 0.030-in. titanium skin over a glass fiber core, and gave a slight indication of a 1/4-in. square void under a 0.040-in. titanium skin. The results compared favorably with those obtained with liquid crystals and thermal phosphors. Tests also showed that temperature differences of 4° or 5° C are sufficient to induce a color reaction in the infrared copy paper (ref. 6).

Liquid Crystals

Liquid crystals were discovered by H. Reinitzer in 1888, but they more or less remained in the laboratory until the 1950's when attempts were made to take advantage of their unique properties (ref. 9). In 1963, a patent was issued involving the use of liquid crystals to measure a thermal pattern. Liquid crystals are so-called because at certain temperatures they exhibit the properties of both a liquid and a crystal; i.e., they are a turbid, mobile liquid, but retain, in part, the ordered molecular structure of a crystal. Liquid crystals were originally classified by Friedel as smectic, nematic, and cholesteric. Although these classifications (particularly the cholesteric phase) have been questioned (ref. 10), Gray maintains that, in view of both the similarities and dissimilarities of the cholesteric with the smectic and nematic phases, Friedel's classification is sufficient. However, the cholesteric phase is presently regarded as a special case of the nematic phase (refs. 11 and 12).

Smectic crystals get their name from *smector*, the Greek word for soap, which they resemble in some ways. They are characterized by cigar-shaped molecules which are arranged in an ordered fashion. The axes of the molecules are parallel to one another and the crystal consists of layers (one molecule thick) of these molecules with their axes perpendicular to the plane of the layer. An example of a smectic liquid is the skin of a soap bubble (ref. 13).

Nematic crystals are also composed of long, cigar-shaped molecules that remain parallel to one another but they are not arranged in layers

TABLE 6-1.—Performance of Thermally Sensitive Papers (ref. 6)

Papers tested	Paper darkening		Core definition through 0.020 in.-Ti	Comments
	Complete in 1 sec	Visible after 5 sec		
1. Meltable organic coating	*65° C		None	(a) Heavier than other papers. (b) Heats irregularly with radiant heat sources. (c) Most expensive paper tested.
2. Heat-sensitive oscillograph paper A.	140° C	119° C	None	(a) More irregular image than IR copy papers. (b) Plastic adheres to PVA. (c) About 5 cents/sq ft.
3. Heat-sensitive oscillograph paper B.			None	Same as A above.
4. IR copy paper A	99° C	87° C	Good	One of the better IR papers tested for this purpose.
5. IR copy paper B	*90° C	*78° C	Good	(a) One of the better IR papers tested for this purpose. (b) The dye precursors are coated on a plastic film which can be used with a vacuum to achieve contact with the test surface. (c) About 5 cents/sq ft.
6. IR copy paper C	94° C		Fair	Costs about 2.7 cents/sq ft.
7. IR copy paper D	*75° C	*68° C	Poor	
8. IR copy paper E	*84° C	*72° C	Good	More expensive than B.
9. IR copy paper F				Poor contrast, darkens irregularly.
10. IR copy paper G			Poor	Poor contrast, thermally sensitive material on both sides.
11. IR copy paper H			Good	These papers, except the J, resemble the A paper. The J is a heavy paper and not suitable for this work.
12. IR copy paper I			Good	
13. IR copy paper J			None	
14. IR copy paper K			Good	

*Manufacturer's data.

as in the smectic phase. Nematic crystals derive their name from the Greek word *nematos* which means thread-like. This characterizes the appearance of nematic crystals that form thread-like structures.

The other type of liquid crystal is the cholesteric, so called because the molecular structure is similar to cholesterol; cholesterol itself does not have a liquid crystal phase. Cholesteric liquid crystals have been described as a twisted nematic phase (ref. 11). The molecules are arranged in layers as in the smectic phase but the layers are quite thin since the molecules are arranged with their long axes parallel to the plane of the layer. Within each layer, the axes

of the molecules are parallel to one another, as in the nematic phase, but in each succeeding layer the molecular axes have a slight angular displacement. Thus, a path through the layers generates a helix.

The three molecular forms of liquid crystals are illustrated in figure 6-6. In general, liquid crystals are characterized as being waxy substances having very weak chemical bonds. Because of the weak chemical bond, they are easily disturbed by almost all forms of energy; thus they may be used to detect and sometimes quantify impinging energy in various forms. In nondestructive testing, only the optical properties of cholesteric liquid crystals have thus

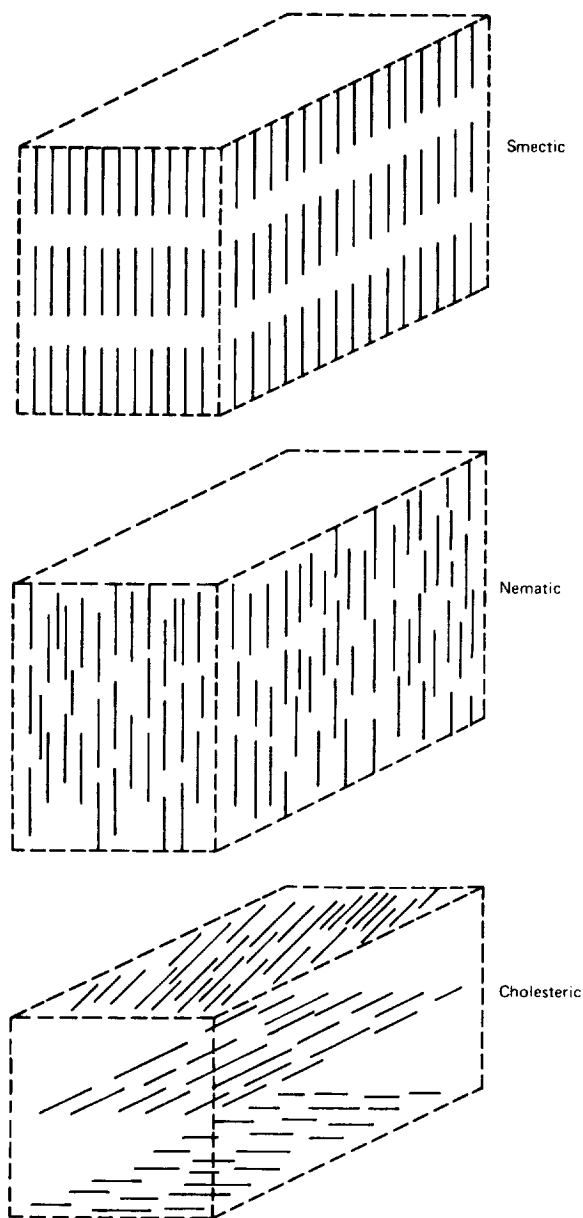


FIGURE 6-6.—Liquid crystal molecular forms.

far been exploited. Most liquid crystals are birefringent, i.e., they refract unpolarized light into two beams that are linearly polarized at right angles to each other. Only cholesteric liquid crystals are dichroic, which means that when they are struck by unpolarized light, the light is broken into two components; one of these components is circularly polarized clockwise and the other, counterclockwise. One com-

ponent is transmitted and the other reflected. It is this reflected component that gives the cholesteric liquid crystal its unique property of producing a color when illuminated by white light (ref. 13).

Thermal reaction of cholesteric liquid crystals.—The pitch of molecular layers within the cholesteric crystals is strongly dependent on temperature (refs. 12 and 14). The pitch, in turn, determines the wavelength at which the polarized beam is reflected. If the wavelength happens to be in the visible range, then the crystals appear to change color as they undergo a temperature change. As they reach their melting point, they become a liquid in which they are essentially colorless and enter into the smectic phase. Further heating causes a “color play” which continues until the isotropic liquid temperature is reached. In the color-play region they may turn from clear to red, yellow, green, blue, violet, and clear again as they are heated. Not all liquid crystals undergo this particular sequence, but may change from red to green to red or several other color sequences (ref. 9). A typical heated spot has the appearance indicated in figure 6-7.

In nondestructive testing it is desirable to have the color play slightly above room temperature, which eliminates the need for extensive heating and cooling. Mixtures of cholesterol oleyl carbonate and cholesterol nonanoate are commonly used. (ref. 14). Cholesterol oleyl carbonate has a color play at 20.5° C. which can be increased with the addition of cholesterol nonanoate. It is possible to prepare or purchase many different cholesteric com-

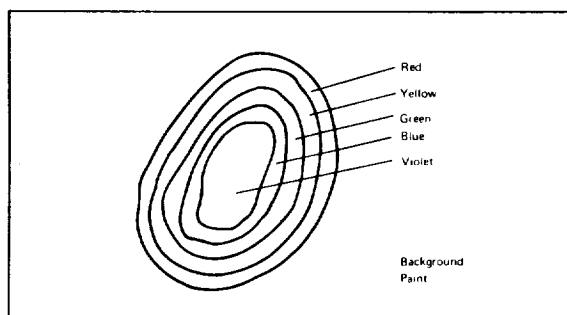


FIGURE 6-7.—Typical appearance of liquid crystal coating when heated.

pounds which exhibit color play at any temperature from -20° to $+250^{\circ}$ C. These mixtures have color-play ranges extending from 30° C down to 1° C (ref. 15). The response time, i.e., the time to change the reflected color, is from about 0.1 to 0.2 sec.

Other reactions of cholesteric liquid crystals.—Cholesteric liquid crystals are very easily disturbed by a number of influences. That is, the color-play temperature may be shifted up or down, or brightness may be markedly reduced depending upon ambient conditions. Some chemical vapors can have a pronounced effect on the color produced at a given temperature, so much so that liquid crystals may be used as leak detectors for certain of these vapors. If the crystals act as a solvent for the vapor, its effects are reversible. If the gas reacts with the crystals, its effects are permanent. Substances that react with the liquid crystals cause color changes at much lower concentration than those in which the crystals act as a solvent. Further, the reacting substances tend to diffuse over a relatively wide area, thus producing a significant indication of its presence. Only a few parts-per-million vapor concentration is required for detection (ref. 16). Eight parts per million of HCl or HF was reported to cause a color shift of 12° C on a cholesterol nonanoate-cholesterol oleyl carbonate mixture; acetone vapor was also detected with liquid crystals (ref. 17). Liquid crystal contamination is generally undesirable in that the color intensity is often reduced over a period of time, thus requiring that the crystals be protected from contaminants when in use.

Mechanical stress, electromagnetic radiation, and polarizing electric fields affect liquid crystals although the effects are not so pronounced as those produced by temperature changes. If the crystals are heated beyond the transition point into an isotropic liquid, the return to the highly colored state upon cooling will be delayed. Exposure to ultraviolet radiation will also degrade performance.

Use and application.—Cholesteric liquid crystals may be painted, sprayed, or dipped on the surface to be examined. Since they function by reflecting light, they are more easily seen

against a dark background. If the surface is not ordinarily dark, it is recommended that it be painted a dull black. If necessary, the paint used may be of a water soluble type so that it can be easily washed off. The applied film of liquid crystals must be very smooth and even; otherwise, the colors will be irregular. The resultant film should generally be between 10 and 20 mils thick (refs. 14 and 18). Successive layers should not be allowed to dry between coatings as this will result in an uneven film and a noticeable pattern irregularity (ref. 19). The coating is sufficient when it has a dull, low-gloss appearance when viewed in oblique light. A 20-mil film has a heat capacity of about 3×10^{-3} J/cm²; the heat capacity of the surface to be measured should be greater than this for good sensitivity. By way of comparison, the heat capacity of 0.5-mm titanium sheet is 1×10^{-1} J/cm².

Since liquid crystals are dissolved in a solvent so they can be easily applied, it is important that the paint used as a background not react with the solvent. Some of the common solvents used are chloroform and petroleum ether. Also, rough, absorbent paint is not desirable as an undercoating because it normally results in a poor surface coverage. On the other hand, high-gloss surfaces will produce specular reflections and interfere with the cholesteric crystal reflection.

The high cost of liquid crystals presently tends to preclude their use on large structures. One gram of the material may cost as much as 50 cents although in large quantities this cost may drop to 12 to 15 cents. One gram will cover about one square foot of surface. As an economic measure, the liquid crystals may be reused by washing them off the surface, filtering out the background paint, dissolving the crystals, and recrystallizing them in an ice bath (ref. 18). To facilitate both the recovery of the crystals and protection from loss of sensitivity due to contamination, the liquid crystals may be sandwiched between 1- or 2-mil plastic films, encapsulated in a gelatin, used in tapes, or placed in an emulsion (refs. 6, 9, and 19). These films are quite stable with shelf life of up to two years without noticeable degradation.

Liquid crystals may be used to observe the thermal pattern of almost any object. They have been used to check certain aircraft structural elements since 1963 (ref. 19). They can also be used to determine temperature abnormalities in electric circuits and human skin. Additionally, surface cracks and unbonds in bonded honeycomb structures can be investigated with liquid crystals.

For temperature measurement, the liquid-crystal color play should be calibrated occasionally against a known temperature standard. Since the index of refraction controls the refracted wavelength, attention must also be given to the angle of incident illumination and viewing angle if precise measurement of temperature is required.

The chief advantage of liquid crystals is their initial low cost in comparison to infrared detectors, and the low operator skill involved. The accuracy is comparable with other thermal methods and is quite repeatable and reliable.

Many of the basic factors to be considered when using liquid crystals to examine bonded structures have resulted from NASA programs (refs. 18 and 19). As a part of this work such factors as sensitivity, liquid crystal recovery, liquid crystal properties, test rigs, background paint, and the type of materials which are adaptable to liquid crystal inspection were investigated.

Sensitivity.—The factors affecting the sensitivity of liquid crystals are the same as those of any other thermal method. Higher thermal con-

ductivity materials yield poorer results than lower thermal conductivity materials; the larger the flaw and the closer it is to the surface, the easier it is to detect. Careful control of the entire thermal regime of the test item is necessary for highest sensitivity.

Under typical conditions, liquid crystals can detect a temperature difference of about 0.2°C , although less sensitive mixtures are often used to achieve a longer time duration of the color play. The best description of the sensitivity that can be achieved with liquid crystals is available in the work of a number of investigators experimenting with several materials. Some of these data are summarized in table 6-2.

NONCONTACT THERMOGRAPHIC DETECTORS AND METHODS

(Infrared Imaging)

As has been shown earlier in this chapter, any object at a temperature above absolute zero will radiate energy in the infrared bandwidth. A large number of devices will respond to this radiation and convert it to a proportional electric signal that may then be displayed. This may be a numerical readout as in the case of a pyroelectric thermometer; it may be a line graph of temperature versus position, as in the case for some IR microscopes; or a thermal "picture" can be made with a scanning IR camera or microscope in which the various temperatures are represented by gray or color scales. Another form of producing a thermograph is

TABLE 6-2.—*Defect Sizes Which Have Been Found With Liquid Crystals*

Material	Minimum detectable defect	Reference
60-mil Al skin over Al honeycomb.....	$\frac{3}{16} \times \frac{3}{16}$ in.....	14
190-mil Al skin over Al honeycomb.....	1 in. ²	14
50-mil Ti skin over Ti honeycomb.....	$\frac{1}{8}$ -in. severance.....	16
50-mil Al skin over phenolic honeycomb.....	$\frac{1}{2}$ -in. adhesive void.....	19
63-mil Al skin over phenolic honeycomb.....	1-in. adhesive void.....	19
63-mil Al skin over Al honeycomb.....	$\frac{1}{2}$ -in. adhesive void, $\frac{1}{4}$ -in. inclusion, $\frac{3}{4}$ -in. crushed core.....	19
30-mil Al skin over Al honeycomb.....	$\frac{1}{2}$ -in. delaminations, $\frac{1}{4}$ -in. crushed core.....	19
12-mil fiber glass over fiber glass honeycomb.....	$\frac{3}{16}$ -in. cells.....	19
Up to 40-mil Ti skin over Ti honeycomb.....	$\frac{1}{4}$ -in. flaw.....	6

with photographic film. A black and white IR sensitive film that responds in the bandwidth of 0.07 to 0.9 μ is available. Color IR films that produce a false color in both the visible and infrared regions are also available.

Advantages and Disadvantages

The greatest advantage of noncontact methods is that the thermal output may be detected remotely. Therefore, the thermal pattern is not disturbed; moreover, inaccessible or difficult spots can be monitored so long as there is a clear field of view between the spot and the sensor. Other advantages of IR methods are that measurements may be made quite rapidly, accurately, and (in certain temperature ranges) temperature differences as small as 0.2° C can be resolved.

The major disadvantage of using infrared imaging equipment is that the surface emissivity of the test object must be known if the temperature is to be measured, since the amount of emitted radiation is a direct function of emissivity. Also, some attention must be given to absorption of infrared by the transmitting media. In other words, if measurements are to be made over considerable distances, a measuring wavelength must be chosen that is not absorbed between the emitter and the receiver. In the atmosphere, for example, water vapor and CO₂ are strong IR absorbers; however, there is a large "window" between 8 and 13 μ where IR transmission is almost 100 percent. Additionally, if the IR measurement is to be made through a piece of visible-wavelength-transparent material such as plastic or glass, or from a reflecting surface, filters must be used to restrict the received radiation to that bandwidth where the emissivity is near 1.0 (ref. 20).

Infrared Detectors

There are two basic types of infrared detectors: (1) photon-effect devices and (2) thermal devices. The response of the photon-effect devices depends on the wavelength of the received radiation; therefore the output signal is dependent upon the wavelength of the IR signal.

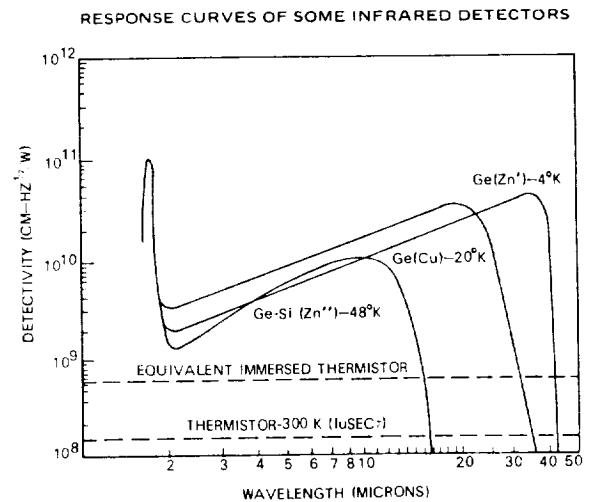


FIGURE 6-8.—Response of photon-effect detectors and thermal detectors.

Thermal detectors on the other hand respond only to the heating caused by the incoming radiation, and the output signal is largely independent of the radiation wavelength. The response of a few photon-effect detectors and of a thermistor-type thermal detector is shown in figure 6-8. At certain wavelengths the photon-effect devices will produce a much larger signal than thermal detectors.

Infrared scanning microscopes and cameras require a very rapid detector response time because the resultant thermograph is actually nothing more than a series of many temperature measurements. If a "flicker free" picture is to be produced, the entire field of view must be scanned rapidly. For instance, some instruments produce 16 pictures per second. Therefore most of these instruments use the high sensitivity and fast response time of photon-effect devices.

Photon-Effect Devices

Photon-effect devices produce voltage, current, or resistance changes when impacted by photons. In general, the response time is very fast and of greater magnitude than thermal devices. The following paragraphs list the characteristics of some of these devices.

Photoemissive detectors.—Photoemissive effects were discovered by Hertz. They result

from a material that emits electrons from the surface when irradiated by a wavelength below a critical value. The energy of the emitted electron was defined by Einstein through the following formula:

$$E = \frac{1}{2}mv^2 = h\mu - \phi$$

where:

- $\frac{1}{2}mv^2$ = kinetic energy of the photoelectron
- μ = frequency of the radiation
- h = Planck's constant
- ϕ = constant determined by the medium (work function).

Photoemissive cells are primarily responsive through the visible wavelengths down to approximately one micron. Hence, their use in infrared detection is not extensive.

A photoemissive cell in its simplest form is an evacuated tube with a photocathode and an anode. The spectral response of the tube is determined by the material used as the photocathode. Photons striking the surface of the cathode cause electron emission, a portion of which is captured by the anode. These tubes have a response time of less than 10^{-8} seconds. Some photoemissive cells contain an inert gas, and may have outputs on the order of 10 to 150 $\mu\text{A}/\text{lm}$, or about three times that of a vacuum-type cell (ref. 21). Photomultiplier tubes are vacuum photoemissive cells with a number of secondary emitters (dynodes). The electrons emitted from the photocathode are attracted toward the first dynode where secondary emission takes place; the secondary emission from the first dynode releases a larger number of electrons that are attracted toward the second dynode and so forth. As many as 10 or 12 dynodes may be placed in the tube so that the final output is quite large.

Photoconductive detectors.—Photoconductors are materials which change their electric conductance when photons fall upon them. The response time is very fast; times shorter than one microsecond have been observed (ref. 22). Their spectral range is narrow, but the many photoconductive materials have overlapping spectral ranges. To obtain a large change in conductance with radiation changes, it may be necessary to cool the semiconductor to reduce

thermal noise. This is often done in infrared detection equipment particularly if temperatures are to be observed near or below room temperature.

Photovoltaic detectors.—Photovoltaic cells produce a voltage when excited by photons. Such cells consist of a photosensitive *p-n* junction. The light illuminates the junction between a layer of metal (*n*-type material) and a layer of *p*-type material. One of the materials is made especially thin so that light may penetrate it. Phototransistors that have a narrower *p-n* junction have also been developed. When light strikes the *p-n* junction the resulting energy transfer creates electron hole pairs within the junction, the rate of pair production being proportional to the light intensity. It is also possible to apply a bias voltage to the junction of a photovoltaic cell in a reverse direction and detect current change as a function of light intensity. When this is done, the device is known as a photodiode.

Equipment

A large assortment of thermographic infrared radiation measuring equipment, ranging from simple photographic film cameras to complex thermal imaging cameras is now available. The IR equipment basically is of two types: (1) microscopes for looking at very small objects such as microcircuits and (2) cameras which have a relatively large field of view with focusing distances extending to infinity.

The microscopes generally have a minimum spatial resolution from 0.0003 in. to about 0.002 in. and a temperature resolution approaching 0.2°C . The scanning of a surface can be accomplished either manually or with a motorized substage. The movements of the substage can be synchronized with a display screen such that a thermal image of a considerable area can be plotted. The response time of some microscopes is as short as one microsecond. One such microscope, built for NASA, scanned by means of rotating mirrors located within the microscope housing. A functional diagram of the instrument is shown in figure 6-9 (ref. 23). This microscope was later built into a circuit containing

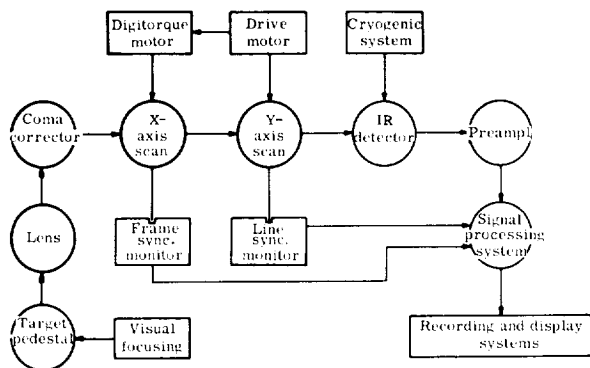


FIGURE 6-9.—Diagram of fast scan infrared microscope.

a color cathode-ray tube so that various isotherms could be displayed in different colors (ref. 24).

Infrared cameras that present a thermal "picture" of the object being viewed are commercially available. This picture is in gray tones which can be translated into temperatures. The temperature resolution is about 0.2°C . The sensitivity is variable and can be as small as 1°C from black to white. By using color filters, color photographs can be produced depicting each isotherm as a different color. One of these cameras is shown in figure 6-10.

Other types of IR cameras that will scan an object from longer distances (1 meter to infinity) and present an X-Y display on a cathode-ray tube are also available.

Applications

The most frequent use of infrared detection in nondestructive testing is probably in the examination of microcircuits and small electronic components. Investigators have met with varying degrees of success in this application. Some of this variance was undoubtedly caused by the limitations of IR test equipment performance. In the early 1960's the fast-scanning, rapid-reaction equipment was not available and results were undoubtedly less satisfactory than can be obtained with present equipment. With proper technique, it appears that IR can be used for qualification, failure analysis, and screening of semiconductor devices (ref. 24). The successful use of infrared was also re-

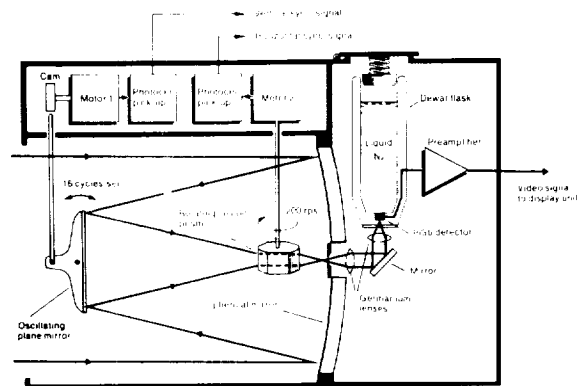
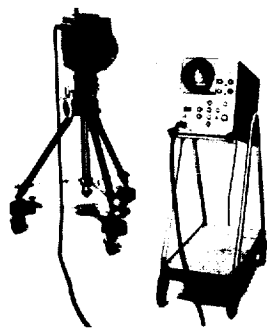


FIGURE 6-10.—Scanning infrared camera. (Courtesy of AGA Corp.)

ported in diagnosing electronic modules (ref. 25), integrated circuit bonds (ref. 26), evaluating electrical designs (ref. 27), detecting flaws in multilayered boards (ref. 28); and it is apparently feasible for use in examining microwelds (refs. 29 and 30). A contribution of NASA in this area was a program conducted to evaluate high-emissivity coatings for use on printed circuit boards and electronic components (ref. 31). Infrared scanning of a surface yields little meaningful data, however, unless the emissivity is constant. Components of printed circuit boards vary widely in their emissivity and it is therefore necessary that they be coated prior to infrared scanning. The materials shown in table 6-3 were found to be satisfactory for this purpose with only minor deficiencies in adhesion, water absorption, elevated temperature, electric properties, and outgassing.

NASA has sponsored several programs for infrared nondestructive testing of electronic assemblies. They included investigations of

TABLE 6-3.—*Suitable Emissivity Coatings for Electronic Components (Ref. 31)*

<i>Manufacturer's designation</i>	<i>Generic name</i>
Hysol, PC 16.....	Epoxy.
Hysol, PC 22.....	Polyurethane.
Magnolia Plastics, Inc., Magobond 39.	Epoxy-polysulfide.
Products Research, PR 1538.....	Polyurethane.
Uralane, 5712.....	Polyurethane.
Dow Corning Corp., Q92-009.....	Silicone.
General Electric Co., SS 4090.....	Silicone.
Martin emissivity coating.....	Acrylic.
Minnesota Mining and Manu- facturing Co., 3M280.	Epoxy.
Humiseal 1A27.....	Polyurethane.

microwelds and microwelding techniques to establish the relationships between the infrared pattern given off during welding and joint strength; automated microweld inspection equipment; and microweld quality as a combined function of infrared radiation and weld-voltage waveform (refs. 30, 32, 33, and 34). In addition, a relation was found between life expectancy of electronic components on a circuit board and infrared radiation given off during operation. It was shown that infrared "finger printing" of the operating components was feasible and that improved packaging could extend the life of the components (ref. 35).

Infrared techniques are also useful for detecting defects in bonded honeycomb materials (refs. 36, 37, 38, and 39). For instance, voids on the order of 0.3 cm were detected beneath a 1.3-mm aluminum-faced honeycomb structure. Shallow subsurface and surface fatigue cracks have been detected using a moving heat source and infrared detector (ref. 40).

In addition, thermography can be used for medical diagnoses. Human skin has an infrared emissivity of 0.99, which is almost that of a perfect blackbody. Furthermore, pigmentation, skin blemishes, suntan, and other off-color areas have emissivities close to 1.0 (ref. 41). Therefore, thermographs of the human body are accurate indicators of skin temperature. If the subject is allowed to remain at rest for a short time in a cool room (to allow for skin tempera-

ture stabilization that might be disturbed by activity), it is possible to determine those body areas having anomalous heat conductivity or abnormal heat supply. For instance, if the room temperature is held below body temperature, dead tissue areas tend to approach room temperature. Thus, areas having low blood circulation and low thermal conductivity such as is typical of bruises, fatty tissue, cysts and benign inactive processes can be located.

Infrared film cameras record wavelengths only in the near-infrared region between 0.7 and 0.9 μ . It is impractical to go beyond this range because of the radiated heat which would fog the film. Since infrared emulsions are sensitive to violet, blue, and red as well as infrared, it is therefore necessary to use a visible-light blocking filter on either the camera lens or the light source. Infrared film cameras are often used outdoors to photograph vegetation to determine diseased areas not revealed by visible light. The military has also used these cameras to photograph suspected camouflaged areas because dyes used in camouflage coverings do not radiate IR in the same manner as natural vegetation. Infrared film cameras are also used for detecting forgeries of art and printed material because the inks and paints used by the forger do not have the same IR signature as the original material.

Quantitative temperature measurements may also be made using IR film cameras. A system was developed to measure turbine-blade temperatures using infrared film and determining temperature as a function of film density. This particular system mapped temperature in the 1000° F (540° C) to 2500° F (1350° C) range with a 1-percent accuracy of the calibration point temperature (ref. 42).

There have been other systems developed to make thermographs for special purposes. For instance, NASA has found that a standard closed-circuit television camera could detect hydrogen fires when equipped with a vidicon that responds from the near infrared to 2.1- μ wavelengths. By placing infrared filters in front of the camera lens, a good contrast is produced between the hydrogen fire and the background (ref. 43).

CONTACT THERMOMETRIC METHODS AND MATERIALS

There are several basic thermal detectors: (1) bolometers, (2) thermistors, (3) thermocouples, and (4) thermopiles. For the most part, they can be used in direct contact with the test item or as a radiation detector. These devices can detect both short- and long-wavelength infrared radiation and very low-temperature or low-radiation levels without cryogenic cooling. The use of these devices as contact thermometers is discussed in this section.

Thermocouples and Thermopiles

Thermocouples consist of a junction of two dissimilar metals. As the junction temperature is raised, a thermoelectric emf is produced. Thermocouples are always used in pairs in a bridge circuit so that the measured temperature is a direct function of the emf produced by the sensing thermocouple as subtracted from the emf produced by a reference thermocouple that is held at a known temperature. As with all thermal detectors, thermocouples may be used as a contact sensor or they can be used in non-contact applications to sense infrared radiation only. When used to sense radiation only, as in a radiometer, the reference junction is mounted in the same detector head as the radiation detecting junction; however, the reference junction is shielded from incoming radiation. Thus, both junctions are in the same ambient temperature and automatic compensation is achieved since only the temperature rise caused by the incoming radiation is measured. Thermocouples have a varying response time that is largely dependent upon the mass of the junction. By the use of very fine wires, response times may be several hundredths of a second.

Thermopiles are merely a series of thermocouple junctions; they produce an increase in emf as a direct function of the number of junctions. While thermopiles do have a higher output signal, the response time is reduced because of the increased mass which must be heated.

A number of significant developments have been made by NASA in the field of special purpose thermocouples. These have been summa-

rized in a NASA Special Publication entitled *NASA Contributions to the Development of Special-Purpose Thermocouples* (ref. 44). This document describes special-purpose thermocouples [such as one that can measure temperatures from -250°F (-120°C) to $+5000^{\circ}\text{F}$ ($+2760^{\circ}\text{C}$) (ref. 45) (fig. 6-11)] and NASA developed techniques in which multiple thermocouples are used with only one reference junction (ref. 46), methods for installing thermocouples in difficult places (ref. 47), and improved thermally conductive adhesives for attaching thermocouples to brittle surfaces (ref. 48). Some special-purpose thermocouple transducer units that can operate under water at 1000 psi, and in the presence of strong magnetic fields have also been developed by NASA (ref. 49). The latter device is shown in figure 6-12.

Bolometers

Bolometers are thermal detectors that are based on the principle that the resistance of a material changes as it is heated. The bolometer allows the radiation to impinge on a very fine wire or a thin metallic film, blackened to increase absorption. The resistance change is then a direct function of the radiation absorbed. The temperature coefficient of a bolometer is from 0.3 to 0.5%/°C. The detector, along with the

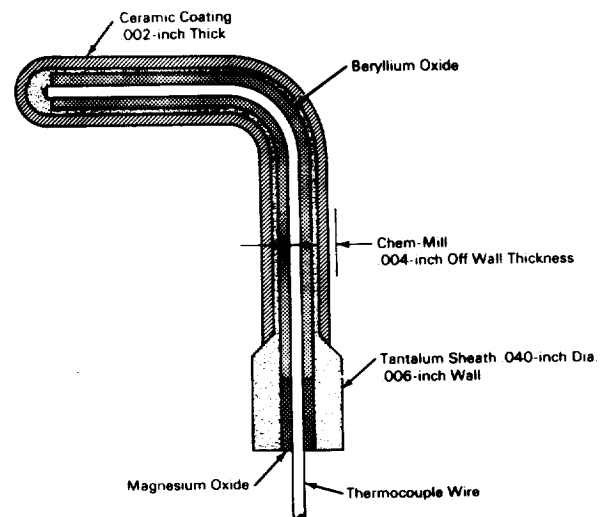


FIGURE 6-11.—Modified thermocouple which measures temperature from -120° to $+2760^{\circ}\text{C}$.

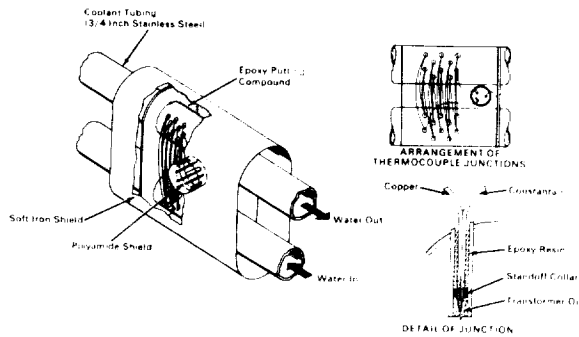


FIGURE 6-12.—Transducer which measures temperature difference in strong magnetic field.

associated circuitry, has a sensitivity equivalent to that achieved with a thermistor-type bolometer (ref. 50).

Thermistor Bolometers

Thermistors, or thermally sensitive resistors, are semiconductors that undergo a reduction in resistance as their temperature rises. Their temperature coefficient is approximately $4\%/^{\circ}\text{C}$. The limiting factor of the thermistor is thermal noise. A thermistor flake having a nominal resistance of 10^6 ohms may only change its resistance 0.04 ohm when used to detect radiation. To detect resistance changes of this level, a dc bias voltage is usually applied and the thermistor is arranged in a bridge circuit.

Capacitance Detectors

While working with thin dielectric films, NASA workers found that a large temperature variation in capacitance could be obtained in thin-film capacitors when a fixed ionic space charge was present in the film. Detectors based on these findings equal or exceed other types of thermal detectors in performance. The high-temperature response, on the order of $100 \text{ mV}/^{\circ}\text{C}$, makes it potentially attractive for applications such as thermal imaging (ref. 51).

Meltable Substances

Wax-like crayons that melt between 38° to 1760°C are commercially available. These crayons have a melting point within a nominal tolerance of ± 1 percent of the rated tempera-

ture value. They are normally used by making a mark with one or more of them on a surface before it is heated. Upon heating, they may gradually change color or color intensity, but this is not a temperature indication. The true temperature indication occurs only when the mark melts, which is readily observable. By using an appropriate range of these crayons arranged in a suitable pattern, general observations can be made regarding the isothermal pattern (or thermograph) of a heated area.

Lacquers, pellets, and small cones containing materials similar to that used in crayons are also available. The lacquer may be brushed, dipped, or sprayed on a smooth surface; upon drying, it has a characteristic dull appearance. After heating, or upon reaching its melting point, the lacquer takes on a glossy appearance that is retained when the surface cools. The pellets (and cones) are placed on the surface to be tested and melt as they reach their rated temperature; the pellets melt between 38° and 1760°C . These substances were made for use where the observation must be made some distance away from the actual operation.

Any substance whose melting point can be predicted can be used as a thermal detector. A NASA contractor has shown how braze alloys and solder may be used. The material is put on the test surface in small patches. The surface is scribed before heating as an aid in revealing which spots have melted. The thermal coefficients of these substances are higher than those of the waxes, which should make them more sensitive to the true surface temperature (ref. 52).

NONCONTACT THERMOMETRIC INSTRUMENTS

These temperature-measuring devices depend upon response of a thermal detector to infrared radiation. They are particularly useful when it is necessary to monitor or measure surface temperatures remotely.

Radiometers

These instruments are used to measure incident radiation. For the most part they consist of some type of hollow cavity with an aperture

in one end and a thermal detector mounted internally. The thermal detector is so located that the radiation is focused on it. Since thermal detectors have a uniform response without regard to infrared wavelength, the radiometer is often used to measure total radiation. If the radiometer has a lens system, it will be restricted to the infrared transmission characteristics of the lenses.

Because of the slow response time of the thermal detector, radiometers are used in nondestructive testing to measure relatively constant temperature processes. They are quite useful for measuring temperature remotely and are often employed to measure temperatures in such severe environments as rocket exhausts.

NASA has developed a number of radiometers and radiometer accessories. For instance, a radiometer was developed in which two thermal detectors were used in combination with gold-coated mirrors that can focus incoming radiation and radiation from an internal reference source on the detectors. The two-detector system has a theoretical signal-to-noise ratio 1.4 times that of a single detector system (ref. 53). An improved cavity radiometer was developed that measures radiation to an accuracy of 1% or 2 percent when operated at a vacuum of 10^{-5} torr or lower (fig. 6-13). The basic device is not new but represents an application of up-to-date materials and electronics. It is estimated to act as a blackbody for more than 99.5 percent of all wavelengths between 0.2 and 40 μ (ref. 54).

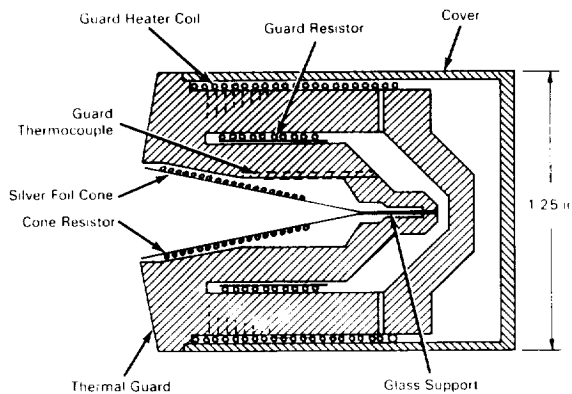


FIGURE 6-14.—Rapid-response blackbody cavity radiometer.

A rapid-response radiometer was made by winding a bifilar-wound resistance thermometer in the shape of a conical cavity and encasing it in a conductive material such as metallic silver (fig. 6-14). Radiant energy is measured by monitoring the power required to hold the shell at a constant high temperature. Response times of fractions of a millisecond are possible (ref. 55).

A reference blackbody, developed by NASA, was built to operate over a wide range of incident angles. It is composed of stacks of razor blades with a black oxide coating (ref. 56). As illustrated in figure 6-15, the deep notches absorb almost all of the incident radiation because of the multiple reflections within the small apex angle.

Pyrometers

Pyrometers (or infrared thermometers) are used in nondestructive testing in much the same way as are the scanning devices previously discussed. These instruments are not as accurate as other scanning devices, but they are simpler, more rugged, more portable, and less expensive. There is a wide variety of this type of equipment on the market with a corresponding variety of performance. Pyrometers are available in the form of infrared microscopes, medium-focusing range thermometers, and long-distance focusing thermometers. Various instruments that will measure temperatures from well below 0°C to above 3000°C are available. An infrared thermometer is illustrated in figure 6-16 (ref. 57).

The accuracy of these instruments is typically several tenths of a degree Celsius, and the response time may range from microseconds to

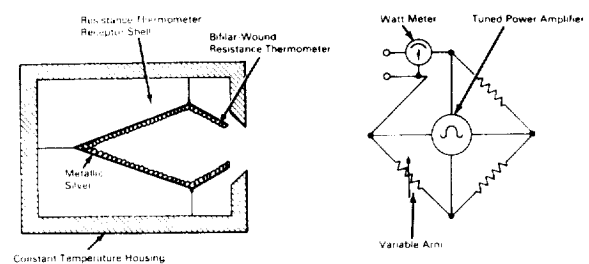


FIGURE 6-14.—Rapid-response blackbody cavity radiometer.

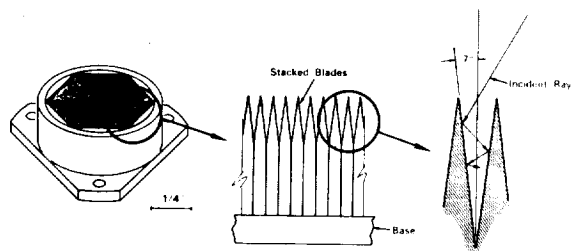


FIGURE 6-15.—Reference blackbody.

tenths of seconds. The faster instruments are readily adapted to automatic data plotting and isotherm location. They are used in many non-destructive tests in which the temperature of only small areas must be monitored or measured.

REFERENCES

1. DEAN, H. F.; AND HARPER, K. F.: Reliability Screening and Step-Stress Testing of Digital-Type Microcircuits. NELC Rept. 1512, Naval Electronics Lab. Center for Command Control and Communications (San Diego), Sept. 1967.
2. MCGONNAGLE, WARREN J.: Nondestructive Testing. McGraw-Hill Book Co., Inc., 1961.
3. VOGEL, PAUL E. J.: Infrared Multiple-Scan Bond Inspection System. U.S. Army Materials Research Agency, Watertown, Mass.
4. BYLER, W. H.; AND HAYS, F. R.: Fluorescence Thermography. Nondestructive Testing, May-June 1961, pp. 177-180.
5. SEARLES, CHARLES E.: Thermal Image Inspection of Adhesive Bonded Structure. American Society for Nondestructive Testing Symposium on NDT of Welds and Materials Joining (Los Angeles), Mar. 1968.
6. WOODMANSEE, W. E.: Contact Thermographic Materials Applied to Nondestructive Testing. Paper presented at the 7th Symposium on Nondestructive Evaluation of Components and Materials in Aerospace, Weapons Systems, and Nuclear Applications. Sponsored by South Texas Section, American Society for Nondestructive Testing, Inc., and Southwest Research Institute, San Antonio, Apr. 23-25, 1969, pp. 43-57. (Available from Western Periodicals Co., North Hollywood, Calif.)
7. ANON.: Thirteenth Semiannual Report to Congress. National Aeronautics and Space Administration, Jan. 1-June 30, 1965.
8. ANON.: Symposium on Nondestructive Tests in the Field of Nuclear Energy. American Society for Testing Materials (Philadelphia), Mar. 1958.
9. FERGASON, JAMES L.: Liquid Crystals and Their Applications. *Electro-Technology*, Jan. 1970, pp. 41-50.
10. GRAY, G. W.: Molecular Structure and the Properties of Liquid Crystals. Academic Press, Inc. (London and New York), 1962, p. 40.
11. SAUPEI, A.: Recent Results in the Field of Liquid Crystals. *Angewandte Chemie Journal (International Edition in English)*, Academic Press, Inc. (New York), vol. 7, no. 2, 1968, pp. 97-112.
12. BROWN, GLENN H.: Liquid Crystals and Some of Their Applications in Chemistry (Report for Analytical Chemists). *Analytical Chemistry*, vol. 41, no. 13, pp. 26A-39A, 1969.
13. FERGASON, JAMES L.: Liquid Crystals, *Scientific American*, vol. CCXL, no. 2, 1964, pp. 77-85.
14. FERGASON, JAMES L.: Liquid Crystals in Nondestructive Testing. *Applied Optics*, vol. 7, no. 9, 1968, pp. 1729-1737.
15. BROWN, SHELBA P.: Detection of Flaws in Metal-Honeycomb Structures by Means of Liquid Crystals. Rept. RS-TR-67-5, Structures and Mechanics Lab. U.S. Army Missile Command (Redstone Arsenal, Al.), June 1967.
16. ARTHAL, JOHN F.: Liquid Crystals as a Nondestructive Inspection Tool, Feasibility Study. Rept. NAEC-AML-2634, U.S. Naval Air Engineering Center (Philadelphia), June 1967.
17. WOODMANSEE, W. E.; AND SOUTHWORTH, H. L.: Detection of Material Discontinuities with Liquid Crystals. *Materials Evaluation*, vol. XXVI, no. 8, 1968, pp. 149-154.
18. SABOURIN, LAMARR: Nondestructive Testing of Bonded Structures with Liquid Crystals. Paper presented at the Structural Adhesive Bonding Conference, MSFC, March 15-16, 1966.
19. COHEN, SHERMAN E.: The Application of Liquid Crystals for Thermographic Testing of Bonded Structures. NASA CR-88196.
20. BERMAN, HERBERT L.; AND WANK, MARTIN R.:

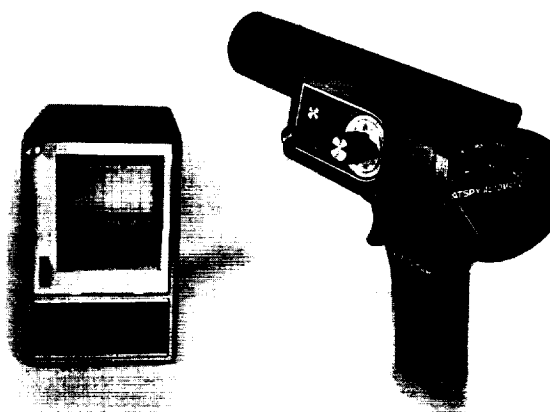


FIGURE 6-16.—Infrared thermometer. (Courtesy of William Wall Corp.)

- Using Infrared Thermometers Effectively. Optical Spectra, July-Aug. 1969, pp. 77-80.
21. HEINZ, ALFRED: Selecting Photosensors. IEEE, vol. 12, no. 10, 1964.
 22. ANON.: Photoconductive Detectors for Infrared. Electronic Industries, vol. 24, no. 11, 1965, pp. 118-121.
 23. ANON.: Nondestructive Testing: Trends and Techniques. NASA SP-5082, 1966, p. 104.
 24. BERGER, W. M.; AND SOLTAU, R. H.: Final Report on the Study of Infrared Evaluation in Qualification and Failure Analysis of Semiconductor Devices. (NAS8-21219) Philco Ford Corp., Microelectronics Division (Blue Bell, Pa.), June 10, 1969.
 25. CHAPNICK, NEWTON N.; AND FAGIN, LEONARD L.: Infrared Thermography for Diagnostic Evaluation of Electronic Modules. Materials Evaluation, June 1967, pp. 164-168.
 26. BRINTON, JAMES: Analyzer Universe Junctions' Secrets. Electronics, Feb. 1970, pp. 158-160.
 27. ANON.: Infrared for Electronics Reliability. Engineering Design News, vol. 10, no. 8, 1965.
 28. JONES, R. W.; AND WHITE, L. M.: Infrared Evaluation of Multilayer Boards, Materials Evaluation, vol. 27, Feb. 1969, pp. 37-41.
 29. ALZOFON, F. E.; AND McDONALD, A. D.: Infrared Evaluation of Microweld Quality. Materials Evaluation, Aug. 1967, pp. 183-184.
 30. HOWARD, RONALD G.: Infrared In-Process Micro-Weld Evaluator. (NAS8-20639 and NAS8-21221) Martin Marietta Corp., Manufacturing Research and Technology Division, (Orlando, Florida).
 31. CHADDERDON, G.; AND HARTMAN, T.: Infrared Testing of Electronic Components, Phase II Report. (NAS8-20131) Martin Marietta Corp. (Orlando, Florida) Jan. 1966.
 32. YATES, G. D.: Establishment of Standards for Compatibility of Printed Circuit and Component Lead Materials, Final Report. (NAS8-20390) Martin Marietta Corp. (Orlando, Florida), Aug. 1967.
 33. SNEDEKER, D. A.: Study on Development of Techniques for Resistance Welding, Phases I and II, Final Report. NASA CR-89649, 1967.
 34. ANON.: Study and Development of Nondestructive Weld Inspection Techniques. NASA CR-73207, 1968.
 35. RANDLE, W. R.: Infrared Testing of Electronic Components, Final Report. NASA CR-76080, 1966.
 36. VOGEL, PAUL E. J.: Evaluation of Bonds in Armor Plate and Other Materials Using Infrared Non-destructive Testing Techniques. Applied Optics, vol. 7, no. 9, 1968, pp. 1739-1742.
 37. KUTZSCHER, E. W.; ZIMMERMANN, KARL H.; AND BOTKIN, JOSEPH L.: Thermal and Infrared Methods for Nondestructive Testing of Adhesive Bonded Structures. Paper presented at the 27th National Fall Conf., Society for Nondestructive Testing, (Cleveland, Ohio), Oct. 16-19, 1967.
 38. KUTZSCHER, EDGAR W.; AND ZIMMERMANN, KARL H.: A Scanning Infrared Inspection System Applied to Nondestructive Testing of Bonded Aerospace Structures. Applied Optics, vol. 7, no. 9, 1968, pp. 1715-1720.
 39. BARTON, E. J.: Thermal Inspection of Adhesive Bonded Structures. Paper presented at conference on NDT of Plastic/Composite Structures, Air Force Materials Lab., The Aerospace Corp., University of Dayton, (Dayton, Ohio), Mar. 1969.
 40. KUBIAK, EDWARD J.: Infrared Detection of Fatigue Cracks and Other Near-Surface Defects. Applied Optics, vol. 7, no. 9, 1968, pp. 1743-1747.
 41. BARNES, R. BOWLING: Thermography of the Human Body. Science, vol. 140, May 1963, pp. 870-877.
 42. POLLACK, FRANK G.; AND HICKEL, ROBERT O.: Surface Temperature Mapping with Infrared Photographic Pyrometry and Turbine Cooling Investigations. NASA TN D-5179, 1969.
 43. ANON.: Infrared Television Used to Detect Hydrogen Fires. NASA Tech Brief, 66-10363, 1966.
 44. MOELLER, C. EUGENE; ET AL.: NASA Contributions to Development of Special-Purpose Thermocouples. NASA SP-5050, 1968.
 45. ANON.: Modified Thermocouple is Effective from -250° to 5000°F. NASA Tech Brief, 66-10461, 1966.
 46. ANON.: Multiple Temperatures Sampled Using Only One Reference Junction. NASA Tech Brief, 66-10260, 1966.
 47. ANON.: Thermocouples Easily Installed in Hard-To-Get-To-Places. NASA Tech Brief, 66-10653, 1966.
 48. ANON.: Compound Improves Thermal Interface Between Thermocouple and Sensed Surface. NASA Tech Brief, 66-10121, 1966.
 49. ANON.: Transducer Measures Temperature Differentials in Presence of Strong Electromagnetic Fields. NASA Tech Brief, 65-10089, 1965.
 50. SCHWARZ, FRANK.: Infrared Detectors. Electro-Technology, vol. 72, no. 5, 1963.
 51. ANON.: Thin Film Thermal Detector. NASA Tech Brief, 67-10505, 1967.
 52. ANON.: Braze Alloys Used as Temperature Indicators. NASA Tech Brief, 66-10274, 1966.
 53. ANON.: Infrared Radiometer. NASA Tech Brief, 67-10422, 1967.
 54. ANON.: Improved Cavity-Type Absolute Total-Radiation Radiometer. NASA Tech Brief, 67-10557, 1967.
 55. ANON.: Blackbody Cavity Radiometer has Rapid Response. NASA Tech Brief, 66-10679, 1966.
 56. ANON.: Reference Black Body is Compact, Convenient to Use. NASA Tech Brief, 63-10004, 1964.
 57. ANON.: Heat Spy Automatic Infrared Thermometer. Revision B, William Wahl Corp. (Los Angeles).

CHAPTER 7

Microwave Techniques

William L. Rollwitz

The band of frequencies of microwaves is usually considered to be between 300 MHz and 300 GHz, corresponding to wavelengths, *in vacuo*, of 1 m to 1 mm (fig. 7-1). It has become conventional to designate specific subintervals of the microwave frequency band by various letters of the alphabet. Table 7-1 contains the more common ones and their letter designations. Although the general nature of microwaves has been known since the time of Maxwell, it was not until World War II that microwave generators and receivers useful for material testing became available. Since the first important use of microwaves was for radar, it is not surprising that their first use in nondestructive evaluation was for components such as waveguides, attenuators, cavities, antennas, and antenna covers (radomes). For example, it was found that the best test for thickness and voids in radomes was the microwaves themselves. Both

TABLE 7-1.—Letter Designations of Major Subintervals of the Microwave Frequency Band

Letter	Frequency band, GHz	Wavelength band <i>in vacuo</i> , cm
L	0.390 to 1.550.....	76.9 to 19.3.
S	1.550 to 5.200.....	19.3 to 5.77.
X	5.200 to 10.900.....	5.77 to 2.75.
K	10.900 to 36.000.....	2.75 to 0.834.
Q	36.000 to 46.000.....	0.834 to 0.652.
V	46.000 to 56.000.....	0.652 to 0.536.
W	56.000 to 100.000.....	0.536 to 0.300.

continuous and pulsed incident waves (reflected and transmitted) were used in these tests.

The use of microwaves for the evaluation of material properties and defects in materials other than radomes began in the late 1950's and early 1960's. The first such evaluation was that of the concentration of moisture in dielectric materials. Microwaves of an appropriate wavelength were found to be strongly absorbed and scattered by water molecules. When the dry host material is essentially transparent to the microwaves, the moisture measurement is readily made.

Next, the thickness of thin metallic coatings on nonmetallic substrates and the thickness of dielectric slabs were measured. Here, incident

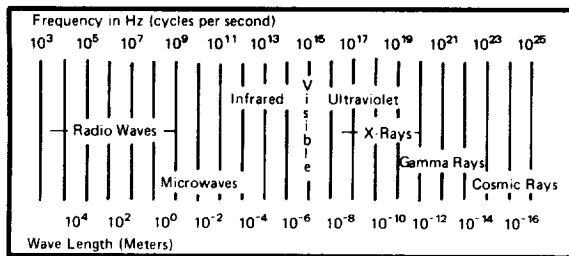


FIGURE 7-1.—The portion of the electromagnetic spectrum from 10³ to 10²⁵ Hz.

and reflected waves were allowed to combine to form a standing wave. Measurements were then made on the standing wave since it provided a scale sensitive to the material thickness.

The measurement of thickness was followed by determination of voids, delaminations, macroporosity, inclusions, and other flaws in plastic or ceramic materials. With the advent of bonded honeycomb structures and fiber-wound and laminar composite materials, microwave techniques were also used to detect flaws in these materials. For most measurements, the reflected wave was found to be most useful, and the use of frequency modulation provided the necessary depth sensitivity. Success in these measurements also indicated that microwave techniques could give information that would be related to changes in chemical or molecular structure which affect the dielectric constant and dissipation of energy at microwave frequencies. Some of the properties measured include polymerization, oxidation, esterification, distillation, and vulcanization.

Microwaves are essentially electromagnetic waves, the velocity and attenuation of which are dependent upon the properties of the medium through which they are propagating. Hence, they can be used to determine changes in material properties. Since the material properties that influence the microwaves are different from those that most strongly affect ultrasonic waves or X-rays, they cannot be directly compared. What can be compared are the characteristics of the measurement techniques.

The main difficulties with the ultrasonics are (1) lack of a wideband frequency response of the transducers, (2) coupling difficulties and contamination by couplant materials, and (3) high reflection at the first interface.

A major limitation of X-rays is that only a transmission factor can be readily obtained. By comparison with ultrasonics and X-rays, the advantages of microwave testing are

- (1) Wideband frequency response of the coupling antennas
- (2) Efficient coupling through air from the antennas to the material
- (3) No material contamination problem caused by the coupling means

(4) Microwaves readily propagate through air, so successive reflections are not obscured by the first one

(5) Both amplitude and phase information about propagating microwaves are readily obtained.

An important limitation to the use of microwaves is their inability to penetrate deeply into conductors or metals. This means that non-metallic materials inside a metallic container cannot be inspected through the metallic container. Another limitation of microwaves is their comparatively low power of resolving localized anomalies. If a receiving antenna of practical size is used, an anomaly whose effective dimension is significantly smaller than the wavelength of the microwaves used cannot be resolved, i.e., distinguished as a separate, distinct flaw. At present, the shortest wavelengths for which practical microwave apparatus exist are of the order of several millimeters. Consequently, microwave testing is not presently suited where flaws are significantly smaller than 1 mm.

PHYSICAL PRINCIPLES

In free space, an electromagnetic wave is transverse, i.e., the oscillating electric and magnetic fields that compose it are transverse to the direction of travel of the wave. The relative directions of these two fields and that of direction propagation of the wave are shown schematically in figure 7-2. As the wave travels along the Z-axis, the electric and magnetic field intensities at an arbitrary fixed location in space vary in magnitude. A particularly simple form of propagating an electromagnetic wave is the linearly polarized, plane sinusoidal wave illustrated in figure 7-3. Such an electromagnetic wave can be described mathematically by equations (1) and (2):

$$E(Z, t) = E_{\max} \sin \left[2\pi \left(\frac{Z}{\lambda} - ft \right) \right] \quad (1)$$

$$H(Z, t) = H_{\max} \sin \left[2\pi \left(\frac{Z}{\lambda} - ft \right) \right] \quad (2)$$

with

$$H_{\max} = \sqrt{\frac{\epsilon_0}{\mu_0}} E_{\max}$$

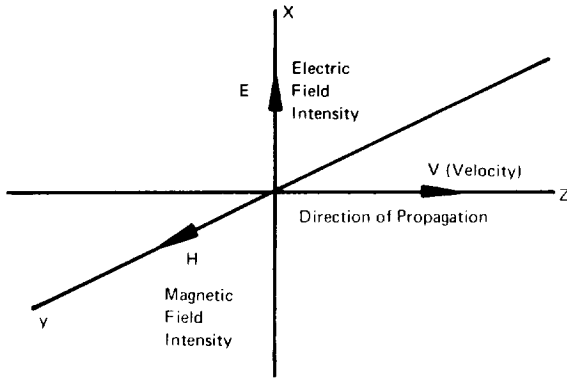


FIGURE 7-2.—Relative directions of the electric field intensity, E , the magnetic field intensity, H , and the direction of propagation, Z , for a linearly polarized, plane electromagnetic wave.

The quantity, λ , is the wavelength of the wave; f is its frequency; μ_0 and ϵ_0 are, respectively, the permeability and dielectric coefficient *in vacuo*. The speed with which a wavefront travels along the Z -axis is given by the familiar relation $v = f\lambda$. In free space, this speed is the speed of light, usually designated by the letter c and having the value 2.998×10^8 m/sec.

For most cases of practical interest in microwave testing, a homogeneous material medium may be characterized in terms of a magnetic permeability, μ , a dielectric coefficient, ϵ , and an electric conductivity, σ . In general, these quantities are themselves functions of the frequency, f ; moreover, μ and ϵ must sometimes be treated as complex quantities, rather than as purely real ones, to account for certain dissipative effects (e.g., the dielectric absorption of microwave energy by water molecules). However, a wide variety of applications occur in which μ and ϵ may be regarded as purely real and constant in value. The magnetic permeability, μ , usually differs but slightly from its value *in vacuo*, while the dielectric coefficient, ϵ , usually lies between one and ten times its value *in vacuo*. The electric conductivity, σ , ranges in value from practically zero ($<^{-17}$) for good insulators up to the order of 10^6 (ohm-cm) $^{-1}$ for good conductors such as copper.

Plane electromagnetic waves propagating through a conductive medium diminish in amplitude as they propagate, falling to 37% of their amplitude at a reference position in a dis-

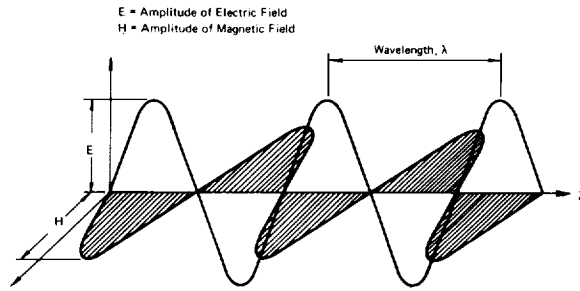


FIGURE 7-3.—Schematic representation of a linearly polarized, sinusoidally varying, plane electromagnetic wave propagating in empty space.

tance, δ (called the skin depth), measured along the direction of propagation. It may be shown that the skin depth is given by the relation:

$$\delta = \sqrt{\frac{2}{\mu\sigma\omega}} \quad (3)$$

The velocity of an electromagnetic wave propagating in a nonconductor is given by the relation:

$$v = \frac{1}{\sqrt{\mu\epsilon}} \quad (4)$$

It is often convenient to express this velocity relative to the velocity of electromagnetic waves *in vacuo*, the ratio being the index of refraction, n , where

$$n = \frac{c}{v} = \sqrt{\frac{\mu\epsilon}{\mu_0\epsilon_0}} \quad (5)$$

The phase velocity of a plane harmonic electromagnetic wave propagating in a conductive medium may be shown to be given by the relation:

$$v = \omega\sigma = \sqrt{\frac{2\omega}{\mu\delta}} \quad (6)$$

where δ is the skin depth, given by equation (3). Thus, v in this case depends strongly on the frequency, ω , even if μ and σ do not themselves depend upon ω . Because of this, a conductive medium is said to be highly dispersive, since a wave packet, which comprises sinusoidal components of many different frequencies, "disperses," or spreads, as it propagates. It may further be shown that in conductive

media the magnetic component of an electromagnetic wave does not propagate in phase with the electric component.

The wavelength of an electromagnetic wave propagating in a weakly conductive medium is given approximately by the relation :

$$\lambda \simeq \frac{\lambda_0}{n} \left\{ 1 - \frac{1}{8} \left(\frac{\sigma}{\epsilon\omega} \right)^2 \right\} = \frac{\lambda_0}{n} \left\{ 1 - \frac{1}{32\pi^4} \left(\frac{\lambda_0}{n\delta} \right)^4 \right\} \quad (7)$$

where λ_0 is the wavelength of the wave *in vacuo*, n is the index of refraction of the medium as defined by equation (5), and δ is the skin depth defined by equation (3). Equation (7) is sufficiently accurate for most materials whose conductivity is low enough for practical microwave testing involving transmission. The criterion for its validity is that the "nonattenuative" wavelength, λ_0/n , be short compared to the skin depth, δ .

Reflection and Refraction

The laws of reflection and refraction of microwaves at interfaces between media of differing electromagnetic properties are essentially the same as those for the reflection and refraction of visible light. The angle of refraction is determined by Snell's law,

$$n_2 \sin \phi = n_1 \sin \theta$$

where n_1 and n_2 are, respectively, the indices of refraction of the two media, θ is the angle of incidence, and ϕ is the angle of refraction. The medium in which the incident ray occurs is arbitrarily designated by the subscript 1, and the other medium by the subscript 2.

It may be shown that, for linearly polarized plane waves incident normally upon an interface separating two dielectric media, the amplitudes of the reflected and transmitted waves, respectively, are given by the relations :

$$E_{\text{max, reflected}} = \frac{n_2 - n_1}{n_1 + n_2} E_{\text{max, incident}}$$

$$E_{\text{max, transmitted}} = \frac{2n_1}{n_1 + n_2} E_{\text{max, incident}}$$

Analogous relations hold for the amplitudes of the magnetic field. For angles of incidence other than zero, the corresponding relations are more complicated and will not be quoted here. Figure 7-4 shows how the amplitude of reflected and refracted waves vary as a function of the angle of incidence for a typical choice of the ratio n_1/n_2 . The shape of the curves in the figure will vary somewhat with the dielectric constant.

Standing Waves

As shown in figure 7-5, the space on the incident side of a boundary, in general, contains two

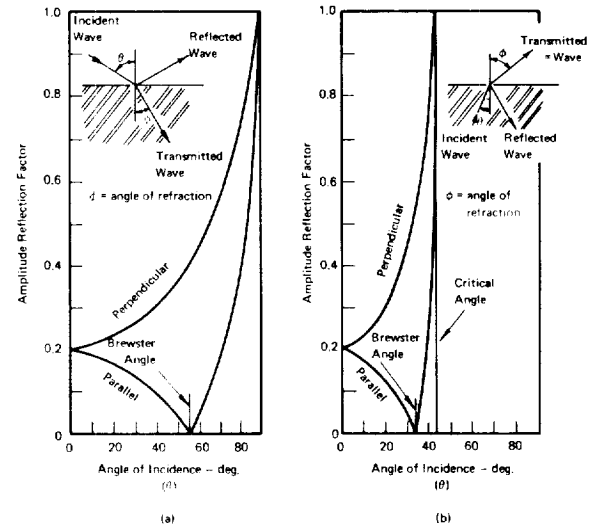


FIGURE 7-4.—Representative reflection of a linearly polarized plane electromagnetic wave at a dielectric interface with electric field parallel or perpendicular to the plane of incidence. [(a) shows wave entering dielectric; (b) shows wave leaving dielectric.] (Courtesy of Royal Radar Establishment, United Kingdom.) (ref. 1)

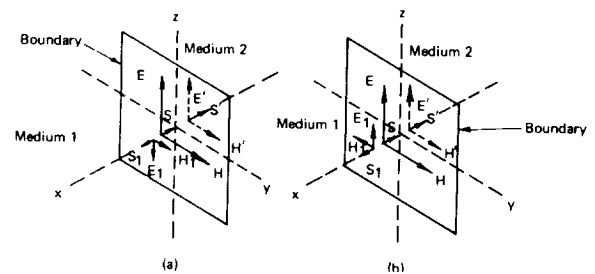


FIGURE 7-5.—Reflection and refraction of an Electromagnetic wave at a boundary surface between two media. [(a) $N_2 > N_1$; (b) $N_2 < N_1$.]

waves: the incident and the reflected wave. Like light waves, the incident and reflected waves may interfere and form standing wave patterns. To have a standing wave, the two or more waves involved must be of the same frequency, and traveling in opposite directions. A graphical representation of a standing wave produced by two equal-amplitude waves going in opposite directions is shown in figure 7-6. The technique in which standing waves are formed with microwave radiation has been used to make accurate measurements of thickness where conventional caliper methods are especially difficult. The technique involved is discussed later in the chapter.

Scattering of Microwaves

In the previous paragraphs, surface irregularities or secondary emitters on the surface and within the material were not considered. When the surface is not smooth on a scale commensurate with the wavelength of the microwaves used, the reflected wave is not a simple single wave, but is essentially a composite of many such waves of various relative amplitudes, phases, and directions of propagation. This effect is greatest when the wavelength is comparable to the dimensions of the irregularities. Under these circumstances, the radiation is said to be scattered. Figure 7-7 shows the scattering behavior of metal spheres having differing ratios of circumference to the wavelength of incident microwave radiation (ref. 1). The scattering is small for values of the circumference-wavelength ratio below 0.3, and varies as the fourth power of this ratio. Ratios below 0.3 lie in what is known as the Rayleigh region. The scattering "cross section" oscillates with decreasing magnitude as the circumference-wavelength

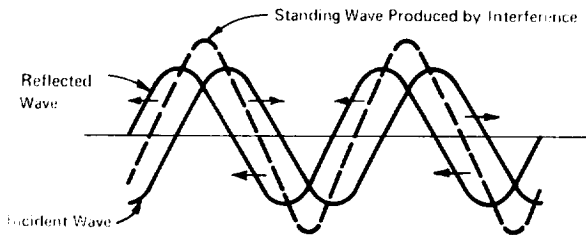


FIGURE 7-6.—Simplified sketch showing the formation of a standing wave by reflection.

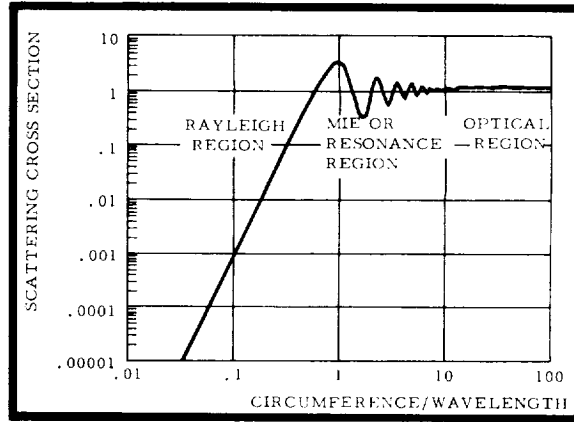


FIGURE 7-7.—Microwave scattering by metallic spheres of various sizes. (Courtesy of Royal Radar Establishment, United Kingdom.)

ratio varies from 0.3 to 10; ratios from 0.3 to 10 are in the resonance region. The maximum scattering occurs where the circumference equals the wavelength. The scattering becomes constant in the optical region for ratios greater than ten.

Absorption and Dispersion of Microwaves

As an electromagnetic wave propagates through a homogeneous medium, part of its energy may be absorbed by the medium. In macroscopic, phenomenological terms, absorption is due to any or all of the following effects: the electric polarization (i.e., electric dipole moment per unit volume) of the material may not vary in phase with the electric field of the wave; the magnetization (magnetic dipole moment per unit volume) may not vary in phase with the magnetic field of the wave; and if the material is electrically conductive, induced currents will dissipate energy by electric resistive loss mechanisms. To account for the first of these absorption mechanisms, it is customary to represent the electric field intensity (at some point within the medium) in the complex harmonic form,

$$E = E_0 e^{i\omega t}$$

Under steady state conditions, the electric displacement (which is proportional to the electric

polarization) is also harmonically varying, but with a phase different from that of E :

$$D = D_0 e^{i(\omega t + \delta)}$$

The complex permittivity ϵ (or dielectric coefficient) is then defined by the equation:

$$\epsilon \equiv \epsilon' + i\epsilon'' = \frac{D}{E} = \frac{D_0}{E_0} e^{i\delta} = \frac{D_0}{E_0} (\cos \delta + i \sin \delta)$$

The tangent of the phase angle δ is referred to as the dielectric loss tangent, and, thus, is given by the relation:

$$\tan \delta = \frac{\epsilon''}{\epsilon'}$$

It can be shown that the average rate of dissipation of energy (per unit volume of dielectric) is given by the expression:

$$\frac{1}{2} D_0 E_0 \omega \sin \delta$$

which, for small values of ϵ''/ϵ' , is approximately the same as

$$\frac{1}{2} D_0 E_0 \omega \frac{\epsilon''}{\epsilon'}$$

In general, both ϵ' and ϵ'' are functions of the frequency, ω . They are not, however, independent of one another. In fact, it can be shown that if one is known (as a function of ω for all values of ω), then the other is mathematically determined. Furthermore, in any frequency interval in which ϵ' is a rapidly changing function of ω , ϵ'' must also be rapidly changing. Since changes in ϵ' affect the velocity of the electromagnetic wave (or, equivalently, the index of refraction of the medium), it follows that at frequencies, ω , at which the medium has a rapidly changing absorption, it will also be highly dispersive, i.e., waves of slightly different wavelength will travel at appreciably different velocities. This effect is of considerable practical importance, especially when short pulses of microwaves propagate through absorptive media, since the shape of the pulse may be appreciably altered by the effects of dispersion. Figure 7-8 shows ϵ' and ϵ'' for water as a function of fre-

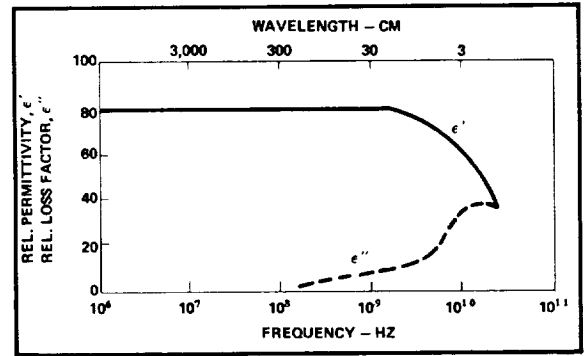


FIGURE 7-8.—Microwave moisture measurement is possible because of relaxation of the water molecule at microwave frequencies (ref. 2). (Courtesy of Lake Publishing Corp. and Plastics Design and Processing; copyright 1968.)

quency. This is an important practical case since ϵ'' has a pronounced peak at frequencies just above 10 GHz (i.e., at wavelengths of the order of 1 cm). This resonance occurs because the polar water molecule has a characteristic rotational relaxation time of about 3×10^{-10} sec. This microwave absorptive property of water is the basis of both microwave cooking and microwave moisture meters.

Special Techniques of Microwave Testing

The following general approaches have been used in the development of microwave nondestructive testing:

- (1) Fixed-frequency continuous wave transmission
- (2) Swept-frequency continuous wave transmission
- (3) Pulse-modulated transmission
- (4) Fixed-frequency continuous wave reflection
- (5) Swept-frequency continuous wave reflection
- (6) Pulse-modulated reflection
- (7) Swept-wavelength continuous wave reflection
- (8) Fixed-frequency standing waves
- (9) Fixed-frequency reflection scattering.

Each of these techniques makes use of one or more of the several processes by which materials can interact with microwaves, i.e., reflection, re-

fraction, scattering, absorption, and dispersion. These nine techniques will be briefly described from the instrumentation standpoint, grouped in four areas: transmission, reflection, standing wave, and scattering.

Transmission Techniques

The general features of the transmission technique are shown in figure 7-9. A microwave generator feeds both a transmitter horn (or other antenna) and a phase-sensitive detector (or comparator). The transmitter horn produces the electromagnetic wave that is incident upon the first face of the material to be tested. At the surface, the incident wave is split into a reflected wave and a transmitted wave. The transmitted wave goes through the material into the receiver horn. The transmitted wave will not all get through the second face of the material because some of it will be reflected at the second surface. The microwave signal from the receiver horn may be compared in amplitude and phase with the reference signal taken directly from the microwave generator.

The reference signal may be taken to be of the form $V \text{ ref} = V_0 \cos \omega t$. The received signal is then of the form,

$$V_{\text{rec}} = V' \cos (\omega t + \phi) = (V' \cos \phi) \cos \omega t + (V' \sin \phi) \sin \omega t$$

Because it is the coefficient of the term that varies in phase with the reference signal, the

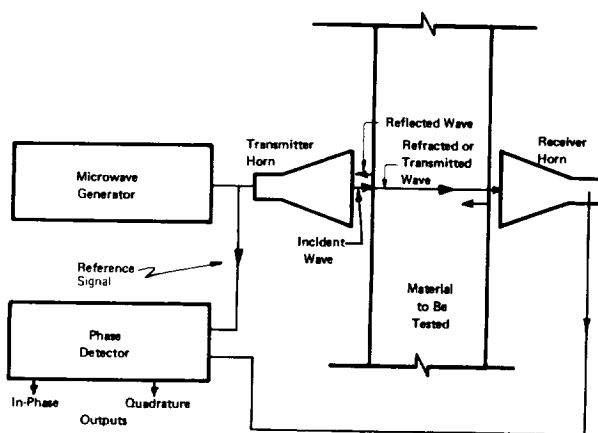


FIGURE 7-9.—Basic components of the transmission technique.

quantity $V \cos \phi$ is referred to as the in-phase component, while the quantity $V' \sin \phi$ is termed the quadrature component. Standard electronic phase-sensitive detectors are available which measure each of these components separately.

The transmission technique can have three variations: fixed-frequency cw, variable-frequency cw, and pulse modulated wave. Each of these variations will be described briefly.

Fixed-frequency cw transmission.—In this technique, the frequency of the microwave generator is fixed. This technique is usually used either when the band of frequencies required for the desired interaction is very narrow, or when the band of frequencies is so broad that the changes with frequency are very small and, therefore, not especially frequency sensitive. The fixed-frequency continuous wave transmission technique is the only one of the transmission techniques in which both components (in-phase and quadrature) can be detected with little mutual interference. Thus, when separation (the ability to get one component alone) is important, this technique is generally used.

Swept-frequency cw transmission.—Some microwave interactions are frequency sensitive in that their resonant frequency shifts with changes in material properties. For others, the response as a function of frequency over substantial bandwidth must be used. The swept-frequency cw transmission technique provides for a transmission measurement over a selected range of frequencies. Because of fundamental limitations on the ability of wideband systems to maintain a fixed phase relationship for all frequencies, phase-sensitive detection is not feasible. A straight amplitude detector that gives an output proportional to the peak amplitude of the transmitted signal is used. The fixed-frequency microwave generator shown in figure 7-9 is replaced with a swept-frequency generator, i.e., a generator the frequency of which is programmed to vary automatically. With presently available generators, a frequency band of one octave can be electronically swept (from 1 to 2 GHz, for example). The availability of wideband amplifiers of low noise and high gain also makes it possible to detect transmitted

signals through materials having quite high attenuation.

Pulse-modulated transmission.— Although phase measurements can be made on the transmitted wave, they are only relative to the reference wave and there is no simple method for tagging a particular sine-wave crest relative to another to measure transmission time. Therefore, when a measurement of the time-of-transmission is required, the pulse-modulated technique is called for. To produce the pulse modulation, the microwave generator is itself gated on and off. Also for this application, the phase-sensitive detector in the receiver is usually replaced by a peak-value detector. Thus, the receiver output will consist of pulses that are delayed a finite time relative to the transmitted pulse. An oscilloscope with an accurate horizontal sweep rate can be used to display these pulses.

Reflection Techniques

The reflection techniques are of two types: single-antenna and dual-antenna (fig. 7-10). Figure 7-10(a) illustrates the single-antenna system in which incident and reflected waves are both transmitted down the waveguide from the microwave generator to the antenna. The phase detector is set so that it compares the phase of the reflected wave with that of the incident wave, and gives two output signals which are respectively proportional to the in-phase and quadrature components in the reflected wave. Such a system works well only for normal or near normal incidence.

The dual-antenna reflection system (fig. 7-10b) operates at any angle of incidence for which there is appreciable reflection. A comparison of figure 7-10(b) with figure 7-9 shows that the dual-antenna reflection equipment is essentially the same as that used for transmission measurements. In the transmission technique the reflected wave is not used; in the reflection technique, on the other hand, the transmitted wave is usually not used except as a reference.

Because of the boundary conditions which must be complied with at the surface of the

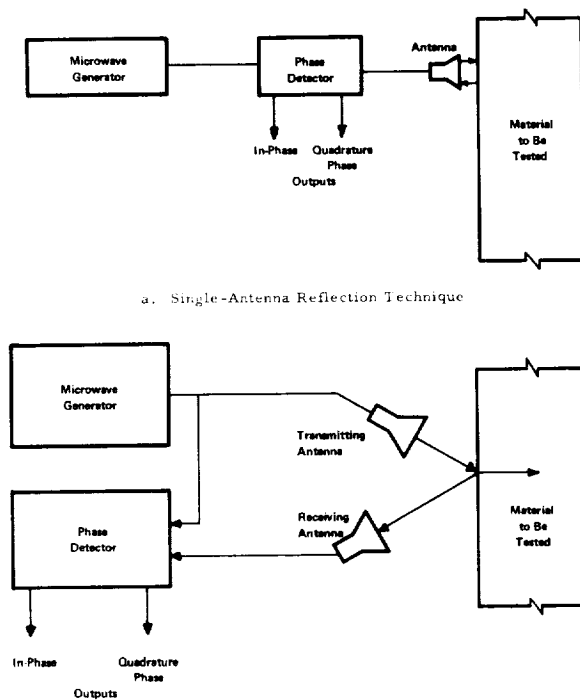


FIGURE 7-10.—Basic reflection techniques.

material, the reflected wave, in principle, has the same information about the bulk microwave properties of the material that the refracted wave does. However, the first surface wave will not contain any information about the inhomogeneous properties of the material within the sample being tested. There will be further reflections from any internal discontinuities or boundaries, which will ultimately add to the surface reflected wave when refracted at the surface. In this way, properties beneath the surface can be sensed. If the component being tested is a plate which has been backed with a layer of conductive metal, then the wave reflected from this metal face will have traversed the material twice, and it too will add to the surface reflected wave to provide information about the interior of the material.

Fixed-frequency cw reflection.—The simplest microwave reflectometer is based on the fixed-frequency technique. The microwave signal is incident upon the material from an antenna; the reflected signal is picked up by that same antenna. Although both the in-phase and the quadrature components of the reflected wave

can be determined, in practice, most such techniques have used only the amplitude of the reflected signal. The dual-antenna reflection technique (fig. 7-10b) can also be used at a fixed frequency. The fixed-frequency cw technique has two notable drawbacks: (1) the depth of a flaw cannot be determined and (2) the frequency response of the material being investigated cannot be determined. For these reasons, a swept-frequency technique may be more useful.

Swept-frequency cw reflection.—When the interaction between a material and microwaves is frequency sensitive, a display of reflection as a function of frequency may be valuable. Since phase-sensitive detection over a wide range of frequencies is difficult, only the amplitude of the reflected signal as the output of the measurement is usually used in swept-frequency techniques.

The measurement of depth can be made with a swept-frequency technique if the reflected signal is mixed with the incident signal in a non-linear element that will produce the difference signal. The difference frequency, then, is a measure of how much farther the reflected signal has traveled than the incident signal. Thus, not only can the presence of an internal reflector be determined, but also its depth.

Pulse-modulated reflection.—The depth of a reflection, in principle, can also be determined by pulse modulating the incident wave. When the reflected time-delayed pulse is compared in time with the incident pulse, and when the velocity of the wave in the material is known, then the depth to the site of the reflection can be determined. In both frequency and time-domain modulation, the nature of the reflector is determined by the strength of the reflected signal. The limitation of pulse modulation is that the pulses required are very narrow if shallow depths are to be determined. For this reason, the use of frequency modulation has been developed and used.

Swept-frequency reflection.—This technique uses a low frequency sweep to identify specific layers of several closely spaced layers of material. The reflection at even multiples of quarter wavelength is larger than at odd multi-

ples of quarter wavelength. The reflected signal will identify specific frequencies for which the layer spacing is an odd integral multiple of the wavelength. This same effect is used, for example, to reduce reflection from lenses by coating them with layers of dielectric.

Standing-Wave Techniques

A standing wave is obtained from the constructive interference of two waves traveling in opposite directions. The result is a standing wave in space, that is, if a small antenna is placed at a fixed point in space, a voltage of constant amplitude and frequency is detected. Moving the antenna to another place would give a voltage of a different but constant amplitude, with the same frequency. The graph of the amplitude of the voltage as a function of position along a standing wave is shown in figure 7-11. One antenna is needed to produce the incident wave, which can interact with the reflected wave to produce the standing wave; another antenna or probe is needed to make measurements along the standing wave. Thus, the dual-antenna reflection system in figure 7-10(b) could be used to both make and measure microwave standing waves. The receiver antenna must not interfere with the incident wave.

Scattering Techniques

The dual-antenna system diagrammed in figure 7-10(b) must be used for scattering measurements because the angles of the diffused or reradiated waves can be over a solid angle of $4\pi sr$. To measure all of the scattered radiation, the entire sphere around the irradiated object or material should be scanned and the detected signal graphed as a function of position.

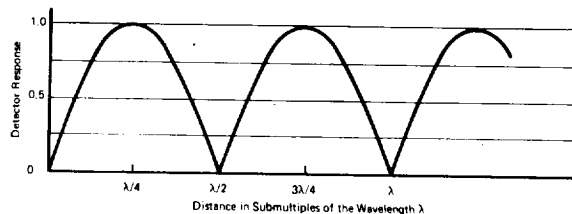


FIGURE 7-11.—Electromagnetic wave amplitude as a function of distance along a standing wave.

APPLICATIONS OF MICROWAVE TECHNIQUES

Thickness Gaging

Thickness measurements may be made with microwave techniques on both metals and non-metallic materials. For metals, use is made of two reflected waves, one from each side of the specimen, the measurement being made by means of the standing wave technique. In order to see how these measurements are made, what happens to a microwave signal incident upon a material (fig. 7-12) should be examined. Two cases are to be considered: (1) incidence upon a conductor and (2) incidence upon a nonconductor. When the wave is incident upon a conductor, most of the wave is reflected; only a small amount is transmitted. The transmitted wave is highly attenuated in the conductor within the first skin depth. For the nonconductors, however, the reflected wave is much smaller than the incident wave so that any standing wave that may be developed does not have a large amplitude. As is seen in figure 7-13, the distance between the minima of the standing wave is equal to one-half wavelength. That is, when a detector antenna moves a distance of one-half wavelength along a standing wave, the amplitude changes as shown. Thus, with a reflectometer (fig. 7-14), the thickness can be measured by forming a standing wave in the

Material	Relative Magnitudes	
	Reflected Wave	Refracted Wave
Conductor	Large	Small
Nonconductor	Small	Large

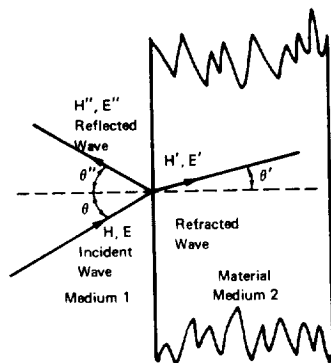


FIGURE 7-12.—Waves at a boundary and their relative magnitudes for conductors and nonconductors.

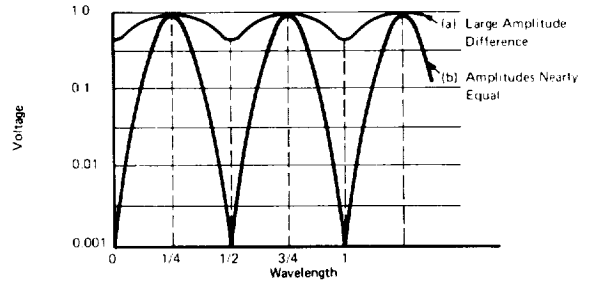


FIGURE 7-13.—Response of a detector moved along the path of interfering waves for: (a) large amplitude difference and (b) amplitudes nearly equal.

detector arm of a “hybrid tee,” a standard microwave device. The wave from the generator is split by the hybrid tee into two waves of equal amplitude. Each of these waves travels down separate waveguides, is reflected from the metal surface, and travels back through the waveguide to the hybrid tee. The hybrid tee then recombines the two reflected waves, directing them into the detector. One arm of the system has been changed in length to allow the sample to be inserted. When the difference between the respective “round trip” distances traveled by the two waves is one-half wavelength, the two waves interfere destructively and the detector reads a minimal voltage. The frequency of the generator can be adjusted in

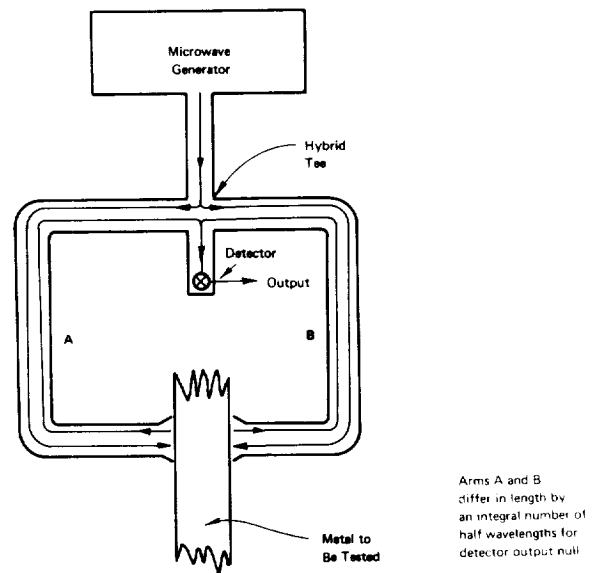


FIGURE 7-14.—Microwave metal thickness gage.

order that a minimal voltage is obtained for any particular thickness of specimen. The thickness of the specimen can then be calculated since the wavelength is known and the distance to one side of the sample is measured or calibrated.

The gage (fig. 7-14) can also be adapted to measure the thickness of a nonconductive material if one side is coated with a thin film of a conductive material. The difference between the two lengths then would be a distance equivalent to twice the thickness of the nonconducting material. If the velocity of the wave in the material and the frequency are known, then the thickness can be computed.

Provided the dielectric material whose thickness is being measured also has absorption, then the reflected wave will be reduced in amplitude so that a smaller amplitude standing wave will be obtained. The smaller amplitude decreases the accuracy of the measurement of the position of the minimum. A comparison of the standing waves for low and high absorption is given in figure 7-15 (ref. 1).

The range over which the simple thickness meter of figure 7-14 can be used unambiguously is approximately one-quarter of the wavelength of the microwaves in the material being tested. If the thickness varies more than one-quarter wavelength, ambiguous results will be obtained. The nominal thickness of most materials can usually be estimated or is known within manufacturing tolerances to within \pm one-eighth wavelength so that the ambiguity can be resolved.

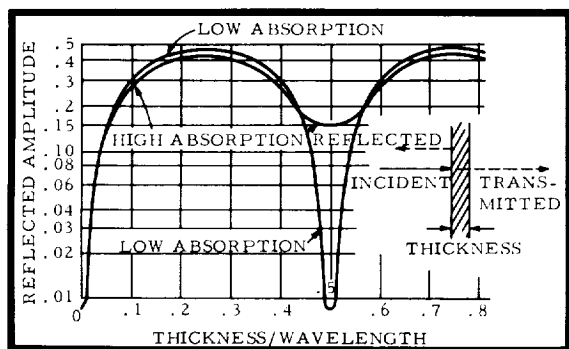


FIGURE 7-15.—Amplitude of reflected microwaves as a function of material thickness. (Courtesy of Royal Radar Establishment, U.K.)

A diagram of another simple thickness meter is shown in figure 7-16 (ref. 3). This meter does away with the hybrid tee and uses a direct waveguide to the material, which must be backed by a thin metallic coating. The standing wave that is set up in the waveguide is detected by a probe in the waveguide itself. If the probe were movable, it would trace out a curve similar to those in figure 7-15; however, in practice, the probe is fixed, and the frequency meter is used for calibration. A reference thickness of material is inserted and the frequency and sweep width for the microwave generator are adjusted until a single half-wavelength standing wave is observed on the oscilloscope. Also observed on the oscilloscope will be the output signal from the frequency meter, which occurs as a sharp peak when the frequency of the oscillator passes through the frequency to which the meter is set. This absorption peak appears superimposed on the standing wave as a pulse (fig. 7-17) (ref. 3). When the equipment is properly set, the peak will not be seen except at the null of the standing wave as shown in figure 7-17(b). When the reference material is replaced by one which is thinner, the peak will appear on the standing wave as shown in figure 7-17(a). When the material is too thick, the display will be as shown in figure 7-17(c). By observing the movement of the peak with respect to the standing wave, the material can be calibrated in thickness relative to the reference thickness.

A series of tests were conducted to determine the sensitivities on a typical sample, which was divided into four areas denoted by letters A, B, C, and D (fig. 7-18) (ref. 3). The instrument indicated that the material was 0.002 in. thinner after the 0.027-in. diam hole was drilled.

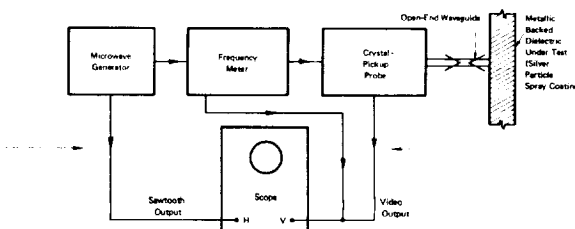


FIGURE 7-16.—“Single-side” microwave thickness gage.

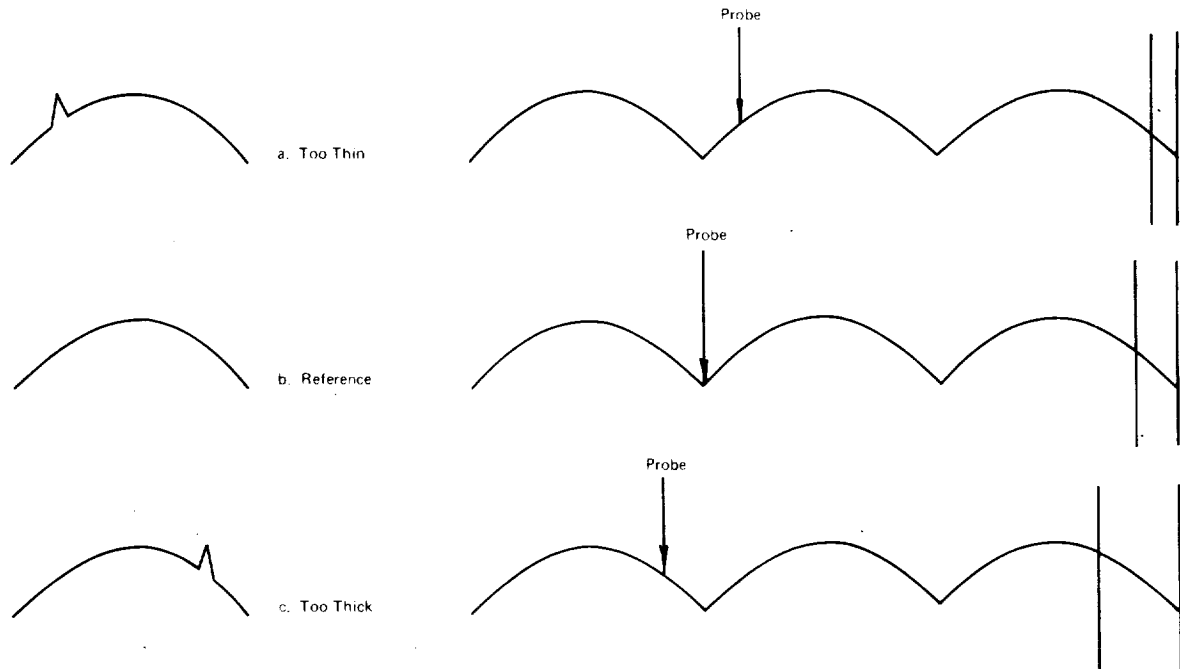


FIGURE 7-17.—Scope display and standing-wave relationship for "single-side" microwave thickness gage.

Larger holes gave a larger indication of thickness change. As shown in figure 7-18, the long dimension of the probe was along the long dimension of the hole. In B, the probe was at 90° to the hole with less indication than before, presumably caused by the polarization. In C, the results were similar to those from area B. D, which contained a delaminated area, gave an indication of an apparent increased thickness. Tests also performed on a piece of circuit board material indicated results similar to those obtained in D (ref. 3).

The use of a microwave thickness gauge in a variety of production operations has demonstrated its suitability for nondestructive testing and quality control of dielectric components. The data for the graph in figure 7-19(a) were obtained from polyethylene coating on common aluminum-foil wrapping material. Measurements were made on coatings of thicknesses of 1.0, 1.5, 1.75, and 2.0 mils. The data for the graph in figure 7-19(b) were obtained from a plate that is a glass fiber reinforced-resin structure used for fabricating boat hulls. The data for the graph in figure 7-19(c) were ob-

tained from aluminum-backed thick polyurethane foam used as a thermal insulation blanket for space vehicles. All of the data graphed in figure 7-19 were taken with a simple amplitude-sensitive reflectometer operating at 9.4 GHz. An antenna (a 1-in.² horn) was used to obtain the data in figures 7-19(b) and (c). The data in figure 7-19(a) were obtained with an antenna known as a short-field probe (ref. 2).

Microwave Flaw Detection

Flaws can be classified as (1) discontinuities and (2) gradual variations. Under these two classes, specific types of flaws may be grouped as:

- (1) Class I—Discontinuities
 - (a) Cracks
 - (b) Delaminations or separations
 - (c) Voids
 - (d) Inclusions
- (2) Class II—Gradual variations
 - (a) Porosity (macroporosity)
 - (b) Defective material regions (departures from nominal composition).

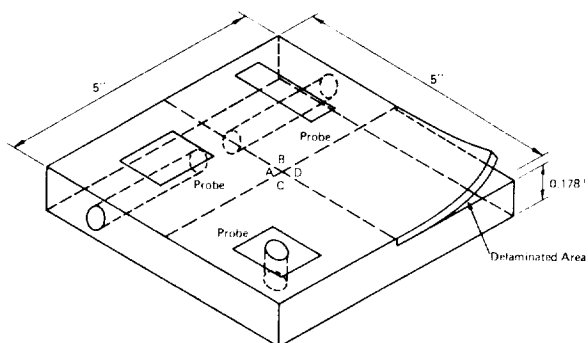


FIGURE 7-18.—Fiber glass laminate test sample for evaluating microwave thickness measurement.

The Class I flaws predominantly reflect or scatter electromagnetic waves. Wherever there is a crack, delamination, void, or inclusion, there is a more or less sharp boundary between two materials having markedly different velocities for electromagnetic waves. At these boundaries, which are usually thin compared to the wavelength of electromagnetic radiation being used, the electromagnetic wave is reflected and refracted or scattered. The reflected or scattered radiation will have appreciable amplitude only if the minimum dimension of the discontinuity is larger than about one-half the wavelength of the incident radiation in the material in question.

The Class II flaws are more gradual than those of Class I. They do not produce strong reflection or scattering, but they do influence the attenuation and the velocity of the electromagnetic wave. When there is absorption, the transmitted wave has an exponential decay with respect to the distance traveled.

CW reflectometer.—This reflectometer, in which the amplitude of the standing wave is measured by a detector in a combination send-receive, slotted microwave coaxial transmission line, can be used to detect flaws in glass-filament solid-rocket motor chambers (fig. 7-20) (ref. 4). The frequency used was in the 12.4- to 18.0 GHz band. Reflections from internal flaws change the amplitude of the standing wave measured by the detector and give a change in the output. When the material is scanned and the reflectometer signal is recorded by intensity-modulating a pen recorder, the flaws can be observed as

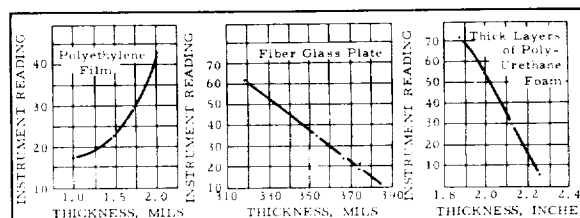


FIGURE 7-19.—Readings of an amplitude sensitive reflectometer as a function of film thickness for (a) polyethylene, (b) fiber glass plate, and (c) polyurethane (ref. 2). (Courtesy of Lake Publishing Corp. and Plastics Design and Processing; copyright 1968.)

light or dark areas. This type of "C-scan," when connected with level-sensing equipment, can be used to record only variations above or below a certain level, thus showing only the flaws. For test purposes, separations were represented by insulation patches made with various defects and bonded to the inside of the rocket case with rubber cement.

Typical C-scan recordings, made with the equipment pictured in figure 7-20, are shown in figure 7-21 (ref. 4). Some of the cutouts or unbonded areas are also shown, although the distortion makes it difficult to actually discern shapes. However, the detection of these patches led to the expectation that irregularities in the case-insulation and insulation-propellant bonds could be detected in motors loaded into the glass-filament chambers.

In order to verify this expectation from the patch tests, a special motor specimen, consisting of a 3-ft. length of the cylindrical section of a glass-filament chamber cast with solid propellant was made. The full-scale section has a case-insulation separation, a bond-insulation patch, an unbonded patch, insulation-propellant separations, and propellant voids. The insulation-propellant separations were made by attaching steel shims to the case wall and withdrawing them after cure. Shims ranging from 0.025- to 0.002-in. thickness were used. Voids of 1- to 3-in. diam were made by casting polystyrene foam balls into the grain, and fine voids were introduced by imbedding samples of porous, vacuum-cured propellant into the grain. After curing, the specimen was placed on a turntable and scanned.

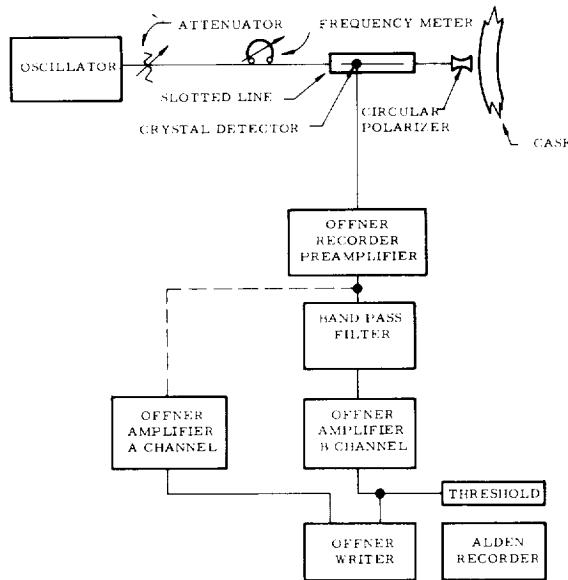


FIGURE 7-20.—CW microwave system used to detect flaws. (Courtesy of Am. Soc. NDT, Inc.)

The detection of the voids depends on the change in the wave reflected into the antenna due to the added reflection from the discontinuity caused by the voids. The system (fig. 7-20) was modified for these measurements by substituting a directional coupler for the slotted line. This coupler allows the output signal to be proportional only to the amplitude of the reflected signal. The reflected signal consists of a large reflection from the outer surface of the case plus smaller ones from the glass-insulation and the insulation-propellant interfaces. At any void or unbonded area, an additional reflection occurs which increases the overall reflection into the antenna. A standing wave can be set up by the reflection in the material in order that, at some frequencies, complete cancellation could occur for reflections one-fourth wavelength apart. Because of this possibility, frequencies were carefully chosen; several frequencies were used to assure that no cancellation occurred.

To make a measurement, the area of the motor casing was scanned around the circumference, and the amplitude of the reflected wave was recorded as a function of the distance around the circumference. The casing was then raised and another circumferential recording made. The re-

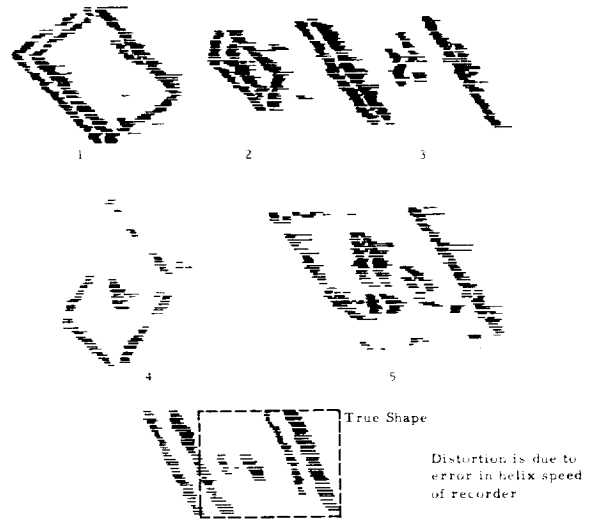


FIGURE 7-21.—C-scan of simulated defects. (Courtesy of Am. Soc. NDT, Inc.)

sults of a typical C-type scan for the areas having insulation-propellant separations are shown in figure 7-22 (ref. 4). The two areas, one each side of the central area, 6 in. wide, are the bonded or unbonded areas. The central portion, where the reflection increases, is that area where there is a 0.025-in. separation between the insulation and the propellant.

While the cw reflectometer could detect the larger voids, the propellant voids and porosity could not be detected. The variations in the reflections from surface irregularities were larger than the variations from the smaller voids and porosity. Therefore, some method was sought to eliminate the surface reflection from the output. Pulse modulation would accomplish this, but

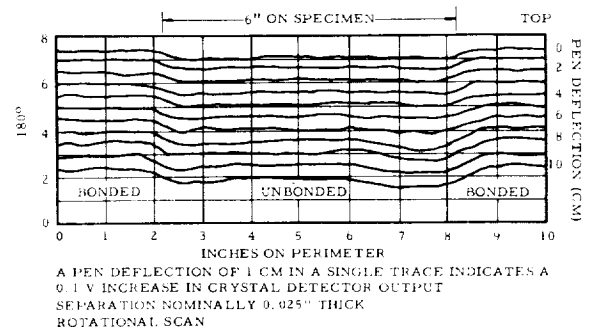


FIGURE 7-22.—Scans of separated propellant-insulation interface. (Courtesy of Am. Soc. NDT, Inc.)

the pulse widths required for the shallow depths were prohibitive. The swept-frequency (or frequency-modulated) reflectometer offered a realizable and useful alternative.

FM reflectometer.—In the FM microwave reflectometer, (ref. 4) a linear sweep is made of the entire frequency range of two generators: 1 to 2 GHz and 12.4 to 18 GHz (roughly the L band and the Ku band, respectively). A separate system was used for each band; each band was swept at a rate of 40 sweeps per second. The basic elements of the FM reflectometer are shown in figure 7-23(a). A graph of the signal at the detector as a function of time is shown in figure 7-23(b). The transmitted signal from the antenna is reflected back into the antenna and the detector from targets 1 and 2. The reflected signals also vary in frequency, just as do the transmitted signals, but, at the detector, *P*, they will be displaced in time as shown by the dashed lines in figure 7-23(b). Thus, at any instant of time, there are three signals at the detector: the first from the transmitted wave, the second from target no. 1, and the third from target no. 2. Each of these signals is of a different frequency, corresponding to the different

propagation times involved. The frequency difference, Δf , is equal to the rate-of-sweep (in Hz) times the delay in seconds. The other terms are defined according to figure 7-23(b). The phase of the reflected signal, ϕ , relative to the reference (transmitted signal) is

$$\phi = (2\pi f) \frac{2D}{c}$$

Both the frequency and the phase of the reflected signals are proportional to the distance to the respective reflectors. Small changes in the position of the reflector cause relatively large changes in phase, which, in turn, cause large changes in the shape of the signal obtained at the crystal detector. As the reflector moves through a distance equal to phase shifts of 0° , 90° , 180° , and 270° , the output of the detector changes in shape as shown by the curves in figure 7-24 (ref. 4).

The final L-band experimental arrangement for this investigation is shown schematically in figure 7-25 (ref. 4). In this scheme separate antennas are used for sending and receiving. The detector senses both the transmitted signal and the reflected signals. These are mixed in the

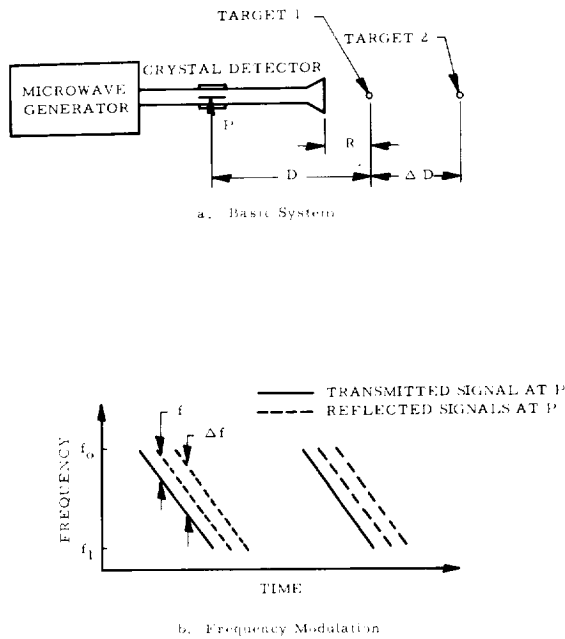


FIGURE 7-23.—Basic FM technique (ref. 4). (Courtesy of Am. Soc. NDT, Inc.)

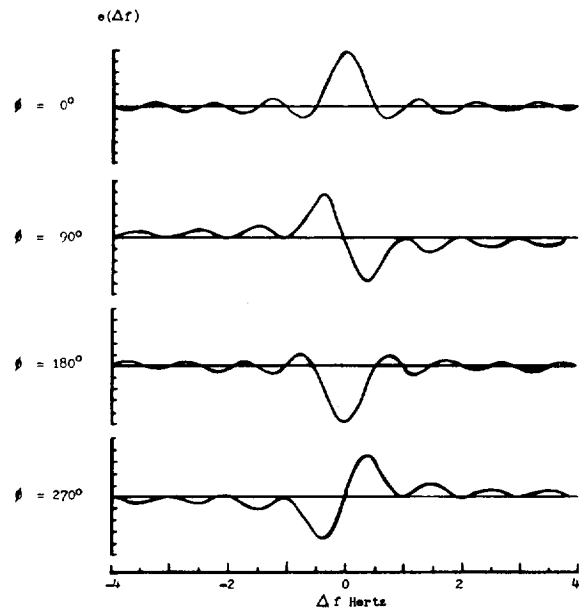


FIGURE 7-24.—Theoretical indications of reflections. (Courtesy of Am. Soc. NDT, Inc.)

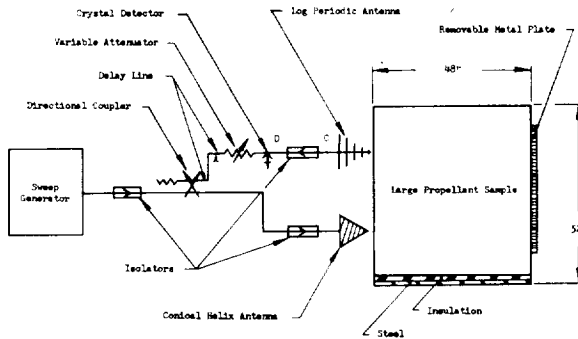
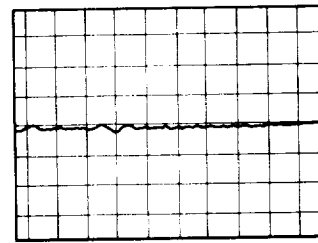


FIGURE 7-25.—L-band experimental arrangement. (Courtesy of Am. Soc. NDT, Inc.)

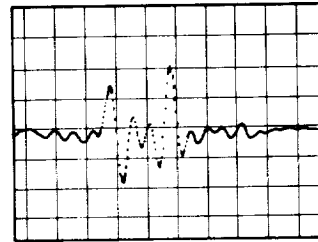
detector to produce a difference frequency equal to the reflected wave frequency, f , less the reference, f_0 , generated by the swept oscillator. A separate beat frequency is developed for each reflected signal. For the case of two discrete reflectors, the output signal of the crystal detector will comprise two frequencies, one for each target.

To determine the number of reflected objects and their locations, the signal from the detector is passed through a cross-correlation spectrum analyzer. The readout of the signal processor is a plot of the amplitude of the detector signal as a function of frequency. To accomplish this, the signal is chopped into many segments of equal duration. If the spacing of these segments corresponds to one of the frequency components of the signal, there will be an output. The spacing of these segments is varied by the long, sawtooth voltage, A , so that all of the possible frequencies in the signal will be swept through. Thus, the output will contain a voltage for each of the frequency components of the signal. Each component is displayed as a dot on an oscilloscope. The vertical displacement of this dot is proportional to the amplitude reached by the integrator for that particular frequency in the integration time.

The Ku-band equipment was similar to that used with the L-band except that waveguide was used rather than coaxial cable. The signals obtained from the Ku-band FM reflectometer through air and through a 2-in. propellant sample, respectively, are shown in figure 7-26 (ref. 4). Figure 7-26(b) shows the return from



a. Horn radiating into air



b. 2-in. propellant sample with metallic reflector on the back surface

FIGURE 7-26.—Ku-band experimental results. (Courtesy of Am. Soc. NDT, Inc.)

a 2-in. sample of propellant backed by a metal reflector on the side opposite to the antenna.

The horizontal axis for the traces in figure 7-26 can be calibrated in frequency (and, hence, depth). The trace shows that there are two main frequencies present, corresponding to reflections from two depths. The first is from the front surface of the sample; the second is from the back surface. A smaller indication is the first multiple reflection from the front surface back to the back surface again.

Further tests of the FM interferometer as an inspection device are reported in reference 5. Experience with the defect standards had shown that the scanning and specimen handling procedures were not separable from instrumentation problems. The production components examined were the Titan III ablative skirt, aircraft tires, and the Polaris A3 first-stage nozzle receptacles. As a result of the tests described below, it is believed that the FM interferometer can be successfully used in non-destructive testing.

1. *The Titan III ablative nozzle skirt.* Figure 7-27 shows the skirt and the inspection fixture (ref. 5). The skirt has an ablative liner: an inner shell of glass cloth and honeycomb, and an outer shell of additional glass cloth layers. At the aft end, there is a segmented flange of aluminum that is imbedded in the structure of

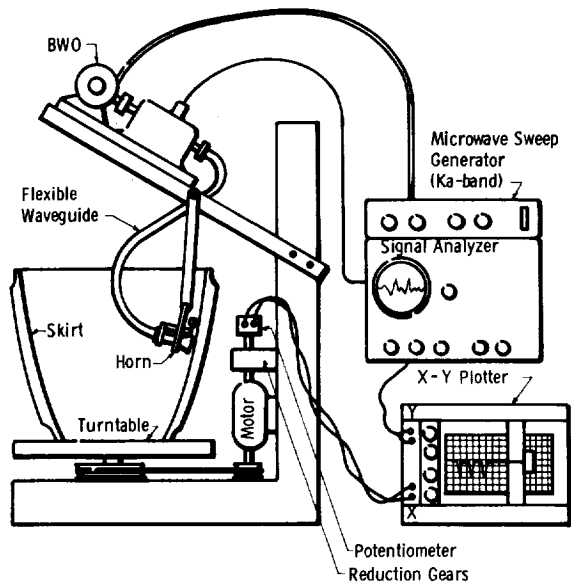


FIGURE 7-27.—Inspection of Titan III ablative nozzle skirt.

the skirt and contains bolt holes for attaching an aft closure. The closure is removed by explosive charges prior to ignition of the motor. An examination for defects of the entire skirt was performed, but, initially, the major effort was concentrated on the region of the segmented ring where damage in handling and in the explosive removal of the closure is possible. For this reason, skirts have been examined before and after tests during which the closures were explosively ejected.

During the test, the skirt was placed with the aft end up on a motor-driven turntable. The turntable drive was geared to a precision potentiometer to produce a voltage for the x-axis of an X-Y plotter to obtain a defect map of the flange area.

When the signal analyzer was put on manual depth scan and set to the depth corresponding to the flange-to-liner interface, the basic display was switched from the oscilloscope to the X-Y plotter and a plot was made of reflected signal vs. angular position on the skirt. Some typical results obtained are shown in figure 7-28. The dips are the gaps between flange segments where the reflection should diminish. The scan covers a region where there is no separation at the inner surface of the flange. The marked sections

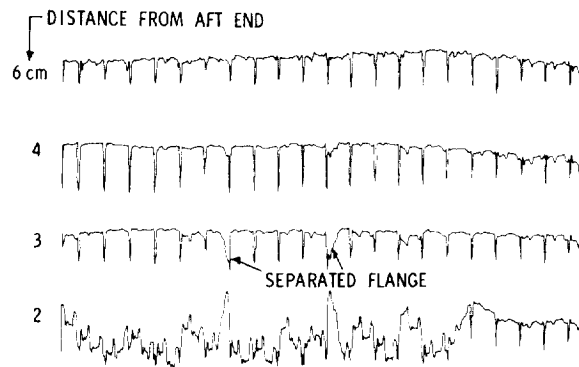


FIGURE 7-28.—Microwave inspection of Titan III-M skirt.

in figure 7-28 show regions where there are indications of some structural anomalies (ref. 5). The signal strength reflected from the inner surface of the flange segments did not return to the base line as rapidly as that from a normal section. One possible explanation is that a crack had started between the segments and had extended for a short distance along the bond between the flange segment and liner. On this basis, suspected defects were reported. Subsequent visual examination showed that the ends of the suspect segments were out of line at the surface, and radiographs confirmed that the concealed portions of segments in question were separated from the liner.

2. *Aircraft tires.* Another potential use of the FM reflectometer is the inspection of military and commercial jet aircraft tires. A full-scale tire with delaminations deliberately built in at various depths in the tread and sidewall was manufactured. Bonded and unbonded balance pads and patches were also applied to the inner surface. All laminar-type defects were detected by slowly scanning and observing the full-depth trace on the CRT of the signal analyzer.

3. *Polaris A3 first-stage nozzle receptacle.* The Polaris A3 first-stage motors have four nozzles, which are recessed into the case of the motor, except for the exit cones. The receptacle is protected by thick insulation to prevent the flame front from reaching any part of the nozzle other than the entrance cone. Separations between any part of the chamber insulation and the propellant grain are considered critical.

These separations are ordinarily detected by tangential betatron (radiographic) inspection, but, in the nozzle receptacle area, the thick, complex structure precluded a reliable inspection. In order to more readily inspect these separations, a special microwave probe that fits into the nozzle receptacle was constructed. (The K-band system (18 to 26 GHz) was used for the Polaris inspection.) The microwave probe was rotated around the nozzle in increments, and, at each increment, the phase control was rotated through 360°. The horn can be set to the desired depth in the nozzle receptacle. The charts were produced by an X-Y plotter. The detection of a 0.003-in. simulated separation was demonstrated.

As a result of these studies, it was concluded that the frequency-domain microwave interferometer is suitable for nondestructive testing. As might be expected, there are many technique variations to be investigated and since there have been continuous improvements, no definite set of performance limits is yet available. The most promising applications involve laminar dielectric structures in which separations and delaminations are the common defects. Epoxies, phenolics, and similar resins are quite transparent to microwaves, and, if they are reinforced with filaments, cloths, or tapes of glass, asbestos, or some similar materials, they remain so. (Metallic or carbon fibers, being conductive, will make the composite opaque to microwave energy.) Voids, and regions in which the resin does not fully impregnate the filler or reinforcement, can be detected as flaws. Some bulk properties can also be measured; for example, the microwave refractive index.

The knowledge derived from these NASA-sponsored NDT microwave studies has been incorporated into an applications guide (ref. 6). This guide is designed to assist the NDT engineer in determining the applicability of microwave testing to particular inspection and development problems.

Microwave Detection of Surface Cracks in Metals

When an electromagnetic wave is incident upon a metallic surface that has slits or cracks,

the metallic surface reradiates (reflects) a signal because of induced current. Under the proper conditions, the reflected wave will combine with the incident wave to produce a standing wave. The reflection from a surface without a crack will be different from that surface with a crack, and will depend upon the direction of the incident wave polarization relative to the crack. When the crack is long and narrow, and the polarization is parallel to the length of the crack, the reflected wave (and thus any standing wave) will be affected by the presence of the crack. The amount of change can be used to determine the size and the depth of the crack.

Standing waves, contacting.—The most sensitive means of detecting the small crack-related changes in the standing wave is to use the standing wave in a resonant cavity (ref. 7). Such a resonant system is also sensitive to variables other than surface cracks. However, a “non-resonant” standing-wave system may be used as demonstrated at the NASA Ames Research Center. One such system is shown in figures 7-29(a) and 7-29(b). Figure 7-29(a) shows the detection head with the test specimen forming one end of the system. The excitation is fed into two slots while the receiver is fed from two other slots. Figure 7-29(b) shows the total microwave circuit used. The test specimen is mounted so that it can be rotated. The variation of the received signal (as the specimen with a 0.010-in. groove is rotated 360°) (ref. 7) is shown in Figure 7-30. Measurements were made at other groove depths and the graph of the results is given in figure 7-31 (ref. 7). The presence of a crack in the fatigue specimen in figure 7-32 was shown by the results given in figure 7-33 (ref. 7).

In the system described above, the test surface acts as a short for one end of the waveguide section. In order that the only waves present in the waveguide section are those incident upon and reflected from the test specimen, the opposite end of the waveguide section is made nonreflective by means of a matching horn and absorbing material. The exciter slots are so arranged that the cylindrical transverse electric (TE_{11}) standing wave is set up by the reflection from a flat (crack-free) test specimen.

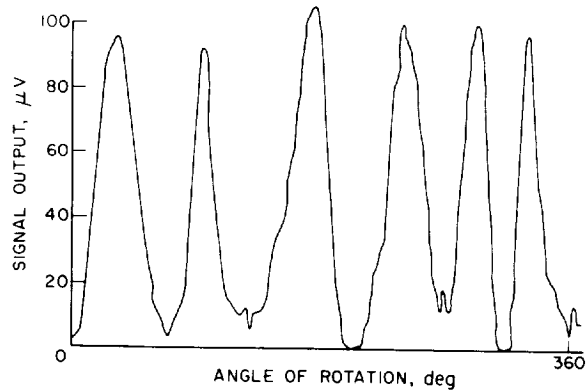
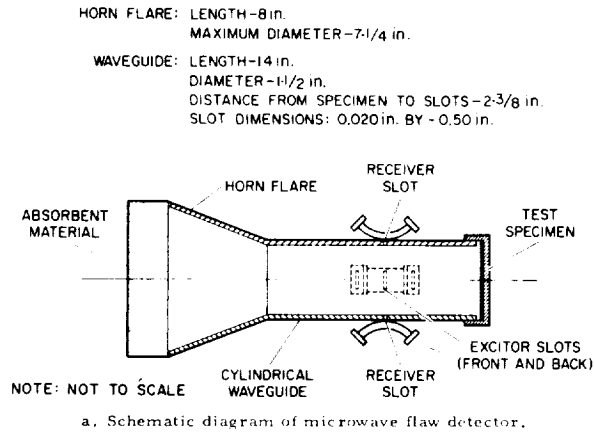


FIGURE 7-30.—Output signal for 0.010-in.-deep groove. (Courtesy of Am. Soc. NDT, Inc.)

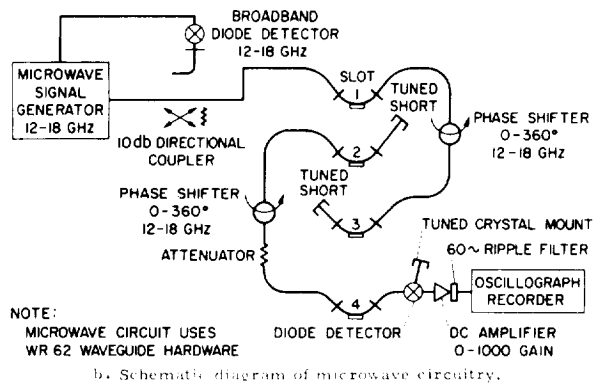


FIGURE 7-29.—Standing-wave surface flaw detection system (ref. 7). (Courtesy of Am. Soc. NDT, Inc.)

The goal of the design is to have none of the transverse magnetic (TM_{11} or TM_{21}) modes excited when the test specimen is crack-free. The presence of a crack in the surface of the test specimen disturbs the flow of current in the end required by the transverse electric mode so that the higher order transverse magnetic modes will be excited. Since the higher modes are specifically caused by the currents due to the crack in the end plate, when the end plate is rotated, these modes will also rotate past the receiver slots. With the TM_{11} mode, the receiver output shows two peaks for a 360° rotation; with the TM_{21} mode, four peaks are obtained from a full rotation. A crack at the exact center of the test surface does not produce a signal. The presence of six peaks as shown in figure 7-33 is probably caused by a mixture of the two

TM modes rather than higher transverse magnetic modes.

A suitable operating frequency was found by sweeping the frequency while the sample, with a groove 0.8 in. long and 0.030 in. deep, was being rotated. The correct value was indicated by a zero-dc level and a signal response to rotation of the groove that established the reference signal level. The microwave circuits were then tuned to this frequency. For the groove that was 0.8 in. long and 0.010 in. deep, a frequency of 15.965 GHz was used.

The influence of burrs was studied with a burr 0.00035 in. high on a groove 0.003 in. deep. The average signal with the burr had a peak-to-peak value of 15 μ V while the average signal

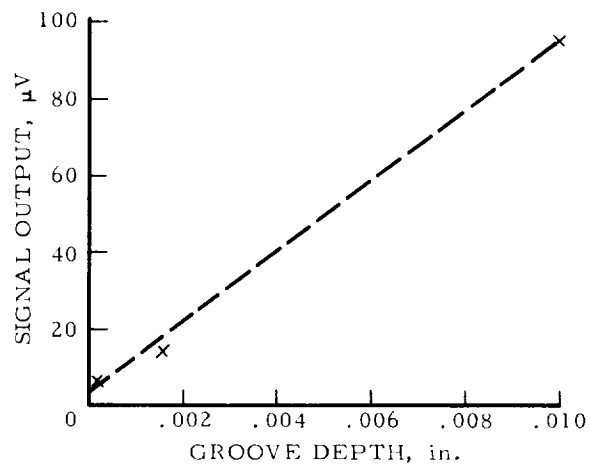


FIGURE 7-31.—Amplitude of output signal for various groove depths. (Courtesy of Am. Soc. NDT, Inc.)

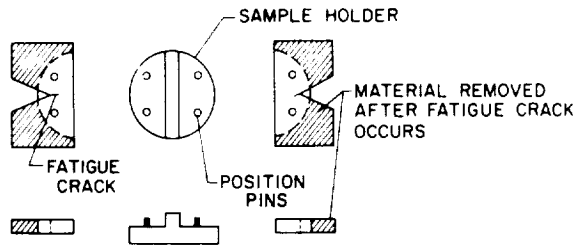


FIGURE 7-32.—Fatigue crack sample holder with samples. (Courtesy of Am. Soc. NDT, Inc.)

without the burr was $6 \mu V$. When the peak-to-peak variation from the various grooves was graphed as a function of the groove depth, the results shown in figure 7-31 were obtained. The straight dotted line fits the data but is not completely defined by the data.

The variations from the fatigue cracks shown in figure 7-32 are shown in figure 7-33. The fatigue cracks were much smaller than the notches used for calibration, being approximately 0.125 in. long and 50μ in. wide. The fourfold variation [fig. 7-33(a)] was caused by the asymmetry of the interfaces between the sample holder and the sample. The presence of one

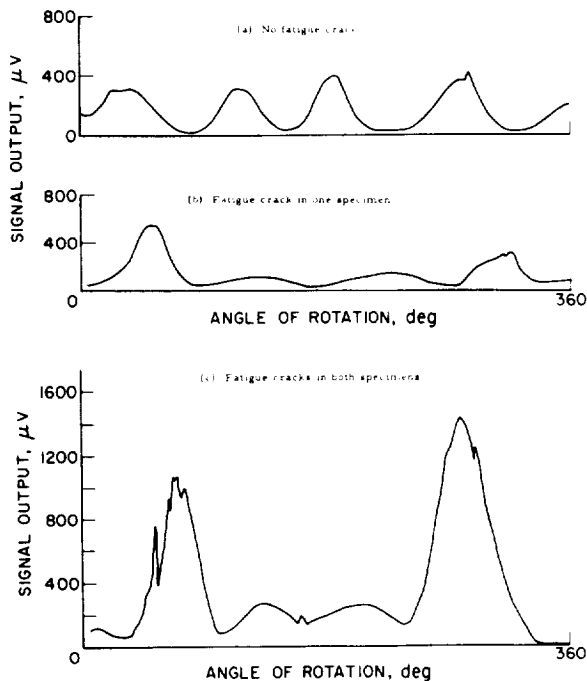


FIGURE 7-33.—Signal output for side-notched specimens. (Courtesy of Am. Soc. NDT, Inc.)

crack gave the results shown in figure 7-33(b). When a second crack was added, the results in figure 7-33(c) show that the two outside variations were increased in value.

Experimental data on the standing-wave, contacting system are summarized below:

- (1) Signal strength increased with increasing crack depth
- (2) Signal strength increased with decreasing skin depth
- (3) Signal strength was apparently unaffected by crack width
- (4) Microwaves can be adapted to the detection of surface cracks on metal specimens
- (5) Flaws or scratches as small as 100μ in. can be detected with the microwave standing wave
- (6) Proper design should increase the sensitivity by at least a factor of 10
- (7) The microwave system should be adapted to noncontact measurements.

Standing waves, noncontacting (ref. 8).—In a further development, noncontacting measurements were made using the apparatus illustrated in figures 7-34 and 7-35 (ref. 8). The details of the microwave mode converter used are shown in figure 7-36 (ref. 8). The mode converter causes the incident wave to be a higher order cylindrical mode composed of TM_{01} or TE_{01} modes. A crack, groove, or other surface defect causes the higher order mode to “degenerate” to the fundamental TE_{11} cylindrical mode that will pass through the mode filter and rotator to produce an output signal. The mode filter is modulated at 1 kHz, and, as a consequence, only the TE_{11} mode signal will have the proper 1-kHz modulation to pass through the narrow-band amplifier tuned to 1 kHz. Grooves with nominal widths of 50μ m were electromachined in a test specimen. Graphs of the results obtained from different groove depths in aluminum are shown in figure 7-37 (ref. 8). A curve is shown for each of the two cylindrical modes used. The largest variation was obtained with the TE_{01} mode.

For steel, the graph of output as a function of crack depth is shown in figure 7-38; the TM_{01} mode produced the widest variations (ref. 8). Contrarily, the opposite was true in aluminum.

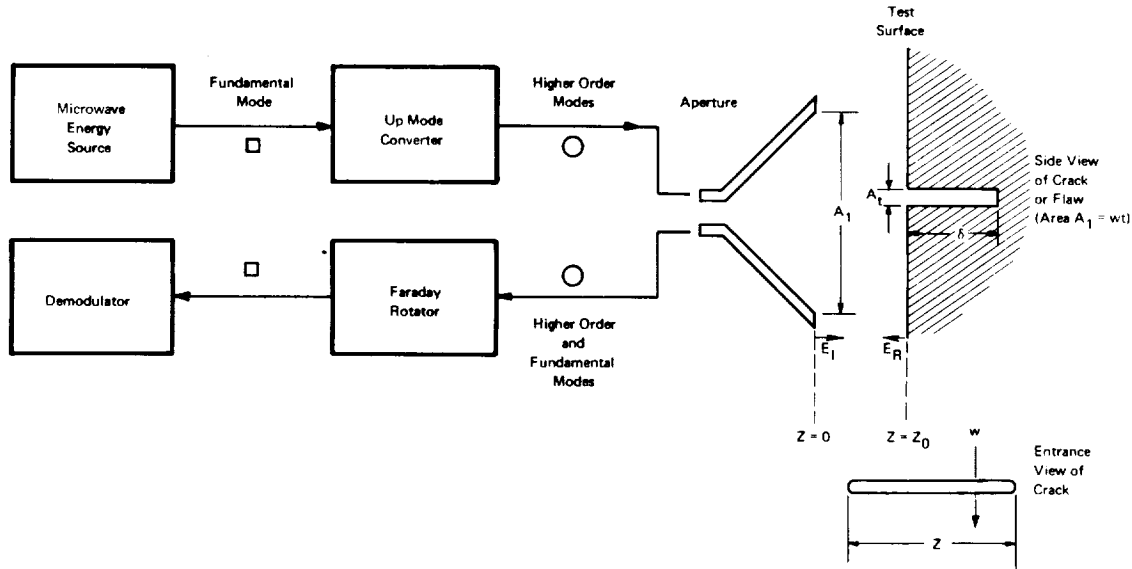


FIGURE 7-34.—Schematic of aperture and crack. (Courtesy of J. Rev. Sci. Instrum.)

Chemical Composition

In many instances, chemical changes in dielectrics, such as plastics, can be detected or even continuously monitored by the use of microwaves; also, the results of chemical changes can be measured. The criterion is that the chemical change must affect the dielectric properties (dielectric constant and/or loss tangent) of the material for electromagnetic frequencies in the microwave region. Some of the chemical or molecular-level applications that have been successfully investigated include:

- (1) Polymerization and degree of cure
- (2) Oxidation
- (3) Esterification
- (4) Distillation
- (5) Vulcanization
- (6) Evaporation
- (7) Titrations (end points).

Microwave techniques have been successfully used to measure specific gravity, homogeneity during blending, and vibration (or displacement). Several investigators have measured the glass-to-resin ratio of some types of aerospace composites (ref. 5).

Studies of the foregoing type can be made with either a through-transmission system or a reflectometer, as previously described, since the

changes in chemical composition will cause a change in the velocity of propagation. The changes in propagation velocity will change the amount and angle of the reflected and transmitted energy.

Moisture Analysis

The free (unbound) moisture content of many dielectric materials can be accurately measured with microwave techniques. Microwaves are strongly absorbed and scattered by water molecules because water exhibits a broad-

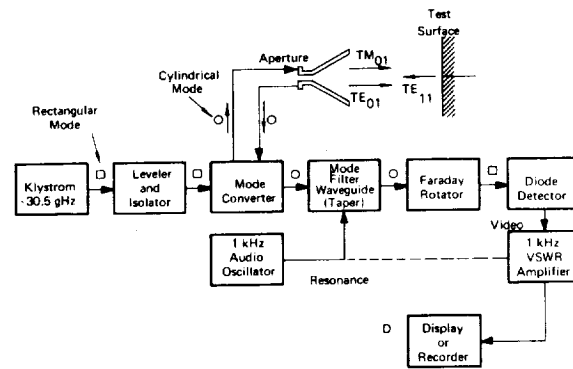


FIGURE 7-35.—Schematic for microwave crack depth measuring system. (Courtesy of J. Rev. Sci. Instrum.)

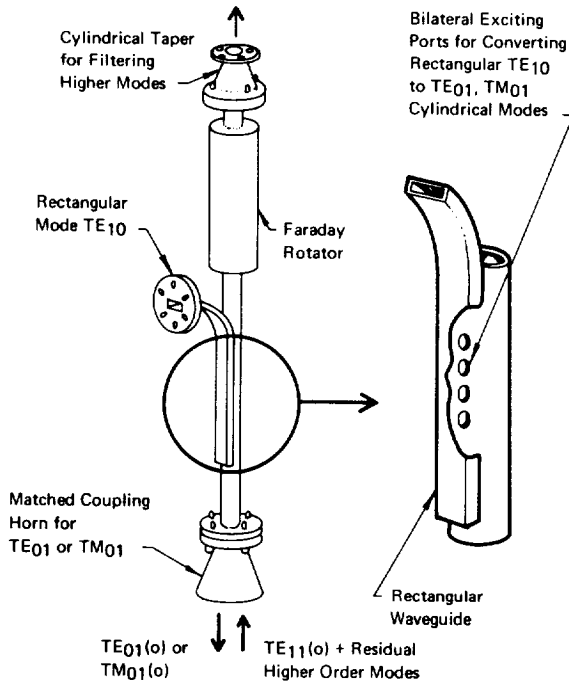


FIGURE 7-36.—Mode converter and taper. (Courtesy of J. Rev. Sci. Instrum.)

band rotational relaxation in the microwave region. Since many completely dry host materials are quite transparent in the same frequency range, a moisture-measuring technique is possible. This technique has found wide use on both a continuous process and laboratory sample basis, especially for plastic and ceramic materials. Figure 7-39 shows the microwave moisture measurement of polyethylene powder;

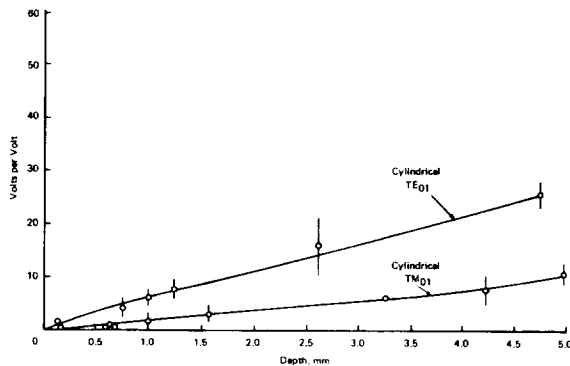


FIGURE 7-37.—Experimental slot depth vs signal strength for aluminum. (Specimen aperture separation = 5mm.) (Courtesy of J. Rev. Sci. Instrum.)

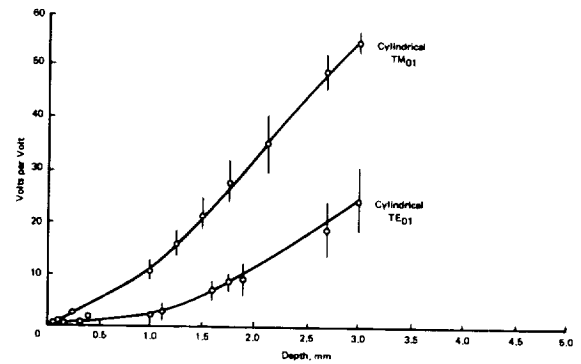


FIGURE 7-38.—Experimental crack depth vs signal strength for steel. (Specimen aperture separation = 5mm.) (Courtesy of J. Rev. Sci. Instrum.)

the plastic was tested by through-transmission techniques at a frequency of 9.4 GHz (ref. 2). Measurements similar to those for the plastic powders can also be obtained for solid shapes, slurries, and liquids. The technique (as described here) is not applicable for gases.

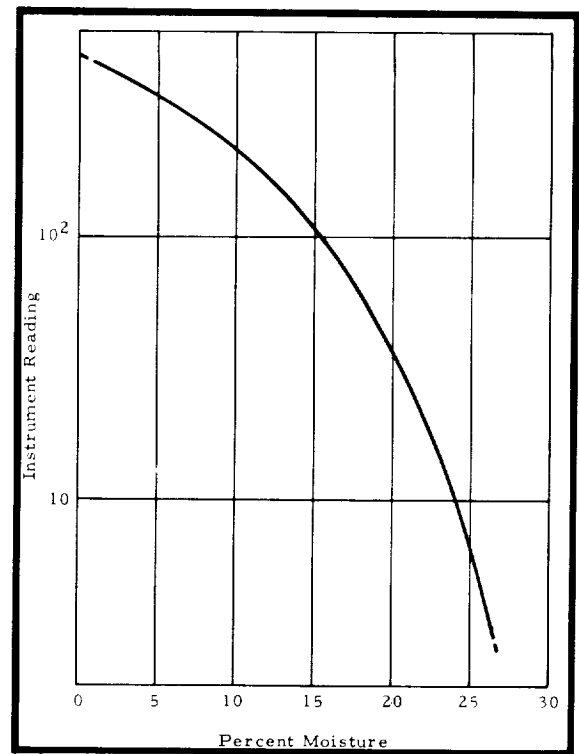


FIGURE 7-39.—Moisture measurement of polyethylene powder. (Courtesy of Lake Publishing Corp. and Plastics Design and Processing; copyright 1968.)

Since water is a polar molecule, its dielectric properties are a function of temperature, and, therefore, if substantial material temperature changes occur, compensation is necessary in the instrument calibration. For example, a change of -12°C will normally cause an error of $\pm 0.2\%$ in the moisture readout. The effect is more pronounced in materials possessing high moisture. Fortunately, the product temperature of most plastic process lines is kept reasonably constant at a given location. The temperature effect is also even less of a problem with plastics because they are relatively dry at the point of measurement.

Microwave Measurement of Material Anisotropy

The directionally dependent properties of some materials can be measured by the use of linearly polarized microwaves. Measurements of anisotropy, on both the molecular scale and macroscopic scale, are made by rotating the sensing head relative to the material under test and observing the signal as a function of polar angle. Certain linearly oriented polymers can be used as examples of molecular level measurements, while wood and glass-fiber-resin structures are examples on the macroscopic level. The direction of glass fibers can be readily determined.

Fiber-matrix composites have also been measured successfully for directionality. One example was a multiple-ply composite having a glass-fiber-resin matrix and unidirectional boron filaments. The boron filaments, of approximately 0.005-in. diam, contained in a tungsten fiber center (0.0005 in. in diam) onto which the boron had been deposited. Being electrically conductive, the overall composite acted on the microwaves very much like a diffraction grating. It was quite easy to detect alignment shifts of only a few degrees by monitoring either the reflected or transmitted microwave component. When the boron filaments were per-

pendicular with respect to the polarization of the microwave beam (electric field vector), a maximum amount of energy was transmitted (or a minimum amount of energy reflected). When the boron filaments and the polarization were parallel, the reverse was true. By continuously rotating the sample, a sinusoidal pattern of filament direction vs signal amplitude was obtained.

REFERENCES

1. HARVEY, A.: *Microwave Engineering*. Academic Press, Inc., 1963.
2. BORSO, RON J.: *Nondestructive Testing of Plastics with Microwaves*, Part 1 and Part 2. *Plastic Design and Processing*. [Reprinted from Nov. and Dec. 1968 Issues, Lake Publishing Corp. (Libertyville, Ill.).]
3. LEONARD, J. D.; AND STROPKI, G. T.: *Quality Control and Nondestructive Testing of Dielectric Components Using the Microwave Thickness Gauge*. Proc. of the 7th (Vol. 5) Symposium on Electromagnetic Windows. Sponsored by the USAF and Ohio State Univ. (Columbus, O.), June 2-4, 1964. (Available from AIAA in microfiche, A65-11107).
4. LUCIAN, A. D.; AND CRIBBS, R. W.: *The Development of Microwave NDT Technology for the Inspection of Nonmetallic Materials and Composites*. Proc. of the 6th Symposium on Nondestructive Evaluation of Aerospace and Weapons Systems Components and Materials, 1967, pp. 199-232. [Available from Western Periodicals Co. (North Hollywood, Calif.)]
5. STANDART, M. W.; LUCIAN, A. D.; ECKERT, T. E.; AND LAMB, B. L.: *Development of Microwave NDT Inspection Techniques for Large Solid Propellant Rocket Motors*. (NAS7-544) Final Rept. 1117, Aerojet-General Corp. (Sacramento, Calif.), June 15, 1969.
6. ANON.: *Microwave Inspection Applications Guide*. NASA CR-107670, 1969.
7. FEINSTEIN, L.; AND HRUBY, R. J.: *Surface-Crack Detection by Microwave Methods*. Proc. of the 6th Symposium on Nondestructive Evaluation of Aerospace and Weapons Systems Components and Materials, 1967, pp. 92-106. [Western Periodicals Co. (North Hollywood, Calif.)]
8. HRUBY, R. J.; AND FEINSTEIN, L.: *A Novel Nondestructive Noncontacting Method of Measuring the Depth of Thin Slits and Cracks in Metals*. *Rev. Sci. Instrum.*, vol. 41, no. 5, 1970, p. 679.

|

N13- 28525
PRECEDING PAGE BLANK NOT FILMED

CHAPTER 8

Magnetic Testing

Richard L. Pasley and John R. Barton

In the broadest sense, magnetic testing comprises all methods in which magnetic fields play an essential role. However, some that might logically be included under the heading of magnetic testing are generally given an independent status. The division is usually made on the basis of frequency. If the magnetic fields involved are static or oscillate at low frequency, the method is classified as a magnetic field method; if the fields oscillate at a high frequency, the method is not so classified. Hinging as it does upon the arbitrary division between low and high frequencies, the foregoing criterion is not always applied in the same way. Microwave radiation, nuclear magnetic resonance (NMR), and electron paramagnetic resonance (EPR) are distinctly high-frequency methods. On the other hand, magnetic-particle inspection and the related magnetometric methods of mapping magnetic field perturbations, as well as tests based on hysteresis characteristics of ferromagnetic materials, use static or vlf fields and are therefore classed as magnetic field methods. Some confusion arises, however, in the classification of methods in which the essential magnetic field involved arises from an electric current induced or injected in a specimen. In such methods, either currents of quite low frequency (even a constant current) or currents of quite high frequency are used, and in principle include eddy-

current methods. However, the basic eddy-current method and its close satellites are rightly accorded an independent status. Certain induced or injected current techniques that might reasonably be classed with eddy-current methods are treated here as magnetic field methods; the decision to do so is based on the essential commonality of their associated techniques of measuring and mapping magnetic fields with those of methods clearly recognized as magnetic field methods.

Magnetic testing probably began by using naturally occurring magnets to separate those metals attracted by magnets from those which are not. Flaws were detected by magnetic methods as early as 1868 when Saxby used an ordinary magnetic compass to locate defects and inhomogeneities in iron gun barrels. Although Saxby attempted to explain the principles behind his test method, many unknowns about magnetism existed at that time. The next notable development was made in 1876 by Ryder, who employed a magnetic method for evaluating the carbon content of ferrous metals. In 1879, Herring was granted a patent for detecting defects using a compass needle. The magnetic induction balance was introduced in 1879 as a means to distinguish between hard and soft steel specimens. Introduced by Hughes, this device was based on the use of alternating

currents to establish magnetic fields in the test specimens, and a pair of earphones to give the test operator an audible indication of the induction balance. The U.S. Bureau of Standards became interested in magnetic testing, and in 1911 undertook an investigation of the mechanical and magnetic properties of spring steels. Following closely in this interest was the American Society for Testing Materials which established, in 1916, a committee on magnetic analysis.

About 1917, Hoke in the United States and metal workers in England noticed that iron particles accumulated around cracks in ferromagnetic articles that were held in magnetic chucks while being ground. This discovery led to the development of magnetic-particle testing. Around 1928, A. V. de Forest began his pioneering work in developing magnetic-particle methods for nondestructive evaluation. In a series of papers, de Forest described the use of circular magnetization for detection of longitudinal defects. He used currents supplied by storage batteries as the source of magnetism to attract powders of various iron compounds to defects. Recognizing the great technological implications of these developments, de Forest, in association with F. B. Doane, founded the Magnaflux Corp. in 1934, the firm chiefly responsible for the commercial development of the magnetic-particle method in the United States.

By 1926, investigations had been reported that involved studies of permeability, coercivity, and other magnetic properties of ferromagnetic materials. During this early period, the terminology "magnetic analysis" was used to describe all types of magnetic tests; later, this term was restricted to describing magnetic methods for the inspection and evaluation of material properties and material quality as opposed to tests for measuring magnetic properties *per se* (ref. 1).

Beginning with World War II and the vast increase in use of aircraft and other transportation vehicles, the rate of development of magnetic testing rapidly increased, especially for magnetic-particle inspection. Government specifications for the first time required magnetic-particle inspection in the fabrication of many

iron and steel parts; process-control documents were written to regulate inspection. At first, inexperienced inspectors often rejected parts that subsequently proved acceptable. Manufacturers experiencing this type of wastage felt the government regulations were unreasonable, especially those manufacturers who had previously never heard of the method. Eventually, industry grew familiar with the magnetic-particle method and began to accept its use (ref. 2).

Developments, especially within the last two decades, include refinement of magnetic field perturbation methods in which a coil of wire or a Hall effect probe scanning the surface of a specimen is used to locate and map regions of anomalous flux leakage. Also, test methods that depend mainly on bulk ferromagnetic characteristics of the investigated material came into use.

Both magnetic-particle and magnetic field perturbation methods are used primarily for flaw detection. The methods are based on simple principles of mapping magnetic fields and in most cases are easy to use. However, both methods have a major limitation in that the test material must be ferromagnetic. Surface and subsurface flaws can be detected by these methods, although the ability to find a defect diminishes with its depth below the surface. In general, the magnetic-particle method is more widely used than the magnetic field perturbation one because it has been in use longer and because its general-purpose equipment can be used for a variety of tests. On the other hand, magnetic field perturbation methods are more sensitive and much more readily automated.

Hysteresis measurements have occasionally been used for detecting flaws, though they are more commonly used for determining changes in material properties such as hardness, chemical composition, and residual stress. For flaw detection, other methods are generally superior to hysteresis-type measurements.

The electric current perturbation method is used primarily to detect flaws in nonferromagnetic materials. This method can be used for locating both surface and subsurface flaws, but in many applications has the disadvantage of requiring exceptionally clean surfaces for the introduction and exit of current.

Because of the relative complexity of the magnetic testing field, a technical discussion of differences and principles is contained in the material that follows. Readers who are concerned primarily with the results may prefer to start with a later section.

PHYSICAL PRINCIPLES

In contemporary physics, all magnetic phenomena are explained in terms of forces between electric charges in motion relative to one another. Such magnetic forces are found to vanish when two charges are at rest relative to one another, and are therefore to be distinguished from purely electric forces that do not so vanish. The initial discussion is restricted to magnetic interaction between charges that move through electrically conductive matter. Such interactions manifest themselves in the form of net forces between conductors bearing electric currents. Figure 8-1 depicts representative portions of two long, parallel conductive wires, each bearing an electric current. When the currents flow in the same direction, each conductor exerts a net force of attraction upon the other; when the currents flow in opposite directions, the force is of the same magnitude, but is reversed in direction, becoming repulsive. The force is found to be proportional to the product of the magnitudes of the two currents, I_1 and I_2 , and to diminish in strength as the separation between the wires increases. These phenomena provide the basis for the international definition of the unit of current: the ampere is the electric current which, if flowing in each of two long, parallel wires 1m apart, results in each wire exerting a force on the other, the force being of magnitude 2×10^{-7} N/m of wire length.

It is convenient to discuss the mutual interaction of currents in terms of a magnetic induction field, \mathbf{B} , surrounding a distribution of current. The magnetic induction field, \mathbf{B} , may be defined as follows. First, consider a small, plane one-turn coil carrying a current, I amperes, and having a surface area, A . To this coil a vector \mathbf{m} , is assigned, called the magnetic dipole moment, whose orientation is normal to the area of the coil, and whose direction is

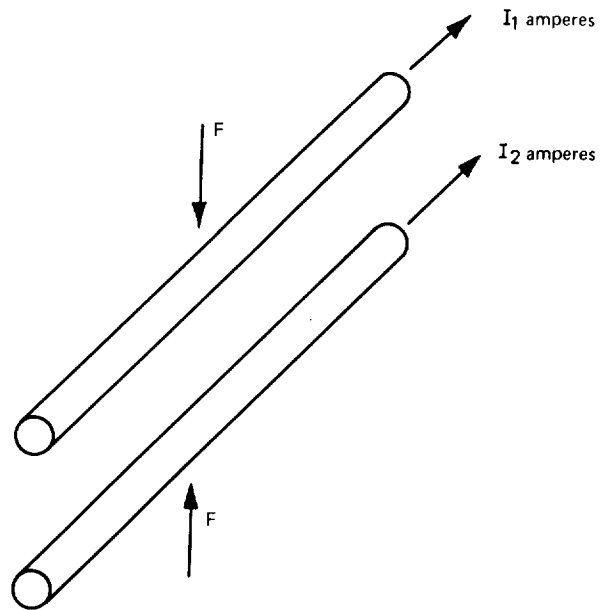


FIGURE 8-1.—Schematic of parallel conductors.

related to the sense of current flow in the coil by the right-hand rule as illustrated in figure 8-2. The magnitude of the vector, \mathbf{m} , is, by definition, the product of the current, I , and the coil area, A , i.e.,

$$|\mathbf{m}| = m = IA$$

It is observed experimentally that a small current loop, as described, behaves in the presence of other current carrying conductors quite like a small permanent magnet. In particular, the coil aligns itself in space so that its vector, \mathbf{m} , is oriented in the same direction as would the south-pole-to-north-pole axis of a small permanent magnet. This suggests that the direction of the magnetic induction field, \mathbf{B} , at a particular point of space be taken as the direction assumed

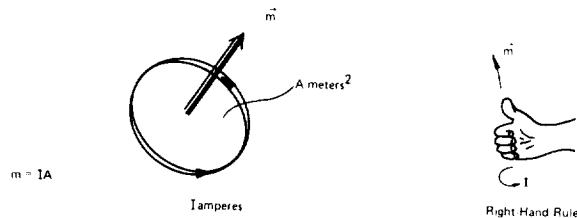


FIGURE 8-2.—Magnetic dipole moment \mathbf{m} of a small current loop.

by the vector \mathbf{m} associated with a small current-carrying test coil. Adopting this definition, it is further found experimentally that if the axis of the coil (i.e., the vector, \mathbf{m}) is forcibly rotated away from its equilibrium direction (which is, by definition, the direction of \mathbf{B}), the torque required to maintain it at an angle, θ , is proportional to the magnitude of \mathbf{m} , and to $\sin \theta$; furthermore, the torque always has a sense tending to return \mathbf{m} to its original direction, as illustrated in figure 8-3. This suggests the definition: the magnitude of the magnetic induction field \mathbf{B} is the torque, L , divided by the product $m \sin \theta$, i.e.,

$$\mathbf{B} = \frac{L}{m \sin \theta} \quad (1)$$

The units in which \mathbf{B} is measured are, by convention, Wb/m^2 , defined as follows: 1 Wb/m^2 is the magnetic induction that will result in a torque of 1 N-m on a coil of the magnetic moment 1 A-m², when placed with its axis perpendicular to the direction of the magnetic induction field. The Wb/m^2 is, of course, not a fundamental physical unit. In fact, from equation (1), it is clear that 1 Wb/m^2 is equivalent to 1 N/A-m.

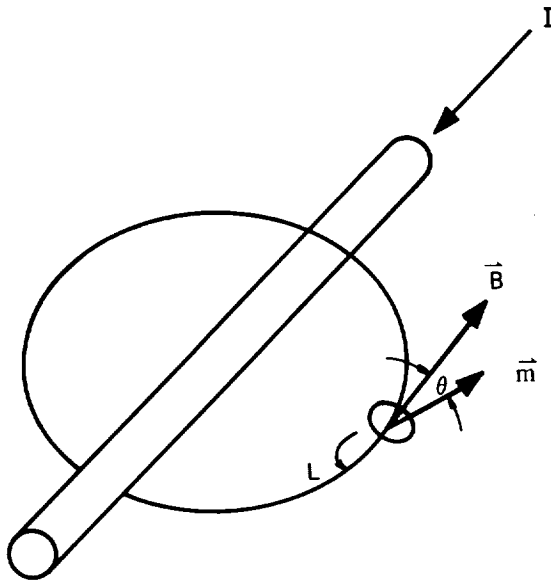


FIGURE 8-3.—A torque is exerted on a magnetic dipole when it is not aligned with the magnetic-induction field. (The magnitude of \mathbf{B} is defined to be the torque per unit dipole moment when the dipole is at right angles with the direction of \mathbf{B} .)

In the foregoing discussion, the only effect that a magnetic-induction field had upon a small magnetic dipole was to exert a torque upon it; this is indeed the case when the field is uniform (i.e., of constant magnitude and direction). Further analysis, however, shows that when the field is nonuniform (in magnitude and/or direction), the field also exerts a net unbalanced force upon the dipole. The net force \mathbf{F} of the dipole is given by the relation:

$$\mathbf{F} = \mathbf{m} \frac{\partial \mathbf{B}_c}{\partial \xi} \quad (2)$$

where ξ denotes a rectangular coordinate along the direction of \mathbf{m} and \mathbf{B}_c is the component of \mathbf{B} along the ξ direction. That is, the force is the product of the magnetic moment and the spatial rate of change (gradient) of the field, in the direction of the moment. The fact that a spatially nonuniform magnetic-induction field exerts a net unbalanced force on a magnetic dipole is the basis of the magnetic-particle inspection method discussed later in this chapter.

Electromagnetic theory provides a basis for calculating the magnetic-induction field arising from an arbitrary distribution of electric currents. For the purposes of the present discussion, the results of such calculations for a few simple current distributions will suffice. The magnetic-induction field surrounding a section of a very long, straight conductor is shown in figure 8-4. The "field lines" are symbolic only, and are used to indicate the spatial direction of the field; they are so drawn that \mathbf{B} at a particular point of space is tangent to the field line drawn through that point. It can be shown that the magnitude of the magnetic-induction field at a perpendicular distance, r , from the center of a long, straight conductor bearing a current, I amperes, is given by the relation:

$$\mathbf{B} = \frac{\mu_0}{4\pi} \left(\frac{2I}{r} \right) \quad (3)$$

The proportionality constant $\mu_0/4\pi$, characteristic of free space (or, for practical purposes, air) surrounding the conductor, has the value 10^{-7} $\text{Wb}/\text{A-m}$; μ_0 is called the magnetic permeability of free space.

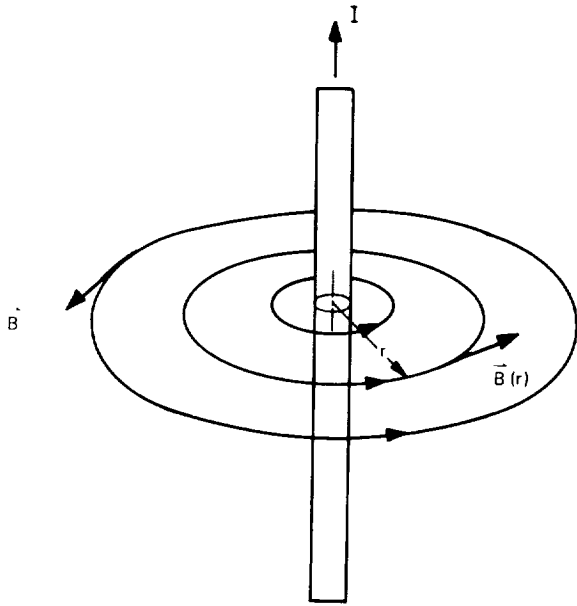


FIGURE 8-4.—Representative magnetic field lines in the magnetic-induction field of a long, straight wire.

The magnetic-induction field at the center of a flat, circular coil of radius, r , comprising N turns each carrying a current, I amperes (in the same sense), has the direction indicated in figure 8-5, its magnitude being given by the relation:

$$B = \frac{1}{2} (\mu_0) \frac{NI}{r} \quad (4)$$

The general distribution and direction of the magnetic-induction field of a flat circular coil is also illustrated in figure 8-5. The general relation for the magnitude of this field at points

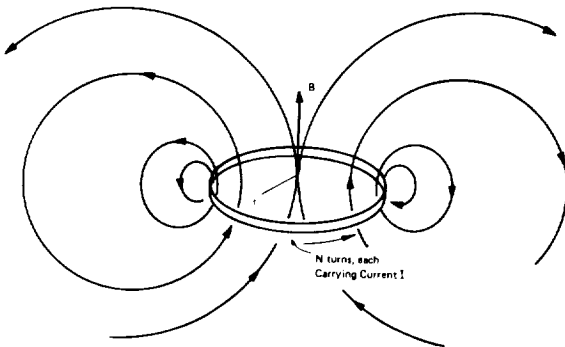


FIGURE 8-5.—Representation of the magnetic-induction field at the center of a flat circular coil.

other than the center of the coil is complicated and will not be given here. As the radius, r , of such a coil becomes small, the coil becomes a magnetic dipole. In the limiting case of a "vanishingly small" coil, its own magnetic-induction field becomes simple as illustrated in figure 8-6. Referred to polar coordinates (also illustrated in figure 8-6), the components of its magnetic-induction field are given by the relations:

$$B_r = \frac{2\mu_0 m}{4\pi} \left(\frac{\cos \theta}{r^3} \right); \quad (5a)$$

$$B_\theta = \frac{\mu_0 m}{4\pi} \left(\frac{\sin \theta}{r^3} \right). \quad (5b)$$

These results are of significance in detecting flaws by magnetic means because, as will be shown later, a small nonmagnetic void or inclusion in an otherwise homogeneous magnetized material presents itself approximately as a "point" magnetic dipole.

It can be shown that the magnetic-induction field within the central region of a long solenoid is uniform in direction and magnitude as illustrated in figure 8-7. The magnitude of the magnetic-induction field is given by the relation:

$$B = \mu_0 NI \quad (6)$$

where N is the number of windings (turns) per meter of coil length, and I is the current (in each turn) in amperes.

Two additional current distributions are of particular interest, namely that of a long, straight, solid cylindrical conductor, and that of an extended flat conductive slab. The magnetic-

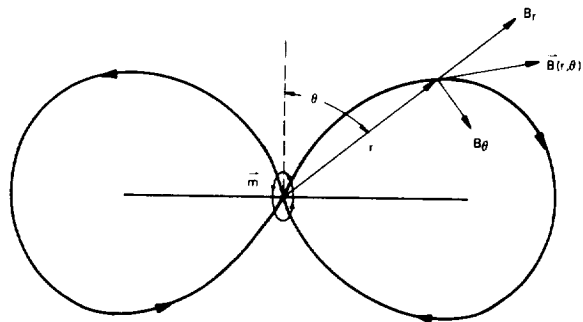


FIGURE 8-6.—Representation of the magnetic-induction field arising from a point magnetic dipole.

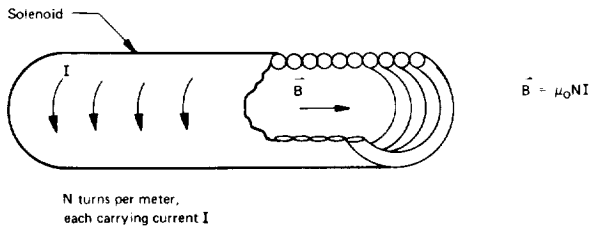


FIGURE 8-7.—Representation of the magnetic-induction field inside a long, straight solenoid.

induction field both inside and outside the conductor carrying a uniform current density, I/A , where I is the total current and A is the cross-section area of the conductor, is illustrated in figure 8-8. The magnetic-induction field near the surface of an infinitely extended flat conductive slab carrying a uniform current density is illustrated in figure 8-9. These two current distributions are of interest in connection with electric current perturbation approaches to magnetic field testing.

Magnetic-Induction Field Lines and Flux Density

As indicated in the preceding paragraphs, it is convenient to represent a magnetic-induction field graphically by drawing continuous lines to which, at any point along such a line, the magnetic-induction field is tangent. This artifice can be extended to permit a graphic portrayal not only of the direction of the field, but of its magnitude as well. This is accomplished by drawing field lines more or less densely, proportional to the strength of the field. Figure 8-10,

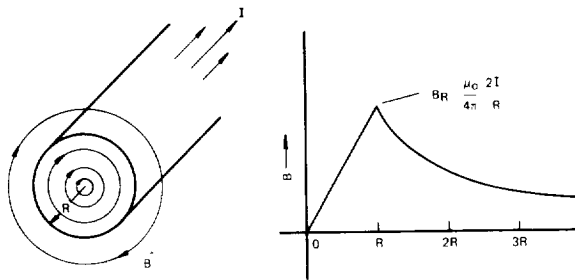


FIGURE 8-8.—Representation of the magnetic-induction field inside and outside a circular conductor (of non-magnetic material) carrying a current, I , uniformly distributed over the cross-sectional area of the conductor.

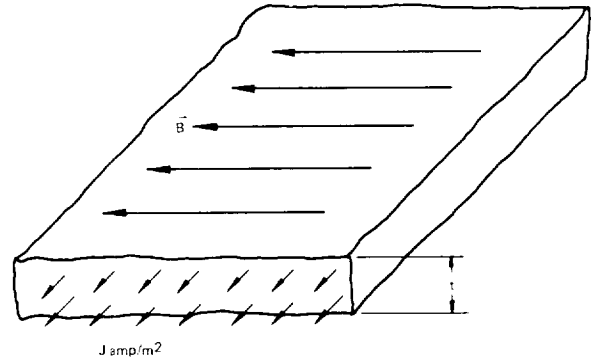


FIGURE 8-9.—A large flat slab bearing a uniform distribution of the current, J amperes/meter², establishes a uniform magnetic-induction field outside the material. [The magnitude of the field immediately at the surface is: $B = (\frac{1}{2}) (\mu_0 J t)$.]

for example, illustrates two uniform magnetic induction fields, one being twice the strength (magnitude) of the other. Figure 8-11 illustrates the magnetic-induction field of a solenoid, with lines drawn to correspond to the reduction in the magnitude of the field outside the solenoid. This artifice will fail, however, unless the area of reference in the determination of the density of field lines is taken to be normal to all the field lines drawn through it.

An important concept related to the foregoing construct is that of magnetic flux. An arbitrary surface introduced into a magnetic-induction field can be thought of as being made up of a large number of small contiguous squares. If, as illustrated in figure 8-12, the magnetic-induction field B is determined at the center of each square, the component of B normal to each square determined and multiplied by the area of the square, and the resulting

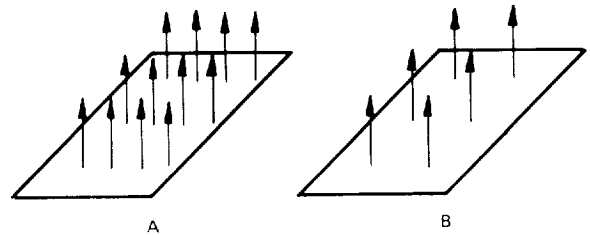


FIGURE 8-10.—Magnetic-induction field magnitude depicted graphically by number of lines per unit area. (The magnitude of field A is twice that of field B; their directions are the same.)

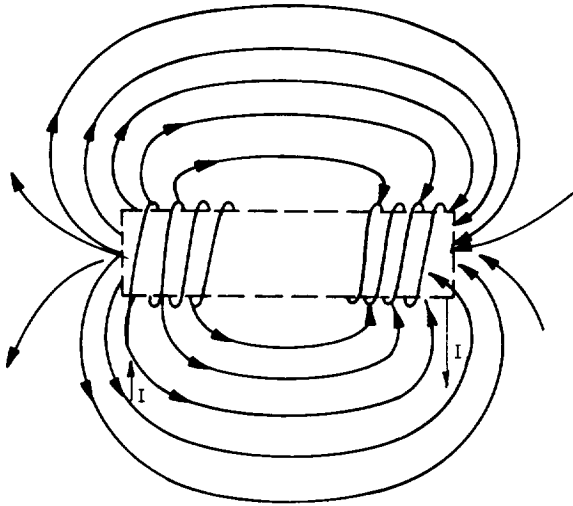


FIGURE 8-11.—Magnetic-induction field of a solenoid illustrated by lines. (Lines are drawn more densely in areas of higher induction fields.)

quantities summed, the result is termed the net magnetic flux through the surface. In the form of an equation, this gives

$$\phi = \sum_{i=1}^N B_i (\cos \theta_i) \Delta A_i \quad (7)$$

(In principle, the limit of the above sum as N approaches infinity and ΔA_i approaches zero should be taken.) Since B is measured in webers/meter², and ΔA_i is measured in meters², it is apparent that ϕ , the magnetic flux, is measured in webers. Thus, the “magnetic induction

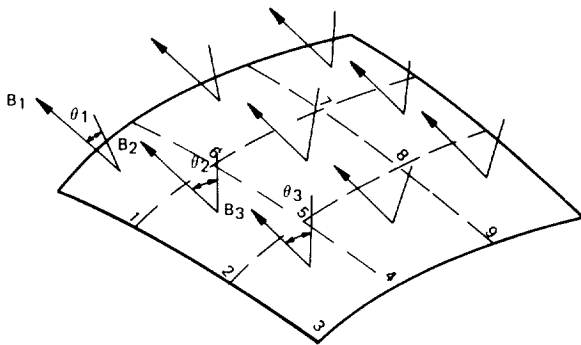


FIGURE 8-12.—Magnetic flux through the curved surface is determined by subdividing into regions small enough to be considered flat. (The normal component of B at the center of each subdivision is then multiplied by the area of that subdivision, and the results summed.)

field” is sometimes referred to as “magnetic flux density,” the two terms being synonymous.

For an open surface (such as a sheet), either side of the surface may arbitrarily be designated the “positive” side; for a closed surface such as a sphere), however, it is conventional to take the outside surface as positive. It has been empirically established that the net magnetic flux through a closed surface is always zero. For this reason, magnetic induction field lines (drawn according to the foregoing conventions as to magnitude and direction of B) must always be drawn as continuous lines that close upon themselves. This fact is in striking contrast to the corresponding circumstances for static electric fields, in which electric field lines (drawn according to conventions analogous to those described above for lines of B) always begin on positive electric charges and always terminate on negative electric charges. The empirically established property of closed lines of B is therefore equivalent to the principle that isolated magnetic “charges” (or “poles”) do not exist. No persuasive empirical evidence for such isolated poles has ever been presented, though very refined experiments have been performed to try to detect them.

The foregoing remarks notwithstanding, it is sometimes both possible and convenient to introduce fictitious magnetic poles, and to relate the actual magnetic field to the fictitious poles as if they were the field’s source. For example, the field of a small current circuit, at points not too near the circuit, may be obtained by imagining the field to arise from two fictitious point magnetic charges of magnitude $+q_m$ and $-q_m$, separated by a displacement l (fig. 8-13). Then assume that each point magnetic charge sets up a surrounding magnetic field that is everywhere

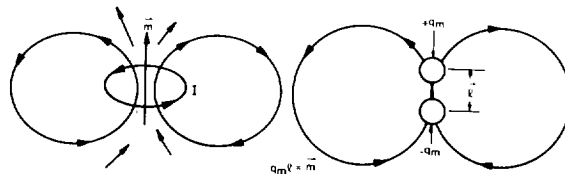


FIGURE 8-13.—The magnetic field attributable to a dipole consisting of two fictitious point magnetic charges of opposite sign is the same as the field arising from a small current loop.

directed radially away from a positive magnetic charge, the direction being reversed for a negative magnetic charge. The magnitude of the field, as a function of distance from the charge, must be taken to be given by an inverse square law,

$$B = \left(\frac{\mu_0}{4\pi} \right) \frac{m}{r^2} \quad (8)$$

If now the magnetic charge, q_m , is taken to be related to the magnetic moment m of the actual current circuit according to the relation:

$$q_m = \frac{m}{\ell} \quad (9)$$

and if the fields from $+q_m$ and $-q_m$ are vectorially combined, then, at distances, r (large compared to ℓ), one obtains as a result exactly the same magnetic field as that of the current circuit given in equations (5a) and (5b). A further analysis shows that any current circuit, whether large or small, can be considered equivalent to two layers of magnetic poles, the layers being of opposite sign (fig. 8-14). The surface magnetic pole density, σ_p , is given by the relation:

$$\frac{dq_m}{ds} = \sigma_p = \frac{I}{\gamma} \quad (10)$$

where I is the current of the circuit in amperes, and γ is the separation of the two fictitious sheets of poles. The magnetic induction field computed from the two fictitious pole layers will be exactly correct everywhere except at the

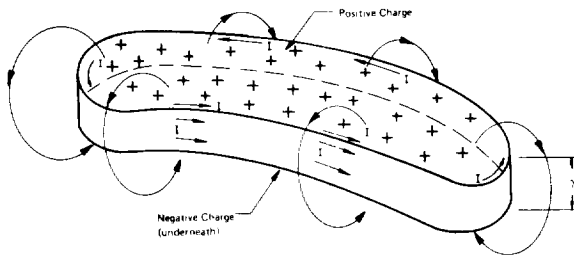


FIGURE 8-14.—A finite current loop gives rise to a magnetic field which is equivalent to the field of a dipolar layer of fictitious magnetic charge. (The field of the fictitious magnetic charges does not correctly represent the true field within the region between the two charge layers.)

pole surfaces or between them. As an application of the foregoing concepts, it can be seen that by slicing a solenoid into thin current circuits, and replacing each current circuit by its equivalent magnetic charge dipole layer, the fictitious charges within the solenoid cancel each other, leaving a uniform layer of (fictitious) positive magnetic poles at one end of the solenoid, and a layer of negative poles at the opposite end (fig. 8-15). (It is important to note, however, that inside the solenoid, the fictitious magnetic pole model of the solenoid not only gives the wrong magnitude for the magnetic field, but also the wrong direction.) The most important utility of the fictitious pole model is in discussing magnetic fields associated with magnetizable materials.

Magnetic Properties of Matter

In the foregoing discussion, magnetic induction fields were related to the flow of macroscopic electric currents that are caused by the

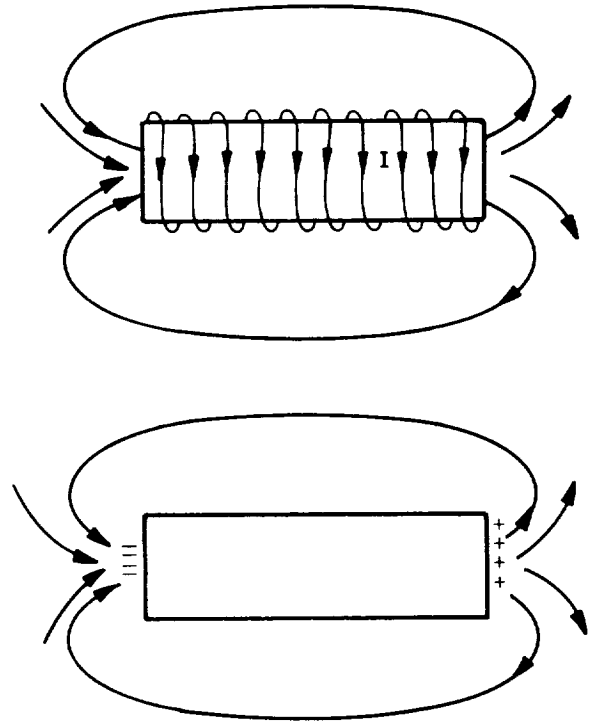


FIGURE 8-15.—The magnetic field exterior to a solenoid can be obtained from an equivalent distribution of fictitious magnetic poles.

drift of electrically negatively charged electrons through a conductor. Similarly, the magnetic properties of matter arise because of microscopic electric currents that take place on an atomic and subatomic scale. In particular, the rotation, or spin, of an electron about its own axis produces an intrinsic magnetic moment. Atoms or molecules that do not exhibit significant magnetic properties are those whose electronic states are such that the spins of the associated electrons are mutually cancelling in their macroscopic effects. Atoms or molecules having an unpaired electron have a net magnetic moment equal to that of the unpaired electron (with a small alteration due to the orbital motion of the electron). The magnetic moments of such electrons tend to align with any externally applied field; however, their net magnetic field is weak. Such materials are said to be paramagnetic.

Even atoms or molecules having no unpaired electrons exhibit a slight magnetic effect. When introduced into a magnetic field, the orbital motions of the electrons are perturbed in such a way as to set up orbital currents whose corresponding magnetic fields are in a direction opposite to that of the inducing field. Such materials are said to be diamagnetic; their magnetic effects are extremely small and insensible with all but very refined apparatus.

The most remarkable magnetic materials are those in which alignment (or "ordering") among individual atomic magnetic moments occurs spontaneously below a certain temperature characteristic of the material. Such ordering, which arises from quantum mechanical coupling among the moments, occurs in a variety of ways, a review of which would be beyond the scope of this survey. Ferromagnetism, ferrimagnetism, and antiferromagnetism are instances of such ordering. Of these, only ferromagnetism is of interest for the present. In ferromagnetic materials, all atomic moments within a certain region (called a domain) are aligned parallel to one another. A domain is large enough to contain on the order of 10^{21} atoms, and is generally commensurate in size with the grains of a polycrystalline material. (However, it has been definitely established

that domains do not correspond to grains, as grains may contain more than one domain and a domain may extend over several grains.) In a normal "unmagnetized" condition, the domains of a ferromagnetic specimen have their respective net magnetic moments aligned at random with respect to one another. When introduced into an external magnetic field, the "walls" separating contiguous domains move in such a way as to increase the volume of domains whose moments are favorably aligned with the external field at the expense of those domains whose moments are unfavorably aligned. Other processes also occur, including the disappearance of some domains, the nucleation of new domains, and the rotation of the moments within domains. (The notion that the domains bodily rotate or flip is erroneous; only the orientation of atomic moments changes.) The magnetic field associated with a magnetized ferromagnetic specimen is typically very large compared with that of nonferromagnetic materials.

Since the magnetic properties of matter arise from a distribution of magnetic dipoles that are individually of atomic dimensions, it is often convenient to discuss microscopic properties in terms of their net magnetic dipole moment per unit volume. This is obtained by vectorially adding the atomic moments within a small volume, and dividing the result by the volume. The volume so used must be large enough to contain a large number of atomic moments, but small enough that its extension can be ignored on a macroscopic scale. This procedure makes it possible to introduce a vector field $\mathbf{M}(\mathbf{r})$, which specifies the magnetic dipole moment per unit volume at a point, \mathbf{r} , within a specimen. Within an individual magnetic domain, $\mathbf{M}(\mathbf{r})$ may for most purposes be regarded as uniform. For many purposes, it is useful to average \mathbf{M} over a region large enough to contain many domains; this procedure results in a magnetization field that is smooth and continuous throughout the specimen. (Such an averaged \mathbf{M} is not appropriate for discussing an experiment in which details on the domain scale are resolved.)

Referring to equations (5a) and (5b), note that if the units of magnetic induction are divided by those of μ_0 , the permeability of free space, the result is the same as the units of magnetic dipole moment per unit volume. For a number of purposes, it is convenient to introduce yet another magnetic field quantity, \mathbf{H} , defined by the following relation:

$$\mathbf{H} = \frac{\mathbf{B}}{\mu_0} - \mathbf{M} \quad (11)$$

\mathbf{H} is usually referred to as the magnetic field intensity or simply the magnetic field (to be distinguished from \mathbf{B} which is the magnetic induction field). \mathbf{H} is also sometimes referred to by the term "magnetizing force," an unfortunate use of the term "force" since \mathbf{H} does not have the appropriate physical units (i.e., it is not measured in newtons or any other force unit).

Many materials are, for practical purposes, magnetically isotropic; i.e., when magnetized, \mathbf{M} , \mathbf{B} , and \mathbf{H} are all collinear at a given point within the material. For such materials, it is convenient to introduce a dimensionless quantity χ_m , called the magnetic susceptibility of the material and defined by the relation:

$$\chi_m = \frac{H}{M} \quad (12)$$

Referring to equation (11), note that for isotropic materials it can therefore be rewritten as

$$\mathbf{B} = \mu_0(1 + \chi_m)\mathbf{H} \quad (13)$$

For ferromagnetic materials, it is usually more convenient to define the $\mu_0(1 + \chi_m)$ to be simply μ , called the permeability of the material. Thus μ may be defined by the equation:

$$\mu = \frac{B}{H} \quad (14)$$

In the absence of any magnetically permeable materials (i.e., when \mathbf{M} is everywhere zero), \mathbf{B} differs from \mathbf{H} only by the multiplicative (dimensional) factor, μ_0 ; thus a field line representation of the \mathbf{H} -field would be identical with that of the \mathbf{B} -field. In the presence of

permeable materials, however, this is not the case. Analysis of the magnetization, \mathbf{M} , of a specimen in terms of the equivalent fictitious magnetic pole model shows that such a specimen may be thought of as containing a volume distribution, ρ , of fictitious magnetic poles, together with a surface distribution, σ , of magnetic poles. The symbol ρ is a measure of the spatial nonuniformity of \mathbf{M} ; σ is simply the component of \mathbf{M} normal to the surface of the specimen. It can further be shown that each element of fictitious magnetic pole strength (i.e., ρdv and σds , dv and ds being respectively small elements of volume and surface) is the source of an H -field in accordance with the inverse square law, i.e., its field directly radially outward or inward depending upon the sign of ρ and σ its magnitude being given by the relation:

$$dH = \frac{1}{4\pi} \left(\frac{\rho dv}{r^2} \right) \quad (15a)$$

or

$$dH = \frac{1}{4\pi} \left(\frac{\sigma ds}{r^2} \right) \quad (15b)$$

The total H -field arising from the magnetized specimen may be obtained by vectorially summing the contributions from each of the fictitious magnetic pole elements. Thus, static magnetic field intensity lines (H -lines) begin on positive fictitious magnetic poles and end on negative fictitious magnetic poles, in complete correspondence with static electric field lines that begin and end on positive and negative electric charges, respectively. For example, figure 8-16 shows the distribution of fictitious magnetic poles on the surface of a permeable sphere placed in a uniform external magnetic field (the sources of which are not shown). It should be noted that on the interior of the permeable sphere, the H -field, due to the magnetization of the sphere, is oppositely directed to the applied external field; the net \mathbf{H} -field in the interior of the sphere is therefore less than the applied external field. This effect is referred to as demagnetization. In the case illustrated, the internal field due to the magnetization of the sphere is uniform and proportional to the (uniform)

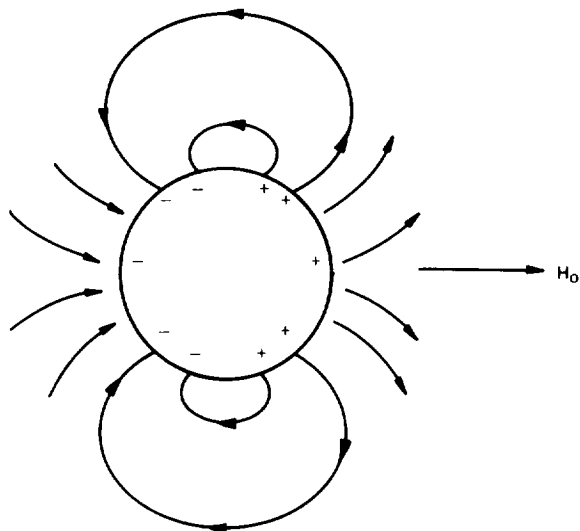


FIGURE 8-16.—A permeable magnetic sphere placed in a uniform external magnetic field is uniformly magnetized throughout its volume, and gives rise to an additional field which may be interpreted in terms of a distribution of fictitious magnetic poles.

magnetization. Hence, a demagnetizing field, H_d may be defined by the relation:

$$H_d = \mathcal{D} M \quad (16)$$

where the proportionality factor, \mathcal{D} , is called the demagnetization factor. The net magnetic intensity inside the sphere is therefore given by the relation:

$$H_i = H_o - H_d = H_o - \mathcal{D} M \quad (17)$$

In turn, the equation:

$$M = \chi_M H_i = \left(\frac{\mu}{\mu_0} - 1 \right) H_i \quad (18)$$

from which these results follow:

$$H_i = \frac{H_o}{1 + \left(\frac{\mu}{\mu_0} - 1 \right) \mathcal{D}} \quad (19)$$

It can be shown that for a sphere, \mathcal{D} is exactly $1/3$. For a long prolate spheroid magnetized along its long axis, \mathcal{D} approaches zero. For a thin prolate spheroid magnetized along its short axis, \mathcal{D} approaches unity. For specimens of shapes other than some instance of a general

ellipsoid, or for nonuniform applied fields, it is not possible to define a demagnetization factor in a manner precisely comparable to the example given above. It should be clear, however, that whenever a specimen is magnetized by introducing it into an external magnetic field, the appearance of fictitious magnetic poles within and on the surface of the specimen will always result in an internal magnetic intensity less than that of the applied field, i.e., a demagnetizing effect takes place. Under unfavorable circumstances, the specimen may be only weakly magnetized. Thus, demagnetization is an important effect that must often be taken into account in magnetic field testing.

Magnetic Hysteresis

A familiar phenomenon is that some ferromagnetic materials when magnetized by introducing them into an external field do not return to a completely unmagnetized state when removed from that field. In fact, they must be subjected to a reversed field of a certain strength to demagnetize them (discounting heating the specimen to a characteristic temperature, called the Curie point, above which ferromagnetic ordering of atomic moments is thermally destroyed, or mechanically working the material to reduce the magnetization). If an external field (that can be varied in a controlled way) is applied to completely demagnetized ("virgin") specimen, and if instrumentation for measuring the magnetic induction within the specimen is at hand, the magnetization curve of the material may be determined. A representative magnetization curve for a ferromagnetic material is shown in figure 8-17. There are a number of important parameters defined in terms of the features of this curve, including (1) the initial permeability, μ_a ; (2) the differential permeability, μ_{diff} ; (3) the incremental (or reversible) permeability, μ_{Δ} ; (4) the total permeability (usually called just "the permeability"), μ_T ; (5) the maximum permeability, μ_{max} ; (6) the residual magnetic induction; and (7) the coercive magnetic field intensity (sometimes called the coercive force"). The initial permeability is simply the slope of the virgin

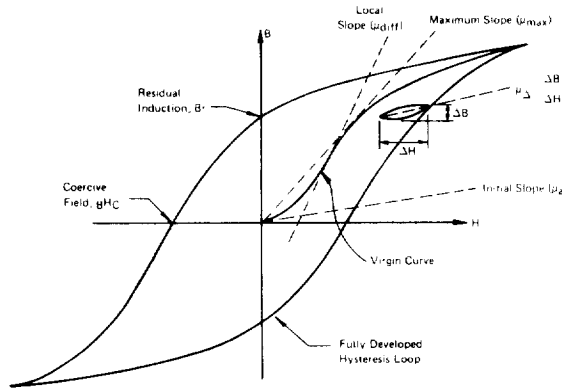


FIGURE 8-17.—A generic hysteresis curve for ferromagnetic materials. (Important parameters defined with respect to the curve are indicated.)

magnetization curve at the origin. The differential permeability is the slope of a line drawn tangent to the magnetization curve at any point in question. If a "minor" hysteresis loop is generated by reducing H (on the "upward" half of the fully developed hysteresis curve) or increasing H (on the "downward" half of the fully developed hysteresis curve) by a small but finite amount, and subsequently changing H so as to return the specimen to the original state, the ratio of the decrement (or increment) in B , (ΔB), to the corresponding change in H , (ΔH), is called the incremental permeability. The incremental permeability is of importance in discussing small oscillatory variations of the magnetization when the specimen has been pre-magnetized as, for example, in magnetoabsorption. The limit of the incremental permeability as ΔH becomes very small is called the reversible permeability (and is not equal to the differential permeability at the point on the magnetization curve in question). The total permeability is simply the ratio B/H at any point of the virgin curve. The maximum permeability is the largest value of the total permeability that occurs along the virgin curve. Once H reaches a value such that the incremental permeability becomes simply the free space permeability, μ_0 , the specimen is said to be magnetically saturated (recalling that demagnetizing effects are presumed negligible). If H is then reduced to zero, it is found that B is

not reduced to zero (because M is not reduced to zero). The residual value of B is called the residual induction. The value of H (applied in a sense opposite to B required to reduce B to zero is called the induction coercive force, denoted by BH_C . (The magnetic field intensity required to reduce the magnetization M to zero is called the magnetization coercive force, denoted by MH_C . (Note that BH_C does not equal MH_C .)

All of the foregoing parameters are defined for quasi-static variations in H , B , and M ; a more elaborate discussion is required to explain rapid changes or high-frequency oscillations of these quantities.

Barkhausen Jumps

The foregoing discussion indicates that M (or B) varies smoothly and continuously with H . This is the case, however, only if the test apparatus cannot resolve small, rapid changes in M (or B). Using refined apparatus it can be shown that the magnetization takes place as a succession of small, rapid jumps that are now known to be associated with discontinuous, irreversible movements of magnetic domain walls (as well as sudden domain nucleation, and possibly abrupt magnetization rotation processes). Such jumps in M are called Barkhausen jumps after their discoverer, and the phenomenon is called the Barkhausen effect. Certain characteristics of the Barkhausen effect are dependent upon the state of mechanical stress of a specimen; efforts are being made to exploit this dependence as a means of indirectly and nondestructively measuring applied and residual stresses in ferromagnetic materials.

Magnetic Circuits

A closed path through one or more magnetic materials is called a magnetic circuit. The total magnetic flux through a cross section of the toroid (fig. 8-18) is given by the relation:

$$\phi = BA = \mu HA = \mu nIA \quad (20)$$

If one multiplies the value of H inside the toroid by its mean circumference, l , the result

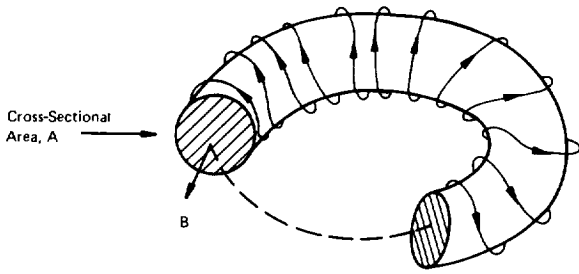


FIGURE 8-18.—Representation of a toroidal coil with a ferromagnetic core.

is called the magnetomotive, \mathcal{M} , of the magnetic circuit :

$$\mathcal{M} = \text{magnetomotive} = Hl \quad (21)$$

Hence, the relation :

$$\phi = \mu \frac{\mathcal{M}}{l} \quad A = \frac{\mathcal{M}}{\frac{l}{\mu A}} \quad (22)$$

In this example, the flux, ϕ , may be considered to be analogous to an electric current, \mathcal{M} to an electromotive (voltage), and the quantity $(l/\mu A)$ to an electrical resistance. The quantity $(l/\mu A)$ is called the reluctance, \mathcal{R} , of the magnetic circuit. Hence, the relation :

$$\phi = \frac{\mathcal{M}}{\mathcal{R}} \quad (23)$$

or, in other words, the magnetic flux in the circuit is equal to the magnetomotive of the circuit divided by the reluctance of the circuit. This analogy may be generalized, and is frequently useful in determining by observation the distribution of flux in an approximate way when an exact determination is too complex to be practical. For example, the magnetomotive of the circuit in figure 8-19 is also Hl ; the total reluctance of the circuit is

$$\mathcal{R} = \mathcal{R}_1 + \mathcal{R}_2 \quad (24)$$

where

$$\mathcal{R} = \frac{l_1}{\mu_1 A} + \frac{l_2}{\mu_2 A} \quad (25)$$

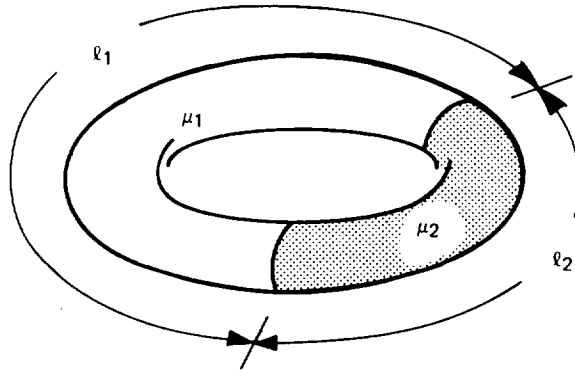


FIGURE 8-19.—A toroidal core with two segments of different permeabilities. (For clarity the toroidal current windings are not shown.)

Hence, the magnetic flux in the circuit is

$$\phi = \frac{\mu}{\mathcal{R}} = \frac{Hl_0}{\frac{l_1}{\mu_1 A} + \frac{l_2}{\mu_2 A}} \quad (26)$$

If $\mu_1 = \mu$, and $\mu_2 = \mu_0$, corresponding to an air gap in a ferromagnetic toroid, the following relation results :

$$\phi = nIA \left[\frac{\mu_0 \mu}{\frac{l_1 \mu_0}{l_1 + l_2} + \frac{l_2 \mu}{l_1 + l_2}} \right] \quad (27)$$

Note that if $\mu \gg \mu_0$ (as is the case for ferromagnetic metals), a small air gap drastically reduces the flux ; in other words, an air gap has a high reluctance.

It can be shown that the reluctance of parallel flux paths add reciprocally, i.e., for two such paths :

$$\frac{1}{\mathcal{R}_T} = \frac{1}{\mathcal{R}_1} + \frac{1}{\mathcal{R}_2} \quad (28)$$

Note that the flux referred to here is that of magnetic induction, \mathbf{B} , not magnetic intensity, \mathbf{H} . The distinction is essential, for it will be recalled that \mathbf{B} is sourceless, while \mathbf{H} is not. Thus the flux of \mathbf{B} is analogous to a conserved current, while that of \mathbf{H} is not.

The value of the magnetomotive used in practical circumstances is usually quite easy to obtain : it can be shown that the total magnetomotive to be attributed to any closed path

(portions of which may lie in magnetically permeable material) is exactly equal to the number of ampere-turns of electric current threading the closed path. As an illustrative example (fig. 8-20), consider determining the number of ampere-turns required to magnetically saturate a short length of steel tubing. Since the tube is very much more permeable than the surrounding air, it will "conduct" essentially all the magnetic flux, which, for simplicity, is considered uniform over the cross-sectional area of the cylinder wall. Just at magnetic saturation, the total flux "conducted" by the tube is

$$\phi = B_{\text{sat}}(tL) \quad (29)$$

where t and L are the thickness and length of the cylinder wall, respectively. The reluctance of the flux "conductor" is given by

$$\mathcal{R} = \frac{l}{\mu_{\text{sat}}A} = \frac{2\pi a}{\mu_{\text{sat}}tL} \quad (30)$$

where a is the mean radius of the cylinder, and μ_{sat} is the permeability of the steel just at magnetic saturation. The required number of ampere-turns is thus:

$$M = \phi \mathcal{R} = \frac{B_{\text{sat}}(tL)2\pi a}{\mu_{\text{sat}}(tL)} = 2\pi a \frac{B_{\text{sat}}}{\mu_{\text{sat}}} \quad (31)$$

Numerical values for B_{sat} and μ_{sat} may be obtained from a valid magnetic hysteresis curve for the steel in question. Unfortunately, such curves are frequently unavailable in practice, resulting in trial-and-error procedures that are time consuming and seldom yield optimum test conditions.

The foregoing considerations have numerous practical consequences for magnetic field methods among which two are especially important. First, whenever it is necessary to magnetize a specimen, it is usually most efficient to make it part of a complete ferromagnetic circuit. Second, the high reluctance of such flaws as cracks, voids, or nonmagnetic inclusions in ferromagnetic materials is responsible for the magnetic field perturbations associated with them; hence, the specimen should be magnetized in such a direction as to cause a given flaw to present the maximum possible reluctance.

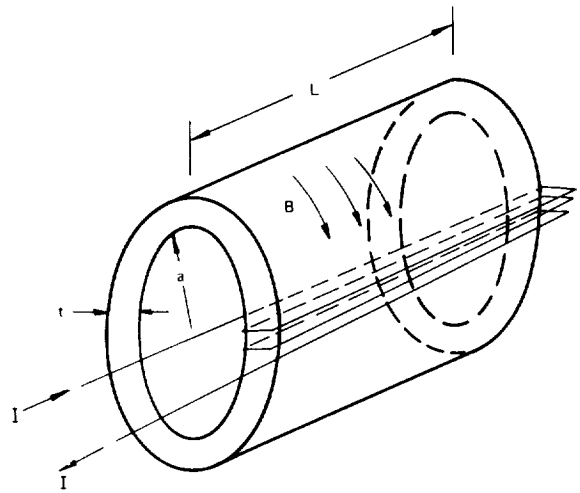


FIGURE 8-20.—A practical magnetic field testing problem.

Perturbation of Magnetic Fields

Any localized region of a magnetically permeable medium, in which the value of the magnetic permeability departs significantly from that of the bulk material, is said to be a permeability anomaly. When the bulk material is "smoothly" magnetized, the magnetic-induction field is altered, or perturbed, in magnitude or direction in the vicinity of such permeability anomalies. In mathematical terms, the vector field, $\mathbf{B}_0(\mathbf{r})$, that would exist if the anomaly were not present is shifted to $\mathbf{B}_0(\mathbf{r}) + \Delta\mathbf{B}(\mathbf{r})$, $\Delta\mathbf{B}(\mathbf{r})$ being the field perturbation. The magnitude and direction of $\Delta\mathbf{B}$ as a function of the position, \mathbf{r} depends upon the size, shape, and orientation of the anomaly, as well as upon the value (or range of values) of permeability that apply to the anomaly. The magnetic field perturbations associated with two general types of flaws in ferromagnetic materials are shown in figures 8-21 and 8-22.

To be detectable, a flaw must produce a significant perturbation of the magnetic induction field at or near the surface of the article being inspected. Much of the technique associated with the magnetic field method is concerned with applying the external magnetizing field in such a way as to maximize the surface field perturbation caused by a given flaw. The sensitivity of virtually all practical magnetic

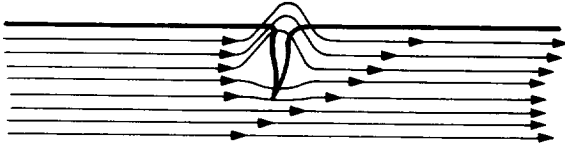


FIGURE 8-21.—Magnetic field perturbation caused by a surface flaw in a ferromagnetic material.

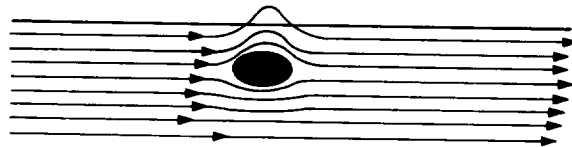


FIGURE 8-22.—Magnetic field perturbation caused by a subsurface inclusion in a ferromagnetic material.

field methods (including the magnetic-particle method and electronic methods of sensing field perturbations) does not depend upon the absolute magnitude of ΔB , but rather upon its spatial gradient. Hence, in practice, an attempt is made to adjust the magnitude and direction of the applied field so that (1) the nominal field has as little gradient as possible along the surface of the specimen and (2) flaw-related perturbations produce as large a local gradient as possible. An elementary example is that of the long, straight cracks in an approximately planar surface of a specimen. If the crack is parallel to the nominal direction of the magnetic field, it produces a comparatively minor perturbation; if, on the other hand, it is transverse to the nominal direction of the field, the same crack produces a somewhat more significant perturbation, and is much more readily detected either by magnetic particles or by electronic field gradient sensors.

The theoretical determination of the field perturbation caused by a prescribed flaw is, in general, mathematically very difficult, and little attention has been devoted to the problem even for flaws of idealized size and shape. Optimum test conditions are usually determined empirically.

Action of Magnetic Field Gradient on Magnetic Particles

The particles used in the magnetic-particle method of flaw detection are not composed of pure iron, but of various inert compounds of iron. The common oxides of iron, Fe_2O_3 and Fe_3O_4 , are used for such powders, as are certain other compounds of iron. When sufficiently finely divided, particles of these materials exist as single magnetic domains, i.e., each is essentially a small (but rather weak) permanent

magnet. Thus, in accordance with equation (2), each particle experiences a net force when it is located in a region of a magnetic field gradient. Under the influence of the gradient, a particle will tend to move toward the region where the magnetic field is strongest. Under appropriate conditions of magnetization of a specimen, substantial field gradients will exist only in the immediate vicinity of a flaw; hence the particles, if free to do so, will move toward and congregate at such flaws.

Powders in the dry form can be used for flaw detection, but measures must be taken to agitate the particles on the surface of a specimen in order to permit them to move under the influence of any field gradient that may be present. It is also possible to suspend the powders in an appropriate liquid where thermal agitation is effective in making them mobile. Practical aspects of the use of magnetic particles for flaw detection are further discussed later in this chapter.

Perturbation of Electric Current Distributions

If a stationary (i.e., constant or periodic in time) current distribution is established in a material that is nominally homogeneous with respect to electric conductivity, localized regions of the material that have anomalous values of electric conductivity will produce corresponding perturbations of the current distribution. Cracks, voids, and nonconductive (or poorly conductive) inclusions in an otherwise homogeneous metal matrix are instances of such anomalies. There are two essentially distinct methods of nondestructively sensing such flaw-related conductive anomalies. One of these, the basic eddy-current approach, entails inductively coupling a "primary" coil, carrying an alternating current, to the metal substrate that

acts as a "secondary"; regions of anomalous conductivity are detected through their effects upon the apparent electric properties of the primary coil. The other approach consists in directly measuring perturbations of the magnetic field accompanying the (correspondingly perturbed) electric current distribution. Approaches do exist that are more or less intermediate between the two foregoing ones. Eddy-current approaches are discussed in a separate chapter of this survey, and will therefore not be treated here.

As the term is used here, the electric current perturbation method will not apply to ferromagnetic materials. Although it is sometimes convenient to magnetize a ferromagnetic article by directly passing an electric current through it, the very large magnetic field amplifying effect of the permeability of ferromagnetic materials has the result that field perturbations due to permeability anomalies will ordinarily vastly outweigh any effect directly caused by a perturbation of the electric current distribution.

Magnetic field gradients brought about by flaw-related perturbations of electric current distributions in nonferromagnetic materials are typically several orders of magnitude smaller than gradients caused by comparable flaws in magnetized ferromagnetic materials. This is so, even for maximum practical values of electric current density. For such low field gradients, magnetic particles are practically ineffective. Magnetometers, entirely adequate for the detection of field perturbations in ferromagnetic materials, may lack the sensitivity needed to detect electric current perturbations. Adequate sensitivity for practical use rests on the application of state-of-the-art electronic methods of enhancing the signal-to-noise ratio of probes of the inductive coil type.

Magnetometer Probes

Two types of electronic magnetic field (or field gradient) sensors can be used in magnetic field methods: (1) the inductive wire coil and (2) Hall effect devices.

The inductive wire-coil sensor is based on

Faraday's law of induction, which may be written as

$$V = -N \frac{d\phi}{dt}$$

where V is the electromotance induced in the coil, N is the number of turns comprised in the coil, and ϕ is the magnetic flux through the area bounded by the coil (fig. 8-23). In order for such a coil to detect perturbations in a magnetostatic field, the coil itself must be moved relative to the field (fig. 8-24). In some cases, it is more practical to move the specimen relative to the coil than vice versa. The electromotance induced in the coil then becomes

$$V = -NA \frac{v dB_{n, \text{avg}}}{dx}$$

where N is the number of turns comprised in the coil, A is effective area of the coil, v is the velocity of the coil relative to the specimen surface, $B_{n, \text{avg}}$ is the component of the magnetic induction field normal to the effective plane of the coil (averaged over the effective area of the coil), and $dB_{n, \text{avg}}/dx$ is the spatial gradient of $B_{n, \text{avg}}$ along the direction of motion of the coil. Thus, for a prescribed field gradient, the corresponding electromotance is proportional to (1) the number of turns comprised by the coil, (2) the velocity of the coil with respect to the field, and (3) the spatial gradient of the field.

(It is not quite correct to say that the V is proportional to the coil area A . What counts is the product $AB_{n, \text{avg}}$; increasing A may not in-

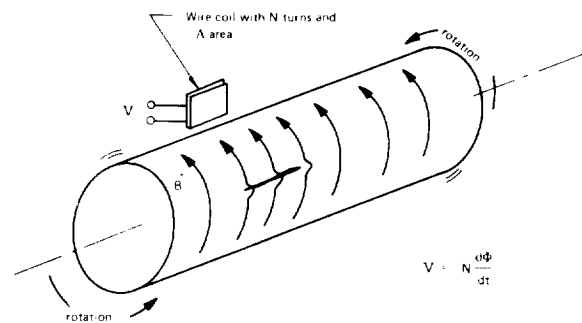


FIGURE 8-23.—A stationary coil of wire with N turns placed in a time-varying magnetic field, $B(t)$, will have induced across its terminals an electromotance of $V = N d\phi/dt$.

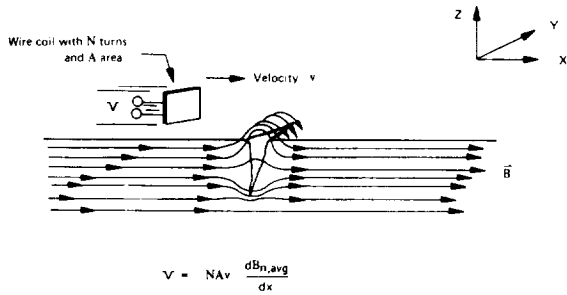


FIGURE 8-24.—Whenever the magnetic field varies over a distance but is constant in time, a wire coil may be moved through the field. (The electromotance induced in the coil is $V = -NAv dB_{n,avg}/dx$.)

crease the product proportionately, since $B_{n, avg}$ depends upon A . In practice, a coil area is quickly reached beyond which no benefit is derived from a further increase.) The theoretical “signal” or “signature” produced by scanning a dipolar perturbation field along a trajectory parallel to the axis of the dipole is shown in figure 8-25.

Hall-effect devices depend on the influence of a magnetic field upon the flow of current through a conductor. The Hall coefficient, characteristic of individual conductive materials, is defined by the relation :

$$\Pi_H = \frac{E_z}{J_x B_y}$$

the terms being defined in figure 8-26. Experimentally, both positive and negative values of Π_H occur. Bismuth is commonly used as an active material in Hall-effect magnetic field sensors.

Commercially available Gauss meters used for measuring magnetic field intensity are generally not suitable for measuring magnetic field perturbations. Suitable sensors must be small (for adequate spatial resolution), and, for adequate sensitivity, must usually be used in matched pairs in a differential arrangement for which the Hall voltages of the two components cancel when in the presence of a purely uniform magnetic field.

The Hall effect probes do not depend upon relative motion for their sensitivity and can be scanned at any rate that is mechanically convenient. However, they are difficult to fabricate,

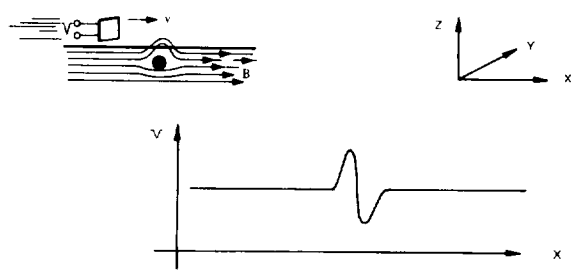


FIGURE 8-25.—The induced electromotance of a wire coil passing through a magnetic field perturbation which is bipolar in the direction of travel will have the characteristic shape indicated.

are somewhat delicate, and require considerable auxiliary electronic apparatus.

THE MAGNETIC-PARTICLE METHOD

The magnetic-particle method of nondestructive inspection consists of magnetizing the test specimen, applying powders of certain iron compounds to the test specimen, and then examining the surface for areas of clustered powder.

The present state of development in magnetic particle equipment and materials allows inspection through a variety of techniques that may be classified according to the following considerations.

(1) The magnitude of the magnetizing current, which would indicate whether low, medium, or high current levels are used.

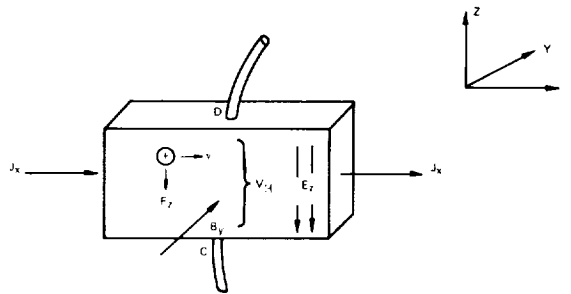


FIGURE 8-26.—A Hall-effect magnetic field sensor. [An electric current in the +X direction corresponds to an effective position charge carrier drift in the -X direction. A magnetic field in the +Y direction exerts a force on the electrons in the +Z direction. The effect is equivalent to an electric field, E_z , and results in a potential difference (called the Hall voltage) between points C and D. For a fixed value of current, H_z , the Hall voltage, V_H , is proportional to the magnetic induction field B_y .]

(2) The type of magnetizing current, which would specify whether direct current, half-wave current, pulsating direct current, or alternating current is used.

(3) The type of the magnetic powder, which would identify the color, shape, and size of the particles. These particles are available either colored with a bright dye or treated with a fluorescent pigment. Also, these particles are available in different sizes ranging from 60- to 40- μ (about 0.0025- to 0.0015-in.) diam to a maximum limited by the ability of the magnetizing apparatus to cause the particles to be attracted and held by flaws. In addition, these particles may be round or elongated. Round particles move more freely over the test surface than the elongated but are not held as strongly to flaws as the elongated. Sometimes a mixture of shapes is used (ref. 2).

(4) The magnetic powder vehicle that would specify whether the particles are applied as a loose dry powder or as a suspension in a liquid. (The respective names of the above are "dry method" and "wet method.")

(5) The particle application procedure that would specify whether the particles are applied while magnetizing current is flowing, or applied after the current has stopped. (These methods are respectively described as being "continuous" and "residual.")

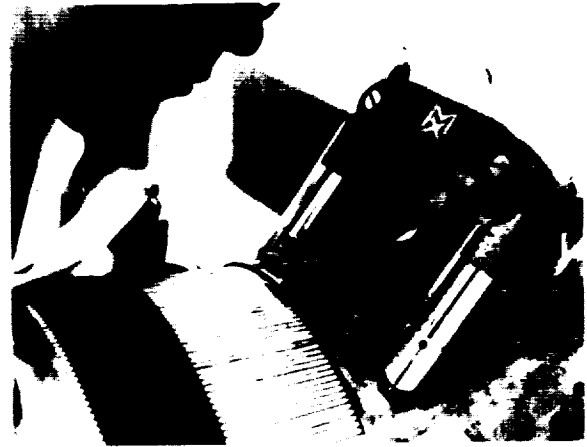
(6) The direction of magnetization with respect to the specimen, which would be specified as "circular" or "longitudinal."

(7) The sensitivity level which would identify the smallest flaw detectable but would be controlled by adjustment in any or all of the above parameters (ref. 2).

Basic Inspection Procedures

The basic steps for all techniques of magnetic-particle inspection are essentially the same, the differences among techniques coming from variations within the steps. The steps (three of which are shown in figure 8-27) include (ref. 2):

- (1) Preparation of the test surface
- (2) Magnetization of the test article
- (3) Application of the magnetic particles



(a) Magnetization of Liquid Fuel Rocket Engine Chamber



(b) Applying Magnetic Particles



(c) Yoke for Demagnetization

FIGURE 8-27.—Basic steps of magnetic particle inspection. (Courtesy of Magnaflex Corp.)

(4) Inspection for flaw indications

(5) Demagnetization of the part.

Surface preparation.—In the preparation of the test surface, dirt, grease, or other contamination that might prevent magnetic particles from moving freely on the surface or from clinging to a flaw region are removed. Non-magnetic contaminants inside surface flaws are not a serious hindrance. However, if current is to be injected into the surface, the injection area should be well cleaned to allow good electric contact.

Magnetization.—The method selected to magnetize the test article depends upon the expected orientation of the flaws and whether or not the flaws are subsurface. Magnetic particle inspection is most effective whenever the magnetic field direction is perpendicular to the longest dimension of a flaw. For subsurface flaws, alternating current techniques are not very effective, whereas filtered direct currents or pulsed direct currents may be used very effectively. The methods of magnetization are to:

(1) Inject an electric current through the item

(2) Pass an electric current through a cable that is either wound around or threaded through the item

(3) Pass an electric current through the coil windings of a magnetic yoke placed on the item.

Each of these methods of magnetization is illustrated in figure 8-28 (ref. 3). Of these methods, magnetization by injecting current into the test item is usually preferred whenever maximum sensitivity to tiny flaws is desired or whenever a magnetic field cannot be conveniently induced in the test item by other methods. However, if the part under inspection is magnetized by injecting current into its surface, care must be taken to avoid arcing as this may severely damage the surface, particularly whenever hand-held prods are used to inject current. Arcing tends to occur whenever the current contacts are dirty or are moved during excitation. A simple way around the arcing problem is to securely clamp the contacts to a clean area. When magnetization is induced by placing the part in an external magnetic field, the arcing problem does not occur.

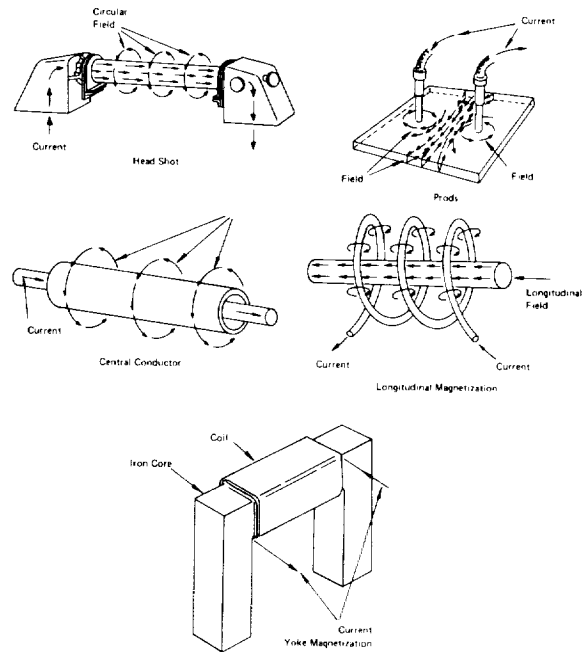


FIGURE 8-28.—Magnetization may be accomplished by (1) injecting an electric current through the object, (2) passing current through a cable that is either wound around or threaded through the item, or (3) passing current through the windings of a magnetic yoke placed on the item. (Courtesy of General Dynamics, Convair Div.)

A critical factor in successful inspection, regardless of the method of magnetization, is the proper choice of magnetizing current level. With too little magnetizing current, the field gradient around flaws will not be of sufficient magnitude to hold the particles in place. On the other hand, if magnetizing current is too high, the field gradient may be strong enough, even in flawless areas, to attract and hold particles over the entire surface, obscuring genuine flaw indications. Obviously there will be an optimum current level for finding various flaws; for each inspection situation, this optimum must usually be found experimentally (ref. 3).

Application of magnetic particles.—The use of either wet or dry magnetic particles depends mainly on the type of flaw sought and the size, shape, and portability of the test article. Dry powders are more effective for subsurface flaws and are more convenient for inspection under field conditions. The wet method is usually su-

perior for detecting fine and shallow flaws (ref. 2).

The dry magnetic-particle powders may be applied by sprinkling from shaker cans, spraying from puff bottles, or spraying from blowers. In any of the above cases, the particles are airborne until coming in contact with the metal surface where they will be attracted to varying degrees all over the current-carrying areas. By blowing, either by mouth, with fans, or with a powder applicator, the loosely held particles are swept away; the remaining particles cluster, indicating the presence of a flaw. The particle color that will best contrast with the surface under test should be used. Generally, the dry powders are not supplied in fluorescent form and must be used in well-lighted areas.

When dry powders are used, either the continuous or residual method of magnetization may be employed. When the continuous method is used, the current flow is maintained through the test article or magnetizing coil, whichever is the case, until after the particles have been applied and the excess, or loose particles have been blown away. The current is then shut off and the part inspected. With the residual method, the current is allowed to flow in the test article or magnetizing coil; the current is then shut off, the particles applied, the excess blown away, and the part inspected. The choice of continuous or residual magnetism methods depends on the retentivity of the specimen material. If the specimen will not retain magnetism, the residual magnetism method probably will be ineffective (ref. 2).

Wet particles are applied by pouring onto the surface area a liquid that contains magnetic particles in suspension. The particles remain in suspension until they are attracted by the magnetic field gradient over the surface of the test article. The particles, which are free to move about in the liquid vehicle, will congregate about the fringing magnetic field of a surface flaw and remain there while the liquid carries away excess particles. The particle color that will best suit the inspection should be used. The colors include black, red, or a fluorescent blue- or yellow-green.

In the application of wet particles during the continuous method, current flow is maintained while a steady stream of the particle mixture is poured over the specimen surface. After the liquid flow is stopped, the magnetizing current is halted. With the residual method of magnetization, the specimen is first magnetized and then either the particle liquid is caused to flow over the specimen surface or the specimen is dipped into the wet particle mixture. Again, as in the case of the dry-particle method, if the specimen has low residual magnetism, this method works poorly.

Inspection.—An experienced inspector with good eyesight is required for examining (in good lighting) surfaces for flaw indications. Some typical flaw indications are shown in figure 8-29. Wherever clusters of powder are found, visual examination with a magnifying glass may be used to determine if there is a surface flaw. If there is doubt, the inspector may repeat the test steps to satisfy himself that the results he is interpreting can be repeated. Subsurface indications often resemble extraneous indications; an experienced inspector will observe the powder as it is first blown over the part surface and notice if some powders tend to cling in any one area. Sometimes the leakage field of subsurface flaws will lightly attract the iron particles but will not be strong enough to hold enough to indicate a definite cluster. Or, if the wet method is being employed, an experienced inspector will give the article an extra shot of current after the particles have already been applied to further strengthen the flaw indication.

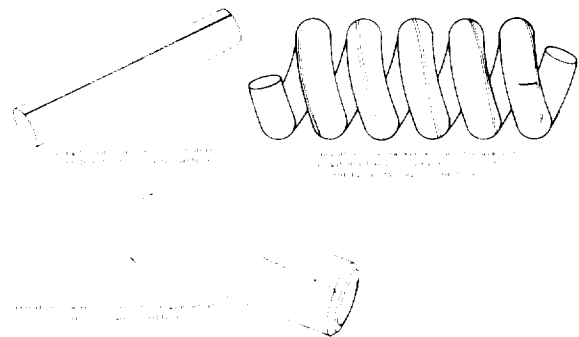


FIGURE 8-29.—Typical magnetic-particle flaw indications.

Demagnetization.—All materials inspected by the magnetic-particle method will retain some residual magnetism after being inspected. The amount of residual magnetism will depend upon the shape of the magnetic hysteresis curve of the material, the amount of magnetizing force used during magnetization, and the direction of the magnetizing field with respect to the specimen geometry. If this residual magnetism will not interfere with the subsequent use of the article under test, there is no need to consider demagnetizing. In most applications, however, there is an increasing concern about the presence of stray magnetic fields. Hence, in most cases, the article will have to be demagnetized. Several methods for demagnetizing parts are now available. One method in which the material is heated to the Curie temperature (at which all ferromagnetic properties disappear) is rarely used. For iron, this temperature is 770° C. A better method is to place the article inside a solenoid powered by a 60-Hz alternating current. The current, which must be of sufficient magnitude to magnetically saturate the article, is then gradually reduced to zero. The residual magnetic induction is reduced as shown in figure 8-30.

The solenoid may also be powered by direct current. In this method, the specimen is placed in the solenoid and magnetized to saturation. The current is turned off, the electrodes reversed, the current magnitude control adjusted downward, and current is caused to flow again in the solenoid. This procedure is repeated until the magnetizing current level is zero. This dc method of demagnetizing is more thorough than the 60-Hz ac method because the ac fields in general do not extend as deeply into the metal; however, the dc method is undesirably slow in comparison. Automatic demagnetizing features are available in some of the magnetic-particle equipment. In this demagnetizing operation, the magnetizing current is replaced by a 60-Hz current of equal magnitude, and a motorized control automatically reduces the current magnitude to zero. Test articles may also be demagnetized using alternating currents of frequency less than 60 Hz, but the required equipment is more complex and expensive.

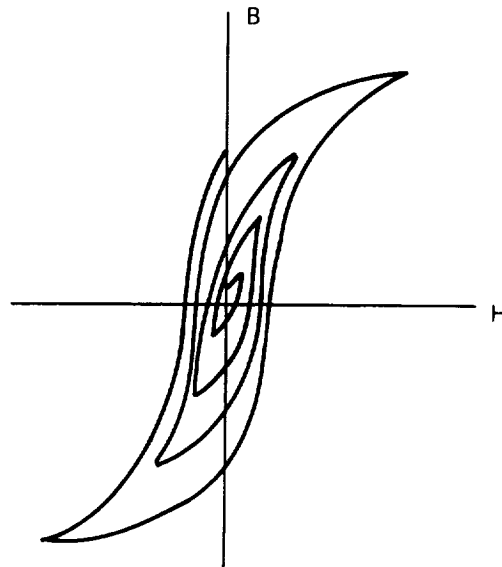


FIGURE 8-30.— B - H curve showing demagnetization.

Specifications and Standards

In order to control a method of inspection that is so dependent upon the operator skills and knowledge as is the magnetic-particle method, instructions in the form of written specifications are widely employed. These specifications range in content from a set of broad operational guidelines to instructions specifying almost every possible detail for performing a given magnetic-particle inspection. These specifications, usually written by technical societies, mainly educate or familiarize the neophyte. They are not intended to be imposed on inspection jobs. More complex specifications are usually written by companies engaged in magnetic-particle testing. Such specifications are also broad but differ from those generated by professional societies mainly in that only those areas in which the company is engaged are covered. In addition to the company specifications, a series of specifications written around single industries and one-type products are available. For instance, U.S. Air Force Technical Orders are produced in terms of aerospace hardware. Likewise, companies that test castings would be expected to prepare specifications solely for inspecting castings. The most restrictive type of specification that can be produced is

one that prescribes precisely the stepwise procedures for testing a single article. Also included in this specification are the standards of acceptance and rejections as well as the recommended disposition of rejectable items. This type is referenced in purchase documents to show advance agreement between buyer and seller regarding what constitutes acceptable practice.

A complete set of detailed procedures that covers all aspects of magnetic-particle testing has not been written or assembled; instead, most existing comprehensive documents contain broad and general descriptions of the utility of the method, the equipment required, and the basic procedural steps involved. A great deal is left to the operator. The difference between "specifications" and "standards" is that the specifications generally explain how the test method is to be accomplished, whereas standards are concerned with what is the best interpretation (ref. 2).

The list in table 8-1 gives a few representative specifications prepared by both industry, professional societies, and government. A more complete listing of specifications may be found in reference 4.

Commercially Available Magnetic-Particle Equipment

Essentially all that is required to perform a magnetic-particle inspection is a source of

electric current and a supply of powders. Commercial equipment, however, provides conveniences that facilitate the inspection. For instance, equipment that can remotely and accurately control the magnitude of current may allow inspection by an unassisted technician. Available equipment may be portable, mobile, or stationary.

The portable magnetic-particle testing units are available as hand-portable current sources or as hand-held magnetic yokes. A typical portable magnetic-particle unit (current source) is shown in figure 8-31 (ref. 3). These portable units are generally designed for operating on 110 or 220 V ac and supplying 500 and 1000 amperes. The output voltage will range from 5 to 25 V depending upon the current level being supplied. Portable units are especially desirable for inspecting small items and for inspecting in remote areas.

Except for added features of demagnetizing circuits, the mobile equipment may be best described as heavy-duty portable equipment on wheels. The electronic circuitry is generally designed to provide heavy currents ranging up to 3000 amperes. Since heavier transformer wires and connectors are required to carry these currents, and cooling fans are added to aid in cooling, the equipment weight becomes excessive. However, such equipment may still be used effectively in many different locations by rolling on wheels. A typical mobile magnetic-particle test unit is shown in figure 8-32 (ref. 3).

TABLE 8-1.—*Selected Representative Magnetic-Particle Inspection Specifications (ref. 4)*

Issuing agency or organization	Date	Title
Atomic Energy Commission.....	1969	Nondestructive Evaluation, Supplementary Criteria for Use of ASME Sec. III (ref. 5).
American Society of Mechanical Engineers..	1968	Sec. VIII, Boiler and Pressure Vessel Code (Unfired Pressure Vessels) (ref. 6).
American Society for Testing and Materials..	1961	A275-61T, Magnetic-Particle Testing and Inspection of Heavy Steel Forgings (ref. 7).
Department of Defense.....	1967	MIL-I-6868C and Amendment 1, Magnetic-Particle Inspection Process (ref. 8).
Society of Automotive Engineers.....	1961	AMS-2300A, Magnetic-Particle Inspection, Premium Aircraft Quality Steel Cleanliness (ref. 9).
United States Air Force.....	1963	T.O. 33B2-1-1, Inspection of Material, Magnetic Inspection Method (ref. 10).

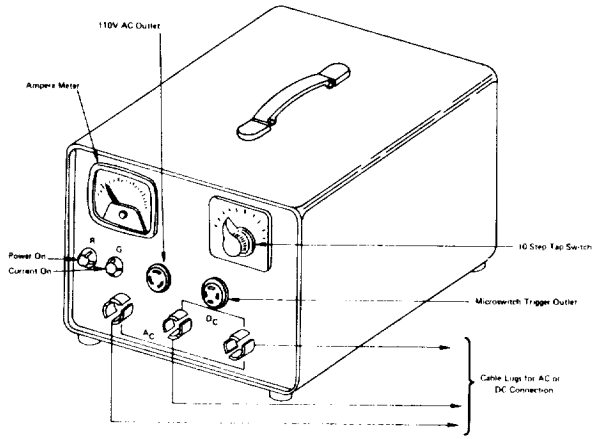
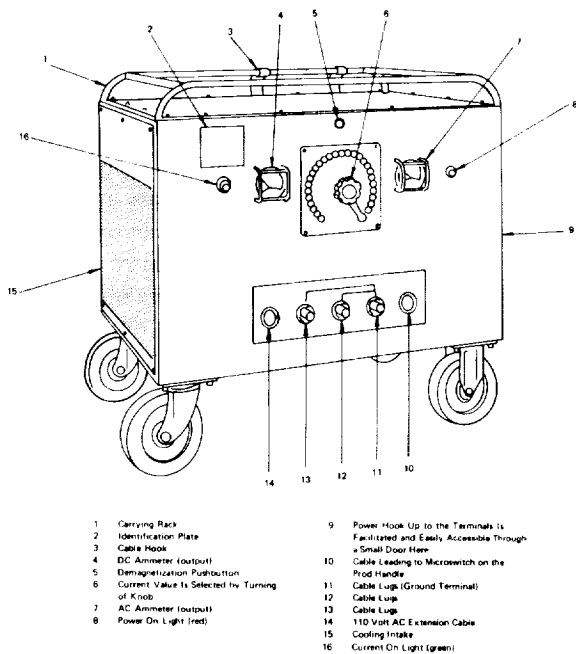


FIGURE 8-31.—Portable magnetic-particle current source. (Courtesy of General Dynamics, Convair Div.)

Stationary magnetic-particle test equipment may be obtained as either general-purpose or special-purpose inspection units. The general-purpose unit is primarily for use in the wet method, and has a built-in tank that contains the wet-particle bath pump which continually agitates the bath and forces the fluid through hoses onto the test article. In addition, curtains and



- | | |
|--|---|
| 1 Carrying Rack | 9 Power Hook Up to the Terminals is Facilitated and Easily Accessible Through a Small Door Here |
| 2 Identification Plate | 10 Cable Leading to Microswitch on the Front Handle |
| 3 Cable Hook | 11 Cable Lugs (Ground Terminal) |
| 4 DC Ammeter (output) | 12 Cable Lugs |
| 5 Demagnetization Pushbutton | 13 Cable Lugs |
| 6 Current Value Is Selected by Turning of Knob | 14 110 Volt AC Extension Cable |
| 7 AC Ammeter (output) | 15 Cooling Intake |
| 8 Power On Light (red) | 16 Current On Light (green) |

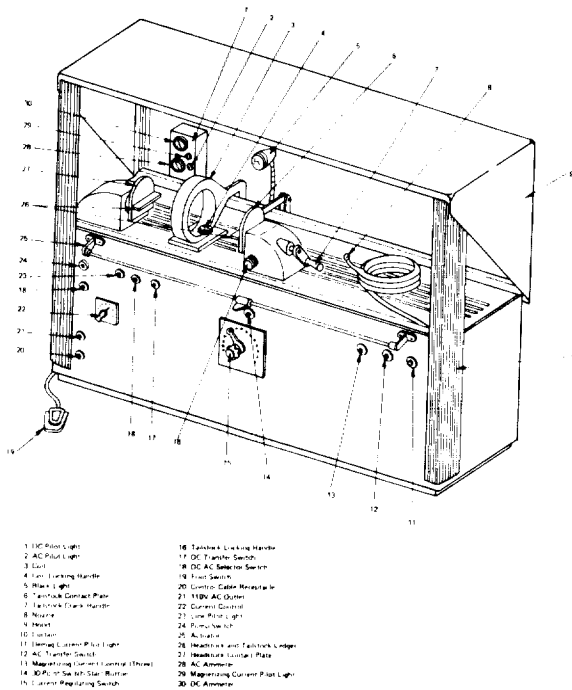
FIGURE 8-32.—Mobile magnetic-particle test unit. (Courtesy of General Dynamics, Convair Div.)

an ultraviolet light are provided for inspection whenever fluorescent particles are used. A general-purpose stationary unit is shown in figure 8-33 (ref. 3).

Special-purpose stationary units are designed for handling and inspecting large quantities of similar items. Generally, conveyors, automatic markers, and alarm systems are included in such units to expedite the handling and disposition of parts. Two special-purpose stationary magnetic-particle test units are shown in figure 8-34 (ref. 2).

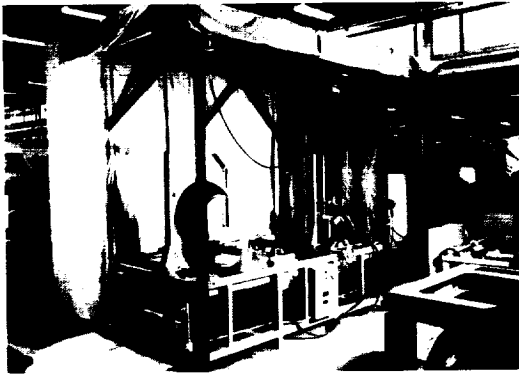
MAGNETIC-HYSTERESIS MEASUREMENTS

The magnetic-hysteresis methods include all the procedures that relate a measurable parameter of the hysteresis loop of a ferromagnetic specimen to a physical or metallurgical property of the specimen. For instance, high-magnetic coercive forces are often associated with mechanically hard steels. The magnetic parameters that may be measured and used in nondestructive evaluation include coercive force, maxi-

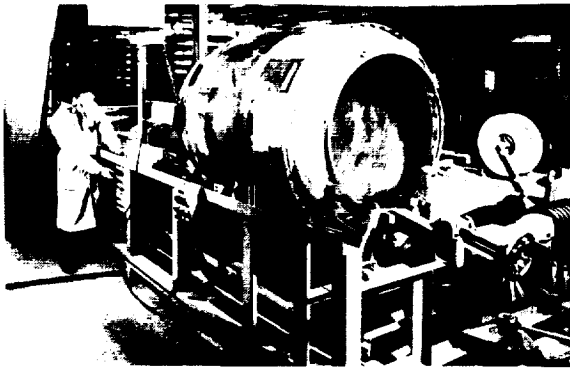


- | | |
|--|------------------------------------|
| 1 110V Pilot Light | 16 Tankless Locking Handle |
| 2 AC Pilot Light | 17 DC Tap Switch |
| 3 Cool | 18 DC AC Selection Switch |
| 4 Tank Locking Handle | 19 Tank Switch |
| 5 Main Light | 20 Control Cable Receptacle |
| 6 Tanklock Contact Plate | 21 110V AC Outlet |
| 7 Tanklock Drain Header | 22 Current Control |
| 8 Noise | 23 Low Pilot Light |
| 9 Heat | 24 Pilot Light |
| 10 Fan | 25 Actuator |
| 11 Spring Loaded Pilot Light | 26 Headstock and Tanklock Ledges |
| 12 AC Tap Switch | 27 Headstock Control Panel |
| 13 Magnetizing Current Control (Therm) | 28 AC Ammeter |
| 14 110V AC Extension Cable | 29 Magnetizing Current Pilot Light |
| 15 Current Releasing Switch | 30 DC Ammeter |

FIGURE 8-33.—General-purpose stationary magnetic-particle test unit. (Courtesy of General Dynamics, Convair Div.)



Special Unit for Inspection of Domes and Nozzles



Special Unit Designed for Inspection of Solid Fuel Missile Motor Cases

FIGURE 8-34.—Special-purpose stationary magnetic-particle test units. (Courtesy of Magnaflux Corp.)

mum-flux density, maximum permeability, retentivity, hysteresis power loss, the Barkhausen effect, and magnetoabsorption. The procedure of measuring any of these quantities usually includes cycling the material in some manner through its magnetic-hysteresis cycle. Depending on what is to be measured, the magnetizing force will then be halted at some predetermined level, will be completely removed, or will continue cycling at a set rate. Then, in any of the methods, the resultant magnetic field or a certain component of the magnetic field is measured.

B-H Curve Tracing

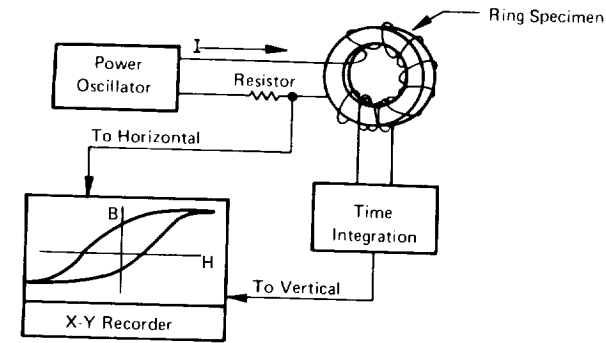
The most direct method of magnetic hysteresis measurement is simply to obtain or trace the

magnetic-hysteresis curve of the material. Because of demagnetizing effects, the graph of flux density, B , vs the magnetizing force, H , will not in general be the intrinsic, characteristic hysteresis curve of the material, but for comparison tests it is usually sufficient. The method of obtaining the $B-H$ curve for both a ring-shaped and a rod-shaped specimen is shown in figure 8-35. The ring method of obtaining hysteresis curves is very accurate when the magnetizing current rate of change is sufficiently slow to prevent errors from eddy currents in the specimen. The rod method of obtaining hysteresis curves is very dependent on the ratio of the length (L) and diameter (D) of the test specimen. For L/D ratios of 10 and higher, this method is sufficiently accurate for most purposes; however, for lower ratios, the hysteresis curve will appear skewed, and complicated formulae must be used to determine the intrinsic hysteresis parameters if these are desired. $B-H$ curve tracing is generally recommended for the screening of materials for gross anomalies in alloy composition or heat treatment but is not recommended for determining subtle changes in any of the magnetic parameters. Instruments for tracing magnetic-hysteresis curves are commercially available; however, in many cases, it is easier to use one of the simple setups illustrated in figure 8-35.

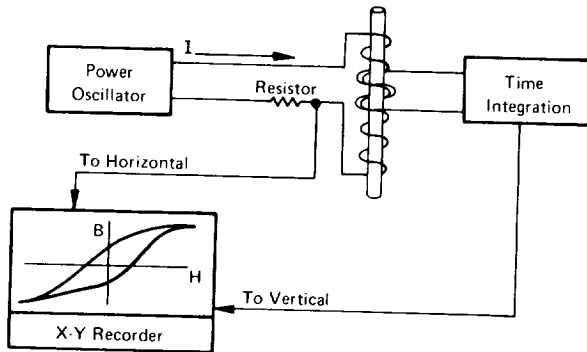
Any material change that would affect one of the magnetic properties will usually have a pronounced effect on the hysteresis curve, and with appropriate experimental techniques may be detected. However, it is usually easier to determine the portion of the B vs H curve that is most affected, and thereafter to measure only that portion. This is exactly what is done when measuring such properties as coercive force and permeability, which are described in the following paragraphs.

Coercive Force

Measurements of the magnetic coercive force may be used as an indirect measure of such properties as hardness, tensile strength, depth of case hardening, alloy content, and aging conditions. Because coercive force has proved very sensitive to changes in most of the above physi-



(a) Setup for Ring-Shaped Specimen



(b) Setup for Rod-Shaped Specimen

FIGURE 8-35.—Method for obtaining B - H curves of ring-shaped and rod-shaped ferromagnetic specimen.

cal factors and is easy to measure, its measurement is one of the more popular methods of hysteresis testing. The correct procedure for measuring coercive force of a material is first to magnetize the material to its saturation condition, then reduce the magnetizing force, H , to zero. At that time, simultaneously monitoring the flux density, B , and gradually increasing the magnetizing field, H , in a direction opposite to the original direction, cause B to decrease to zero. The amount of magnetizing force required to reduce B to zero is the coercive force. This method obviously is extremely slow and very difficult to automate with reasonable accuracy. In practice, most measuring systems do not bother with the step of increasing a magnetizing force opposite to the original field; instead, this step is simply omitted. The theory behind this is that for most ferromagnetic materials commonly encountered, the retentivity is very

nearly directly proportional to the coercive force. Hence, the preferred method is to magnetize the specimen to saturation and then measure its residual magnetism and relate this to coercive force. The procedure for measuring residual magnetism is either to scan the specimen surface with a field-measuring device, or if the object is small, simply to drop it through an inductive coil and measure the voltage impulse. (See ref. 11.)

Permeability

Instead of plotting the hysteresis loop for each specimen, an easier method of comparing magnetic properties is to make measurements that yield the material permeability (B/H) at a preselected, constant value of H . The procedure for doing this is to introduce the specimen into a known external magnetic field and then measure the flux density, B , of the specimen. The external magnetic field may be generated by electromagnetic yokes or by hand-held magnets, and the measurement of B may be made by induction coils or with Hall-effect devices. A convenient measuring method is shown in figure 8-36. In this method, the test specimen is made part of a magnetic circuit; changes in permeability will affect the flux density in the area of the Hall effect device.

Waveform Analysis

This analysis is based on the use of the specimen magnetic material essentially as the core of a transformer arrangement made up of testing coils. As shown in figure 8-37, the specimen is magnetized in an encircling coil arrangement with a sinusoidal magnetizing current. The induced voltage of the pickup coil is determined by the equation $V = -N (d\phi/dt)$ where N is the number of turns in the pickup coil and ϕ is the value of flux. Since the magnetic flux of the specimen material exhibits a hysteresis effect, the induced voltage of the pickup coil is modulated as indicated. This periodic voltage, if examined with a frequency spectrum analyzer, is found to contain a strong second harmonic component (as well as higher harmonics). One

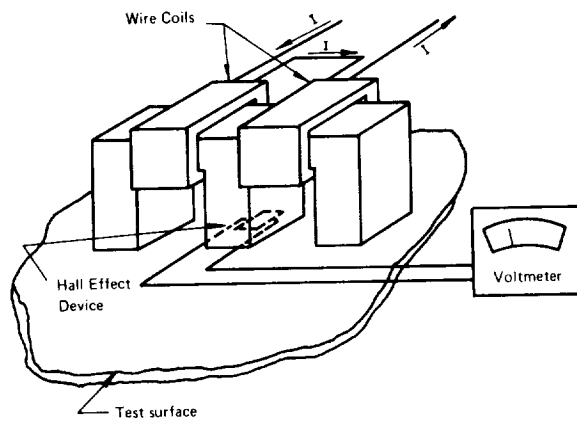


FIGURE 8-36.—Magnetic permeability may be measured by monitoring the flux-density level.

method of waveform analysis is to simply monitor the magnitude of this second harmonic component and relate this to a physical property. Another method of waveform analysis is a comparison technique in which a standard specimen and a test specimen are simultaneously magnetized in identical coil arrangements; the induced voltages from identical pickup coils on each specimen are subtracted and the difference displayed on an oscilloscope. Whenever the waveform of the test specimen is identical to that of the standard specimen, a zero net voltage will occur. However, whenever there is a difference in waveforms, this difference will be displayed.

Barkhausen Noise

Barkhausen-noise measurements are made by slowly magnetically cycling a specimen while monitoring high-frequency changes in the specimen flux. The source of these high-frequency changes are small, abrupt jumps in the magnetization of the specimen. In this method, observations are made of the voltage pulses that occur in a secondary pickup coil near the specimen surface as the specimen is being magnetized. Barkhausen-noise measurements have been related to applied and residual stresses in ferromagnetic materials. This method, though promising, is still being developed, and has thus far found only limited application (refs. 11 to 16).

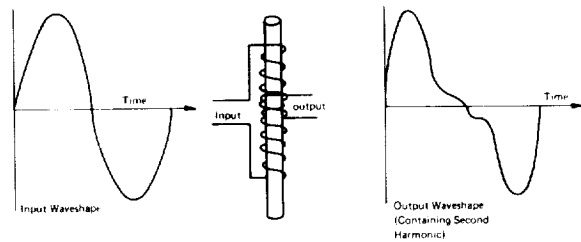


FIGURE 8-37.—The induced voltage from a ferromagnetic specimen in a transformer arrangement as shown here will be distorted because of the material hysteresis. (This induced voltage can be shown to contain harmonics of the fundamental magnetizing frequency.)

Magnetoabsorption

A piece of ferromagnetic material in the presence of two different magnetic fields, one of which is constant and the other varying at radio frequency rates, will apparently absorb energy from the varying field at a rate dependent upon the magnitude of the constant field. This method which is still being developed, has been investigated for measuring the effect of stress and cold work in ferromagnetic specimens (refs. 17 to 21).

MAGNETIC FIELD PERTURBATION

As used here, the expression "magnetic field perturbation method" refers to the use of various magnetometer probes to scan the surface of a magnetized ferromagnetic specimen, thereby enabling the construction of a map of the magnetic induction field of the surface of the specimen. The magnetic-particle method is itself a magnetic field perturbation method. However, inserting a string of precise qualifiers to distinguish the methods results in unwieldy expressions; therefore, the foregoing convention will be adhered to. Other expressions which have been used in the literature include "de search-coil method," "magnetic field scanning method," and (by the Russians) "ferroprobe method." The restriction of the expression "magnetic field perturbation method" to ferromagnetic specimens is intentional; the material property with respect to which a flaw-related anomaly produces a field perturbation is magnetic permeability. As will be developed in a

subsequent section, the same general kind of instrumentation (i.e., scanning magnetometers) is also employed in the method referred to as the "electric current perturbation method," which is applicable only to nonferromagnetic materials. In that case, detected flaws correspond to electric conductivity anomalies, and a distinguishing name for the method is clearly needed.

Only two types of magnetic field sensors (magnetometers) have found any appreciable use in the magnetic field perturbation method, namely the inductive coil and the Hall effect probe. The operation of these has previously been discussed in this chapter.

The first of these sensors to be used was the inductive coil. As early as 1931, patents were issued for the inspection of railroad track by magnetizing the rail (by injected dc current) and scanning along its length with a (rather large) inductive "search coil." Another early application of this method (and a continuing one) is the quality control inspection of steel pipe and tubing (ref. 11).

As a part of its continuing research on the causes and mechanisms of degradation and failure of rolling element antifriction bearings, NASA-Lewis Research Center (through a contractor) has made a limited study of the use of the magnetic field perturbation method for the inspection of ball bearing rings. The circular configuration of such rings, as well as their general size, lends itself to scanning since the probe can be held fixed (with provision for indexing to successive parallel tracks) while the bearing ring is rotated at high speed on a concentric axle. The essential apparatus used (fig. 8-38), shows a scan recording with a "signature" (fig. 8-39) which, from pre- and post-failure metallographic analyses, was correlated with a subsurface nonmetallic inclusion. The use of this method indicates that under favorable circumstances it is possible to infer from these recordings both the approximate size and depth of such flaws.

Perhaps the most ambitious use of the magnetic field perturbation method to date is an automatic system for inspecting steel "D" spars (the main structural members) of fully assembled helicopter rotor blades. In this method,

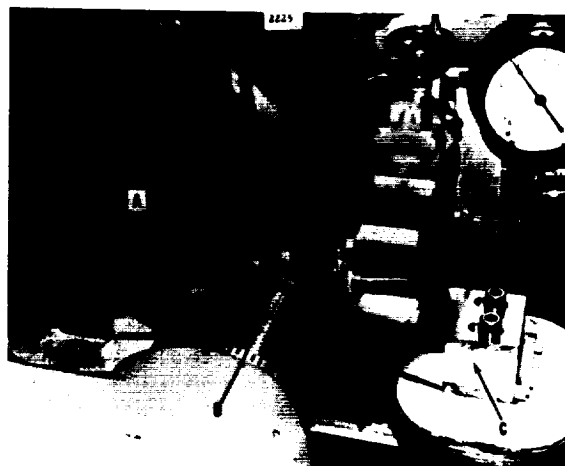


FIGURE 8-38.—Magnetic field perturbation apparatus used for inspection of ball bearing rings. (A—rotatable air coupled probe; B—bearing race; C—marking yoke; D—angle mark generator; E—locating holes for marking fixture.)

some forty individual induction coil probes are used, which scan the interior surface of the spar. Figure 8-40 is a photograph of this system. The original work on the method was commercially sponsored and the instrumentation was developed during separate programs under sponsorship of the U.S. Navy and the U.S. Air Force Office.

ELECTRIC CURRENT PERTURBATION

If a distribution of electric current is established by induction or direct injection through electrodes in a nonferromagnetic material, regions of anomalous electric conductivity (as opposed to magnetic permeability) will locally perturb the otherwise regular current-flow pattern. Since an electric current is accompanied by a magnetic field, a perturbation of the current-flow pattern will be reflected as a perturbation



FIGURE 8-39.—Typical magnetic field perturbation scan recording of a ball bearing ring showing a "signature" which was correlated with a subsurface nonmetallic inclusion.

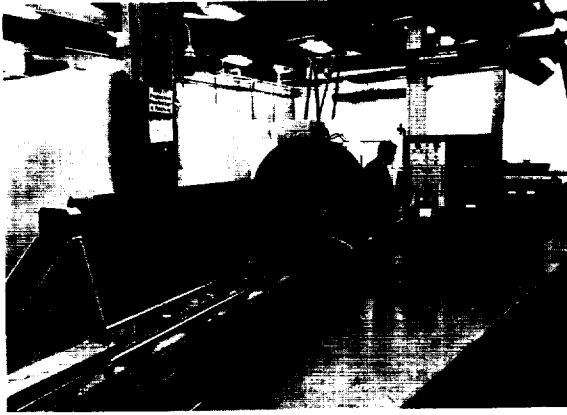


FIGURE 8-40.—Automatic magnetic field perturbation equipment for inspection of helicopter rotor blades.

of the magnetic field at the surface of the material. Open cracks, voids, and refractory inclusions have essentially zero electric conductivity. A "closed" crack may have a conductivity ranging from near zero to the value of the bulk material itself. For practical values of electric current density in nonferromagnetic engineering metals, the magnitude of the accompanying magnetic field and field perturbations is typically several orders of magnitudes smaller than is encountered in magnetic field perturbation inspection of ferromagnetic materials. Hence, the magnetic field sensors (and their associated electronics) typically used in magnetic field perturbation inspections are generally not sufficiently sensitive to be used directly to sense field perturbations associated with electric conductivity anomalies. However, techniques have been developed for substantially increasing the signal-to-noise ratio of inductive coil probes, the details of which have not been made public. Well-known state-of-the-art means of electronic signal-to-noise enhancement are available, which might be used in electric current perturbation inspections.

The electric current perturbation method has not yet been as widely used as has the magnetic field perturbation method. It would appear, however, to hold considerable promise for the inspection of articles made of aluminum, magnesium, titanium, and other conductive, nonferromagnetic metals and alloys. A sketch of an

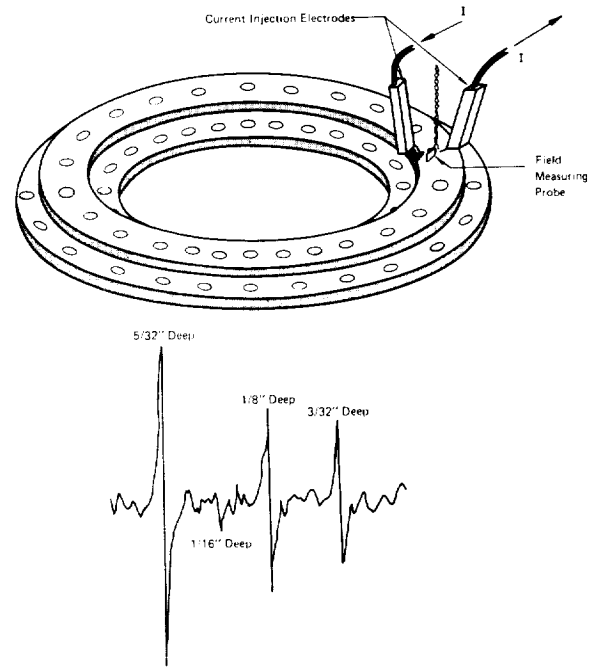


FIGURE 8-41.—Electric current perturbation methods are used to measure defects in aluminum valve flange. (Recording shows typical indication of 0.30-in.-long grooves in various depths.)

aluminum valve flange (from NASA-Marshall Space Flight Center) casting being inspected by the electric current perturbation method along with a recording of data is shown in figure 8-41.

LIMITATIONS AND ADVANTAGES

The magnetic-particle method has the following notable limitations and disadvantages.

- (1) It is limited to inspecting ferromagnetic materials.
- (2) Its effectiveness is substantially dependent upon the skill, experience, and attentiveness of the operator.
- (3) For applications requiring magnetizing current, access to electrical power is required.
- (4) It is somewhat messy.

On the other hand, the method is generally more sensitive to surface flaws than liquid penetrants, and has the further advantage of being sensitive to at least some subsurface flaws.

The magnetic field perturbation method has the following major drawbacks.

(1) The specimen must be scanned by a sensor; this operation requires a more or less complex electromechanical scan generator for each class of articles if they are substantially dissimilar in size or geometry.

(2) Associated electronic data acquisition, processing, and display apparatus is somewhat complex.

The major advantages of the magnetic field perturbation method are:

(1) In its most refined form, it is probably the most sensitive method for the detection of surface and shallow subsurface cracks and flaws.

(2) It lends itself to automation.

(3) It is substantially independent of an operator.

The electric current perturbation method has advantages and limitations closely paralleling those of the magnetic field perturbation method, with one major exception: Electric current perturbation can be used only to inspect nonferromagnetic, electrically conductive metals. In this sense, it is complementary to the magnetic field perturbation method.

Magnetic-hysteresis methods of characterizing ferromagnetic materials have a basic limitation in that indications are usually ambiguous, i.e., a given parameter of the hysteresis curve is usually strongly influenced by two or more equally significant factors. Thus, it is usually assumed that all variables are held constant except the one being monitored. If a heat-treatment process is being monitored by a measuring residual magnetism for example, other metallurgical properties such as chemical composition must usually be presumed to be invariable. In other respects, magnetic-hysteresis measurements require comparatively simple electronic apparatus, and automation is often practical.

REFERENCES

1. LEWIS, D. M.: *Magnetic and Electrical Methods of Nondestructive Testing*. George Allen & Unwin Ltd., Ruskin House (London), 1951, p. 10.
2. BERZ, C. E.: *Principles of Magnetic Particle Testing*. Magnaflux Corp. (Chicago), 1967.
3. ANON.: *Magnetic Particle Testing—Classroom Training Manual*. NASA CR-61227, 1967 (N68-28789).
4. ANON.: *Commonly Used Specifications and Standards for Nondestructive Testing*. *Materials Evaluation*, Aug. 1968, pp. 30-35A.
5. ANON.: *Nondestructive Evaluation, Supplementary Criteria for Use of ASME, Section III, Division, Reactor Development and Technology*, Atomic Energy Commission, 1969.
6. ANON.: *Boiler and Pressure Vessel Code (Section VIII)*. American Society of Mechanical Engineers, 1968.
7. ANON.: *Magnetic Particle Testing and Inspection of Heavy Steel Forgings*. American Society for Testing and Materials, A275-68, 1968.
8. ANON.: *Inspection Process, Magnetic Particle, Military Inspection*. MIL-I-6868C, Feb. 2, 1965, and Amendment 1, *Inspection Process, Magnetic Particle*, Feb. 17, 1967.
9. ANON.: *Magnetic Particle Inspection, Premium Aircraft Quality Steel Cleanliness*. Society of Automotive Engineers Material Specifications AMS-2300A, July 15, 1961.
10. ANON.: *Inspection of Material, Magnetic Particle Method*. U.S. Air Force Tech. Order 33B2-1-1, Apr. 1, 1963.
11. MCMASTER, ROBERT C.: *Nondestructive Testing Handbook, Vol. II*. The Ronald Press Co., 1963, pp. 30.1-35-22.
12. STIERSTADT, K.: *Der Magnetische Barkhausen-Effekt*. Springer Tracts in Modern Physics, Vol. 40, Springer-Verlag (Berlin), 1966, pp. 2-106.
13. LEEP, R. W.: *The Barkhausen Effect and Its Application in Nondestructive Testing*. Proc. of the Symposium on Physics and Nondestructive Testing (Dayton, O.) 1964, pp. 439-453. Available from Gordon and Breach Science Publishers, Inc. (New York), 1967.
14. DONALDSON, W. L.; AND PASLEY, R. L.: *A New Method of Nondestructive Stress Measurement*. Proc. of the 6th Symposium on Nondestructive Evaluation of Aerospace and Weapons Systems Components and Materials, 1967, pp. 563-575. Available from Western Periodicals Co. (Los Angeles), 1967.
15. LEEP, R. W.; AND PASLEY, R. L.: *Method and System for Investigating the Stress Condition of Magnetic Materials*. U.S. Patent 3,427,872, Oct. 5, 1966.
16. CARY, R.; AND ISAAC, E. D.: *Magnetic Domains and Techniques for Their Observation*. Academic Press, Inc. (New York), 1966.
17. ROLLWITZ, WILLIAM L.: *Magnetoabsorption Measurements of Stress*. Proc. of the 6th Symposium on Nondestructive Evaluation of Aerospace and Weapons Systems Components and Materials, 1967, pp. 36-59. (Available from Western Periodicals Co., Los Angeles)
18. ROLLWITZ, WILLIAM L.: *Magnetoabsorption Measurements in Nickel and Iron Wires*. Symposium on Physics and Nondestructive Testing (Dayton, O.), Sept. 29-Oct. 1, 1964, pp. 405-437. [Available from Western Periodicals Co., Los Angeles]

- able from Gordon and Breach Science Publishers, Inc. (New York), 1967.]
19. ROLLWITZ, WILLIAM L. ; AND CLAASSEN, J. P. : Magnetoabsorption Techniques for Measuring Material Properties. AFML-TR-65-17, 1965.
20. ROLLWITZ, WILLIAM L. ; AND CLAASSEN, J. P. : Magnetoabsorption Techniques for Measuring Material Properties. AFML-TR-66-76, May 1966.
21. ROLLWITZ, WILLIAM L. : Magnetoabsorbtion Techniques for Measuring Material Properties, Part II—Measurements of Residual and Applied Stress. AFML-TR-66-76, Part II, June 1968.

CHAPTER 9

Leak Testing

Robert E. Engelhardt

For as long as men have used vessels to hold liquids, they have engaged in leak testing; thus, it can perhaps be labeled the oldest branch of nondestructive evaluation. Advances in this method of NDT have, by and large, been closely linked with progress in the technology of containment, transport, and use of fluids (both liquids and gases) on the one hand, and the technology of exclusion of fluids from a given vessel (as in the case of boats and vacuum systems) on the other hand. Despite its evident practical importance, leak testing remained until quite recently largely unrecognized as an independent technical discipline. Even today there are remarkably few individual published works which cover the field in a systematic, comprehensive, and up to date manner. Of these, the most current and perhaps the most complete is the *Leakage Testing Handbook* (ref. 1).

Historically, leak detection was initially used for liquid systems, first for water and later for other liquids. Systems for the accumulation, storage, and distribution of water for human consumption, irrigation, and power generation are examples. The development of closed, pressurized distribution systems increased the importance of leak detection. Leaks were found largely by visual inspection, however, until the development of effective pumps for compressing air

into or evacuating it from a closed system. Gross leaks in such systems were detectable from the sound made by air rushing out of (or into) the system; even the presence of quite small leaks could be sensed by observing the gradual falling (or rising) of pressure by means of a manometer or pressure gage. Both these methods, in refined forms, are of contemporary importance. It is not known when the idea occurred for testing a pressurized vessel by submerging it in water and observing the formation of bubbles, but a U.S. Patent was issued in 1885 covering the use of this method for detecting leaks in certain items. The earliest use of soap solutions that form visible bubbles when freshly coated onto the surface of a region from which a gas is escaping is also unknown, but the earliest recorded U.S. Patent for such a preparation was issued in 1934 (ref. 2).

The development of steam power in the late eighteenth century and throughout the nineteenth century and the attendant progress in pressure-vessel technology stimulated a number of primitive NDE methods, including leak testing. Within the last century, the rise in the industrial production and use of fluids that are explosive, flammable, chemically reactive, toxic, or otherwise hazardous stimulated the development of leak detecting methods of great sensitivity, the so-called trace-sensitive methods. The

widespread use of closed refrigerant systems also created a market for simple and reliable detectors sensitive to trace leaks.

Ultrasensitive leak-testing methods, however, were not required until the advent of modern vacuum technology that began with the introduction of the rotary oil-sealed pump during the late nineteenth century. Such early pumps were capable of generating vacuums of about 10^{-4} atm, and could be used in the evacuation of incandescent lamps and X-ray tubes. Gaeder's mercury-vapor diffusion pump, introduced in 1915, and Langmuir's condensation pump, which were capable of generating vacuums of 10^{-9} atm, produced the vacuums required for electron vacuum tubes. Large-volume high vacuums were required for nuclear particle accelerators, the development of which dates from the mid 1930's. Until the development of sensitive mass spectrometers for residual gas analysis, leak testing of such systems was done mainly by monitoring vacuum (i.e., gas-density) gauges. Large-volume, high vacuum technology and its attendant leak-testing technology was remarkably advanced by NASA's requirements for space simulation systems. The development of both manned and unmanned spacecraft and launch vehicles for them created unprecedented requirements for leak testing. Whether in propellant or oxidizer tankage, piping in a launch vehicle, spacecraft attitude control systems, hermetically sealed electronic components, or life support systems a leak more often than not means serious trouble on a spaceflight.

As leak testing has advanced, it has become clear that the notion of a "leak-free" or "zero-leakage" containment system is merely a concept. All containment systems leak; the only rational requirement that can be imposed is that such a system leak at a rate no greater than some finite maximum allowable rate, however small that may be, as long as it is within the range of sensitivity of a measuring system.

As in most technologies, leak testing has specialized terminology with which a newcomer must become familiar. It has become conventional to use the term "leak" to refer to an actual discontinuity or passage through which a fluid flows or permeates. "Leakage" refers to the

fluid that has flowed through a leak. "Leak rate" refers to the rate of fluid flow per unit of time under a given set of conditions, and is properly expressed in units of mass per unit time. Often, however, it is more convenient to express leak rate in other units that are equivalent to mass per unit time. At a given temperature, the product of pressure and volume of a given quantity of gas is proportional to its mass. Hence, leak rate is often expressed as the product of some measure of pressure and volume per unit time, for example torr-liters/sec, micron-liters/sec, and atm-cc/sec; the exact significance of these terms is treated in the section on Physical Principles.

There are two basic types of leaks. One is an essentially localized leak, i.e., a discrete passage through which fluid may flow (crudely, a hole). Such a leak may take the form of a tube, crack, orifice, or the like. A system may also leak through permeation of a somewhat extended barrier; such a leak is called a distributed leak. Gases may flow through a solid having no holes large enough to permit more than a small fraction of the gas to flow through any one hole. This process involves diffusion through the solid and may involve various surface phenomena such as absorption, dissociation, migration, and desorption of gas molecules (ref. 3).

A distinction may be drawn between "real" and "virtual" leaks. Real leaks are the type described above; "virtual leak" refers to gradual desorption of gases from surfaces or components within a vacuum system. It is not uncommon for a vacuum system to have real and virtual leaks simultaneously.

Before discussing specific leak-testing methods, it will be helpful to review briefly some pertinent results from fluid dynamics.

PHYSICAL PRINCIPLES

As a physical phenomenon, leakage falls generally within the discipline of fluid dynamics. Only the rudiments of this branch of physics, however, are needed for most of the practical requirements of leak testing. Gas systems are somewhat more susceptible of reasonably exact theoretical treatment than are liquid systems.

It is in the testing of gas systems that mathematical models are of greatest utility, and the ensuing discussion is mainly concerned with such systems.

The equation of state of an ideal gas (i.e., a gas made up of perfectly elastic "point" particles) is

$$PV = NRT \quad (1)$$

where

P is the gas pressure

V is the volume of the vessel containing the gas

T is the absolute temperature of the gas

N = number of moles of gas

$$= \frac{\text{mass of the gas in grams}}{\text{gram-molecular weight of the gas}}$$

R = the universal gas constant, the same for all (ideal) gases, the numerical value of which depends upon the system of units in which P , V , and T are measured.

The gram-molecular weight of a gas is simply the number of grams numerically equal to the molecular weight of the gas. Regardless of the molecular weight, one mole of a gas always contains 6.023×10^{23} (Avogadro's number) molecules.

Fundamentally, pressure is a force per unit area, directed normally to the area. In the cgs system of units, pressure is measured in dynes/cm². In leak testing, however, it is conventional to measure pressures in terms of atmospheric pressure. By international compact, the pressure of the standard atmosphere is 1.013×10^6 dynes/cm², being equivalent to the pressure exerted by a column of mercury of 760 mm in height, at 0° C, under a standard acceleration of gravity of 980.665 cm/sec². Another unit of pressure commonly used, especially in vacuum technology, is the torr, which is defined to be $1/760$ of a standard atmosphere, and is equivalent to 1 mm of mercury.

The numerical value of the gas constant, R , in two useful sets of units is

$$R = \frac{0.08207 \text{ atm-liter}}{\text{mole } ^\circ\text{K}} = \frac{62.37 \text{ torr-liter}}{\text{mole } ^\circ\text{K}} \quad (2)$$

For many practical purposes, any real gas may be treated as an ideal gas provided the gas is sufficiently dilute, i.e., when the density of the gas is much less than the density of the condensed phase of the gas. When this is not the case, it may be necessary to use an equation of state more exact than that of an ideal gas.

The primary use to which such equations of state are put in leak testing is in determining from measurements of pressure, volume, and temperature the total quantity of gas in a closed system. The quantity of gas of a given composition may be expressed in terms of (1) the total number of molecules, (2) the total mass of gas, or (3) any quantity proportional to these. For example, suppose a pressure vessel of volume, V , is pressurized to a pressure, P , (greater than atmospheric pressure), at a temperature, T , and allowed to stand for a period of time, say 24 hours. At the end of this period, the pressure is found to have dropped to P_2 (less than P_1). If the temperature of the system is unchanged, and if the vessel may be assumed not to have expanded in volume, then the drop in pressure must be due to a loss of gas; and a leak must be presumed to be present. If, however, the temperature, T_2 , is less than T_1 , the drop in pressure may be due to cooling. If the quantity of gas has indeed not changed, it follows from equation (1) that P_1, V_1, P_2, V_2 , and T_2 must satisfy the relation:

$$\frac{P_1 V_1}{T_1} = \frac{P_2 V_2}{T_2} \quad (3)$$

If $V_1 = V_2$, as assumed, then the following relation exists:

$$\frac{P_1}{T_1} = \frac{P_2}{T_2} \quad (V \text{ constant}) \quad (4)$$

Thus, if P_2 has fallen in proportion to the drop in temperature, the system may be presumed not to have leaked at a rate discernible with the pressure gage and thermometer used to monitor the system. If the precision and drift of these instruments are known, a maximum leak rate consistent with their indication of "no leaking" can be computed.

If the reduction in pressure cannot be accounted for by the reduction in temperature

[i.e., equation (4) is found not to be satisfied], then a leak may be presumed present, and the leak rate may be determined by computing the loss in quantity of gas. Referring to equation (1), note that the loss of gas (expressed in number of moles) is given by

$$\Delta N = N_2 - N_1 = \left(\frac{P_2}{T_2} - \frac{P_1}{T_1} \right) \frac{V}{R} \quad (5)$$

where again V is presumed constant.

If desired, ΔN may be converted to mass by multiplying by the mean gram-molecular weight of the gas. When ΔN is divided by the time span between measurements (24 hr in this example), the average leak rate is obtained.

In the example given above, the volume of the system was assumed to be constant. For most systems, this is an adequate approximation. All pressure vessels do, however, expand by some amount when they are pressurized; moreover, their volume may vary with temperature caused by the thermal expansion or contraction. In some cases where very precise estimates of leak rate are required explicit corrections for these effects must be made.

It is sometimes convenient to measure the rate of leaking of a system under one pressure gradient, and from this predict what the leak rate will be at another pressure gradient. Additionally, having determined a leak rate with some convenient gas, it is sometimes useful to be able to predict the leak rate to be expected for another gas. It is not always possible to do either of these in an accurate and reliable way; in general, it cannot be done if the physical size or shape of the leak path is explicitly pressure dependent. Even in cases where this difficulty does not arise, an exact theoretical description of the gas flow may, at certain pressures, temperatures, and pressure gradients, be prohibitively complicated. Frequently, however, a satisfactory result can be obtained from the considerations below.

Fluid flow may be classified into the following discrete regimes: molecular, laminar, turbulent, and sonic. As the flow changes from one regime to another, it goes through transitional regimes during which it exhibits some of the

characteristics of both the higher and lower flow regimes. A given leak may exhibit several of these flow types depending upon the pressure gradient, temperature, and fluid composition. It is, therefore, important to identify the type of flow that exists in order to predict the effect of changing these variables. Conversely, with a constant temperature, pressure, and fluid composition, the geometry of the leak will determine the type of flow. Since the leak may be a crack, hole, permeation, or a combination of these, its geometry is often impossible to ascertain, but general empirical guidelines can establish the type of flow for gases. If the leak rate is:

(1) Less than 10^{-6} atm-cc/sec, the flow is usually molecular

(2) 10^{-4} to 10^{-6} atm-cc/sec, it is usually transitional

(3) 10^{-1} to 10^{-6} atm-cc/sec, it is usually laminar

(4) Greater than 10^{-2} atm-cc/sec, it is usually turbulent (ref. 1).

These types of gas flow are more accurately described by the Knudsen number:

$$N_K = \lambda/d \quad (6)$$

where

N_K = Knudsen number

λ = mean free path of the gas

d = diameter of the leak.

The relation between N_K and flow regime is:

$N_K < 0.01$ laminar (or a higher regime)

$0.01 > N_K > 1.00$ transitional

$N_K > 1.00$ molecular.

The mean free path of the gas is the average distance the gas molecules travel before colliding with another molecule. Values of mean free path for various gases and pressures may be found in reference 4. In a vacuum system, the mean free path will vary from inches to many feet; when the mean free path is very long, collisions with the chamber surfaces are more frequent than collisions between molecules.

This, in part, explains why neither gases nor leakage diffuse evenly throughout a vacuum system at a rate as rapid as may be expected. The flow of gases in a vacuum is analogous to current flow in an electrical system. Every

baffle or restriction in the system acts as an impedance to gas diffusion. Consequently, if there are many impedances between the leak and the leak detector that reflect or absorb the molecules, movement of the gas molecules to the leak detector does not follow theoretical diffusion rates; instead, it is greatly dependent upon system geometry.

The level of vacuum is almost universally described in terms of pressure. However, it is the mean free path or concentration of molecules that controls such vacuum properties as viscosity, thermal conductance, and dielectric strength. Further, very few vacuum gages actually measure pressure, but instead measure the concentration of molecules. Therefore "pressure" in a vacuum system is largely an inaccurate term although it remains in popular usage.

Molecular Flow of Gases

Gas flow is said to be molecular when the mean free path of the gas is greater than the largest cross-sectional distance of the leak. Thus, flow is propagated through the leak by collisions of the gas molecules with the leak wall. If the gas flow is molecular, Knudsen's equation for flow in a long pipe is often used to describe it as

$$Q = \frac{1}{6} \sqrt{\frac{2\pi RT}{M}} \left(\frac{d^3}{L}\right) (P_1 - P_2) \quad (7)$$

where

- Q = rate of flow, micron cc/sec
- R = universal gas constant, 8.3149 joules/mole, °K
- M = molecular weight of gas, g/mole
- d = pipe diam, cm
- L = pipe length, cm
- P_1 = upstream pressure, microns of mercury
- P_2 = downstream pressure, microns of mercury
- T = absolute temperature, °K

If one measures a molecular flow leak rate, Q_1 using a gas of molecular weight, M_1 , at temperature, T_1 , with a pressure drop, ΔP_1 , across the leak, then, by using equation (6), the leak rate of another gas of molecular weight, M_2 , temperature, T_2 , and pressure drop, ΔP_2 , can be predicted (assuming the leak geometry

and the flow regime to be unchanged). The resulting relation is:

$$Q_2 = Q_1 \sqrt{\frac{M_1 T_2}{M_2 T_1}} \left(\frac{\Delta P_2}{\Delta P_1}\right) \quad (8)$$

Laminar Flow of Gases

As the pressure increases and the mean free path of the gas molecules decreases, molecule-to-wall collisions no longer predominate, and molecule-to-molecule collisions become the primary mode of flow propagation. This is called laminar or viscous flow, and is characterized by smooth streamlines, the velocity profiles across the leak being parabolic. If the flow is laminar, Poiseuille's equation for flow in a long tube may be used:

$$Q = \frac{\pi}{8\eta L} \left(\frac{d}{2}\right)^4 P_a (P_1 - P_2) \quad (9a)$$

or

$$Q = \frac{\pi d^4}{128\eta L} \left(\frac{P_1^2 - P_2^2}{2}\right) \quad (9b)$$

where

P_a = average of upstream and downstream pressure

η = gas viscosity in poise, at gas temperature

The other units are the same as defined for equation (7). It is assumed that in laminar flow, the flow is essentially isothermal and no temperature change occurs that might be caused by expansion of the gas.

Laminar flow under different conditions is expressed by the relation:

$$\left[\frac{Q_1 (P_1^2 - P_2^2)}{\eta_1} \right] \text{condition 1} = \left[\frac{Q_2 (P_1^2 - P_2^2)}{\eta_2} \right] \text{condition 2}$$

where $(P_1^2 - P_2^2)$ at condition 1 and at condition 2 are the pressure differentials at conditions 1 and 2, respectively. Values for viscosity may be found in such handbooks as reference 5.

Transitional Flow of Gases

Knudsen developed a very complex formula for the transition between turbulent and lami-

nar flow in tubes. It tends to approach the value of a molecular-flow equation for low pressure differences and approaches the value of a laminar-flow equation for high pressure differences. Additional transitional flow equations exist but they are all empirical and must be used with caution. Transitional flow is not well understood and is usually avoided wherever possible by altering system operating conditions.

Turbulent and Sonic Flow of Gases

Turbulent and sonic flows of gases are only encountered at very high flow rates; their value as a function of leak geometry and gas property is not often calculated. The onset of turbulent flow depends upon the value of a dimensionless parameter called the Reynolds number that is a function of the gas velocity, length of the tube, gas mass density, and gas viscosity. Sonic flow is that which occurs when the flow velocity reaches the speed of sound at the leak orifice or nozzle throat. Sonic speed is a function of the specific heat of the gas at constant volume and pressure, the mass density of the gas, the pressure differential across the orifice, and orifice discharge coefficient, and the throat area. It should be noted that the gas velocity will not go above sonic velocity; therefore, an increase of pressure will have no effect on flow. Further details on turbulent and sonic flow may be found in references 4 and 6.

Flow of Liquids

Laminar flow of liquids can be calculated by using Poiseuille's equation for liquid flow

$$Q = \frac{\pi d^4}{128} \left(\frac{P_1 - P_2}{L} \right) \quad (10)$$

the units for which are the same as defined for equation (7).

Turbulent flow of liquids, like gases, is a function of the Reynolds number, and calculations of turbulent flow in the field of leak testing are not accomplished easily because of the lack of knowledge about the leak geometry.

Additional Comments on Flow

The conductance value of a gas flow is obtained by dividing the quantity of gas flowing in a line by the pressure differential. Thus, the flow equations previously given may be converted to leak conductance by dividing them by $(P_1 - P_2)$. In some cases, such as molecular flow, the leak conductance is constant as long as the flow regime is constant. In other flow regimes, leak conductance is a function of average upstream and downstream pressures.

All of the equations cited were for long circular tubes or capillaries. Other geometrical forms will produce different flow rates and a number of equations have been developed for some standard shapes. Some of these are discussed in the *Handbook of Physics* (ref. 7).

It is good practice for correlations to be made in order that the predicted leak will be equal to or larger than the actual leak. If there is doubt about the flow that will occur under working conditions as compared to test conditions, it is suggested that (1) if the pressure under working conditions is increased, calculate the flow using laminar-flow equations, (2) if the pressure is decreased, use molecular-flow equations, and (3) if the gas is changed, use molecular-flow equations (ref. 1). Correlation by pressure differential is sometimes inaccurate if the leaks change geometry with pressure due to stress in the vessel, if they become self-cleaning, or if they only appear above a certain pressure.

RELATIONS OF LEAK-TESTING METHODS AND INSTRUMENTATION

This section contains a general orientation with respect to currently available leak-testing methods and instrumentation. Details of the mode of operation of specific instruments, their relative advantages and disadvantages, and the strategy of solving particular leak-testing problems are treated in detail in subsequent sections.

For purposes of the ensuing discussion, it is convenient to categorize leak-testing methods according to whether the method is primarily applicable to the testing of internally pressurized systems or to vacuum systems. It is also use-

ful to distinguish methods used primarily in connection with gas systems from those used with liquid systems. (Several methods fall into more than one of these categories.) Another useful way of classifying leak-detecting methods is according to their range of sensitivity, i.e., the largest and smallest leak rates for which they are suited. The maximum sensitivities mentioned in the text are achievable only under ideal conditions and should not be expected unless such conditions exist.

There are two basic ways to detect leaks in internally pressurized gas systems: (1) any reduction in the total quantity of gas contained within the system may be detected and (2) the escaping gas may itself be detected. A loss in the original quantity of gas contained in a vessel may be detected either by actually weighing the vessel and its contents, or by deducting such a loss from changes in the internal pressure of the vessel as measured with a suitable pressure gage, consideration being given to any change in temperature.

Directly weighing a vessel is practical only if the vessel is of reasonable size and can be placed on a suitable scale. The sensitivity and accuracy of this method is limited by that of the scale; in general, this method is poor unless the weight of the vessel is comparable to or smaller than the weight of its contents. This method has been used to good effect in testing for leaks in the fire extinguisher carried aboard the Apollo spacecraft command module. The pressure vessel of the extinguisher, with attachments, weighs 1.76 kg when empty, and 3.60 kg when fully charged. Thus, periodic weighing of the charged extinguisher on a balance of sensitivity of 1 part in 20 000 is a practical means for ensuring its freedom from unacceptable leakage.

The principles involved in determining leak rates of a gas-filled enclosure by measuring changes in the pressure and temperature of the system were discussed in the section on physical principles. Monitoring with a pressure gage is almost certainly the most frequently used method of detecting the presence of a leak in a gas system. Its disadvantages are that it (1) requires a considerable length of time to establish definitely the presence of a very small (i.e.,

slow) leak and (2) gives no information on the location of the leak. The sensitivity and accuracy of the method are determined essentially by the sensitivity and accuracy of the pressure gage and thermometer used.

A particularly sensitive means of detecting a leak by sensing a pressure drop is the so-called differential pressure method whereby a gage sensitive only to a pressure difference between two ports is connected between an internally pressurized system (to be tested) and a reference vessel (assumed to be leak free) pressurized to the same pressure. Loss of gas from the vessel under test results in a pressure imbalance which is sensed by the differential pressure gage. This null method is in principle intrinsically more sensitive than an absolute pressure gage method.

For small leaks in pressurized gas systems, some method of directly sensing the escaping gas is usually necessary, especially when it is essential to locate the leak. The general methods available for doing this are:

- (1) Listening
- (2) Submergence bubble testing
- (3) "Soap"-bubble testing
- (4) Flow detection
- (5) Specific gas detectors.

The flow of a gas through an orifice always produces a certain amount of acoustic energy. The audible sound made by gas escaping from a gross leak under a moderate to high pressure differential is familiar to most people. Listening for leaks with the unaided ear is a surprisingly sensitive method of leak detection when a noisy background or other interference is not present. The use of an ordinary stethoscope greatly increases the sensitivity of listening, and is virtually a necessity if background noise is present. The aid of an electronic sound detector raises this method from a gross leak method to a fine one; the extension of the frequency response of such systems into the ultrasonic range improves their sensitivity still further. Instruments based on these principles are commercially available.

Submergence bubble testing is accomplished simply by submerging a pressurized vessel in a liquid bath and visually observing the forma-

tion of bubbles as the gas escapes from a leak. This very old method, commonly associated with the testing of pneumatic tires and inner tubes, is capable of considerable refinement through the proper choice of the liquid bath and attention to details.

When submergence of a pressurized vessel or system is impractical, "soap"-bubble testing may be used instead. The method involves coating a suspect area with a thin film of a solution that forms bubbles by entrapping gas escaping from a leak. Originally, soap solutions were used for this purpose—hence its name; special preparations are now commercially available. By adjusting the properties of the solution (e.g., its surface tension and viscosity), a range of sensitivities can be achieved; a crude but useful leak-rate calibration is also possible.

If an internally pressurized vessel or system can conveniently be enclosed within a larger vessel that can be closed except for a small duct, leakage from the vessel under test will result in an increase in pressure within the larger enclosing vessel, and a flow of gas through the attached duct will occur. If a device sensitive to the movement (i.e., flow) of gas is installed in the attached duct, it can serve as a leak-rate indicator. Positive-displacement flow meters that are extremely sensitive have been developed for this purpose. A slight variant of this approach is the use of a volumetric-displacement meter instead of a flow meter. The volumetric-displacement meter consists essentially of a cylinder with a movable piston. When attached to the duct from a vessel enclosing a leaking system, the piston moves as the pressure of the enclosing vessel rises, effectively increasing the volume of enclosing vessel and returning the internal pressure to the ambient atmospheric pressure. The piston must offer little resistance to movement (i.e., it must be very nearly free of frictional drag), and its motion must be accurately horizontal. Sensitive volumetric-displacement meters are equipped with micrometric cathetometers by means of which extremely small displacements of the piston can be accurately measured.

Perhaps the simplest example of leak detection and measurement by measuring flow is the

bubble tube. If the end of the duct from the outer enclosing vessel is introduced into a liquid bath, appreciable leakage will result in bubbles being generated. Even quite small leak rates can be detected simply by the movement of the liquid meniscus in the tube.

A large and ever increasing number of leak-detecting instruments and materials are presently available; they depend for their operation on some response to a specific property of a leaking gas, that is, they work only as detectors of a single specific gas or a family of gases that are closely related either chemically or physically. The most important of these are:

- (1) The human nose
- (2) Materials that undergo a change of color by chemical reaction with a gas
- (3) Instruments used primarily to detect halide gases
- (4) Instruments that detect combustible gases by oxidizing them under controlled conditions
- (5) Instruments that sense changes in the molecular composition of an air-gas mixture by monitoring the thermal conductivity of the mixture
- (6) Detectors based on the characteristic absorption of infrared radiation by specific molecules
- (7) Instruments based on some form of mass spectrometer, which is selectively sensitive to atoms or molecules of specific molecular weights
- (8) Gas chromatographs
- (9) Nuclear radiation detectors used in conjunction with a radioactive tracer gas.

Smelling, of course, is not a quantitative method and depends upon the escaping gas having a characteristic odor. The method is not to be dismissed lightly, however, for certain gases (mercaptans, for example) have been shown to be detectable by smelling in concentrations (at atmospheric pressure) as small as one part per billion, a sensitivity which is not exceeded even by mass spectrometers.

Products, generally liquids or pastes, which change color in the presence of gases that are acidic or basic are commercially available. Such materials are referred to as being pH sen-

sitive (pH being the chemical scale of basicity—acidity). For example, carbon dioxide is acidic and ammonia is basic; special color-changing preparations for their detection are commercially available.

One of two common types of halogen detectors is the halogen (or halide) torch in which a small flame heats a copper plate. If a gas containing one of the halogens (i.e., one of the elements fluorine, chlorine, bromine, iodine, or astatine) is introduced into the flame in the presence of the copper plate, a chemical reaction results in the emission of light of a characteristic hue that is visually observed. Such torches are commonly used to test refrigeration or air-conditioning systems for refrigerant leaks.

The other common type of halogen detector is the so-called heated-anode detector. In the presence of a halogen, the anode to cathode electric current increases.

Combustible gas detectors, widely used in checking for leaks in systems containing gaseous or volatile-liquid hydrocarbons, generally operate by sensing a small increase in the temperature of a heated element that catalyzes the oxidation of the combustible gas.

The thermal conductivity of a gas at a fixed pressure and temperature depends upon the molecular composition of the gas. Instruments in which this property is exploited for leak-detection purposes (called thermal-conductivity leak detectors) usually have an electrically heated element over which a stream of sampled gas is drawn at a constant rate of flow. Changes in the molecular composition of the gas change the rate at which heat is conducted away from the element. Such detectors are most sensitive to leaking gases that have molecular weight which differs substantially from the mean molecular weight of air.

Although not widely used, leak detectors that sense the presence of a specific gas by looking for a characteristic absorption of infrared radiation are commercially available. They measure (in essence) the fractional concentration (or partial pressure) of a particular molecular species.

Various forms of mass spectrometers are frequently used in leak detection. The simplest of

these works only in conjunction with helium and is therefore usually called a helium leak detector. Helium leak detectors can be used both at atmospheric pressure (to detect helium escaping from an internally pressurized system) and in vacuum systems where it detects helium entering the system. Mass spectrometers more complex than the helium leak detector are also used; in fact, mass spectrometers, as a class, are the most sensitive leak detectors available. All of them work by ionizing the atoms or molecules of an incoming stream, and subsequently separating these ions according to their electric charge-to-mass ratio, after which they are sensed by some form of ion detector.

The gas chromatograph has also been used as a form of leak detector. Gas collected from a leaking system is condensed to a liquid in a cold trap, subsequently removed, evaporated, and analyzed in a conventional analytical gas chromatograph. These devices separate molecular species according to molecular weight by utilizing their differences in release from an adsorbent-packed column.

Finally, for certain specialized problems, the radioactive gas krypton 85 has been successfully used as a tracer gas for leak detection. It is detected with nuclear radiation detectors.

Systems filled with liquids and internally pressurized may, if the liquid is volatile, be tested externally with an appropriate specific gas detector. Apart from this, such systems are usually tested either by simple visual inspection (sometimes aided by the use of a visible dye or fluorescent material added to the filling liquid) or, if the liquid is acidic or basic, a pH detecting paste. If the system is pressurized, a pressure gage is quite sensitive to liquid leaks since a small reduction in the quantity of liquid results in a very large pressure drop (liquids being essentially incompressible). Other somewhat specialized direct methods of detecting liquids are also available.

The leak testing of vacuum systems makes use of several specially adopted versions of specific gas detectors. Also, a newly constructed vacuum system will be tested for gross leaks first by internal pressurization. The presence of a substantial leak can also be detected by the "pump-

down" time required to achieve a certain vacuum level. In general, the "vacuum gage" by which a vacuum is monitored is in itself the most widely used leak detector for vacuum systems.

Specific gas detectors such as helium detectors, halogen detectors, mass spectrometers, and thermal-conductivity detectors, are often used with a specific "tracer" gas to test vacuum systems. The detector is installed at an appropriate location, ordinarily near the vacuum-pump port. A tracer gas is then sprayed on suspect regions of the exterior surface of the system; detection of the tracer gas by the interior detector establishes the presence of a leak and its location if due allowance is made for the time lag between application of the tracer gas and its subsequent detection.

A categorization of leak-testing methods is summarized in figure 9-1, and table 9-1 indicates in qualitative terms the relative sensitivity of the principal leak-testing methods.

DETAILS OF LEAK-TESTING METHODS AND INSTRUMENTATION

Leak-testing methods can be divided or grouped according to the pressure and fluid in the system. The following paragraphs contain a description of most of the common leak-test methods and instruments in the general order shown in figure 9-1.

Pressurized Gas Methods

Acoustic methods.—Turbulent flow through a leak produces sound of both sonic and ultrasonic frequencies. If the leak is large, it may be

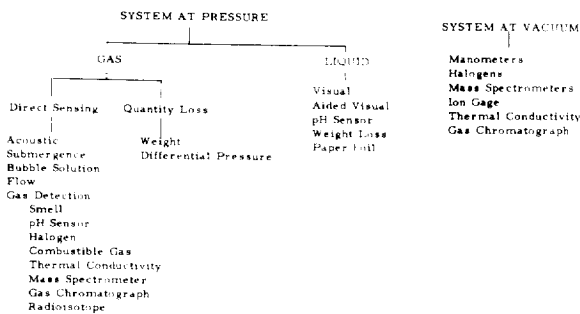


FIGURE 9-1.—Leak-testing methods.

TABLE 9-1.—Relative Sensitivity of Leak Detection Methods and Equipment

Unaided senses	↑ Low ↓ Moderate ↓ High ↓
Eyes	
Ears	
Nose (usual)	
Aided senses	
Bubble solutions	
Penetrants	
Chemical indicators	
Stethoscopes	
Halide torch	
Mass, flow, or pressure change	
Thermal conductivity	
Acoustic emission	
Vacuum gage	
Halogen detector	
Ion gage	
Radioactive isotope	
Mass spectrometer	

detected with the ear. Otherwise, sonic emissions are detected by such instruments as stethoscopes or microphones that have a limited ability to locate as well as determine the approximate size of a leak. Stethoscopes and electronic transducers (microphones) serve to enhance detection sensitivity. While there may be a tendency to discount the human ear, this is an error; "listening" for a leak is an economical and fast method for finding gross leaks.

Smaller leaks may be found with ultrasonic probes operating in the range of 35 to 40 kHz, although the actual emission from the leak ranges up to about 60 kHz (ref. 8). Ultrasonic detectors are considerably more sensitive than are sonic detectors, and are said to be capable of detecting air leaking through a 0.010-in. hole at 5 lb/sq in. pressure from distances of 50 ft (ref. 9). The performance of an ultrasonic leak detector as a function of detection distance, orifice diameter, and internal air pressure is shown in figure 9-2 (ref. 9). It should be noted that the sound level produced is an inverse function of the molecular weight of the leaking gas. Thus, a given flow rate of a gas such as helium will produce more sound energy than the same flow rate of a heavier gas such as nitrogen, air, or carbon dioxide. If background noise is low, ultrasonic detectors can detect turbulent leaks on the order of 10⁻² atm-cc/sec.

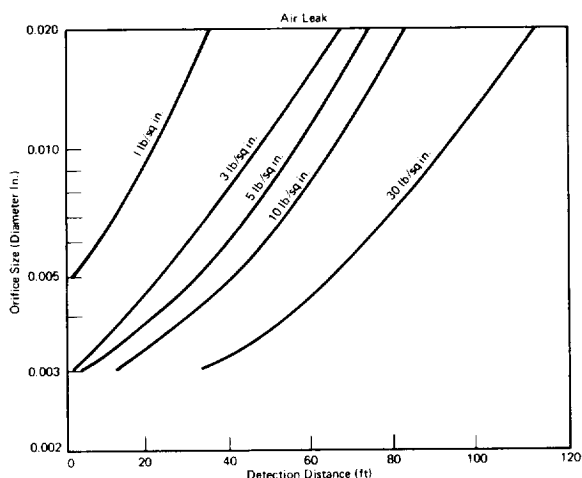


FIGURE 9-2.—Detection distance with an ultrasonic leak detector.

Submergence testing.—One of the simplest methods for leak testing small vessels pressurized with any gas is to submerge them in a liquid and observe bubbles. If the test vessel is sealed at atmospheric pressure and it is desired to test for leaks by submerging it, a pressure differential may be obtained by pumping a partial vacuum over the liquid or by heating the liquid. The sensitivity of this test is increased by reducing

- (1) The pressure above the liquid
- (2) The liquid density
- (3) The depth of liquid immersion
- (4) The surface tension of the liquid.

It is evident from this list that oils are a more sensitive medium than water. Because of this, it is common practice to test electric components in a bath of hot glycerin [as described, for example, in MIL-STD-202 (ref. 10)]. When testing by reducing the pressure over the liquid, several precautions must be observed, particularly if the reduced pressure brings the liquid close to its boiling point. Otherwise, the liquid will begin to boil, giving a false leak indication. The test vessel must be thoroughly cleaned to increase surface wetting, to prevent the clinging of bubbles to its surface, and to prevent contamination of the fluid. If water is used, it must be distilled or deionized and should be handled with a minimum amount of sloshing to reduce the absorbed

TABLE 9-2.—Bubble Formation Time of Freon 12

Leak rate, atm-cc of air	Bubble formation time, sec.
1.8×10^{-2}	1.3
1.8×10^{-3}	13.3
1.8×10^{-4}	145
1.8×10^{-5}	1440
1.8×10^{-6}	14400
1×10^{-10}	239×10^7 (7.6 yr)

gas content. A small amount of wetting agent such as Triton X-100* is normally added to water to reduce surface tension.

Some general idea of the sensitivity of submergence testing can be obtained from table 9-2, which shows the time for a bubble of Freon 12 to form when directed through a $\frac{3}{32}$ -in. diam tube, submerged $\frac{1}{4}$ to 1 in. under water (ref. 11). It is obvious that if high sensitivity is desired, several minutes must be used to observe each suspected area.

Immersion testing may in principle be used on any internally pressurized item that would not be damaged by the test liquid. It is commonly used to detect gross leaks. This method is inexpensive, requires little operator skill for low sensitivity testing, and will accurately locate a leak.

Bubble solutions.—Bubble forming solutions may be applied to the surface of a pressurized vessel if it is too large or unwieldy for submergence. However, care must be taken to insure that no bubbles are formed from the process itself. Spraying the bubble solution is not recommended; it should be flowed onto the surface. Sensitivities on the order of 10^{-4} atm-cc/sec are possible with this method, with prudent observation. Sensitivity may drop to about 10^{-2} atm-cc/sec with an unskilled worker, with 10^{-3} atm-cc/sec being an average value (ref. 8).

Like immersion testing, the use of bubble forming solutions is inexpensive and does not require extensive training of the inspector. One disadvantage is that it will normally not determine the size of a leak. However, a basis for

*Registered trademark of Rohm and Haas Corp.

quantitative judgment of leak rate around threads and flanges using a bubble solution has been developed by NASA (ref. 12). Table 9-3 gives a comparison of bubble appearance vs leakage flow; the typical appearances of "soap bubbles" produced by threaded-type and flange-type leaks are shown in figures 9-3 to 9-6 (ref. 12).

Flow.—Another method of detecting gas loss from a pressurized container is to place the container inside a leak-free enclosure with a single attached duct. Any leakage from the container will cause a corresponding fluid flow through the duct, which can be monitored with sensitive flow detectors. These flow detectors include such devices as bubble tubes and instruments measuring flow by the expansion of bellows, the movement of a piston in a cylinder, and positive-displacement rotary-vane arrangements. Some volumetric displacement meters will detect leaks of about 10^{-5} atm-cc/sec (fig. 9-7). This is a very simple method to use when it is inconvenient to measure directly the pressure change of the container under test. For example, during one stage of the manufacture of a fire extinguisher for the Apollo command module, an inner bag is tested for leaks by attaching a submerged tube to an outer enclosure and pressurizing the inner bag. Any leaking of the inner gas is indicated by bubbles coming from the submerged tubes.

Specific gas detectors.—Many available types of leak detectors will react to either a specific gas or a group of gases having in common some specific physical or chemical property. Some of the more commonly used gas detectors are described below.

(1) *The human nose.* Like listening, the human sense of smell can and should be used to locate odorous gross leaks. The olfactory nerves are quite sensitive to certain substances and, although not especially useful for leak location, they will determine the presence of strong odors. However, the olfactory nerves fatigue quite rapidly and if the leakage is not noted immediately, the nose may quickly go "dead" and the leakage can no longer be detected.

(2) *pH sensors.* Chemically reactive solutions can be formulated that will change color due to a change in pH. They may be made up in the form of a paste or paint and applied to the external surface of the test vessel. Pressurization with an acid gas such as carbon dioxide or a basic gas such as ammonia will indicate the leak location when using the appropriate external indicator solution. Ambient contamination sometimes reduces the sensitivity of this method.

(3) *Halogen detectors.* Two distinct types of halogen detecting devices are in common use: (1) the "hot-anode" detector and (2) the "halide-torch" detector. The hot-anode detector (fig. 9-8) contains a hot platinum or ceramic element that readily ionizes halogen atoms. In the presence of halogen vapors, the rate of ion current between the anode and the cathode is increased (ref. 1). The sensitivity of halogen detectors operating at atmospheric pressure is about 10^{-9} atm-cc/sec, but this will vary dependent upon the specific gas being used (refs. 1 and 13). As with any sensitive detector, halogen detectors are subject to saturation in the vicinity of large leaks. Dual ranges are avail-

TABLE 9-3.—Bubble Appearance Leak Rate

Leak type	Leak class	Appearance	Leak rate, std in. ³ /min
Threads.....	I	Small uniform bubbles, 1/16-in. diam, persistent.....	1×10^{-3} to 4×10^{-1} .
Threads.....	II	Random sized bubbles, reasonably persistent.....	4×10^{-1} to 2.8.
Threads.....	III	Large, fast-forming bubbles that break quickly.....	2.8 to 47.0.
Flanges.....	I	Very small bubbles, milky appearance, like shaving cream.	1×10^{-3} to 1.3.
Flanges.....	II	Random sized bubbles, moderate persistence.....	1.3 to 4.0.
Flanges.....	III	Large, fast-forming bubbles of short duration.....	4.0 to 50.0.

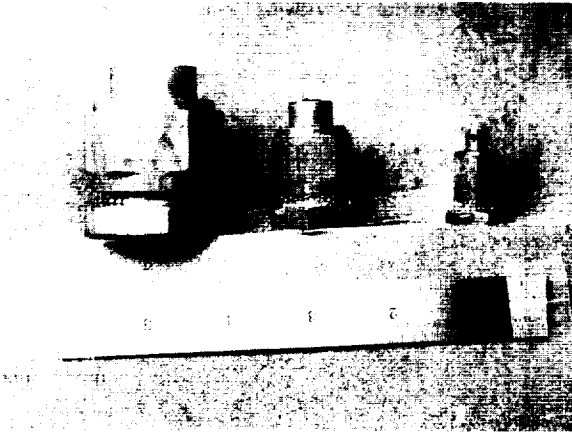


FIGURE 9-3.—Typical appearance of soap bubbles produced by threaded leak, class I.



FIGURE 9-5.—Typical appearance of soap bubbles produced by flange leak, class I.

able on some instruments to reduce this problem and to allow their use in a contaminated atmosphere. Since halogen-containing gases are generally heavy and have low diffusion rates, some care is required in their use as a tracer gas.

Another device for detecting the presence of a gas containing halogens is the halide torch (fig. 9-9). This device consists of a flame-heated copper plate. The flame changes color in the presence of a halogen gas that is drawn into the flame through a probe tube by convection. This apparatus has about the same speed and sensitivity as soap bubble tests, i.e., 10^{-4} atm-cc/sec (ref. 1). The halide torch is used as a probing device, and is used almost exclusively to test refrigerant systems for leaks. It is very

portable, has a low initial cost, and is simple to operate. Its disadvantages are that it cannot be used in an explosive atmosphere, and since refrigerant tends to accumulate in pockets, detection of a leak location in these areas is difficult.

(4) *Combustible gas detectors.* Combustible gas detectors are often used in areas such as the basements of buildings where combustible fumes are likely to accumulate. These instruments measure the combustible gas concentration by sensing the temperature of a heated catalytic element whose temperature will rise in the presence of a combustible gas. They will detect combustible gas mixtures well below the dangerous concentration level. The heated cat-

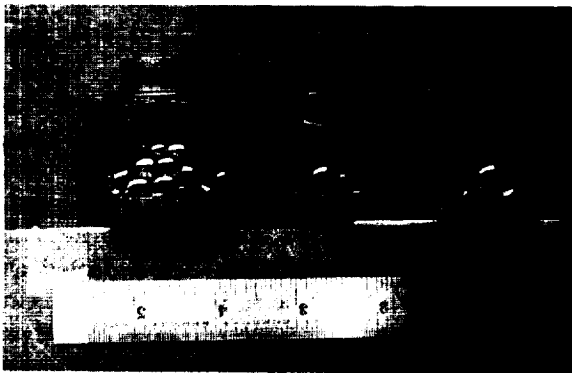


FIGURE 9-4.—Typical appearance of soap bubbles produced by threaded leak, class II.



FIGURE 9-6.—Typical appearance of soap bubbles produced by flange leak, class II.

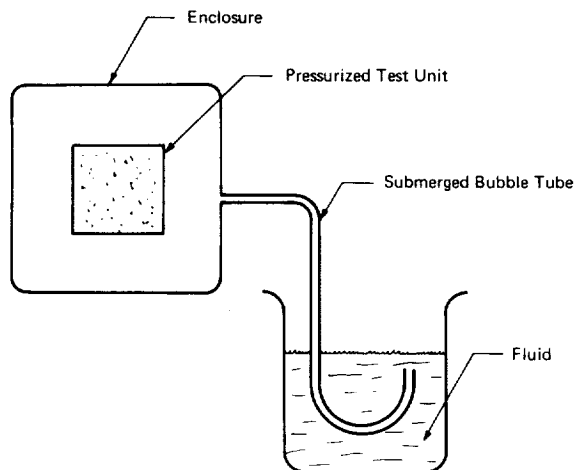


FIGURE 9-7.—Detection of leakage by observing flow out of enclosures.

alyst operates at a temperature below the ignition temperature of combustible gases. Should the instrument malfunction and ignite the gas, flame propagation to the atmosphere is prevented by a metal mesh. Combustible gas detectors are approved for use in hazardous environments.

(5) *Thermal-conductivity detectors.* Thermal-conductivity detectors detect a change in the thermal conductivity of a gas mixture by means of two filaments, thermocouples, or thermistors connected into a bridge circuit. In



FIGURE 9-8.—Hot-anode halogen leak detector.

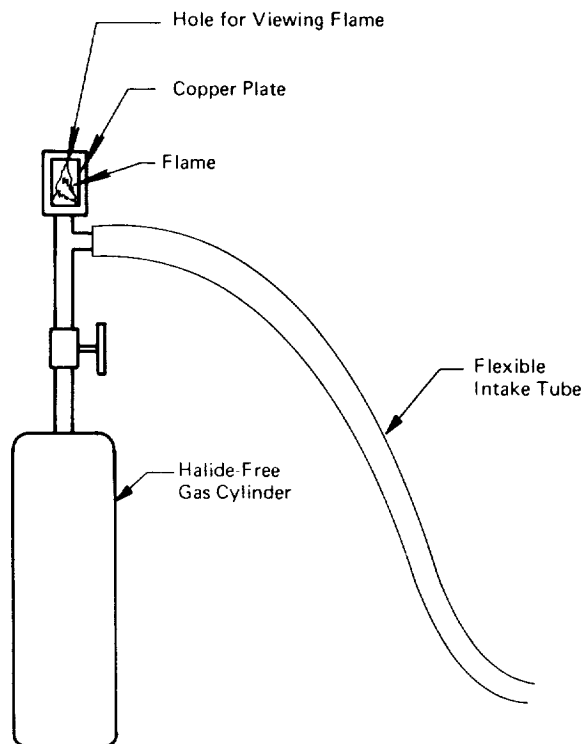


FIGURE 9-9.—Halide torch.

one type, the tracer gas is drawn over one filament and atmospheric gas or air over the other, thus reducing contamination background effects. It is often used as a portable unit with the sensing elements mounted in the hand-held portion to which a probe is attached. It will react to many gases and may be used at vacuum or atmospheric pressure. Its maximum sensitivity of about 10^{-4} atm-cc/sec is achieved with helium.

(6) *Mass spectrometers.* A mass spectrometer detects the presence of tracer gases by ionization of the molecules of the tracer gas in an evacuated tube. As the molecules enter the tube, they are ionized and accelerated down the tube toward a collector or grid at the other end. Through adjustment of voltage, frequency, or magnetic field, the molecules are deflected as they pass down the tube so that some of them will hit the target and some will miss. Whether or not they hit the target is a function of their momentum or mass. Those ionized molecules impacting the target will cause a current to flow

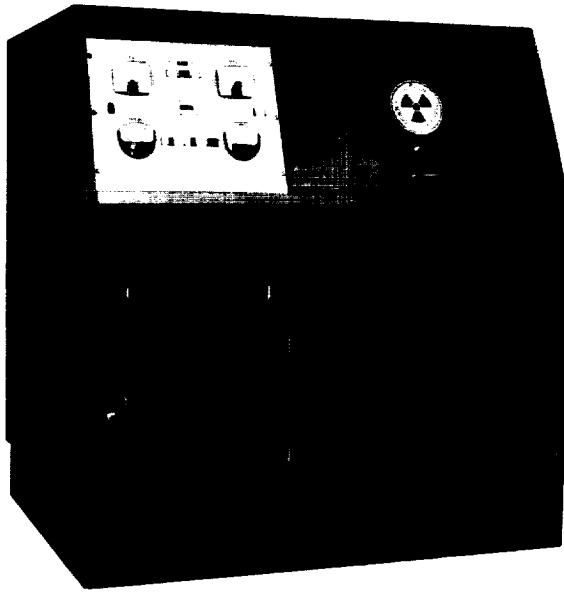


FIGURE 9-11.—Radiflo instrument.

measured with a radiation counter. A Radiflo* instrument (fig. 9-11) is used in this method. Under carefully controlled conditioning, the Radiflo has a sensitivity about equal to the helium mass spectrometer, i.e., 10^{-12} atm-cc/sec. The Radiflo is highly automated and therefore lends itself to rapid, sensitive testing of large quantities of small parts such as transistors. One disadvantage is that organic coatings on the parts might absorb the krypton 85, thus giving a false leak indication.

(8) *Gas chromatographs.* The gas chromatograph, which is very simple in principle, is sometimes useful for leak detecting. In this instrument, a carrier gas is made to flow through an adsorbent column, and a sample gas is then injected into the carrier ahead of the adsorbent column. Next, the gas sample is fractionated into its constituents as a function of the residence time of each constituent in the adsorbent column. The constituents are detected as they leave the adsorbent column usually by thermal-conductivity instruments, but they may also be detected by such devices as infrared analyzers and vapor-density balances. The advantage of

*Registered trademark of the Consolidated Electrodynamics Corp.

the gas chromatograph is that with proper calibration, it will identify the search gas as a compound rather than by an individual molecule as does the mass spectrometer. This can be very beneficial if there are several gases in the system; their identification will often materially aid in locating the source of the leakage. A gas chromatograph has been used to detect leakage in a fire extinguisher used on the Apollo command module (fig. 9-12).

Methods of applying specific gas detectors.—The proper method for using a specific gas detector is based on the function of the leak detector, the fluid which is leaking, and the type of vessel being tested. Some of the more important considerations in determining the best method of using leak detectors are discussed below.

(1) *Probing.* Probes, which will react to a number of gases, may be used in two ways; one is in a probe mode and the other is to monitor an enclosure placed around the pressurized item. In the probe mode, the external surface of the pressurized vessel is scanned with either a portable detector having a short probe attached, or a probe is connected to a stationary leak detector by means of tubing (fig. 9-13). In general, the connection of long probes to a stationary detector reduces sensitivity; leak location is therefore difficult since it requires a correspondingly longer time for the gas to flow up the tube to the leak-detector sensing element. Sensitivity is reduced because of "hang up" which is the slow release of sorbed gases in the probe tubing, resulting in a high leak-detector background reading. Another undesirable feature of

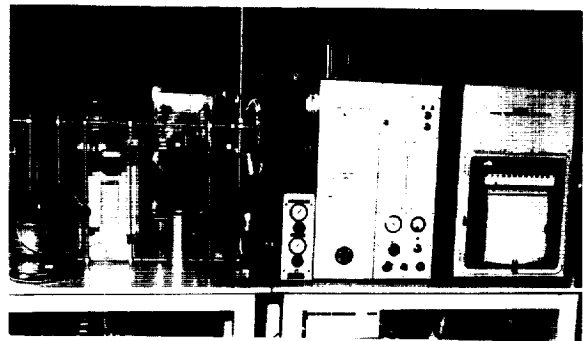


FIGURE 9-12.—Gas chromatograph used to detect leakage of the Apollo fire extinguisher.

long probes is the long "cleanup time." This occurs when a rather large leak is encountered and the probe tubing becomes filled with a high concentration of the search gas. A minute or more may be required for the leak-detector pump to clear the search gas from the sensing element. This in turn reduces scanning speed.

There are means for offsetting some of the disadvantages of long probes. When using a helium mass spectrometer, CO₂ may be introduced in the probe line near the tip. The CO₂ will act as a carrier fluid for the helium thus purging the tube walls and, in conjunction with a high capacity pump, will carry the helium search gas to the leak detector very rapidly. The CO₂ is then selectively trapped with liquid nitrogen, leaving the helium. A probe of this type is said to be several times faster than conventional probes and provides a reduction in background buildup (ref. 14). A rather obvious disadvantage of the long probe is that the person handling it cannot observe the leak-detector reaction. This can be circumvented by earphones, audible signals, and lights, but such devices must be triggered at some threshold level of detector response that may not correspond to the desired leak size. Of course, two persons can be used, but it is more desirable if the probe operator can visually monitor the readout of the leak detector.

Probing has disadvantages where accurate measurements of leak rate are desired; as previously mentioned, background buildup and sensitivity losses will occur. Measurement of leak rate however, can be accomplished by placing a calibrated leak over the probe tip to calibrate the leak-detector-tube-probe system. The leakage may then be measured by placing a suc-

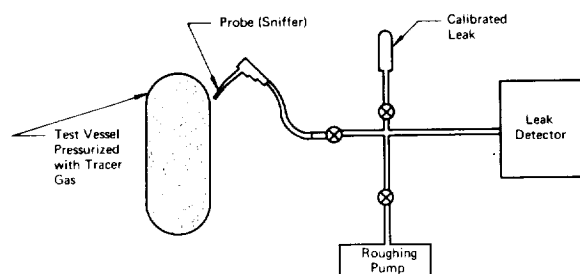


FIGURE 9-13.—Connection of probe to detect leaks with a stationary leak detector.

tion cup on the probe and applying it to the leak area.

(2) *Enclosures.* The second way in which a search-gas leak detector may be used is to monitor an enclosure that is used to accumulate the leakage (fig. 9-14). This method does not provide a means for locating the leak but it is preferred with respect to leakage measurement and, in many cases, for leak detection.

Large enclosures may be tested by enclosing them in a plastic bag. Accumulation of the search gas in the bag is monitored by a leak detector connected to the bag by a short sampling probe or by piping. Leakage measurement involves the insertion of a calibrated leak into the enclosure and comparison of the test leak rate with the calibrated leak rate. One of the problems associated with this method is the construction of a bag that does not leak and has low permeability with respect to the search gas.

Small units are tested with this method by placing them in an enclosure such as a sealed bell jar; the enclosure is monitored for search gas accumulation. Depending upon the type of leak-testing instrument used, the enclosure may be placed under a vacuum. If relatively large leaks are expected, a supply of search gas must be connected to the unit under test to insure that the concentration of the internal search gas of the test item and pressure drop across the leak are constant.

(3) *Back pressuring.* This method of pressurized testing is normally used with small hermetically sealed electronic components such

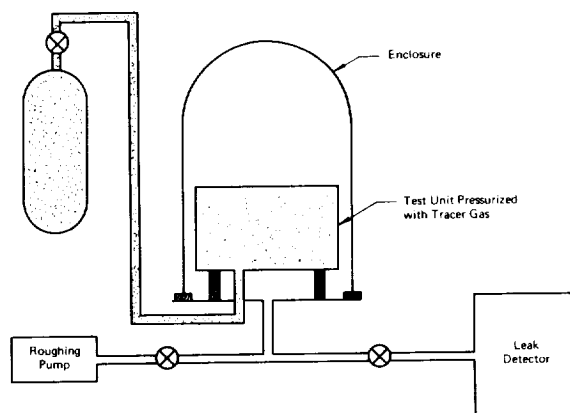


FIGURE 9-14.—Leak detection using an enclosure.

as integrated circuits, relays, and transistors. In this method, test units are placed in a pressurized container that is filled with a tracer gas. This condition is maintained for a period of time sufficient for the tracer gas to flow into the tested article through any leak that may be present. Since leaks are expected usually to be quite small, very sensitive tracer-detector combinations must be used. The tracer gas used is normally helium or Krypton 85 and detection is respectively by use of a helium mass spectrometer or a nuclear radiation detector. Absolute values of the size of the leak are sometimes difficult to determine with back pressuring due to adsorption and absorption of the tracer gases and change in detector response time caused by leak direction.

One unique application of back pressuring is to pressurize each sealed component of a complex system with a different tracer gas. Leak detection with a residual-gas analyzer will both detect the leak and allow a determination to be made of which components are leaking (ref. 15).

In using back pressuring, care must be taken to insure that the leaking components do, in fact, contain tracer gas. Therefore, it is important that the time be suitably controlled between back pressuring and leak testing. For example, in a test specification for transistors by the Jet Propulsion Lab., the transistors are subjected to a helium pressure of 100 psig for 16 hr, air washed for 4 min and then leak tested within 3 hr (ref. 16). If more than 3 hr elapse before leak testing, the transistors are pressurized again. If there is doubt as to how much search gas will flow into the components under back pressurization, the following expression may be used for estimation purposes (ref. 17):

$$P_i = P_0 \left(1 - e^{-\frac{AT}{V}} \right) \quad (11)$$

where

P_i = partial pressure of tracer gas, inside the component at T , atm

P_0 = the pressure of the tracer gas surrounding the component, atm

A = the conductance of the leak with a pressure differential of 1 atm-cc/sec

V = component internal free volume, cc

T = time that pressure P_0 is applied, sec.

(4) *Quantity loss.* One of the more commonly used methods for detecting leaks in pressure vessels is by monitoring the change in the total quantity of the internal charge of gas. The concepts of this method have been discussed under Physical Principles of this chapter. In summary, gross tests may be carried out by determining system pressure loss, while more accurate results are obtained using the perfect gas laws and calculating loss of gas mass. For the highest accuracy, it may be necessary to use equations of state better than that of the ideal gas.

(5) *Differential-pressure measurement.* Gas quantity loss can also be determined by the differential-pressure method. This is done by connecting two identical containers together with a differential-pressure gage between them (fig. 9-15). Differential-pressure gages are quite sensitive to small pressure differences; therefore, if the two containers are maintained at equal ambient conditions, leaks as small as 10^{-4} atm-cc/sec can be detected in systems operating at pressures up to 6000 psig (ref. 18). The primary advantages of this method are (1) temperature effects are largely cancelled and (2) the actual working fluid may be used.

Pressurized Liquid Methods

Visual detection of liquid leakage.—The simplest method for checking a liquid-filled vessel for leaks is visual observation. As with the case of listening and smelling, this is a simple and quick method for gross leak testing of liquid-filled containers.

Aided visual detection of liquid leakage.—Visual methods may be enhanced either by the addition of dye to the liquid or by using a pure dye penetrant. The basic difference between the liquid-penetrant method used here and that discussed in chapter 2 is that leak testing is basically a two-step process. The penetrant is applied to the high-pressure side of the leak, commonly by filling the test vessel with penetrant. The developer is then applied to the outside of the vessel and visually observed for the pres-

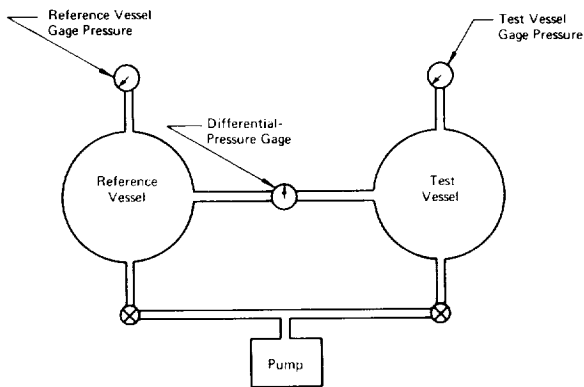


FIGURE 9-15.—Diagram showing use of a differential-pressure gage to detect leaks.

ence of a dye indication. Either visible or fluorescent dyes may be used. Water-washable systems are more common, although some increase in sensitivity is obtained with solvent-removable systems. When both sides of the pressure vessel are accessible, the liquid penetrant may be sprayed, dipped, or painted on the vessel; then pressure may be applied to speed the rate of penetrant flow. The penetrant will also flow through the leak by capillary action, providing sufficient penetrant is available. A disadvantage of dye penetrants is that they may tend to plug smaller leaks making them difficult to locate with more sensitive, subsequently used test methods.

pH sensing of liquids.—A pH-sensitive coating can also be used to detect the presence of liquid leakage. By coating the outside of the vessel with pH sensitive paint, paste, or tape, the appearance of either an acidic or basic liquid will be visually indicated.

Liquid quantity loss.—Since liquids are, for leak detection purposes, incompressible, pressure change of a vessel filled with liquid can be used to locate leaks that are quite small. If the vessel is such that it can be filled completely, leaving no gas pockets, large pressure changes will result from quite small leaks. If the test units are small, leakage can also be detected by direct weighing to determine loss of quantity. The sensitivity of this latter method is largely dependent upon the weight of the liquid as compared to the total weight of the system

since analytical scales or balances are accurate to about 1 part in 20 000 or 0.005% of full scale.

Paper-foil method.—One rather ingenious method of detecting water leakage, developed by a NASA contractor, consists of placing over weld joints a water-soluble strip of paper with a strip of aluminum foil bonded to the back of the paper. In the presence of a leak, the water-soluble paper will dissolve thus locating the leak. By monitoring the electric resistance between the aluminum foil and the vessel, a leak can be detected (ref. 19).

Instruments for Detecting Systems Under Vacuum

Manometers.—Perhaps the most straightforward manner of testing for leaks in systems under vacuum is by observing the manometers installed on the system. While this technique is not as adaptable to locating a leak as regular leak detectors, some indication can be attained. Since most vacuum gages will react or change their reading in the presence of a search gas, spraying tracer gases over individual portions of the vacuum system will produce a gage response and give some indication of leak location. The location can also be roughly established by isolating various portions of the system by valving and observing the gage reaction. The primary evidence of the existence of a leak in the system is failure of the system to achieve anticipated pressure levels in a certain pumping time as based on past or calculated performance. However, due consideration must be given to other gas loads (virtual leaks) that may exist in the system. Sources of these gas loads are (1) system contamination such as water, (2) outgassing of chamber surfaces and of test items, and (3) outgassing of entrapped areas such as unvented O-ring grooves.

Pressure-change gages having a pressure-change sensitivity of 10^{-6} torr are available for vacuum applications. Ion gages will measure vacuums to 10^{-14} torr and can be used to measure changes in pressure. The sensitivity of all pressure-change methods is time dependent, that is, the mass changes per unit of time; therefore, the

longer the test duration, the more sensitive the method.

Leak detection by monitoring changes in pressure of the internal fluid is often used when leak detection equipment *per se* is not immediately available. For the most part, it can be accomplished with instruments that are already installed on the system.

Halogen detectors.—The heated-anode halogen detectors can also be used on vacuum systems. With special adaptors, they can be used down to 10^{-3} torr. Leaks are detected by using an externally applied search gas.

Mass spectrometers.—Mass spectrometers are in many ways ideally suited for use as leak detectors on vacuum systems because the detector tube of a mass spectrometer must be maintained at a vacuum. Further, mass spectrometers usually have built-in vacuum pumping systems that can be directly coupled to the system under test. Helium mass spectrometers are most commonly used. Leaks are detected by spraying or enveloping the outer surface of the system with helium.

Ion gages.—In addition to detecting leaks in vacuum systems by pressure-change instruments, ion gages can be used to detect the presence of specific tracer gases. Since each gas passing through the gage ionizes differently, equal flows of different gases will produce variable readings. Leak rates may be related to ion-gage readings in response to a tracer gas through the equation (ref. 20):

$$Q_a = \frac{\Delta R S_a}{\sigma - 1} \quad (\text{molecular flow}) \quad (12)$$

or

$$Q_a = \frac{\Delta R S_a}{\frac{\sigma v}{\mu} - 1} \quad (\text{laminar flow}) \quad (13)$$

where

- Q_a = flow of air, torr liters/sec
- ΔR = change in ion-gage reading
- S_a = pumping speed, liters/sec
- σ = gage-sensitivity factor
- $v = \frac{\eta_a}{\eta_t}$; η_a = viscosity of air; η_t = viscosity of tracer gas

$$\mu = \left(\frac{M_a}{M_t} \right)^{1/2}; M_a \text{ is molecular weight of air}$$

and M_t is molecular weight of tracer gas.

Table 9-4 contains values of $\sigma - 1$ and $\frac{\sigma v}{\mu} - 1$ for several gases and values of σ for ion gages (ref. 20.).

Thus, by spraying search gas on the outside of a vacuum system, leaks can be located by observing the ion-gage response. The gage should decrease its reading in the presence of gases having a negative parameter value and increase for gases having a positive value (table 9-4).

The palladium-barrier gage is a modified ionization gage that has a palladium barrier in front of the ionization chamber. Since heated palladium is permeable to hydrogen but no other gases, only hydrogen will be passed through to the ionization chamber, thus allowing hydrogen to be used as a search gas.

Thermal-conductivity gages.—Since the thermal conductivity of a gas is a function of its mean free path, it follows that gages measuring the thermal conductivity of the gas as it passes over a heated filament will indicate vacuum. Several types of these gages, including the well-known Pirani gage, are now available.

Gas chromatographs.—Gas chromatographs may be used as leak detectors in vacuum systems by condensing in a cold trap a sample of gas drawn from the vacuum system with a vacuum pump. The cold trap is then isolated from the vacuum system with valves and the frozen

TABLE 9-4.—Tracer Gas Factors

Gas	σ	Gas factor	
		Molecular $\sigma - 1$	Viscous $\frac{\sigma v}{\mu} - 1$
Helium.....	0.17	-0.83	-0.93
Argon.....	1.3	0.3	0.85
Carbon dioxide.....	1.4	0.4	0.4
Water vapor.....	0.9	-0.1	-0.72
Hydrocarbons.....	3-10	2.9	1-10
Hydrogen.....	0.5	-0.5	-0.94

gas released to the chromatograph by warming the trap. The sensitivity of this instrument is limited essentially by the volume of sample drawn into the cold trap, the volume being proportional to elapsed time.

Tracer Gases Used in Testing Vacuum Systems

Vacuum systems are normally tested in the vacuum condition, rather than being internally pressurized. As mentioned earlier, since some leaks, particularly small ones, are directional, it is desirable to test with the leakage flowing in the operational direction. There are two ways in which a search gas may be used in this situation. One is to envelop the entire test vessel (or a particular portion of it) in a bath of tracer gas by the use of either rigid or flexible (bag) enclosures (fig. 9-16). The other approach is to probe for the leak by spraying tracer gas over the outer surface of the vessel (fig. 9-17). Calibration is accomplished by injecting the tracer gas into the vacuum system or by attaching a calibrated leak. Instrument calibration is discussed later in this chapter.

Helium is one of the most common tracer gases used. It is basically inert and safe; its molecular size is small (thereby allowing it to flow through very small leaks), and its diffusion rate is high. It is also easily detected by a mass spectrometer; this instrument has the additional advantage of operating under vacuum. In testing a vacuum system, the smallest leaks are important since they have a great influence on the ultimate vacuum that the system can reach. Therefore, the most sensitive test method is normally used; that is, one in which helium tracer gas is utilized in combination with a helium mass spectrometer.

While a general review of high-vacuum technology will not be given here, there are certain characteristics of high vacuums and high-vacuum systems that must be recognized and understood prior to testing such a system for leaks. These characteristics are briefly discussed below.

(1) *Tracer-gas diffusion.* Tracer-gas diffusion rates are highly variable and are dependent upon the type of gas and the geometry of the

system. The diffusion rates of gases such as helium and hydrogen are generally eight or nine times higher than the Freons.

(2) *Tracer-gas freeze-out.* If the system is being cryogenically pumped and/or has liquid nitrogen traps, the tracer gas may be trapped by the cryogenic surfaces or at least reduced in concentration.

(3) *Leak-detector connection.* Mass spectrometers have their own pumping systems that may be used to maintain the vacuum if small systems are under test and the leakage is small. On large systems, it may be necessary to operate the system diffusion pumps and forepumps while the system is under test. In general, the leak detector should be connected to the fore line of the diffusion pumps, and in parallel with the forepumps as shown in figure 9-18. In this manner, the leak detector will experience an amount of tracer gas that is proportional to the pumping rate of the leak detector and the forepump according to the following relation:

$$\%TG = (100) \frac{LD}{FP + LD} \quad (14)$$

where

$\%TG$ = percentage of total tracer-gas leakage flowing to leak detector

LD = leak-detector pumping speed

FP = forepump pumping speed.

If the leak detector is connected directly to the vacuum chamber, it will experience only a small

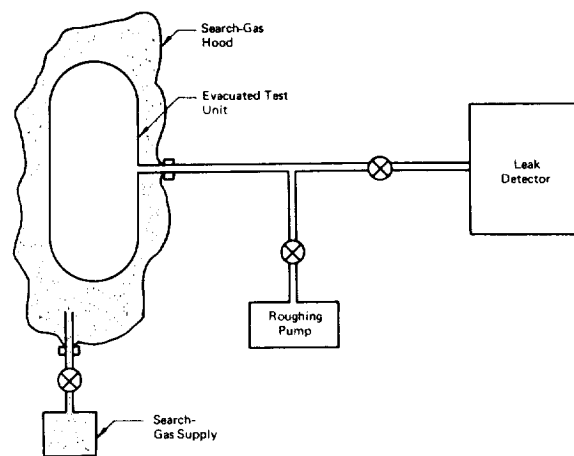


FIGURE 9-16.—Measurement of leakage using a hood filled with search gas.

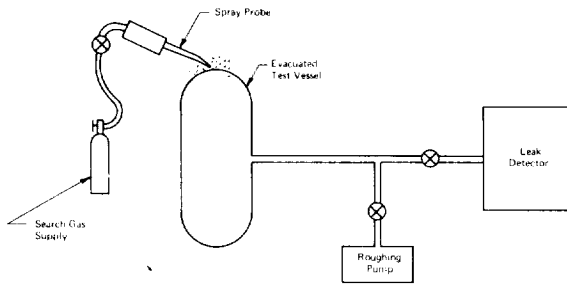


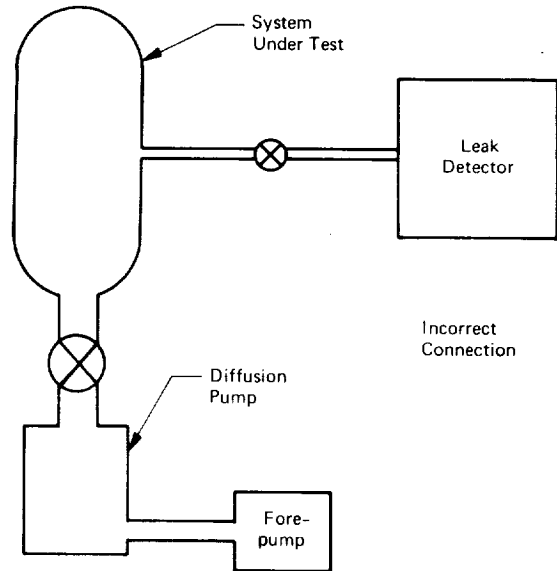
FIGURE 9-17.—Measurement of leakage by spraying search gas over an evacuated system.

amount of tracer gas since the leak-detector pumping speed is generally far less than that of the vacuum-chamber diffusion pumps. If the system throughput is small, however, the system diffusion pumps and roughing pumps can be valved off or backed by the leak-detector pumps which in turn will maintain the desired vacuum.

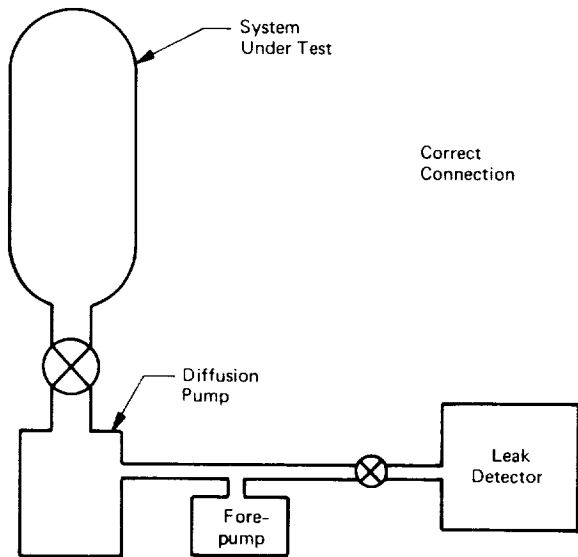
(4) *System materials and cleanliness.* The system should be maintained in a very clean state; otherwise, contaminant outgassing will result, thus reducing the system vacuum. The proper materials must also be selected to reduce hang-up of the tracer gas, glass or stainless steel being used as much as possible. In particular, grease coatings on seals and the use of rubber should be held to a minimum since they will readily absorb helium and then slowly release it giving a high background count.

(5) *Temperature and tracer-gas concentration.* For leak testing it is important that the temperature be held constant and preferably at the expected operating temperature of the item to be checked. Also, the concentration of tracer gas should be as high as possible to insure a sufficient detector response.

Since small leaks are important in vacuum systems, a great number of papers and several books have been devoted to the general subject of vacuum technology, including the prevention of leaks. These include design of vacuum systems, pumping systems, sealing techniques, and vacuum measurement. Several references, which are quite thorough, may be consulted for further information (e.g., refs. 4, 20, and 21).



Incorrect Connection



Correct Connection

FIGURE 9-18.—Proper connection of a mass spectrometer into a vacuum system.

STRATEGY OF LEAK TESTING

Factors Influencing Choice of Method

There are three major factors that determine the leak-testing method to be used: (1) the size of the anticipated leak; (2) the size and physical characteristics of the item to be tested for leaks; and (3) the reason for conducting the

test, whether it be to locate, detect, or to measure leak rate.

General characteristics of the leaking system.—The size and physical characteristics of the system play a large role in the selection of applicable leak detection methods. If a search fluid, either gas or liquid, is used, it must be non-reactive with the test item or system components. In general, it is desirable to leak test the items or systems with the actual working fluid. This eliminates any errors that might be caused by converting from search-fluid leakage to working-fluid leakage. It is also possible that search-fluid leakage may occur while working-fluid leakage will not occur and vice versa.

If search gas is to be used, consideration should be given to the characteristics of the gas. In most instances, high diffusion rates and small molecular size are desirable. Hydrogen and helium are two of the best gases that meet these requirements. On the other hand, when probing the surface of a container filled with search gas, it may be desirable to use a persistent gas or a gas with a low-diffusion rate. A persistent gas will remain in the leak area longer and may facilitate leak detection and location through an increase of search-gas concentration.

Location of the leak.—If the leak location is the purpose of the test, methods that include the use of probes or portable detectors are necessary in order that the test vessel surface may be scanned. With vacuum systems, a reverse process may be used by spraying search gas over the surface and detecting its entry point by observing the leak-detector reaction as the search-gas spray is moved along the vessel surface. Bubbles, immersion, liquid penetrant, and chemical indicators will provide means for locating leaks through visual observation.

Leak size.—Insofar as size of the leak is concerned, the method and instrument must match or be responsive to the size of the leakage. Figure 9-19 contains the approximate working range of several leak detectors. If the leakage is too great, the leak detector will be swamped. This case is normally self-evident because the detector will “peg” or go to full scale and stay there until it is removed from the leakage source. Some combustible-gas detectors, how-

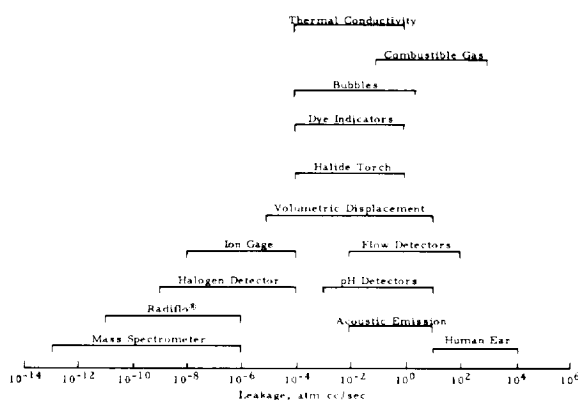


FIGURE 9-19.—Approximate range of various leak detectors.

ever, may return to zero in the presence of a high concentration of leakage. For example, if the vapor/air ratio of gasoline vapor becomes richer than about one part vapor to nine parts air, the mixture is no longer combustible and the detector may indicate zero or some nominal value, despite the fact that high concentrations of hydrocarbon vapor exist.

Small leaks may not produce any response on a given detector, thus eliminating any possibility of finding the leak. It should not be assumed, however, that the leakage is zero. There is a universal agreement that the term “zero” leakage or no leakage is inaccurate. Specifications or test procedures containing such terms are considered to be illogical. It is preferred to define leakage in terms such as “less than minimum detectable leakage” or less than some specified leak rate.

The minimum detectable leakage (MDL) is the smallest leakage to which the detector will respond and is measured by observing leak-detector reaction to a calibrated or known leakage. When calculating the MDL of a mass-spectrometer leak detector, it is conventional that the noise and random background count rate be doubled (ref. 22). The mass-spectrometer detector sensitivity is defined by the equation:

$$S = \frac{Q}{D - B}, \quad (15)$$

where

S = detector sensitivity, atm-cc/sec/scale division

D = total deflection produced by calibrated leak, scale divisions

Q = calibrated leakage flow, atm-cc/sec

B_s = steady background reading, scale division.

Then in terms of S , the MDL may be expressed as

$$\text{MDL} = 2(N + B_R)(S) \quad (16)$$

N = scale deflection produced by instability or noise in system, scale divisions

B_R = random background deflection, scale divisions.

System response.—The response of a leaking system to a leak is a major factor in leak testing because if the response were to be too slow, it could be very time-consuming to locate the leak or the leak could be missed. Any number of characteristics affect system response, including the size of the leak, diffusion rate of the leakage, absorption and adsorption of the leakage, clean-up time of the detector, pumping speed, loss of the search gas in an enclosure, and volume of test vessel. It is obvious that attention must be given to these characteristics in order to achieve minimum possible response time. They have already been mentioned but a few additional pertinent observations about them are given below.

(1) *Size of the leak.* Theoretically, the size of the leak does not affect system response time; it only affects the magnitude of detector readout. However, if some type of leakage-accumulation (or mass-loss) method is being employed, then size of the leak will affect response time in that sufficient leakage must be accumulated (or lost) for the detector to respond.

(2) *Search-gas diffusion.* In large open vessels, gas diffusion is not a major problem. However, in tortuous systems, one investigator found that even after 24 hr neither helium nor Freon had evenly diffused throughout the system (ref. 23).

(3) *Absorption and adsorption of search gases.* Absorption and adsorption are respon-

sible for hang-up in the system; they may also materially reduce search-gas concentration. Permeation is another factor causing difficulties, for example, helium permeates through a 1-in. diam O-ring in about 1 hr, thus producing a detectable reading in the system (ref. 20).

(4) *Detector cleanup time and pumping speed.* It can be shown that if:

$$\frac{V}{S} = t \quad (17)$$

where

V = system volume, liters

S = detector pumping speed, liters/sec

t = characteristic evacuation time, sec,

then, the leak detector will reach 63% of its maximum value at time, t , which is known as the response time. Conversely, the time for it to decay to 37% of its maximum value is known as the cleanup time. Increasing the pumping speed will reduce time, but will introduce a corresponding signal reduction. Also, increasing the pumping speed by a factor of 10 will reduce the readout deflection of the detector by a factor of 10, which may cause problems. The calculation of the response time is quite useful because it gives some idea of how long a search gas should be sprayed over the external surface of a vessel under vacuum in order to detect a leak. For instance, if the vessel has a volume of 1000 liters and the leak detector has a pumping speed of 5 liters/sec, then the suspected leak area should be sprayed with search gas for about 200 sec for the detector to reach 63% of its maximum value.

(5) *System volume.* The larger the volume, the smaller the concentration of leakage will be. This may be alleviated by closing off part of the system when possible. If enclosures are being used to trap the leakage, they should be as small as possible. For example, if the leakage of search gas is 10^{-5} atm-cc/sec, the enclosure volume minus the test unit volume is 10^6 cc, and the detector can detect 1 ppm of search gas, then 28 hr will be required to reach a detectable search-gas concentration.

Leak-Rate Measurement Using Calibrated Leaks

Leak-rate measurement can be accomplished using almost any of the standard leak-detecting

methods in conjunction with a calibrated or known leak. If the leakage is inward into the test vessel, it may be measured by search-gas concentration inside the vessel or system vacuum. If the leakage is outward, it may be collected in an enclosure and the concentration rise within the enclosure monitored; it can also be measured by placing the leak detector probe directly over the leak and isolating the surrounding area with a suction cup. In addition, leaks may be measured by mass-change methods.

In order to calibrate a leak-test instrument for purposes of measuring leakage rates, it is necessary that its response to a known leakage be found. Further, it should be calibrated with a leakage that is the smallest to which it will respond, preferably using the fluid that will be utilized during testing since most leak detectors respond differently to each type of fluid. Leak detectors for measuring gross mass changes or flow may be calibrated in a conventional manner using deadweight testers, nozzles, orifices, and manometers. The more sensitive gas or search-gas detectors may be calibrated by injecting slugs of known volumes of search gas into the system (refs. 23 and 24) or by using standard and/or calibrated leaks.

One form of a standard leak can be made by constructing a device with a small orifice or nozzle; by maintaining constant upstream pressure, the flow will be constant. Another approach is to maintain the upstream pressure at a level high enough to produce flow of sonic velocity at the nozzle throat, thus making the leakage independent of upstream pressure. Very small, calibrated leaks are produced by flow through a capillary tube or permeation through a membrane (normally glass). The capillary type may or may not have a self-contained gas supply. There is a certain advantage to those not having a self-contained gas supply in that a variety of gases can be used with them, although a constant search-gas pressure must be supplied. Capillary tubes may be purchased with leak rates ranging from about 10^{-2} to 10^{-7} atm-cc/sec. Specific leak sizes are also available; these calibrated leaks can normally be supplied to match any specified leakage within about 20%. Permeation type standard leaks are

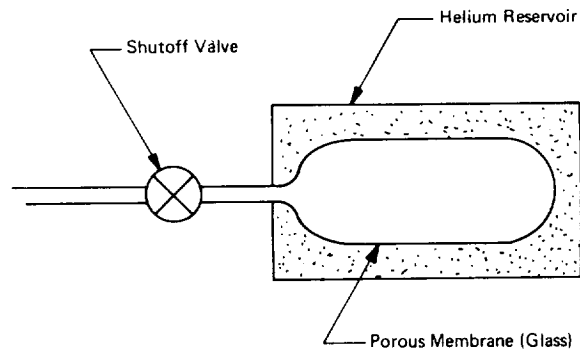


FIGURE 9-20.—Porous membrane calibrated leak.

supplied with their own self-contained gas supply, usually helium (fig. 9-20). Although the flow through the membrane is molecular and therefore pressure dependent, they typically have a helium loss of only 10% in 10 years. These leaks have a flow in the range of 10^{-6} to 10^{-10} atm-cc/sec.

Common Errors Made in Leak Testing

It is generally agreed that the most common errors in leak testing are (1) using a method that is too sensitive and (2) using only one leak-testing method. It is good practice for leak testing to be conducted in two or more stages beginning with gross testing and graduating to the more sensitive methods (ref. 8). The reasons for this procedure are rather obvious in that the sensitive methods cannot be used in the presence of gross leaks. Therefore, savings in both time and money are achieved by testing initially for gross leaks.

An additional common error is one in which the environment is not controlled in the vicinity of the leak. This environmental control may consist of a number of steps depending upon the test method employed. If a search gas is being used it might mean control of the atmosphere to prevent contamination by the search gas that might be detected as an erroneous leak. If sonic or ultrasonic methods are being used, control of background noise is necessary. If small leaks are present, many types of airborne contaminants may cause temporary plugging of the leak. For example, breathing on a molecular leak may

cause it to plug from the water vapor in the breath. Naturally, particulate matter in the air may plug or partially plug a leak.

NASA CONTRIBUTIONS

The major contributions of NASA to leak testing have been indirect. The huge purchases by NASA and NASA contractors of electronic components having low leakage rates have brought about improvements in both technology and instrumentation for testing these components. Even greater impact was felt by the many firms dealing with vacuum technology. The requirements of NASA for space simulation chambers and equipment that must operate in near perfect vacuum led to many advances in leak testing of high and ultrahigh vacuum systems. Similarly, NASA's demands for space pressure vessels has brought about significant contributions to leak testing of pressure vessels. The NASA contributions cited below are based on a literature search conducted over a period of several months. They are illustrative of the many contributions leading to advances in leakage testing.

A useful contribution by NASA to leakage testing is the *Leakage Testing Handbook* (ref. 1). This 392-page document is extremely thorough (and was used liberally in the preparation of this chapter). It contains a large bibliography and is highly recommended as a general information source on the subject.

Testing of sealed integrated circuits.—A three-stage test for sealed integrated circuits

was developed to check them for leakage down to 10^{-8} atm-cc/sec. The three stages consisted of (1) back-pressuring test unit with nitrogen and submergence in hot glycerin, (2) back-pressuring test unit with helium and submergence in alcohol, and (3) use of the Radiflo instrument (ref. 25).

Soluble paper for detecting water leaks.—A method of detecting leaks was developed consisting of an aluminum strip laid over a wider strip of water-soluble paper (fig. 9-21). The strips are then laid over the seams of a water-filled vessel. If a leak occurs, the water-soluble strip will dissolve indicating the leak location and the aluminum foil will be in electric contact with the vessel, thus indicating that a leak has occurred by a corresponding change in resistance (ref. 19).

Dye detector for CO₂.—Test strips to detect variable concentrations of CO₂ using basic fuchsine dye were made. This dye is more color sensitive to CO₂ concentration than the methyl violet crystals previously used. The bleaching agent is also nontoxic (ref. 26).

Ultrasensitive ionization gage.—An ionization gage that will detect pressures down to 10^{-14} torr has been made. This gage is constructed of stainless steel which avoids electrically charged surfaces that distort the internal electric field (fig. 9-22) (ref. 27).

Capacitive system for detecting liquid leaks.—A weld-inspection system was produced by bonding a conductive film to the pressure vessel by electrically insulating the film from the vessel as shown in figure 9-23. When leakage

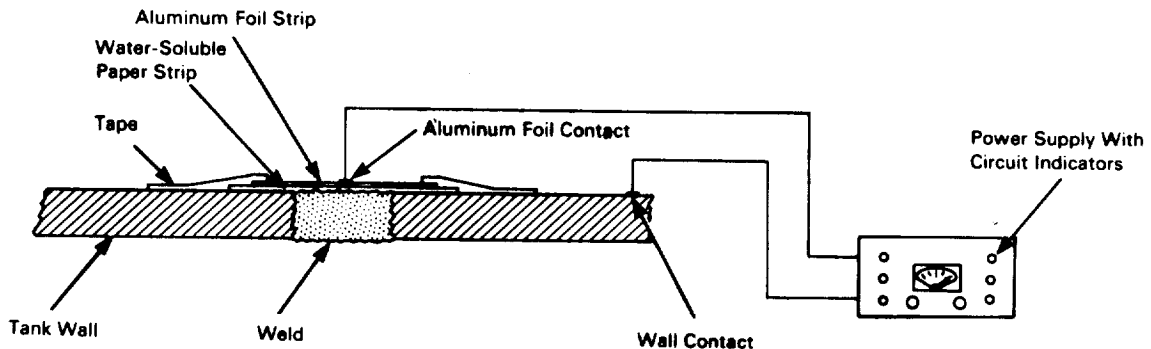


FIGURE 9-21.—Detection of leaks with water-soluble paper and aluminum foil.

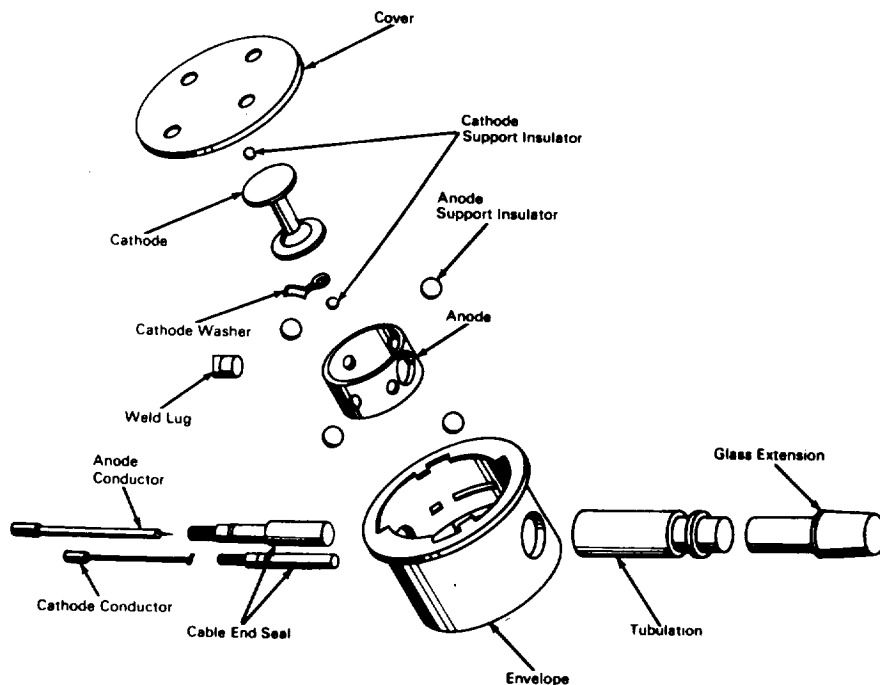


FIGURE 9-22.—Exploded view of ion gage capable of detecting pressure down to 1×10^{-14} torr.

occurs, the film breaks, thus reducing capacitance between the film and the vessel, indicating a leak has occurred; the amount of reduction in capacitance will locate the leak (ref. 28).

Portable hydrogen leak detector.—A portable hydrogen detector that consisted of a glass tube through which the sample gas was drawn has been constructed (fig. 9-24) (ref. 29). The glass

tube was packed with glass fiber and palladium black. The outside of the tube was painted with a thermochromic paint and a temperature sensor was imbedded in the palladium black. When

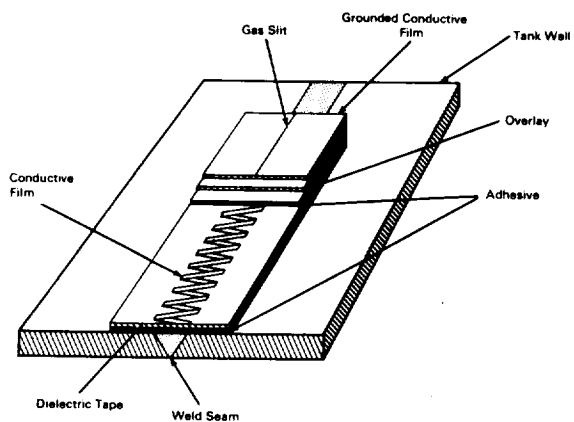


FIGURE 9-23.—The use of conductive film to detect leaks by change in capacitance.

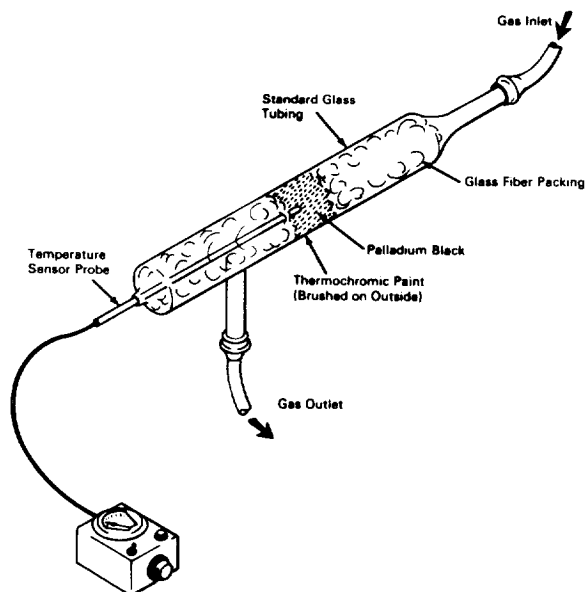


FIGURE 9-24.—Portable hydrogen leak detector.

hydrogen was present in the sample gas, the palladium temperature rose thus producing a readout from the temperature sensor and a color change in the thermochromic paint (ref. 29).

Measurement of leak rate using a calibrated enclosure.—Rapid and accurate procedures were developed for determining leak rates using a calibrated enclosure. The governing equations for these procedures were also developed. The injection of a slug of search gas (He) was found to be the most rapid and convenient method. However, accuracy of the injection method was improved by making several runs. Attention was given to the practical aspects of operating techniques and the theoretical aspects of enclosure-volume-time relations and permeation (ref. 24).

Simple differential-pressure gage.—A differential-pressure gage was developed that detects differential pressures down to 10^{-3} torr (fig. 9-25) (ref. 30). It consists of a bellows to which strain gages are attached. Movement of bellows will cause strain-gage response.

Portable helium leak detector.—A portable helium leak detector has been constructed that

has a sensitivity of 10^{-3} to 10^{-6} atm-cc/sec. It is a thermal-conductivity instrument and has its own calibrated leak source (fig. 9-26) (ref. 31).

Fixture for leak testing pipe welds.—A rubber torus that could be clamped around a pipe weld has been made. Leak testing was then carried out by attaching a leak detector to the torus as shown in figure 9-27. Previously, a polyethylene bag was taped around the weld; this arrangement was unsatisfactory (ref. 32).

Calibrated leak.—A calibrated leak device was built to produce controlled flows on the order of 10^{-4} atm cc/sec (fig. 9-28) (ref. 33).

Dispersion and diffusion data.—Dispersion and diffusion data for Freon and helium were developed for open and tortuous systems. It was shown that in such systems, the diffusion did not occur as predicted and was unreliable (ref. 23).

"Calibrated" bubbles.—A method of realizing quantitative data on leakage flow from the appearance of bubbles was also developed (ref. 12). This has been discussed previously in this chapter.

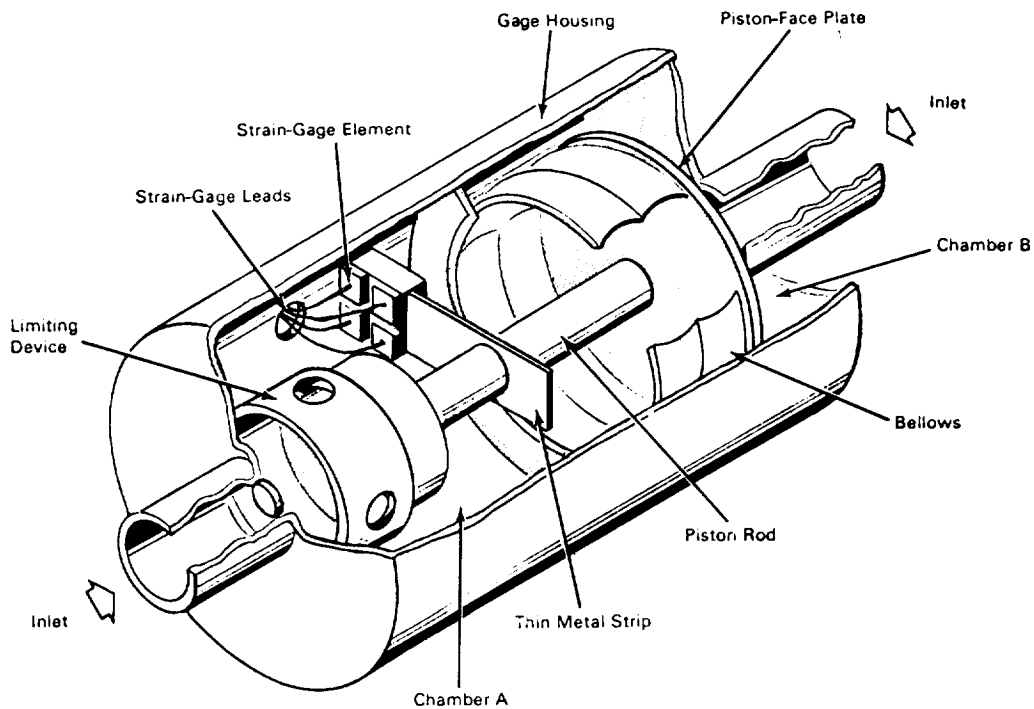


FIGURE 9-25.—Differential-pressure gage with expanding bellows and strain-gage system.

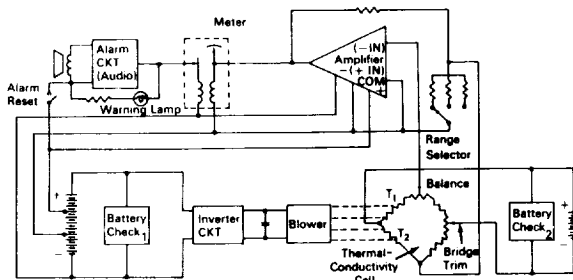


FIGURE 9-26.—Diagram of portable helium leak detector.

Ultrasonic leak detectors.—Two types of ultrasonic leak detectors were evaluated resulting in data showing orifice diameter vs. pressure and detectable distance, frequency response, leak frequency spectrum, pressure vs. sound level, and similar information (ref. 9). Investigations of the factors affecting the accuracy of leak detection by mass-change methods were carried out. The results indicated that the perfect gas law was not always sufficiently accurate (ref. 34).

In 1967, a NASA sponsored contractor published a valuable reference report. It contains a listing of commercially available leak detectors and gives data on each of these including operating principle, manufacturer, response time, environmental effects, fail-safe character-

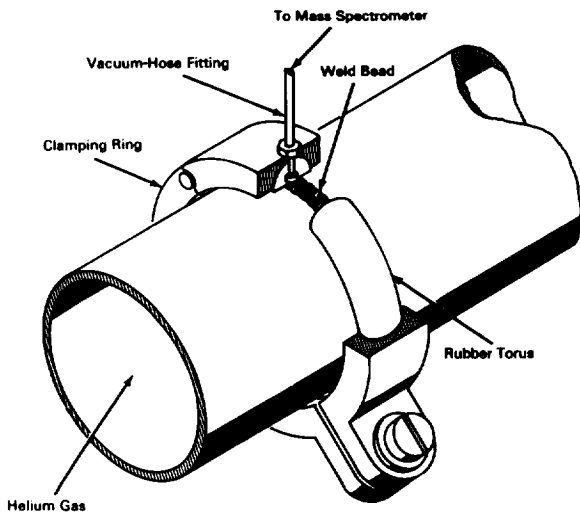


FIGURE 9-27.—Rubber torus used to check weld leaks.

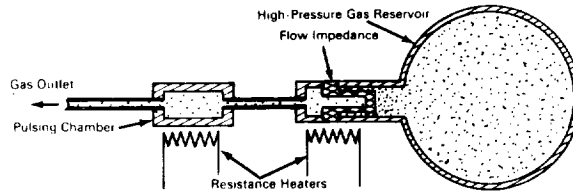


FIGURE 9-28.—Controlled leakage device.

istics, life expectancy, portability, size, weight, time on market, price, delivery time, and remarks (ref. 13). A state-of-the-art summary has also been produced for leak testing of alkaline cells (ref. 35).

REFERENCES

- MARR, J. WILLIAM: Leakage Testing Handbook. NASA CR-952, 1968. (N68-20389)
- ANON.: Symposium on the Role of Non-Destructive Testing in the Economics of Production. American Society for Testing Materials (Philadelphia), Feb. 1951.
- ANON.: Glossary of Terms Used in Vacuum Technology. American Vacuum Society, Pergamon Press (New York), 1958.
- DUSHMAN, SAUL: Scientific Foundation of Vacuum Technique. Second ed., John Wiley and Sons, Inc., 1962.
- WEAST, ROBERT C., ED.: Handbook of Chemistry and Physics. Fiftieth ed., The Chemical Rubber Co. (Cleveland), 1969.
- STREETER, VICTOR L.: Fluid Mechanics. Second ed., McGraw-Hill Inc., 1958.
- CONDON, E. U.; AND ODISHAW, HUGH, ED.: Handbook of Physics. McGraw-Hill Book Co. Inc., 1958, pp. 5-78-5-80.
- WELLS, FREDERIC E.: A Survey of Leak Detection for Aerospace Hardware. American Society for Nondestructive Testing, 28th National Conference (Detroit, Mich.), Oct. 1968.
- ANON.: Final Report on Hazards Monitoring at NASA Merritt Island Launch Area, Vol. II, Task B—Ultrasonic Leak Detectors for Cryogenics and Gases. NASA CR-81124, 1965.
- ANON.: Test Methods for Electrical Component Parts. MIL-STD-202C, Sept. 1963.
- HUTCHINS, WARREN C.: Leak Test Specifications. Instruments and Control Systems, vol. 35, Apr. 1962, pp. 107-110.
- DECASTRA, J. E.; AND WELLS, F. E.: Proposed Standards Describing and Estimating Leaks in Aerospace Hardware. NASA TM X-53692, 1968.
- BIALOUS, A. J.: Characteristics and Sources of Commercially Available Leak Detectors. Rept. 67-6-278 (NAS7-396), General Electric Co., Elec-

- tronic Physics Lab. (Schenectady, N.Y.), July 1967.
14. ANON.: Complete High Vacuum Catalog. Veeco Instruments Inc. (Plainview, N.Y.), 1969.
 15. FISHER, F.: Vacuum and Room Temperature Leak Test Procedure for the OAO-PEP Spectrometer/Fine Guidance and Focus Drive Subassemblies, Prototype. NASA-Goddard Space Flight Center, Greenbelt, Md., Feb. 1966.
 16. ANON.: General Specification No. NPQ-2451-GEN, Qualification Testing Requirements Methods and Procedures for Transistors. Jet Propulsion Lab., California Inst. of Technol., Jan. 1966.
 17. PANZA, PRISCO A., JR.: Improved Fine and Gross Leak Test Methods for Electronic Components. American Society for Non-destructive Testing, 28th National Conference (Detroit, Mich.), Oct. 1968.
 18. SKOLNICK, EDWARD: Finding Leakage by Differential Pressure. *J. Environmental Sciences*, vol. 7, no. 2, 1964, p. 35.
 19. ANON.: Weld Leaks Rapidly and Safely Detected. NASA Tech Brief 65-10265, 1965.
 20. SANTELER, DONALD J.; HOLKEBOER, DAVID H.; JONES, DONALD W.; AND PAGANO, FRANK: Vacuum Technology and Space Simulation. NASA SP-25, 1966.
 21. ROTH, A.: Vacuum Sealing Techniques. Pergamon Press, Inc., 1966.
 22. WINKELMAN, GLAUDE R.; AND WILSON, NORMAN G.: An Analytical Method for Mass Spectrometer Leak Detection. Los Alamos Scientific Lab., Univ. of California (Los Alamos), June 1968.
 23. BROWN, JAMES L.: Diffusion of Trace Gases for Leak Detection in Aerospace Systems. NASA TM X-53742, 1968.
 24. MANGANARO, J. L.; AND HOLLINGER, D. L.: Quantitative Leak Test Design Guide. NASA CR-88504, 1967.
 25. LOMBARDI, I.; McDONOUGH, L.; AND PADDEN, H.: High Reliability Screening of Semiconductor and Integrated Circuit Devices. NASA CR-721, 1967. (N67-23322)
 26. ANON.: Test Strips Detect Different CO₂ Concentrations in Closed Compartments. NASA Tech Brief 65-10390, 1965.
 27. ANON.: Cold Cathode Ionization Gauge Has Rigid Metal Housing. NASA Tech Brief 66-10041, 1966.
 28. ANON.: Capacitive System Detects and Locates Fluid Leaks. NASA Tech Brief 66-10099, 1966.
 29. ANON.: "Sniffer" Used as Portable Hydrogen Leak Detector. NASA Tech Brief 66-10356, 1966.
 30. ANON.: Differential Pressure Gauge Has Fast Response. NASA Tech Brief 65-10285, 1965.
 31. ANON.: Portable Detector Set Discloses Helium Leak Rates. NASA Tech Brief 67-10065, 1967.
 32. ANON.: Fixture Facilitates Helium Leak Testing of Pipe Welds. NASA Tech Brief 67-10178, 1967.
 33. ANON.: Device Provides Controlled Gas Leaks. NASA Tech Brief 68-10142, 1968.
 34. SOLDEBERGREN, JAN H.: Criterion for Mass Drop-Off Measurements Based Upon Precise Pressure and Temperature Measurements. NASA TM X-53551, 1966.
 35. ANON.: A Study of the State of the Art of Hermetic Seals for Secondary Alkaline Spacecraft Cells. NASA CR-97888, 1968.

Strain Sensing

Robert R. King and Felix N. Kusenberger

All real solid objects undergo changes in geometrical configuration when subjected to mechanical loads. In analytical terms, such loads are expressed in terms of stresses; the corresponding changes in configuration are expressed in terms of strains. An unrestrained body will, in general, also undergo strains as a consequence of other changes in its physical state, such as a temperature change. The methodology by which the relation between stresses and corresponding strains is empirically studied is called experimental stress analysis, although the emphasis is, in fact, upon the determination of strain. This chapter is concerned with the three most generally used practical methods of strain sensing—brittle coatings, photoelastic coatings, and resistance strain gages. The use of these methods does not normally compromise the fitness for service of the test article; when so used, they are correctly considered to belong to the discipline of nondestructive evaluation.

Experimental stress analysis plays an essential role in contemporary mechanical engineering, and especially so in aerospace engineering. There are many reasons, such as economy, ease of handling, and minimizing energy requirements, for keeping the functional components of any structure or machine as small and light as possible. This, in effect, requires that materials be utilized at the highest permissible

values of stress consistent with the required reliability (or integrity) of the part. Significant stress parameters are embodied in theories of yielding, fracture, and fatigue in materials. These modes of failure stimulate interest in the accurate determination of strains and stresses in load-bearing components.

Although the fundamental relation between stress and strain is of primary importance in determining the load-bearing capability of a part, there are also functional relations between strain and other physical parameters that may characterize a particular material. For example, temperature changes may cause a material to undergo thermal expansion or contraction; a change in the state of magnetization will cause a magnetostrictive material to change dimensions; similarly, a change in electric polarization can produce strain in some materials. From a chemical viewpoint, a change of state (atomic or molecular arrangement) in the material or a change of chemical composition (such as moisture absorption) may produce dimensional changes in the body. Conversely, forcibly straining a body may influence some properties of the material from which it is made. These properties may be mechanical, electrical, magnetic, thermal, optical, or chemical in nature. Some specific examples are:

- (1) Overall part dimensions

- (2) Modulus of elasticity (in nonlinear portions of stress-strain curves)
- (3) Electrical resistivity
- (4) Magnetic susceptibility
- (5) Thermal conductivity
- (6) Optical index of refraction
- (7) Melting point.

Certain of these properties exhibit very dramatic changes with changes in strain. When such an effect is repeatable and the existing technology makes it readily measurable, a strain-sensing method based on the functional relation between this parameter and strain may be devised. Several general methods for making strain measurements are based on the use of the following:

- (1) Brittle coatings
- (2) Photoelastic coatings
- (3) Resistance strain gages
- (4) X-ray diffraction
- (5) Extensometers.

Of these methods, only three at present have been developed sufficiently so that the cost of equipment, and the complexity, availability, and reliability of measurements encourage wide usage in practical NDE. These are brittle coatings, photoelastic coatings, and resistance strain gages. The discussion in the ensuing sections will introduce and briefly describe each of the above methods. The use of brittle coatings, photoelastic coatings, and resistance strain gages will be subsequently discussed in greater detail.

It should be emphasized that any given test method may well be considered nondestructive when used with one specimen, while being considered highly destructive when applied to a specimen of a different kind. Another point of vital importance, particularly in making precise measurements, is that the device or material being employed in making the measurement may be influenced by environmental conditions other than that which is the basis of the method. In general, such effects cannot be totally eliminated and must be considered and corrected for when analyzing the data acquired.

It is beyond the scope of this chapter to develop systematically and thoroughly the theoretical formalism in terms of which experi-

mental stress analysis is guided and interpreted. The purpose of this section is simply to review from an elementary viewpoint those physical concepts (and their mathematical formulations) that are essential for a useful understanding of the subsequent discussion of strain-sensing methods. The discussion is restricted to isotropic materials.

The intensity of the force (force applied per unit area) acting on the surface of a body (or a specified subregion of that body) is called a stress. It can be shown that such a stress can be resolved into three mutually orthogonal components, one of which is normal to the surface (at the location in question), the other two being tangent to that surface. A small (in principle, infinitesimally small) cubical volume which may be considered to be within a larger body, the orientation of which is arbitrary, and for which the stresses acting on each surface are resolved into normal and tangential components is illustrated in figure 10-1. Normal components of stress that act inward with respect to the surface of the cube are said to be compressive; those that act outward are said to be tensile. The tangential components of stress are called shearing stresses. It can be shown that at any point within (or on the surface of) a body in mechanical equilibrium, it is always possible to

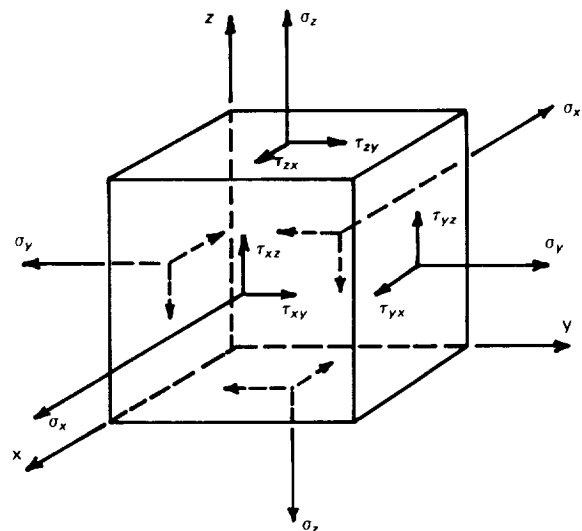


FIGURE 10-1.—Elementary cubical volume and associated stresses.

orient a small reference cube (whose center coincides with the point of interest) so that the shear stresses on the surfaces of the cube all vanish. When so oriented, the three mutually orthogonal axes normal to the faces of the cube are called the principal directions of stress; the corresponding three mutually orthogonal stress components are called the principal stresses. Only three components of stress must be specified since the condition of equilibrium requires that the stresses on opposite faces of the cube be equal in magnitude and oppositely directed.

The deformation of a solid body subject to a prescribed distribution of stress may be specified entirely in terms of the deformation of the material within a small cube located at any point in the stress field. The deformation of an arbitrarily oriented cube is, in general, complex; however, if the reference cube is taken so that the three lines normal to its surfaces coincide with the local principal directions of stress, its deformation is simple to describe. Furthermore, such a description is sufficient since it can be shown that it is possible to derive the deformation of an arbitrarily oriented cube from this case. The deformation of a suitably oriented reference cube when two of the principal stresses vanish is illustrated in figure 10-2; such a stress field is said to be locally uniaxial. For definiteness, the stress shown in the figure is chosen to be tensile. As illustrated, the reference cube elongates in the direction of the tension and contracts in the transverse directions. The longitudinal strain is defined to be the longitudinal extension of the cube divided by the original length of the cube edge; the transverse strain is defined in an analogous way. Extensions are taken to be positive, and contractions to be negative.

If the strain of the reference cube is directly proportional to the stress, the material is said to obey Hooke's law, and to be elastic. Many engineering materials, including most metals, are very nearly elastic within a limited range of strain values characteristic of the respective material. A schematic stress vs. strain graph with features typical of mild steels is shown in figure 10-3 (ref. 1). (The figure also contains a non-rigorous definition of the commonly used terms

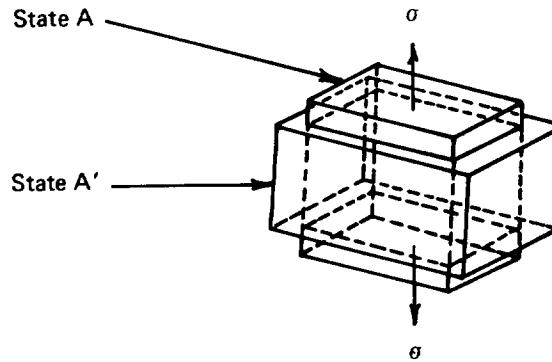


FIGURE 10-2.—Deformation of a cubical volume in axial stress field.

yield point and ultimate strength.) Within the range in which Hooke's law is observed, the ratio of principal stress to principal strain (for a uniaxial stress) is a constant, i.e.,

$$\frac{\sigma}{\epsilon} = E$$

The constant E is called Young's modulus or the modulus of elasticity and is characteristic of the material in question. The ratio of the transverse strain to the corresponding longitudinal strain (for the case under discussion) is also a constant, μ , called Poisson's ratio:

$$\mu = \frac{\epsilon_{\text{transverse}}}{\epsilon_{\text{longitudinal}}}$$

When more than one of the principal stresses does not vanish, the corresponding strains are additive, resulting in the basic set of equations:

$$\epsilon_x = \frac{\sigma_x}{E} - \mu\epsilon_y - \mu\epsilon_z$$

$$\epsilon_y = \frac{\sigma_y}{E} - \mu\epsilon_x - \mu\epsilon_z$$

$$\epsilon_z = \frac{\sigma_z}{E} - \mu\epsilon_x - \mu\epsilon_y$$

In experimental stress analysis, the major interest is in mapping the strains (and the corresponding inferred stresses) at unconstrained surfaces of test specimens. It can be shown that a normal to such a surface is a principal direction of stress, and that the corresponding prin-

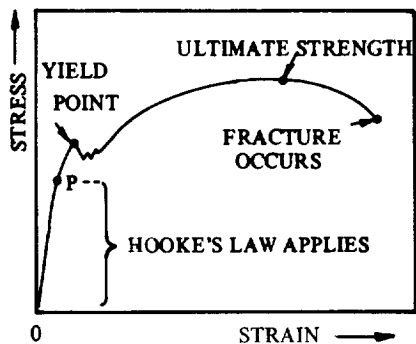


FIGURE 10-3.—Stress vs strain graph for mild steel. Courtesy of Mac-Millan and Co., Ltd. and Strain Gauges and Uses, H.K.P. Neubert.)

principal stress vanishes (neglecting atmospheric pressure). The two remaining principal stresses must therefore be tangential to the surface at the location in question. Hence, the problem reduces to that of determining a two-dimensional (biaxial) field of strain.

While a small unit surface oriented normally with respect to a principal stress direction experiences no shearing force, it does experience a shear if otherwise oriented. A simple graphical device is available with which to determine both the normal and the shearing stress on a small surface in a two-dimensional stress field. This device, called Mohr's stress circle, is schematically illustrated in figure 10-4 (ref. 2). The radius of the circle is one-half the difference between the principal stresses, which can be shown to equal the maximum shearing stress. A strain circle precisely analogous to the stress circle also exists. Thus, if the strain analyst can determine the magnitude and direction of the principal strains at each point on the surface of a mechanically loaded component, he can infer the corresponding stress field. With sufficiently complete data regarding the fundamental stress-strain relation for the material in question at his disposal, he can evaluate the structural component under test in terms of its ability to function satisfactorily under its operational load.

It must be recognized that the foregoing discussion of stress-strain analysis is greatly oversimplified; anyone contemplating such an

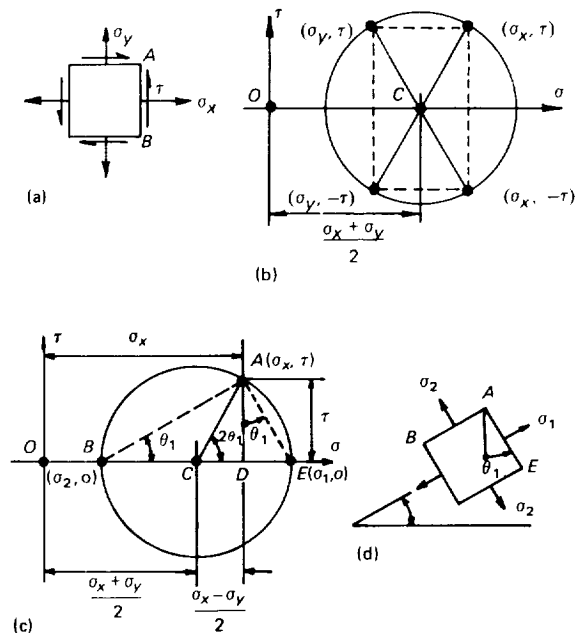


FIGURE 10-4.—Mohr's stress circle. (Courtesy of Prentice-Hall, Inc. and Mechanics of Materials, E.P. Popov.)

analysis and not already expert in the field should, of course, consult a more thorough and detailed treatment (ref. 3).

PHYSICAL PRINCIPLES

The physical principles of some major non-destructive strain-sensing methods are introduced below. Immediately following these discussions, concise operating characteristics are tabulated for each of the methods described, for the purpose of comparison.

Brittle coatings.—The use of brittle coatings is based on the principle that, when strained only very slightly, a brittle substance will crack along a direction normal to the direction of maximum tensile strain. Coatings are formulated to crack at various values of strain, calibration being made on a standardized cantilever beam at the time of the test. It is assumed that under similar strain on the test structure, cracks will begin to appear in the coating when the strain threshold has been reached. Brittle coatings commonly used are either of a resin base (lacquers) or a glass base (ceramics).

Photoelastic coatings.—The use of these coatings is concerned with the strain-optical property (birefringence) of certain materials. The birefringent coating (normally plastics) is applied to the surface of a part to be inspected and illuminated with polarized light. When the coating is viewed through a second polarizing lens (analyzer), interference fringes are seen, the pattern depending upon the type of light used and the relative orientation of the polarizer and analyzer. From the observed fringes, the direction of the principal strains can be determined and their magnitudes calculated, in principle.

Strain gages.—Many strain-measuring methods utilize some means of converting strain information into an electric signal that is easily amplified and displayed. However, “electric strain gages” operate by direct interaction of electric energy with the strain field of the sensor. This applies to the electron current in metal wires (wire- or foil-resistance strain gages) as well as the more complex conduction of electrons and holes in semiconductors (semiconductor strain gages). It is also apparent in piezoelectric strain gages, where distortions of crystal lattice generate surface charges. Inductance and capacitance strain gages are effective through variation of their electromagnetic fields.

The conventional bonded resistance strain gage consists of a wire or foil grid which, when cemented to the test structure, undergoes changes in electrical resistance in direct proportion to the changes in strain in the structure. Semiconductor strain gages are usually made of a piezoresistive semiconductor material whose electric resistance is extremely sensitive to changes in strain. Resistance changes from either type gage may be measured using a Wheatstone bridge arrangement or by amplifying a signal from the gage and displaying it on conventional electric readout equipment.

X-ray diffraction.—When X-rays having wavelengths comparable with the atomic spacing in a crystal are incident on the crystal surface, diffraction occurs and a kind of interference pattern is obtained, which contains information on the actual atomic spacing within

the material. Measurements of radiation intensities in the diffraction pattern can be made from an exposed and developed photographic film or by using a goniometer in conjunction with X-radiation intensity measuring devices. This pattern reveals the relative location of atoms in the crystal structure to a depth of about 0.0001 in.; changes in the pattern may be used to calculate the strain in the test piece (ref. 4).

Extensometers.—The method in which extensometers are used differs from the aforementioned strain-measuring methods in that the quantity measured is the change in length, Δl , of a discrete macroscopic segment of the test specimen. If the segment is of length l , the average strain in the segment is calculated as

$$\epsilon_{\text{avg}} = \frac{\Delta l}{l}$$

Many extensometers have been developed in which pneumatic, acoustic, mechanical, electrical, and optical means of detecting and magnifying the change in linear separation of two points on the surface of the test specimen are used. Some general categories into which these may be divided and an example of each are:

- (1) Mechanical levers (screw micrometer).
- (2) Optical levers (deflection of light beam by a mirror).
- (3) Optical interferometry (interference holography).
- (4) Electrical extensometers (differential transformer).
- (5) Grid systems (Moiré fringe method).
- (6) Acoustic gages (sensing frequency of a vibrating wire).

Tables 10-1 and 10-2 are adapted from those printed in the October 16, 1961 issue of *Product Engineering* (ref. 5). The quantitative data presented should be considered as approximate values, not representing any particular commercial product.

BRITTLE COATINGS

Historical Background

It was recognized at a very early date that a thin brittle coating in intimate contact with a

TABLE 10-1.—Operating Characteristics of Some NDE Strain-Measuring Methods (Reprinted from the October 16, 1961 issue of *Product Engineering*; copyright 1961 by McGraw-Hill, Inc.)

	Approximate max. strain sensitivity, min./in.	Usual gage length, in.	Approximate range, % strain	Indicates direction of max. principal stress	Displays entire field	Determines strain at points	Indicates strain gradient	Direct reading
Brittle coatings								
Resin based (room temp.)								
Macrotechnique	500	Very small	0.3	Yes	Yes	No	Yes	No.
Microtechnique	800-1000	Very small	0.3	Yes	Yes	No	Yes	No.
Glass-based (elevated temp.)	200	Very small	0.2	Yes	Yes	No	Yes	No.
Bonded strain gages								
Wire and foil								
Single element	5	1/4 to 1	2.0	No	No	Yes	No	Yes.
Rosettes (all types)	5	1/8 to 1	2.0	Yes	No	Yes	No	Yes.
High elongation	5	1/16 to 1	15.0	No	No	Yes	No	Yes.
Dynamic (isostatic)	5	1/16 to 1	2.0	No	No	Yes	No	Yes.
Transistors (piezoresistive)—								
Single element	1	1/4 to 1/2	0.6	No	No	No	No	Yes.
Photoelasticity—Photoelastic								
coatings	10	Very small	3-50	Yes	Yes	No	Yes	No.
X-ray diffraction	± 100	Lattice spacing.	Elastic	Yes	No	Yes	No	No.
Extensometers	1-100	Varies	Varies	No	No	Yes	No	No.

TABLE 10-1.—Operating Characteristics of Some NDE Strain-Measuring Methods (Reprinted from the October 16, 1961 issue of *Product Engineering*; copyright 1961 by McGraw-Hill, Inc.)—Continued

Remote indicating	Complexity of equipment 1 to 4	Readout instrument	Required operator experience 1 to 4	Laboratory or field	Operating environment A=air W=water O=oil	Required calculations short-long 1 to 4	Estimated time delay from first operation to first measurement hr.
Brittle coatings							
Resin based (room temp.)							
Macrotechnique-----	No-----	1,2 Strain scale-----	1,2	L,F	A,W	1	8 to 10.
Microtechnique-----	No-----	1,2 Strain scale-----	3,4	L	A,W	1	½ to 2.
Glass based (elevated temp.).	No-----	1,2 Strain scale-----	2,3	L,F	A,W,O	1	1 to 10.
Bonded strain gages							
Wire and foil							
Single element-----	Yes-----	1,2,3 Strain indicator-----	1,2	L,F	A,O	1	¼ to 24.
Rosettes (all types)-----	Yes-----	1,2,3 Oscillograph-----	1,2,3	L,F	A,O	3,4	¼ to 24.
High elongation-----	Yes-----	1,2,3 Oscilloscope-----	1,2	L,F	A,O	1	2 to 24.
Dynamic (iselaastic)-----	Yes-----	1,2,3 Punch card or print out.	1,2	L,F	A,O	1	¼ to 24.
Transistors (piezoresistive)---Single element.	Yes-----	1,2,3-----	1,2	L,F	A,O	1	¼ to 24.
Photoelasticity—Photoelastic coatings.							
X-ray diffraction-----	No-----	4 Goniometer (film).	4	L	A	2,3	½ to 1.
Extensometers-----	No-----	1,2,3,4 Strain scale-----	1,2,3	L,F	A	None	¼→.

TABLE 10-1.—Operating Characteristics of Some NDE Strain Measuring Methods—Continued

	Triaxial (internal) stresses									
	Static temp °F (max.)					Dynamic temp °F (max.)				
	<0	100	200	600	1000	<0	100	200	600	1000
Brittle coatings:										
Resin based (room temp.)										
Macrotechnique.....										
Microtechnique.....										
Glass based (elevated temp.).....										
Bonded strain gages:										
Wire and foil (metallic):										
Single element.....		✓				✓				
Rosettes (all types).....										
High elongation.....										
Dynamic (isostatic).....										
Semiconductors (piezoresistive)—single element.....										
Photoelasticity—Photoelastic coatings.....										
X-ray diffraction.....										
Extensometers.....										

	Shear (surface) stresses, $e_1 - e_2$									
	Static temp °F (max.)					Dynamic temp °F (max.)				
	<0	100	200	600	1000	<0	100	200	600	1000
Brittle coatings										
Resin-based (room temp.)										
Macrotechnique.....		✓				✓				
Microtechnique.....		✓				✓				
Glass based (elevated temp.).....	✓	✓	✓	✓		✓	✓	✓	✓	
Bonded strain gages										
Wire and foil (metallic)										
Single element.....										
Rosettes (all types).....	✓	✓	✓	✓		✓	✓	✓	✓	✓
High elongation.....										
Dynamic (isostatic).....										
Semiconductors (piezoresistive)—Single element.....										
Photoelasticity—photoelastic coatings.....		✓	✓			✓	✓			
X-ray diffraction.....	✓	✓	✓	✓	✓					
Extensometers.....										

TABLE 10-2.—*Applications and Limitations of Some NDE Strain-Measuring Methods (Reprinted from the October 16, 1961 issue of Product Engineering; copyright 1961 by McGraw-Hill, Inc.)*

	Typical applications	Operating limitations
Brittle coatings: macro	Machinery, structures, pressure vessels	No extremely thin membranes in bending.
Micro	Thin membranes, small parts	Only for thin or small parts.
Glass-based	Turbine wheels, engines, heat exchangers	Materials heated to glazing temp(1000°F).
Strain gages: single	Machinery, structures, pressure vessels	Protect against electrical instability.
Rosettes	Machinery, structures, pressure vessels	Protect against electrical instability.
High elongation	Machinery, structures, pressure vessels	Protect against electrical instability.
Dynamic (isostatic)	Machinery, structures, pressure vessels	Protect against electrical instability.
Semiconductors	Machinery, structures, pressure vessels	No high-strain level or sharp bends.
Photoelasticity coatings	Actual machinery, parts, pressure vessels.	No extremely thin membrane in bending.
X-ray diffraction	Specimens, small parts	Small parts only.
Extensometers	Mechanical tests, primary measurements	Sharp curvatures difficult.

stressed metal part furnishes a means of detecting loaded regions and of determining the direction of strains in a part. Probably the first brittle coating used was simply the oxide scale on hot rolled and annealed steel structures such as wrought iron bridges. Various methods have been devised to enhance such indications, the most useful one being that of liquid penetrants. Attempts were made to use varnish, lacquer, or resins as brittle coatings as early as 1925, but wide application, particularly in elastic-strain regions, did not start before 1937. Under the supervision of the late A. D. deForest, of the Massachusetts Institute of Technology, Greer Ellis developed the forerunner of the present day commercial product known as Stresscoat*, manufactured and marketed by the Magnaflux Corp. The sensitivity of the early lacquers was dependent upon the environmental humidity and temperature at which the test was performed. Recent formulations are somewhat less dependent upon humidity.

Another method for applying resin coatings to structural objects was developed by B. P. Haigh and used later by J. S. Blair. This method consists of mildly heating the test pieces and then spraying a dust of a powdered resin upon the surface of the object. The powder has a low melting point and melts on contact with the heated surface, forming a thin, uniform coating. Such a coating is marketed by Soci t 

*Registered trade name.

National Etude Construction Material Aviation (SNECMA) in France (ref. 1).

The development of ceramic brittle coatings has extended their useful operating range to temperatures up to 700° F. When fired, the coatings are glass-like and brittle, and are less fragile than lacquers (though not less strain sensitive).

Brittle coatings are most useful in exhibiting the general stress-distribution pattern over the surface of a complex structure and are particularly useful for locating areas of high-stress concentrations and their directions. A primary use is the application to a specimen prior to the attachment of electric strain gages.

Advantages and Disadvantages of Brittle Coatings

Some of the major advantages of the brittle-coating method for measuring strain are enumerated below.

- (1) It is one of the simplest means available for locating regions of strain concentration.
- (2) It can be used on essentially any material which can be spray-painted (metals, glass, wood, and certain plastics, for example).
- (3) Both tensile and compressive strains can be investigated.
- (4) Quantitative strain values within about $\pm 10\%$ accuracy are possible. (A high degree of skill and very well-controlled environmental conditions are required for better results.)

(5) The glazed ceramic-based coatings require no special protection from oil, water, or reasonable mechanical handling.

Some of the important disadvantages of the brittle-coating method are given below.

(1) The commonly used resin lacquers are sensitive to humidity and temperatures and are easily scratched. Temperature changes during a test of $\pm 5^\circ \text{F}$ prevent any quantitative conclusions being made from the results (ref. 3).

(2) With the lacquer coatings, carbon disulfide, a highly flammable and poisonous compound, is employed as a solvent (ref. 6).

(3) Ceramic based coatings require that the test specimen be heated to approximately 1000°F , the glazing temperature for the coating.

(4) On thin specimens, this method is best used only qualitatively since the reinforcing and loading effects of the coating itself are difficult to determine accurately.

Physical Principles of Brittle Coatings

Strain measurement by brittle coatings is based upon these properties: (1) the coatings fracture without appreciable deformation, (2) fracture occurs when the maximum tensile strain in the coating reaches a certain limiting value, and (3) fracture occurs normal to the direction of maximum tensile strain. When a brittle coating is applied evenly over the surface of a specimen the specimen may be deformed to produce a crack pattern in the coating. If the strains of interest are compressive, the specimen may be deformed first, then the coating applied, and, later, the specimen allowed to return to its equilibrium position. In this way, compressive strains in the specimen will induce tensile strains in the coating and affect its cracking. The crack patterns may be observed during or after the deformation of the specimen to reveal useful information on the two-dimensional (biaxial) strain pattern existing at the surface of the specimen during its deformation. Drawings indicative of some typical crack patterns on a cantilever beam loaded in various ways by forces or moments are shown in figure 10-5 (ref. 1). For a quantitative analysis of crack patterns, a control specimen with known strain distributions (usually a cantilever beam) may

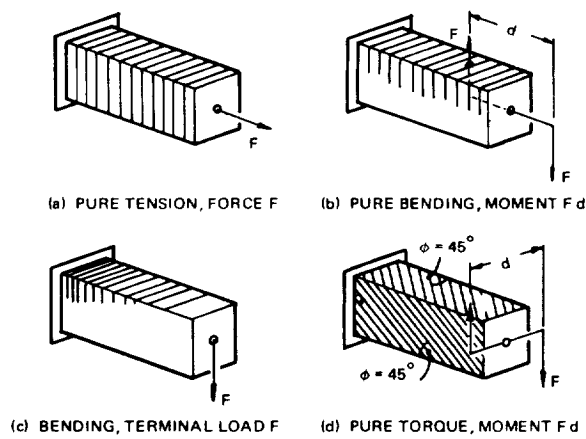


FIGURE 10-5.—Representations of typical crack patterns in a brittle coating. (Courtesy of MacMillan and Co., Ltd. and Strain Gauges and Uses, H.K.P. Neubert.)

be covered with a brittle coating identical to that on the specimen. With conditions similar to those experienced by the test specimen, the cantilever is deflected as shown in figure 10-5 (c). For any given deflection from its rest position, the strain at any point along the length of the beam can be determined theoretically. Of primary importance is the strain associated with the cracks most recently formed when the beam is deflected. This strain value is known as the strain threshold for the particular coating under the prevailing environmental conditions; it is assumed that under similar strain on the test structure, cracks will begin to appear in the coating when this strain threshold has been reached. If the strains are increased in small increments, the cracks spread and the limit of the propagation always marks the line along which the extensional strains are approximately equal to the strain threshold. While it is generally true that the crack density is greatest in regions of greatest strain, comparisons of crack density on the test specimen with those on the calibration bar seldom give better results than about $\pm 20\%$ accuracy (ref. 1). Consequently, the "crack-density method" is seldom used for quantitative measurements.

Best results are usually obtained from brittle coatings that have been sprayed on a specimen, introducing a uniform distribution of fine air bubbles into the coating, which contrib-

utes appreciably to the consistency of crack formation in the coating. The bubbles appear to have two functions: (1) they facilitate an even drying of the coating and (2) they prevent the cracks from spreading into regions where the strain is below the normal threshold sensitivity of the coating (ref. 3).

Although the lacquer coatings are brittle, they are quite plastic and will creep under prolonged straining. In such cases, the amount of strain necessary to initiate cracking of the coating varies with time, making it essential to make corrections for creep in order to obtain reliable quantitative results. Charts are supplied by the manufacturer for this purpose.

Brittle coatings flake off when the compressive strains in the specimen reach approximately 1%. Thus, because of the transverse compression occurring when a specimen is tensioned, flaking will usually occur near the yield point for most structural materials. When coatings are selected to give flaking indications, they are usually the more sensitive coatings and tend to craze (contain minute cracks) so completely during drying that they are no longer useful to indicate elastic strains (ref. 7).

Typical Materials and Instrumentation

At the present time, the only commercial supplier of brittle coatings in the U.S. is the Magnaflux Corp. It manufactures both lacquer and ceramic coatings under the names Stresscoat, Stresscoat ST-101, and Stresscoat All-Temp*, each of which is available in formulations of varied strain sensitivity. A lacquer coating is made by SNECMA in France, and may be obtained in liquid or powder form, the latter being spread by the application of heat (ref. 1). Other brittle coatings have also been used; however, most of these were either experimental or special-purpose coatings developed by the individual user.

The Magnaflux coatings are described briefly below.

(1) Stresscoat

Type: Lacquer coating.

Characteristics: Brittleness is affected by humidity and temperature during drying and testing. Charts are available for use in selecting the coating with the desired strain sensitivity. These charts are based upon wet and dry bulb readings from a sling psychrometer.

Maximum strain sensitivity: 500 μ in./in.

Strain range: 0.3%

Application to specimen: Air-spray gun; air dry for about 18 hr

(2) Stresscoat ST-101

Type: Lacquer coating

Characteristics: Brittleness is affected by temperature only

Maximum strain sensitivity: 200 μ in./in.

Strain range: 0.2%

Application to specimen: Air-spray gun or aerosol-spray containers; air dry for about 12 to 18 hr

(3) Stresscoat All-Temp

Type: Ceramic coating

Characteristics: These coatings are designed to match the mean linear thermal coefficient of expansion of the metal being tested over the temperature range at which tests are performed. For a given specimen, the coatings of different expansion coefficients will have different threshold strains due to the sign and magnitude of strains that are locked into the coating during cooling from glazing temperatures. These coatings are not subject to creep when strain is applied slowly or for a long period of time.

Maximum strain sensitivity: 200 μ in./in.

Strain range: 0.2%

Application of coating: Air-spray gun; heat to approximately 1000° F glazing temperature and cool to testing temperature (less than or equal to 700° F)

There are several materials and methods available to aid the observer when he inspects the crack patterns in the coatings. The first of these is an aluminum-colored undercoating that will reflect light through the cracks and make them more visible. Another aid is the dye etchant that is a fluid containing a dye that can selectively etch cracks in the brittle coatings leaving a residue of the visible dye in the cracks. This method has one distinct disadvantage in that it destroys the further usefulness of the coating by chang-

*Registered trade names.

ing its strain sensitivity through the etching process. To overcome this difficulty the electrified particle inspection method may be used. In this method, a special liquid electrolyte is applied to the coating and then enters the cracks. Excess electrolyte is removed from the surface of the part which is then covered with positively charged powder that is attracted to the negative ions in the electrolyte left trapped within the cracks (ref. 6). Since the coating is not harmed, the specimen may be further deformed and the coating again inspected for cracks. It should be noted that the ceramic coatings need no electrolyte to collect the powder about the cracks.

Any good commercial spray gun can be used to apply the resin-based coatings to a specimen, and a shop air supply is satisfactory for spraying purposes provided no oil or water droplets are entrained. It is imperative that the air supply be free of moisture because excess moisture will be trapped in the coating and affect its strain sensitivity. The ceramic-based coatings require the additional use of an oven to bring the specimen and coating up to the glazing temperature. If the spraying is done indoors, a commercial spray booth should be used because the liquid vehicles are toxic and flammable. The ceramic powders (frits) are suspended in a hydrocarbon vehicle, and there is a tendency for the suspended powders to settle out. Consequently, the spray mixture must be continuously agitated or circulated to keep the particles suspended. A photograph of a complete Stresscoat Kit, including those materials and apparatus needed for a majority of field tests, is shown in figure 10-6 (ref. 7).

Testing Procedures

In the following discussion, general procedures are outlined for using the brittle-coating method for sensing strains. These are not detailed, exhaustive instructions, but are indicative of those procedures typically required when utilizing the method.

Preparation of specimen.—In general, the procedure for preparing a specimen for brittle coating is the same as for any other type spray-paint application. Surfaces should be clean,

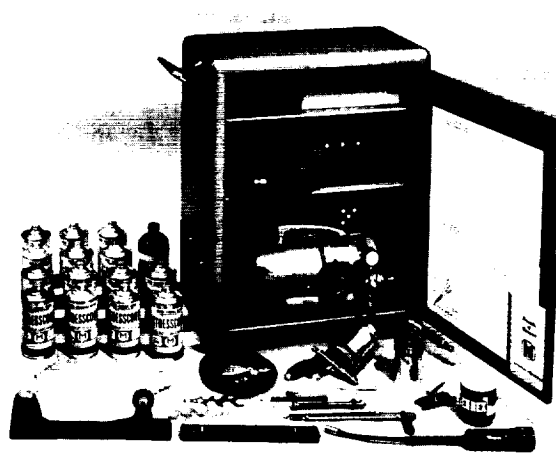


FIGURE 10-6.—A complete Stresscoat® kit commonly used throughout industry. (Courtesy of Magnaflex Corp.)

smooth, and free of grease, oil, rust, and scale. Grit-blasting or the use of a wire brush is a good means of acquiring the necessary surface finish, providing these are not in themselves harmful to the specimen being tested. An aluminum pigmented undercoat is often applied before the lacquer-based coatings to provide a uniform reflective surface to aid in crack detection. After this, the lacquer coating is best sprayed upon the specimen and allowed to dry at a temperature slightly higher than that expected during the test. The coating is generally of proper thickness when its appearance changes from clear to a distinct yellowish tinge (ref. 7). Coatings should be applied as uniformly as possible; but the thickness does not affect the threshold strain appreciably, providing the thickness lies within 0.004 to 0.008 in. for lacquers and 0.003 to 0.005 in. for ceramics.

The ceramic-based coatings consist of a suspension of finely divided ceramic particles that must be fused into a smooth, glossy coating by heating to approximately 1000° F in an oxidizing atmosphere. This is conveniently done in an electric furnace. When fired to a glossy smooth coat, the parts may be air-cooled to the testing temperature.

Preparation of testing apparatus.—The apparatus needed for examining and analyzing brittle-coating indications is simple. Indeed, all that is needed other than equipment for spray-

ing (and firing) the coating are: (1) a means for inducing strain into the specimen (usually mechanical loading jigs) and (2) calibration bars to be coated at the time and under the same conditions as was the specimen, by which the strain threshold of the coating may be determined.

Data acquisition.—Acquiring data from brittle-coating tests consists of observing and recording the location and orientation of cracks in the coating. The cracks of interest in making a quantitative strain measurement are those that were last formed (threshold cracks) after each incremental change in deformation of the specimen. To obtain the best results in static tests, it is generally best to (1) deform the specimen in step fashion and allow it to return to its rest position after each deformation or (2) deform the specimen at a steady rate and make corrections for creep using available charts.

Under moderate strains, the coatings will crack and stay open for visual inspection, with proper lighting. However, with high-threshold strains, the cracks are closed very tightly when the specimen is allowed to return to its rest position and will not reflect light. To improve the inspection in such cases, the observer may use the dye etchant or electrified particle method to enhance the crack patterns as previously described. The patterns thus made visible can be photographed or preserved with transparent coatings as a record of the test.

Restoration of specimen for service.—The major part of the previously applied brittle coatings may be removed mechanically by scraping, wire brushing, or grit blasting. Vapor degreasers and solvent cleansers may be used to remove residual materials from the lacquer coatings.

Interpretation of results.—Crack patterns in brittle coatings must be interpreted in light of the physical principles previously discussed. However, certain precautions are necessary to assure that quantitative data from the tests are valid. As mentioned before, the strain threshold of the various types of brittle coatings is dependent upon temperature, humidity, or both. Consequently, these environmental conditions

must be maintained within those limits given by the manufacturer for each coating throughout the duration of the test. If the specimen is coated with a lacquer coating and is deformed for more than 10 sec, the effects of creep on threshold strain should be taken into account by means of correction charts.

Frequently, it is desirable to extrapolate strain measurements made at one value of mechanical load to other values of load. This is valid only if the two conditions are satisfied: (1) the material of the specimen must remain in its linear elastic range and (2) the distribution of loading must not change. Then, it may be assumed that all the measured strains vary directly in proportion with the load (ref. 7).

Current State of the Art

The following discussions include some applications, special techniques, and recent developments in brittle-coating, strain-measuring technology. They are intended to present the current state of the art in brittle coatings.

Brittle-coating tests of honeycomb panels.—The results of brittle-coating tests performed on honeycomb panels by a NASA contractor are shown in figure 10-7 (ref. 8). The panels were strained by such means as internal pressurization to give quick visual indications of unbonded areas in the structure. Although the information contained in these tests is used only qualitatively, the process is reported to be of considerable value in evaluating the integrity of honeycomb structures (ref. 8).

Measuring compressive strains.—To measure compressive strains in a specimen, either of two approaches may be used in lacquer coatings: (1) deform the specimen and then apply the coating—when the coating is dry, return the specimen to its rest position and check for crack indications and (2) apply and dry the coating before the specimen is deformed to take advantage of the creep property of these coatings—this property causes relaxation of compressive strains produced in the coating when the specimen is deformed. After about two hours, the load may be removed and the coating inspected in the usual manner. When ceramic coatings are used only the former method is

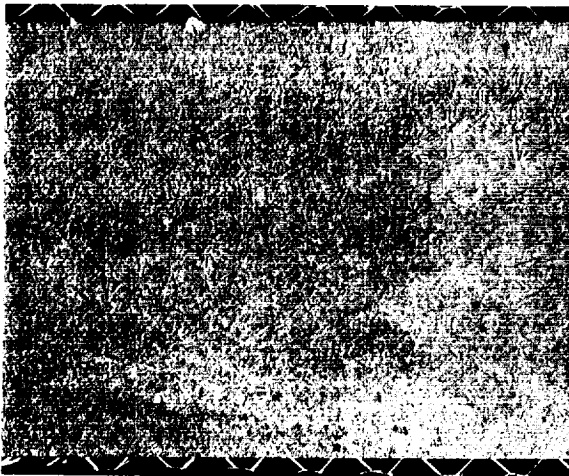


FIGURE 10-7.—Brittle-coating tests of honeycomb panels. (Courtesy of General American Transportation Corp.)

applicable because these coatings do not creep appreciably.

Sensitized brittle coatings.—Brittle coatings can be sensitized (made to crack at lower threshold strains) by two means: (1) chilling the coating or (2) etching the coating with a dye etchant. Results obtained by such means are chiefly qualitative and are used primarily to indicate the direction of strains in less highly strained areas of the specimens.

Dynamic brittle-coating tests.—When static testing conditions may not satisfactorily dupli-

cate conditions of loading in service, loads can be applied dynamically and the crack patterns observed either statically after the loading or during loading under a stroboscopic light to obtain quantitative data. The most often encountered problem in dynamic tests is that of temperature rises in the test sample. The effects of an excessive temperature rise may be reduced by sprinkling water over the test sample and calibration bars, or by placing the sample in a water bath. The specific coating used should be selected along the 100% humidity line (on the coating selection chart) for the temperature of the water used in the test (ref. 7).

Measuring residual surface strains.—Residual strains of appreciable amounts can be measured using the trepanning method in which small holes are drilled in the surface of the test piece. The removal of material at the location of the hole permits the relaxation of strains in the material near it. Results can be obtained only by sensitizing the coatings with a dye etchant. This method might not be nondestructive to all specimens (ref. 7).

Recent developments.—The brittle-coating method was developed almost to its present state more than two decades ago. Since then, there seems to have been very little interest in further development of it. Indeed, only two developments of significance have been made since 1960: the Stresscoat ST-101 coatings (described earlier) and the micromethod.

The micromethod employs extremely thin microcoatings for use on small, thin-walled parts such as a tiny watch gear or thin diaphragm. The standard coatings are thinned and sprayed to a thickness of 0.0003 to 0.001 inch. The sensitivity of the thinner coating is less than that of the usual coating so that the more sensitive lacquers must be used, and even these are sometimes chilled to increase their sensitivity (ref. 6).

PHOTOELASTIC COATINGS

Historical Background

The photoelastic effect is related to the change in the velocity of light that occurs in some materials as a result of strains within the material.

Sir David Brewster is credited with the discovery of the effect through his work in 1816 when he was examining stressed glass with polarized light. He observed fringe patterns exhibited by the glass similar to those in figure 10-8 (ref. 9). The underlying theory explaining these patterns was developed by Maxwell, Neumann, Wertheim, and others. They interpreted the patterns as being interference patterns resulting from optical retardation related to strains in the glass.

The use of this phenomenon for strain measurement first appeared in the engineering world around the turn of the century and was developed mainly by Professor E. G. Coker and L. N. G. Filon, both of the University of London. Since that time, much effort has been expended by other workers (notably M. M. Frocht in the U.S.) to further develop and promote this science. Around 1930, A. Mesnager first suggested the use of a coating of photoelastic material applied to a reflective metal surface, greatly broadening the scope of applications for the photoelastic strain-measuring method.

Significant progress has been made in perfecting the techniques and improving the required equipment. In recent years, the development of new synthetic transparent resins that possess desirable photoelastic characteristics has made the method applicable to an even wider variety of problems. The continuing development of sprayable photoelastic coatings promises to be usable for even larger more complex-shaped structures. The invention of Polaroid polarizing filters has greatly enhanced the utility of the method because it provides a relatively inexpensive means of producing large beams of polarized light (ref. 3).

Only photoelastic coatings will be discussed in the remaining portions of this section, because the basic theory and equipment utilized in photoelastic model methods are not too different from those for photoelastic coatings. Also, only the coatings are applicable to the majority of nondestructive tests. Details concerning the model methods may be found in references 3 and 10.

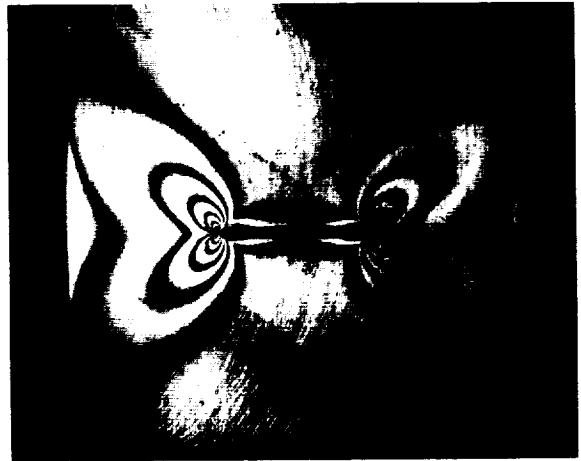


FIGURE 10-8.—Photoelastic-fringe patterns about a crack. (Courtesy of Jet Propulsion Lab., California Institute of Technology.)

Advantages and Disadvantages of Photoelastic Coatings

Some of the advantages of photoelastic coatings for making strain measurements are given below.

(1) Photoelastic coatings provide for the rapid location of high-strain concentrations on the surface of a specimen, giving the overall picture of the principal strain difference ($\epsilon_p - \epsilon_q$).

(2) Photoelastic coatings can be applied to most structural materials (metal, concrete, wood, glass, rubber, and bone, for example).

(3) Measurements can be made under a variety of environmental conditions, even when the plastic is immersed in some transparent liquids such as water, oil, and liquid hydrogen.

(4) Measurements can be made remotely by direct observation or by the use of a camera, television, or other photosensitive devices.

(5) Large strains are measurable making possible the determination of yielding in the tested specimen.

(6) The magnitudes of principal strains may be determined to within $\pm 10 \mu$ in./in. and their directions may be established to within $\pm 2^\circ$.

Some disadvantages of the photoelastic-coating strain-measuring method are as follows:

(1) Separation of the principal strains requires (a) more than one measurement in the

oblique-incidence method, or (b) the determination of the principal strain difference ($\epsilon_p - \epsilon_q$) from a photoelastic measurement and the utilization of some other experimental technique to determine either of the principal strains alone or, perhaps, their sum ($\epsilon_p + \epsilon_q$).

(2) Areas of interest on the test specimen must be accessible to light.

(3) Correction factors must be introduced for (a) measurements at temperatures above about 100° F, (b) reinforcement of the specimen by the coating, and (c) birefringent effects attributable to large curvature or high-strain gradients (ref. 11).

(4) When measurements are made under oblique incidence, the strain is averaged over some finite length dependent upon the coating thickness (i.e., the gage length is considerably greater than zero).

Physical Principles of Photoelastic Coatings

The strain-measuring method, in which photoelastic coatings are used, makes use of the strain-optic property (birefringence) possessed by some transparent plastics. A coating of the special plastic is bonded to the specimen to be tested so that when the specimen becomes deformed, strains are transmitted to the coating. The coating breaks up a normally incident ray into two orthogonal components, each of which is plane polarized, so that the planes of vibration of these two components are coincident with the directions of the principal strains. The two rays travel in the birefringent material with different speeds that are dependent upon the properties of the particular photoelastic material and the magnitudes of the principal strains. Stating this another way, the material possesses two different indices of refraction as signified by the term "birefringent." Because the two light waves travel at different speeds, the optical-path lengths for the two waves passing through the coating differ so that in general there will be a difference in phase of the two waves as they emerge from the birefringent material. The strain-optic law relating the principal strains to the relative retardation of the two

components may be stated mathematically for a biaxial strain field as

$$R_T = 2K_t (\epsilon_p - \epsilon_q)$$

in which R_T is the relative retardation of the wave components, K is the constant known as the strain-optic coefficient characteristics of the particular coating being used, t is the thickness of the coating, and ϵ_p and ϵ_q are the principal strains.

Figure 10-9 is a schematic representation of how this phenomenon may be used in making strain measurements (ref. 12). A monochromatic light source is shown for simplicity.

The analyzer transmits only those components of the light waves that are coincident with the polarizing axis of the analyzer. Thus, one observes the interference and reinforcement of the two wave components in a particular plane by rotating the axis of the analyzer to that inclination. These are seen as light and dark fringes (as shown previously in figure 10-8) representing a retardation of $1/2$ a wavelength for each change from a light fringe to a dark fringe. Such fringes are called isochromatics, and the principal strain difference ($\epsilon_p - \epsilon_q$) is a constant along any particular one of these isochromatic fringes.

If the axis of the analyzer is crossed (turned 90°) to that of the polarizer, a set of rather broad dark bands will be observed superimposed upon the isochromatic fringe pattern. At any point in the coating where a principal strain axis is parallel to the plane of vibration of the incident light, the wave passes through the coating unaffected. Since the analyzer is set 90° to this plane, it will extinguish the ray regardless of the strain within the coating. This set of bands, called isoclinics, corresponds to

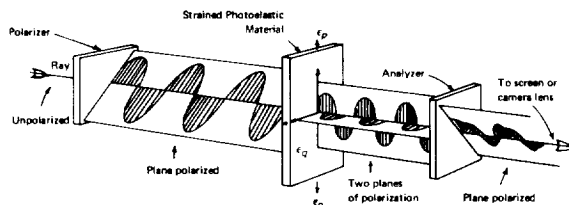


FIGURE 10-9.—Representation of light waves within a simple polariscope. (Courtesy Product Engineering; copyright Product Engineering.)

those locations where an axis of one of the principal strains has a constant direction that is parallel to the axis of the polarizer. White light is generally used when examining the isoclinics so that the dark isoclinics can be more easily distinguished from the colored isochromatics. The usual practice is to trace the isoclinics for several orientations of the crossed polarizer and analyzer. These data are then used to determine the directions of principal strains at the points of interest.

It is usually desirable to eliminate the isoclinics in attempting to analyze the isochromatics. This can be done by placing a quarter-wave retardation plate between each polarizer and the part coated with the photoelastic material. Such a plate splits incident light into two linearly polarized components with polarization axes perpendicular to each other, and with a relative retardation of $\frac{1}{4}$ wavelength. The light emerging from the combination of a plane polarizer and the quarter-wave plate with their planes of polarization set at 45° to each other (fig. 10-10) (ref. 12) is known as circularly polarized light. Such light entering the coating will be resolved into two components regardless of the orientation of the strain in the coating. The components upon emerging and passing through the second quarter-wave plate (with its slow axis oriented at 90° to that of the first quarter-wave plate) and then through the plane analyzer will be extinguished only when affected by the birefringence in the coating. Consequently, there are no isoclinics.

For measuring very small fractional retardations, optical instruments called compensators are used in conjunction with the polariscope.

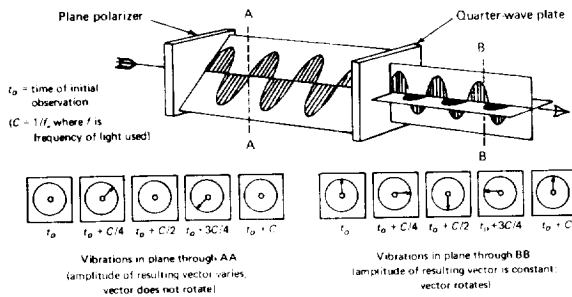


FIGURE 10-10.—Representation of circularly polarized light. (Courtesy of McGraw-Hill, Inc.)

The most common of these is the Babinet compensator (fig. 10-11) (ref. 3). It consists of a pair of wedge-shaped polarizing crystals with their axes so arranged that the relative retardation of light waves traversing the pair is dependent upon the distance travelled in each wedge. In moving the wedges relative to each other, the interference-fringe pattern can be displaced and the relative retardation produced by the compensator can be measured according to the equation:

$$R_c = \lambda \left(\frac{M}{M_0} \right)$$

where R_c is the retardation produced by the compensator, λ is the wavelength of light used, M_0 is the wedge displacement necessary to produce one wavelength retardation, and M is the measured wedge displacement. The color of light transmitted (dark or light fringe in the case of monochromatic light) determines the total relative retardation of the two wave components which must equal the sum of the retardation produced in the compensator and that produced in the coating.

Typical Materials and Instrumentation

A birefringent coating that may be applied to the test specimen and a reflection polariscope are needed to perform a photoelastic-coating strain measurement. Several different arrangements of the basic optical components in a reflection polariscope are shown in figure 10-12. Reflection polariscopes are quite varied in construction. The simplest device, a polarizing quarter-wave viewer, consists of a polarizing plate (Polaroid sheet) bonded to a quarter-wave plate whose optical axis is set at 45° to the transmission axis of the polarizer. This assembly may be

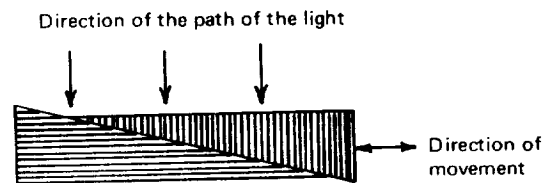


FIGURE 10-11.—Diagram of a Babinet compensator. (Courtesy of John Wiley and Sons, Inc.)

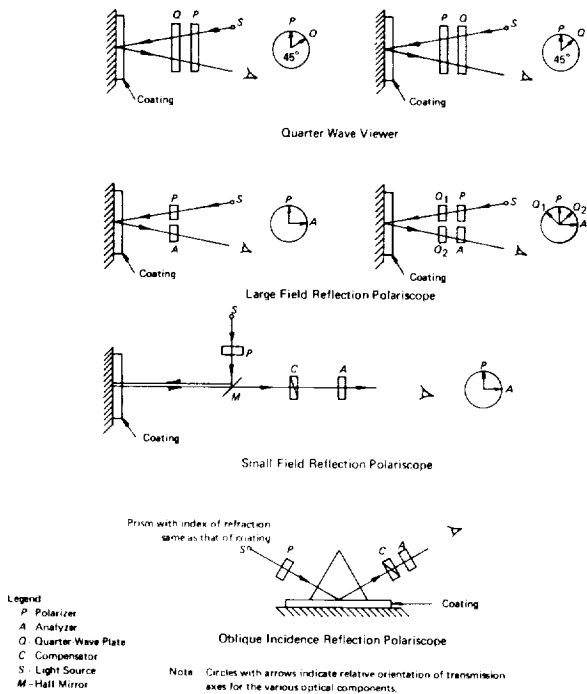


FIGURE 10-12.—Diagrams of reflection polariscopes used with photoelastic coatings.

placed against the plastic coated specimen and viewed under room light. Typical accuracies obtained while using such a device is $\pm 10^\circ$ for direction of principal stresses and strains and $\pm 80 \mu$ in./in. for magnitude of strain. Other instruments are of increasing complexity, with provisions being made for one or more of the following:

- (1) The inclusion of an oblique incident prism
- (2) Compensators for measuring small relative retardation in the wave components
- (3) Stroboscopic light sources for dynamic observations
- (4) Photocell attachments for measuring light intensities
- (5) A camera attachment for recording fringe patterns.

Such instruments may have strain sensitivities as high as $\pm 10 \mu$ in./in., depending upon the coating material used, and will determine the principal strain direction within $\pm 2^\circ$. A representative commercially available polariscopes is shown in figure 10-13.



FIGURE 10-13.—Commercially available large field reflection polariscopes.

It is convenient to have the polariscopes equipped with sources of both white and monochromatic light which can be interchanged quickly and easily. For white light, an incandescent projector type bulb of about 500 w capacity is satisfactory for most applications. Monochromatic light can be obtained from a dc mercury-arc lamp, but a filter should be used to mask out radiation other than green light. Sodium-vapor lamps can be utilized but generally do not have a concentrated source of sufficiently high intensity for photographic work (ref. 3).

Photoelastic coatings have been developed for a wide variety of specimen materials and analysis conditions. They may be applied to flat, curved, or irregular shaped surfaces; some have been successfully used on metals, concrete, plastics, ceramics, rubbers, plaster, glass, wood, and tile. This versatility is obtained by making the coatings available in three general forms: (1) flat sheets (commonly 0.030 to 0.250 in. thick), (2) liquids for casting contoured sheets, and (3) sprayable liquids.

Many plastics exhibit the photoelastic property of birefringence but only a relative few have sufficiently large birefringent effects to be useful to the strain analyst. Recently, interest has focused upon several two-part epoxies and some urethane polymers that are promising for contoured sheets and spray-on applications. Presently, the coating materials seem to be di-

vidable into two general groups: (1) low elongation materials (1% to 3%) and (2) high-elongation materials (some manufacturers claim as much as 85%). The strain-optic coefficient of the high-elongation materials is usually only 10% to 25% that of the low-elongation plastics. Developments are being made so rapidly in coating materials, especially in sprayable coatings, that it is advisable to consult the current literature for available materials.

Testing Procedures

The general procedures required when using the photoelastic-coating method to make strain measurements are outlined in this section. These are not detailed instructions, but are indicative of the procedures typically required.

Preparation of specimen.—The surface of the test specimen must be thoroughly cleaned with a good degreaser to insure proper adhesion of the coating. The surface must be reflective or made to be reflective in one of the following ways:

- (1) Polishing the surface (the finish obtained using sandpaper or by rough grinding is usually adequate)
- (2) Spraying with a reflective undercoat
- (3) Bonding the plastic sheets to the test specimen with a reflective cement
- (4) Using flat, photoelastic sheets with metallized reflective backings.

The coatings are applied to this prepared surface with special adhesives. However, when a contour sheet must be used, the liquid plastic is mixed with a hardener and poured to the desired thickness in a level mold. Before the plastic completely hardens, it is removed from the mold and carefully shaped directly on the surface to be tested. In this way, a sheet is produced which has uniform thickness and is free of residual birefringence. Once the contoured sheet is fully hardened, it is bonded to the surface in a manner similar to that for the flat sheet. The sprayable coatings are generally epoxies with good adhesive qualities and require no other cement. A single coat may be as thin as 0.003 in. but additional coats may be applied to any desired thickness (ref. 13).

Preparation of testing apparatus.—The testing apparatus consists of the reflection polariscope and the loading jigs used to deform the specimen. To make a photoelastic-strain measurement, it is necessary that the coated specimen be loaded and the reflection polariscope positioned for lighting and viewing the areas of interest. A typical arrangement employed by a NASA contractor is shown in figure 10-14 (ref. 15).

Unless the strain-optic properties of the coating used are known, it is necessary to make calibration measurements. Because the specimen in general is of a complex shape, it cannot be easily used to calibrate the coating. Test samples are taken from the coating material and are loaded so as to give a simple, prescribed strain field. From this, the strain-optic coefficient may be determined.

Data acquisition.—In photoelastic analysis, data acquisition begins by illuminating the specimen with plane polarized white light and viewing the field through a "crossed" analyzer (axis 90° to polarizer axis). The dark isoclinics for the angle at which the analyzer happens to be set will be seen superimposed over colored isochromatics. A complete survey of principal strain orientations is usually made by rotating the axes of the crossed system to various settings at each of which the isoclinics are sketched or photographed. Once this is done, the quarter-wave plates can be inserted into the polariscope

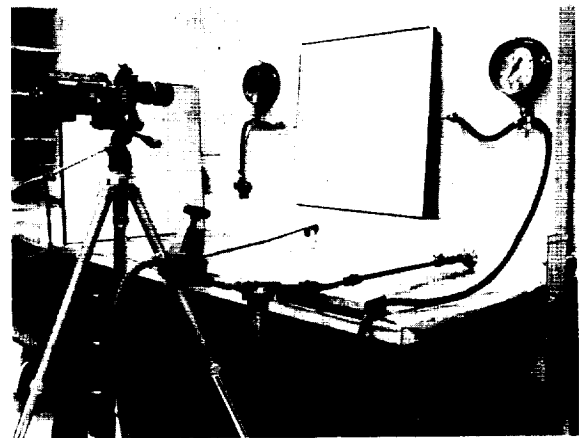


FIGURE 10-14.—Arrangement for inspecting honeycomb panels. (Courtesy of Lockheed-Georgia Co.)

so that only the isochromatic fringes are visible. Points of known zero strain and locations of obvious strain concentration are used as references. The number of fringes (if monochromatic light is chosen for the isochromatic analysis) or the successions of color spectra (in white light analysis) which lie between these two points is counted to determine the relative retardation at the point of interest. In monochromatic analysis, more precise measurements of the relative retardation at discrete points are made with a compensator, usually attached directly to the polariscope. When the fringe pattern is viewed through this, a dark fringe moves across the isochromatics as the compensator is adjusted. The compensator may be calibrated so that the principal strain difference associated with those areas covered by the dark fringe is indicated directly. It may even be connected to an electronic readout device so that the relative retardation or the associated strain difference is presented in analog or digital form. Once the relative retardation has been determined, it is a simple calculation to find the principal strain difference ($\epsilon_p - \epsilon_q$). The oblique-incidence method requires that measurements of relative retardation be made at two oblique-incidence angles (fig. 10-12) from which the separate principal strains can be calculated (ref. 14).

Restoration of specimen for service.—Coatings for NDE must be removable without damaging the underlying structure. This is not an easy task since the adhesives used are necessarily quite strong so that they always transmit strains to the coating. Commercially available strippers in which the coating swells and destroys the bond after approximately 24 hours can be used. Associated with this swelling is an increased toughness that allows the coating to be peeled away in large pieces. Heating affects the coating and bonding agent similarly. Sometimes a cold thermal shock can be of benefit in coating removal because it crazes the coating and partially destroys the bond (ref. 15).

Interpretation of results.—The determination of the directions of the principal strains by viewing the isoclinics (as described previously) is relatively simple; determination of the magnitudes of the principal strains, how-

ever, is more complex and requires that the analyst beware of several pitfalls. Birefringent coatings carry a portion of the load that would otherwise be borne by the structure so that strains at the structure-coating interface may be somewhat less than those in an uncoated part. The modulus of elasticity for the low-elongation coatings is on the order of 500 000 psi, enough to carry an appreciable amount of the load, especially on thin test specimens. In some cases, especially those involving thin test pieces, the coating will cause a shift in the strain distribution within the test specimen (for example, a shift in its neutral axis) unless it is coated on both sides to maintain a symmetrical cross section.

Strain gradients through the coating thickness must also be considered because of the averaging effect that influences the measured strain values (ref. 16). The observed birefringence is directly proportional to the surface strain at a point only so long as the strain is uniform on the surface or changes little over distances comparable to the thickness of the coating. In such cases, it is relatively easy to determine the strain. However, in the presence of high-strain gradients at the metal surface or if the surface is highly curved, the deformation of the coating will vary across its thickness and the observed birefringence will depend on the magnitudes of the strain and its gradient (ref. 11).

Thermal effects are also of importance in making quantitative stress measurements in which photoelastic coatings are used. Existing photoelastic coatings are relatively good thermal insulators compared to metallic specimens. Consequently, the coating may alter the temperature distribution and the thermally induced strains within the part. Another closely associated problem is the birefringence exhibited by the coating due to different thermal expansions of the coating and test specimen (ref. 17).

All these complications do not, however, preclude the use of the photoelastic strain-measuring method to a large portion of the important engineering applications, since correction factors exist in the literature for most of the above mentioned difficulties (refs. 11, 16, 18, and 19).

Even when correction factors are not available, the method can often yield strain values as good or better than those which can be inferred from other means.

Current State of the Art

In the following paragraphs several applications, special techniques, and recent developments in photoelastic-coating strain-measuring technology are given to indicate the current state of the art.

Evaluation of bonded honeycomb structures.—A method devised especially for detecting unbonded regions in bonded structures with perforated honeycomb core was developed at NASA-Marshall Space Flight Center. An epoxy-type birefringent coating which can be used with conventional paint-spray equipment was developed. The method is based on applying air pressure to the perforated cellular structure of an edge-sealed honeycomb structure. Nonuniform deflection of the panel skin occurs in areas where there is no bond of the face sheet to the core. By coating the skin with a strain-sensitive plastic film prior to the pressurization, defective areas thus deflected can easily be located (fig. 10-15) with the reflection polariscope (refs. 15 and 20).

Strain analysis of solid propellants.—A way of determining the stresses and strains in actual solid propellants without the use of models is to cement on the surface of the propellants a thin photoelastic coating that follows the deformations of the propellant. The birefringence of the coating can then be used as an index of the state of strain in the propellant. If the coating material has a modulus of elasticity equal to or lower than the modulus of elasticity of the propellant, the interpretation of the fringes obtained is simple. In cases when the coating has a reinforcement effect on the propellant or when the loading is thermal and the thermal properties of the coating and the propellant are not the same, the interpretation of the fringe pattern obtained becomes more complicated and the approach less practical (ref. 21).

Simultaneous recording of isoclinics and isochromatics.—The Jet Propulsion Lab. designed an inflated cylinder test (simulating the normal

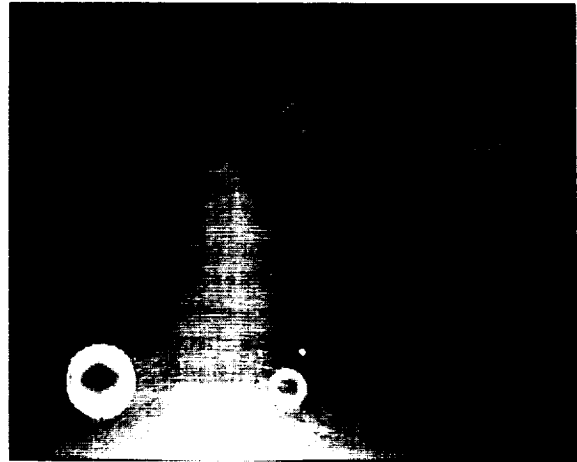


FIGURE 10-15.—Photoelastic indications from voids in honeycomb panels. (Courtesy of Lockheed-Georgia Co.)

loading of a solid-propellant rocket) that enables reasonable measurements to be made of the biaxial surface layer strains of a viscoelastic material as a function of time. A problem arises when the photoelastic-coating method is used to measure time-dependent strains in that the position of both the isoclinics and isochromatics must be recorded as a function of time. One solution to this problem requires simply that a number of preset polariscopes (fig. 10-16) (ref. 22) be indexed to record the isoclinics in a short period (ideally an instant of time). In this manner, groups of readings may be taken at different intervals of time. The

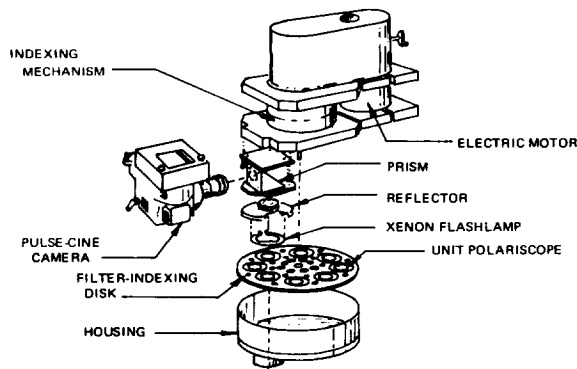


FIGURE 10-16.—Indexing-reflection polariscope for simultaneous recording of isoclinics and isochromatics. (Courtesy of Society for Experimental Stress Analysis.)

extension of this experimental method to the temperature and dynamic-loading regimes is readily apparent (ref. 22).

Thermal effects in photoelastic tests.—If photoelastic coatings exhibited thermal conductivity and thermal expansion equal to that of structural materials and if strain-optic sensitivity did not vary with the temperature, photoelastic-coating analysis could be conducted in thermal fields exactly as in room-temperature tests. Analytically and empirically derived factors to account for birefringence resulting from differential thermal expansion of coating and specimen are available for some cases. Measurements of surface strains introduced by external loading and thermal stresses have been performed in the temperature range of -60° to $+350^{\circ}$ F for tests of extended duration and to $+500^{\circ}$ F for brief periods (ref. 17).

Dynamic photoelastic methods.—In recent years, a large number of investigators have used photoelastic methods to solve transient stress problems. The means of recording the fringe patterns have varied appreciably, at least four different recording systems having been used. In one method, very high-speed full-field cameras were used. In another method, streak cameras have provided a continuous record of the fringe pattern along a line on the model. Photographs of the fringe patterns may be recorded with ordinary cameras if a flash-type light source (about $2\text{-}\mu$ sec duration) is used. Some investigators have used a photomultiplier

in conjunction with a dynamic polariscope to record fringe changes electronically (ref. 23).

Low-temperature photoelastic studies.—A special cryostat was fabricated by a NASA contractor so that photoelastic measurements could be made at cryogenic temperatures. The cryostat incorporates a large glass Dewar, which permits visual observation to be made of the test specimen submerged in the cryogen. It can be assembled in a test machine, and the test specimen loaded mechanically through a self-reacting frame without introducing any loads in the glass Dewar. The cryostat was sealed at the junction of the glass Dewar and the vent line directed upward and away from the cryostat to minimize frosting of the outer surface of the Dewar during test (ref. 24).

Photoelastic strain gages.—PHOTO-STRESS* strain gages consist of a piece of photoelastic plastic with a reflective surface bonded to one side and a polarizing material bonded to the other. Each gage also includes a graduated scale. The gages have been manufactured under conditions of prestress that produce permanent color bands or fringes in the plastic. These fringes are always visible in the gage even when it is unstrained. In use, the gages are bonded to a test specimen; when the load is applied, the fringes in the gage shift position, the displacement being directly proportional to the magnitude of strain. In the case of the rosette gages, the separate magnitude and directions of the principal strains are directly indicated. The main limitation of these gages is that they do not perform accurately in areas of high strain gradients (ref. 14).

Sprayable photoelastic coatings.—Considerable emphasis has recently been placed on the development of sprayable coatings. It is desirable that such coatings consist of premixed components, and that they be useable in conventional paint-spray equipment. For large areas of coverage, a pot life of several hours is desired; however, a short cure time is desired when the material is sprayed. To accomplish this, ketimines have been utilized as a primary curing agent or hardener. Ketimines have a very low level of reactivity with the resin in

*Manufactured by Chapman Lab., Inc.

the absence of moisture; however, moisture converts the ketimines to a polyamine and a ketone. The ketone is released and the polyamine functions as a reactive cross-linking agent for the resin in the same manner as the conventional amine curing agents (ref. 15).

Infrared photoelastic studies.—The extension of photoelastic methods to spectral ranges other than the visible offers several interesting possibilities. These include a clearer understanding of the phenomenon of birefringence and its relationship to material structure and behavior, an increase in the number and types of useful photoelastic materials, and improved measurement of photoelastic-material behavior, including wavelength dependence. Although the principles of measurement and the interpretation of data are not dependent upon wavelength, several problems arise when nonvisible radiation is used in photoelastic investigations. Apparatus and experimental procedures have been developed for studies in which monochromatic radiation of wavelengths up to $2 \mu\text{m}$ is employed. It is believed that the basic techniques may be applied throughout an even broader spectrum; equipment is being developed for use with radiation in wavelengths of more than 2 micrometers. The most serious problem in instrumentation for infrared photoelasticity is the fact that the radiation is not visible. Observation and recording of data are accomplished by means of infrared photographs and point-sensing techniques in which a modulated infrared beam is used. An additional possibility for detecting infrared and ultraviolet photoelastic effects is afforded by closed-circuit television and video tape (ref. 25).

Lasers as light sources for photoelastic studies.—Lasers have a great potential in photoelasticity since they are extremely intense, very nearly monochromatic, highly collimated, and especially coherent. Short pulses attainable by certain lasers should be valuable for dynamic work (ref. 26).

RESISTANCE STRAIN GAGES

Historical Background

The basic operating principle of wire- and foil-resistance strain gages was noted as early

as 1856 when Lord Kelvin reported that certain metallic conductors when subjected to mechanical strain exhibited a corresponding change in electric resistance, but it was not used commercially for another seventy-five years. During the past twenty-five years, there have been numerous developments and improvements that have contributed to making the bonded-resistance strain gage into the precise, versatile, and reliable instrument which it is today. Outstanding among these developments are the following (ref. 27):

- (1) The use of a sensing element in the form of a very fine wire which can be cemented directly to the surface of a specimen and then forced by the cement to follow the strains of the specimen surface
- (2) Premounting the sensing element on a paper or plastic carrier to facilitate installation
- (3) Development of the foil gage
- (4) Development of the semiconductor gage.

Advantages and Disadvantages of Resistance Strain Gages

The resistance strain gage closely meets the criteria for an ideal strain-measuring method. Some of the advantages of the resistance strain gage are listed below (ref. 13).

- (1) They have been used to measure strains as low as a fraction of a millionth of an inch per inch and up to 23% on rubbers and plastics.
- (2) They have been used in temperatures from -458°F (liquid helium) to 2000°F .
- (3) They may be used submerged in water and have been used as long as a year and a half in sea water.
- (4) They have been used in hydrostatic environments at pressures above 50 000 psi.
- (5) They may be used from zero to over 50 000 Hz.
- (6) They may be used on almost all metals, concrete, cement, brick, bones, wood, rubber, and plastics, and have even been woven into fabrics.

Some disadvantages of strain gages are listed below.

- (1) The strain-resistance effect is not completely linear, especially at high elongations for

the wire type. Semiconductor strain gages are inherently nonlinear though compensations can be made in the ancillary electronic circuitry used.

(2) Low outputs from some of the gages require that the signal leads be well shielded from external fields.

(3) Resistance strain gages indicate the strain at points or small areas only, and do not indicate the strain gradient in the field.

Physical Principles of Resistance Strain Gages

When a metal is strained, its electrical resistivity is directly influenced by distortions in the atomic lattice. There is also another source of the resistance change when a wire becomes strained, which is associated with the geometry of the wire. This change occurs because the wire becomes longer and thinner as illustrated in figure 10-17. The basic relation between the electrical resistance of a conductor and the factors on which it depends is expressed by the equation:

$$R = \rho \left(\frac{L}{A} \right)$$

where R represents the resistance of the wire, ρ the resistivity of the material, L the original length of the wire, and A the cross-sectional area of the wire. The strain sensitivity factor for the wire, S , is defined by the relation:

$$S = \frac{\Delta R/R}{\epsilon} = \frac{\Delta R/R}{\Delta L/L}$$

and ϵ is the strain.

It can be shown from the above relation for R , and using Poisson's ratio, μ , that

$$S = 1 + 2\mu + \frac{\Delta \rho / \rho}{\Delta L / L}$$

The term $(1 + 2\mu)$ corresponds to the dimensional changes in length and cross-sectional area of the wire. These changes alone would make S equal to roughly 1.6, since for most metals μ is approximately equal to 0.3; however, experimental evidence shows that S lies between -12 and $+6$ so that, in general, the direct effect of

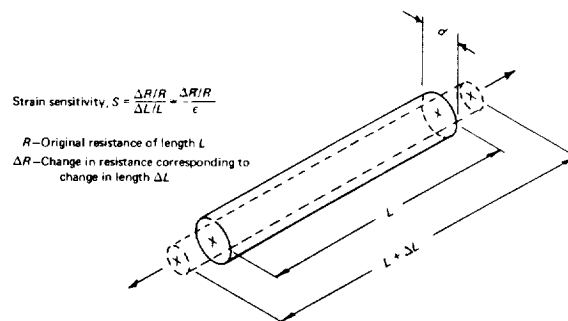


FIGURE 10-17.—Dimensional changes in a strained-cylindrical conductor.

strain on resistivity must be an important part of the strain sensitivity of the material.

The strain-sensitivity factor for a semiconductor gage can be written in a form similar to that for wire gages, namely, $S = 1 + 2\mu + M$ where M represents that part of S dependent upon changes other than those which are geometrical in nature. For germanium and silicon, μ lies between 0.3 and 0.6; in most commercially available semiconductor strain gages, S lies between 50 and 200 so that the factor M (which is related to the electric conductivity of the semiconductor material) is found to make by far the more important contribution to the strain sensitivity. The electric resistivity of semiconductor materials is inversely proportional to the product of the number of charge carriers and their average mobility. When the semiconductor material is strained, both the number of carriers and their average mobility change; the magnitude and the sign of the change are dependent upon the semiconductor material, its carrier concentration, and its crystallographic orientation with respect to the applied strain (ref. 28).

When a strain gage is constructed, its overall strain coefficient (gage factor), K , depends upon several factors, including:

- (1) Strain sensitivity of the sensing element material,
- (2) Geometry of the sensing element, and
- (3) Direction of strain relative to the gage axis.

Gage factor is an overall coefficient relating the change in resistance of the gage to strains ap-

plied along its axis only and is established by the manufacturer according to the relation :

$$K = \frac{\Delta R/R}{\epsilon_{axial}}$$

where R is the gage resistance, K is the gage factor, and ϵ_{axial} is the strain applied along the longitudinal axis of the gage (ref. 29).

For the resistance change of a gage under strain to be of value, a means must be available to detect and measure the amount of resistance change. Since ΔR is so small, conventional ohmmeters are not capable of measuring the change in resistance with sufficient precision. There are, however, several acceptable means available for measuring ΔR . By far the most widely employed circuit for use with all types of resistance strain gages is the Wheatstone bridge. As illustrated in figure 10-18, bridge circuits can be made using one to four strain gages, at least one of which is active, that is, it changes resistance with strain in the specimen (ref. 30). Such circuits in essence translate the resistance change of the gage into a corresponding voltage change. A well-regulated voltage is normally imposed across the two opposite corners of the Wheatstone bridge to energize it, and the bridge is then balanced, i.e., bridge resistors are adjusted so that output voltage is zero. A voltage change proportional to the product of the excitation voltage and the resistance changes of the strain gages will appear across the output terminals of the Wheatstone bridge. For conventional wire and foil gages, the signal level is on the order of millivolts. Semiconductor strain gages can produce signals up to several volts (ref. 28). Beginning with the bridge initially balanced, it can be shown from an analysis of the bridge circuit that

$$\Delta E \cong \epsilon \left(\frac{KV}{4} \right)$$

where ϵ is the strain in the gage and the remaining factors are those defined in figure 10-19. In a similar manner, it can be shown that if two or four arms of the bridge are made active, the output will be respectively two or four times that for a single gage, provided the signs of the strains are opposite in adjacent

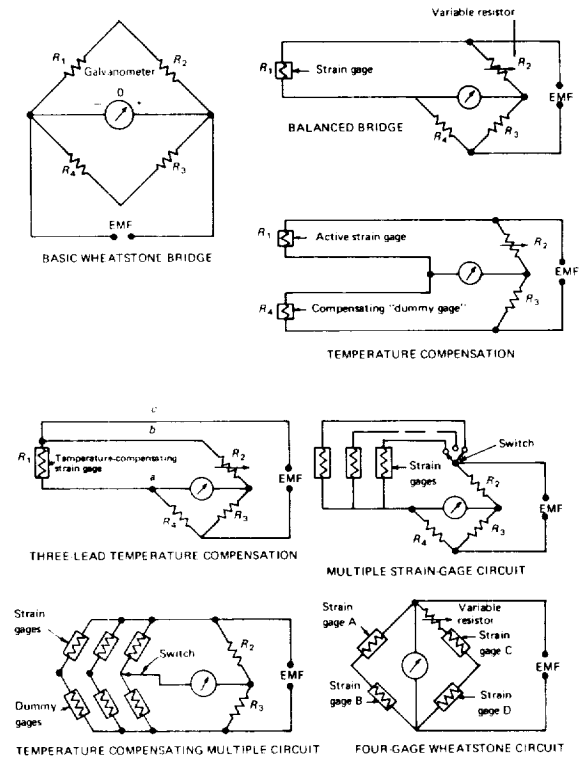


FIGURE 10-18.—Wheatstone bridge circuits for use with resistance strain gages. (Courtesy Product Engineering; copyright Product Engineering.)

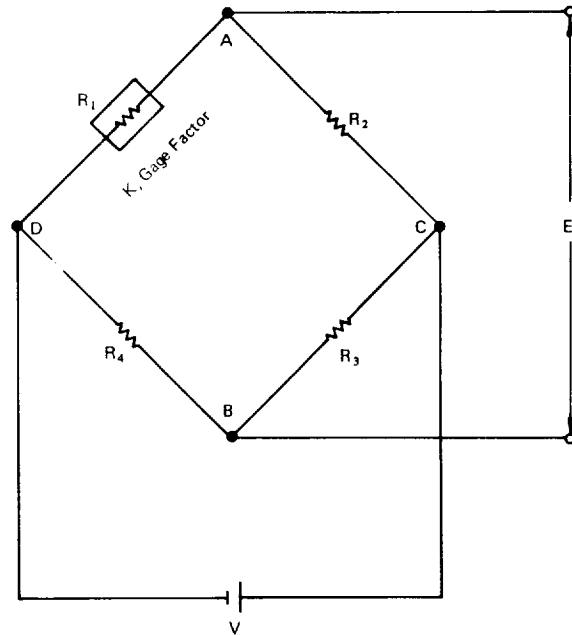


FIGURE 10-19.—Typical bridge circuit with single active gage.

bridge arms (ref. 3). That the resistance changes in the various arms of the bridge can be made to add or subtract is very useful. It is immediately evident that multiple-gage techniques offer the possibility of selecting gages and circuit configurations in which compensations can be made for such things as temperature-induced changes in gage resistance or gage factor. This is accomplished by using gages with opposing effects in the bridge so that their undesired effects cancel one another.

There is another circuit, the potentiometer circuit (fig. 10-20), which is commonly employed for making dynamic strain measurements. This circuit will respond to dynamic strains or the dynamic component of combined strains. The purpose of the coupling capacitor is to prevent the passage of any direct current. An analysis of the potentiometer circuit results in the following relation:

$$\Delta E = \epsilon KV \left(\frac{R_b R_g}{(R_b + R_g)^2} \right)$$

Signals from either of the circuits described can be amplified for display or recording, or the signal can be used to modulate a carrier wave which can be amplified (ac amplification) and then demodulated for display. The latter technique can be further instrumented to provide telemetering signals over large distances.

Typical Materials and Instrumentation

Resistance strain gages are perhaps the most useful instruments for strain measuring available at the present time. Their wide range of application is made possible through the production of gages in a broad range of sensitivities, sizes, and geometrical configurations (some of these details were indicated previously in table 10-1). Several designs have evolved in the production of strain gages, many of which are special-purpose or special-feature devices. The temperature-compensated gage composed of wires of two different materials whose temperature effects tend to cancel one another is an example of such a design. Another example is the weldable gage with a quick and rugged installation that will remain intact even when

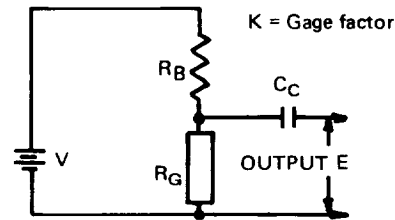


FIGURE 10-20.—Potentiometer circuit for sensing dynamic strain.

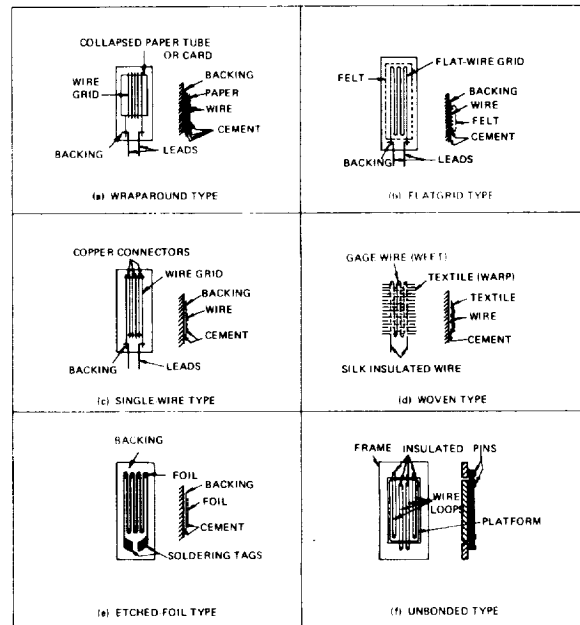


FIGURE 10-21.—Basic types of wire and foil strain gages. (Courtesy of MacMillan and Co., Ltd. and Strain Gauges and Uses, H. K. P. Neubert.)

exposed to severe environments (such as extremely high or low temperatures, severe vibrations, and some corrosive atmospheres). Some of these gages are shown in figure 10-21 (ref. 1). The high-sensitivity semiconductor strain gages are of the general construction illustrated in figure 10-22 (ref. 31).

A series of strain gages mounted adjacent to or overlapping each other are illustrated in figure 10-23 (refs. 29 and 32). These arrays of gages, called rosettes, have their axes oriented so that the strains indicated by each element of the rosette may be used collectively to calculate the magnitudes of the principal strains and their directions. For the general case of plane

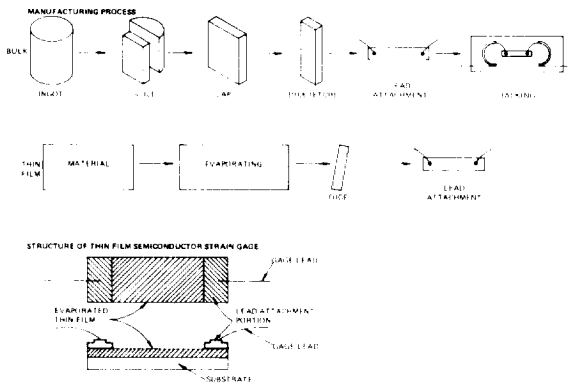


FIGURE 10-22.—Structure of semiconductor strain gages. (Courtesy Product Engineering; copyright Product Engineering.)

stress, it is necessary that strains be measured in at least three directions in order to find the principal strain magnitudes and directions. Strain rosettes, therefore, commonly consist of three gages. If a strain reading is obtained in a fourth direction, the value can be used to simplify the computations for principal strains or as a check on the accuracy of the results obtained from the other three gages. For the case in which the principal strain directions are known, two strain readings in these directions are sufficient for the determination of the principal strains (ref. 32).

For a convenient comparison of the relevant characteristics of wire and semiconductor gages, the major mechanical and electrical properties of two representative samples (a typical constantan-wire gage and a general-purpose *p*-silicon semiconductor gage) are listed in table 10-3 (ref. 1). The values quoted in the table are averages and do not represent any particular commercial product.

Wire or foil grids, as well as the semiconductor elements previously illustrated, are commonly attached by the manufacturer to a carrier or backing to make handling easier. Generally, the gage backing consists of a thin layer of a material such as resin-impregnated paper, sprayed epoxy, elastomer films, or a thin strip of metal. Gages with backings are attached to a specimen with adhesives, or, in some cases, by welding. Such bonding will transmit strains from the specimen, forcing the gages to follow these strains. Thermosetting, thermo-

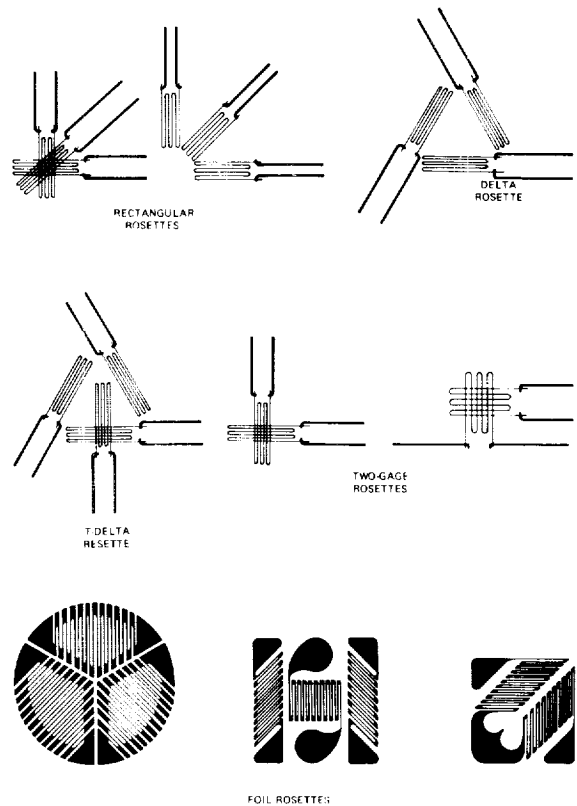


FIGURE 10-23.—Strain-gage rosette configurations. (Courtesy of Instrument Society of America and The Strain Gage Primer, Perry and Lissner; copyright 1962 by McGraw-Hill Book Co., Inc.; used with permission of McGraw-Hill Book Co., Inc.)

plastic, and ceramic cements have been used with strain gages. The approximate temperature ranges of application for the various bonding agents are (ref. 13):

- (1) Thermoplastic cements (room temperature to 130° F)
- (2) Thermosetting cements (elevated temperatures to 600° F)
- (3) Ceramic cements (high temperature to 1800° F)
- (4) Welding (high temperatures to 1800° F).

Each type of bonding medium has characteristics such as shearing strength, curing temperature, and curing time, which must be reviewed and evaluated for a specific application. The scope of this chapter does not allow a detailed examination of these cements, but special mention should be made of the acrylic-based ce-

TABLE 10-3.—Comparison of Typical Wire- and Semiconductor-Resistance Strain Gage Characteristics

	Units	Wire gage	Semiconductor gage
<i>A. Mechanical properties</i>			
Filament material.....		Constantan	<i>p</i> -silicon
Young's modulus.....	10^{10} N/m ²	16	—19
Poisson's ratio.....		0.33	0.18
Max. breaking strength.....	10^9 N/m ²	4.6	20
Min. radius of curvature.....	10^{-3} m	0.5	3
Max. strain.....	10^{-3} m/m	50	4
Max. elastic strain.....	10^{-3} m/m	1	4
Min. filament cross section.....	10^{-10} m ²	1	2
Min. gage length.....	10^{-3} m	2	2
Fatigue life at $e = \pm 10^{-3}$	cycles	$>10^7$	$>10^7$
<i>B. Electrical properties</i>			
Gage factor.....		2	120
Useful linear range (uncompensated).....	10^{-3} m/m	± 1 (50)	± 0.5 (—0.5 to +3)
Temperature coefficient of gage factor (uncompensated; constant-voltage operation).	$10^{-6}/^\circ\text{C}$	<1	—3500
Temperature coefficient of gage factor (uncompensated; constant-current operation).	$10^{-6}/^\circ\text{C}$	<1	—750
Useful temperature range (acceptable temperature stability).	$^\circ\text{C}$	—80 to +250	—40 to +100
Operational temperature range (stable gage bonding).	$^\circ\text{C}$	—80 to +250	—80 to +250
Resistivity.....	10^{-6} Ωm	0.45	200
Temperature coefficient of resistivity.....	$10^{-4}/^\circ\text{C}$	± 0.2	+10
Apparent strain on aluminum (uncompensated).	$10^{-3}/^\circ\text{C}$	0.015	2.6
Gage resistance.....	Ω	10^2 to 10^3	10^2 to 10^4
Normal gage current (on metals).....	10^{-3} A	20	20
<i>C. Miscellaneous</i>			
Ruggedness in handling.....		good	fair
Cost per gage.....	shilling	5 to 10	60 to 120

ments whose cure time is extremely short (1 to 5 min). These cements are useful in a broad range of applications at room temperatures up to 150° F, and have made the use of bonded strain gages much more attractive.

A number of considerations enter into the selection of the type of strain gages for any given strain measurement. The following list includes the major factors that must be considered in making such a selection:

- (1) Type of strain to be measured (static or dynamic)
- (2) Form of strain-indication record desired
- (3) Accuracy requirements

(4) Number of simultaneous strain measurements to be made

(5) Equipment and budget restrictions.

It is possible to arrive at the desired results by using any of several different instruments or a combination of instrument components. It will generally be necessary to make some compromise among the above factors, but instruments or components must be selected for compatibility. Each instrument has certain electric characteristics such as frequency response, input and output impedances, and voltage or current limitations. It is necessary for satisfactory results that each element involved in a com-

plete sequence have characteristics that properly match those of the associated elements in that sequence.

A block diagram of the essential components which together make up the most important strain-gage instrumentation systems in current use is presented in figure 10-24 (ref. 32). Apparatus for making strain measurements often can be used to perform more than one or even all of the functions indicated in the diagram.

Testing Procedures

The following discussion includes the general procedures for using electric-resistance strain gages. These procedures are merely indicative

of the steps typically required when making strain measurements with such gages.

Preparation of specimen.—The surface of a specimen to which a bonded-resistance strain gage is to be applied must be carefully prepared to provide for good adhesion between the specimen and gage in order that the strain in the specimen is reliably transmitted to the gage. All loose scale and oxides must be removed and the surface made smooth and even. A roughened surface such as that left by emery paper, grinding, or sand blasting is usually adequate. The surface is then thoroughly cleaned with a solvent degreaser.

Preparation of testing apparatus.—The preparation of testing apparatus for making a

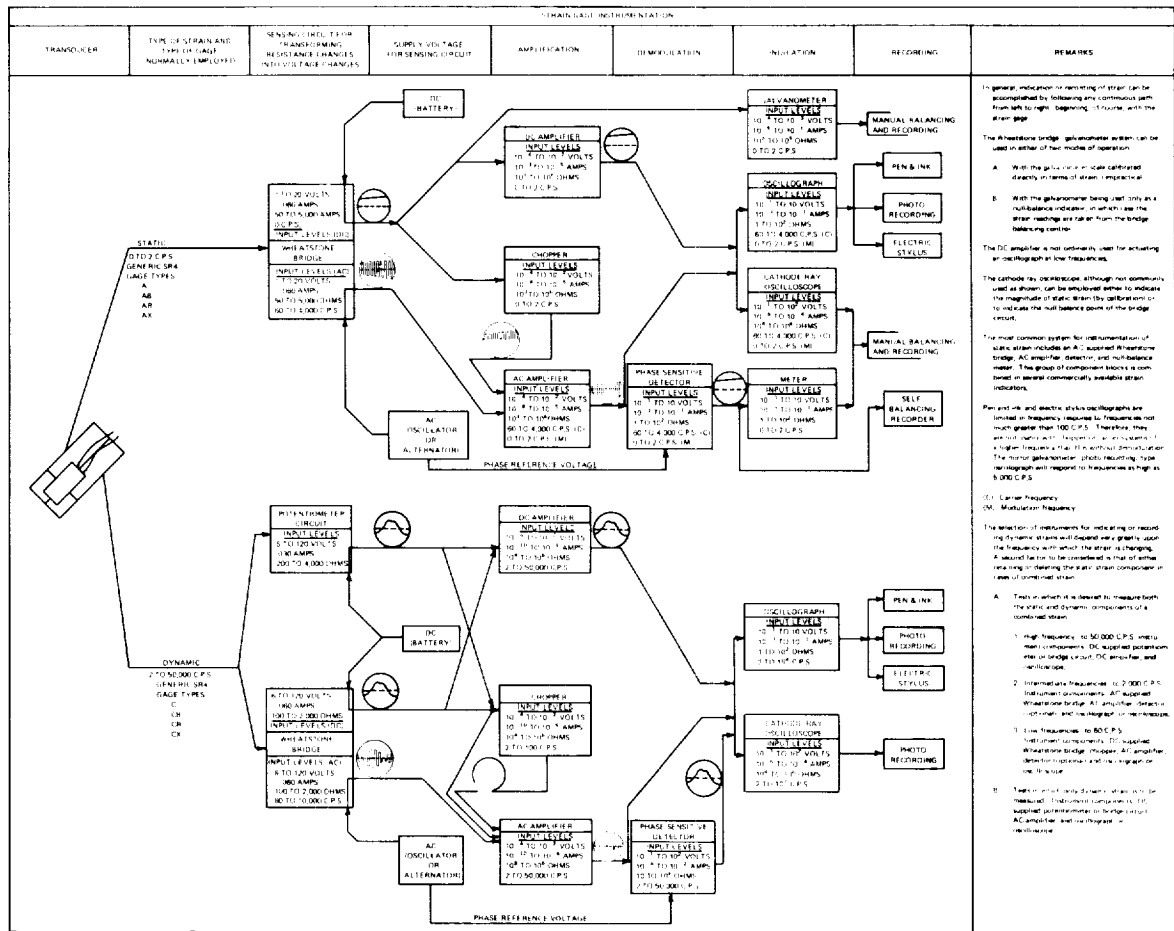


FIGURE 10-24.—Strain-gage instrumentation diagram. (Courtesy of Instrument Society of America and The Strain Gage Primer, Perry and Lissner; copyright 1962 by McGraw-Hill Book Co., Inc.; used with permission of McGraw-Hall Book Co., Inc.)

bonded resistance strain gage measurement may be summarized as follows:

- (1) Bond the gage to the specimen
- (2) Solder leads to the gage and provide strain relief for the leads
- (3) Moisture-proof the gage (cover gage and soldered connections with grease, wax, varnish, or a synthetic rubber compound to seal the gage and leads from moisture)
- (4) Calibrate all electronic instruments that are to be used in the measurement, following instructions provided by the manufacture.

Some of the tools and materials which are typically used in attaching a gage to a surface, using a cement, are shown in figure 10-25 (ref. 33).

Data acquisition.—Once the specimen and testing apparatus have been prepared normally only the application of a load is necessary to obtain a direct strain indication. As might be expected from the discussion on instrumentation, the details of this strain indication may be quite varied. In the simplest case of measuring a static strain with a single active gage, the measurement may consist simply of rebalancing the Wheatstone bridge after strain in the active gage has altered the initially balanced state of the bridge. The adjustments made to rebalance the bridge are recorded and used to calculate a value for the strain. At the other extreme are the multichannel systems consisting of tens or even hundreds of active strain gages from which signals are received and processed, and a printout of the strain values made by a digital computer. A particular advantage of almost all of these systems is that the indication can usually be made at a site remote from the specimen being tested. Telemetering strain indications over great distances may be accomplished by rather commonplace means, and this has been of vast usefulness in the space exploration program.

Interpretation of results.—Several effects that must be taken into account and either prevented or corrected for precise interpretations include: (1) the temperature dependence of strain gages, (2) the effects of poor bonding of a gage to the specimen surface, and (3) the effects of moisture.



FIGURE 10-25.—Tools and materials commonly used in making strain-gage attachments. (Courtesy of Union Carbide Corp., Oak Ridge Y-12 Plant.)

Temperature changes can cause an erroneous strain indication associated with: (1) the different thermal expansion of the strain gage and that of the material in the test specimen, (2) the thermal coefficient of resistivity for the strain-gage material, and (3) changes in the gage factor with temperature (ref. 13).

An indirect way in which temperature may affect strain indication lies in its effects upon cements that bond the gage to the specimen. At elevated temperatures, some cements soften and begin to creep and in doing so they do not always transmit the strain from the specimen to the gage. This effect would be particularly pronounced in dynamic strain measurements of high-frequency strains.

Moisture effects upon strain indications take the forms of: (1) absorption by the matrix or the adhesive causing a reduction in the resistance to ground, (2) absorption by the adhesive causing a reduction of mechanical strength in the bond layer, and (3) electrolysis of the conducting materials when a current is passed through the gage causing corrosion of leads or the gage filament (ref. 13). If such moisture effects are encountered, corrective action must be taken before meaningful data can be acquired.

As illustrated in figure 10-26, the resistance strain history of a bonded-wire resistance strain gage exhibits hysteresis and zero shift in the first few strain cycles (ref. 1). The major source

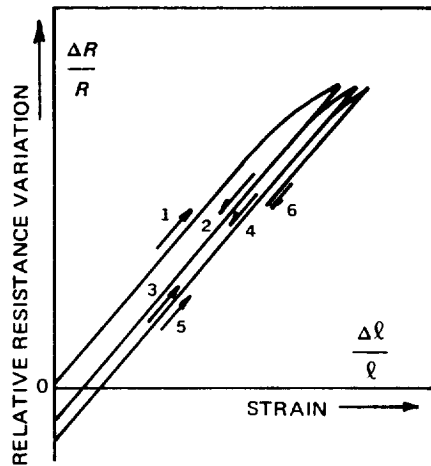


FIGURE 10-26.—Resistance vs strain history graph for a bonded-wire-resistance strain gage. (Courtesy of MacMillan and Co., Ltd. and Strain Gauges and Uses, H. K. P. Neubert.)

of this property lies in the bonding of the gage to the specimen. Residual stresses that remain in the bond when it is cured are relieved in the initial strain cycles; they depend on

- (1) the degree of cure of the bond
- (2) the gage length
- (3) the number of strain cycles applied
- (4) the direction of the preceding strain cycle (ref. 13).

The hysteresis and zero shift from commercially available gages is usually negligible; excessively high values of hysteresis found in practical tests are almost invariably due to imperfect bonding (ref. 1).

As was discussed in the theory, materials used to make strain gages are sensitive to transverse strains. Similarly, the gage factor of a strain gage is dependent to some degree upon the transverse strain experienced by the gage. This transverse sensitivity, which is largely dependent upon the geometry of the gage, can usually be obtained from the manufacturer's literature. If the gage is located in an area of high-transverse strain, this effect cannot be neglected when interpreting the indications from the gage.

Current State of the Art

Several applications of resistance strain

gages, special techniques, and recent developments that suggest the extensive utilization of resistance strain gages today are discussed below.

Strain gages used in building construction.—The Blair High School project, conducted jointly by the Jet Propulsion Lab. and the California Institute of Technology under the overall supervision of the architectural firm Neptune and Thomas Associates, is an example of the transfer of NASA generated technology to a nonaerospace operation. This project entails transferring to the structural engineering field an instrumentation approach that was initially developed for the testing of space vehicles. The objective of this project was to assess (1) the static characteristics of the planned high school building structural frame by quantitatively determining the response of the structure to such steady loading factors as its own weight; and (2) the dynamic characteristics of the structure and its response and resistance to earthquakes. It is the instrumentation concept, itself, that is of primary importance in the potential technology transfer; and, in particular, it is the JPL strain gage data processing and analysis routine that constitutes a significant advancement. Strain gage outputs are scanned continuously and are acquired by a multichannel recorder while the structure is being loaded. The analog data are digitized and then fed into a computer using the JPL-developed computer routine to make a thorough analysis in a manner not previously employed in architectural design. The computer program developed specifically for this instrumentation system uses the taped data to match and compare the outputs of the various strain-gage readings. A more thorough evaluation is accomplished by the new technique, using one installation of gages, than can be accomplished by the traditional technique of making repeated changes in connections to the gages (ref. 34).

Device for measuring coefficient of static friction.—A NASA-developed device that can accurately measure the coefficient of static friction of magnetic tape by using a strain gage to measure the force of friction between a reference surface and the tape drawn over that surface at a

constant velocity is illustrated in figure 10-27 (ref. 35). The device is mounted so that the test surfaces are enclosed in an environmental chamber. A sample of tape to be tested is clamped at its upper end to a cantilever spring containing a strain gage. The base of the cantilever spring is mounted on the drive block of a motor-driven lead-screw mechanism. The tape with the precision weight secured to its lower end is suspended over a rounded face block made of any desired metal. For testing the tape against other materials, a cap made of the desired material can be placed over the metal block and held in position as the tape is drawn over it (ref. 35).

Measurement of plant leaf movements.—Dr. T. Hoshizaki of the University of California and Dr. K. Yokoyama of NASA-Ames Research Center have used strain gages to measure leaf movements (fig. 10-28) (ref. 36). Strain gages bonded directly to the leaf of a plant are used to measure leaf movements in experiments testing the effects of light and dark cycles on the leaf movements of pinto beans, apparently causing little adverse effect to the plant.

Uniaxial stress transducer for internal measurements.—A NASA-developed miniature transducer for measuring stress, which employs a semiconductive piezoresistive element that is stress sensitive along a specific axis only, is shown in figure 10-29 (ref. 37). A semiconductor transducer is fashioned from a *p*-silicon splinter embedded in a high-density, polyethylene cylinder. The silicon splinter is grown in a selected crystallographic orientation so as to be favorably piezoresistive along that axis. The mechanism of measurement is based on the compressive deformation of the transducer as a

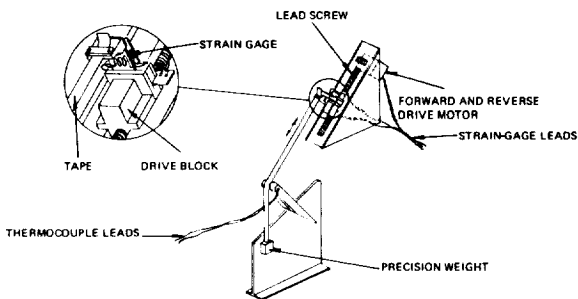


FIGURE 10-27.—Device for measuring static friction of magnetic tapes.

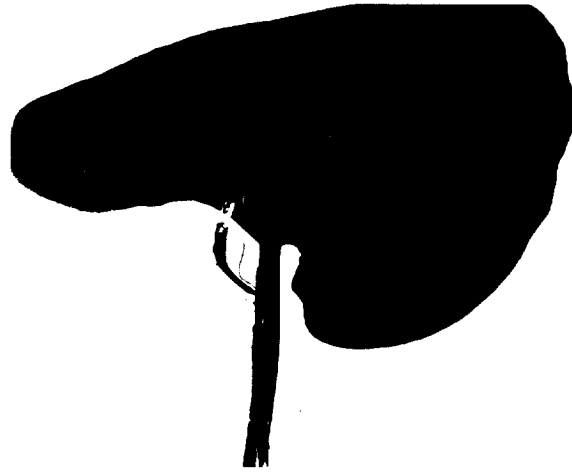


FIGURE 10-28.—Strain gage mounted on leaf of a pinto bean. (Courtesy of Dr. T. Hoshizaki, University of California and Dr. K. Yokoyama, NASA-Ames Research Center.)

whole. Loading of the transducer cylinder along the selective axis of the piezoresistor changes the resistance of the silicon splinter in direct relation to the amount of stress applied. Various deformation sensitivities are possible by using cylinders of differing Young modulus values. Such transducers may be implanted within a mass to measure internal stresses (ref. 37).

Tunnel diode strain gages.—The tunnel diode is an active device with a characteristic curve at constant strain and temperature (fig. 10-30) (ref. 38). A portion of the characteristic curve in region I is of interest here. If a uniaxial strain is applied in the plane of a tunneling junction, the effect is a shift in the current-voltage characteristic along the current axis. The effect is most pronounced in the vicinity of the peak-tunneling curves. For maximum sensitivity, the voltage bias for the diode is important. Biasing the diode slightly beyond the peak current into the negative-resistance region produces an enhancement of the sensitivity to both tension and compression. The tunnel diode can be employed as a linear strain gage in a bridge configuration similar to that used for conventional piezoresistive semiconductor- or wire-resistance strain gages. The advantage of the tunnel diode is its higher resolution (ability to detect lower strain levels), although its maximum output is comparable to that of the wire

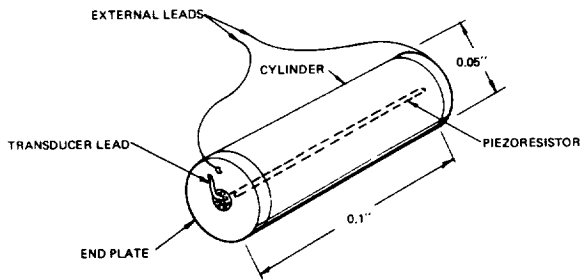


FIGURE 10-29.—Miniature uniaxial transducer for measuring internal stresses.

gage and requires external amplification. Tunnel diodes can also be employed as strain-modulated oscillators. The serious drawback of the strain-sensitive oscillator is the fact that the parameters that allow the oscillator to be strain sensitive are the parameters that are susceptible to temperature and bias variation (refs. 38 and 39).

Fatigue-life gages.—A fatigue-life gage, called the *S/N gage*, is a special strain gage to aid in assessing incipient fatigue failure in critical structural members. When bonded to a test specimen, it accumulates a change in electric resistance as it undergoes successive strain cycles. This resistance change is attributed to strain hardening of the grid material. Since the amount of strain hardening is dependent on the magnitude of strain and the number of strain cycles, the fatigue gage in essence records the strain history of the material on which it is mounted. A correlation is then attempted between resistance change of the gage and the amount of fatigue damage experienced by the material (ref. 40). The resistance change in the gage is permanent and irreversible; consequently, a continuous connection to electronic circuitry such as recorders and other instrumentation is not required. The fatigue history experienced by the gage can be monitored at will simply by measuring the gage resistance in the normal way. The total resistance change may be over 10%, which is many times larger than the full-scale resistance change produced by straining a gage under normal structural-loading conditions (ref. 31).

Strain-sensitive junction on the apex of a needle.—A novel design developed under a

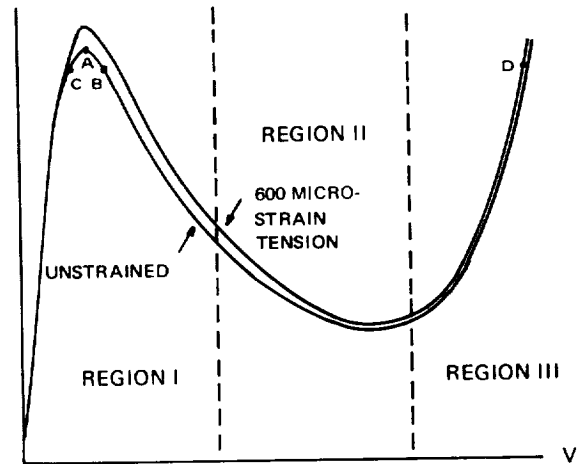


FIGURE 10-30.—Tunnel diode characteristic current vs voltage curve. (Courtesy of Instrument Society of America and The Strain Gage Primer, Perry and Lissner; copyright 1962 by McGraw-Hill Book Co., Inc.; used with permission of McGraw-Hill Book Co., Inc.)

NASA-sponsored project consists of a *p-n junction* (fabricated from a semiconductor material) made on the apex of a needle. This can be forced against a conductive surface so that the transmitted force proceeds to change the electrical characteristics of the *p-n junction*. The change is proportional to the applied force and can be measured with suitable electronic means. The device can be used to fabricate force sensors, strain sensors, and displacement sensors (ref. 41).

Physiologically implantable telemetering system used with strain gages.—Under a NASA contract, Case Western Reserve University developed multichannel, physiologically implantable telemetering systems for biological measurements. The design is flexible, allowing several channels of information to be handled simultaneously, and can telemeter a wide range of physiological signals, including strain gage measurements. An improved transmitter oscillator was developed using silicon-controlled switches as the memory elements. This circuitry allowed two oscillator stages to be wired in one flat pack thereby increasing the packing density for the completed transmitter. A 4-channel strain-gage transmitter was constructed and tested using the new oscillator stages and im-

stallation is immersed in liquid hydrogen, the outer protective layer of silicone lacquer may develop cracks, which destroy its waterproofing characteristics. Therefore, when the gage is to be used for strain measurements in water and in liquid hydrogen, the measurements in water must take precedence (ref. 45).

Temperature compensation by electron irradiation.—Beneficial radiation effects on semiconductor strain gages have been reported at the NASA-Langley Research Center. The temperature coefficients of resistance and gage factor of some *n*-type and *p*-type silicon strain gages are readily reduced by exposing them to high-energy electron radiation. The semiconductor strain gages are placed in the homogeneous beam of electrons whose energies are between 1 and 3 MeV and are irradiated until their temperature coefficients of resistance at room temperature are reduced to zero. This method of reducing the temperature coefficients yields the best results for *n*-type silicon gages whose resistivity is between 0.05 and 1.0 ohm-cm, and for *p*-type silicon gages whose resistivity is between 5.0 and 10.0 ohm-cm. After irradiation, the gages are heated to 175° C for a 24-hr period to stabilize their temperature coefficients (ref. 46 and private correspondence with JPL).

Use of strain gages in radiation environments.—As the application of strain gages has branched into new fields, the importance of the various radiation effects to strain-gage indications has been made evident. Studies by the Atomic Energy Commission reveal that transient radiation can produce extraneous signals in strain gages by several methods (ref. 47).

(1) Spurious currents are produced by secondary electron absorption in and ejection from conductors.

(2) Changes in the resistance of insulation materials, the strain-gage elements, and lead conductors are caused by gamma heating and radiation-induced changes in the free-charge carrier densities of the material.

(3) Thermal strains are produced by gamma heating of the various components used in the construction of the transducer.

From the results of in-pile applications of re-

sistance strain gages, the following conclusions can be made (ref. 48).

(1) Resistance strain gages are a possible means for in-pile strain measurements.

(2) Weldable strain gages of the coaxial type are very promising for such applications.

(3) Normal compensation techniques are also efficient for radiation-induced parasitic effects.

REFERENCES

1. NEUBERT, H. K. P.: Strain Gauges Kinds and Uses. MacMillan and Co., Ltd., (London) and St. Martin's Press (New York), 1967.
2. POPOV, E. P.: Mechanics of Materials, Prentice-Hall, Inc., 1952.
3. HETENYI, M.: Handbook of Experimental Stress Analysis. John Wiley & Sons, Inc., 1950.
4. VAUGHAN, D. A.; AND CRITES, N. A.: Measurement of Stress by X-Ray Diffraction. Product Engineering, Sept. 30, 1963, pp. 43-50.
5. CRITES, N. A.: Which Type of Stress-Analysis Method? Product Engineering, Oct. 16, 1961, pp. 90-96.
6. CRITES, N. A.: For Stress Analysis Brittle-Coating Methods. Product Engineering, Nov. 27, 1961, pp. 63-72.
7. ANON: Principles of Stresscoat, a Manual for Use with Brittle Coating Stress-Analysis Method. Magnaflux Corp., Chicago, Ill., 1967.
8. SCHMITZ, G.; AND FRANK, L.: Nondestructive Testing for Evaluation of Strength of Bonded Material. NASA CR-67983, 1965.
9. GERBERICH, W.: Stress Distribution about a Slowly Growing Crack Determined by the Photoelastic Coating Method. Rept. 32-208 (NAS 7-100), Jet Propulsion Lab., Calif. Inst. of Technology.
10. FROCHT, M. M.: Photoelasticity. Vol. I. John Wiley & Sons, Inc., 1941.
11. DUFFY, J.: Effects of the Thickness of Birefringent Coatings. Experimental Mechanics, vol. I, no. 3, 1961, pp. 74-82.
12. CRITES, N. A.; GROVER, H.; and HUNTER, A. R.: Experimental Stress Analysis by Photoelastic Techniques. Product Engineering, Sept. 3, 1962, pp. 57-69.
13. ANON: Photostress—Photoelastic Stress Analysis Products. Catalog 18-3000, Materials Evaluation Group, Automation Industries, Inc., Phoenixville, Pa., 1969.
14. MCMASTER, R. C.: Nondestructive Testing Handbook, Vol. II. The Ronald Press Co., 1959.
15. MCGEE, W. M.: Final Engineering Report 8379, Birefringent Coatings for Nondestructive Testing of Honeycomb Sandwich Structures. NASA CR-77759, 1966.

16. ZANDMAN, F.; REDNER, S. S.; AND REIGNER, E. I.: Reinforcing Effect of Birefringent Coatings. *Experimental Mechanics*, vol. 2, no. 2, 1962, pp. 55-64.
17. ZANDMAN, F.; REDNER, S. S.; AND POST, D.: Photoelastic-Coating Analysis in Thermal Fields. *Experimental Mechanics*, vol. 3, no. 9, 1963, pp. 215-221.
18. POST, D.; AND ZANDMAN, F.: Accuracy of Birefringent-Coating Method for Coatings of Arbitrary Thickness. *Experimental Mechanics*, vol. 1, no. 1, 1961, pp. 21-32.
19. LEE, T. C.; MYLONAS, C.; AND DUFFY, J.: Thickness Effects in Birefringent Coatings with Radial Symmetry. *Experimental Mechanics*, vol. 1, no. 10, 1961, pp. 134-141.
20. BEAL, J. B.: New Testing and Inspection Techniques. Paper presented at the Technology Utilization Conference, Berry College (Rome, Ga.), June 9, 1967.
21. DURELLI, A. J.: Recent Advances in the Application of Photoelasticity in the Missile Industry. School of Engineering and Architecture, The Catholic Univ. of America, Oct. 1962.
22. SAN MIGUEL, A.; AND SILVER, R. H.: A Normal-Incidence Reflective Polaroscope for Viscoelasticity Measurements. *Experimental Mechanics*, vol. 5, no. 10, 1965, pp. 345-352.
23. DALLY, J. W.; RILEY, W. F.; AND DURELLI, A. J.: A Photoelastic Approach to Transient Stress Problems Employing Low-Modulus Materials. *J. of Applied Mechanics*, Dec. 1959, pp. 613-620.
24. FEHER, S.: Research Study of Common Bulkhead and Manufacturing Technology Improvement Program for Saturn Stages. NASA CR-85369, 1967.
25. CLOUD, G. L.; AND PINDER, J. T.: Techniques in Infrared Photoelasticity. *Experimental Mechanics*, May 1968, pp. 193-201.
26. TAYLOR, C. E.; BOWMAN, C. E.; NORTH, W. P.; AND SWINSON, W. F.: Applications of Lasers to Photoelasticity. Department of Theoretical and Applied Mechanics, Univ. of Illinois, Mar. 1965.
27. MURRAY, Dr. W. M.: What are Strain Gages—What Can They Do? *ISA Journal*, vol. 9, no. 1, 1962, pp. 30-36.
28. ANON: Semiconductor Strain Gages. Bulletin KSG-5, Kulite-Bytrex Corp., Newton, Mass.
29. MURRAY, Dr. W. M.: Strain Gage Types and Basic Circuits. *ISA Journal*, vol. 9, no. 2, 1962, pp. 47-51.
30. CRITES, N. A.: Equipment and Application—Today's Strain Gages. *Product Engineering*, Mar. 19, 1962, pp. 85-93.
31. CHIRONIS, N. P.: Changes in Strain Gages. *Product Engineering*, Dec. 6, 1965, pp. 83-88.
32. PERRY, C. C.; AND LISSNER, H. R.: The Strain Gage Primer. McGraw-Hill Book Co., Inc., 1955.
33. MUZZALL, C. E.: Compendium of Gas Autoclave Engineering Studies. Union Carbide Corp., Oak Ridge, Tenn., Nov. 2, 1964.
34. KASTEL, D.: Stress Measurements on Blair High School Gymnasium: A Demonstration of Space Technology Transfer. NASA CR-68996, 1965.
35. ANON: Device Measures Static Friction of Magnetic Tape. NASA Tech Brief 67-10586, 1967.
36. HOSHIZAKI, Dr. T.; AND YOKOYAMA, Dr. K.: Recording Leaf Movements with a Strain Gauge. NASA CR-59801, 1964.
37. ANON: Miniature Stress Transducer Has Directional Capability. NASA Tech Brief 65-10023, 1965.
38. KIGGINS, T. R.; AND MILNES, A. G.: A Solid-State Tunnel-Diode Strain Gage. *Trans. ISA*, vol. 3, no. 3, 1964, pp. 229-237.
39. RINDNER, W., GARFEIN, A., PITTELLI, E., AND IANNINI, A.: A Miniature Electromechanical Tunnel-Diode Transducer. NASA-Electronics Research Center, Cambridge, Mass., TN C-87, July 1969.
40. HARBERT, J. D. AND STEPHENS, R. I.: S/N Fatigue Gage Response to Cumulative Damage. Proc. of the 7th Symposium on Nondestructive Evaluation of Components and Materials in Aerospace, Weapons Systems and Nuclear Applications. Sponsored by South Tex. Section. Am. Soc. for Nondestructive Testing, Inc. and Southwest Research Inst., Apr. 23-25, 1969. (Available from Western Periodicals Co., Hollywood, Calif.)
41. WORTMAN, J. J. AND STOCKARD, R. R.: Semiconductor p-n Junction Stress and Strain Sensor. Research Triangle Inst., NASA-Case XLA-4980, Mar. 11, 1969.
42. KO, W. H., YON, E., AND RAMSETH, D.: System Design and Fabrication Technique for Multi-channel, Physiologically Implantable, Telemetering Systems for Biological Measurements. NASA CR-100920, 1969.
43. ANON: Strain Gage Network Distinguishes Between Thermal and Mechanical Deformations. NASA Tech Brief 66-10280, 1966.
44. ANON: Forming Blocks Speed Production of Strain Gage Grids. NASA Tech Brief 65-10009, 1965.
45. ANON: Coating Permits Use of Strain Gage in Water and Liquid Hydrogen. NASA Tech Brief 66-10192, 1966.
46. ANON: Radiation Used to Temperature Compensate Semiconductor Strain Gages. NASA Tech Brief 66-10186, 1966.
47. TERRY, F. D., KINDRED, R. L., AND ANDERSON, S. D.: Transient Nuclear Radiation Effects on Transducer Devices and Electrical Cables. Phillips Petroleum Company, Idaho Falls, ID., Nov. 1965.
48. WELTEVREDEN, P.: In-Pile Application of Strain Gauges—Preliminary Results. Joint Nuclear Research Center, Ispra Establishment, Italy, 1966. (N66-28099)

|

PRECEDING PAGE BLANK NOT FILLED

CHAPTER 11

Developmental Methods

C. Gerald Gardner

This chapter includes brief accounts of three nondestructive evaluation methods that have been introduced within the past few years: (1) acoustic emission, (2) the use of coherent (laser) light, and (3) ultrasonic holography. The fact that these methods are already being used with available commercial apparatus indicates the rapid pace at which NDE is progressing. While these methods have played no significant role in NASA reliability and quality assurance programs to date, they are being studied for future applications. There is little doubt that by the time the space shuttle becomes a reality, these methods will have been standardized.

ACOUSTIC EMISSION

When a metal is deformed, various internal processes result in the generation of elastic stress waves. At the microscopic level, the formation and movement of dislocations generates stress waves of low amplitude; at the macroscopic level, the propagation of cracks generates stress waves of much larger amplitude. These waves consist of more or less sharply defined discrete pulses that propagate outward from localized sources. Such a pulse is a superposition of sinusoidal components, the individual frequencies of which cover a broad range from es-

entially zero Hz to many MHz. The process of generation and propagation of these stress waves is called acoustic emission, despite the fact that in most practical cases only the ultrasonic components are detected. The prospect of "listening" to acoustic emission with appropriate instrumentation and thereby nondestructively characterizing a specimen is apparent. Although of significant interest from a fundamental point of view, the detection of low-level acoustic emission associated with individual dislocation processes is at present useful only under controlled laboratory conditions. On the other hand, the detection of acoustic emission from a propagating macroscopic crack has proved to be practical. Instrumentation for this purpose, of varying degrees of sophistication and complexity, is commercially available from a few firms. In addition, some firms provide, on a contract basis, field service units of the most complex type.

Figure 11-1 is a diagram of the usual components in a simple, single-channel acoustic emission monitoring system. Various types of sensors are in use, essentially all of which are based on piezoelectric materials. The differences among these are in natural frequency, bandwidth (produced by damping, at the expense of sensitivity), and vibratory mode (longitudinal or shear). It is important to recognize that the

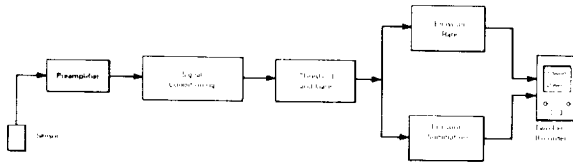


FIGURE 11-1.—Elementary single-channel acoustic emission monitoring system.

output signal from such a transducer is not in general a precise reproduction of the elastic stress wave impinging upon it. When affected by a stress-wave packet of short duration, a high- Q (narrow bandwidth) detector is simply shocked into vibration at its natural frequency, and thereafter “rings down,” the damping time being inversely related to Q . A damped, low- Q detector, while less sensitive, produces an output that is a more precise analogue of the stress wave. Piezoelectric accelerometers have been used as acoustic emission detectors in the low to intermediate frequency range. The bandwidth and transfer function of the amplifiers and the filters used also affect the signal finally observed. A high-gain, low-noise, wide-band preamplifier properly matched to the transducer is especially important if the spectral properties of the acoustic emission are of interest.

At present, most acoustic emission monitoring systems are based on the simplest possible signal processing, i.e., merely registering the arrival of a discrete stress-wave packet. Systems differ in ability to distinguish the arrival of a new packet from a variation in amplitude of a single packet of complex shape.

It has been experimentally demonstrated that the rate of emission of stress-wave pulses, as detected by acoustic emission monitors, increases with the rate of growth of a macroscopic crack in a variety of materials. Hence, one application of acoustic emission monitoring is the surveillance of structures subject to possible catastrophic fracture, important examples of which are pressure vessels and airframes.

Another application of acoustic emission monitoring is the location of propagating cracks by detecting a stress-wave pulse with an array of two or more transducers. By measuring the differences in times of arrival of the stress wave

at each of the transducers, the source may be located geometrically by triangulation. Rather elaborate systems employing many transducers and a digital computer programmed to perform the triangulation calculations on structures of considerable complexity (e.g., intersecting cylinders) have been developed. A diagram of such a system is shown in figure 11-2. Major applications to date have been on large storage tanks and on nuclear reactor pressure vessels during proof tests.

Further effort is being devoted to (1) the development of better transducers, coupling methods, and signal analysis, (2) studying the effect of material properties and specimen geometry on the propagating stress wave, and (3) the correlation of the rate of emission and other signal characteristics with the flaw type, size, rate of propagation, and the like.

NASA Contributions

The potential of acoustic emission monitoring for surveillance of rocket motor cases during pressure testing has been investigated by a NASA contractor. The contractor concluded that a “critical stress-wave signature” was present, the detection of which would indicate imminent failure in sufficient time to permit reduction of the pressure and thus prevent catastrophic destruction of defective motor cases (ref. 1).

In a further investigation by the same contractor, the correlation of stress-wave-emission

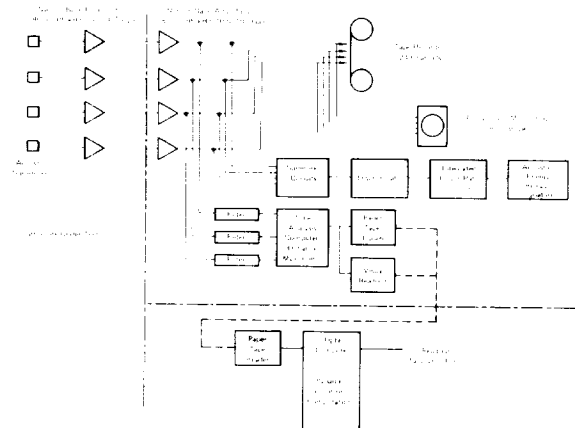


FIGURE 11-2.—Multichannel acoustic emission monitoring and flaw-location system.

characteristics with fracture in aluminum alloys was studied, in which standard laboratory, precracked, flat tensile specimens were used. Typical results obtained are shown in figures 11-3 and 11-4 (ref. 1). The cumulative stress-wave-emission count and the crack length of the test specimen as functions of the applied tensile load for the representative single-edge-notch specimen of 2014-T651 aluminum are illustrated in figure 11-3. Figure 11-4 contains a graph of stress-wave-emission rate, accumulated stress-wave emission, and crack opening displacement (COD), versus applied load, for a specimen of the same alloy having a part-through crack. From this and similar data, the contractor determined that stress-wave emission accompanying crack growth could be used as a precursor to the onset of a critical stress-intensity failure condition, although substantial differences in stress-wave-emission characteristics were found among different aluminum alloys tested (refs. 2 and 3).

COHERENT LIGHT METHODS

A number of related NDE methods based on the coherence of laser light are being developed. The most important of these thus far are holographic interferometry and multifrequency contouring. Optical correlation and laser speckle effects are still essentially confined to the laboratory. All of these methods are based on the idea of sensing more or less subtle features of the surface of a specimen. If a flaw or damage mechanism does not (or cannot non-destructively be made to) alter the shape of the surface of the specimen, coherent light methods are inapplicable (excluding the case of transparent materials). Holographic interferometry provides a means of comparing an object either with a holographically recorded image of itself, or with that of another closely similar object, thus making evident regions where the shapes differ. Multifrequency contouring provides a means of making a "relief map" of the surface of an object, with the capability of making evident very minute relief features. Optical correlation provides a means of comparing a surface with a holographic record of the same surface at

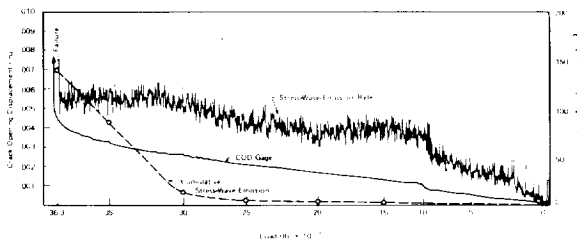


FIGURE 11-3.—Stress-wave emission rate and cumulative count, and crack opening displacement for 2014-T651 aluminum.

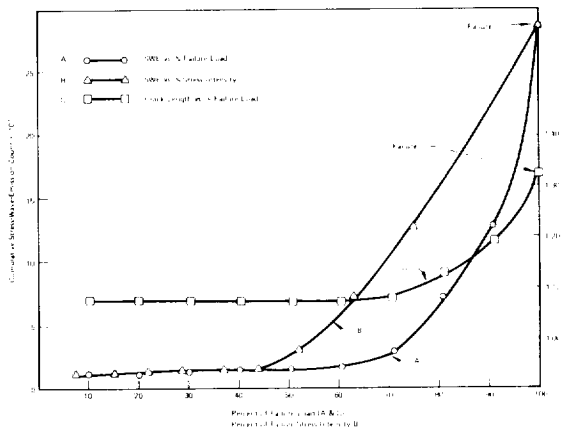


FIGURE 11-4.—Cumulative stress-wave emission count and crack lengths vs % failure stress intensity and load for 2014-T651 aluminum.

a previous time, the comparison being on the microscopic scale of crystalline dislocation features; in the method presently employed an electronic signal is produced; its amplitude is proportional to the degree of similarity (i.e., correlation). Speckle effects provide much the same sort of information as optical correlation but require only an ordinary photograph of the laser-illuminated surface rather than a hologram of it.

Holographic Interferometry

A hologram is a photographic* recording of the interference pattern created in the photographic emulsion by two beams of light, one of which is reflected by a particular subject, and

*Media other than photographic emulsions are being explored, but are not in common use.

the other of which is a reference beam. The basic arrangements for recording and reconstructing a hologram are shown in figure 11-5a and 11-5b. When the exposed photographic plate is developed the resultant image of the interference pattern is essentially a somewhat complicated transmission grating that can diffract a transmitted beam of light. If the hologram is illuminated by the original reference beam used in making it, that beam is so diffracted that the light diffracted on either side of the directly transmitted ("zero order") beam has wavefronts corresponding precisely to the wavefronts originally emanating from the subject. The eye (or a lens) sees these reconstructed wave fronts as images of the original subject. One of the images is "virtual," that is, it appears to be behind the hologram in the location of the original object; the other is "real," that is, it appears in front of the hologram and can be displayed on a screen or viewed as a "space image." Only the virtual image is used in holographic interferometry. Since the holographically reconstructed wave fronts that produce the images have all the features of the wave fronts that originally emanated from the object, the images are truly three-dimensional; when viewed by the eye such an image has the appearance of depth and parallax.

Holographic interferometry is accomplished by replacing the developed hologram in its original position with respect to the object, the reference beam, and the illumination beam. Under conditions of precise repositioning, the virtual image of the object spatially overlaps the object itself, and, to the eye or camera, appears to merge with it. If, however, the object itself has changed dimensionally, a ray radiating from a point on the illuminated object, and passing through the hologram directly to the eye or camera, will in general differ in path length from that of the corresponding ray from the virtual image of the object. Because of this difference in path length, a corresponding phase difference exists, and an interference fringe pattern occurs. The observed fringe pattern can be analyzed to yield the deformation of the object with respect to its original form at the time its hologram was made.

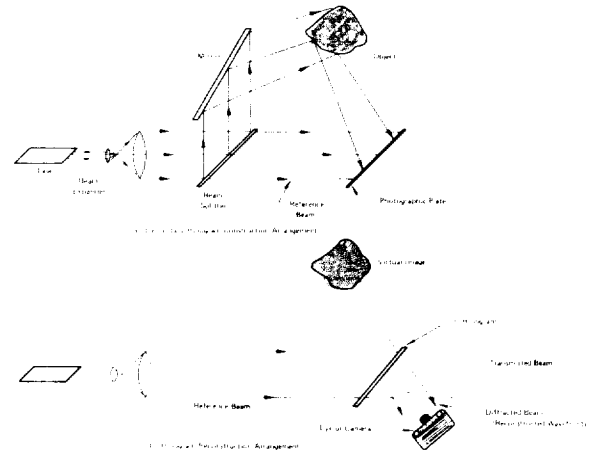


FIGURE 11-5.—Basic arrangements for recording and reconstructing a hologram.

As described above, the interference fringe pattern can be observed or photographed in real time; thus this method lends itself to the study of deformations induced by applied mechanical loads or by thermal stressing. An alternate method (called the double-exposure method) is to record on a photographic plate the hologram of the object in its reference condition, and subsequently record in the same (undeveloped) plate the hologram of the deformed object (being careful to preserve the arrangement of object, light beams, and photographic plate). When developed and illuminated with the reference beam (this time with the actual object removed), the reconstruction contains the superimposed images of the object in the two conditions to be compared, and an interference fringe pattern is also constructed.

Figure 11-6a is a photograph of a real-time holographic interferogram of a portion of the inner surface of an automobile tire. The larger contours are not indicative of flaws; however, the chain of small, fine contours is indicative of localized ply separations. Figure 11-6b is a photograph of a section through the same tire showing the actual ply separations nondestructively indicated in figure 11-6a.

Real-time holographic interferometry is being used, on an experimental basis, to detect flaws in pneumatic tires, disbanded regions in honeycomb composite structures, and the like. It is also being investigated as an approach to com-

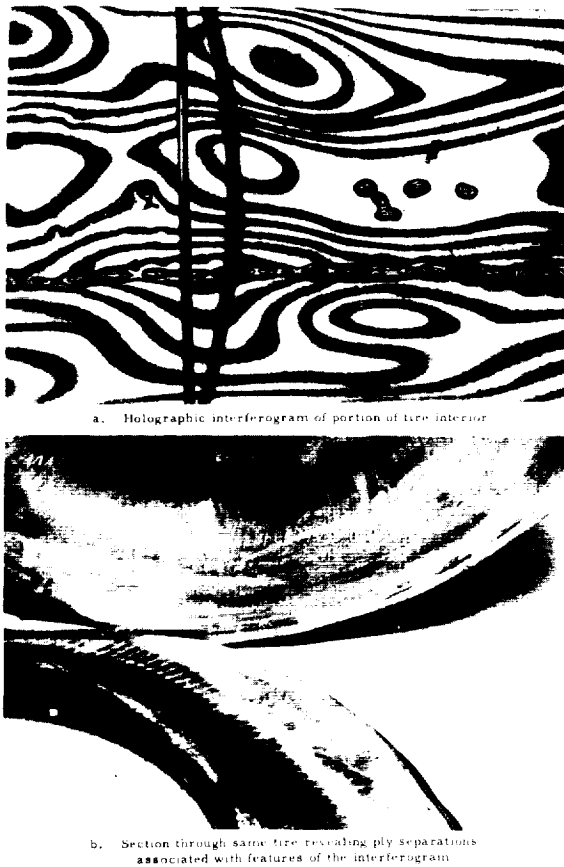


FIGURE 11-6.—Tire flaws detected by holographic interferometry. (Courtesy of GCO, Inc.)

pare the shape of production line items of precision shape with a holographically recorded “master template.”

Holographic Vibration Analysis

If a time-exposure hologram is made of an object undergoing cyclic vibration, the resultant time-averaged hologram, when reconstructed, shows a time-averaged fringe pattern that defines the vibrational modes of the surface and their nodal regions. This holographic approach to vibrational analysis can also be used to detect flaws that produce vibrational anomalies. The method is, however, not a real-time method; it requires development and reconstruction of the time-averaged hologram.

An alternative, real-time approach to holographic vibrational analysis is to prepare a reference hologram of the object at rest, set up the system for conventional real-time interferometry, set the object to vibrating, and then stroboscopically observe the dynamic interference fringe pattern.

Holographic Contouring

If simply a “relief map” of a surface is desired, holographic differential interferometry need not be used. More direct ways have been developed, one of which is the dual-source method in which a hologram of an object is prepared using two mutually coherent point sources of laser light as the illumination beam. The interference pattern of the two sources, formed on the surface of the object, appears in the reconstructed holographic image as contours defining the relief features of the surface. An alternative, and generally superior, approach is to use an illumination beam and a reference beam each made up of two wavelengths rather than one. (Several lasers are available that provide such beams.) When the resulting hologram is illuminated by a single-frequency laser beam, two images with slightly different positions are produced. These two images interfere, and (for appropriate geometries) the resulting image contours are accurate indications of surface relief. A two-frequency contour map of the surface of a coin is shown in figure 11-7. The two wavelengths used were 6328 Å and 6118 Å. Each fringe interval represents a depth difference of 9.25 micrometers.

So far, holographic contouring has not been as promising as an NDE method as has holographic interferometry. The surface strains associated with fatigue damage, however, is now being studied in the laboratory. Holographic contouring may also be used to evaluate the perfection of precision parts, such as roller bearing components.

Optical Correlation

With the real-time holographic interference arrangement, if the light passing through the

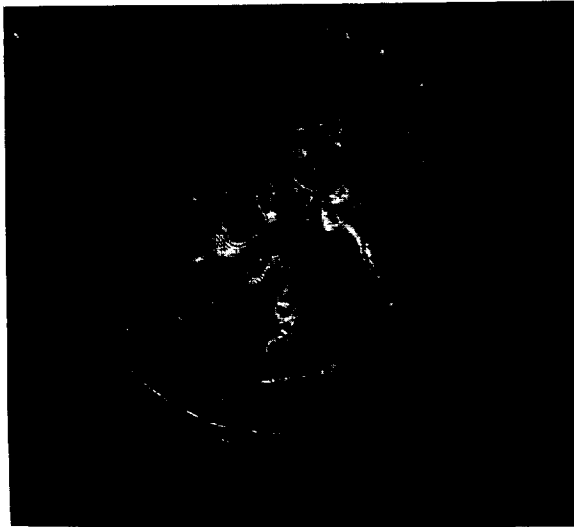


FIGURE 11-7.—Two-frequency holographic contour map. (Courtesy of Dr. J. R. Varner, Univ. of Michigan.)

hologram is brought to a focus by a single lens, the intensity of light at the focal spot is proportional to the degree of correlation of the real object and its virtual image. Thus, a photometer located at the focus of the lens can, in effect, produce a signal proportional to the degree of correlation. It has been demonstrated (in the laboratory) that by this method fatigue-induced changes in the surface microstructure of a fatigue specimen can be detected and measured prior to the onset of visible cracking.

NASA Activities

NASA-sponsored work in holographic instrumentation through 1969 has been reviewed elsewhere (ref. 4). Only some highlights of potential importance in NDE will be mentioned here.

The visualization of fluid flow fields by holographic techniques has been investigated both at NASA Centers and by NASA contractors. The potential advantage would appear to be in very low-pressure gases, characteristic of the upper atmosphere. Holographic vibrational analysis is also being studied for application to aerospace structures. An investigation of considerable interest for NDE is the use of coherent

light to create visual images from microwave holograms. All these investigations are presently in exploratory or early developmental phases.

ULTRASONIC HOLOGRAPHY

Optical holography was made possible by the development of practical sources of coherent light. Sound, like light, is a wave phenomenon, though of an entirely different kind; furthermore, sources of coherent sound have been available for centuries. Yet, strangely, no one appears to have thought of making "sound holograms" until after optical holography was developed. Although sound holograms could in principle be made using sound of any frequency, ultrasonic frequencies are most useful for NDE; hence the term "ultrasonic holography" is preferred over the term "acoustical holography" which is sometimes used.

An ultrasonic hologram is made similarly to an optical hologram; ultrasonic waves simply take the place of light waves in the illumination beam and the reference beam. Of course, photographic film cannot be used directly to record the resulting interference pattern. While various schemes have been proposed for recording ultrasonic holograms, the only one to meet with any significant degree of success is the so-called ripple tank. The hologram is produced by action of the interfering ultrasound beams impinging on the water surface to produce a steady-state ripple pattern, the hologram. This may be photographed (under appropriate illumination) to give a permanent hologram from which the image can be reconstructed and made visible by illumination with a visible-light laser beam. This method of reconstruction is somewhat impractical because the reconstructed image is smaller in lateral dimensions than the original scene by the ratio of the wavelength of the light used to the wavelength of ultrasound used, a very small fraction. A more practical method, which also has the advantage of being a real-time method, is to illuminate the ripple pattern with a coherent light beam and view the hologram by reflection (fig. 11-8). The demagnification effect still takes place; however, this may be overcome by viewing the recon-

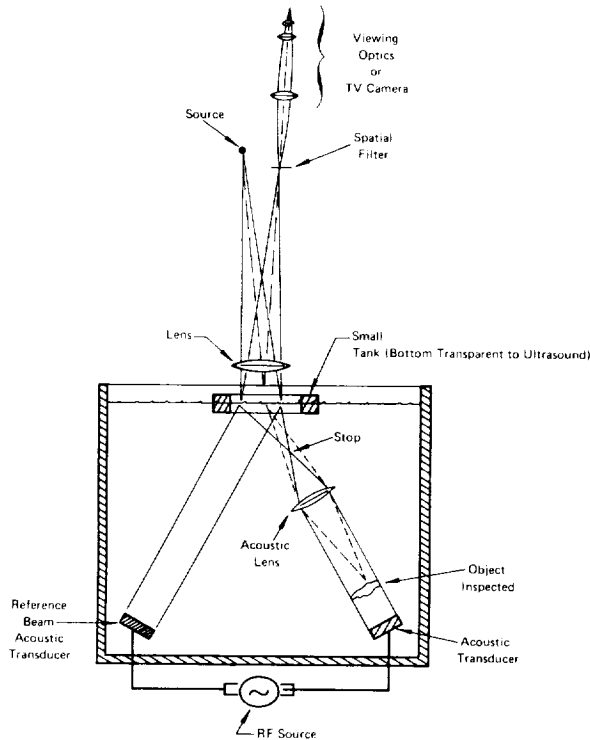


FIGURE 11-8.—Diagram of ripple tank arrangement for real-time ultrasonic holography.

structured scene through appropriate magnifying optics. A closed-circuit television system may also be used to view the image. A system incorporating these features is now commercially available.

Ultrasonic holography has the advantage of presenting a visual image of what the ultrasound "sees" in the bulk of an inspected object, a very useful feature. However, the method also has disadvantages. First, the resolving power of the system is intrinsically limited by the wave-

length of the ultrasound used. Second, it is difficult to apply the method to objects of irregular shape; mode conversion at the interface of the water and the inspected object and multiple internal reflections and scattering create problems. Third, the size of the object that can be inspected is limited by the size of the water tank available and by attenuation in the inspected object. These disadvantages are subject to improvement through further research and development, and it appears likely that ultrasonic holography will in the future be widely used in NDE.

An alternative, essentially nonholographic, method of using ultrasound and laser light to create a visual image of the interior of an object has also been developed. This method, which depends on Bragg diffraction of light by the sound beam, is still in the research stage; commercial versions have not appeared yet (ref. 5).

REFERENCES

1. GREEN, A. T.; LOCKMAN, C. S.; BROWN, S. J.; AND STEELE, R. K.: Feasibility Study of Acoustic Depressurization System. NASA CR-54472, 1966.
2. GREEN, A. T.; AND CRIMMINS, P. P.: Correlation of Stress-Wave-Emission Characteristics with Fracture in Aluminum Alloys. (NAS8-21405) Rept. 1246-Q-2, Aerojet-General Corp. (Sacramento, Calif.), March 1969.
3. CRIMMINS, P. P.: Correlation of Stress-Wave-Emission Characteristics with Fracture in Aluminum Alloys. (NAS8-21405) Rept. 1246-Q-3, Aerojet-General Corp. (Sacramento, Calif.), June 1969.
4. RAGENT, BORIS; AND BROWN, RICHARD M.: Holographic Instrumentation Applications. NASA SP-248, 1970.
5. APRAHAMIAN, R.; AND BHUTZ, P. G.: NDT by Acousto-Optical Imaging. *Materials Evaluation*, vol. 29, no. 5, 1971, pp. 112-116.

|

Bibliography

CHAPTER 2

- ALBURGER, JAMES R.: Porosity Detection and Suppression in Penetrant Inspection Processes. *Materials Evaluation*, vol. 23, Aug. 1965, pp. 385-390.
- ALBURGER, JAMES R.: Theory and Applications of Liquid Tracers. *Nondestructive Testing*, vol. 20, Mar.-Apr. 1962.
- ALBURGER, JAMES R.: Two New Approaches to the Design of Lox-Usage Inspection Penetrant Systems. Paper presented at American Society for Nondestructive Testing, 28th National Conference (Detroit, Mich.), Oct. 14-17, 1968. (Available in microfiche from AIAA, Number A68-44057.)
- ANON.: Advances in Penetrant Methods and Materials. Shannon Luminous Materials Co. (Los Angeles, Calif.), Bulletin No. 640223.
- ANON.: An Aid in the Selection of Nondestructive Testing Methods, Procedures and Specifications. NASA Reliability and Quality Assurance Office (Code KR), Washington, D.C., 20546.
- ANON.: Crack Detection Method Is Safe in Presence of Liquid Oxygen. NASA Tech Brief 65-10107, 1965.
- ANON.: Inspection Requirements, Nondestructive: For Aircraft Materials and Parts. Military Specification, MIL-I-6870B (ASG), Feb. 25, 1965.
- ANON.: Penetrant Inspection Method, Standard for. MSFC-STD-366, NASA/Marshall Space Flight Center, Oct. 27, 1964.
- ANON.: Penetrant Maintenance, Tests—Procedures. Shannon Luminous Materials Co. (Los Angeles, Calif.), Bulletin No. 640110.
- ANON.: Penetrant Parameters. Shannon Luminous Materials Co. (Los Angeles, Calif.), Bulletin No. 651118.
- ANON.: Super-Sensitive Inspection Penetrant Processes. Uresco, Inc. (Downey, Calif.), Bulletin No. 661007.
- ANON.: Surfactant for Dye-Penetrant Inspection Is Insensitive to Liquid Oxygen. NASA Tech Brief 10131, 1966.
- CAMPBELL, WILLIAM B.; AND MCMASTER, ROBERT C.: Derivation of Penetrant-Developer Resolution. *Materials Evaluation*, May 1967, pp. 126-128.
- HENEGHAN, PAUL S.: Some Observations of Phenomena Related to Penetrant Detection of Cracks. *Nondestructive Testing*, Mar-Apr., 1960, pp. 121-123.
- LOMERSON, EDWIN O., JR.: Statistical Method for Evaluating Penetrant Sensitivity and Reproducibility. Paper presented at the American Society for Nondestructive Testing, 28th National Conference (Detroit, Mich.), Oct. 14-17, 1968. (Available in microfiche from AIAA, Number A68-45210.)
- MCFAUL, HOWARD J.: Effect of Finishing Processes on Detectability of Surface Flaws by Penetrant Process. *Materials Evaluation*, Dec. 1965, pp. 577-582.
- MCGONNAGLE, WARREN J.: *Nondestructive Testing*. McGraw-Hill Book Co., Inc., 1961.
- OFFNER, W. W.: Committee Chairman: Guide for Interpretation of Nondestructive Tests of Welds in Ship Hull Structures. Report No. SSC-177, prepared for the Ship Structure Committee by the Weld Flaw Evaluation Committee, National Academy of Sciences, National Research Council, Washington, D.C., Sept. 1966. Contract No. NObS-90310 between Bureau of Ships, Department of the Navy, and The National Academy of Sciences.
- RODGERS, ERNEST H.; AND MERHIB, CHARLES P.: A Report Guide to Liquid Penetrant Literature. U.S. Army Materials Research Agency (ARMA), Nondestructive Testing Information Center, AMRA MS 64-12, Aug. 1964. (AD 612-044.)
- STINEBRING, R. C.; AND ZURBRICK, J. R.: Properties Determination and Process Control of Boron Filament Composites Using Nondestructive Test Methods. Proceedings of the Society of Aerospace Material and Process Engineers, 10th National Symposium, Nov. 9-11, 1966 (A67-13447.)
- SWAMY, S. G. N.: Indigenous Dye-Penetrants. Central Mechanical Engineering Research Institute (Durgapur 9, India), Feb. 1967. (N68-16235)
- WOLFORD, ROY: Automated Penetrant Inspection Systems—How Practical? Presented at American Society for Nondestructive Testing, 28th National Conference (Detroit, Mich.), Oct. 14-17, 1968. (Available in microfiche from AIAA, Number A68-45208.)

CHAPTER 3

- ANON.: Supplement C, Ultrasonic Testing Method. Recommended Practice No. SNT-TC-1A (1968 Edition), American Society for Nondestructive Testing.
- ANON.: Commonly Used Specifications and Standards for Nondestructive Testing. Materials Evaluation, Aug. 1968.
- BLITZ, J.: Fundamentals of Ultrasonics. Butterworths (London), 1963.
- FOWLER, KENNETH A.; AND MERHIB, CHARLES P.: A Report Guide to Ultrasonic Testing Literature, Vol. V. U.S. Army Materials Research Agency (Watertown, Mass.), AMRA MS 67-06, June 1967.
- GOOBERMAN, G. L.: Ultrasonics: Theory and Application. Hart Publishing Co. (New York), 1968.
- KRAUTKRAMER, J.; AND KRAUTKRAMER, H., in collaboration with Grabendorfer, W.; and Niklas L.: Ultrasonic Testing of Materials. Springer-Verlag (New York), 1969.
- MCMASTER, ROBERT C.: Nondestructive Testing Handbook, Vol. II, The Ronald Press Co. (New York), 1959.
- MERHIB, CHARLES P.: A Report Guide to Fatigue Testing Literature. U.S. Army Materials Research Agency (Watertown, Mass.), AMRA MS 67-05, May 1967.
- MERHIB, CHARLES P.; AND RODGERS, ERNEST H.: A Report Guide to Ultrasonic Testing Literature, Vol. I. U.S. Army Materials Research Agency (Watertown, Mass.), AMRA MS 66-02, Mar. 1966.
- MERHIB, CHARLES P.; AND RODGERS, ERNEST H.: A Report Guide to Ultrasonic Testing Literature, Vol. III. U.S. Army Materials Research Agency (Watertown, Mass.), AMRA MS 66-11, Dec. 1966.
- RODGERS, ERNEST H.: A Report Guide to Ultrasonic Attenuation Literature. U.S. Army Materials Research Agency (Watertown, Mass.), AMRA MS 65-09, Dec. 1965.
- RODGERS, ERNEST H.; AND MERHIB, CHARLES P.: A Report Guide to Ultrasonic Testing Literature, Vol. II. U.S. Army Materials Research Agency (Watertown, Mass.), AMRA MS 66-05, June 1966.
- RODGERS, ERNEST H.; AND MERHIB, CHARLES P.: A Report Guide to Ultrasonic Testing Literature, Vol. IV. U.S. Army Materials Research Agency (Watertown, Mass.), AMRA MS 67-03, Apr. 1967.
- STENTON, FREDERICK G.; AND MERHIB, CHARLES P.: A Report Guide to Ultrasonic Testing Literature, Vol. VI. U.S. Army Materials and Mechanics Research Center (Watertown, Mass.), AMMRC MS 69-03, Apr. 1969.

CHAPTER 4

- ANON.: Radiography in Modern Industry. Third ed. with supplements, Eastman Kodak Co. (Rochester, N.Y.), 1969.
- BERGER, H.: Neutron Radiography. American Elsevier Publishing Co. (New York), 1965.

- CLARK, G. L.: Applied X-Rays. Fourth ed., McGraw-Hill Book Co., Inc., 1955.
- DER BOGHOSIAN, SATRAK: A Report Guide to Radiographic Testing Literature, vol. III. U.S. Army Materials and Mechanics Research Center (Watertown, Mass.), Sept. 1968. (AD 676835)
- DER BOGHOSIAN, SATRAK, AND RODGERS, ERNEST H.: A Report Guide to Gamma Radiographic Literature. U.S. Army Materials Research Agency (Watertown, Mass.), Aug. 1964 (AD 612042)
- HALMSHAW, R. ED.: Physics of Industrial Radiology. American Elsevier Publishing Co. (New York), 1966.
- MCMASTERS, ROBERT C.: Nondestructive Testing Handbook, vol. I. The Ronald Press Co., 1963, sections 13-27.

CHAPTER 5

- ANON.: Supplement E, Eddy American Society for Nondestructive Testing, Current Testing Method. Recommended Practice No. SNT-TC-1A (1968 Edition).
- ANON.: Braze Joint Quality Tested Electromagnetically. NASA Tech Brief 67-10333, 1967.
- ANON.: Commonly Used Specifications and Standards for Nondestructive Testing. Materials Evaluation, Aug. 1968, pp. 30A-35A.
- ANON.: Eddy Current. Vol. I—Basic Principles. NASA CR-61207, 1967.
- ANON.: Eddy Current, Vol. II—Equipment, Methods and Applications. NASA CR-61208, 1967.
- ANON.: Eddy Current Probe Measures Size of Cracks in Nonmetallic Materials. NASA Tech Brief 67-10645. 1967. (N67-10645)
- ANON.: Introduction to Nondestructive Testing. NASA CR-61204, 1967.
- ANON.: Materials Testing and Malfunction Investigation Capability. NASA TM X-59274, 1965. (N67-14940)
- ANON.: Nondestructive Testing. A Demand Bibliography. NASA TM X-61424, Dec. 1968. (N69-14767)
- ANON.: Standard Method for Measuring Impedance of Anodic Coatings on Aluminum. 1968 Book of ASTM Standards, Part 6, American Society for Testing and Materials (Philadelphia), pp. 489-493.
- ANON.: Study and Development of Nondestructive Weld Inspection Techniques. NASA CR-73207, 1968. (N68-21683)
- ANON.: Proc. of Symposium on Nondestructive Tests in the Field of Nuclear Energy. American Society for Testing Materials (Philadelphia), Mar. 1958.
- ANON.: Tentative Recommended Practice for Measuring Coating Thickness by Magnetic or Electromagnetic Methods. 1964 Book of ASTM Standards, Part 31. American Society for Testing and Materials (Philadelphia), pp. 602-604.
- ANON.: Trade Names of Nondestructive Test Equipment and Materials. Materials Evaluation, Mar. 1969, pp. 33A-38A.

- BARRY, R. C.: Evaluation of Welds. Proc. of Symposium on Weld Imperfections, (Palo Alto, Calif.), Sept. 19-21, 1966. Addison Wesley, 1968, pp. 49-74.
- BEAL, J. B.: The Challenge of Nondestructive Testing in Outer Space. Proc. of the Sixth Symposium on Nondestructive Evaluation of Aerospace and Weapons Systems Components and Materials. Western Periodicals Co. (North Hollywood, Calif.), 1967, pp. 440-464.
- BENSON, R. W.: Development of Nondestructive Methods for Determining Residual Stress and Fatigue Damage in Metals. NASA CR-79304, June 1966. N67-12227)
- BENSON, R. W.; CHAPMAN, J. R.; HUFFMAN, H. F.; AND PEARSALL, S. H.: Final Report, Development of Non-Destructive Methods for Determining Residual Stress and Fatigue Damage in Metals, Mar. 8, 1968. (N68-21875)
- BENSON, R. W.; CHAPMAN, J. R.; HUFFMAN, H. F.; AND PEARSALL, S. H.:—Final Report, Development of Non-Destructive Methods for Determining Residual Stress and Fatigue Damage in Metals.
- BIRCHON, D.; BROMLEY, D. C.; AND WINGFIELD, P. M.: Some Recent Developments in Non-Destructive Testing. The Engineer, Nov. 3, 1967, pp. 590-592. (Available from AIAA in Microfiche, A68-11107.)
- BROWN, R. L., JR.; AND LIBBY, H. L.: Detection of Anisotropic Conditions Using Eddy Currents. Nondestructive Testing, vol. 20, no. 5, 1962, pp. 339-342.
- COOPER, R. G.; AND ZORAN, W. A.: Potential Problems of In-Space Nondestructive Testing. Proceedings of the Sixth Symposium on Nondestructive Evaluation of Aerospace and Weapons Systems Components and Materials. Western Periodicals Co. (North Hollywood, Calif.), 1967, pp. 503-520.
- COX, T. A.: Electromagnetic Inspection of Hardened Steel. Memorandum Report M67-24-1, Frankford Arsenal (Philadelphia), Apr. 1967. (N67-32844)
- COX, T. A.: Phase Sensitive Eddy Current Test Equipment. Report No. M66-2-1, Frankford Arsenal (Philadelphia), Fire Control Engineering Directorate, Aug. 1965. (N66-13631)
- DICK, P.: Nondestructive Test Equipment for Predicting and Preventing Failure. ASME Publication No. 65-MD-26. (Available from AIAA in Microfiche, A65-28612.)
- DODD, C. V.: Applications of a Phase Sensitive Eddy Current Instrument. Materials Evaluation, June 1964, pp. 260-262 and 272.
- FANNELLI, L. H.; AND MCKOWN, R. D.: Prediction of Strength of Graphitic Material by Nondestructive Test Techniques. Nondestructive Testing of Nuclear Graphite, ASTM STP 439, American Society for Testing and Materials, 1968, pp. 48-60. (Available from AIAA in Microfiche, A68-40696.)
- FORD, R. M.; AND EDENBOROUGH, N. B.: A Low-Cost, Phase-Measurement Device for Eddy Current Systems. Materials Evaluation, Jan. 1969, pp. 23-24.
- GIBSON, J. A.: Review of Nondestructive Testing Techniques for Detecting Lack of Penetration in Aluminum Fusion Welds. (Columbus, Ohio), Battelle Memorial Institute (Contract No. DAAH01-67-C-1921), Oct. 1967.
- GRUBINSKAS, R. A.; AND MERHIB, C. P.: A Report Guide to Literature in the Field of Electromagnetic Testing. Report No. AMRA MS 65-03, Nondestructive Testing Information Center, U.S. Army Materials Research Agency (Watertown, Mass.), Apr. 1965.
- HAGEMAIER, D.; AND KLEINT, R.: Evaluating Aluminum Alloys by Nondestructive Tests. Metals Progress, May 1964, pp. 15-18.
- HAGEMAIER, D.; AND BASL, G. J.: Evaluation of Mechanical Properties of 2014-T6 Weldments by Non-destructive (Eddy Current) Methods. Materials Evaluation, vol. 25, Jan. 1967, pp. 1-7.
- HAGEMAIER, D.: Nondestructive Testing of Space Vehicle Liquid Propellant Rocket Engines. Proceedings 1968 Symposium on the NDT of Welds and Metals Joining, ASNT, pp. 107-137.
- HAGEMAIER, D.: Testing Rocket Engine Materials. Metal Progress, Aug. 1968, pp. 87-88 and 90. (Available from AIAA in microfiche, A68-37511.)
- HOCHSCHILD, R.: Mathematical Foundations of Non-Destructive Testing by Eddy Current Methods. (Oak Ridge, Tenn.) Technical Information Service, Report No. NYO-3576 to United States Atomic Energy Commission), Mar. 18, 1953.
- JUDD, T. W.: Orbitest for Round Tubes. Materials Evaluation, vol. 28, no. 1, 1970, pp. 8-12.
- KARLOV, G. I.; AND BYSTRUSHKIN, G. S.: Nondestructive Method for Checking the Early Stages of Fatigue Damage. Translated from Zavodskaya Laboratoriya, vol. 34, no. 7, July 1968, pp. 866-868. (Available from AIAA in microfiche, A69-10316.)
- KLEINT, R. E.; AND HAGEMAIER, D. J.: Relationship of Standards and Specifications to Nondestructive Testing. Presented at the Reliability and Industrial Courses, University of California (Los Angeles).
- LAMBERT, J. A. B.; AND TROUGHTON, A. J.: The Importance of Service Inspection in Aircraft Fatigue. Aircraft Engineering, vol. 39, Oct. 1967, p. 14, 17-20, 25-28, 31 and 32. (Available from AIAA in microfiche, A67-42442.)
- LEWIS, D. M.: Magnetic and Electrical Methods of Non-Destructive Testing. Simson Shand Ltd. (London and Hertford), 1951.
- LIBBY, H. L.: An Improved Eddy Current Tubing Test. Materials Evaluation, vol. 23, no. 4, 1965, pp. 181-187.
- MARTIN, G.: Nondestructive Testing in the Aerospace Industry. The British Journal of Non-Destructive Testing, vol. 9, no. 2, 1967, pp. 27-60.
- MCCLUNG, R. W.; AND DOUGLAS, D. A., JR.: Nondestructive Testing of Irradiated Materials in the United States. (Contract W-7405-eng-26), Oak Ridge National Laboratory, Apr. 1965. (N66-20488)

- McGONNAGLE, W.; AND PARK, F.: Nondestructive Testing. *Materials Evaluation*, vol. 22, Dec. 1964, pp. 561-575.
- McGONNAGLE, W.: *Nondestructive Testing*. McGraw-Hill Book Company, Inc., 1961.
- MERHIB, C. P.: A Report Guide to Fatigue Testing Literature. Report No. AMRA MS 67-05, U.S. Army Materials Research Agency (Watertown, Mass.), May 1967.
- MOORE, J. F.; AND MARTIN, G.: Development of Non-destructive Testing Techniques for Honeycomb Heat Shields. NASA CR-78681, 1966. (N66-38920)
- MORAN, J. H.; AND KUNZ, K. S.: Basic Theory of Induction Logging and Application to Study of Two-Coil Sondes. *Geophysics*, vol. 27, no. 6, Part I, 1962, pp. 829-858.
- MULLINS, L.: The Scope of Non-destructive Testing. *Transactions*, vol. 78, no. 10, Institute of Marine Engineers, 1966, pp. 426-434.
- MUSSER, C. W.: Integrated NDT Systems for Establishing Weld Integrity of Space Vehicles. Proc. of 4th Space Congress: The Challenge of the 1970's Canaveral Council of Technical Societies, pp. 27-1 to 27-16. (Available from AIAA in microfiche, A67-36586.)
- MUSSER, C. W.: NDT Systems for Establishing Weld. *Materials Evaluation*, Feb. 1969, pp. 42-48. (Available from AIAA in microfiche, A69-19699.)
- NEUSCHAEFER, R. W.: Improvements in Structural Non-destructive Testing. *Research Achievements Reviews*, vol. 1, NASA TMX-53620, 1967. (N67-30570 thru N67-30574)
- NEUSCHAEFER, R. W.: Assuring Saturn Quality Through Nondestructive Testing. *Materials Evaluation*, vol. 27, no. 7, 1969, pp. 145-152.
- ONO, K.; AND MCGONNAGLE, W.: Pulsed Eddy Current Instrument for Measuring Sodium Levels of EBR-II Fuel Rods. Report No. ANL-6278, Argonne National Laboratory, July 1961.
- ORD, R. N.; AND RICHARDSON, R. L.: Eddy Current Test Pattern Recognition Program. Report No. BNWL-942, Battelle Memorial Institute, Pacific Northwest Laboratory (Richland, Washington), Nov. 1968. (N69-23430)
- PADILLA, V. E.; AND PARKS, J. W.: Definition of Fatigue Crack Geometry by Eddy Current Techniques. Proc. of the Seventh Symposium on Nondestructive Evaluation of Components and Materials in Aerospace, Weapons Systems and Nuclear Applications, Apr. 23-25, 1969. Western Periodicals Company (North Hollywood, Calif.), pp. 79-84.
- RENKEN, C. J.; AND MYERS, R. C.: A Double Pulse Eddy Current Testing System. Report No. ANL-5935, Argonne National Laboratory, June 1959.
- RENKEN, C. J.: Progress Report on Nondestructive Testing by Electromagnetic Methods. Report No. ANL-6414, Argonne National Laboratory, July 1962.
- RENKEN, C. J.; MYERS, R. G.; AND MCGONNAGLE, W. J.: Status Report in Eddy Current Theory and Application. Argonne National Laboratory (Lemont, Ill.), Nov. 1958.
- RENKEN, C. J.: A Through Transmission System Using Pulsed Eddy Current Fields. *Nondestructive Testing*, vol. 18, no. 4, 1960, pp. 234-236.
- ROSS, J. D.: Electromagnetic Testing of Reactor Components. Proc. of the Symposium on Nondestructive Testing Trends in the AEC Reactor Program, Atomic Energy Commission Headquarters Building (Germantown, Md., May 20, 1960, pp. 65-73.
- RUMMEL, W. D.: Monitor of the Heat Affected Zone in 2219-T87 Aluminum Alloy Weldments. Proc. of Symposium on NDT of Welds and Materials Joining. American Society for Nondestructive Testing (Los Angeles, Calif.), Mar. 1968. (Available from AIAA in microfiche, A68-23206.)
- SAWYER, H. F.; AND MULKERN, J. R.: In-Process Non-Destructive Microweld Inspection Techniques. Report No. 680798 (Contract No. NAS2-4166), Walter V. Sterling Inc.
- SCHALL, W. E.: *Nondestructive Testing*. The Machinery Publishing Co., Ltd. (Graphic Art Services (Brighton) Ltd., Great Britain), 1968.
- SCHMITZ, G.; WIECZOREK, A.; AND LEVINE, M.: Development of Nondestructive Testing Methods for the Evaluation of Thin and Ultrathin Sheet Materials. Technical Documentary Report No. ML TDR 64-278, General American Transportation Corp. (Niles, Ill.), Sept. 1964. (N65-10276)
- SMILEY, R. W.: Polaris Takes a Second Look at NDT. *Materials Evolution*, vol. 24, Dec. 1966, pp. 679-682.
- SMITH, G. H.; AND McMASTER, R. C.: Current Aerospace Applications Using MRA Eddy Current Test Systems. *Materials Evaluation*, Dec. 1967, pp. 283-288. (Available from AIAA in microfiche, A68-14526.)
- TERRY, D.: The Development of Eddy-Current Testing Techniques for Tube Inspection. *Journal Brit. I.R.E.*, Nov. 1963, pp. 373-382.
- WELDON, W. J.: Nondestructive Testing Application Techniques That Are Peculiar to Airline Maintenance Inspection. Proceedings of the Seventh Symposium on Nondestructive Evaluation of Components and Materials in Aerospace Weapons Systems and Nuclear Applications, Apr. 23-25, 1969. Western Periodicals Company (North Hollywood, Calif.), pp. 415-419.
- WITZELL, W. E.; AND KROPP, C. J.: Weldment Flaw Growth Characteristics of 2219-T81 Aluminum Alloy. NASA CR-72288, 1967.
- ZOLLER, L. K.: Prospectus for NDT in the Saturn and Advanced Space Flight Programs. *Materials Evaluation*, vol. 24, Nov. 1966, pp. 637-640. (Available from AIAA in microfiche, A67-12631.)
- ZORAN, W. A.: Nondestructive Testing for Space Application, Feasibility and Preliminary Design Study, Phase I Report. NASA CR-84442, 1966. (N67-27429)

CHAPTER 6

- ALZOFON, F. E.:** Analysis of Three Modes of Cooling In Infrared Nondestructive Testing. Paper presented at the 27th National Fall Conf., Society for Non-destructive Testing (Cleveland, O.), Oct. 16-19, 1967.
- ANON.:** AGA Thermovision Advance Information on Model LS-1 Infrared Line-Scanner. AGA Infrared Instruments Department (Lidingo, Sweden).
- ANON.:** AGA Thermovision Model 661, 665 and 669. AGA Publication 556/A102.
- ANON.:** Applied Infrared Photography. Kodak Technical Publication, M26, Eastman Kodak Co. (Rochester, N.Y.), 1968.
- ANON.:** Conference on NDT of Plastic/Composite Structures, 1969. Sponsored by Air Force Materials Lab. (MAMN), The Aerospace Corp., Univ. of Dayton (Dayton, O.), Mar. 18-20, 1969.
- ANON.:** Current Infrared Papers Presented at the IR & T sessions of SNT 25th National Convention (Detroit); the 1966 Spring Convention of SNT (Los Angeles); and the SNT 26th National Conference (Chicago), Oct. 1966.
- ANON.:** A DDC Bibliography on Liquid Crystals. Vol. I of three volumes, DDC-TAS-68-11, Defense Documentation Center, July 1968.
- ANON.:** Ferroelectric Bolometer Measures RF Absolute Power at Submillimeter Wavelengths. NASA Tech Brief, 66-10051, 1966.
- ANON.:** Foil Radiometer Accessory Improves Measurements. NASA Tech Brief, 67-10448, 1967.
- ANON.:** Graphite Element Serves as Radiant Heat Source. NASA Tech Brief, 65-10218, 1965.
- ANON.:** Hot Parts Checked Remotely by New Meter. Product Engineering, vol. 40, no. 9, 1969, pp. 64-65.
- ANON.:** Inexpensive Infrared Source Improvised from Flashlight. NASA Tech Brief, 66-10096, 1966.
- ANON.:** Infrared Fiber Optics. Electrical Design News, vol. 10, no. 10, 1965.
- ANON.:** Infrared Solves Plastic-Pouch Packaging Problem. Design News, June 9, 1969.
- ANON.:** Infrared Television System for Fault Detection, Alternate I—Contract System. NASA CR-62578, 1965.
- ANON.:** Infrared Thermography Evaluates Space Suits. Design News, vol. 25, no. 2, 1970, p. 8.
- ANON.:** Infrared Thermometer, New Products and Services. Materials Evaluation, June 1969, p. 44A.
- ANON.:** IR-Transmission Glasses Formed From Oxides of Bismuth and Tellurium. NASA Tech Brief, 65-10190, 1965.
- ANON.:** Internal Cooling Increases Range of Immersion-Type Temperature Probe. NASA Tech Brief, 65-10157, 1965.
- ANON.:** Liquid Crystals—A Step Closer to Low-Voltage Displays. The Electronic Engineer, Aug. 1968, p. 17.
- ANON.:** Measuring Microheat. Electro-Technology, July 1969.
- ANON.:** Metal Sheath Improves Thermocouple Using Graphite in One Leg. NASA Tech Brief, 65-10051, 1965.
- ANON.:** Method of Measuring Thermal Conductivity of High Performance Insulation. NASA Tech Brief, 68-10013, 1968.
- ANON.:** Miniature Bioelectronic Device Accuracy Measures and Tele-Meters Temperature. NASA Tech Brief, 66-10057, 1966.
- ANON.:** Miniature Pyrometer. New Products and Services. Materials Evaluation, Feb. 1969, p. 40A.
- ANON.:** Optical Integrating Sphere Operates at Visible and Infrared Wavelengths. NASA Tech Brief, 68-10126, 1968.
- ANON.:** Photo/Thermochromic Non-Destructive Inspection Coatings. Air Force Materials Lab., Materials Support Division, Jan. 28, 1970. (Source: Sid Allinikov, Wright-Patterson Air Force Base, O.)
- ANON.:** Portable Pyrometer. Materials Evaluation, June 1968, p. 37A.
- ANON.:** Precision Bolometer Bridge. NASA Tech Brief, 68-10156, 1968.
- ANON.:** Preparation of NDI Paint. Air Force Materials Lab., Jan. 28, 1970. (Source: Sid Allinikov, Wright-Patterson Air Force Base, O.)
- ANON.:** Proceedings of the 6th Symposium on Nondestructive Evaluation of Aerospace and Weapons Systems, Components and Materials. Sponsored by South Texas Section of the Society for Nondestructive Testing, Inc., and Southwest Research Institute (San Antonio, Tex.), 1967.
- ANON.:** Research Achievements Review Series No. 10. NASA TM X-53466, 1965.
- ANON.:** Research Achievements Review Vol. II, Report 5, Quality and Reliability Assurance Research at MSFC. NASA TM X-53620, 1966.
- ANON.:** Research Achievements Reviews, Vol. II, Series 1 through 12. NASA TM X-53793, 1968.
- ANON.:** Space Programs Summary 37-43, Vol. IV, Supporting Research and Advanced Developments for the Period Dec. 1, 1966 to Jan. 31, 1967. Jet Propulsion Lab., Calif. Inst. of Technology (Pasadena, Calif.), Feb. 28, 1967.
- ANON.:** Study of Fast Response Thermocouple Measurement of Temperatures in Cryogenic Gases. NASA Tech Brief, 66-10661, 1966.
- ANON.:** The Symposium on Physics and Nondestructive Testing. Preliminary Program, Sheraton-Dayton Hotel (Dayton, O.), Sept. 1965. Sponsored by IIT Research Institute.
- ANON.:** Taking Mars Temperature. Design News, May 26, 1969.
- ANON.:** Testing System Uses a Camera to Scan Tire Interior for Flaws. The New York Times, July 27, 1969.
- ANON.:** Thermal and Infrared. Current Literature on Nondestructive Testing. Materials Evaluation, June 1967, p. 30A.

- ANON.: Twin Helix System Produces Fast Scan in Infrared Detector. NASA Tech Brief, 66-10638, 1966.
- ANON.: Wedge Immersed Thermistor Bolometer Measures Infrared Radiation. NASA Tech Brief, 65-10330, 1965.
- ANON.: Wide-Angle Sensor Measures Radiant Heat Energy in Corrosive Atmospheres. NASA Tech Brief, 65-10019, 1965.
- ANNABLE, R. V.; LEITER, H. A.; LODDER, J. F.; and JUAREZ, D. J.: Second Quarterly Report for a Day-Night High Resolution Infrared Radiometer Employing Two-Stage Radiant Cooling. (NAS5-10113) ITT Industrial Lab. (Fort Wayne, In.), June 24, 1966—Oct. 1, 1966.
- ASTHEIMER, R. W.; AND SCHWARZ, F.: Thermal Imaging Using Pyroelectric Detectors. Applied Optics, vol. 7, no. 9, 1968, pp. 1687-1695.
- BASEMORE, THOMAS R.: An Infrared Scanning System for Inspection of Printed Circuits. Proc. of the 7th Symposium on Nondestructive Evaluation of Components and Materials in Aerospace, Weapons Systems and Nuclear Applications. Sponsored by South Texas Section, American Society for Nondestructive Testing, Inc., and Southwest Research Institute, Apr. 23-25, 1969, pp. 388-394. (Available from Western Periodicals Co., North Hollywood, Calif.)
- BERGER, HAROLD; AND KRASKA, I. R.: Characteristics of an Infrared Vidicon Television System. Materials Evaluation, Apr. 1966, pp. 197-200.
- BERGSTROM, LEIF; AND BAEU, DIETRICH: Nondestructive Testing by High-Speed Thermography. Materials Evaluation, May 1969.
- BERKEBILE, M. J.; AND LARACUENTE, F.: Optical Scanning of Infrared Emission Aids Microcircuit Reliability.
- BERRYMAN, G.; AND EDWARDS, T. R.: Evaluation of Semiconductor Devices Using the Scanning Electron Microscope. Marshall Space Flight Center, Huntsville, Ala.
- BOBO, S. B.; AND CROWLEY, A. H.: Use of Contiguous Optical Fibers as a Means of Carrying Thermal Information from Welds. Applied Optics, vol. 7, no. 7, 1968, pp. 1839-1844.
- BOLLINGER, L. E.: Transducers for Measurement, Part III, Temperature From One Extreme to the Other. ISA Journal, Oct. 1964.
- BOLWELL, A. J.: Fiber Optics Improve Efficiency of Image Intensifier Tube. Design News, July 7, 1969, p. 65.
- BORG, SVEN-BERTILE: Thermal Imaging with Real-Time Picture Presentation. Applied Optics, vol. 7, no. 9, 1968, pp. 1697-1703.
- BRANSTETTER, J. ROBERT: Some Practical Aspects of Surface Temperature Measurement by Optical and Ratio Pyrometers. NASA TN-D-3604, 1966.
- BRINTON, JAMES: Monitor Keeps IC From Losing Its Header. Electronics, Dec. 22, 1969, pp. 133-135.
- BRITTEN, E. ROBERT: The Development of An Infra-Red Signature Analysis Technique, A Non-Destructive Testing Tool. Paper presented at 5th Conference/Exhibit, Temperature Measurements Society (Hawthorne, Calif.), Mar. 14-15, 1967.
- BROWN, SHELBA P.: Cholesteric Crystals for Nondestructive Testing. Paper presented at Symposium on NDT of Welds and Materials Joining, American Society of NDT, Inc. (Los Angeles, Calif.), Mar. 1968.
- CARSLAW, H. S.; AND JAEGER, J. C.: Conduction of Heat in Solids. Clarendon Press (Oxford), 1959.
- COHEN, SHERMAN E.: Nondestructive Testing for Evaluation of Strength of Bonded Material (Metallic). NASA-CR-61503, 1966.
- CON, G. K. T.; AND AVERY, D. G.: Infrared Methods—Principles and Applications. Academic Press, Inc. (New York and London), 1960.
- EISNER, LEONARD: Infrared: What's Ahead. Electronic Products, vol. 7, no. 9, 1965.
- ERTHAL, JOHN F.: Liquid Crystals as a Nondestructive Inspection Tool, Feasibility Study. Rept. NAEC-AML-2634, U. S. Naval Air Engineering Center (Philadelphia), June 1967.
- EXTON, REGINALD J.: Theory and Operation of a Variable Exposure Photographic Pyrometer Over the Temperature Range 1800° to 3600° F (1255° to 2255° K). NASA TN D-2660, Mar. 1965.
- FLORANT, L. E.: Testing Using Infrared. ISA Journal, July 1964, pp. 61-64.
- FRAZER, R. M.: Thermal Infrared Radiometers as Instruments for Nondestructive Reliability Testing. U. S. Navy Electronics Lab., (San Diego), May, 1966.
- GATES, DAVID M.: Sensing Biological Environments with a Portable Radiation Thermometer. Applied Optics, vol. 7, no. 9, 1968, pp. 1803-1809.
- GLICKSMAN, RICHARD: Integrated Circuit Technology: Instrumentation and Techniques for Measurement, Process, and Failure Analysis. Instrumentation for Advanced Microelectronic Measurements, McGraw-Hill Book Co., Inc., 1967, pp. 231-259.
- GREEN, D. R.; AND DAY, C. K.: Infrared Testing of Bonds Between Graphite and Protective Coatings. Paper presented at Symposium on Nondestructive Testing of Nuclear Graphite, ASTM STP no. 439.
- GREEN, DONALD R.: Principles and Applications of Emittance—Independent Infrared Nondestructive Testing. Applied Optics, vol. 7, no. 9, 1968, pp. 1779-1789.
- GREEN, DONALD R.: Thermal Surface Impedance Method for Nondestructive Testing. Materials Evaluation, Oct. 1967, pp. 231-236.
- GRIFFIN, D. D.: Infrared Techniques for Measuring Temperature and Related Phenomena of Microcircuits. Applied Optics, vol. 7, no. 9, 1968, pp. 1749-1755.
- HAMITER, LEON: Infrared Techniques for the Reliability Enhancement of Microelectronics. SCP and Solid State Technology, Mar. 1967, pp. 41-49.

- HAMLIN, WILLIAMS O.: Infrared Temperature Measurements. *Electronics World*, vol. 79, no. 2, 1968, pp. 34-36.
- HERMAN, RUTH A.: Aspects of Using Infrared for Electronic Circuit Diagnosis. *Materials Evaluation*, Sept. 1967, pp. 201-206.
- HORMUTH, GUSTAVE A.: Temperature Measurement in Environmental Testing, Part V. *Test Engineering*, Nov. 1969, pp. 22-23.
- HORMUTH, GUSTAVE A.: Temperature Measurement in Environmental Testing, Part VII. *Test Engineering*, Feb. 1970, pp. 12, 13 and 17.
- HORMUTH, GUSTAVE A.: Temperature Measurement in Environmental Testing, Part VIII. *Test Engineering*, Mar. 1970, pp. 12-13.
- KENDALL, J. M., SR.: Primary Absolute Cavity Radiometer. NASA CR-103422, 1969.
- KING, J.; LIMPERIS, T.; MORGAN, J.; POLCYN, F.; AND WOLFE, W.: Infrared. *International Science and Technology*, no. 16, Apr. 1963.
- KINGSBURY, J. E.; AND CLOTFELTER, W. N.: Nondestructive Testing—The Road to Quality. Paper presented at Symposium on Technology Status and Trends (Huntsville, Ala.), Apr. 21-23, 1965.
- KLASS, PHILIP J.: Component Failures Predicted by Infrared. *Aviation Week and Space Technology*, Dec. 3, 1962, pp. 85-90.
- KREITH, FRANK.: Principles of Heat Transfer, Second ed., International Textbook Co. (Scranton, Pa.), 1965.
- KRUSE, PAUL W.; MCGLAUCHLIN, LAURENCE D.; AND MCQUISTAN, RICHMOND B.: Elements of Infrared Technology—Generation, Transmission and Detection. John Wiley & Sons, Inc., 1962.
- LAWLER, A. E.; AND PIRZADEH, N.: Measurement of Anodic Coating on Aluminum by Emissivity. *Materials Evaluation*, May 1969, pp. 118-120.
- LEFTWICH, RICHARD F.; AND ORDWAY, GEORGE B.: Optical Activities in Industry. *Applied Optics*, vol. 7, no. 9, 1968, pp. 1853-1856.
- LEMASTER, EDMOND.: Quality Assurance Testing of Metal to Metal Bonding for Aircraft Structures. Procedures and Engineering Branch, AF Plant 13, Wichita, Kansas.
- LEVIT, A. D.: Programming and Graphic Support for Infrared Thermal Plotters. *Materials Evaluation*, Sept. 1968, pp. 180-186.
- LYNNWORTH, LAWRENCE C.; AND BENES, JAMES J.: Design Guide Measuring Temperature. *Machine Design*, vol. 41, no. 26, 1969, pp. 190-204.
- MERHIB, CHARLES P.; AND RODGERS, ERNEST H.: A Report Guide to Thermal Testing Literature. Nondestructive Testing Information Center, AMRA MS 64-14, Aug. 1964.
- MUSSER, C. W.: Integrated NDT Systems for Establishing Weld Integrity of Space Vehicles. The Boeing Co. (New Orleans).
- NANDA, M. M.; CORL, E. A.; AND SILVERMAN, S. L.: Infrared Analysis Technique for Determining Aluminum-Phosilicate Reaction. IBM Components Division (Hopewell Junction, N.Y.).
- OVREBO, P. J.; SAWYER, R. R.; OSTERGREEN, R. H.; POWELL, R. W.; AND WOODCOCK, E. L.: Industrial, Technical, and Medical Applications of Infrared Techniques. *IRE Proceedings*, vol. 47, Sept. 1959, pp. 1629-1645.
- PERRON, R. R.: Infrared Scanning Apparatus for Flaw Detection Using Duplicate Parallel Detectors (3,210-546). What's New in NDT Patents? *Materials Evaluation*, June 1966, p. 321.
- RANDLE, WILLIAM R.: The Application of Infrared Measurement Techniques to Electronic Design and Testing. *Applied Optics*, vol. 7, no. 9, 1968, pp. 1797-1801.
- REVESZ, GEORGE; AND MARKS, BRUCE G.: Testing Components by Thermal Plotter. *Electro-Technology*, vol. 76, no. 2, 1965.
- RICHARDSON, NORMAN R.: Project Fire Instrumentation for Radiative Heating and Related Measurements. NASA TN D-3646, 1966.
- SABOURIN, LA MARR: Nondestructive Testing of Bonded Structures with Liquid Crystals. Paper presented at Conference on Structural Adhesive Bonding, Mar. 15-16, 1966.
- ST. CLAIB, J. C.: An Infrared Method of Rocket Motor Inspection. *Materials Evaluation*, Aug. 1966, pp. 425-430.
- SAUL, ROBERT: Infrared Measurements and Techniques. *Electro-Technology*, vol. 74, no. 4, 1964.
- SCHLEGEL, EARL S.: Apparatus for Determining Temperature Profiles in Misconstructures. *Review of Scientific Instruments*, vol. 34, no. 4, 1963, pp. 360-361.
- SCHULTZ, A. W.: A Novel Infrared Nondestructive Testing Technique for Determining the Thermal Conductivity of Graphite, Paper presented at Symposium on Nondestructive Testing of Nuclear Graphite, ASTM STP no. 439.
- SCHULTZ, ARNOLD W.: An Infrared Transient Method for Determining the Thermal Inertia, Conductivity and Diffusivity of Solids. *Applied Optics*, vol. 7, no. 9, 1968, pp. 1845-1851.
- SCHUMACHER, DAVID H.: Measuring Microbond Integrity with an Infrared Microradiometer. *Materials Evaluation*, Dec. 1968, pp. 257-260.
- SCHWARTZ, SEYMOUR: Integrated Circuit Technology: Instrumentation & Techniques for Measurement, Process and Failure Analysis. *Infrared Testing and Mask Alignment*. McGraw-Hill Book Co., Inc., 1967, pp. 158-191.
- SELIKSON, DR. BERNARD; AND DIMAURO, JOSEPH.: Reliability Screening Using Infrared Radiation. RADC-TR-66-360, Sylvania Electric Products, Inc., Oct. 1966.
- SKINNER, KENNETH L.; ET AL.: Passive Instrumentation and Stimuli Generation for Saturn IB Equipment Checkout. NASA CR-76404, 1966.

- SMITH, R. A.; JONES, F. E.; AND CHASMAR, R. P.: The Detection and Measurement of Infra-red Radiation. Clarendon Press (Oxford), 1958.
- SUNDSTROM, ERIK: Wide-Angle Infrared Camera for Industry and Medicine. Applied Optics, vol. 7, no. 9, 1968, pp. 1763-1779.
- TURNER, VERNON D.; AND BLOCK, LOUIS: Infrared Radiation. Electronic Industries, vol. 21, no. 2, 1962.
- TURNER, VERNON D.; AND BLOCK, LOUIS: Measuring Infrared Radiation. Electronic Industries, vol. 21, no. 2, 1962, pp. 96-98.
- VANZETTI, RICCARDO: Infrared Techniques Enhance Electronic Reliability. Solid-State Design, Aug. 1963, pp. 29-37.
- WALKER, M.; ROSCHEN, J.; AND SCHLEGAL, E.: An Infrared Scanning Technique for the Determination of Temperature Profiles in Microcircuits. Trans. IEEE on Electronic Devices, vol. ED-10, no. 4, 1963, pp. 263-267.
- WASHINGTON, SHELTON: An Improved Method for Inspection Solder Connections. Paper presented at the 18th Annual Defense Conference on Nondestructive Testing, U.S. Army Materials Research Agency, Picatinny Arsenal, N.J.
- WITZELL, W. E.; HERSH, M. S.; AND ANDERSON, R. T.: A Survey of Welding and Inspection Techniques for 2219-T81 Aluminum Alloy. NASA CR-72-97, 1967.
- WOODMANSEE, W. E.: Aerospace Thermal Mapping Applications of Liquid Crystals. Applied Optics, vol. 7, no. 9, 1968, pp. 1721-1727.
- WORMSER, ERIC M.: Sensing the Invisible World. Applied Optics, vol. 7, no. 9, 1968, pp. 1667-1671.
- YODER, JOHN R.: Temperature Measurement with an Infrared Microscope. Applied Optics, vol. 7, no. 9, 1968, pp. 1791-1796.
- ANON.: Ferroelectric Bolometer Measures RF Absolute Power at Submillimeter Wavelengths. NASA Tech Brief 66-10051, 1966.
- ANON.: Filling an Information Gap—NDT and the Apollo-Saturn V Program. Materials Evaluation, Mar. 1969.
- ANON.: Flange on Microwave Antenna Subreflector Cuts Ground Noise. NASA Tech Brief 63-10229, 1964.
- ANON.: Highly Stable Microwave Delay Line. NASA Tech Brief 67-10642, 1967.
- ANON.: Letter Symbols for Aeronautical Sciences. (ASA Y10.7-1954) American Society of Mechanical Engineers (New York City), 1954.
- ANON.: Liquid Hydrogen Densitometer Utilizes Open-Ended Microwave Cavity. NASA Tech Brief 67-10115, 1967.
- ANON.: Microwave Technique Measures Plasma Characteristics. NASA Tech Brief 65-10122, 1965.
- ANON.: Modified Filter Prevents Conduction of Microwave Signals Along High-Voltage Power Supply Leads. NASA Tech Brief 63-10091, 1964.
- ANON.: Nondestructive Testing—A Demand Bibliography. NASA-TM-X-61424, 1968. (N69-14767)
- ANON.: Novel Horn Antenna Reduces Side Lobes, Improves Radiation Pattern. NASA Tech Brief 63-10264, 1964.
- ANON.: Scanning Means for Cassegrainian Antenna. NASA Tech Brief 67-10174, 1967.
- ANON.: Silicon Oxide Films Grown in Microwave Discharge. NASA Tech Brief 68-10171, 1968.
- ANON.: Terms of Reference, International Committee for Nondestructive Testing. Materials Evaluation Feb. 1968.
- ANON.: Trade Names of Nondestructive Test Equipment & Materials. Materials Evaluation, Mar. 1969, pp. 33A-38A.
- ANON.: Traveling-Wave Tube Circuit Simplifies Microwave Relay. NASA Tech Brief 65-10127, 1965.
- ANON.: Warpage Eliminated in Copper-Clad Microwave Circuit Laminates. NASA Tech Brief 67-10454, 1967.
- BALDANZA, NICHOLAS T.: A Review of Nondestructive Testing for Plastics: Methods and Applications. Plastics Technical Evaluation Center, Picatinny Arsenal, (Dover, N.J.), Aug. 1965.
- BALLARD, DOUGLAS W.: NDT Nondestructive Testing. Industrial Research, Oct. 1965, pp. 68-72.
- BALLARD, DOUGLAS W.: New Frontiers for Nondestructive Testing in the Nuclear Age. Sandia Laboratories (Albuquerque, N. Mex.), Apr. 1965. (N66-18760)
- BEAL, JAMES B.: New Testing and Inspection Techniques. Paper presented at the Technology Utilization Conference (Berry College, Rome, Ga.), June 9, 1967.
- BENSON, ROBERT W.; ET AL.: Development of Non-Destructive Methods for Determining Residual Stress and Fatigue Damage in Metals. NASA CR-79304. (N67-12227)

CHAPTER 7

- ANON.: An Aid in the Selection of Nondestructive Testing Methods, Procedures and Specifications. NASA Reliability and Quality Assurance Office (Code KR), Wash., D.C.
- ANON.: The British Journal of Non-Destructive Testing, vol. 9, no. 2, 1967.
- ANON.: Commonly Used Specifications and Standards for Nondestructive Testing. Materials Evaluation, Aug. 1968.
- ANON.: Compact Microwave Mixer Has High Conversion Efficiency. NASA Tech Brief 66-10625, 1966.
- ANON.: Composite Filter Steepens Rejection Slopes in Microwave Application. NASA Tech Brief 66-10393, 1966.
- ANON.: Conference on NDT of Plastic/Composite Structures, 1969. Sponsored by Air Force Materials Laboratory (MAMN), The Aerospace Corp. and Univ. of Dayton (Dayton, O.), Mar. 18-20, 1969.
- ANON.: Double-Throw Microwave Device Switches Two Lines Quickly. NASA Tech Brief 63-10258, 1964.

- BENSON, ROBERT W.; ET AL.: Development of Non-Destructive Methods for Determining Residual Stress and Fatigue Damage in Metals. Robert W. Benson and Associates, Inc. (Nashville, Tenn.), Mar. 8, 1968. (N68-21875)
- BILLETER, T. ROGER; BROWN, D. P.; AND SPEAR, W. G.: Microwave Techniques for Measuring High Temperatures and Coolant Impurities. Nuclear Applications, vol. 6, Jan. 1969, pp. 73-80.
- BRANDON, W. W., JR.: Applications of Microwaves in the Non-Destructive Testing of Solid Propellants. [DA-01-021-ORD-12341(Z)] Rohm & Haas Co., Redstone Arsenal Research Div. (Huntsville, Ala.), Nov. 2, 1964. (AD 609 982)
- COFIELD, R. E.: Thickness Measurements by Nondestructive Testing Methods. Union Carbide Corp., Nuclear Div., Y-12 Plant, June 21, 1966. (N66-36284)
- CRIBBS, R. W.; LAMB, B. L.; AND LUCIAN, A. D.: Development of Microwave NDT Inspection Techniques for Large Solid Propellant Rocket Motors. (NAS 7-367) Final Rept. 0948 Phase I, Aerojet-General Corp. (Sacramento, Calif.), Dec. 31, 1965.
- DEAN, D. S.: Microwave Techniques. Technical Information Service, American Institute of Aeronautics and Astronautics (New York). (A70-11395)
- DRAYER, D. W.; AND BOWDEN, W. J.: Evaluation of Filament Wound Epoxy Composites. [AT(29-1)-789] Final Rept., Bendix Corp., Kansas City Div., Feb. 1967. (N67-29953)
- EPSTEIN, GEORGE; AND ROWAND, RICHARD R.: NDT Methods for Composites, Reinforced Plastics. Materials Engineering, vol. 70, no. 4, 1969, pp. 59-62.
- FEINSTEIN, LESTER; AND HRUBY, RONALD J.: Microwave Detection of Surface Cracks on Metals. (AIAA Paper no. 68-321) Proc. of 9th Conference on Structures, Structural Dynamics, and Materials. Sponsored by AIAA and ASME (Palm Springs, Calif.), Apr. 1-3, 1968. (A68-24274)
- FOWLER, K. A.; ET AL.: Detection of Voids and Inhomogeneities in Fiber Glass Reinforced Plastics by Microwave and Beta-Ray Backscatter Techniques. Springfield Armory (Springfield, Mass.), May 20, 1966. (AD 644 419)
- GIBSON, JOHN A.: Review of Nondestructive Testing Techniques for Detecting Lack of Penetration in Aluminum Fusion Welds. (DAAH01-67-C-1921) Battelle Memorial Institute (Columbus, O.) Oct. 11, 1967. (AD 661 044)
- GRUBINSKAS, ROBERT C., ET AL. A Report Guide to Literature in the Field of Electromagnetic Testing. AMRA-MS-65-03, Nondestructive Testing Information Center, Apr. 1965. (AD 615 346)
- HABORAK, R. C.: Nondestructive Testing (NDT) Acousto-Optical Imaging. (NAS7-747) First Quarterly Progress Rept., TRW Systems Group (Redondo Beach, Calif.), Oct. 13, 1969.
- HABORAK, R. C.: Nondestructive Testing (NDT) Acousto-Optical Imaging. (NAS7-747) Monthly Progress Rept. no. 3, TRW Systems Group (Redondo Beach, Calif.), Nov. 5, 1969.
- HABORAK, R. C.: Nondestructive Testing (NDT) Acousto-Optical Imaging. (NAS7-747) Second Quarterly Progress Rept., TRW Systems Group (Redondo Beach, Calif.), Jan. 5, 1970.
- HALL, ELIZABETH H.: Non-Destructive Testing—A Report Bibliography. Defense Documentation Center, Cameron Station (Alexandria, Va.), Nov. 1963.
- HOGARTH, C. A.; AND BLITZ, J.: Techniques of Non-Destructive Testing. Butterworths (London), 1960.
- KLEINT, R. E.; AND HAGEMAIER, D. J.: Relationship of Standards and Specifications to Nondestructive Testing. Materials Evaluation, Aug. 1965.
- LUCIAN, A. D.; AND CRIBBS, R. W.: The Development of Microwave NDT Technology for the Inspection of Nonmetallic Materials and Composites. (NAS7-367) Aerojet-General Corp. (Sacramento, Calif.), June 1, 1967.
- MCFAUL, H. J.; AND WEBB, C. W.: Quality and Economic Improvement in Nondestructive Testing. Nondestructive Testing, vol. 19, no. 5, 1961, pp. 327-328.
- MCMMASTER, ROBERT C.: Management Use of Nondestructive Tests. Nondestructive Testing, vol. 19, no. 2, 1961, pp. 116-123.
- MCMMASTER, ROBERT C.: Nondestructive Testing Handbook. Vol. I, The Ronald Press Co., 1963.
- MULLINS, L.: The Scope of Non-Destructive Testing. Institute of Marine Engineers—Transactions, vol. 78, no. 10, 1966, pp. 426-434.
- NEUSCHAEFER, ROBERT W.: Assuring Saturn Quality Through Nondestructive Testing. Material Evaluation, vol. 27, no. 7, 1969, pp. 145-152.
- SMILEY, ROBERT W.: Polaris Takes a Second Look at NDT. Materials Evaluation, vol. 24, Dec. 1966, pp. 679-682.
- VOGEL, PAUL E. J.: Paper 3—Infrared Multiple-Scan Bond Inspection System. U.S. Army Materials Research Agency (Watertown, Mass.).
- WALKER, B. E., JR.; AND EWING, C. T.: Nondestructive Testing for Void Content in Glass-Filament-Wound Composites. Naval Research Lab. (Washington, D.C.), Oct. 1968. (N69-17406)
- ZURBRICK, J. R.: The Mystery of Reinforced Plastics Variability: Nondestructive Testing Holds the Key. Materials Research and Standards, vol. 8, July, 1968, pp. 25-36. (A68-33849)

CHAPTER 8

- ANON: An Aid in the Selection of Nondestructive Testing Methods, Procedures and Specifications. NASA Reliability and Quality Assurance Office (Code KR), Wash., D.C.
- ANON: Fundamentals of Welding. Welding Handbook, Sixth ed., Section One, American Welding Society, 1968.
- ANON.: Inspection Procedure for Determining the Magnetic Permeability of Wrought Austenitic Steels. MIL-STD-288, July 26, 1956.

- ANON.: Inspection Requirements, Nondestructive: For Aircraft Materials and Parts. MIL-I-6870B (ASG), Feb. 25, 1956.
- ANON.: Magnetic Inspection Units. MIL-M-6867C, Jan. 27, 1969.
- ANON.: Magnetic Particle Indications on Steel Nuts. MS-17980 (SHIPS), Sept. 21, 1962.
- ANON.: Magnetic-Particle Inspection; Process, for Ferromagnetic Materials. MIL-M-11472 (ORD), Sept. 24, 1951.
- ANON.: Magnetic-Particle Inspection; Soundness Requirements for Weldments. MIL-M-11473 (ORD), Sept. 24, 1951.
- ANON.: Magnetic Particle Inspection Unit, Lightweight. MIL-M-23527 (SHIPS), Dec. 17, 1962.
- ANON.: Magnetic Particle Method, Supplement B. American Society for Nondestructive Testing, Recommended Practice no. SNT-TC-IA, 1968.
- ANON.: Magnetic Particle Testing. NASA CR-61206, 1967. (N68-28778)
- ANON.: Nondestructive Testing Requirements for Metals. MIL-STD-271D (SHIPS), Mar. 11, 1965.
- ANON.: Operating and Servicing Manual for NASA-ARC Portable Magnetic Test Unit. Rept. A-13050, NASA-Ames Research Center, Oct. 8, 1968.
- ANON.: Steel Forgings, Carbon and Alloy, for Shafts, Sleeves, Couplings, and Stocks (Rudders and Diving Planes). MIL-S-23284 (SHIPS), June 29, 1962.
- BARRY, R. C.; AND HEISER, G. G.: Evaluation of the Quality of Electron Beam Butt Welds in High Strength Maraging Steel Rings. Symposium on Nondestructive Testing of Welds and Materials Joining (Los Angeles). Sponsored by Am. Soc. NDT, Mar. 11-13, 1968.
- BASTOW, JOSEPH G.: Proceedings of the Magnetics Workshop. NASA CR-67986, 1965.
- FOWLER, KENNETH A.: Magnetic Methods for Crack Detection in Cannon Bores. U.S. Army Materials Research Agency (Watertown, Mass.), Feb. 1967.
- GRUBINSKAS, ROBERT A.; AND MERHIB, CHARLES P.: A Report Guide to Literature in the Field of Electromagnetic Testing. Rept. AMRA MS65-03, Nondestructive Testing Information Center, U.S. Army Materials Research Agency (Watertown, Mass.), Apr. 1965.
- HARRIS, CHARLES A.: Magnetic Field Restraints for Spacecraft Systems and Subsystems. Rept. X-325-67-70, NASA-Goddard Space Flight Center, Feb. 1967.
- HAYES, D. A.: The Use of Mechanized Nondestructive Testing in Quality Control. Science and Technology, vol. XIII, no. 9, 1966.
- HENDRON, J. A.: Automated Magnetic Particle Inspection of Pressure Vessels. Nondestructive Testing, Jul.-Aug., 1963.
- KONOVALOV, E. G.; AND OREKHOV, G. T.: A Residual Stress Gauge (RSG). (In Russian) Akademiia Nauk BSSR, Doklady, vol. 12, Nov. 1968.
- KARLOV, G. I.; AND BYSTRUSHKIN, G. S.: Nondestructive Method for Checking the Early Stages of Fatigue Damage. Translated from Zavodskaya Laboratoriya, vol. 34, no. 7, 1968.
- KLEINT, R. E.; AND HAGEMAIER, D. J.: Relationship of Standards and Specifications to Nondestructive Testing. The Reliability and Industrial Statistics Courses, Univ. of Calif. (Los Angeles).
- LAMBERT, J. A. B.; AND TROUGHTON, A. J.: The Importance of Service Inspection in Aircraft Fatigue. Aircraft Engineering, vol. 39, Oct. 1967.
- MARTIN, G.: British Journal of Nondestructive Testing, vol. 9, no. 2, 1967.
- MCGONNAGLE, WARREN J., Nondestructive Testing. McGraw-Hill Book Company, Inc., 1961.
- MCMASTER, R. C.: A New Eddy Current Nondestructive Test. Metals Engineering Quarterly, vol. 6, May 1966, pp. 32-49.
- MIROSHIN, I. V.: The Formation of a Defect Field of Magnetization of a Specimen by a Moving Field From a Localized Source. National Lending Library for Science and Technology, Boston Spa (Yorkshire, England).
- NAZAROV, S. T.: Ways for the Automation of Nondestructive Weld-Joint Inspection Methods. Foreign Technology Division, Wright-Patterson AFB, Ohio, May 1965.
- PARSONS, C. L.; AND HARRIS, C. A.: Component Magnetic Test Facility Operations and Test Procedure Manual. NASA TM X-55495, 1965.
- RODGERS, ERNEST H.; AND MERHIB, CHARLES P.: A Report Guide to Magnetic Particle Testing Literature. Rept. AMRA MS-65-04, U.S. Army Materials Research Agency (Watertown, Mass.), June 1965.
- ROLLWITZ, WILLIAM L.: Magnetoabsorption. Progress in Applied Materials Research, vol. 6, 1964. [Available from Gordon and Breach Publishers, Inc. (New York)].
- SKINNER, KENNETH L., ET AL.: Passive Instrumentation and Stimuli Generation for Saturn IB Equipment Checkout. NASA CR-76404, May 1966.
- SKINNER, KENNETH L., ET AL.: Passive Instrumentation and Stimuli Generation for Saturn IB Equipment Checkout. NASA CR-76403, May 1966.

CHAPTER 9

- ADAMS, C.; HAGEMAIER, D.; MAYER, J.: Nondestructive Testing of Brazed Rocket Engine Components. (NASS-18734). Paper presented at the American Welding Society, 6th Western Welding Technical Conference (Palo Alto, Calif.), May 1968.
- ANON.: Leak Detection Manual. Rept. 99249-0011, Consolidated Electrodynamics Corp., Apr. 1967.
- ANON.: Leak Locator for Vacuum Jacketed Pipelines Eliminates Need for Removal of Outer Jacket. NASA Tech Brief 66-10412, 1966.
- ANON.: Research Achievements Review Series No. 10. NASA TM X-53466, 1965.

- ANSLEY, S. P., JR.; AND WILLIAMS, R. B.: Vacuum Leak Detection as Applied to Major Space Environmental Chambers. Rept. AEDC-TDR-63-142, ARO Inc., Aug. 1963.
- BAIN, J. A.; AND LANIEWSKI, J. P.: Zero Leakage Design for Ducts and Tube Connections for Deep Space Travel—Fundamental Investigations. NASA CR-93925, 1967.
- BAIN, J. A.; AND LANIEWSKI, J. P.: Zero Leakage Design for Ducts and Tube Connections for Deep Space Travel—Tube Connector Design Principles and Evaluation. NASA CR-93924, 1967.
- BLOCK, M. N.; AND DEGREEFF, J. O.: Research and Determination of Rates of Leakages of Nuclear Fuel Elements. Translated from Eurotom Communication 688, Jan. 1964.
- COOPER, R. M.; AND NAGY, A. J.: Leak Testing of Aerospace Components Subsystems and Systems. Spacecraft Department, MSD, General Electric Co.
- McGONNAGLE, WARREN J.: Nondestructive Testing. McGraw-Hill Book Co., Inc., 1961.
- MANGANARO, J. L.; HOLLINGER, D. L.; AND KOCK, E. F.: Mass Spectrometer Leak Testing by a Calibrated Enclosure Method. Materials Evaluation, Dec. 1968.
- MANN, C. A.; AND CAMPSIE, I. C.: The Non-Destructive Testing of Fuel Elements and Their Components for the U.K. Power Reactor Development Programme. United Kingdom Atomic Energy Authority, 1965.
- PAPPIN, W.: Helium Leak Detection Techniques. Symposium in Nondestructive Tests in the Field of Nuclear Energy, ASTM STP no. 233, 1958.
- PAULK, J. I. ET AL.: Hermetic Seal Evaluation for Electronic Components. NASA CR-61225, 1968.
- ROEHRS, ROBERT J.: Leak Testing Cryogenic Vessels, Part II. Cryogenic Engineering News, May 1969.
- ANON.: Strain Gages—First in Strain Measurement. BLH Electronics, Inc. (Waltham, Mass.).
- ANON.: Strain Gage Handbook. BLH Electronics, Inc. Waltham, Mass.
- ANON.: Strain Gage Pressure Transducer, Final Data Report. Aerojet-General Corp. (Sacramento, Calif.), Feb. 1967.
- ANON.: Understanding Photoelasticity. Machine Design, Oct. 24, 1968.
- ANON.: Weldable Strain Gages. Microdot Inc., South Pasadena, Calif.
- BECKER, HERBERT; AND TANG, C. N.: Investigation of Stresses in the Algol II-B Rocket Nozzle Model. NASA CR-5191, 1966.
- BOHLEN, J. C.: Process Development of Large Photoelastic Birefringent Plastic Sheets. Department of Forestry and Rural Development (Vancouver, B.C.), June 1968.
- CRITES, N. A.: Your Guide to Today's Strain Gages. Product Engineering, Feb. 19, 1962.
- DEAN, M., III; AND DOUGLAS, R. D.: Semiconductor and Conventional Strain Gages. Academic Press (New York), 1962.
- DEAN, M., III: Techniques for Protecting and Waterproofing Resistance Wire Strain Gages. R & D Rept. no. 797, The David W. Taylor Model Basin, U.S. Navy (Wash., D.C.), Mar. 1956.
- FROCHT, M. M.: Photoelasticity. The MacMillan Co., 1963.
- GINSBURG, V. L.: Stress Analysis by the Optical Method. NASA TT F-9327, Apr. 1965.
- HOFFMAN, I. S.: Wind-Tunnel Evaluation of a Parachute Instrumentation Concept. Rept. LWP-531, NASA-Langley Research Center, Dec. 20, 1967.
- HOSHIZAKI, T.; AND YOKOYAMA, DR. K.: Recording Leaf Movements with a Strain Gauge. Nature, vol. 207, 1965, pp. 880-881.
- MASUBUCHI, KOICHI: Nondestructive Measurement of Residual Stresses in Metals and Metal Structures. NASA CR-64918, 1965.
- MURRAY, W. M.; AND STEIN, P. K.: Lectures and Laboratory Exercises on Strain Gage Techniques. Paper presented at the Dept. of Engr., Univ. of Calif. (Los Angeles), Aug. 21-Sept. 1, 1961.
- NALLE, D. H.: Fundamentals of Strain Measurement and Recording. Part I, Equipment, Nov. 1961, pp. 51-55; Part III, Equipment, Feb. 1962; and Part IX, Equipment, May 1962.
- POPOV, E. P.: Mechanics of Materials. Prentice-Hall, Inc., 1952.
- SANCHEZ, J. C.; AND WRIGHT, W. V.: Semiconductor Strain Gages—What Can They Do? ISA Journal, vol. 9, no. 5, 1962.
- SAN MIGUEL, A.; AND DURAN, E. N.: Some Low-Modulus Birefringent Resins. Experimental Mechanics, vol. 4, no. 3, 1964.

CHAPTER 10

- AKHMETZIANOV, M. KH.: Application of Photoelastic Coatings in the Investigation of Shells. Translation from Izvestiya An SSSR, Mekhanika, no. 6, pp. 84-86, 1965. (N66-22282)
- AKHMETZIANOV, M. KH.: Application of the Method of Photoelastic Coatings to the Determination of the Stresses and Deformations in Flexible Plates and Shells. Translation from Izvestiya Akademii Nauk SSSR, Mekhanika, Mashinostroyeniye, no. 1, pp. 199-201, 1964. (N64-25055)
- ANON.: The Development and Evaluation of an Inorganic Bonding Method for Semiconductor Strain Gages for Space and Ultra High Vacuum Applications. NASA CR-100015, 1968. (N69-19138)
- ANON.: Procedure for Installation of Strain Gages. NASA-MSFC-SPEC-10M01691, Apr. 2, 1963.
- ANON.: Micro-Measurements Catalog and Technical Data Binder. Vishay Intertechnology, Inc. (Romulus, Mich.).
- ANON.: Miniature Telemetry System Accurately Measures Pressure. NASA Tech Brief 66-10624, 1966.

- SCHUERER, P. H.; AND SIMPSON, W. G.: Evaluation of Strain Indicator Coatings for Application in Detecting Voids and Bonded Honeycomb Sandwich Structures. NASA TM X-53135.1, 1964.
- SCOTT, I. G.: Creep of Resistance Strain Gauges at Elevated Temperatures. Dept. of Supply, Australian Defense Scientific Service, Aeronautical Research Lab., Melbourne, May 1968.
- SCOTT, I. G.: Pre-Attachment Matching of Resistance Strain Gauges on a Temperature Coefficient Basis. Dept. of Supply, Australian Defense Scientific Service, Aeronautical Research Lab., June 1968.
- SLOT, T.: Reflection Polariscope for Photography of Photoelastic Coatings. *Experimental Mechanics*, vol. 2, no. 2, 1962.
- TENNYSON, R. C.: A Review of the Theory of Photoelasticity. Inst. of Aerophysics, Univ. of Toronto, UTIA Review no. 23, Dec. 1962.
- THOMPSON, W. H.: Photoelastic Analysis of Stress Waves Resulting from Exploding Wires. Union Carbide Corp., Oak Ridge, Tenn., July 1, 1966.
- WRIGHT, R. R.: Semiconductor Pressure Transducers. Sandia Lab., Albuquerque, N. Mex., Sept. 1965.
- GRANT, R. A.; AND BROWN, G. M.: Holographic Non-destructive Testing (HNDT). *Materials Evaluation*, vol. 27, no. 4, 1969, pp. 79-84.
- GOODMAN, J. W.: *Introduction to Fourier Optics*. McGraw Hill Book Co., Inc., 1968.
- JOLLY, W. D.: The Application of Acoustic Emission to In-Process Inspection of Welds. *Materials Evaluation*, vol. 28, no. 6, 1970, pp. 135-139.
- KERSCH, L. A.: Advanced Concepts of Holographic Nondestructive Testing. *Materials Evaluation*, vol. 29, no. 6, 1971, pp. 125-129.
- KREUZER, J. L.: Ultrasonic Holography for Nondestructive Testing. *Materials Evaluation*, vol. 26, no. 10, 1968, pp. 197-203.
- MAROM, E.; AND MUELLER, R. K.: Nondestructive Early Fatigue Detection. Proceedings of the 6th Symposium on Nondestructive Evaluation of Aerospace and Weapons Systems Components and Materials, 1967, pp. 79-91. [Available from Western Periodicals Co. (Los Angeles, Calif.)]
- METHEREL, A. F., ed.: *Acoustical Holography*. Proceedings of the International Symposium on Acoustic Holography. vol. 1, 1969, vol. 2, 1970, and vol. 3, 1971. [Available from Plenum Press Corp. (New York).]
- NAKAMURA, Y.: Acoustic Emission Monitoring System for Detection of Cracks in a Complex Structure. *Materials Evaluation*, vol. 29, no. 1, 1971, pp. 8-12.
- ROMRELL, D. M.; AND BUNNEL, L. R.: Monitoring of Crack Growths in Ceramic by Acoustic Emission. *Materials Evaluation*, vol. 28, no. 12, 1970, pp. 267-270.
- SMITH, H. W.: *Principles of Holography*. Wiley-Interscience (New York), 1969.
- SHARPE, R. S., ed.: *Research Techniques in Nondestructive Testing*. Academic Press (London and New York), 1970.
- WAITE, E. V.; AND PAIRY, D. L.: Field Evaluation of Heavy-Walled Pressure Vessels Using Acoustic Emission Analysis. *Materials Evaluation*, vol. 29, no. 6, 1971, pp. 117-124.

CHAPTER 11

- BREDEN, B. E.: Acoustical Holography as a Tool for Nondestructive Testing. *Materials Evaluation*, vol. 27, no. 6, 1969, pp. 140-144.
- CHAUNG, K. C.: Application of the Optical Correlation Measurement to Detection of Fatigue Damage. *Materials Evaluation*, vol. 26, June 1968, pp. 116-119.
- DUNEGAN, H. L.; HARRIS, D. O.; AND TETELMAN, A. S.: Detection of Fatigue Crack Growth by Acoustic Emission Techniques. *Materials Evaluation*, vol. 28, no. 10, 1970, pp. 221-227.
- FREDERICH, J. R.: Acoustic Emission as a Technique for Nondestructive Testing. *Materials Evaluation*, vol. 28, no. 2, 1970, pp. 43-47.
- GABOR, D.; KOCK, W. E.; AND STROKE, G. W.: Holography. *Science*, vol. 173, July 2, 1971, pp. 11-22.

○